

***β /MESO-FUNCTIONALIZED PORPHYRINS: SYNTHESSES
AND THEIR UTILIZATION IN ANION SENSING, NLO
AND COMPLEXATION WITH FULLERENES***

Ph.D. THESIS

by

PINKI RATHI



**DEPARTMENT OF CHEMISTRY
INDIAN INSTITUTE OF TECHNOLOGY ROORKEE
ROORKEE-247667 (INDIA)
AUGUST, 2019**

***β /MESO-FUNCTIONALIZED PORPHYRINS: SYNTHESSES
AND THEIR UTILIZATION IN ANION SENSING, NLO
AND COMPLEXATION WITH FULLERENES***

A THESIS

*Submitted in partial fulfilment of the
requirements for the award of the degree*

of

DOCTOR OF PHILOSOPHY

in

CHEMISTRY

by

PINKI RATHI



DEPARTMENT OF CHEMISTRY
INDIAN INSTITUTE OF TECHNOLOGY ROORKEE
ROORKEE-247667 (INDIA)
AUGUST, 2019



**©INDIAN INSTITUTE OF TECHNOLOGY ROORKEE, ROORKEE-2019
ALL RIGHTS RESERVED**



Dedicated
to
my Parents

ACKNOWLEDGEMENTS

Ph.D. is a project complemented with a great deal of intricacy, foiling, effort, trust and support of a number of associates. I want to convey modicum of deep sense of gratitude from the core of heart to all who helped me to reach this magical day.

First and foremost, I bow my head before the highly benevolent and merciful almighty, the God for all his divine blessing showered on me to reach at this brink of giving a final shape to my dream.

*It gives me immense pleasure in expressing a deep sense of gratitude to my supervisor, **Dr. M. Sankar**, who exemplified to me the meaning of research. At the verge of this wonderful day, when I pause to look back to my research period, I feel equally glad for his perpetual encouragement, prudent guidance and dynamic interest throughout my research work. I am highly grateful for his placid and benign behavior, his patience in correcting mistakes during my research period. Further, this feat was possible only because of his unconditional support. My heartfelt thanks to Mrs. Ananthalakshmi Sankar, for her care, kindness and providing homely atmosphere.*

I would also like to express my sincere thanks to Prof. K. R. Justin Thomas (present) as well as Prof. M. R. Maurya (former), Head, Department of Chemistry and all other faculty members for providing me the essential infrastructural facilities to carry out research investigations. I am grateful to my research committee members, Prof. M. R. Maurya (Chairman), Department of Chemistry, Dr. Parsenjit. Kar (Internal member), Department of Chemistry, and Dr. P. Gopinath (External member), Centre of nanotechnology, IIT Roorkee, for their valuable suggestions and encouragement to carry out this work.

My heartfelt thanks to Mr. Madan Pal and Mr. Ramesh Department of Chemistry, for their technical help during my presentations in the department. Further, I express my gratitude to the Head, IIC, IIT Roorkee for providing necessary instrumentation facilities. My sincere thanks to the Head, Department of Biotechnology for providing MALDI mass spectral facility to carry out this research work. I am thankful to Ms. Neetu Singh and Prof. U. P. Singh, IIT Roorkee, for single crystal X-ray data collection.

“The love of a family is life’s greatest blessings”. I would like to express special thanks and sincere gratitude to my parents Smt. Kusum and Sh. Yashpal Singh for their immense love, support and prayers during all the tough times. I am extraordinary privileged in having Dr. Arun

Kumar and Aaditya Rathi as my brothers without their prior teachings, guidance and ceaseless encouragement, I could never have embarked and started this journey. I am fortunate in having Mr. Chirag Malik my husband who is a pillar of support during all the stressful time and has always been there for me. I want to express sincere gratitude to my in-laws Smt. hariendr and Sh. Rampal Singh for their constant love, support and care during my research time. I feel a deep sense of gratitude to my sisters Neetu, Madhu, Archna, Pooja, Meenu for their constant support. Also, I want to express my immense love to my niblings Tanvi, Raghav, Kitto, Rudhra and Sanchi. Their cuteness always makes my day cheerful.

No research is possible without a good company of friends. I am truly thankful to my close friends Renu Saini and Sandeep. Their endless support, valuable advice and concerning behavior turned my all days intensely delightful and certainly unforgettable. I would like to express my warm thanks to my labmates and friends Dr. Ravi Kumar, Dr. Pinky Yadav, Dr. Nitika Grover, Dr. Kamal Prakash, Dr. Nivedita Chaudhari, Dr. Mandeep K. Chahal, Dr. Tawseef, Ashwin, Mohina, Amit Saxena, Madhusudan, Dr. Pinky Singh, Sandeep, Renu Rohal, Inderpal, Soni, Aamir, Nivedita, Tasleem, Ankit Sharma, Ekta, Teena and Sonia for their friendly behavior. My sincere acknowledge to my all cousins, friends, batchmates and whose names have been unknowingly left, thank you very much for your prayers. My sincere apologies if I have missed someone, but I am grateful for their support.

Last but not the least I feel privileged for my stay at IIT Roorkee and providing a healthy environment and a wonderful ambience. I fare-a-diu to this prestigious Institute fully satisfied and take an oath to serve for the mankind of my nation and the whole world with whatever the knowledge and wisdom. I possess and will acquire in future by virtue of furtherance of my research work and results thereof.

Pinki Rathi

ABSTRACT

Porphyrins are naturally occurring tetrapyrrolic pigments. They are highly π -conjugated system which makes them interesting and versatile. In living systems, porphyrins are very vital to biomolecules and many enzymes which play significantly important physiological process like redox reaction, photosynthesis, gas transport and so on. Porphyrins are chemically versatile molecule due to chemical and thermal stabilities and conformational flexibility. Porphyrins have optical, photophysical and electrochemical redox properties which make them robust precursor for obtaining medicinally, scientifically and industrially suitable materials. The photophysical and electrochemical redox properties of porphyrins can be altered by fine tuning in structural modification and electronic nature of *meso*/ β -substituents. β -Substituents exerts much larger electronic and steric effects in comparison to substitution at *meso*-positions since they are in direct conjugation with porphyrin π -system. Various β -substituted porphyrins are utilized for NLO, PDT, ion sensing, catalytic and DSSCs applications. Herein, we report the synthesis of *meso*/ β -functionalized porphyrins and their utilization in various application such as anion sensing, NLO and complexation with fullerene. We have organized this thesis into following 8 chapters.

Chapter 1 describes the basic introduction about porphyrins, their synthetic methods and their applications in different arena such as catalysis, NLO, DSSC, anion sensing and PDT.

Chapter 2 includes the synthesis of mixed β -substituted arylaminoporphyrins and N-fused porphyrins (MTPP(NHPh) X_2 and MTPP(N-fused) X_2 , X = H, Br, Ph, PE and M = 2H, Co(II), Ni(II), Cu(II), Zn(II)). These porphyrins exhibited interesting photophysical and electrochemical redox properties. Single crystal X-ray study revealed twist conformation of H₂TPP(N-fusedPh)Br₂. Photoinduced electron transfer study of ZnTPP(N-fused) X_2 , X = H, Br, Ph, PE was carried out *via* axial coordination of C₆₀Im and C₆₀Py which exhibited 1:1 supramolecular dyads formation. These porphyrins exhibited very low oxidation potential due to intramolecular charge-transfer from β -arylamine group to porphyrin core. Efficient fluorescent quenching was observed for Zn(II) N-fused porphyrins while titrating with C₆₀ derivatives due to axial coordination of C₆₀Im/C₆₀Py to Zn(II) porphyrin. The first oxidation potential of supramolecular dyads are anodically shifted (\sim 0.10 V) as compared to C₆₀Im/C₆₀Py free Zn(II)porphyrins which exhibited supramoleccular interaction between Zn(II) porphyrins and C₆₀Im/C₆₀Py system in ground state.

Chapter 3 describes the synthesis of tetrabenzoquinone appended Ni(II) and Cu(II) porphyrins. These porphyrins exhibited strong solvatochromism behavior in nitrogenous base through axial coordination. We studied the F⁻ and CN⁻ anion sensing properties of these porphyrins. The electrochemical studies revealed that tetrabenzoquinone appended metalloporphyrin is electron deficient by ~1.1 V as compared to TDtBPPM (M = Cu, and Ni) and nearly 0.94 V as compared to oxoporphyrinogen respectively and therefore binds to less basic F⁻ ions also in addition to highly basic CN⁻ ions through axial ligation mechanism. They act as F⁻ and CN⁻ chemosensor in nonaqueous media and selective CN⁻ sensor in aqueous media due to high solvation of F⁻ ions in aqueous media.

Chapter 4 describes the synthesis of two new series of unsymmetrically nonplanar mixed β -octasubstituted porphyrins (MTPP(Ph₂)Br₅X, X = NO₂, Br and M = 2H, Co(II), Ni(II), Cu(II), Zn(II)) and studied their structural, photophysical and electrochemical redox properties. Single crystal X-ray study of H₂TPP(NO₂)Ph₂Br₅ exhibited saddle shape nonplanar conformation with deviation of 24 core atoms ($\Delta 24 = \pm 0.558 \text{ \AA}$) and displacement of β -carbons ($\Delta C_{\beta} = \pm 1.23 \text{ \AA}$) from the mean plane of porphyrin core. So H₂TPP(NO₂)Ph₂Br₅ exhibited highly nonplanar conformation as compared to precursor (H₂TPP(NO₂)(Ph)₂) ($\Delta C_{\beta} = \pm 0.671 \text{ \AA}$ and $\Delta 24 = \pm 0.320 \text{ \AA}$) due to the effect of five β -bromo substituents at periphery of the porphyrin. H₂TPP(Ph₂)Br₅X, X = NO₂, Br exhibited 53-61 nm and 90-95 nm bathochromic shift in the Soret band and Q_{x(0,0)} band, respectively as compared to H₂TPP. They are exhibited higher protonation and deprotonation constant due nonplanar conformation of macrocyclic core and electronic nature of β -substituents. HOMO-LUMO energy gap of CuTPP(Ph₂)Br₆ and CuTPP(NO₂)Ph₂Br₅ decreased to 0.55 V and 0.62 V as compared to CuTPP, respectively .

Chapter 5 presents the synthesis of *meso*-tetraalkylporphyrin and their Zn(II) derivatives. Single crystal X-ray structure of *meso*-tetrapropylporphyrin revealed the orientation of alkyl chains and planar conformation of porphyrin macrocycle. Photophysical, spectroscopic and electrochemical redox properties of self-assembled donor-acceptor dyads formed by *meso*-tetraalkylporphyrin and fullerene C₆₀ were investigated. The binding of C₆₀ with porphyrins (H₂TMeP, H₂TtP and H₂TPrP) and their Zn derivatives was determined by UV-Vis, fluorescence and ¹H NMR analyses. The stoichiometry of complexation between C₆₀ and porphyrin was found to be 1:1. The determined association constants of (K) follow the order: H₂TMeP > H₂TtP > H₂TPrP > H₂THexP > H₂TPP. The effect of alkyl chain length on porphyrin-fullerene complexation were

investigated. The oxidation potentials of dyads anodically shifted (20-100 mV) as compared to corresponding *meso*-tetraalkylporphyrins indicating supramolecular interaction between the constituents in ground state. Optimized geometry of H₂TMeP:C₆₀ revealed the formation of supramolecular dyads and charge transfer interaction between porphyrin host and fullerene (C₆₀) guest.

Chapter 6 encompasses the synthesis of mixed β -trisubstituted (MTPP(TPA)₂X, (where M = Co, Ni, Cu, Zn and X = NO₂/CHO) porphyrins with their photophysical, electrochemical redox properties and DFT studies. H₂TPP(TPA)₂X, (X = NO₂/CHO) exhibited ~22 nm and 31-39 nm red shift in Soret and Q_{x(0,0)} bands, respectively than H₂TPP due to effect of β -substituents and nonplanarity of macrocycle. The push-pull effect of NO₂/CHO and TPA affect the HOMO-LUMO energy gap. H₂TPP(TPA)₂NO₂ and H₂TPP(TPA)₂CHO exhibited large resultant dipole moment values 7.62 D and 4.55 D, respectively as compared to H₂TPP (0.052 D).

Chapter 7 presents the synthesis of antipodal β -tetrasubstituted porphyrins and characterized by using various spectroscopic techniques. Due to β -tetrasubstitution they exhibited tunable redox potentials and moderate nonplanar conformation. These porphyrins are easy to oxidize as compared to MTPPs. NiTPP(TPA)₄ exhibited 0.15-0.29 V and 0.03-0.04 V cathodic shift in first oxidation potential and first reduction potential, respectively as compared to NiTPP and NiOPP due to destabilization of HOMOs.

Chapter 8 summarizes the results obtained from the present thesis with future perspectives.

List of Publications (Published/Communicated/Prepared)

1. **P. Rathi** and M. Sankar* Highly Electron Deficient Tetrabenzoquinone appended Ni(II) and Cu(II) Porphyrins: Spectral, Solvatochromism, Electrochemical Redox and Tuneable F⁻ and CN⁻ Sensing Properties. *New J. Chem.* **2017**, *4*, 11962-11968.
2. N. Grover, **P. Rathi** and M. Sankar* Spectral Investigations of *Meso*-Tetraalkylporphyrin-Fullerene Host-Guest Complexes. *J. Porphyrins Phthalocynines.* **2015**, *19*, 998-1006.
3. R. Kumar, P. Yadav, **P. Rathi** and M. Sankar* Photophysical, Electrochemical Redox, Solvatochromism and Anion Sensing Properties of β -Tetra- and -Octaphenylethynyl Substituted *meso*-Tetraphenylporphyrins. *RSC Adv.* **2015**, *5*, 82237-82246.
4. P. Yadav, **P. Rathi** and M. Sankar* Facile Generation of A₂B Corrole Radical using Fe(III) salts and its Spectroscopic Properties. *ACS Omega*, **2017**, *2*, 959-965.
5. **P. Rathi** and M. Sankar* Unsymmetrical Nonplanar ‘Push-Pull’ β -Octasubstituted Porphyrins: Facile Synthesis, Structural, Photophysical and Electrochemical Redox Properties *Dalton Trans.* **2019**, DOI: 10.1039/C9DT02792K.
6. **P. Rathi**, S. Seetharaman, M. Sankar,* F.D’Souza* Synthesis, Structural, Spectral and Electrochemical Redox Properties of N-Fused Porphyrins and Their Photoinduced Electron Transfer Studies with C₆₀ Derivatives (Manuscript under preparation).
7. F. D’Souza, K. Prakash, A. Z. Alsaleh, **P. Rathi**, A. Sharma and M. Sankar* Synthesis, Spectral, Electrochemical and Photovoltaic Studies of A₃B Porphyrinic Dyes having Peripheral Donors *ChemPhysChem* **2019**. <https://doi.org/10.1002/cphc.201900604>.
8. **P. Rathi** and M. Sankar* β -Functionalized ‘Push-Pull Porphyrins: Synthesis, Photophysical and Electrochemical Redox Properties (Manuscript under preparation).
9. **P. Rathi** and M. Sankar* A Synthetic Approach toward the Mixed β -substituted Arylamino porphyrins: Synthesis, Photophysical and Electrochemical Redox Properties (Manuscript under preparation).

Poster presentation at International and National Conferences

- 1. P. Rathi** and M. Sankar* ‘Regioselective Synthesis and Studies on β -functionalized ‘Push-Pull’ Porphyrins poster presentation at National Conference on Organic Molecules as Synthons and Reagents for Innovations held at IIT Roorkee on February 8-10, 2019.
- 2. P. Rathi** and M. Sankar* ‘A Synthetic Approach toward the Mixed β -Substituted Arylamino porphyrins: Structural, photophysical and Electrochemical studies’ to be presented at the 10th International Conference on Porphyrins and Phthalocyanines (ICPP-10) held at Munich, Germany during July 1-6, 2018.
- 3. P. Rathi** and M. Sankar* ‘Synthesis, Spectral and Electrochemical Redox Properties of Asymmetrical β -Substituted’ Porphyrins poster presentation at ‘ACS on Campus -2018’ held at IIT Roorkee on February 7, 2018.
- 4. P. Rathi**, T. A. Dar and M. Sankar* ‘Sterically Crowded Porphyrins: Synthesis and Their Catalytic Applications’ poster presentation at Modern Trends in Inorganic Chemistry (MTIC-XVII) held at CSIR-NCL, Pune and IISER, Pune during December 11-14, 2017.
- 5. P. Rathi**, N. Grover and M. Sankar* ‘Spectral Investigation of *Meso*-Tetraalkylporphyrins-Fullerene Host-guest Assemblies’ poster presentation at the 18th CRSI National Symposium in Chemistry (NSC-18) held at INST Mohali and Punjab University, Chandigarh, during February 5-7, 2016.

TABLE OF CONTENTS

Title	Page No.
Candidate's declaration	
Acknowledgement	i
Abstract	iii
List of Publications	vi
List of Conferences	vii
Table of Contents	viii
List of Charts	xiv
List of Schemes	xv
List of Figures	xvi
List of Tables	xxi
CHAPTER 1. Introduction	
1.1 General Introduction to Tetrapyrrolic Pigments	2
1.2 Synthetic Tetrapyrrole Analogues	3
1.3 Synthesis of Porphyrin in Laboratory	4
1.4 Functionalization of Tetrapyrroles	6
1.4.1 Nitration and Bromination of Tetrapyrroles	7
1.4.2 β -fused Porphyrin	8
1.5 Some Applications of Porphyrin and their Analogues	10
1.5.1 Porphyrins as Catalysts	10
1.5.2 Porphyrins in Photodynamic Therapy	11
1.5.3 DSSCs Application of Porphyrins	15

1.5.4 Porphyrins as Sensors for Analytes	18
1.5.5 Porphyrins as NLO Material	19
1.5.6 Porphyrins Intraction with Fullerenes	20
1.6 Objectives and Future Implications of Present Work	21
1.7 References	25
CHAPTER 2. Synthesis, Structural, Spectral and Electrochemical Redox Properties of β-Arylamino and N-fused Porphyrins and Photoinduced Electron Transfer Studies on N-fused Porphyrins With C₆₀ Derivatives	
2.1 Introduction	39
2.2 Experimental Section	41
2.2.1 Reagents	41
2.2.2 Instruments and Methods	41
2.2.3 Synthesis of MTPP(NHPh)X ₂ (X = H, Br, Ph, PE and M = 2H, Co, Ni, Cu, Zn) Derivatives	42
2.2.4 Synthesis of MTPP(N-fusedPh)X ₂ (X = H, Br, Ph, PE and M = 2H, Co, Ni, Cu, Zn) Derivatives	46
2.3 Results and Discussion	51
2.3.1 Synthesis and Characterization	51
2.3.2 Crystal Structure Discussions	52
2.3.3 Electronic Absorption Spectral Studies	53
2.3.4 Emission Spectral Discussions	56
2.3.5 DFT Studies	58
2.3.6 Electrochemical Redox Studies	60
2.3.7 Chemical Oxidation Studies	62
2.3.8 ¹ H NMR Studies	63
2.4 Conclusions	66

2.5 References	66
----------------	----

CHAPTER 3. Highly Electron Deficient Tetrabenzquinone Appended Ni(II) and Cu(II) Porphyrins: Spectral, Solvatochromism, Electrochemical Redox and Tuneable F⁻ and CN⁻ Sensing

3.1 Introduction	72
3.2 Experimental Section	74
3.2.1 Reagents	74
3.2.2 Instrumentation and Methods	74
3.2.3 Synthetic Procedure	75
3.3 Results and Discussion	75
3.3.1 Synthesis and Characterization	75
3.3.2 Cyclic Voltammetric Studies	77
3.3.3 Solvatochromism Studies	78
3.3.4 Anion Binding Studies	79
3.3.5 Computational Studies	84
3.3.6 Cyanide Sensing in Aqueous Media	84
3.4 Conclusions	86
3.5 References	86

CHAPTER 4. Highly Nonplanar, Asymmetrical, β -octasubstituted Porphyrins: Synthesis, Structural, Photophysical and Electrochemical Redox Properties

4.1 Introduction	91
4.2 Experimental Section	92
4.2.1 Reagents	92
4.2.2 Instrumentation and Methods	93
4.2.3 Synthetic Procedure	93
4.3 Results and Discussion	96

4.3.1 Synthesis and Characterization	96
4.3.2 Single Crystal X-ray Structure	97
4.3.3 Electronic Spectral Studies	98
4.3.4 Protonation and Dprotonation Studies	100
4.3.5 Electrochemical Redox Properties	102
4.3.6 DFT Studies	105
4.4 Conclusions	107
4.5 References	107
CHAPTER 5. Spectral Investigation of <i>Meso</i>-Tetraalkylporphyrin-Fullerene Host-Guest Complexes	
5.1 Introduction	112
5.2 Experimental Section	114
5.2.1 Reagents	114
5.2.2 Instrumentation and Methods	114
5.2.3 Synthetic Procedure	114
5.3 Results and Discussion	116
5.3.1 Synthesis and Characterization	116
5.3.2 Crystal structure study of H ₂ TPrP	117
5.3.3 UV-Visible Spectral Studies	118
5.3.4 Fluorescence Spectral Studies	121
5.3.5 Cyclic Voltammetric Studies	123
5.3.6 ¹ H NMR Studies	124
5.3.7 Computational Studies	125
5.4 Conclusions	126
5.5 References	126

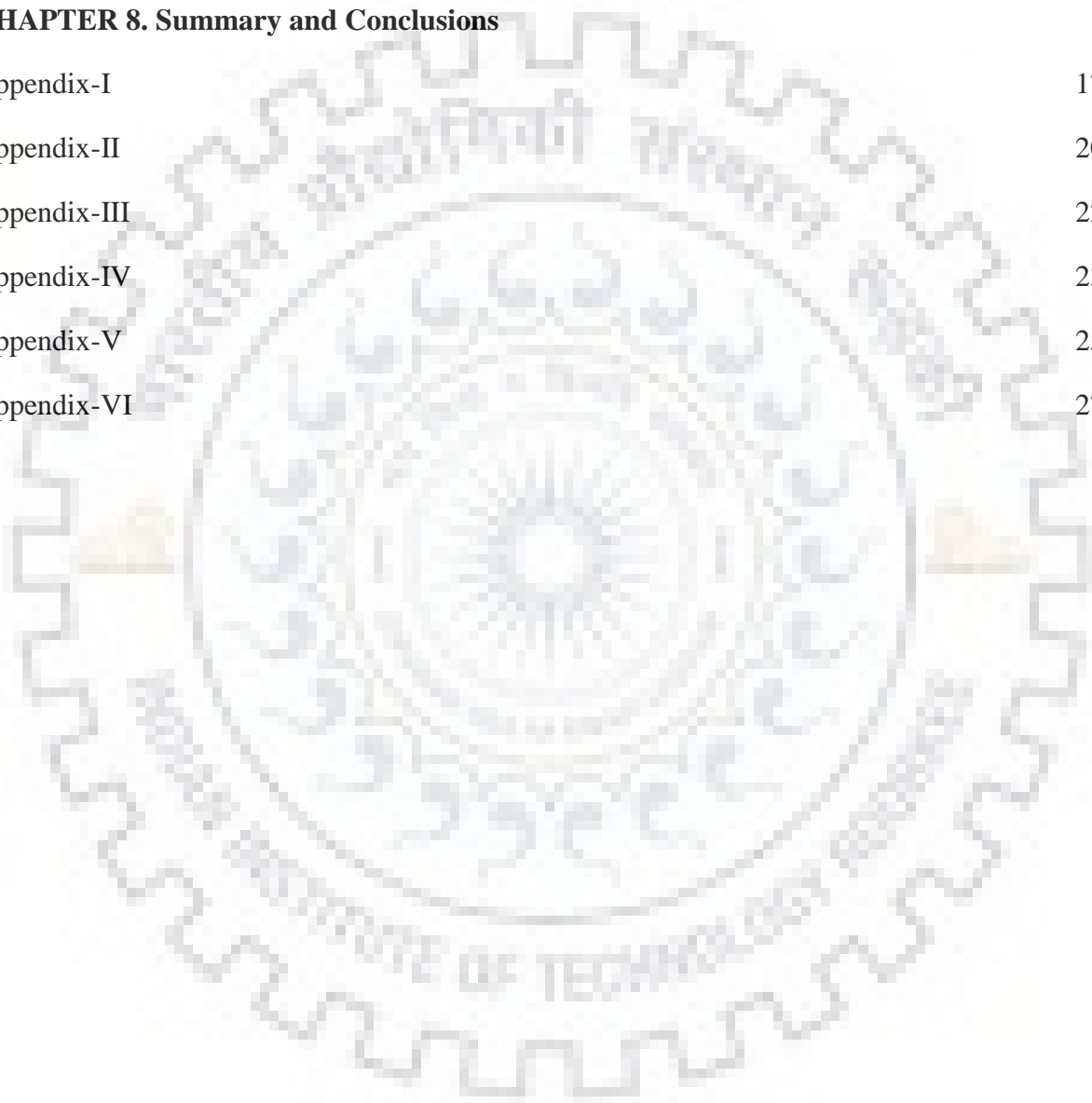
CHAPTER 6. β -Functionalized ‘Push-Pull’ Porphyrins: Synthesis, Photophysical, Electrochemical Redox Properties and NLO Studies

6.1 Introduction	131
6.2 Experimental Section	133
6.2.1 Reagents	133
6.2.2 Instrumentation and Methods	133
6.2.3 Synthetic Procedure	134
6.3 Results and Discussion	137
6.3.1 Synthesis and Characterization	137
6.3.2 Optical Absorption and Emission Spectral Studies	138
6.3.3 NLO Studies using Femtosecond Pulses	140
6.3.4 Electrochemical Redox Properties	142
6.3.5 DFT Studies	146
6.4 Conclusions	147
6.5 References	148

CHAPTER 7. Antipodal β -Tetrasubstituted Triphenylaminoporphyrins: Synthesis, Spectral and Electrochemical Redox Studies

7.1 Introduction	152
7.2 Experimental Section	153
7.2.1 Reagents	153
7.2.2 Instrumentation and Methods	154
7.2.3 Synthetic Procedure	154
7.3 Results and Discussion	156
7.3.1 Synthesis and Characterization	156
7.3.2 Absorption Spectral Studies	157

7.3.3 DFT Studies	158
7.3.4 Electrochemical Redox Studies	160
7.4 Conclusions	162
7.5 References	163
CHAPTER 8. Summary and Conclusions	
Appendix-I	174
Appendix-II	208
Appendix-III	227
Appendix-IV	239
Appendix-V	259
Appendix-VI	273



List of Charts

CHAPTER 2		Page
		No.
Chart 2.1	Molecular Structure of Synthesized β -Arylamino porphyrin and β -N-fused porphyrin.	40
CHAPTER 3		
Chart 3.1	Molecular Structure of Synthesized Porphyrins.	74
CHAPTER 4		
Chart 4.1	Molecular Structure of Synthesized β -Octasubstituted Porphyrins.	92
CHAPTER 5		
Chart 5.1	Molecular Structure of Synthesized <i>Meso</i> -Tetraalkylporphyrins.	113
CHAPTER 6		
Chart 6.1	Molecular Structure of Synthesized Tri β -substituted 'Push-Pull' Porphyrins.	132
CHAPTER 7		
Chart 7.1	Molecular Structure of Antipodal β -Tetrasubstituted Triphenylaminoporphyryns.	153

List of Schemes

CHAPTER		Page No.
CHAPTER 2		
Scheme 2.1	Synthetic Routes to Mixed β -Arylamino porphyrin and N-fused Porphyrins.	51
CHAPTER 3		
Scheme 3.1	Synthetic Routes to Ni-diOxP (1) and Cu-diOxP (2) under β -Nitration Condition.	76
CHAPTER 4		
Scheme 4.1	Synthesis of Mixed β -Substituted Porphyrins.	96
CHAPTER 5		
Scheme 5.1	Synthesis of <i>Meso</i> -Tetraalkylporphyrins (1-3) and Their Corresponding Zn(II) Complexes.	117
CHAPTER 6		
Scheme 6.1	Synthesis of Mixed β -Substituted Porphyrins.	137
CHAPTER 7		
Scheme 7.1	Synthesis of H ₂ TPP(TPA) ₂ NO ₂ and Their metal Derivatives.	156

List of Figures

CHAPTER 1		Page
		No.
Figure 1.1	The Basic Structure of Porphyrin.	2
Figure 1.2	Chemical Structure of Naturally Found Tetrapyrrolic Pigments.	3
Figure 1.3	Synthetic Analogues of Tetrapyrrole.	4
Figure 1.4	Synthetic Routes for the Preparation of Uroporphyrin-III.	5
Figure 1.5	Functionalization of Porphyrins.	7
Figure 1.6	Synthetic Routes For β -Bromosubstituted Porphyrins.	8
Figure 1.7	Synthesis of β -Arylamino porphyrins.	9
Figure 1.8	Oxidative C-N Fusion of Pyridinyl Porphyrin.	9
Figure 1.9	β -Octachlorovanadylporphyrin.	10
Figure 1.10	Porphyrin Catalyzed Organic Reactions.	11
Figure 1.11	Mechanism in Photodynamic Therapy.	12
Figure 1.12	Structure of porphyrin photosensitizers used in PDT as drugs.	13
Figure 1.13	Structure of 10, 15, 20-Tritolylporphyrin-5-(4-Amidophenyl)-[5-(4-phenyl)-10, 15, 20-Tritolylporphyrin.	13
Figure 1.14	Structure of Porphyrin-Ferrocene Conjugate (TNCF).	15
Figure 1.15	(a) Dye Sensitized Solar Cell (b) Working Principle of DSSC	16
Figure 1.16	Molecular Structure of <i>Meso</i> -and β -Substituted Porphyrin Based Dyes.	17
Figure 1.17	Molecular Structure of Trans-A ₂ BC dyes.	18
Figure 1.18	Porphyrin Based Anion and Cation Sensors.	19
Figure 1.19	Structure of ZnTPP Coordinated Pyridyl Fulleropyrrolidine Dyad and ZnNC Coordinated with Phenylimidazolyl Fulleropyrrolidine Dyad.	21
CHAPTER 2		
Figure 2.1	ORTEP Diagram Showing Top and Side Views of H ₂ TPP(N-fusedPh)Br ₂ , Hydrogen Atoms are Omitted for Clarity. In the Side View, <i>Meso</i> -Phenyls are Omitted for Clarity.	52

Figure 2.2	UV-Visible Spectra of (a) ZnTPP(N-fusedPh) and ZnTPP(N-fusedPh)Ph ₂ , (d) ZnTPP(N-fusedPh)Br ₂ and ZnTPP(N-fusedPh)PE ₂ .	54
Figure 2.3	UV-Visible Titration of ZnTPP(N-fusedPh)PE ₂ with (a) C ₆₀ Im and (b) C ₆₀ Py in <i>o</i> -Dichlorobenzene at 298 K.	56
Figure 2.4	Fluorescence Spectra of (a) ZnTPP(N-fusedPh) and ZnTPP(N-fusedPh)Ph ₂ , (b) ZnTPP(N-fusedPh)Br ₂ and ZnTPP(N-fusedPh)PE ₂ .	58
Figure 2.5	Quenching of Fluorescence Intensity of ZnTPP(N-fusedPh)PE ₂ (4d) in <i>o</i> -Dichlorobenzene at 298 K.	58
Figure 2.6	(a) Optimized Structure (b) Electrostatic Potential map (c) Pictorial Representation of Frontier HOMO (d) LUMO of ZnTPP(N-fusedPh):C ₆₀ Py	60
Figure 2.7	Cyclic Voltammograms of ZnTPP(N-fusedPh) and ZnTPP(N-fusedPh)PE ₂ in Presence and Absence of C ₆₀ Im in <i>o</i> -Dichlorobenzene at 298 K.	62
Figure 2.8	Chemical Oxidation of ZnTPP(N-fusedPh)PE ₂ using NOBF ₄ in <i>o</i> -Dichlorobenzene at 298 K.	63
Figure 2.9	(a) ¹ H NMR spectra of Imine Proton of H ₂ TPP(N-fusedPh), H ₂ TPP(N-fusedPh)Br ₂ , H ₂ TPP(N-fusedPh)Ph ₂ , H ₂ TPP(N-fusedPh)PE ₂ and (b) Comparison Spectra of H ₂ TPP(N-fusedPh)Br ₂ Inner -NH Proton with H ₂ TPP(NHPh)Br ₂ .	64
Figure 2.9	(a) ¹ H NMR Spectra of (a) ZnTPP(N-fusedPh)Ph ₂ :C ₆₀ Im Adduct (b) ZnTPP(N-fusedPh)Ph ₂ in C ₆ D ₆ at 298 K.	65

CHAPTER 3

Figure 3.1	Absorption Spectra of 1-4 Porphyrins in CH ₂ Cl ₂ at 298 K.	76
Figure 3.2	Cyclic Voltammograms of 1-4 in CH ₂ Cl ₂ Containing 0.1 M TBAPF ₆ as Supporting Electrolyte using Ag/AgCl as Reference Electrode.	77
Figure 3.3	Electronic Absorption Spectrum of 1 in Solvents of Various Polarities.	79
Figure 3.4	UV-Visible Titration of 1 (3.14×10^{-5} M) (a) Upon Addition of F ⁻	80

ions ($0-1.14 \times 10^{-3}$ M) and (b) Upon Addition of CN^- ions ($0-1.53 \times 10^{-3}$ M) in Toluene Medium at 298 K. Inset Shows the Corresponding B-H plot.

Figure 3.5	Absorption Spectra of 1 (3.14×10^{-5} M) in the Presence of Different Anions.	81
Figure 3.6	Ratiometric Absorbance Changes (A_{427}/A_{400}) of 1 (3.14×10^{-5} M) on Addition of 4 equiv of CN^- and 10 equiv. of other Anions. Blue Bars Indicate the Blank and in the Presence of other Interfering Anions, and Brown Bars Indicate the Addition of CN^- to the Interfering Anions.	83
Figure 3.7	Ratiometric Absorbance Changes (A_{424}/A_{400}) of 1 (3.14×10^{-5} M) on Addition of Excess equiv of F^- and other Anions. Blue Bars Indicate the Blank and in the Presence of other Interfering Anions, and Brown Bars Indicate the Addition of F^- to the Interfering Anions.	83
Figure 3.8	B3LYP/LANL2DZ-Optimized Geometry Showing (a) Top as well as (b) Side View of Ni-diOxP.2CN ⁻ ; Hydrogen are Omitted for Clarity. In the Side View <i>Meso</i> -Phenyl Substituents is not Shown Omitted for Clarity.	85
Figure 3.9	Pictorial View of Frontier Molecular Orbitals (FMOs) of 1 and 1.2CN⁻	85
Figure 3.10	UV-Visible Spectra of 1 and 1.2CN⁻ After Addition of Aqueous Solution of KCN and 18-Crown-6.	86
CHAPTER 4		
Figure 4.1	ORTEP Digram of $\text{H}_2\text{TPP}(\text{NO}_2)(\text{Ph})_2\text{Br}_5$.	98
Figure 4.2	(a) Optical Absorption Spectra of $\text{H}_2\text{TPP}(\text{NO}_2)(\text{Ph})_2\text{Br}_5$ and $\text{H}_2\text{TPP}(\text{Ph})_2\text{Br}_6$ (b) Emission Spectra of H_2TPP , $\text{H}_2\text{TPP}(\text{NO}_2)(\text{Ph})_2\text{Br}_5$ and $\text{H}_2\text{TPP}(\text{Ph})_2\text{Br}_6$.in CH_2Cl_2 at 298 K.	100
Figure 4.3	UV-Visible Spectral Titration of $\text{H}_2\text{TPP}(\text{NO}_2)(\text{Ph})_2\text{Br}_5$ (a) TFA and (b) TBAOH in Toluene at 298K. Insets Exhibit Hill Plots	102
Figure 4.4	Comparative Cyclic Voltammograms of Porphyrins CuTPP,	106

CuTPPNO₂, CuTPP(NO₂)(Ph)₂, CuTPP(Ph)₂Br₆ and CuTPP(NO₂)(Ph)₂Br₅ using Ag/AgCl as Reference Electrode and 0.1M TBAPF₆ in CH₂Cl₂ at 298 K.

Figure 4.5 HOMO-LUMO Variation of CuTPP, CuTPPNO₂, CuTPP(NO₂)(Ph)₂, CuTPP(Ph)₂Br₆ and CuTPP(NO₂)(Ph)₂Br₅. 106

CHAPTER 5

Figure 5.1 Crystal Structure Data of H₂TPrP (**3**) (a) Top View and (b) Side View 118

Figure 5.2 UV-Vis Spectra of **2** (H₂TetP) and **2a** (ZnTetP) in CH₂Cl₂ at 298 K 119

Figure 5.3 (a) Spectral Changes Observed During the Titration of Fullerene (C₆₀) to the Solution of H₂TPrP (**3**) in Toluene at 298 K. (b) Benesi-Hildebrand Plot Constructed for Evaluating the Binding Constant as well as Stoichiometry for **3**:C₆₀ Host-Guest Complex. 119

Figure 5.4 (a) Fluorescence Spectral Changes Observed During the Titration of Fullerene (C₆₀) to the Solution of H₂TPrP (**3**) in Toluene at 298 K. (b) Stern-Volmer Plot for **3**:C₆₀ Host-Guest complex. 122

Figure 5.5 Bar Graph Represents logK Values of Differ Alkyl Porphyrins and Their Zn(II) Derivatives. 123

Figure 5.6 ¹H NMR Spectra of (a) **1**:C₆₀ Adduct (b) **1** in C₆D₆ at 298 K. 125

Figure 5.7 (a) B3LYP/3-21G Optimized Structure H₂TMeP (**1**):C₆₀ Supramolecular Dyad (b) Frontier HOMO Orbitals (c) Frontier LUMO Orbitals. 126

CHAPTER 6

Figure 6.1 (a) UV-Visible and (b) Fluorescence Spectra of H₂TPP(TPA)₂NO₂ and H₂TPP(TPA)₂CHO in CH₂Cl₂ at 298 K. 139

Figure 6.2 Experimental and Theoretically fitted Z scan data for sample (i) H₂TPP(TPA)₂NO₂ in OA mode at (a) 680 nm (b) 700 nm (c) 750 nm (d) 800 nm (e) 850 nm and CA mode at (f) 750 nm (g) 800 nm (ii) H₂TPP(TPA)₂CHO in OA mode at (a) 680 nm (b) 700 nm (c) 750 nm (d) 800 nm (e) 850 nm and CA mode at (f) 680 nm (g) 700 141

nm (h) 750 nm (i) 800 nm (j) 850 nm.

Figure 6.3	Cyclic Voltammograms of Porphyrins (a) MTPP(TPA) ₂ NO ₂ and MTPP(TPA) ₂ CHO (M = 2H, Co(II), Cu(II), Ni(II), Zn(II)) and in CH ₂ Cl ₂ with a Scan Rate of 0.1 V/s at 298 K.	144
Figure 6.4	Comparative Diagram for HOMO-LUMO Variation of CuTPP, CuTPPNO ₂ , CuTPPBr ₂ NO ₂ , CuTPP(TPA) ₂ NO ₂ , CuTPPCHO, CuTPPBr ₂ CHO and CuTPP(TPA) ₂ CHO.	145
Figure 6.5	Optimized Gas Phase Geometry of H ₂ TPP(TPA) ₂ NO ₂ and H ₂ TPP(TPA) ₂ CHO.	146
Figure 6.6	Theoretically Calculated Dipole Moment Direction of H ₂ TPP(TPA) ₂ NO ₂ and H ₂ TPP(TPA) ₂ CHO.	147
CHAPTER 7		
Figure 7.1	(a) UV-Visible and (b) Fluorescence Spectra of H ₂ TPP(TPA) ₄ and ZnTPP(TPA) ₄ in CH ₂ Cl ₂ at 298 K.	158
Figure 7.2	Optimized Geometry of H ₂ TPP(TPA) ₄ (a) Top View and (b) Side View.	159
Figure 7.3	Frontier Molecular Orbitals of H ₂ TPP(TPA) ₄ .	159
Figure 7.4	Comparative Cyclic Voltammograms of NiTPP, NiOPP and NiTPP(TPA) ₄ in CH ₂ Cl ₂ at 298 K.	161
Figure 7.5	HOMO-LUMO Variation of NiTPP(TPA) ₄ in Comparison to NiTPP and NiOPP.	161

List of Tables

CHAPTER 2	Page No.
Table 2.1	Photophysical Data of Porphyrins (MTPP(NHPh) X_2 and MTPP(N-fusedPh) X_2 (X = 2H, Br, Ph, PE and M = 2H, Zn(II)). 55
Table 2.2	UV-Visible and Fluorescence Titration Data of C ₆₀ ImC ₆₀ Py with ZnTPP(N-fusedPh) X_2 (X = H, Br, Ph, PE) in <i>o</i> -dichlorobenzene at 298 K. 57
CHAPTER 3	
Table 3.1	Electrochemical redox Data (Ag/AgCl) of Synthesized Porphyrin (1-4) in CH ₂ Cl ₂ Containing 0.1 M TBAPF ₆ at 298 K scan rate 0.1 V ⁻¹ . 78
Table 3.2	Binding Constant Data of Electron Deficient Meso-Tetrakis(3,4-benzoquinone) substituted Porphyrins in Toluene at 298 K. 81
CHAPTER 4	
Table 4.1	Photophysical Data of Synthesized Free base and Zn(II) Porphyrins in CH ₂ Cl ₂ at 298 K. 100
Table 4.2	Protonation and Deprotonation Constant Data of H ₂ TPP(NO ₂)(Ph) ₂ Br ₅ and H ₂ TPP(Ph) ₂ Br ₆ in Comparison with H ₂ TPP(NO ₂)Br ₅ in Toluene at 298 K. 102
Table 4.3	Redox Potential Data of Synthesized and Compared Porphyrins (V vs Ag/AgCl) in CH ₂ Cl ₂ Containing 0.1 M TBAPF ₆ with Scan Rate 0.1 V ⁻¹ . 104
CHAPTER 5	
Table 5.1	Association Constant of Porphyrin-C ₆₀ Supramolecular Dyad in Toluene at 298 K. 120
Table 5.2	UV-Visible and Fluorescence Spectral Data of Meso-Tetraalkylporphyrins (1-3 and 1a-3a) in CH ₂ Cl ₂ at 298 K. 121
Table 5.3	Electrochemical Redox Data of 1-3 and 1a-3a in Presence and Absence of C ₆₀ in Benzonitrile at 298K. 124

CHAPTER 6

Table 6.1	Photophysical Data of $H_2TPP(TPA)_2NO_2$ and $H_2TPP(TPA)_2CHO$ ($M = 2H, Co(II), Ni(II), Cu(II), Zn(II)$) in CH_2Cl_2 at 298 K.	139
Table 6.2	NLO coefficient data of $H_2TPP(TPA)_2NO_2$ and $H_2TPP(TPA)_2CHO$.	141
Table 6.3	Electrochemical Redox Data of all Synthesized Porphyrins $MTPP(TPA)_2X$ where ($M = 2H, Co, Ni, Cu$ and Zn ; $X = NO_2$ and CHO) in CH_2Cl_2 at 298 K.	144

CHAPTER 7

Table 7.1	Photophysical Data of $H_2TPP(TPA)_4$ ($M = 2H, Co(II), Ni(II), Cu(II), Zn(II)$) in CH_2Cl_2 at 298 K.	158
Table 7.2	Electrochemical Redox Data of Porphyrins $MTPP(TPA)_4$ where ($M = Cu, Co, Ni$ and Zn) in CH_2Cl_2 at 298 K.	162



CHAPTER 1
INTRODUCTION



CHAPTER 1

INTRODUCTION

1.1 GENERAL INTRODUCTION TO TETRAPYRROLIC PIGMENTS

Porphyryns are the most indispensable chemical units which are required for several processes for life on the earth. In these tetrapyrrolic pigments, four pyrrole rings are linked together by covalent bonds or carbon units in a cyclic form (macrocycle) to give cyclic tetrapyrrole ring system as shown in Figure 1.1 [1,2]. The word of ‘porphyrin’ has been created from “*porphura*” which means purple because of its strong absorption in the visible region [3,4]. Porphyryns are highly colored, stable and aromatic heterocyclic macrocycles. Tetrapyrroles are present in linear form in the bile pigments. Analogues of porphyryns are called porphyrinoids which widely exist in nature. The most important porphyrinoids found in nature are chlorophyll containing chlorin, haemoglobin and cytochrome both contain heme, while bacteria and plants contain bacteriochlorophyll and chlorophyll, respectively. Porphyryns play important role in biological process such as electron transfer, oxygen binding, catalysis and most importantly in photosynthesis [5–7]. Naturally occurring tetrapyrroles are different in peripheral substituents, the oxidation state of core ring and nature of metal ions present in the core of the macrocycles. Porphyrinoids form variety of metal complexes with metals such as Ag^{III} , V^{IV} , Fe^{III} , Fe^{II} , Ni^{II} , Co^{II} , Cu^{II} , Zn^{II} etc [8–12]. Some naturally occurring tetrapyrroles (such as heme, chlorophyll, cytochrome P_{450} and Vitamin B_{12}) are shown in Figure 1.2. Porphyrin exhibits strong absorption band in visible region that imparts deep color to them.

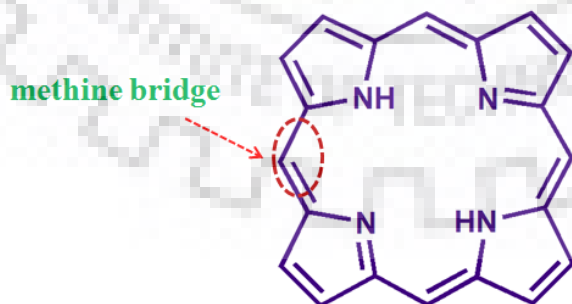


Figure 1.1 The Basic Structure of Porphyrin.

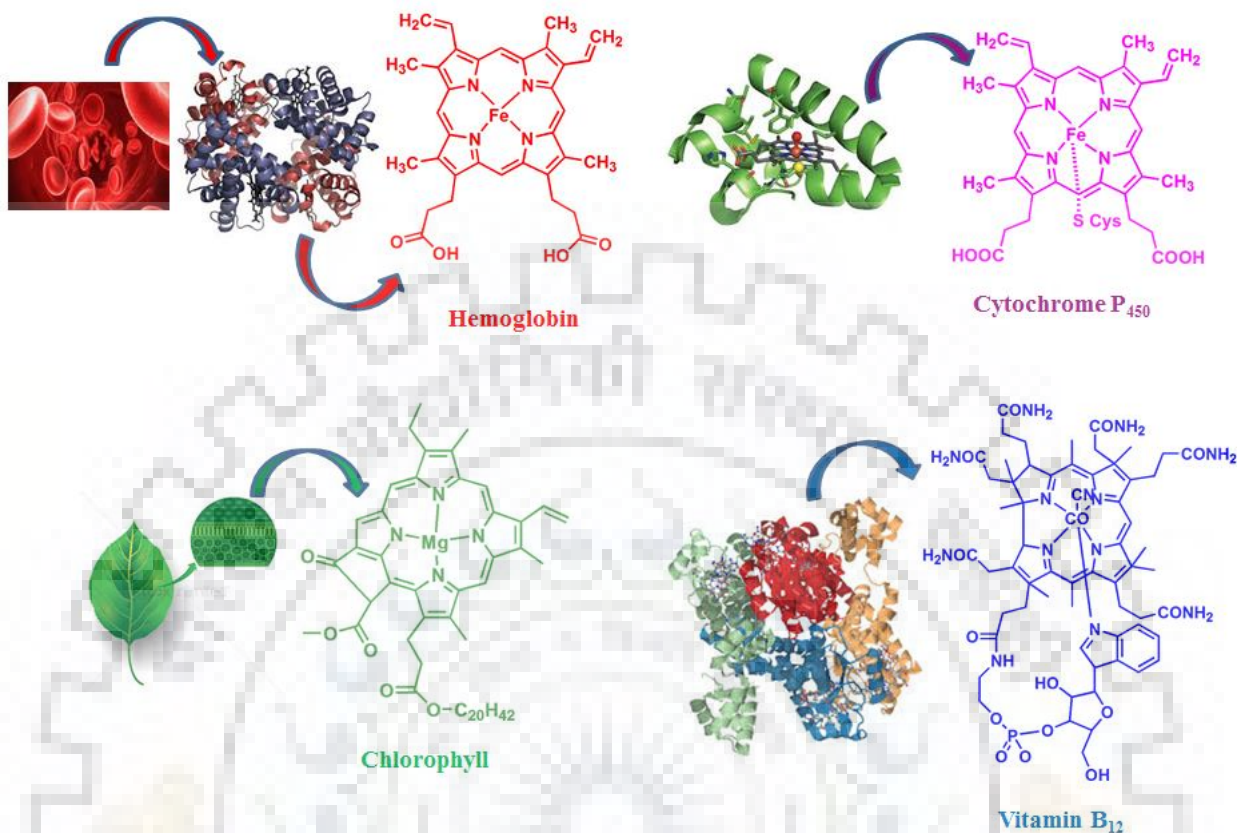


Figure 1.2 Chemical Structures of Naturally Found Tetrapyrrolic Pigments.

1.2 SYNTHETIC TETRAPYRROLE ANALOGUES

A large number of synthetic tetrapyrroles have prepared over the decades to study the porphyrin based naturally occurring system. Porphyrins are chemically versatile and rich molecules that promoted the laboratory synthesis and study of porphyrinoids (porphyrins and their analogues). β -*meso* substituted porphyrins offer great insight to study the physical and chemical properties of the macrocycle. Metalloporphyrins have generated great interest in the area of catalytic process to mimic the enzymes such as peroxidase, cytochrome P₄₅₀, and catalase and as a model for transmembrane electron transporters. The physical and chemical properties of porphyrins can be easily tuned *via* modification in the peripheral substituents. Many research groups have reported wide range of (*meso*/ β) substituted porphyrins [13–15], chlorins with contracted ring system [16–19], core modified [20], π -extended analogues [21–23] and inverted analogues [24–26] of porphyrinoids and utilized them for many applications in several fields. (Figure 1.3)

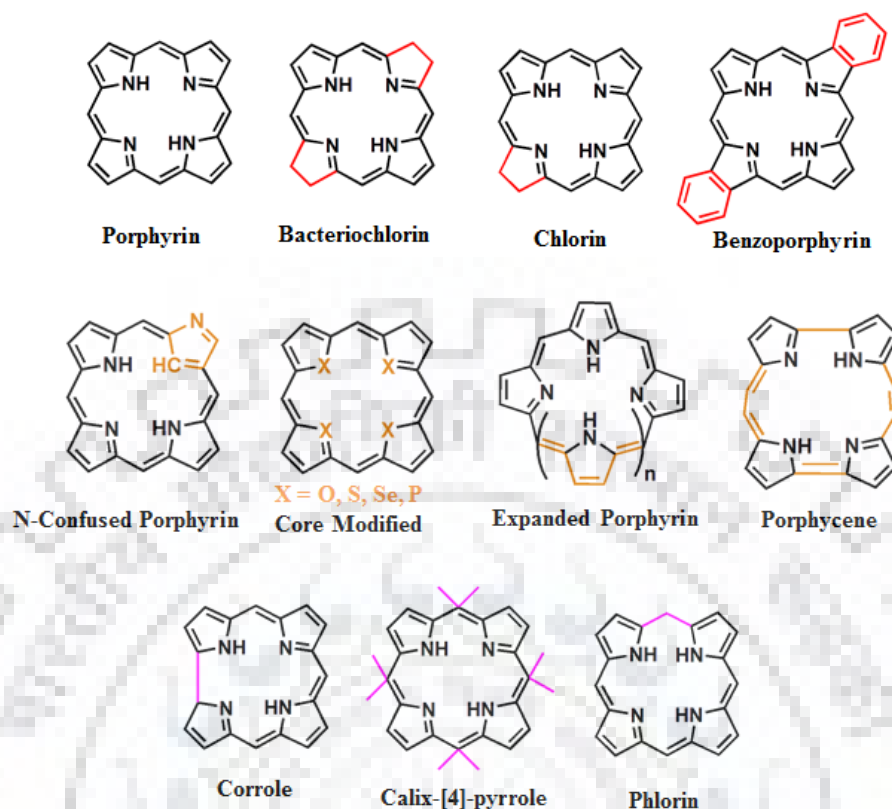


Figure 1.3 Synthetic Analogues of Tetrapyrroles.

5,10,15,20-tetraphenylporphyrin (H_2TPP) and its metal complexes were studied widely because H_2TPP and its metal complexes are used as starting material for further functionalization, since the β /*meso* positions of porphyrin are available for substitution (electron rich and electron withdrawing groups). Functionalized porphyrins revealed unique photophysical and electrochemical properties.

1.3 SYNTHESIS OF PORPHYRIN IN LABORATORY

Fischer and Walach first synthesized porphyrin analogues in 1926 *via* synthesis of octamethylporphine [27]. In this method, the reaction was carried out between dipyrromethenes in molten succinic acid at 180-190 °C and the desired product was formed with very low yield (around 2% only). In 1957, S.F. MacDonald reported the synthesis of stable dipyrromethane (also known as dipyrromethane and pyrromethanes) which were used as good starting materials for the synthesis of A_3B and A_2B_2 types of porphyrins [28]. In 1960, MacDonald reported the synthesis of pure isomeric porphyrins from dialdehyde and dipyrromethane [29,30]. Acetic acid having 0.4% hydroiodic acid was used as solvent in this reaction. By using this method,

Uroporphyrin III was also reported with 55-65% yield as shown in Figure 1.4. The unsubstituted porphyrin are highly planar but substitution at β -position causes nonplanarity of the macrocyclic ring. Adler, Longo and coworkers in 1967 developed an alternative method for the synthesis of *meso*-substituted tetraphenylporphyrin [31]. Adler and Longo's method was a practical version of Rothmund's seal tube method (1963) [32]. This was one pot synthesis acid catalyzed condensation of substituted aldehyde and pyrrole in propionic acid refluxing at 140 °C for 30 min in open air. There were some problems in this methodology. (1) In this method, tar was formed creating purification problem (2) acid sensitive aldehydes were not stable for the synthesis (3) this method was limited for the synthesis of symmetrical porphyrins only. In 1987 another major breakthrough came in the synthesis of porphyrin which is known as 'Lindsey method'. This method provided the large scale synthesis of asymmetrical porphyrin with milder conditions. In this method, the reaction was carried out between aldehyde and pyrrole in inert atmosphere in the presence of chloroform and acid catalyst (BF_3/TFA) at room temperature which leads to formation of porphyrinogen intermediate. After addition of DDQ/*p*-chloranil the intermediate porphyrinogen is converted in to porphyrin *via* oxidation reaction. This method gave very good yield as compared to other methods for the synthesis of porphyrins [33]. Mixed substituted porphyrins exhibited interesting photophysical and electrochemical properties. After substitution *via* bulky groups or increasing the number of groups at periphery of porphyrin causes steric crowding which results into steric repulsive interaction among the substituents at periphery of porphyrins. This repulsion results for nonplanar conformation of macrocycle.

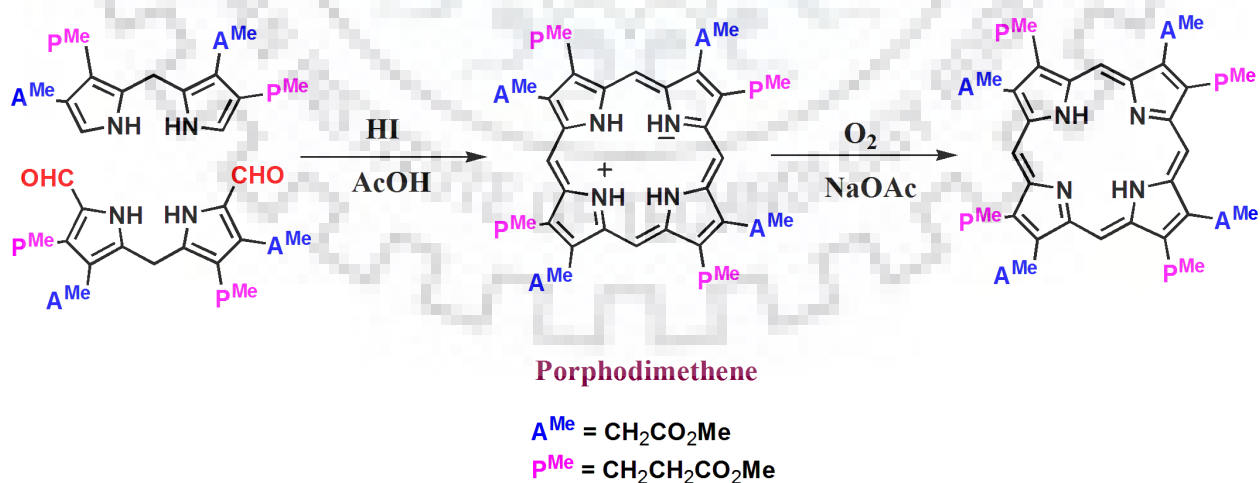


Figure 1.4 Synthetic Routes for the Preparation of Uroporphyrin-III.

1.4 FUNCTIONALIZATION OF TETRAPYRROLES

Porphyrins are thermally and chemically highly stable macrocycles. These are versatile compounds and have flexible conformation. Porphyrins exhibit unique photophysical, optical and electrochemical redox properties which make them good starting candidates for preparing scientific, industrial and medicinally suitable materials. Porphyrins are the most important studied compounds and undergo numerous reactions. *Meso/β*-functionalized macrocycles can be obtained using two types of methods. First include the condensation of substituted aldehyde with functionalized pyrrole or condensation of substituted aldehyde with substituted dipyrromethanes [34,35]. Second method includes the introduction of the substituents or functional groups at periphery of the macrocycle after their synthesis and this method are known as post functionalization (Figure 1.5) [36]. Post functionalization are carried out by two types of methods firstly by appending functional groups at the periphery of the porphyrin and in second method functionalization of porphyrin core. Many chemical reactions have been carried out in the post functionalization of the macrocycle such as metal catalyzed coupling reactions [37,38], nucleophilic substitution [39], electrophilic substitution or addition [40] and transformation of the functional groups [41]. As a result the physical and chemical properties of porphyrins can be tuned by functionalization at *meso/β*-position of the macrocycle. *β*-substituted tetrapyrroles are found in the nature. Unsymmetrical *β*-substituted porphyrins were found to be great interest because these porphyrins can be used to mimic the naturally occurring process such as photosynthesis. Many research groups have reported the synthesis of *β*-substituted porphyrins [42–44]. *β*-Substituted porphyrins can be derived *via* cross coupling reactions and substitution at the periphery of porphyrins. Functionalization of porphyrins has been carried out by using electrophilic substitution reaction such as formylation, nitration and halogenation to give a variety of functionalized porphyrins.

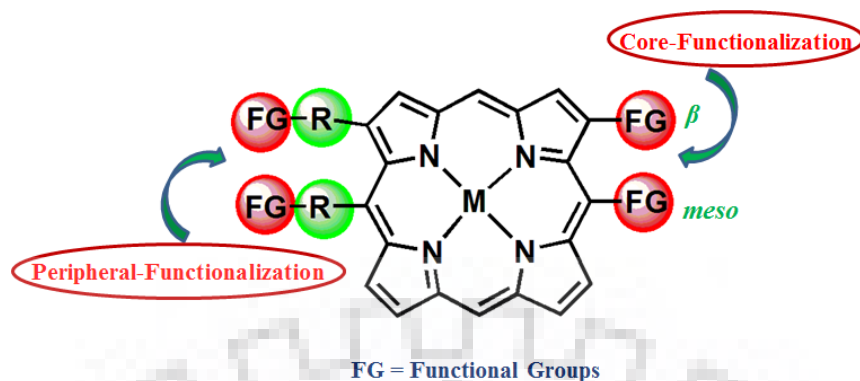


Figure 1.5 Functionalization of Porphyrins.

1.4.1 Nitration and Bromination of Tetrapyrroles

β -Nitroporphyrin is a good starting material for further functionalization of porphyrins with improved properties for various specific applications [15,45]. β -Nitro group activates the pyrrole unit where it is inserted towards the attack by nucleophiles and activates the antipodal pyrrole ring to direct electrophilic substitution reactions. Crossley and coworkers reported the functionalization of β -nitroporphyrin and described the reaction of benzenethiolate and ethanethioalate with β -nitroporphyrin to afford β -thioethers [46,47]. Bromination of porphyrin can be carried out using liquid bromine and NBS (N-bromosuccinamide) [48]. Bromination of porphyrins make them suitable intermediate for the synthesis of higher order porphyrins by metal catalyzed coupling reactions (aryl and alkyl coupling) and these porphyrins are used in various applications like in NLO (non-linear optics) [49,50]. In 1984 Nudy and coworkers reported the formation of mono, di and tri bromo-substituted porphyrins with good yields [51]. Octabromination and modified tetrabromination of porphyrin was reported by Krishnan and Bhyrappa and Kumar *et al.* respectively [52,53]. β -Octasubstituted porphyrins exhibited unique physicochemical properties (Figure 1.6). Kato *et al.* reported the formation of monobromoporphyrin with very good yields. Fischer and Halbig reported the bromination of β -alkylporphyrin [54]. Samuels *et al.* developed the monobromination of porphyrin using NBS (N-bromosuccinimide) in CCl_4 or bromine in CHCl_3 but this method was not more developed due to non-reproducibility [55]. β -Substituents of porphyrins have more effect on electrical and steric properties as compared to *meso*-substituents of porphyrins. Octabromination of porphyrin has been also reported by using NBS in CCl_4 . 2-Nitroporphyrin on bromination with NBS give 2-nitro-12,13-dibromo-*meso*-tetraphenylporphyrin [56].

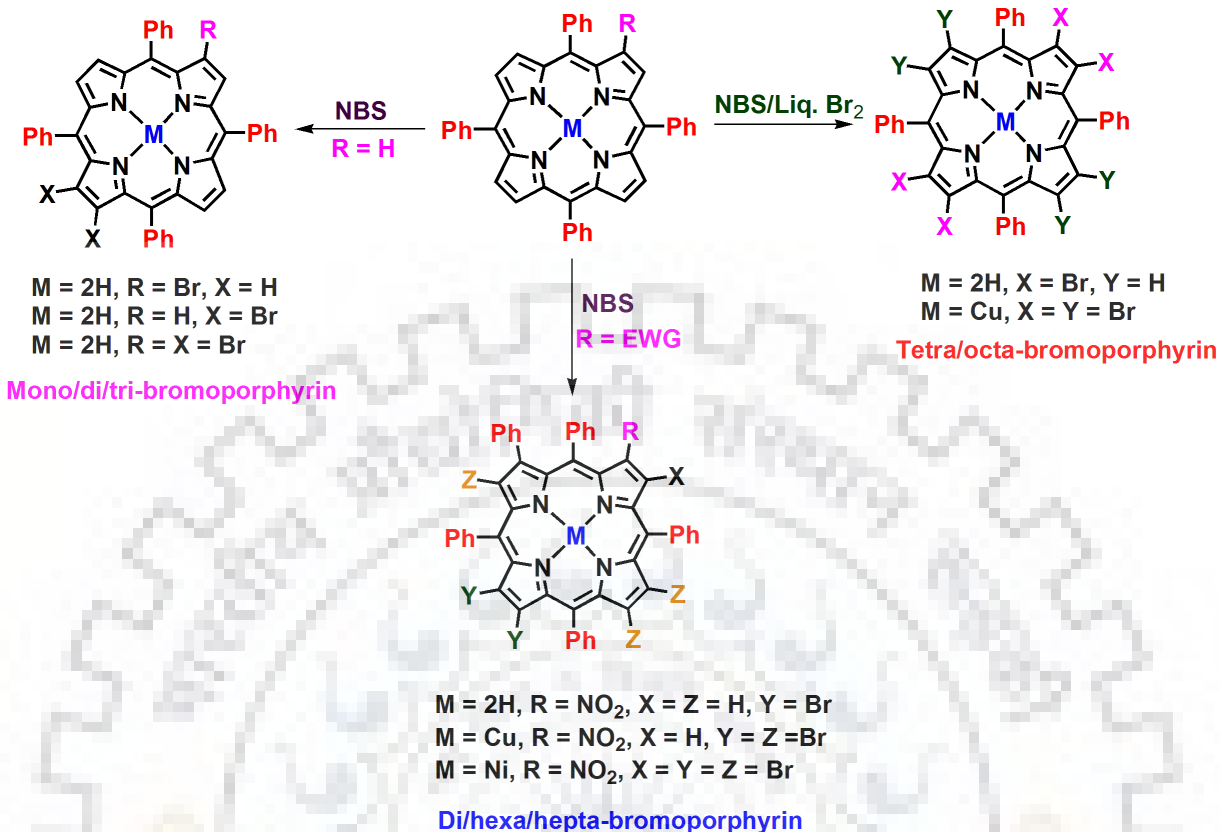


Figure 1.6 Synthetic Routes for β -Bromosubstituted Porphyrins.

1.4.2 β -Fused Porphyrin

Fused π -conjugated porphyrin exhibits unique photophysical and electrochemical properties [57–59]. Notably, β -Meso fusion exhibited more electronic and steric effect at porphyrin π -system as compared to β, β' fusion [60]. The remarkable, electronic and optical properties of fused porphyrin make them appealing candidates for an immense variety of applications. 2-Nitroporphyrin acts as good starting candidate for the formation of 2-arylamino porphyrin and further fusion reaction of 2-arylamino porphyrin in the presence of nitrobenzene [61]. Reduction of nitro group gave access to various interesting derivatives. Mikus and coworkers reported the isomeric form of β, β' -dinitro-5,10,15,20-meso-tetraphenylporphyrin are the good starting material for further transformation reactions [62]. On refluxing 2-nitroporphyrin with excess triethylphosphite in *o*-dichlorobenzene at 155 °C gave the formation of cyclic enamine porphyrin with 70-75% yield [63]. Smith *et al.* reported the synthesis of β -fused pyrroloporphyrins using Barton-Zard condensation of α -isocyanoacetic ester with Ni(II)-2-NO₂TPP in the presence of

DBU [64]. In 2008 Pereira *et al.* reported the reduction of β -nitro group to β -arylamino group by refluxing the free base 2-NO₂TPP in aniline at 180 °C for 20 h and further refluxing in nitrobenzene for 30 h resulted into N-arylquinolino[2,3,4-*at*] porphyrin was formed (Figure 1.7) [61]. In 2013, Kojima *et al.* reported multifused porphyrins and studied the effects of π -extended conjugation on electrochemical and optical properties of porphyrin π -system [65]. Reaction of β -pyrrolic functional group with *meso*-phenyl groups was described by Callot and coworkers [66]. β - β' , β -*meso* and *meso*-*meso* fused porphyrins were reported by Osuka and coworkers [67,68]. In 2018, our research group has reported fused porphyrins and chlorins *via* oxidative fusion [69]. In 2018, Berthelot and coworkers reported the intramolecular oxidative C-N fusion of *meso*-pyridinyl nitrogen and β -pyrrole carbon (Figure 1.8) [70].

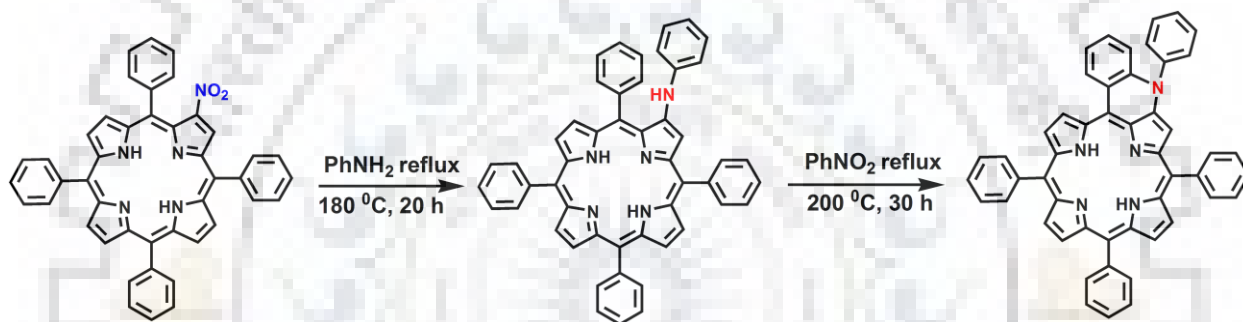


Figure 1.7 Synthesis of β -Arylamino Porphyrin

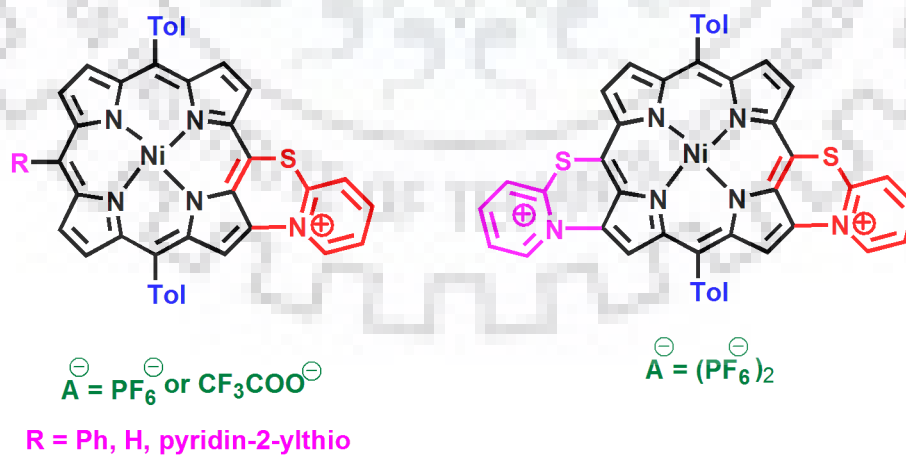


Figure 1.8 Oxidative C-N fusion of Pyridinyl Porphyrin

1.5 SOME APPLICATIONS OF PORPHYRINS AND THEIR ANALOGUES

Synthetic porphyrins are used in several applications due to their strong absorption in visible region, highly conjugated π -electronic system, good thermal, chemical stability and good coordination ability. Some important applications of porphyrins and their analogues are discussed below.

1.5.1 Porphyrins as Catalysts

Naturally occurring catalysts such as peroxidase, catalase, cytochrome P450, cytochrome and superoxide dismutase catalyze different type of biological chemical reactions. Porphyrin is the part of the naturally occurring enzymes. *Meso*-free metalloporphyrin are not able to catalyze C-H oxidation reaction due to their fast oxidative degradation and formation of *meso*-dihydroporphyrin which inactivate its catalytic ability [71]. Therefore introduction of phenyl or other relative groups at *meso*-position of porphyrin protect its active site and make it suitable for catalytic oxidation reaction.

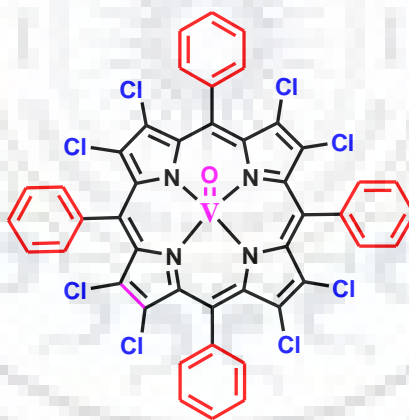


Figure 1.9 β -Octachlorovanadylporphyrin

Dolphin *et al.* classified some metalloporphyrins on the basis of their structural feature which have been used in catalysis. Natural porphyrin (cytochrome, F430 and P450 etc.) are known to be part of enzymes. Synthetic porphyrins are widely explored for their catalytic behavior. The first metalloporphyrin catalyzed the hydroxylation and the epoxidation of the hydrocarbon was reported by Groves and coworkers [72]. Introduction of substituents at *meso*/ β -position of porphyrin make its efficient catalyst to catalyze the various types of reactions. Several types of

reactions such as epoxidation, sulphonation, hydroxylation and carbonylation are catalyzed by porphyrinic catalysts as shown in Figure 1.10 [73]. Epoxidation of styrene catalyzed by water soluble manganese and iron porphyrins was reported by Simonneaux and coworkers [74]. In 2015, our research group also reported the selective epoxidation of olefin by using 2,3,7,8,12,13,17,18-octachloro-*meso*-tetraphenylporphyrinatooxidovanadium(IV)(Figure 1.9) [75]. *Meso*-functionalized porphyrins having mesityl, pentafluorophenyl and 2,6-dichlorophenyl groups have shown excellent catalytic activity [76,77]. Gross *et al.* reported Fe(III) corrole for efficient decomposition of toxic peroxyxynitrite [78]. Manganese and iron-porphyrin complexes worked as efficient homogenous catalyst for oxygenation or oxygen transfer reactions for eg. chloro-substituted Fe(II) porphyrin [79,80]. In 2019, our research group reported selective epoxidation and oxidative bromination reactions catalyzed by electron deficient oxidovanadium (IV) porphyrins in aqueous medium [5].

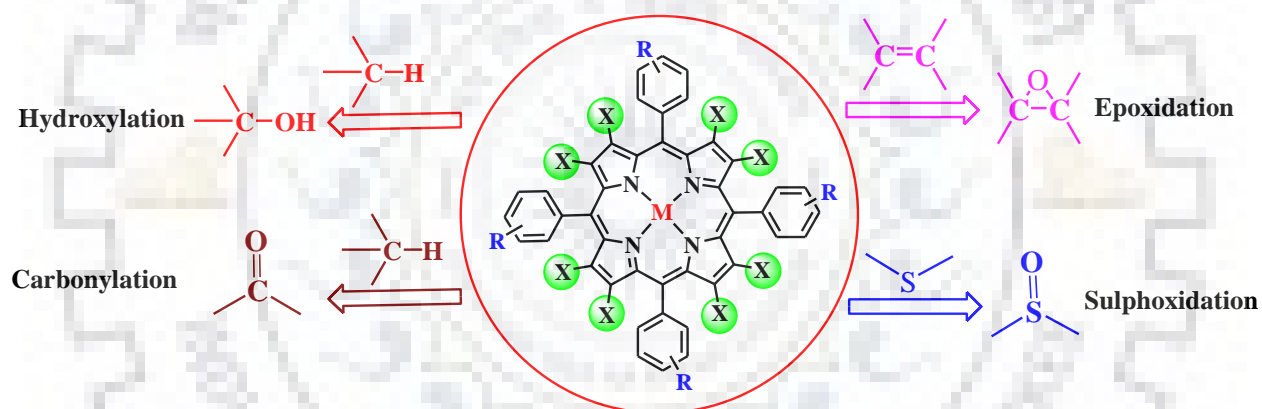


Figure 1.10 Porphyrin Catalyzed Organic Reactions.

1.5.2 Porphyrins in Photodynamic Therapy

At the present time cancer is a very severe disease and for this disease in the research, lots of money has been spent to find out proper treatment. Cancer is a deadly disease and also called malignancy, is an abnormal growth of cells. There are more than 100 types cancer, including skin cancer, breast cancer, colon cancer, lung cancer, prostate cancer and lymphoma. For the treatment of this disease, chemo therapy and radiation therapy have been used which have numerous side effects.

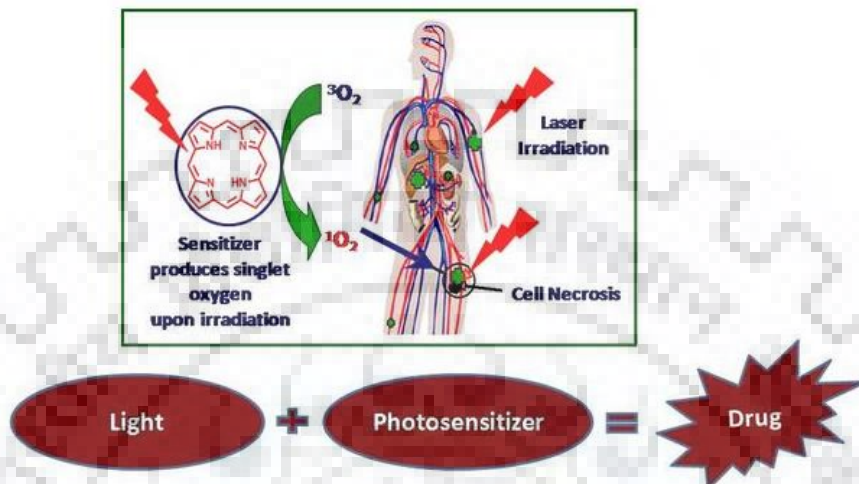


Figure 1.11 Mechanisms in Photodynamic Therapy.

PDT is a medicinal treatment which uses a combination of drugs and light to destroy the unwanted tissues and cancerous cells without any other organ toxicity [81,82]. PDT exhibits dual selective mode of action: photosensitizer (drug) is introduced in the body and assemble where rapid dividing cells exist. Then light activates the photosensitizer and triggers the toxic action. The photosensitizers which absorb the radiations with the higher wavelength (600-800 nm) in the visible region are used in PDT.

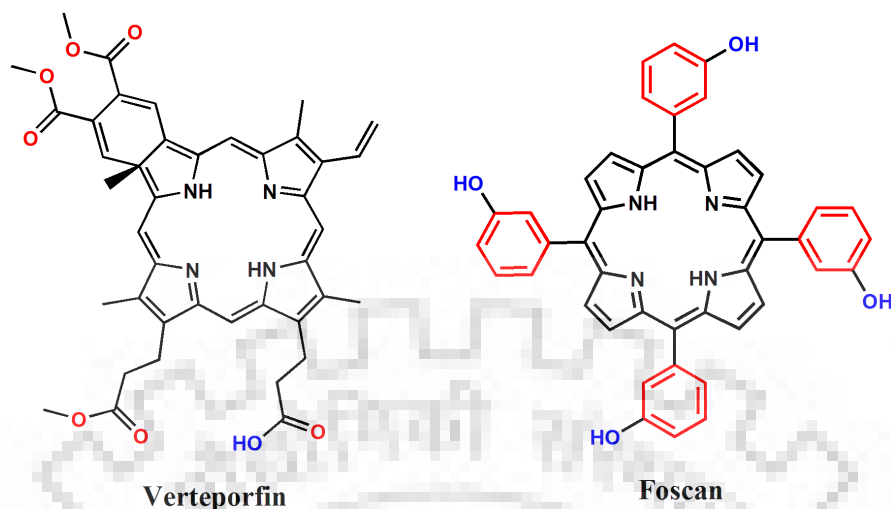


Figure 1.12 Structure of Porphyrin Photosensitizers used in PDT as Drugs.

During the treatment, the toxic cells are damaged and become necrotic after short periods. To destroy the tumor cells, photodynamic therapy (PDT) is one of the best recognized treatments. Esophageal tumor and lung cancer treatment was carried out by using photofrin. PDT treatment can be performed on weak patients and tissues where surgery is not possible.

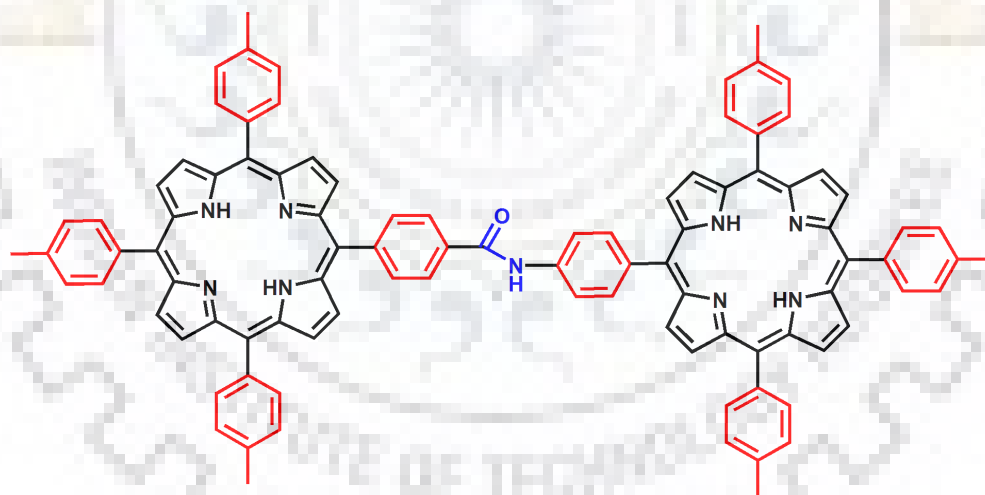


Figure 1.13 Structure of 10,15,20-tritolylporphyrin-5-(4-amidophenyl)-[5-(4-phenyl)-10,15,20-tritolylporphyrin].

Sensitizer is excited to the high energy level and transfers its energy to tissue oxygen thereby generate very reactive singlet oxygen and free radicals, destroy the tumor cells without affecting the normal cells. United States food and drug administration (FDA) approved benzoporphyrin and their derivatives for the treatment of macular degradation. In recent years, many researchers

have reported the activation of autophagic mood of cell death *via* irradiation of the photosensitizer [83,84]. First porphyrin isomer, tetra-*n*-propyl porphycene, was used as photosensitizer for the treatment of tumor. Chlorin, porphyrin and related macrocycles which produce strong absorption in the visible region has been proved as efficient photosensitizer in *vivo* PDT [85,86]. Their synthetic versatility and planar aromatic structure with unique photophysical properties make them a great interest for PDT applications. Porphyrin has more affinity for the tumor sites and form ROS efficiently. PDT effect on melanoma tumors in mice was studied by Buseti and coworkers in 1999. After that Buseti *et al.* used benzoporphyrin derivatives (verteporfin) to eliminate the abnormal blood vessel from the eyes including macular degradation (Figure 1.12). Laserphyrin which is activated in 662-667 nm wavelength range was developed by Japan for the treatment of early stage of lung cancer [87]. One of the most important and promising photosensitizer based on macrocycle texaphyrin known as lutetium texaphyrin was developed which was soluble in the water and absorbs radiations with higher wavelength (700-750 nm) [88]. Researchers have investigated porphyrin dimer (10,15,20-tritolylporphyrin-5-(4-amidophenyl)-[5-(4-phenyl)-10,15,20-tritolylporphyrin) (Figure 1.13) for treatment of melanoma, as PDT agent. Medical community's major area of study is that the diseases which are untreatable from antibiotics that cure from PDT. The great deal of the research is to find out the new PDT agents for the treatment of the tumors. Photofrin is used for the treatment of lung cancer, papillary bladder and esophageal tumour [89,90]. PDT also used for the treatment of intraperitoneal, brain tumor and intrathoracic tumour. In 1990s ophthalmic PDT was developed to treatment of subfoveal choroidal neovascularization (CNV). In 2000 PDT was introduced to ophthalmology. Temoporfin (*meso*-tetrahydroxyphenylchlorin, mTHPC), (Foscan) has been used for treatment of squamous cell carcinoma in the head and neck region and also prostate cancer [91]. In 2018, Andrade and coworkers reported the photodynamic effect of zinc porphyrin on *Leishmania braziliensis* [92]. Lei and coworkers prepared porphyrin-ferrocene conjugates which exhibit potency and efficiency for killing the cancer cells in very low drug doses (Figure 1.14) [93].

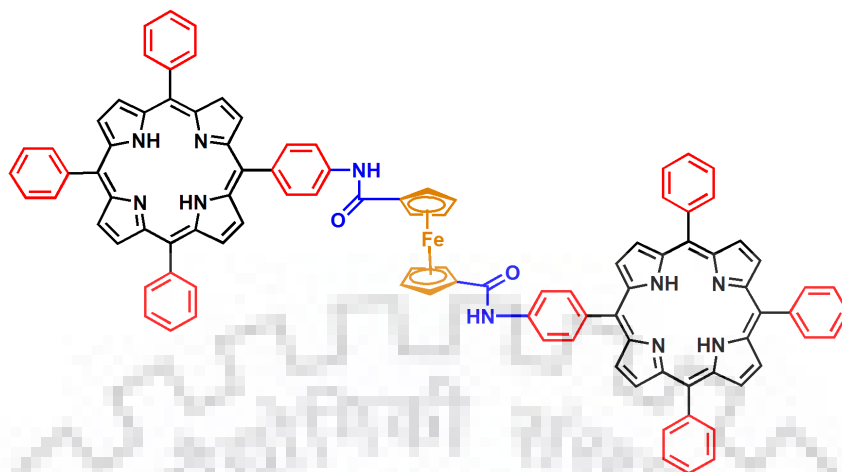


Figure 1.14 Structure of Porphyrin-Ferrocene Conjugate (TNCF).

1.5.3 DSSC Application of Porphyrins

The exponentially growth of population caused the imbalance in environment due to the large consumption of the fossil fuel increase the formation of CO_2 in the environment, which leads to the issue of global warming. So artificial photovoltaic devices and photosynthesis are required to harvest the sun light. Solar energy is one of the most important sources of renewable energy (tidal energy, geothermal energy, wind energy and biomass). Solar energy is an environmentally friendly resource of energy and it also reduces the emission of greenhouse gases. In 1954 the first silicon based solar cell was designed with 6% power conversion efficiency. Silicon based solar cell exhibited maximum 10-20% power conversion efficiency, despite their high utility these sensitizer exhibited several problems such as environmental toxicity, high cost, weak absorption and tedious synthesis. Due to these drawbacks researchers have developed low cost, environment friendly dyes sensitized solar cell (Figure1.15a) which exhibit high photovoltaic achievements. β - and *Meso*-substituted porphyrins are shown in Figure 1.16. DSSCs (Dye-sensitized solar cells) convert the solar energy in to the electrical energy. Several ruthenium based dyes are used as sensitizer in the DSSCs and which produced high power conversion efficiency [94,95]. Porphyrins and phthalocynine have reported as photosensitizer in DSSCs because they exhibit high molar extinction coefficient, high stability and tunability by substitution at periphery of macrocycle [96–100]. Misra and coworkers reported the ferrocenyl

appended triphenylamine based dyes with high efficiency [101]. Figure 1.15b represents the working principle of DSSC.

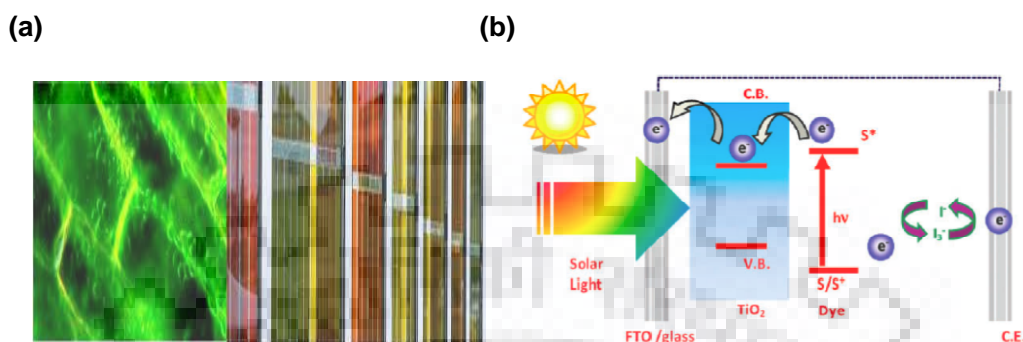


Figure 1.15 (a) Dye Sensitized Solar Cell (b) Working Principle of DSSC

Gratzel and coworkers have reported ruthenium based polypyridyl sensitizer in 1991. Various organic dyes such triphenylamine [102–105], aniline [106], phenothiazine [107,108], indoline [109], carbazole [110], coumarin [111] and fluorene [112] were utilized as electron donating in DSSCs. In 2018, our research group has synthesized *trans*-A₂BC type of porphyrins with 5.3-7.11 % power conversion efficiencies (η) (Figure 1.17) [102]. The main components of DSSCs are working electrode (TiO₂, anode), counter electrode (Pt, cathode), strong absorbing dye and redox electrolyte (iodide). After absorbing the light energy the molecule become excited and lose the electrons in high energy level which are pushed from working electrode from external circuit towards the cathode and the dye molecule get generated by absorbing electron from redox electrolyte (Figure1.15).

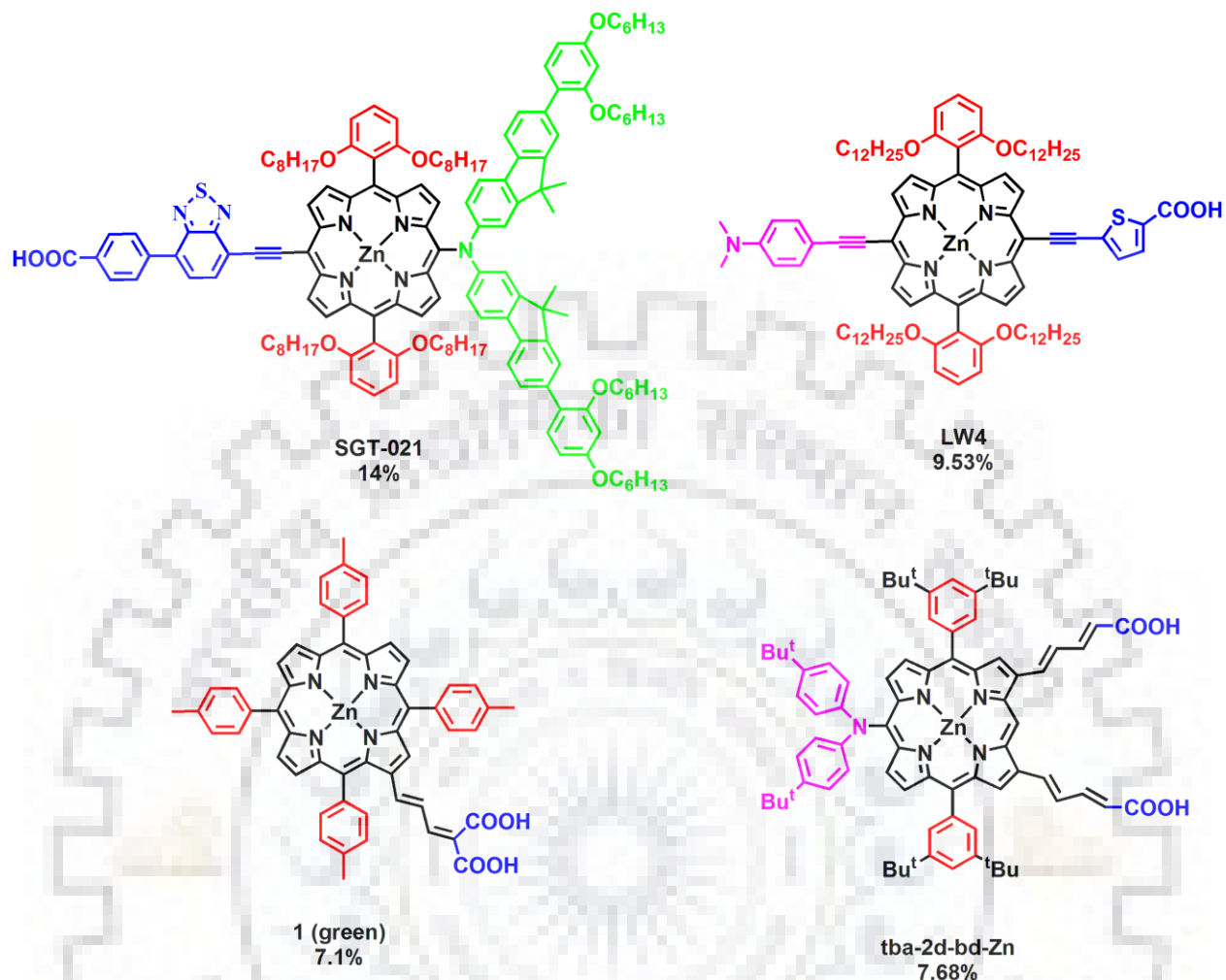


Figure 1.16 Molecular Structure of *Meso* and β -Substituted Porphyrin Based Dyes.

Porphyrin and phthalocyanine have high thermal stability, strong absorption in the visible region, good photochemical stability and large π -conjugated system. The properties of porphyrin can be easily tuned by selective substitution at periphery of the macrocycle and *via* variation in the metal atom at the center of core of porphyrin which made interest to researcher used as sensitizer in the DSSCs application. By using this technique, the efficient conversion of solar energy in to electrical energy takes place and may be used for large scale production in the future. Remarkably, the main objective of the researchers is to prepare the photosensitizer (dye) which absorb the radiation of higher wavelength (600-900 nm) in the visible light where the solar photon flux is the highest.

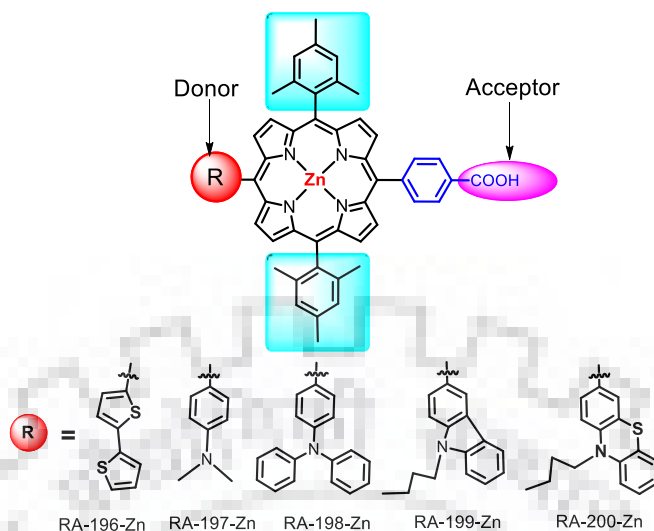


Figure 1.17 Molecular Structure of Trans-A₂BC Dyes.

1.5.4 Porphyrins as Sensors for Analytes

Various toxic species and the pollutants enter in our environment through human activities such as industrialization and by natural process. These toxic species and pollutants affect the human life lethally. So we need material based sensor for the detection of such type of pollutants with highly selectivity, good sensitivity and must be to use [113]. Due to unique photophysical and electrochemical properties of porphyrin make them suitable sensor for the detection of the ions [114,115]. Porphyrin conjugate and coumarin inserted corrole used for the detection of cations and anions and these sensors also used to detecting the mercuric cation by changing the colour in the non-aqueous media [116]. Zn(II)-tetrakis(triarylborane)porphyrin was reported by Thilagar *et al.* which detected cyanide and fluoride ions *via* different ways [117]. The binding of cyanide ions occur to core Zn(II) metal which exhibited predominant change in the absorption spectra. Fluoride ion binds to peripheral boron atom and brings minor change in the absorption spectra. Sapphyrin based fluorescent sensor was developed for the detecting of fluoride ion by Tabata and coworkers [118]. D'Souza, Hill and coworkers reported the anion binding to inner –NH protons exhibited large cathodic shift which endowed it as good electrochemical anion chemosensor [119]. Several porphyrinoids (porphyrins, sapphyrins, oxoporphyrinogens, calixpyrroles and phlorins) have been studied as sensors for many anions by strategies such as chemodosimetry and chemosensing from the last few decades [120–122]. Notably, many metalloporphyrins have been utilized for the detection of CN⁻ ions *via* axially coordination of

CN^- ions to the inner core metal such as rhodium, zinc, nickel and copper. Several types of ‘picket fence’ porphyrins have anion recognition sites which are linked to *meso*-position of Zn(II) porphyrin reported by Beer *et al.*[123]. Many types of porphyrinoids have been reported to recognize the anions such as CN^- , F^- , CH_3COO^- , H_2PO_4^- etc. In 2015, Zhang and coworkers reported a series of expanded anion-porphyrin supramolecular assemblies which exhibited exclusive environmental responsive behavior. Some porphyrin based sensors are shown in Figure 1.18 [124].

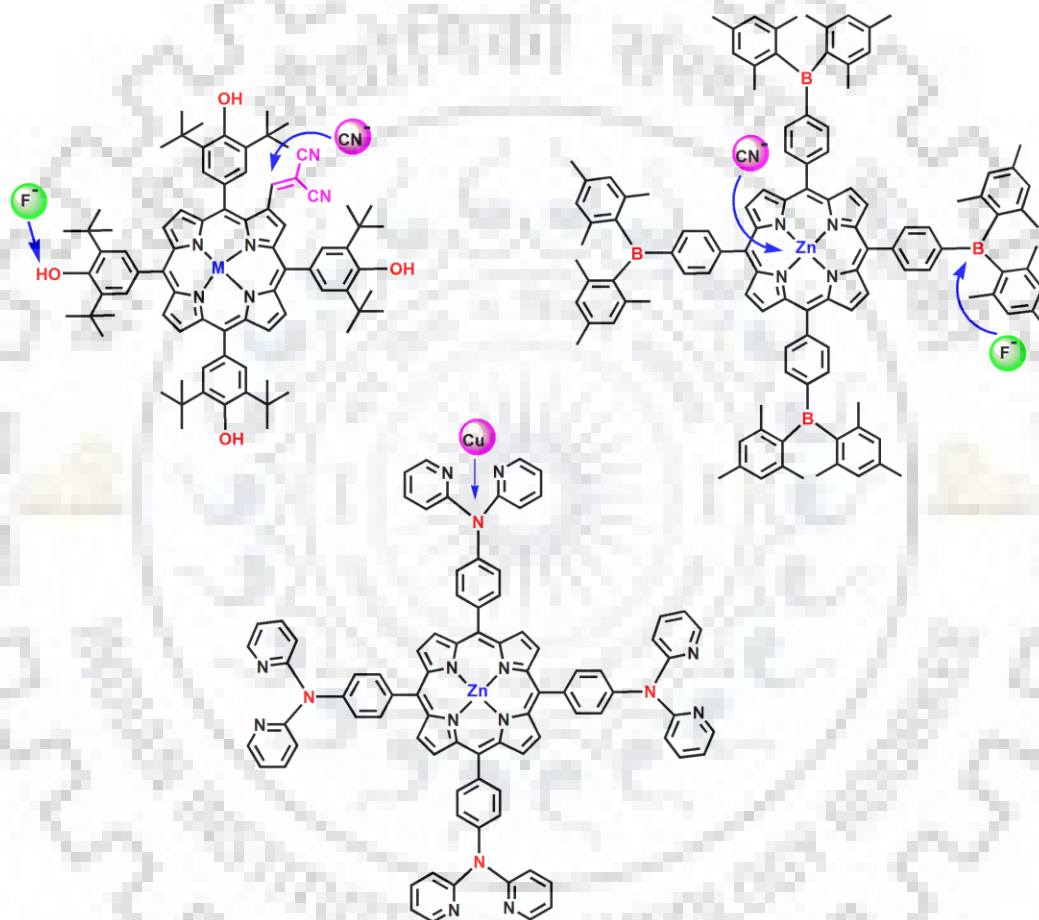


Figure 1.18 Porphyrin Based Anion and Cation Sensors.

1.5.5 Porphyrins as NLO Material

Nonlinear optics (NLO) deals with the study the interaction of the intense radiation with the matter. These materials used in optical limiting devices, data storage, signal processing and optical switching. Optical susceptibility of the medium is directly associated with dielectric constant and refractive index. The molecular polarization of isolated molecule is given as

$$P = \alpha E + \beta E E + \gamma E E E \quad \text{Eq.1}$$

α = linear polarisability, β = quadratic polarizability, γ = cubic polarizability and E = applied electric field

for a molecular group, the polarization can be expressed as

$$P = \chi^{(1)} E + \chi^{(2)} E E + \chi^{(3)} E E E$$

Herein, $\chi^{(1)}$ = linear susceptibility, $\chi^{(2)}$ = second order susceptibility and $\chi^{(3)}$ third order susceptibility.

Upon irradiation of molecule with high electric field, second and third susceptibility are more evident so molecule is nonlinear whereas on applying the low electric field the linear susceptibility is evident and second and third susceptibility negligible. Molecules with asymmetry, large π -electronic conjugation, thermally stable and with permanent dipole moment exhibit good nonlinear optical properties. Porphyrinoids exhibit chemical and thermal stability, permanent dipole moment, tunable optical properties and highly conjugated π -electronic system so these molecules are used in NLO applications [125]. Suslick *et al.* have reported a series of asymmetric porphyrins for NLO application [126]. β -substituted ‘push-pull’ porphyrins have been reported by many research groups for NLO applications. In 2017 a series of β - and *meso*-substituted porphyrins which showed second order of NLO responses have been reported by Gabriele *et al.* Our research group reported asymmetric corroles (A_2B) for NLO applications [127].

1.5.6 Porphyrin Complexation with Fullerenes

Chemists have been inspired by natural photosynthesis to mimic this energy transducing procedure in the laboratory. Fullerene possesses high electron affinity, spherical shape and also required small reorganization energy in various electron transfer reactions and hence these characteristics of fullerene make them well suited for artificial photosynthesis device fabrication. Porphyrin and fullerene bind to each other *via* hydrogen bonding, metal-ligand bond, π - π interaction, ion-dipole and dipole-dipole interaction. Porphyrin and phthalocynine exhibited favorable electrochemical potential and absorbed the radiation with higher wavelength and are good electron donor, so these are used as good biomimicking photosensitizers [128–131]. These

supramolecular dyads are used as solar energy conversion devices such as logic gate function, switching and optoelectronic devices [132,133]. Boyd and coworkers introduced the close association of porphyrin and fullerene molecular packing in crystal structure. D'Souza and coworkers reported several porphyrin-fullerene conjugated supramolecular dyads (Figure 1.19) [134–136]. In 2018, D'Souza *et al.* developed self-assembled bis-crown ether-porphyrinogen with C_{60} alkyl cation and F^- ion binding at porphyrin core that emphasize the ultrafast charge separation in supramolecular dyads *via* binding of F^- ion to porphyrin core [137]. El.Khouly and coworkers reported the intra and intermolecular procedure between imidazole appended fullerene and Zn(II) naphthalocynine where quenching constant was found $5.3 \times 10^8 \text{ M}^{-1}\text{s}^{-1}$ that indicated that the intermolecular electron transfer from triplet excited state of Zn(II) naphthalocynine to $C_{60}\text{Im}$ [138].

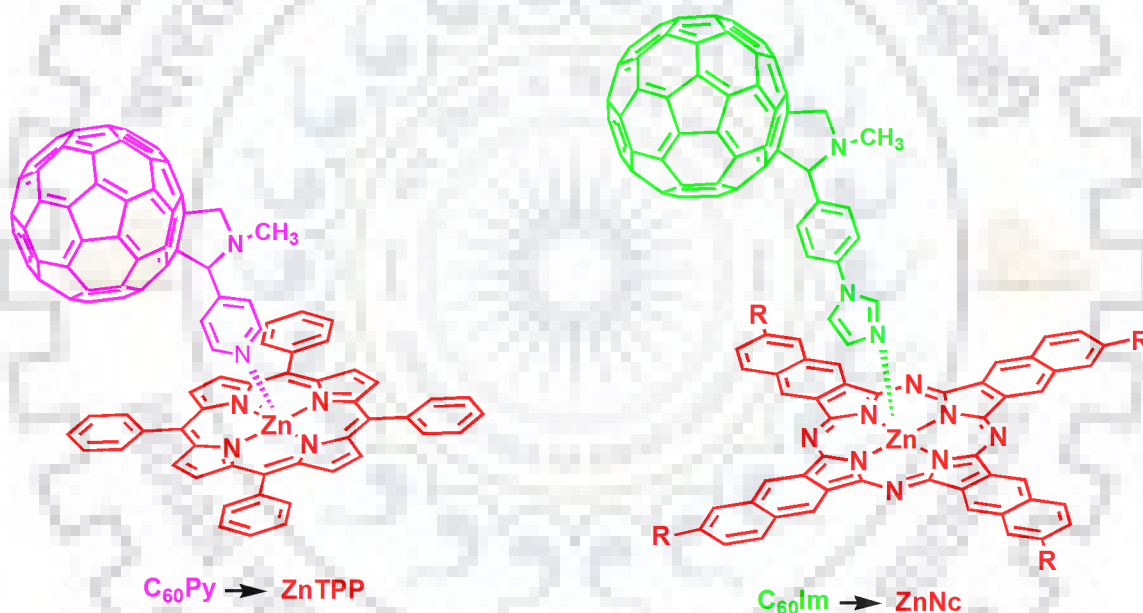


Figure 1.19 Structure of ZnTPP Coordinated with Pyridyl Fulleropyrrolidine Dyad and ZnNc Coordinated with Phenylimidazolyl Fulleropyrrolidine Dyad.

1.6 OBJECTIVES AND FUTURE IMPLICATIONS OF THE PRESENT WORK

Stability of macrocyclic core in porphyrinoids system permits easy modification *via* functionalization at β and *meso* position of the macrocycle which exhibit tunable photophysical and electrochemical properties. Modification of porphyrinoids can also be carried out by (a)

metallation using different types of metals and (b) by axial coordination of several types of ligands to central metal. β -Functionalized porphyrins have huge varieties of application in several field of research such as NLO, sensitizer in the DSSCs, catalysis, for sensing of cations and anions and as PDT agents. β -Functionalization of porphyrins are found to be interesting due to direct conjugation of β -substituents with the porphyrin π -system. The peripheral functionalization of porphyrin show unique electrochemical and photophysical properties by varying shape, size and electronic nature of β -substituents and core metal ions. Lots of chemical reactions can be performed at nitro group of porphyrins. The β -nitro group work as the starting material for synthesis of substituted porphyrins which undergo further use for functionalization *via* nitro group such as reduction, substitution etc. Mixed substituted porphyrins have been widely studied. The photophysical and electrochemical properties of porphyrins can be tuned very easily *via* changing the substituents at the periphery of the porphyrins. Fusion is another important pathway to obtain variety of β -and *meso*-functionalized porphyrins.

In the present work, we have synthesized β -arylamino porphyrins and their corresponding N-fused porphyrins. *Meso*-arylamino porphyrins have been widely explored and lots of literature is also available. However, the facile synthesis of β -arylamino porphyrins is still limited. This is a nucleophilic substitution reaction in which there is direct displacement of the nitro group by arylamino group. The beauty of the reaction is we don't need to add any additional catalyst or reagent because here aniline itself works as solvent and as reagent. These porphyrins exhibited an interesting electrochemical properties and broad absorption spectral features with hypsochromic shift as compared to β -nitroporphyrins. The N-fused porphyrin exhibited great interest in the research due to their binding with $C_{60}Im$ and $C_{60}Py$. Fusion of porphyrin significantly altered the physicochemical properties of macrocycle as their emission and absorption are change drastically as compared to unfused macrocycle. The main purpose of synthesizing these porphyrins was to mimic the photosynthetic process in plants *via* preparing donor-acceptor dyads where porphyrin act as electron donor and fullerene act as electron acceptor. N-fused porphyrins exhibited broad Soret band due intramolecular charge transfer from β -arylamino moiety to porphyrin core. The redox potential of supramolecular dyads are positively shifted (~ 100 mV) as compared to $C_{60}Im/C_{60}Py$ free Zn(II) N-fused porphyrins which exhibited supramolecular interaction between Zn(II) N-fused porphyrins and $C_{60}Im/C_{60}Py$ derivatives in ground state.

Further, we studied the CN^- and F^- ion sensing of highly electron deficient tetrabenzquinone appended Ni(II) and Cu(II) porphyrins. These porphyrins exhibited the hypsochromic shift in Soret band as compared to 5,10,15,20-tetrakis(3,5-di-*t*-butyl-4'-hydroxyphenyl)porphyrin (H_2dtBTPP) and *meso*-tetrakis(3,5-di-*tert*-butyl-4-oxo-2,5-cyclohexadienylidene) porphyrinogen (OxP). Electrochemical properties revealed diOxPM ($\text{M} = \text{Cu}$ and Ni) and $\text{H}_2\text{-dtBTPP}$ exhibit first reduction potential is very much anodically shift ($\Delta E_{\text{redn}} = 1.1 \text{ V}$) as compared to M-dtBTPP ($\text{M} = \text{Cu}, \text{Ni}$) due to strong electron withdrawing effect of cyclohexadienyl groups. These porphyrins exhibited very high binding constant (1.5×10^9 - $2.5 \times 10^7 \text{ M}^{-2}$) with F^- and CN^- . Solvatochromism was combined with anion binding with an attempt to provide the axial ligation mechanism of CN^- and F^- ions and these porphyrins also act as chemosensor in nonaqueous media. These porphyrins preferably detect the CN^- ions over F^- ions in aqueous media due to high solvation of F^- ions in water.

Mixed β -substitution at periphery of the porphyrin exhibits interesting photophysical and electrochemical redox properties. These properties of porphyrin can be tuned *via* different types of substitution at periphery of the macrocycle. Two new families of β -substituted porphyrins have been synthesized and characterized by using various spectroscopic techniques. $\text{H}_2\text{TPP}(\text{Ph})_2\text{Br}_5\text{X}$ ($\text{X} = \text{NO}_2$ or Br) exhibited a significant bathochromic shift ($\Delta\lambda_{\text{max}} = 53\text{-}61 \text{ nm}$) in their Soret band and ($\Delta\lambda_{\text{max}} = 90\text{-}95 \text{ nm}$) in $\text{Q}_x(0,0)$ band as compared to H_2TPP . The higher nonplanarity and electronic nature of β -substituents exhibit higher protonation and deprotonation constants for $\text{H}_2\text{TPP}(\text{Ph})_2\text{Br}_6$ as compared to $\text{H}_2\text{TPP}(\text{NO}_2)(\text{Ph})_2\text{Br}_5$. Single crystal X-ray structure revealed the nonplanar conformation of $\text{H}_2\text{TPP}(\text{NO}_2)(\text{Ph})_2\text{Br}_5$. Tunability in redox potential was achieved by appending either electron donating and/or accepting substituents at MTPP ($\text{M} = 2\text{H}, \text{Co(II)}, \text{Ni(II)}, \text{Cu(II)},$ and Zn(II)) skeleton of the macrocycle. The energy gap between HOMO-LUMO of $\text{CuTPP}(\text{Ph})_2\text{Br}_6$ and $\text{CuTPP}(\text{NO}_2)(\text{Ph})_2\text{Br}_5$ decreased to 550 mV and 620 mV as compared to CuTPP , respectively due to electronic effect of appending β -substituents and the nonplanarity of the porphyrin core.

Porphyrin revealed instance absorption in visible region, so it used as good electron donor and very easily oxidized in photoinduced electron transfer reaction. Electron donating properties of *meso*-alkyl porphyrin make them to bind with fullerene C_{60} . We have synthesized variety of *meso*-alkylsubstituted free base and Zn(II) porphyrins. We studied the π - π interaction of porphyrin with C_{60} which exhibited 1:1 binding of porphyrin with fullerene.

We have synthesized for the first time a new series of β -trisubstituted ‘push-pull’ porphyrins by Suzuki cross-coupling reaction. Redox tunability was achieved by introduction of electron acceptor $-\text{NO}_2$ and strong electron donor triphenylamine groups at the backbone of porphyrin π -system at antipodal position. Synthesized porphyrins exhibited interesting photophysical and electrochemical properties. Due to asymmetry and high dipole moment, these porphyrins exhibited higher order of NLO behaviours.

Steric repulsive interaction between the peripheral substituents causes the nonplanar conformation of porphyrin macrocycle. It reveals that the nonplanarity of porphyrin macrocycle can be modulated by varying the shape, size, and the number of the substituents at periphery of the macrocycle. We report the synthesis, spectral, and electrochemical redox properties of symmetrically β -tetrasubstituted triphenylaminoporphyrin ($\text{H}_2\text{TPP}(\text{TPA})_4$) and its metal derivatives (Co(II), Ni(II), Cu(II) and Zn(II)). All the synthesized porphyrins were characterized by various spectroscopic techniques. β -Tetrasubstituted triphenylaminoporphyrins induced nonplanar conformation which was confirmed by DFT studies. Due the β -substitution, the synthesized porphyrins exhibited tunable redox potential.

The present thesis organized into following eight chapters:

Chapter 1 describes the introduction to *meso*/ β -substituted porphyrins and their application in DSSCs, NLO, ions sensing, PDT and catalysis etc.

Chapter 2 includes the synthesis of mixed β -arylamino porphyrins and N-fused porphyrins and their characterization by using various spectroscopic techniques. Further it describes the photo-induced electron transfer studies of N-fused porphyrins with C_{60}Im and C_{60}Py derivatives.

Chapter 3 indicates the synthesis of highly electron deficient tetrabenzquinone appended Ni(II) and Cu(II) porphyrins. These porphyrins exhibit F^- and CN^- anions sensing and strong solvatochromism behavior with nitrogenous bases.

Chapter 4 encompasses the synthesis, photophysical, electrochemical, protonation and deprotonation studies 2,3,7,8,17,18-hexabromo-12,13-diphenyl-*meso*-tetraphenylporphyrin and 2-nitro-3,7,8,17,18-pentabromo-12,13-diphenyl-*meso*-tetraphenylporphyrin.

Chapter 5 deals with the synthesis and characterization of free base and Zn(II) derivative of *meso*-tetraalkylporphyrins and their donor-acceptor complexation with C_{60} derivatives.

Chapter 6 includes the synthesis of new series of β -trisubstituted ‘push-pull’ porphyrins and their NLO studies.

Chapter 7 exhibits the synthesis, structural, photophysical and electrochemical redox properties of symmetrically β -tetrasubstituted porphyrins.

Chapter 8 provides the conclusion and future scope of the present studies.

1.7 REFERENCES

- (1) Dolphin, D. *The Porphyrins*; Academic Press, **1978**.
- (2) Kadish, K. M.; Smith, K. M.; Gabriel, Â. S.; Guillard, R. *The Porphyrin Handbook*. Academic Press, New York. **2000**.
- (3) Lan, M.; Zhao, H.; Yuan, H.; Jiang, C.; Zuo, S.; Jiang, Y. Absorption and EPR Spectra of Some Porphyrins and Metalloporphyrins. *Dyes and Pigments* **2007**, *74*, 357–362.
- (4) Datta-Gupta, N.; Bardos, T. J. Synthetic Porphyrins. I. Synthesis and Spectra of Some Para-substituted Meso - Tetraphenylporphines. *J. Heterocycl. Chem.* **1966**, *3*, 495–502.
- (5) Dar, T. A.; Uprety, B.; Sankar, M.; Maurya, M. R. Robust and Electron Deficient Oxidovanadium(IV) Porphyrin Catalysts for Selective Epoxidation and Oxidative Bromination Reactions in Aqueous Media. *Green Chem.* **2019**, *21*, 1757–1768.
- (6) Speck, M.; Kurreck, H.; Senge, M. O. Porphyrin-o-Quinones as Model Systems for Electron Transfer and Catecholase Reactions. *Eur. J. Org. Chem.* **2000**, *2000*, 2303–2314.
- (7) Nakashima, H.; Hasegawa, J. Y. A.; Nakatsuji, H. On the Reversible O₂ Binding of the Fe-Porphyrin Complex. *J. Comput. Chem.* **2006**, *27*, 426–433.
- (8) Abeles, R. H.; Dolphin, D. The Vitamin B₁₂ Coenzyme. *Acc. Chem. Res.* **1976**, *9*, 114–120.
- (9) Mohajeri, A.; Hassani, N. Catalytic Activity of Corrole Complexes with Post-Transition Elements for the Oxidation of Carbon Monoxide: A First-Principles Study. *New J. Chem.* **2018**, *42*, 12632–12643.
- (10) Zhou, M.; Zhang, H.; Xiong, L.; He, Z.; Wang, T.; Xu, Y.; Huang, K. Fe-Porphyrin Functionalized Microporous Organic Nanotube Networks and Their Application for the Catalytic Olefination of Aldehydes and Carbene Insertion into N-H Bonds. *Polym. Chem.* **2017**, *8*, 3721–3730.
- (11) Wu, Y.; Jiang, J.; Weng, Z.; Wang, M.; Broere, D. L. J.; Zhong, Y.; Brudvig, G. W.; Feng, Z.; Wang, H. Electroreduction of CO₂ Catalyzed by a Heterogenized Zn-Porphyrin Complex with a Redox-Innocent Metal Center. *ACS Cent. Sci.* **2017**, *3*, 847–852.

- (12) Bahrami, M.; Kraft, S.; Becker, J.; Hartmann, H.; Vogler, B.; Wardelmann, K.; Behle, H.; Elemans, J. A. A. W.; Barke, I.; Speller, S. Correlative Microscopy of Morphology and Luminescence of Cu Porphyrin Aggregates. *J. Phys. B: At. Mol. Opt. Phys.* **2018**, *51*, 144002.
- (13) Hiroto, S.; Miyake, Y.; Shinokubo, H. Synthesis and Functionalization of Porphyrins through Organometallic Methodologies. *Chem. Rev.* **2017**, *22*, 2910–3043.
- (14) Kumar, R.; Sankar, M. Synthesis, Spectral, and Electrochemical Studies of Electronically Tunable β -Substituted Porphyrins with Mixed Substituent Pattern. *Inorg. Chem.* **2014**, *53*, 12706–12719.
- (15) Abdulaeva, I. A.; Birin, K. P.; Michalak, J.; Romieu, A.; Stern, C.; Bessmertnykh-Lemeune, A.; Guilard, R.; Gorbunova, Y. G.; Tsivadze, A. Y. On the Synthesis of Functionalized Porphyrins and Porphyrin Conjugates: Via β -Aminoporphyrins. *New J. Chem.* **2016**, *40*, 5758–5774.
- (16) Phuong, P. T. T.; Lee, S.; Lee, C.; Seo, B.; Park, S.; Oh, K. T.; Lee, E. S.; Choi, H. G.; Shin, B. S.; Youn, Y. S. Beta-Carotene-Bound Albumin Nanoparticles Modified with Chlorin e6 for Breast Tumor Ablation Based on Photodynamic Therapy. *Colloid Surface B.* **2018**, *171*, 123–133.
- (17) Huang, L.; Wang, M.; Huang, Y. Y.; El-Hussein, A.; Wolf, L. M.; Chiang, L. Y.; Hamblin, M. R. Progressive Cationic Functionalization of Chlorin Derivatives for Antimicrobial Photodynamic Inactivation and Related Vancomycin Conjugates. *Photochem. Photobiol. Sci.* **2018**, *17*, 638–651.
- (18) Chaudhri, N.; Grover, N.; Sankar, M. Versatile Synthetic Route for β -Functionalized Chlorins and Porphyrins by Varying the Size of Michael Donors: Syntheses, Photophysical, and Electrochemical Redox Properties. *Inorg. Chem.* **2017**, *56*, 11532–11545.
- (19) Chaudhri, N.; Grover, N.; Sankar, M. Nickel-Induced Skeletal Rearrangement of Free Base Trans-Chlorins into Monofused NiIII-Porphyrins: Synthesis, Structural, Spectral, and Electrochemical Redox Properties. *Inorg. Chem.* **2018**, *57*, 11349–11360.
- (20) Pijeat, J.; Dappe, Y. J.; Thuéry, P.; Campidelli, S. Synthesis and Suzuki-Miyaura Cross Coupling Reactions for Post-Synthetic Modification of a Tetrabromo-Anthracenyl Porphyrin. *Org. Biomol. Chem.* **2018**, *16*, 8106–8114.

- (21) Lang, P.; Habermehl, J.; Troyanov, S. I.; Rau, S.; Schwalbe, M. Photocatalytic Generation of Hydrogen Using Dinuclear π -Extended Porphyrin–Platinum Compounds. *Chem. Eur. J.* **2018**, *24*, 3225–3233.
- (22) Esipova, T. V.; Vinogradov, S. A. Synthesis of Phosphorescent Asymmetrically π -Extended Porphyrins for Two-Photon Applications. *J. Org. Chem.* **2014**, *79*, 8812–8825.
- (23) Guan, H.; Zhou, M.; Yin, B.; Xu, L.; Song, J. Synthesis and Characterization of Π -extended “Earring” Subporphyrins. *Beilstein J. Org. Chem.* **2018**, *14*, 1956–1960.
- (24) Lepper, M.; Köbl, J.; Schmitt, T.; Gurrath, M.; De Siervo, A.; Schneider, M. A.; Steinrück, H. P.; Meyer, B.; Marbach, H.; Hieringer, W. “inverted” Porphyrins: A Distorted Adsorption Geometry of Free-Base Porphyrins on Cu(111). *Chem. Commun.* **2017**, *53*, 8207–8210.
- (25) Wang, L. L.; Peng, S. H.; Wang, H.; Ji, L. N.; Liu, H. Y. Photophysical Properties of Free-Base and Manganese(III) N-Confused Porphyrins. *Phys. Chem. Chem. Phys.* **2018**, *20*, 20141–20148.
- (26) Pushpan, S. K.; Venkatraman, S.; Anand, V. G.; Sankar, J.; Rath, H.; Chandrashekar, T. K. Inverted Porphyrins and Expanded Porphyrins: An Overview. *J. Chem. Sci.* **2002**, *114*, 311–338.
- (27) Fischer, H.; Walach, B. Synthese Des Octamethylporphins, Des Methyl-analogen Des Ätioporphyrins. Mitteilung Über Porphyrinsynthesen. *Liebigs Ann.* **1926**, *450*, 164–181.
- (28) MacDonald, S. F. Dipyrromethanes. *J. Am. Chem. Soc.* **1957**, *79*, 2659–2659.
- (29) Lash, T. D. What’s in a Name? The MacDonald Condensation. *J. Porphyr. Phthalocyanines* **2016**, *20*, 855–888.
- (30) Tarlton, E. J.; MacDonald, S. F.; Baltazzi, E. Uroporphyrin 3. *J. Am. Chem. Soc.* **1960**, *82*, 4389–4395.
- (31) Adleb, A. D.; Longo, F. R.; Finarelli, J. D.; Goldmacher, J.; Assour, J.; Korsakoff, L. A Simplified Synthesis for *Meso*-Tetraphenylporphine. *J. Org. Chem.* **1967**, *32*, 476–476.
- (32) Rothmund, P. Formation of Porphyrins from Pyrrole and Aldehydes. *J. Am. Chem. Soc.* **1935**, *57*, 2010–2011.
- (33) Lindsey, J. S.; Schreiman, I. C.; Hsu, H. C.; Kearney, P. C.; Marguerettaz, A. M. Rothmund and Adler-Longo Reactions Revisited: Synthesis of Tetraphenylporphyrins under Equilibrium Conditions. *J. Org. Chem.* **1987**, *52*, 827–836.

- (34) Hao, E.; Fronczek, F. R.; Vicente, M. G. H. Carborane Functionalized Pyrroles and Porphyrins via the Suzuki Cross-Coupling Reaction. *Chem. Commun.* **2006**, *0*, 4900–4902.
- (35) Temelli, B.; Unaleroglu, C. Synthesis of *Meso*-Tetraphenyl Porphyrins via Condensation of Dipyrrromethanes with *N*-Tosyl Imines. *Tetrahedron* **2009**, *65*, 2043–2050.
- (36) Hiroto, S.; Miyake, Y.; Shinokubo, H. Synthesis and Functionalization of Porphyrins through Organometallic Methodologies. *Chem. Rev.* **2017**, *117*, 2910–3043.
- (37) Hilderbrand, S. A.; Weissleder, R. One-Pot Synthesis of New Symmetric and Asymmetric Xanthene Dyes. *Tetrahedron Lett.* **2007**, *48*, 4383–4385.
- (38) Meijere, A. de.; Diederich, F. *Metal-Catalyzed Cross-Coupling Reactions*; Wiley-VCH, **2004**.
- (39) Yamashita, K. I.; Kataoka, K.; Takeuchi, S.; Sugiura, K. I. Metal-Free Synthesis of *Meso*-Aminoporphyrins through Reduction of *Meso*-Azidoporphyrins Generated in Situ by Nucleophilic Substitution Reactions of *Meso*-Bromoporphyrins. *J. Org. Chem.* **2016**, *81*, 11176–11184.
- (40) Mikus, A.; Zajac, M.; Ostrowski, S. Frontiers in the Electrophilic Nitration of: *Meso* - Tetraphenylporphyrin Derivatives. *Org. Chem. Front.* **2018**, *5*, 2840–2844.
- (41) Mikus, A.; Rosa, M.; Ostrowski, S. Isomers of β,β -Dinitro-5,10,15,20-Tetraphenylporphyrin Derivatives: Valuable Starting Materials for Further Transformations. *Molecules* **2019**, *24*, 838.
- (42) Grover, N.; Sankar, M.; Song, Y.; Kadish, K. M. Asymmetrically Crowded “Push-Pull” Octaphenylporphyrins with Modulated Frontier Orbitals: Syntheses, Photophysical, and Electrochemical Redox Properties. *Inorganic Chemistry* **2016**, *55*, 584–597.
- (43) Reddy, K. S. K.; Liu, Y. C.; Chou, H. H.; Kala, K.; Wei, T. C.; Yeh, C. Y. Synthesis and Characterization of Novel β -Bis(*N,N*-Diarylamino)-Substituted Porphyrin for Dye-Sensitized Solar Cells under 1 Sun and Dim Light Conditions. *ACS Appl. Mater. Interfaces* **2018**, *10*, 39970–39982.
- (44) Fujimoto, K.; Yorimitsu, H.; Osuka, A. Facile Preparation of β -Haloporphyrins as Useful Precursors of β -Substituted Porphyrins. *Org. Lett.* **2014**, *16*, 972–975.
- (45) Hiroto, S.; Miyake, Y.; Shinokubo, H. Synthesis and Functionalization of Porphyrins through Organometallic Methodologies. *Chem. Rev.* **2017**, *117*, 2910–3043.
- (46) Crossley, M. J.; Harding, M. M.; Tansey, C. W. A Convenient Synthesis of 2-Alkyl-

- 5,10,15,20-Tetraphenylporphyrins: Reaction of Metallo-2-Nitro-5,10,15,20-Tetraphenylporphyrins with Grignard and Organolithium Reagents. *J. Org. Chem.* **1994**, *59*, 4433–4437.
- (47) Catalano, M. M.; Crossley, M. J.; Harding, M. M.; King, L. G. Control of Reactivity at the Porphyrin Periphery by Metal Ion Co-Ordination: A General Method for Specific Nitration at the β -Pyrrolic Position of 5,10,15,20-Tetraarylporphyrins. *J. Chem. Soc. Chem. Commun.* **1984**, *0*, 1535–1536.
- (48) Bhyrappa, P. Recent Advances in Mixed β -Pyrrole Substituted *Meso*-Tetraphenylporphyrins. *Tetrahedron Lett.* **2016**, *57*, 5150–5167.
- (49) Tessore, F.; Birolì, A. O.; Di Carlo, G.; Pizzotti, M. Porphyrins for Second Order Nonlinear Optics (NLO): An Intriguing History. *Inorganics* **2018**, *6*, 81.
- (50) Mi, Y.; Liang, P.; Yang, Z.; Wang, D.; Cao, H.; He, W.; Yang, H.; Yu, L. Application of Near-IR Absorption Porphyrin Dyes Derived from Click Chemistry as Third-Order Nonlinear Optical Materials. *ChemistryOpen* **2016**, *5*, 71–77.
- (51) Nudy, L. R.; Hutchinson, H. G.; Schieber, C.; Longo, F. R. A Study of Bromoporphins. *Tetrahedron* **1984**, *40*, 2359–2363.
- (52) Bhyrappa, P.; Krishnan, V. Octabromotetraphenylporphyrin and Its Metal Derivatives: Electronic Structure and Electrochemical Properties. *Inorg. Chem.* **1991**, *30*, 239–245.
- (53) Kumar, P. K.; Bhyrappa, P.; Varghese, B. An Improved Protocol for the Synthesis of Antipodal β -Tetrabromo-Tetraphenylporphyrin and the Crystal Structure of Its Zn(II) Complex. *Tetrahedron Lett.* **2003**, *44*, 4849–4851.
- (54) Fischer, H.; Halbig, P. Über Iso-ätioporphyrin, Sein Tetrabromderivat, Seinen Oxydativen Und Reduktiven Abbau, Sowie Eine Synthese Eines Iso-mesoporphyrins Und Des Opsopyrrols. *Justus Liebigs Ann. Chem.* **1926**, *450*, 151–164.
- (55) Samuels, E.; Shuttleworth, R.; Stevens, T. S. Halogenation of Porphin and Octaethylporphin. *J. Chem. Soc. C: Org.* **1968**, *0*, 145–147.
- (56) Yadav, P.; Kumar, R.; Saxena, A.; Butcher, R. J.; Sankar, M. β -Trisubstituted “Push-Pull” Porphyrins-Synthesis and Structural, Photophysical, and Electrochemical Redox Properties. *Eur. J. Inorg. Chem.* **2017**, *2017*, 3269–3274.
- (57) Bengasi, G.; Baba, K.; Frache, G.; Desport, J.; Gratia, P.; Heinze, K.; Boscher, N. D. Conductive Fused Porphyrin Tapes on Sensitive Substrates by a Chemical Vapor

- Deposition Approach. *Angew. Chem. Int. Ed.* **2019**, *58*, 2103–2108.
- (58) Chen, Q.; Brambilla, L.; Daukiya, L.; Mali, K. S.; De Feyter, S.; Tommasini, M.; Müllen, K.; Narita, A. Synthesis of Triply Fused Porphyrin-Nanographene Conjugates. *Angew. Chem. Int. Ed.* **2018**, *57*, 11233–11237.
- (59) Matsuo, H.; Toganoh, M.; Ishida, M.; Mori, S.; Furuta, H. Stereoretentive Ligand Exchange Reactions of N-Fused Porphyrin Ruthenium(II) Complexes. *Inorg. Chem.* **2017**, *56*, 13842–13851.
- (60) Fox, S.; Boyle, R. W. First Examples of Intramolecular Pd(0) Catalysed Couplings on *Ortho*-Iodinated *Meso*-Phenyl Porphyrins. *Chem. Commun.* **2004**, *4*, 1322–1323.
- (61) Pereira, A. M. V. M.; Alonso, C. M. A.; Neves, M. G. P. M. S.; Tomé, A. C.; Silva, A. M. S.; Paz, F. A. A.; Cavaleiro, J. A. S. A New Synthetic Approach to N-Arylquinolino[2,3,4-*at*]Porphyrins from β -Arylaminoporphyrins. *J. Org. Chem.* **2008**, *73*, 7353–7356.
- (62) Mikus, A.; Rosa, M.; Ostrowski, S. Isomers of β,β -Dinitro-5,10,15,20-Tetraphenylporphyrin Derivatives: Valuable Starting Materials for Further Transformations. *Molecules* **2019**, *24*, 838.
- (63) Richeter, S.; Jeandon, C.; Gisselbrecht, J. P.; Graff, R.; Ruppert, R.; Callot, H. J. Synthesis of New Porphyrins with Peripheral Conjugated Chelates and Their Use for the Preparation of Porphyrin Dimers Linked by Metal Ions. *Inorg. Chem.* **2004**, *43*, 251–263.
- (64) Jaquinod, L.; Gros, C.; Olmstead, M. M.; Antolovich, M.; Smith, K. M. First Syntheses of Fused Pyrroloporphyrins. *Chem. Commun.* **1996**, 1475–1476.
- (65) Ishizuka, T.; Saegusa, Y.; Shiota, Y.; Ohtake, K.; Yoshizawa, K.; Kojima, T. Multiply-Fused Porphyrins - Effects of Extended π -Conjugation on the Optical and Electrochemical Properties. *Chem. Commun.* **2013**, *49*, 5939–5941.
- (66) Richeter, S.; Jeandon, C.; Gisselbrecht, J. P.; Ruppert, R.; Callot, H. J. Syntheses and Optical and Electrochemical Properties of Porphyrin Dimers Linked by Metal Ions. *J. Am. Chem. Soc.* **2002**, *124*, 6168–6179.
- (67) Fukui, N.; Kim, T.; Kim, D.; Osuka, A. Porphyrin Arch-Tapes: Synthesis, Contorted Structures, and Full Conjugation. *J. Am. Chem. Soc.* **2017**, *139*, 9075–9088.
- (68) Fukui, N.; Cha, W.; Shimizu, D.; Oh, J.; Furukawa, K.; Yorimitsu, H.; Kim, D.; Osuka, A. Highly Planar Diarylamine-Fused Porphyrins and Their Remarkably Stable Radical Cations. *Chem. Sci.* **2016**, *8*, 189–199.

- (69) Chaudhri, N.; Grover, N.; Sankar, M. Selective Conversion of Planar Trans-Chlorins into Highly Twisted Doubly Fused Porphyrins or Chlorins via Oxidative Fusion. *Inorg. Chem.* **2018**, *57*, 6658–6668.
- (70) Berthelot, M.; Hoffmann, G.; Bousfiha, A.; Echaubard, J.; Roger, J.; Cattey, H.; Romieu, A.; Lucas, D.; Fleurat-Lessard, P.; Devillers, C. H. Oxidative C-N Fusion of Pyridinyl-Substituted Porphyrins. *Chem. Commun.* **2018**, *54*, 5414–5417.
- (71) Chang, C. K.; Ming-Shang, K. Reaction of Iron(III) Porphyrins and Iodosoxylene. The Active Oxene Complex of Cytochrome P-450. *J. Am. Chem. Soc.* **1979**, *101*, 3413–3415.
- (72) Groves, J. T.; Nemo, T. E.; Myers, R. S. Hydroxylation and Epoxidation Catalyzed by Iron-Porphine Complexes. Oxygen Transfer from Iodosylbenzene. *J. Am. Chem. Soc.* **1979**, *101*, 1032–1033.
- (73) Maurya, M. R.; Kumar, A.; Costa Pessoa, J. Vanadium Complexes Immobilized on Solid Supports and Their Use as Catalysts for Oxidation and Functionalization of Alkanes and Alkenes. *Coord. Chem. Rev.* **2011**, *255*, 2315–2344.
- (74) Stephenson, N. A.; Bell, A. T. Mechanistic Insights into Iron Porphyrin-Catalyzed Olefin Epoxidation by Hydrogen Peroxide: Factors Controlling Activity and Selectivity. *J. Mol. Catal. A: Chem.* **2007**, *275*, 54–62.
- (75) Kumar, R.; Chaudhary, N.; Sankar, M.; Maurya, M. R. Electron Deficient Nonplanar β -Octachlorovanadylporphyrin as a Highly Efficient and Selective Epoxidation Catalyst for Olefins. *Dalton Trans.* **2015**, *44*, 17720–17729.
- (76) Dolphin, D.; Traylor, T. G.; Xie, L. Y. Polyhaloporphyrins: Unusual Ligands for Metals and Metal-Catalyzed Oxidations. *Acc. Chem. Res.* **1997**, *30*, 251–259.
- (77) Dawson, J. H. Probing Structure-Function Relations in Heme-Containing Oxygenases and Peroxidases. *Science* **1988**, *240*, 433–439.
- (78) Avidan-Shlomovich, S.; Gross, Z. Reaction Mechanism for the Highly Efficient Catalytic Decomposition of Peroxynitrite by the Amphipolar Iron(III) Corrole 1-Fe. *Dalton Trans.* **2015**, *44*, 12234–12243.
- (79) Liu, W.; Groves, J. T. Manganese Catalyzed C-H Halogenation. *Acc. Chem. Res.* **2015**, *48*, 1727–1735.
- (80) Green, M. T.; Dawson, J. H.; Gray, H. B. Oxoiron(IV) in Chloroperoxidase Compound II Is Basic: Implications for P450 Chemistry. *Science* **2004**, *304*, 1653–1656..

- (81) Pandey, R. K. Recent Advances in Photodynamic Therapy. *J. Porphyr. Phthalocyanines* **2000**, *4*, 368–373.
- (82) MacDonald, I. J.; Dougherty, T. J. Basic Principles of Photodynamic Therapy. *J. Porphyr. Phthalocyanines* **2001**, *5*, 105–129.
- (83) Kessel, D.; Vicente, M. G. H.; Reiners, J. J. Initiation of Apoptosis and Autophagy by Photodynamic Therapy. *Autophagy* **2006**, *2*, 289–290.
- (84) Kessel, D.; Reiners, J. J. Apoptosis and Autophagy after Mitochondrial or Endoplasmic Reticulum Photodamage. *Photochem. Photobiol.* **2007**, *83*, 1024–1028.
- (85) Pandey, R. K.; Bellnier, D. A.; Smith, K. M.; Dougherty, T. J. Chlorin and Porphyrin Derivatives as Potential Photosensitizers in Photodynamic Therapy. *Photochem. Photobiol.* **1991**, *53*, 65–72.
- (86) Lee, S.-J. H.; Jagerovic, N.; Smith, K. M. Use of the Chlorophyll Derivative, Purpurin-18, for Syntheses of Sensitizers for Use in Photodynamic Therapy. *J. Chem. Soc. Perkin Trans. 1* **2004**, *0*, 2369.
- (87) Song, L. W. K.; Wang, K. K.; Zinsmeister, A. R.; D, P. Hematoporphyrin Derivative (HpD) in Photodynamic Therapy Administered to a Human Cholangiocarcinoma Model. *Soc.* **1998**, *6*, 421–427.
- (88) Dimofte, A.; Zhu, T. C.; Hahn, S. M.; Lustig, R. A. In Vivo Light Dosimetry for Motexafin Lutetium-Mediated PDT of Recurrent Breast Cancer. *Lasers Surg. Med.* **2002**, *31*, 305–312.
- (89) Tian, Y. Y.; Wang, L. L.; Wang, W. Progress in Photodynamic Therapy on Tumors. *Laser Phys.* **2008**, *18*, 1119–1123.
- (90) Sutedja, T.; Baas, P.; Stewart, F.; van Zandwijk, N. A Pilot Study of Photodynamic Therapy in Patients with Inoperable Non-Small Cell Lung Cancer. *Eur. J. Cancer* **1992**, *28*, 1370–1373.
- (91) Moore, C. M.; Nathan, T. R.; Lees, W. R.; Mosse, C. A.; Freeman, A.; Emberton, M.; Bown, S. G. Photodynamic Therapy Using Meso Tetra Hydroxy Phenyl Chlorin (MTHPC) in Early Prostate Cancer. *Lasers Surg. Med.* **2006**, *38*, 356–363.
- (92) Andrade, C. G.; Figueiredo, R. C. B. Q.; Ribeiro, K. R. C.; Souza, L. I. O.; Sarmiento-Neto, J. F.; Rebouças, J. S.; Santos, B. S.; Ribeiro, M. S.; Carvalho, L. B.; Fontes, A. Photodynamic Effect of Zinc Porphyrin on the Promastigote and Amastigote Forms of:

- Leishmania Braziliensis. *Photochem. Photobiol. Sci.* **2018**, *17*, 482–490.
- (93) Lei, Z.; Zhang, X.; Zheng, X.; Liu, S.; Xie, Z. Porphyrin-Ferrocene Conjugates for Photodynamic and Chemodynamic Therapy. *Org. Biomol. Chem.* **2018**, *16*, 8613–8619.
- (94) Krishna, N. V.; Krishna, J. V. S.; Mrinalini, M.; Prasanthkumar, S.; Giribabu, L. Role of Co-Sensitizers in Dye-Sensitized Solar Cells. *ChemSusChem* **2017**, *10*, 4668–4689.
- (95) Carella, A.; Borbone, F.; Centore, R. Research Progress on Photosensitizers for DSSC. *Front. Chem.* **2018**, *6*, 481.
- (96) Maragani, R.; Misra, R.; Roy, M. S.; Singh, M. K.; Sharma, G. D. (D- π -A) 2 - π -D-A Type Ferrocenyl Bisthiazole Linked Triphenylamine Based Molecular Systems for DSSC: Synthesis, Experimental and Theoretical Performance Studies. *Phys.Chem.Chem. Phy.* **2017**, *19*, 8925–8933.
- (97) Huang, Z. S.; Meier, H.; Cao, D. Phenothiazine-Based Dyes for Efficient Dye-Sensitized Solar Cells. *J. Mater. Chem. C* **2016**, *4*, 2404–2426.
- (98) Wang, C. L.; Hu, J. Y.; Wu, C. H.; Kuo, H. H.; Chang, Y. C.; Lan, Z. J.; Wu, H. P.; Wei-Guang Diao, E.; Lin, C. Y. Highly Efficient Porphyrin-Sensitized Solar Cells with Enhanced Light Harvesting Ability beyond 800 nm and Efficiency Exceeding 10%. *Energy Environ. Sci.* **2014**, *7*, 1392–1396.
- (99) Martínez-Díaz, M. V.; De La Torre, G.; Torres, T. Lighting Porphyrins and Phthalocyanines for Molecular Photovoltaics. *Chem. Commun.* **2010**, *46*, 7090–7108.
- (100) Liu, B.; Zhu, W.; Wang, Y.; Wu, W.; Li, X.; Chen, B.; Long, Y. T.; Xie, Y. Modulation of Energy Levels by Donor Groups: An Effective Approach for Optimizing the Efficiency of Zinc-Porphyrin Based Solar Cells. *J. Mater. Chem.* **2012**, *22*, 7434–7444.
- (101) Misra, R.; Maragani, R.; Patel, K. R.; Sharma, G. D. Synthesis, Optical and Electrochemical Properties of New Ferrocenyl Substituted Triphenylamine Based Donor-Acceptor Dyes for Dye Sensitized Solar Cells. *RSC Adv.* **2014**, *4*, 34904–34911.
- (102) Kumar, R.; Sudhakar, V.; Prakash, K.; Krishnamoorthy, K.; Sankar, M. Tuning the Photovoltaic Performance of DSSCs by Appending Various Donor Groups on *Trans*-Dimesityl Porphyrin Backbone. *ACS Appl. Energy Mater.* **2018**, *1*, 2793–2801.
- (103) Mizuno, Y.; Yisilamu, Y.; Yamaguchi, T.; Tomura, M.; Funaki, T.; Sugihara, H.; Ono, K. (Dibenzoylmethanato)Boron Difluoride Derivatives Containing Triphenylamine Moieties: A New Type of Electron-Donor/ π -Acceptor System for Dye-Sensitized Solar

- Cells. *Chem. Eur. J.* **2014**, *20*, 13286–13295.
- (104) Bao, L. Q.; Phuong, H.; Thuy, C. T. T.; Lee, J. W.; Kim, J. H.; Thogiti, S. Synthesis and Investigation of Triphenylamine-Based Double Branched Organic Dyes for p-Type Dye-Sensitized Solar Cells. *Mol. Cryst. Liq. Cryst.* **2017**, *653*, 109–117.
- (105) Tang, Y.; Wang, Y.; Li, X.; Ågren, H.; Zhu, W. H.; Xie, Y. Porphyrins Containing a Triphenylamine Donor and up to Eight Alkoxy Chains for Dye-Sensitized Solar Cells: A High Efficiency of 10.9%. *ACS Applied Materials and Interfaces* **2015**, *7*, 27976–27985.
- (106) Michinobu, T.; Satoh, N.; Cai, J.; Li, Y.; Han, L. Novel Design of Organic Donor-Acceptor Dyes without Carboxylic Acid Anchoring Groups for Dye-Sensitized Solar Cells. *J. Mater. Chem. C* **2014**, *2*, 3367–3372.
- (107) Prakash, K.; Sudhakar, V.; Sankar, M.; Krishnamoorthy, K. Trans-A₂B₂Zn(II) Porphyrin Dyes with Various Donor Groups and Their Co-Sensitization for Highly Efficient Dye-Sensitized Solar Cells. *Dyes Pigm.* **2019**, *160*, 386–394.
- (108) Yang, G.; Tang, Y.; Li, X.; Ågren, H.; Xie, Y. Efficient Solar Cells Based on Porphyrin Dyes with Flexible Chains Attached to the Auxiliary Benzothiadiazole Acceptor: Suppression of Dye Aggregation and the Effect of Distortion. *ACS Appl. Mater. Interfaces* **2017**, *9*, 36875–36885.
- (109) Horiuchi, T.; Miura, H.; Sumioka, K.; Uchida, S. High Efficiency of Dye-Sensitized Solar Cells Based on Metal-Free Indoline Dyes. *J. Am. Chem. Soc.* **2004**, *126*, 12218–12219.
- (110) Luo, C.; Bi, W.; Deng, S.; Zhang, J.; Chen, S.; Li, B.; Liu, Q.; Peng, H.; Chu, J. Indolo[3,2,1-Jk]Carbazole Derivatives-Sensitized Solar Cells: Effect of π -Bridges on the Performance of Cells. *J. Phys. Chem. C* **2014**, *118*, 14211–14217.
- (111) Hara, K.; Wang, Z. S.; Sato, T.; Furube, A.; Katoh, R.; Sugihara, H.; Dan-Oh, Y.; Kasada, C.; Shinpo, A.; Suga, S. Oligothiophene-Containing Coumarin Dyes for Efficient Dye-Sensitized Solar Cells. *J. Phys. Chem. B* **2005**, *109*, 15476–15482.
- (112) Liu, Z.; Xiong, D.; Xu, X.; Arooj, Q.; Wang, H.; Yin, L.; Li, W.; Wu, H.; Zhao, Z.; Chen, W.; et al. Modulated Charge Injection in P-Type Dye-Sensitized Solar Cells Using Fluorene-Based Light Absorbers. *ACS Appl. Mater. Interfaces* **2014**, *6*, 3448–3454.
- (113) Rong, L.; Liu, L. H.; Chen, S.; Cheng, H.; Chen, C. S.; Li, Z. Y.; Qin, S. Y.; Zhang, X. Z. A Coumarin Derivative as a Fluorogenic Glycoproteomic Probe for Biological Imaging.

- Chem. Commun.* **2014**, 50, 667–669.
- (114) Ding, Y.; Zhu, W. H.; Xie, Y. Development of Ion Chemosensors Based on Porphyrin Analogues. *Chem. Rev.* **2017**, 117, 2203–2256.
- (115) Mrinalini, M.; Pathak, S. S.; Achary, B. S.; Panchakarla, L. S.; Prasanthkumar, S. Voltage Stimulated Anion Binding of Metalloporphyrin-Induced Crystalline 2D Nanoflakes. *Chem. Asian J.* **2019**, 14, 537–541.
- (116) Santos, C. I. M.; Oliveira, E.; Menezes, J. C. J. M. D. S.; Barata, J. F. B.; Faustino, M. A. F.; Ferreira, V. F.; Cavaleiro, J. A. S.; Neves, M. G. P. M. S.; Lodeiro, C. New Coumarin-Corrole and Porphyrin Conjugate Multifunctional Probes for Anionic or Cationic Interactions: Synthesis, Spectroscopy, and Solid Supported Studies. In *Tetrahedron* **2014**, 70, 3361–3370.
- (117) Swamy, P. C. A.; Mukherjee, S.; Thilagar, P. Dual Binding Site Assisted Chromogenic and Fluorogenic Recognition and Discrimination of Fluoride and Cyanide by a Peripherally Borylated Metalloporphyrin: Overcoming Anion Interference in Organoboron Based Sensors. *Anal. Chem.* **2014**, 86, 3616–3624.
- (118) Nishimoto, J.; Yamada, T.; Tabata, M. Solvent Extraction and Fluorometric Determination of Fluoride Ion at Ppb Level in the Presence of Large Excess of Aluminum(III) and Iron(III) by Using an Expanded Porphyrin, Sapphyrin. *Anal. Chim. Acta* **2001**, 428, 201–208.
- (119) Schumacher, A. L.; Hill, J. P.; Ariga, K.; D'Souza, F. Highly Effective Electrochemical Anion Sensing Based on Oxoporphyrinogen. *Electrochem. Commun.* **2007**, 9, 2751–2754.
- (120) Wei, K.; Yao, F.; Kang, X. F. Single-Molecule Porphyrin-Metal Ion Interaction and Sensing Application. *Biosens. Bioelectron.* **2018**, 109, 272–278.
- (121) Nishiyabu, R.; Anzenbacher, P. 1,3-Indane-Based Chromogenic Calixpyrroles with Push-Pull Chromophores: Synthesis and Anion Sensing. *Org. Lett.* **2006**, 8, 359–362.
- (122) Chatterjee, T.; Srinivasan, A.; Ravikanth, M.; Chandrashekar, T. K. Smaragdyrins and Sapphyrins Analogues. *Chem. Rev.* **2017**, 117, 3329–3376.
- (123) Cormode, D. P.; Murray, S. S.; Cowley, A. R.; Beer, P. D. Sulfate Selective Anion Recognition by a Novel Tetra-Imidazolium Zinc Metalloporphyrin Receptor. *Dalton Trans.* **2006**, 0, 5135–5140.
- (124) Chahal, M. K.; Sankar, M. Switching between Porphyrin, Porphodimethene and

- Porphyrinogen Using Cyanide and Fluoride Ions Mimicking Volatile Molecular Memory and the “NOR” Logic Gate. *Dalton Trans.* **2016**, *45*, 16404–16412.
- (125) Tessore, F.; Biroli, A. O.; Di Carlo, G.; Pizzotti, M. Porphyrins for Second Order Nonlinear Optics (NLO): An Intriguing History. *Inorganics* **2018**, *6*, 81.
- (126) Suslick, K. S.; Chen, C. T.; Meredith, G. R.; Cheng, L. T. Push-Pull Porphyrins as Nonlinear Optical Materials. *J. Am. Chem. Soc.* **1992**, *114*, 6928–6930.
- (127) Yadav, P.; Anand, T.; Moram, S. S. B.; Bhattacharya, S.; Sankar, M.; Rao, S. V. Synthesis and Femtosecond Third Order Nonlinear Optical Properties of Push-Pull Trans-A₂B-Corroles. *Dyes Pigm.* **2017**, *143*, 324–330.
- (128) Fierro, C.; Anderson, A. B.; Scherson, D. A. Electron Donor-Acceptor Properties of Porphyrins, Phthalocyanines, and Related Ring Chelates: A Molecular Orbital Approach. *J. Phys. Chem.* **1988**, *92*, 6902–6907.
- (129) Borovkov, N. Y.; Kolker, A. M. Aqueous Route to Phthalocyanine-Fullerene Composites with Regular Structure. *J. Phys. Chem. C* **2014**, *118*, 14403–14409.
- (130) Bottari, G.; Olea, D.; López, V.; Gomez-Navarro, C.; Zamora, F.; Gómez-Herrero, J.; Torres, T. Ordering Phthalocyanine-C₆₀ Fullerene Conjugates on Individual Carbon Nanotubes. *Chem. Commun.* **2010**, *46*, 4692–4694.
- (131) Sun, D.; Tham, F. S.; Reed, C. A.; Chaker, L.; Burgess, M.; Boyd, P. D. W. Porphyrin-Fullerene Host-Guest Chemistry. *J. Am. Chem. Soc.* **2002**, *122*, 10704–10705.
- (132) D’Souza, F.; Ito, O. Supramolecular Donor-Acceptor Hybrids of Porphyrins/Phthalocyanines with Fullerenes/Carbon Nanotubes: Electron Transfer, Sensing, Switching, and Catalytic Applications. *Chem. Commun.* **2009**, *0*, 4913–4928.
- (133) Hasobe, T.; Kamat, P. V.; Absalom, M. A.; Kashiwagi, Y.; Sly, J.; Crossley, M. J.; Hosomizu, K.; Imahori, H.; Fukuzumi, S. Supramolecular Photovoltaic Cells Based on Composite Molecular Nanoclusters: Dendritic Porphyrin and C₆₀, Porphyrin Dimer and C₆₀, and Porphyrin-C₆₀ Dyad. *J. Phys. Chem. B* **2004**, *108*, 12865–12872.
- (134) Zarrabi, N.; Obondi, C. O.; Lim, G. N.; Seetharaman, S.; Boe, B. G.; D’Souza, F.; Poddutoori, P. K. Charge-Separation in Panchromatic, Vertically Positioned Bis(Donor Styryl)BODIPY-Aluminum(III) Porphyrin-Fullerene Supramolecular Triads. *Nanoscale* **2018**, *10*, 20723–20739.
- (135) Barrejón, M.; Arellano, L. M.; Gobeze, H. B.; Gómez-Escalonilla, M. J.; Fierro, J. L. G.;

Chapter 1: Introduction

- D'Souza, F.; Langa, F. N-Doped Graphene/C₆₀ Covalent Hybrid as a New Material for Energy Harvesting Applications. *Chem. Sci.* **2018**, *9*, 8221–8227.
- (136) Poddutoori, P. K.; Kandrashkin, Y. E.; Obondi, C. O.; D'Souza, F.; Van Der Est, A. Triplet Electron Transfer and Spin Polarization in a Palladium Porphyrin-Fullerene Conjugate. *Phys. Chem. Chem. Phys.* **2018**, *20*, 28223–28231.
- (137) Webre, W. A.; Gobeze, H. B.; Shao, S.; Karr, P. A.; Ariga, K.; Hill, J. P.; D'Souza, F. Fluoride-Ion-Binding Promoted Photoinduced Charge Separation in a Self-Assembled C₆₀ Alkyl Cation Bound Bis-Crown Ether-Oxoporphyrinogen Supramolecule. *Chem. Commun.* **2018**, *54*, 1351–1354.
- (138) El-Khouly, M. E.; Rogers, L. M.; Zandler, M. E.; Suresh, G.; Fujitsuka, M.; Ito, O.; D'Souza, F. Studies on Intra-Supramolecular and Intermolecular Electron-Transfer Processes between Zinc Naphthalocyanine and Imidazole-Appended Fullerene. *ChemPhysChem* **2003**, *4*, 474–481.



CHAPTER 2

β -N-FUSED PORPHYRINS AND THEIR COMPLEXATION WITH FULLERENES



CHAPTER 2

SYNTHESIS, STRUCTURAL, SPECTRAL AND ELECTROCHEMICAL REDOX PROPERTIES OF β -ARYLAMINO AND N-FUSED PORPHYRINS AND PHOTOINDUCED ELECTRON TRANSFER STUDIES OF N-FUSED PORPHYRINS WITH C₆₀ DERIVATIVES

2.1 INTRODUCTION

Porphyrin has highly conjugated 18 π -electrons in their core structure which play an important role in many vital processes such as electron transfer and oxygen transportation in biological reactions [1-2]. Porphyrin derivatives exhibit variation in chemical and photophysical properties according to the substitution at β and *meso* positions of the macrocycle which make them model compounds for various applications such as PDT (photodynamic therapy), catalysis and as novel functional materials [3-5]. The synthesis of new asymmetrically β -substituted porphyrins can be very useful for NLO applications [6]. Highly conjugated π -extended porphyrins exhibit unique electronic and electrochemical properties which make them promising molecules for material applications. To accomplish these specific applications, structurally diverse porphyrin molecules with exceptional physiochemical properties are required. *Meso*-functionalization of porphyrin core has been extensively elaborated from past few decades. However, the functionalization at periphery of macrocyclic system was recognized as a synthetic approach towards β -substituted macrocyclic system [7-9]. The longer range of absorption wavelength (600- 900 nm) can obtain by expanding the absorption window of porphyrins by extending their aromatic system *via* ring fusion at β - and *meso*-positions [10]. The fusion of porphyrin π -system significantly alters the properties of macrocyclic ring as their absorption and emission pattern drastically changed from the other unfused porphyrin derivatives. From past two decades, a number of fused porphyrins were synthesized and studied [11-12]. Several aromatic ring fused porphyrins (fusion at β - and *meso*-position) such as pyrene, azulene, naphthalene, benzene and anthracene have been synthesized [13-14]. The main purpose of our study is to prepare fused porphyrin which can mimic the photosynthetic reaction system by designing the donor-acceptor dyads where porphyrin act as electron donor and fullerene work as electron acceptor [15]. The porphyrins (host) selectively bind to fullerene (guest) to form supramolecular assemblies (host-guest complex) *via* non-covalent interaction, π - π interaction, ion-dipole, dipole-dipole, hydrogen

bonding, and metal ligand bond, all non-covalent type of interactions which developed inter-molecular building block were used to synthesize advanced functional materials [16-17].

Fullerene is a good electron acceptor with spherical shape and requires small reorganization energy in electron transfer procedure. Two important applications of these models (host-guest complex) are: (i) the conversion of light energy into electrical energy, and (ii) optoelectronic device development [18-19]. The electron accepting nature of fullerene increases the electron transfer in forward direction and reduces in the backward direction which results into the formation of charge separated long lived states [20]. Porphyrin has been extensively used as biomimetic photosensitizing electron donating molecules because these can be easily oxidize in electron transfer reaction and also absorb light of wider wavelength in visible region [21]. D'Souza and co-workers have reported the self-assembled supramolecular conjugates which demonstrated that those assemblies have generated long live charged separated species and were used for light harvesting applications [22-24]. Different types of substituted Zn(II) porphyrin and phthalocynine have been used for the construction of porphyrin/phthalocyanine-fullerene dyads [19,25-28]. In 2018, D'Souza *et al.* reported fluoride ion binding promoted the photoinduced charge separation in supramolecular assemblies of C₆₀ alkyl cation bound bis-crown ether-oxoporphyrinogen. Fluoride anions convert electron-withdrawing oxoporphyrinogen to donor species without affecting the fullerene unit so that charge separation can be easily proceeds [29]. In this work, we reported the synthesis of mixed β -substituted arylaminoporphyrins and N-fused porphyrins and further utilized the Zn(II) N-fusedporphyrins for the complexation with C₆₀Im/C₆₀Py derivatives to form donor-acceptor dyads.

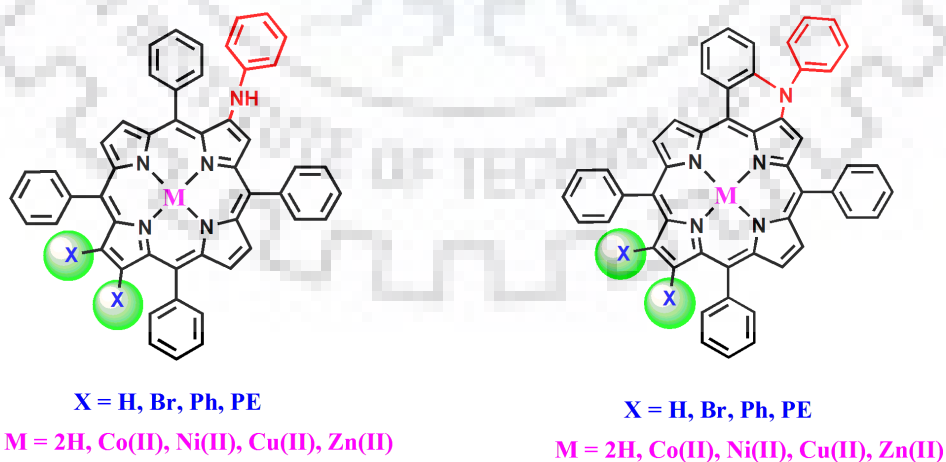


Chart 2.1 Molecular Structures of Synthesized β -Arylamino porphyrins and N-fused porphyrins.

2.2 EXPERIMENTAL SECTION

2.2.1 Reagents

H₂TPP, H₂TPP(NO₂), H₂TPP(NO₂)X₂ (X = Br, Ph, and PE), H₂TPP(NHPh) and their metal derivatives were synthesized according to the reported literature [30,31]. Pyrrole purchased from Alfa Aesar, UK and used without further purification. Aniline and nitrobenzene purchased from Rankem India and used without any further purification. P₂O₅, TBAPF₆, K₂CO₃ and (NBS) N-bromosuccinimide were purchased from HiMedia India. Utilized metal salts including Co(II), Cu(II), Zn(II) and Ni(II) were purchased from HiMedia and Sigma Aldrich, respectively and used as received. Silica gel for column chromatography was purchased from Thomas Baker India and used as received. Before use, NBS was recrystallized in hot water and dried at 72 °C for 7 h under vacuum. Solvents used in this work were distilled and dried before use. Precoated thin layer silica gel chromatographic plates were purchased from E. Merck and used as received. TBAPF₆ for CV studies was recrystallized in hot ethanol and then dried for 2 days at 25 °C.

2.2.2 Instrumentation and Methods

Electronic absorption spectra were recorded on Agilent Cary 100 spectrophotometer using a pair of quartz cells of 3.5 ml volume and 1 cm path length. Fluorescence spectra were recorded on Hitachi F-4600 spectrofluorometer using 1 cm path length quartz cell. ¹H NMR spectra were recorded in CDCl₃ on JEOL ECX 400 MHz spectrometers. MALDI-TOF mass spectra were measured using a Bruker UltrafleXtreme-TN MALDI TOF/TOF spectrometer using HABA (4'-hydroxyazobenzene-2-carboxylic acid) matrix. The ground state geometry optimization in gas phase was carried out by DFT calculations using B3LYP functional with LANL2DZ/6-311G (d,p) basis sets. CH instruments (CHI 620E) were used to electrochemical measurements. A three electrode assembly was used consisted of a Platinum working electrode, Ag/AgCl reference electrode and Pt-wire as a counter electrode. All measurements were performed in distilled CH₂Cl₂ and *o*-dichlorobenzene which was purged with Ar gas, using 0.1 M TBAPF₆ as the supporting electrolyte.

2.2.3 Synthesis of MTPP(NHPh)X₂ (X = H, Br, Ph, PE and M = 2H, Co(II), Ni(II), Cu(II), Zn(II)):

(a) Synthesis of 2-Phenylamino-5,10,15,20-tetraphenylporphyrin and Their Metal Derivatives:

2-Nitro-5,10,15,20-tetraphenylporphyrin (140 mg, 0.220 mmol) was dissolved in aniline (14 mL) and refluxed for 20h at 180 °C under nitrogen atmosphere. After 20h, the reaction mixture was cooled to room temperature and acidified by aqueous saturated citric acid solution. Further the compound was extracted with CH₂Cl₂ and the organic layer was washed with water, dried over anhydrous Na₂SO₄ and evaporated to dryness under reduced pressure. The residue was taken in CH₂Cl₂ and purified by column chromatography by using CH₂Cl₂/hexane as eluent. The first fraction was collected and identified as desired product (arylamino porphyrin). The remaining part obtained as unidentified mixture. The porphyrin was recrystallized from CH₂Cl₂/hexane mixture (1:5, v/v) yielding brown solid with 52% (73 mg, 0.103 mmol) yield.

H₂TPP(NHPh) (I): UV-Vis. λ_{\max} (nm), (log ϵ): 408(5.21), 525(4.38), 569(4.0), 599(3.96), 657(3.62). ¹H NMR in CDCl₃ (400 MHz), δ (ppm): 8.83 (d, J = 8 Hz, 1H, β -H), 8.74-8.79 (m, 4H, β -H), 8.58 (d, J = 4 Hz, 1H, β -H), 8.31 (s, 1H, β -H-3), 8.20-8.23 (m, 8H, *meso*-*o*-Ph-H), 7.85-7.94 (m, 3H, *meso*-*m,p*-20-Ph-H), 7.75-7.79 (m, 9H, *meso*-*m,p*-5,10,15-Ph-H), 7.31 (d, J = 8 Hz, 2H, β -*m*-NHPh-H), 7.04 (d, J = 8 Hz, 2H, β -*o*-NHPh-H), 6.95 (t, J = 8 Hz, 1H, β -*p*-NHPh-H), 6.63 (s, 1H, outer-NH-H). -2.53 (s, 2H, -NH). MALDI-TOF-MS (m/z): found [M+H]⁺ 706.96, calcd. 706.29. Elemental analysis calcd. For C₅₀H₃₅N₅: C, 85.08%; H, 5.00%; N, 9.92% and found: C, 85.28%; H, 5.12%; N, 9.98%.

10 mg (0.0141 mmol) of H₂TPP(NHPh) was dissolved in 7 ml of CHCl₃. To this, 10 eq. of M(OAc)₂.nH₂O (M = Cu(II), Zn(II), Co(II)) in 2 ml of methanol was added and the resulting mixture was refluxed for 35 minutes. After that the mixture was cooled to room temperature and washed with water, organic layer passed through anhydrous Na₂SO₄ and crude product was purified by column chromatographed using CHCl₃ as eluent. Ni(II) metalation has been done by refluxing H₂TPP(NHPh) with 10 eq. of Ni(OAc)₂.2H₂O in DMF for 2h [31]. After completion, the metalated porphyrin was precipitated with water. The crude solid was purified on silica gel column using CHCl₃ as eluent. Yield: 86-95%. **CoTPP(NHPh):** Yield: 92% (9.2mg, 0.012 mmol), UV-Vis. λ_{\max} (nm), (log ϵ): 411(5.12), 534(4.18), 590(4.02). MALDI-TOF-MS (m/z):

found $[M+H]^+$ 763.236, calcd. 763.21. **NiTPP(NHPh)**: Yield: 86% (8.62 mg, 0.011mmol), UV-Vis. λ_{\max} (nm), (log ϵ): 415(5.01), 544(4.28), 582(4.08). ^1H NMR in CDCl_3 (400 MHz): δ (ppm) 8.64-8.70 (m, 4H, β -H), 8.60 (d, $J = 8$ Hz, 1H, β -H), 8.56(d, $J = 8$ Hz, 1H, β -H), 8.26 (s, 1H, β -H-3), 7.96-8.00 (m, 8H, *meso*-*o*-Ph-H), 7.74-7.82 (m, 3H, *meso*-*m,p*-20-Ph-H), 7.64-7.69 (m, 9H, *meso*-*m,p*-5,10,15-Ph-H), 7.24 and 7.28 (s, 2H, β -*m*-NHPh-H), 6.91 (t, $J = 8$, 3H, Hz, β -*m,p*-NHPh-H), 6.38 (s, 1H, outer-NH-H). MALDI-TOF-MS (m/z): found $[M+H]^+$ 762.240, calcd. 762.21. **CuTPP(NHPh)**: Yield: 91% (9.1mg, 0.012 mmol), UV-Vis. λ_{\max} (nm), (log ϵ): 409(5.28), 563(4.29), 590(3.96). MALDI-TOF-MS (m/z): found $[M+H]^+$ 767.205, calcd. 767.21. **ZnTPP(NHPh)**: Yield: 95% (9.5 mg, 0.012 mmol), UV-Vis. λ_{\max} (nm), (log ϵ): 407 (5.46), 560 (4.37), 588 (4.16). ^1H NMR in CDCl_3 (400 MHz): δ (ppm) 8.92 (d, $J = 4$ Hz, 1H, β -H), 8.83-8.89(m, 4H, β -H), 8.64 (d, $J = 4$ Hz, 1H, β -H), 8.47(s, 1H, β -H-3), 8.19-8.22(m, 8H, *meso*-*o*-Ph-H), 7.84-7.94(m, 3H, *meso*-*m,p*-20-Ph-H), 7.72-7.77(m, 9H, *meso*-*m,p*-5,10,15-Ph-H), 7.30(dd, $J = 8$ Hz, 2H, β -*m*-NHPh-H), 7.06(d, $J = 8$ Hz, 2H, β -*o*-NHPh-H), 6.94(t, $J = 8$ Hz, 1H, β -*p*-NHPh-H), 6.64(s, 1H, outer-NH-H) MALDI-TOF-MS (m/z): found $[M + 2H]^+$ 767.205, calcd. 767.20.

(b) Synthesis of 2-Phenylamino-12, 13-dibromo-5,10,15,20-tetraphenylporphyrin and Their Metal Derivatives:

$\text{H}_2\text{TPP}(\text{NHPh})\text{Br}_2$ was prepared from $\text{H}_2\text{TPPNO}_2\text{Br}_2$ (120 mg) using similar synthetic procedure as discussed for the synthesis of $\text{H}_2\text{TPP}(\text{NHPh})$. Yield 50% (60 mg, 0.070 mmol).

$\text{H}_2\text{TPP}(\text{NHPh})\text{Br}_2$: UV-Vis. λ_{\max} (nm), (log ϵ): 417(4.97), 609(3.79). ^1H NMR in CDCl_3 (400 MHz), δ (ppm): 8.80 (d, $J = 4$ Hz, 1H, β -H), 8.74 (d, $J = 8$ Hz, 1H, β -H), 8.67 (d, $J = 8$ Hz, 1H, β -H), 8.50 (d, $J = 4$ Hz, 1H, β - H), 8.12-8.22 (m, 8H, *meso*-*o*-Ph-H), 8.03 (s, 1H, β -H-3), 7.87-7.93 (m, 3H, *meso*-*m,p*-20-Ph-H), 7.72-7.80 (m, 9H, *meso*-*m,p*-5,10,15-Ph-H), 7.29 (d, $J = 8$, 2H, Hz β -*m*-NHPh-H), 6.93 (t, 3H, β -*o,p*-NHPh-H), 6.59 (s, 1H, outer-NH-H), -2.58 (bs, 2H, imino-H). MALDI-TOF-MS (m/z): found $[M]^+$ 863.411, calcd. 863.11. Elemental analysis calcd. For $\text{C}_{50}\text{H}_{33}\text{N}_5\text{Br}_2$: C, 69.54%; H, 3.85%; N, 8.11% and found: C, 69.80%; H, 3.72%; N, 8.09%.

The metal derivatives were synthesized using similar synthetic procedure as described for $\text{MTPP}(\text{NHPh})$, where M = Co(II), Ni(II), Cu(II) and Zn(II). Yields were found to be 83-94%.

CoTPP(NHPh)Br₂: Yield: 91% (11 mg, 0.011 mmol), UV-Vis. λ_{\max} (nm), (log ϵ): 417(4.67), 543(3.79). MALDI-TOF-MS (m/z): found $[M+H]^+$ 921.302, calcd. 921.03. **NiTPP(NHPh)Br₂**:

Yield: 83% (10 mg, 0.01 mmol), UV-Vis. λ_{\max} (nm), (log ϵ): 421(4.56), 600(3.59). ¹H NMR in CDCl₃(400 MHz), δ (ppm): 8.67 (d, J = 4 Hz, 1H, β -H), 8.61 (d, J = 4 Hz, 1H, β -H), 8.46 (t, J = 8 Hz, 2H, β -H), 8.15 (s, 1H, β -H-3), 7.93-7.96 (m, 4H, *meso*-*o*-Ph-H), 7.83 (d, J = 8 Hz, 4H, *meso*-*o*-Ph-H), 7.74-7.80 (m, 3H, *meso*-*m,p*-20-Ph-H), 7.62-7.67 (m, 9H, *meso*-*m,p*-5,10,15-Ph-H), 7.24 and 7.28 (s, 2H, β -*m*-NHPH-H), 6.89-6.95 (m, 3H, β -*m,p*-NHPH-H), 6.35 (s, 1H, outer-NH-H). MALDI-TOF-MS (m/z): found [M]⁺ 919.90, calcd. 919.03. **CuTPP(NHPH)Br₂**: Yield: 92% (11 mg, 0.012 mmol), UV-Vis. λ_{\max} (nm), (log ϵ): 410(4.93), 563(2.97), 595(2.89). MALDI-TOF-MS (m/z): found [M]⁺ 924.50, calcd. 924.03. **ZnTPP(NHPH)Br₂**: Yield: 94% (11.3 mg, 0.0121 mmol), UV-Vis. λ_{\max} (nm), (log ϵ): 412(5.12), 570(3.99), 599 (4.04). ¹H NMR in CDCl₃(400 MHz), δ (ppm): 8.79 (d, J = 4 Hz, 1H, β -H), 8.73 (t, J = 8 Hz, 2H, β -H), 8.55 (d, J = 4 Hz, 1H, β -H), 8.45(s, 1H, β -H-3), 8.14-8.18 (m, 4H, *meso*-*o*-Ph-H), 8.04 (d, J = 8 Hz, 4H, *meso*-*o*-Ph-H), 7.84-7.93 (m, 3H, *meso*-*m,p*-20-Ph-H), 7.67-7.78 (m, 9H, *meso*-*m,p*-5,10,15-Ph-H), 7.30 (dd, J = 8 Hz, 2H, β -*m*-NHPH-H), 7.03 (d, J = 8 Hz, 2H, β -*o*-NHPH-H) 6.95 (t, J = 8 Hz, 1H, β -*p*-NHPH-H), 6.63 (s, 1H, outer-NH-H) MALDI-TOF-MS (m/z): found [M+H]⁺ 927.313, calcd. 927.03.

(c) Synthesis of 2-Phenylamino-12,13-diphenyl-5,10,15,20-tetraphenylporphyrin and Their Metal Derivatives: H₂TPP(NHPH)Ph₂ was prepared using 150 mg of 2-nitro-12,13-diphenyl-5,10,15,20-tetraphenylporphyrin following the similar procedure as described for H₂TPP(NHPH) synthesis. Yield: 47% (70 mg, 0.082 mmol). **H₂TPP(NHPH)Ph₂**: UV-Vis. λ_{\max} (nm), (log ϵ): 414(5.08), 531(4.18), 577(3.93), 603(3.91), 660(3.44). ¹H NMR in CDCl₃(400 MHz), δ (ppm): 8.58 (d, J = 4 Hz, 1H, β -H), 8.51 (d, J = 4 Hz, 1H, β -H), 8.47 (d, J = 4 Hz, 1H, β -H), 8.42 (d, J = 4 Hz, 1H, β -H), 8.18-8.23 (m, 5H, 1H- β -H-3 and , 4H, *meso*-*o*-Ph-H), 7.84-7.92 (m, 3H, *meso*-*m,p*-20-Ph-H) 7.79 (d, J = 4 Hz, 4H, *meso*-*o*-Ph-H), 7.67-7.73 (m, 4H, *meso*-*m*-Ph-H), 7.29 (dd, J = 8 Hz, 2H, β -*m*-NHPH-H), 7.16-7.19 (m, 4H, *meso*-*p*-Ph-H), 6.96-7.02 (t, 3H, β -*o,p*-NHPH-H), 6.90-6.94 (m, 4H, *meso*-*o*-Ph-H), 6.83-6.85 (m, 6H, *meso*-*m,p*-Ph-H), 6.61 (s, 1H, outer-NH), -2.26 (s, 2H, imino H), MALDI-TOF-MS (m/z): found [M+H]⁺ 858.348, calcd. 858.35. Elemental analysis calcd. For C₆₂H₄₃N₅: C, 86.79%; H, 5.05%; N, 8.16% and found: C, 86.87%; H, 5.13%; N, 8.33%.

The metal derivatives were prepared as described for MTPP(NHPH). Yields were found to be 82-94%. **CoTPP(NHPH)Ph₂**: Yield: 90% (9 mg, 0.010 mmol), UV-Vis. λ_{\max} (nm), (log ϵ):

411(4.96), 550(4.02). MALDI-TOF-MS (m/z): found [M+H]⁺ 915.136, calcd. 915.27. **NiTPP(NHPh)Ph₂**: Yield: 82% (8.2 mg, 0.09 mmol), UV-Vis. λ_{\max} (nm), (log ϵ): 417(4.97), 609(3.79). ¹H NMR in CDCl₃(400 MHz), δ (ppm): 8.42 (d, *J* = 4 Hz, 2H, β -H), 8.31 (d, *J* = 8 Hz, 1H, β -H), 8.26 (d, *J* = 4 Hz, 1H, β -H), 8.19 (s, 1H, β -H-3), 7.95 (d, *J* = 8 Hz, 4H, *meso-o*-Ph-H), 7.73-7.80 (m, 3H, *meso-m,p*-20-Ph-H), 7.63 (t, *J* = 8 Hz, 4H, *meso-o*-Ph-H), 7.43 (t, *J* = 8 Hz, 4H, *meso-o*-5,10,15-Ph-H), 7.24 (dd, *J* = 8 Hz, 2H, β -*m*-NHPh-H), 7.15 (t, *J* = 8 Hz, 2H, *meso-m*-5,10,15-Ph-H), 7.04 (t, 3H, β -*o,p*-NHPh-H), 6.83-6.92 (m, 13H, *meso-m,p*-5,10,15-Ph-H and *meso-o,m,p*-Ph-H), 6.34 (s, 1H, outer-NH). MALDI-TOF-MS (m/z): found [M+H]⁺ 914.207, calcd. 914.27. **CuTPP(NHPh)Ph₂**: Yield: 94% (9.4 mg, 0.010 mmol), UV-Vis. λ_{\max} (nm), (log ϵ): 409(5.04), 561(4.16), 589(4.14). MALDI-TOF-MS (m/z): found [M+H]⁺ 919.18, calcd. 919.28. **ZnTPP(NHPh)Ph₂**: Yield: 93% (9.3 mg, 0.010 mmol), UV-Vis. λ_{\max} (nm), (log ϵ): 411 (4.98), 569 (3.89), 592 (3.84). ¹H NMR in CDCl₃(400 MHz), δ (ppm): 8.72 (d, *J* = 4 Hz, 1H, β -H), 8.60 (d, *J* = 8 Hz, 1H, β -H), 8.52-8.55 (m, 2H, β -H), 8.40 (s, 1H, β -H-3), 8.17-8.21 (m, 4H, *meso-o*-Ph-H), 7.82-7.91 (m, 3H, *meso-m,p*-20-Ph-H), 7.71-7.76 (m, 7H, *meso-o,m*-5,10,15-Ph-H), 7.32(dd, *J* = 8 Hz, 2H, β -*m*-NHPh-H), 7.11-7.24 (m, 6H, *meso-m,p*-5,10,15-Ph-H), 7.05 (t, 3H, β -*o,p*-NHPh-H), 6.92-6.98 (m, 4H, *meso-o*-Ph-H), 6.77-6.85 (m, 6H, *meso-m,p*-Ph-H), 6.63 (s, 1H, outer-NH). MALDI-TOF-MS (m/z): found [M+H]⁺ 920.188, calcd. 920.27.

(d) Synthesis of 2-Phenylamino-12,13-diphenylethynyl-5,10,15,20-tetraphenylporphyrin and Their Metal Derivatives:

H₂TPP(NHPh)PE₂ was prepared from the Stille coupling reaction of H₂TPP(NHPh)Br₂. Yield: 47% (76 mg, 0.084 mmol). **H₂TPP(NHPh)PE₂**: UV-Vis. λ_{\max} (nm), (log ϵ): 427(4.96), 524(4.00), 622(3.96). ¹H NMR in CDCl₃(400 MHz), δ (ppm): 8.74 (d, *J* = 4 Hz, 1H, β -H), 8.69 (d, *J* = 4 Hz, 2H, β -H), 8.51 (d, *J* = 8 Hz, 1H, β -H), 8.17-8.25 (m, 8H, *meso-o*-Ph-H), 8.09 (s, 1H, β -H-3), 7.87-7.92 (m, 3H, *meso-m,p*-20-Ph-H), 7.72-7.74 (m, 9H, *meso-m,p*-5,10,15-Ph-H), 7.35-7.38 (m, 4H, β -*o*-PE-H), 7.28 (dd, *J* = 4 Hz, 2H, β -*m*-NHPh-H), 7.14-7.19 (m, 6H, β -*m,p*-PE-H), 6.91-7.00 (m, 3H, β -*o,p*-NHPh-H), 6.59 (s, 1H, β -NH), -2.45 (s, 2H, outer-NH). MALDI-TOF-MS (m/z): found [M+H]⁺ 906.48, calcd. 906.35. Elemental analysis calcd. For C₆₆H₄₃N₅: C, 87.49%; H, 4.78%; N, 7.73% and found: C, 87.55%; H, 4.89%; N, 7.87%.

The metal derivatives were prepared as described for MTPP(NHPh). Yields were found to be 85-95%. **CoTPP(NHPh)PE₂**: Yield: 92% (9.2 mg, 0.009 mmol), UV-Vis. λ_{\max} (nm), (log ϵ): 442(4.90), 602(4.01). MALDI-TOF-MS (m/z): found [M+H]⁺ 963.368, calcd. 963.27. **NiTPP(NHPh)PE₂**: Yield: 85% (8.5 mg, 0.009 mmol), UV-Vis. λ_{\max} (nm) (log ϵ): 442 (4.85), 615 (4.17). ¹H NMR in CDCl₃(400 MHz), δ (ppm): 8.60 (d, *J* = 8 Hz, 1H, β -H), 8.56 (d, *J* = 4 Hz, 1H, β -H), 8.46 (t, *J* = 4 Hz, 2H, β -H), 8.14 (s, 1H, β -H-3), 7.92-7.97 (m, 8H, *meso*-*o*-Ph-H), 7.74-7.80 (m, 3H *meso*-*m*,*p*-20-Ph-H), 7.61-7.64 (m, 9H, *meso*-*m*,*p*-5,10,15-Ph-H), 7.29-7.31 (m, 7H, β -*o*,*m*-PE-H), 7.23-7.28 (m, 5H, β -*m*-NHPh-H and *m*,*p*-PE-H), 6.88-6.93 (m, 3H, β -*o*,*p*-NHPh-H), 6.34 (s, 1H outer-NH). MALDI-TOF-MS (m/z): found [M]⁺ 962.438, calcd. 962.27. **CuTPP(NHPh)PE₂**: Yield: 94% (9.4 mg, 0.010 mmol), UV-Vis. λ_{\max} (nm), (log ϵ): 423(4.85), 574(3.95), 615(4.10). MALDI-TOF-MS (m/z): found [M]⁺ 967.448, calcd. 967.28. **ZnTPP(NHPh)PE₂**: Yield: 95% (9.5 mg, 0.009 mmol), UV-Vis. λ_{\max} (nm), (log ϵ): 426(4.93), 579(4.09), 617(4.22). ¹H NMR in CDCl₃(400 MHz), δ (ppm): 8.73(d, *J* = 8 Hz, 2H, β -H), 8.69 (d, *J* = 4 Hz, 1H, β -H), 8.54 (d, *J* = 4 Hz, 1H, β -H), 8.34 (s, 1H, β -H-3), 8.14-8.19 (m, 8H, *meso*-*o*-Ph-H), 7.83-7.91 (m, 3H, *meso*-*m*,*p*-20-Ph-H), 7.68-7.72 (m, 9H, *meso*-*m*,*p*-5,10,15-Ph-H), 7.38-7.40 (m, 4H, β -*o*-PE-H), 7.27-7.31 (m, 6H, β -*m*,*p*-PE-H), 7.03(d, 3H, NH- β -*o*,*m*-Ph-H), 7.03(d, 3H, *o*,*m*-NHPh-H), 6.94 (t, 2H *m*,*p*-NHPh-H), 6.62 (s, 1H, outer-NH). MALDI-TOF-MS (m/z): found [M+H]⁺ 967.776, calcd. 967.28.

2.2.4 Synthesis of MTPP(N-fusedPh)X₂ (X = H, Br, Ph, PE and M = 2H, Co(II), Ni(II), Cu(II), Zn(II)) Derivatives:

(a) **Synthesis of N-Arylquinolino[2,3,4-at]Porphyrin and Their Metal Derivatives:** A solution of H₂TPP(NHPh) (120 mg, 0.181 mmol) in 10 mL of nitrobenzene was refluxed at 200 °C for 30 h. After 30 h, the reaction mixture was poured on top silica gel chromatographic column. Initially, nitrobenzene was eluted using hexane as eluent then the porphyrin was eluted with CH₂Cl₂/hexane mixture (1:1, V/V). The final product was recrystallized as a dark green solid from CH₂Cl₂/hexane mixture. Yield: 70% (85 mg, 0.120 mmol). **H₂TPP(N-fusedPh)**: UV-Vis. λ_{\max} (nm), (log ϵ): 408 (5.01), 525(4.38), 569(4.0), 599(3.96), 657(3.62). ¹H NMR in CDCl₃ (400 MHz), δ (ppm): 9.68 (d, *J* = 8Hz, 2H, 5'-H and β -H), 8.82 (d, *J* = 4Hz, 1H, β -H), 8.75 (d, *J* = 4Hz, 1H, β -H), 8.68 (d, *J* = 4Hz, 2H, β -H), 8.60 (d, *J* = 4Hz, 1H, β -H), 8.26-8.28, 8.16-8.18, 8.08-8.12, (3m, 6H, *meso*-*o*-Ph-H-5,10,15), 7.64-7.90 (m, 18H, H-3, H-2', 3', 4', *meso*-*m* and *p*-Ph-H-5,10,15 and β -NPh-H), -1.24 (s, 2H, imino-H). MALDI-TOF-MS (m/z): found [M+H]⁺

704.14, calcd. 704.27. Elemental analysis calcd. For C₅₀H₃₃N₅: C, 85.32%; H, 4.73%; N, 9.95% and found: C, 85.44%; H, 4.87%; N, 9.99%.

The metal derivatives were prepared as described for MTPP(NHPh). Yields were found to be 60-80%. **CoTPP(N-fusedPh)**: Yield: 75% (9 mg, 0.011 mmol), UV-Vis. λ_{\max} (nm), (log ϵ): 442(5.13), 641(4.09). MALDI-TOF-MS (m/z): found [M+H]⁺ 761.077, calcd. 761.19 Elemental analysis calcd. For C₅₀H₃₁N₅Co: C, 78.94%; H, 4.11%; N, 9.21% and found: C, 78.98%; H, 4.23%; N, 9.29%. **NiTPP(N-fusedPh)**: Yield: 60% (7.4 mg, 0.009 mmol), UV-Vis. λ_{\max} (nm), (log ϵ): 426(4.98), 555(4.28), 594(3.96), 631(4.03). ¹H NMR in CDCl₃ (400 MHz), δ (ppm): 9.48 (d, *J* = 4Hz, 1H, 5'-H), 8.94 (d, *J* = 8Hz, 1H, β -H), 8.87 (d, *J* = 4Hz, 1H, β -H), 8.57-8.61 (m, 3H, β -H), 8.53 (d, *J* = 4Hz, 1H, β -H), 8.03-8.05, 7.96-7.98, 7.89-7.91 (3m, 6H, *meso-o*-Ph-H-5,10,15), 7.82(d, 3H, β -*m*-NPh-3',4'-H and β -H) 7.54-7.91 (m, 14H, H-3, *meso-m*, *p*-Ph-H-5,10,15 and β -NPh-H), 7.44-7.41 (m, 1H-4' β -NPh-H) MALDI-TOF-MS (m/z): found [M+H]⁺ 760.50, calcd. 760.19. Elemental analysis calcd. For C₅₀H₃₁N₅Ni: C, 78.96%; H, 4.11%; N, 9.21% and found: C, 79.11%; H, 4.25%; N, 9.31%. **CuTPP(N-fusedPh)**: Yield: 79% (9.5 mg, 0.012 mmol), UV-Vis. λ_{\max} (nm), (log ϵ): 403(sh) (4.11), 456(4.98), 561(3.45), 605(3.54), 635(3.76). MALDI-TOF-MS (m/z): found [M+K]⁺ 803.15, calcd. 803.16. Elemental analysis calcd. For C₅₀H₃₁N₅Cu: C, 78.46%; H, 4.08%; N, 9.15% and found: C, 78.52%; H, 4.15%; N, 9.23%. **ZnTPP(N-fusedPh)**: Yield: 78% (9.4 mg, 0.0121 mmol), UV-Vis. λ_{\max} (nm), (log ϵ): 407(sh)(4.09), 460(4.50), 568(3.38), 613(3.53), 645(3.78). ¹H NMR in CDCl₃ (400 MHz), δ (ppm): 9.71 (d, *J* = 4Hz, 1H, 5'-H), 9.57 (d, *J* = 8Hz, 1H, β -H), 8.91 (d, *J* = 4Hz, 1H, β -H), 8.85 (d, *J* = 4Hz, 1H, β -H), 8.76-8.80 (m, 2H, β -H), 8.73 (d, *J* = 4Hz, 1H, β -H), 8.27-8.29, 8.17-8.20, 8.11-8.13 (3m, 6H, *meso-o*-Ph-H-5,10,15), (m, 6H, *meso-o*-Ph-H-5,10,15), 7.57-7.91 (m, 18H, H-3,H-2',3',4', *meso-m* and *p*-Ph-H-5,10,15 and β -NPh-H). MALDI-TOF-MS (m/z): found [M+K]⁺ 804.19, calcd. 804.15. Elemental analysis calcd. For C₅₀H₃₁N₅Zn: C, 78.28%; H, 4.07%; N, 9.13% and found: C, 78.33%; H, 4.12%; N, 9.22%.

(b) Synthesis of N-Arylquinolino[2,3,4-at]-12,13-dibromoporphyrin and Their Metal Derivatives:

H₂TPP(N-fusedPh)Br₂ was prepared from H₂TPP(NHPh)Br₂ (100 mg, 0.115 mmol) according to the similar procedure as discussed for H₂TPP(N-fusedPh) synthesis. Yield: 70% (70 mg, 0.081

mmol). **H₂TPP(N-fusedPh)Br₂**: UV-Vis. λ_{\max} (nm), (log ϵ): 418(4.98), 460(4.72), 621(4.10), 668(4.02). ¹H NMR in CDCl₃ (400 MHz), δ (ppm): 9.68 (d, J = 8 Hz, 1H, 5'-H), 9.46 (d, J = 4 Hz, 1H, β -H), 8.55-8.71 (m, Hz, 3H, β -H), 8.05-8.22 (m, 6H, *meso-o*-Ph-H-5,10,15), 7.64-7.89 (m, 18H, H-3,H-2',3',4', *meso-m* and *p*-Ph-H-5,10,15 and β -NPh-H), -1.15 (s, 2H, imino-H). MALDI-TOF-MS (m/z): found [M+H]⁺ 862.36, calcd. 862.09. Elemental analysis calcd. For C₅₀H₃₁Br₂N₅: C, 69.70%; H, 3.63%; N, 8.13% and found: C, 69.82%; H, 3.76%; N, 8.21%

The metal derivatives were prepared using similar method as for H₂TPP(NHPh) metal complexes. Yield was found to be 62-80%. **CoTPP(N-fusedPh)Br₂**: Yield: 68% (8.2 mg, 0.009 mmol), UV-Vis. λ_{\max} (nm), (log ϵ): 446(4.76), 637(3.28). MALDI-TOF-MS (m/z): found [M+H]⁺ 919.25, calcd. 919.01. Elemental analysis calcd. For C₅₀H₂₉Br₂N₅Co: C, 65.38%; H, 3.18%; N, 7.62% and found: C, 65.45%; H, 3.25%; N, 7.74%. **NiTPP(N-fusedPh)Br₂**: Yield: 62% (7.4 mg, 0.008 mmol), UV-Vis. λ_{\max} (nm), (log ϵ): 433(4.87), 637(4.12). ¹H NMR in CDCl₃(400 MHz), δ (ppm): 9.31(d, J = 4 Hz, 1H, 5'-H), 8.91 (d, J = 4 Hz, 2H, β -H), 8.49 (d, J = 8 Hz, 1H, β -H), 8.42 (d, J = 4 Hz, 1H, β -H), 7.51-7.92 (m, 23H, H-3,H-2',3',4', *meso-o,m* and *p*-Ph-H-5,10,15-H-3,H-2',3' and β -NPh-H), 7.42 (d, J = 8 Hz, 1H, H-4'). MALDI-TOF-MS (m/z): found [M]⁺ 917.02, calcd. 917.01. Elemental analysis calcd. For C₅₀H₂₉Br₂N₅Ni: C, 65.40%; H, 3.18%; N, 7.63% and found: C, 65.49%; H, 3.28%; N, 7.71%. **(CuTPP(N-fusedPh)Br₂**: Yield: 80% (9.6 mg, 0.010 mmol), UV-Vis. λ_{\max} (nm), (log ϵ): 408(sh) (4.18), 463(4.76), 640(3.96). MALDI-TOF-MS (m/z): found [M+K+H]⁺ 961.08, calcd. 961.98. Elemental analysis calcd. For C₅₀H₂₉Br₂N₅Cu: C, 65.05%; H, 3.17%; N, 7.59% and found: C, 65.10%; H, 3.22%; N, 7.64%. **ZnTPP(N-fusedPh)Br₂**: 76% (9.2 mg, 0.010 mmol), UV-Vis. λ_{\max} (nm), (log ϵ): 415(sh)(4.32), 466(4.60), 617(3.94), 650(3.95). ¹H NMR in CDCl₃ (400 MHz), δ (ppm): 9.55 (d, J = 8 Hz, 1H, 5'-H), 9.51 (d, J = 8 Hz, 1H, β -H), 8.77 (d, J = 4 Hz, 1H, β -H),8.61 (s, 2H, β -H), 8.01-8.12 (m, 6H, *meso-o*-Ph-H-5,10,15), 7.64-7.87 (m, 18H, H-3,H-2',3',4', *meso-m* and *p*-Ph-H-5,10,15 and β -NPh-H). MALDI-TOF-MS (m/z): found [M+K+H]⁺ 962.28, calcd. 962.97. Elemental analysis calcd. For C₅₀H₂₉N₅Br₂Zn: C, 64.92%; H, 3.16%; N, 7.57% and found: C, 64.98%; H, 3.25%; N, 7.67%.

(c) Synthesis of N-Arylquinolino[2,3,4-at]-12,13-diphenylporphyrin and Their Metal Derivatives: H₂TPP(N-fusedPh)Ph₂ was prepared from H₂TPP(NHPh)Ph₂ (110 mg, 0.128 mmol) according to the similar procedure as discussed for H₂TPP(N-fusedPh) synthesis. Yield:

67% (74 mg, 0.086 mmol). **H₂TPP(N-fusedPh)Ph₂**: UV-Vis. λ_{\max} (nm), (log ϵ): 417(4.72), 456sh(4.70), 568(3.73), 615(3.90), 672(3.73). ¹H NMR in CDCl₃ (400 MHz), δ (ppm): 9.68 (d, J = 4 Hz, 2H, 5'-H and β -H), 9.40 (s, 1H, β -H), 8.43-8.52 (m, 4H, β -H and *meso-o*-Ph-H-5,10,15), 8.09 (bs, 3H, *meso-o*-Ph-H-5,10,15), 7.64-7.88 (m, 18H, H-3,H-2',3',4', *meso-m* and *p*-Ph-H-5,10,15 and β -NPh-H), 6.81-6.99 (m, 10H, β -Ph-H), -0.93 (s, 2H, imino-H). MALDI-TOF-MS (m/z): found [M]⁺ 856.35, calcd. 856.34. Elemental analysis calcd. For C₆₂H₄₁N₅: C, 86.99%; H, 4.83%; N, 8.18% and found: C, 87.12%; H, 4.89%; N, 8.33%.

The metal derivatives were prepared as discussed for H₂TPP(N-fusedPh). The yields were found to be 60-80%. **CoTPP(N-fusedPh)Ph₂**: Yield: 76% (7.6 mg, 0.008 mmol), UV-Vis. λ_{\max} (nm), (log ϵ): 446(4.88), 641(3.10). MALDI-TOF-MS (m/z): found [M]⁺ 912.27, calcd. 912.25. Elemental analysis calcd. For C₆₂H₃₉N₅Co: C, 81.57%; H, 4.31%; N, 7.67% and found: C, 81.65%; H, 4.43%; N, 7.90%. **(Ni)TPP(N-fusedPh)Ph₂**: Yield: 60% (6.1 mg, 0.007 mmol), UV-Vis. λ_{\max} (nm), (log ϵ): 443(4.98), 561(3.79), 607(3.88), 641(3.99). ¹H NMR in CDCl₃ (400 MHz): (ppm) 9.28 (d, J = 4 Hz, 1H, 5'-H), 8.88 (d, J = 8 Hz, 1H, β -H), 8.49 (d, J = 8 Hz, 1H, β -H), 8.38 (d, J = 8 Hz, 1H, β -H), 8.20 (d, J = 4 Hz, 1H, β -H), 7.88-7.90 (m, 2H, *meso-o*-Ph-H-5), 7.70-7.81(m, 3H, *meso-o*-Ph-H-10,15), 7.68-7.72 (m, 1H, *meso-o*-Ph-H-15), 7.53-7.64(m, 7H, H-3,H-2',3',4', *meso-m*-Ph-H-5,10,15) 7.39-7.48 (m, 5H, *meso-m* and *p*-Ph-H-5,10,15-H), 6.99-7.12(m, 5H, β -NPh-H) 6.75-6.94(m, 10H β -Ph-H). MALDI-TOF-MS (m/z): found [M+H]⁺ 912.66, calcd. 912.26. Elemental analysis calcd. For C₆₂H₃₉N₅Ni: C, 81.59%; H, 4.31%; N, 7.67% and found: C, 81.67%; H, 4.49%; N, 7.90%. **CuTPP(N-fusedPh)Ph₂**: Yield: 80% (8 mg, 0.09 mmol), UV-Vis. λ_{\max} (nm), (log ϵ): 441(4.76), 567(3.43), 610(3.56), 639(3.69). MALDI-TOF-MS (m/z): found [M+H]⁺ 917.34, calcd. 917.26. Elemental analysis calcd. For C₆₂H₃₉N₅Cu: C, 81.16%; H, 4.28%; N, 7.63% and found: C, 81.34%; H, 4.36%; N, 7.78%. **ZnTPP(N-fusedPh)Ph₂**: Yield: 78% (7.8 mg, 0.008 mmol), UV-Vis. λ_{\max} (nm), (log ϵ): 415(4.37sh), 465(4.80), 574(3.66), 748 (4.02). ¹H NMR in CDCl₃ (400 MHz), δ (ppm): 9.54 (d, J = 4 Hz, 2H, 5'-H and β -H), 8.65-8.62 (m, 2H, β -H), 8.48 (d, J = 4 Hz, 1H, β -H), 8.10 (bs, 2H, *meso-o*-Ph-H-5), 7.56-7.92 (m, 17H, H-3,H-2',3',4', *meso-o,m* and *p*-Ph-H-5,10,15), 6.84-7.21 (m, 15H, β -NPh-H and β -Ph-H). MALDI-TOF-MS (m/z): found [M+MeOH+H]⁺ 950.88, calcd. 950.28. Elemental analysis calcd. For C₆₂H₃₉N₅Zn: C, 80.99%; H, 4.28%; N, 7.62% and found: C, 81.22%; H, 4.34%; N, 7.76%

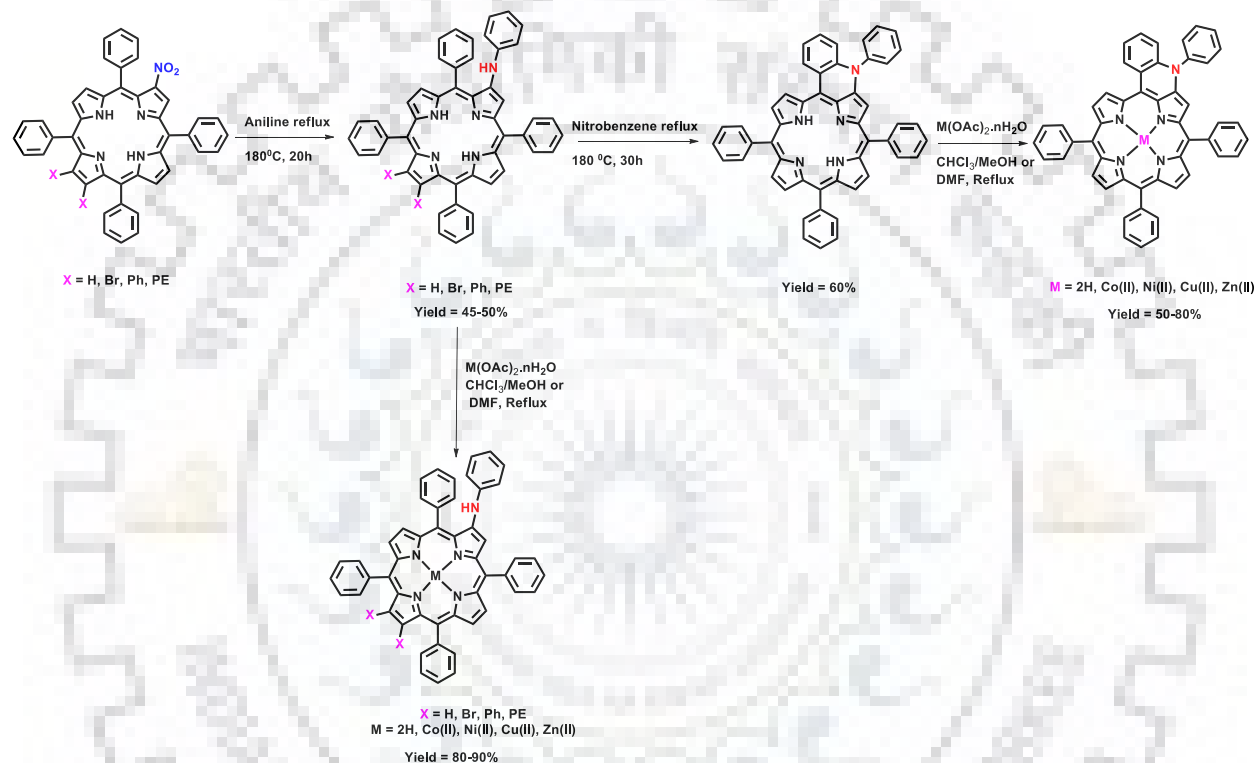
(d) Synthesis of N-Arylquinolino[2,3,4-at]-12,13-diphenylethynylporphyrin: H₂TPP(N-fusedPh)PE₂ was prepared from H₂TPP(NHPh)PE₂ (120 mg, 0.132 mmol) using the similar procedure as followed for H₂TPP(N-fusedPh) synthesis. Yield: 66% (80 mg, 0.089 mmol). **H₂TPP(N-fusedPh)PE₂:** UV-Vis. λ_{\max} (nm), (log ϵ): 426(4.90), 474(sh) (4.80), 568(3.96), 628(4.04), 683(3.99). ¹H NMR in CDCl₃ (400 MHz), δ (ppm): 9.67 (d, $J = 8$ Hz, 1H, 5'-H), 9.55 (d, $J = 4$ Hz, 1H, β -H), 8.69 (d, $J = 4$ Hz, 2H, β -H), 9.58 (s, 2H, β -H), 8.30-8.33, 8.20-8.22, 8.06-8.09 (3m, 6H, *meso-o*-Ph-H-5,10,15) 7.64-7.88 (m, 18H, H-3,H-2',3',4', *meso-m,p*-Ph-H-5,10,15 and β -NPh-H), 7.34-7.39 (m, 4H, β -*o*-PE-H), 7.27-7.30 (m, 6H, β -*m,p*-PE-H), -1.04 (s, 2H, imino-H). MALDI-TOF-MS (m/z): found [M+H]⁺ 904.94, calcd. 904.34. Elemental analysis calcd. For C₆₆H₄₁N₅: C, 87.68%; H, 4.57%; N, 7.75% and found: C, 87.75%; H, 4.66%; N, 7.87%

The metal derivatives were prepared with similar method as described for MTPP(NHPh). The yields were found to be 63-80%. **CoTPP(N-fusedPh)PE₂:** Yield: 72% (7.2 mg, 0.008 mmol), UV-Vis. λ_{\max} (nm), (log ϵ): 464(4.80), 645(3.45). MALDI-TOF-MS (m/z): found [M+H]⁺ 961.41, calcd. 961.25. Elemental analysis calcd. For C₆₆H₃₉N₅Co: C, 82.49%; H, 4.09%; N, 7.29% and found: C, 82.55%; H, 4.21%; N, 7.33%. **NiTPP(N-fusedPh)PE₂:** Yield: 63% (6.3 mg, 0.007 mmol), UV-Vis. λ_{\max} (nm), (log ϵ): 465(4.98), 553(4.03), 589(4.11), 640(4.72). ¹H NMR in CDCl₃ (400 MHz), δ (ppm): 9.34(d, $J = 4$ Hz, 1H, 5'-H), 8.91 (d, $J = 8$ Hz, 1H, β -H), 8.84 (d, $J = 4$ Hz, 1H, β -H), 8.49 (d, $J = 4$ Hz, 1H, β -H), 8.42 (d, $J = 4$ Hz, 1H, β -H), 8.00-8.02, 7.95-7.97, 7.86-7.88 (3m, 6H, *meso-o*-Ph-H-5,10,15) 7.79-7.81 (m, 4H, H-3,H-2',3',4') 7.55-7.73 (m, 14H, *meso-m* and *p*-Ph-H-5,10,15 and β -NPh-H), 7.51 (s, 1H, β -*o*-PE-H), 7.41 (d, 2H, β -*o*-PE-H), 7.33-7.36 (m, 2H, β -*o* and *m*-PE-H), 7.28-7.31 (m, 3H, β -*m*-PE-H), 7.24-7.25 (m, 2H, β -*p*-PE-H). MALDI-TOF-MS (m/z): found [M+H]⁺ 960.44, calcd. 960.26. Elemental analysis calcd. For C₆₆H₃₉N₅Ni: C, 82.51%; H, 4.09%; N, 7.29% and found: C, 82.64%; H, 4.14%; N, 7.34%. **CuTPP(N-fusedPh)PE₂:** Yield: 77% (7.7 mg, 0.008 mmol), UV-Vis. λ_{\max} (nm), (log ϵ): 417(sh) (4.11), 481(4.79), 555(3.67), 597(3.69), 645(3.96). MALDI-TOF-MS (m/z): found [M+K]⁺ 1003.27, calcd. 1003.22. Elemental analysis calcd. For C₆₆H₃₉N₅Cu: C, 82.10%; H, 4.07%; N, 7.25% and found: C, 82.65%; H, 4.12%; N, 7.33%/. **ZnTPP(N-fusedPh)PE₂:** Yield: 80% (8 mg, 0.008 mmol), UV-Vis. λ_{\max} (nm), (log ϵ): 426 (4.60), 486 (5.00), 606 (3.97), 649 (4.30). ¹H NMR in CDCl₃ (400 MHz), δ (ppm): 9.58(d, $J = 8$ Hz, 1H, 5'-H), 9.50 (d, $J = 8$ Hz, 1H, β -H), 8.74(d, $J = 4$ Hz, 1H, β -H), 8.58-8.63 (m, 2H, β -H), 8.24-8.26,

8.16-8.18, 8.05-8.09 (3m, 6H, *meso*-*o*-Ph-H-5,10,15) 7.65-7.90 (m, 18H, H-3,H-2',3',4', *meso*-*m,p*-Ph-H-5,10,15 and β -NPh-H) 7.39-7.41 (m, 4H, β -*o*-PE-H), 7.27-7.30 (m, 6H, β -*m,p*-PE-H). MALDI-TOF-MS (m/z): found [M+K]⁺ 1004.067, calcd. 1004.21. Elemental analysis calcd. For C₆₆H₃₉N₅Zn: C, 81.94%; H, 4.06%; N, 7.24% and found: C, 82.12%; H, 4.14%; N, 7.34%.

2.3 RESULTS AND DISCUSSION

2.3.1 Synthesis and Characterization



Scheme 2.1 Synthetic Routes to Mixed β -Arylamino and N-fused Porphyrins.

2-Nitro-TPPs are good precursor for the further functionalization of macrocycle. Further, these molecules have been used for specific applications in various fields. Functionalization of β -nitroporphyrin was first measured by Crossley and co-workers [32]. H₂TPP(NO₂)Br₂ was utilized for palladium coupling reactions such as Suzuki and Stille coupling reactions which resulted into the formation of H₂TPP(NO₂)Ph₂ and H₂TPP(NO₂)PE₂, respectively. H₂TPP(NO₂)X₂ (X = 2H, Br, Ph and PE) was used as starting material for the synthesis of H₂TPP(NHPh)X₂ (X = H, Br, Ph, and PE). Refluxing of H₂TPP(NO₂)X₂ (X = H, Br, Ph, and PE) in aniline (as solvent) for 20h resulted into the direct nucleophilic displacement of nitro group by aniline at higher temperature (180 °C). Further, the synthesized H₂TPP(NHPh)X₂ (X = H, Br, Ph, PE) were utilized as

precursor for fusion reaction. Refluxing of H₂TPP(NHPh)X₂ (X = H, Br, Ph, and PE) in nitrobenzene for 30h at 200 °C resulted into fusion of β -arylamine group with *ortho* position of *meso*-phenyl ring and yielded H₂TPP(N-fusedPh)X₂ (X = H, Br, Ph, and PE) in good yields (65-70%). Zhang and co-workers have also reported the synthesis of β -arylamino porphyrin from mono-bromoporphyrin by using Pd(OAc)₂ and BINAP in the presence of Cs₂CO₃ in THF [33]. The reaction was completed in 24h and the product was formed with 48% yield. However, our method is cost-effective and simple as compared to Zhang and coworkers.

2.3.2 Crystal Structure Discussion

The structural identification of H₂TPP(N-fusedPh)Br₂ was carried out by single crystal X-ray study. The X-ray quality single crystals of H₂TPP(N-fusedPh)Br₂ were grown by vapor diffusion of methanol onto the porphyrinic solution in CH₂Cl₂ at room temperature. Figure 2.1 represents the ORTEP diagrams showing top and side views of crystallized porphyrin. Figure 2.1 shows that the bromo substitution at antipodal position of N-fused β -arylamine pyrrole. Selected average bond lengths and bond angles of H₂TPP(N-fusedPh)Br₂ is listed in Table A1, Appendix-I. H₂TPP(N-fusedPh)Br₂ have been crystallized with *P*1 space group in triclinic system. H₂TPP(N-fusedPh)Br₂ revealed twisted form of macrocycle core with the magnitude of displacement of β -carbon atoms ($\Delta C_{\beta} = \pm 0.385 \text{ \AA}$) and deviation of 24 core atoms ($\Delta 24 = \pm 0.220 \text{ \AA}$) from the mean plane. The average C _{α} -C _{β} bond length of substituents bearing pyrrole ring is higher as compared to C _{α'} -C _{β'} average bond length (not bearing β -substituents). The crystallographic data of H₂TPP(N-fusedPh)Br₂ is listed in Table A2, Appendix-I. Figure 2.1 exhibits the twisted conformation of porphyrin at the fused sight due to tilted orientation of pyrrole ring above and below from the mean plane of the porphyrin macrocycle.

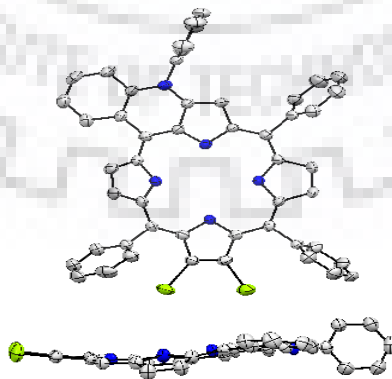


Figure 2.1 ORTEP Diagram Showing Top and Side Views of H₂TPP(N-fusedPh)Br₂, Hydrogen Atoms are Omitted for Clarity. In The Side View, *meso*-Phenyls are Omitted for Clarity.

2.3.3 Electronic Absorption Spectral Studies

Electronic spectral studies of synthesized porphyrins were recorded in CH_2Cl_2 at 298 K. Electronic absorption spectra of the synthesized porphyrins were influenced due to asymmetrical β -substitution at the periphery of the macrocycle. H_2TPP exhibited one B-band and four Q-bands. Further, β -nitration ($H_2TPP(NO_2)$) exhibited red shift in both B-band and Q-bands as compared to H_2TPP . The photophysical properties of β -arylamino porphyrins are quite different from β -nitro-porphyrin which making them interesting molecules for further studies. $H_2TPP(NHPh)$ exhibited 18 and 8 nm hypsochromic shift in the Soret and last $Q_{x(0,0)}$ band, respectively as compared to H_2TPPNO_2 due external charge transfer from amino group to the porphyrin core which resulted the increment in the HOMO-LUMO gap. The Soret bands of $H_2TPP(NHPh)X_2$ ($X = H, Br, Ph$ and PE) are located in the range of 408-427 nm, whereas Q bands are observed in the range of 524-693 nm. Due to the electron-withdrawing nature and extended π -conjugation of phenylethynyl substituents, $H_2TPP(NHPh)PE_2$ exhibits 10-19 nm red shift in the optical absorption spectra as compared to other synthesized porphyrins. N-fused porphyrins exhibited very broad Soret band as compared to parent molecules i.e. $H_2TPP(NHPh)X_2$ ($X = H, Br, Ph$ and PE) possibly due to fusion and external charge transfer from amino group to porphyrin core. Table 2.1 lists the UV-Vis. spectral data of free base and Zn(II) derivatives of synthesized porphyrins. Soret band of N-fused porphyrins are observed in the range 412-426 nm and Q bands in the range of 568-683 nm. $H_2TPP(N-fusedPh)PE_2$ exhibits 5-14 nm bathochromic shift in the Soret band and 11-20 nm in Q-bands relative to other synthesized fused porphyrins i.e. ($H_2TPP(N-fusedPh)$, $H_2TPP(N-fusedPh)Br_2$ and $H_2TPP(N-fusedPh)Ph_2$). As shown by FWHM, $H_2TPP(NHPh)X_2$ ($X = H, Br, Ph$ and PE) and $H_2TPP(N-fusedPh)X_2$ ($X = H, Br, Ph$ and PE) exhibited higher value of full width at half maximum (58-81 nm) as compared to H_2TPP (14 nm) that revealed the extent of external charge transfer from β -arylamino group to porphyrin core. The Soret band of these porphyrins was found to be broader with respect to H_2TPP . UV-Visible absorption spectra of synthesized Zn(II)N-fused porphyrins and $H_2TPP(NHPh)X_2$ ($X = H, Br, Ph$ and PE) are shown in Figures 2.2 and A17, Appendix-I.

Host-guest complex formation of $C_{60}Im/C_{60}Py$ with Zn(II) N-fusedporphyrins was studied by UV-visible titration in a non-coordinating solvent such as *o*-dichlorobenzene at 298 K. Figure 2.3 shows the UV-Visible spectral titration of $ZnTPP(N-fusedPh)PE_2$ with $C_{60}Im/C_{60}Py$ in *o*-

dichlorobenzene. The sequential addition of C₆₀Im/C₆₀Py to the Zn(II) complexes shows the decrement in Soret band of porphyrins (ZnTPP(N-fusedPh)X₂, X = H, Br, Ph and PE) and red shift in Q-bands, which evidences for the formation of supramolecular assembly. The association constants of these Zn(II) porphyrins:fullerene dyads were calculated by using Benesi-Hildebrand plot. The association constants of ZnTPP(N-fusedPh)PE₂:C₆₀Im and ZnTPP(N-fusedPh)PE₂:C₆₀Py were found to be $1.24 \times 10^5 \text{ M}^{-1}$ and $7.59 \times 10^3 \text{ M}^{-1}$ respectively, with 1:1 stoichiometry. The observed association constant (K) values of other synthesized Zn(II)N-fused porphyrins were found within the range of 2.22×10^4 to $4.51 \times 10^5 \text{ M}^{-1}$ with C₆₀Im and 5.39×10^3 to 1.02×10^4 with C₆₀Py as listed in Table 2.2. Similar results were obtained for other synthesized Zn(II)-N-fusedporphyrins i.e. (ZnTPP(N-fusedPh), ZnTPP(N-fusedPh)Br₂ and ZnTPP(N-fusedPh)Ph₂) as shown in Figures A18-A23, Appendix-I. The K values for axial coordination of imidazole-functionalized fullerene and pyridine-functionalized fullerene to synthesized Zn(II)N-fusedporphyrins are 10-100 times higher compared to the axial coordination of pyridine functionalized fullerene to ZnTPP. Similarly, the K values are also 10-100 times greater than the K values for fullerene (without functionalized) binding with Zn(II) *meso*-tetraalkyl porphyrin [34,35]. BH plots of N-fused porphyrins exhibited 1:1 stoichiometry of all the synthesized Zn(II)N-fusedporphyrins with C₆₀Im and C₆₀Py. The association constants values of imidazole analogs are higher than pyridine analogs due to higher basicity of imidazole than pyridine.

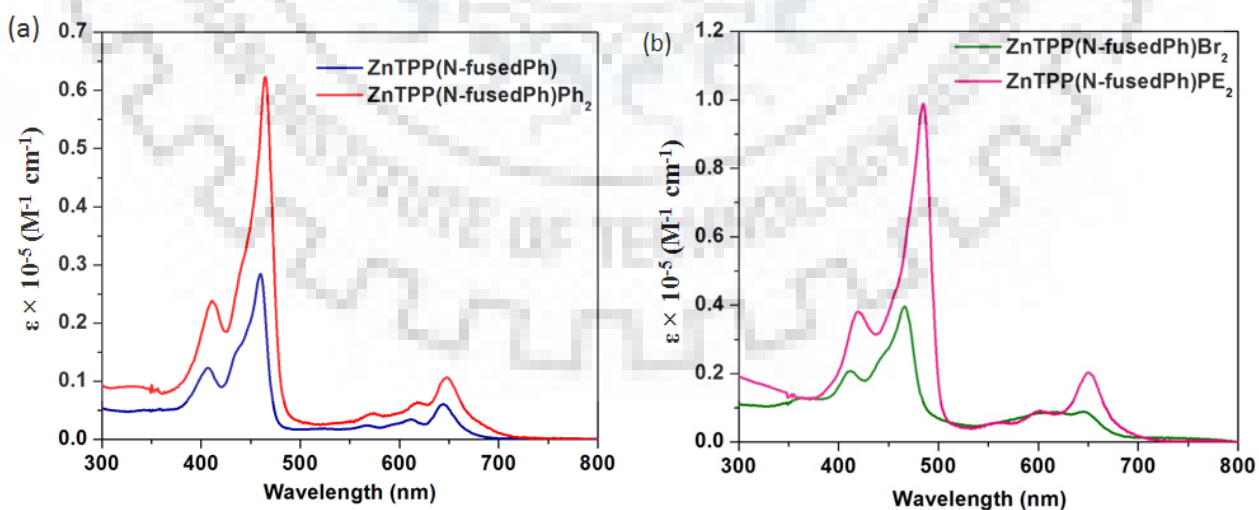


Figure 2.2 UV-Visible Spectra of (a) ZnTPP(N-fusedPh) and ZnTPP(N-fusedPh)Ph₂, (b) ZnTPP(N-fusedPh)Br₂ and ZnTPP(N-fusedPh)PE₂.

Table 2.1 Photophysical Data of Synthesized Porphyrins (MTPP(NHPh) X_2 and MTPP(N-fusedPh) X_2 (X = H, Br, Ph, PE and 2H, Zn(II)) in CH_2Cl_2 at 298 K.

Por.	B band (nm)	Q band(s) (nm)	$\lambda_{\text{emission}}$ (nm)	Φ_f	τ (nm)	FWHM
H₂TPP(NHPh)	408(5.21)	525(4.38), 569(4.0), 599(3.96), 657(3.62)	667, 735	0.098	0.196	53
H₂TPP(NHPh)Br₂	417(5.00)	525(4.22), 612(3.98), 693(3.792)	656, 713	0.009	0.005	41
H₂TPP(NHPh)Ph₂	414(5.08)	531(4.18), 577(3.39), 603(3.91), 660(3.44)	676, 741	0.033	0.014	74
H₂TPP(NHPh)PE₂	427(5.01)	524(4.10), 622(3.96)	702, 762	0.023	0.209	58
ZnTPP(NHPh)	407 (5.46)	560(4.33), 588 (4.16)	627, 679	0.043	1.62	45
ZnTPP(NHPh)Br₂	412(5.12)	570 (3.99), 599 (4.04)	635, 687	0.007	0.05	31
ZnTPP(NHPh)Ph₂	411(5.11)	569 (3.89), 592(3.84)	632, 685	0.034	1.36	70
ZnTPP(NHPh)PE₂	426 (5.05)	579(4.07), 617 (4.22)	643, 701	0.044	1.32	80
H₂TPP(N-fusedPh)	412 (4.93), 451(4.68)	594(4.05), 609(4.05), 663(3.99)	671	0.025	6.62	72
H₂TPP(N-fusedPh)Br₂	418(4.98), 460(4.72)	621(4.10), 668(4.02)	670	0.008	2.48	78
H₂TPP(N-fusedPh)Ph₂	417(4.72), 456(4.70)	568(3.73), 615(3.90), 672(3.76)	682	0.021	1.20	86
H₂TPP(N-fusedPh)PE₂	426(4.90), 474(4.78)	568(3.96), 628(4.04), 683(3.99)	688	0.042	3.35	95
ZnTPP(N-fusedPh)	407(4.09), 460(4.50)	568(3.38), 613(3.53), 645(3.78)	659	0.067	1.41	38
ZnTPP(N-fusedPh)Br₂	415(4.32), 466(4.60)	617(3.94), 650(3.95)	658	0.009	2.44	49
ZnTPP(N-fusedPh)Ph₂	415(4.37), 465(4.80)	574(3.66), 617(3.80), 648(4.02)	660	0.041	2.96	36
ZnTPP(N-fusedPh)PE₂	426(4.60), 486(5.00)	606(3.97), 649(4.30)	647	0.039	2.00	36

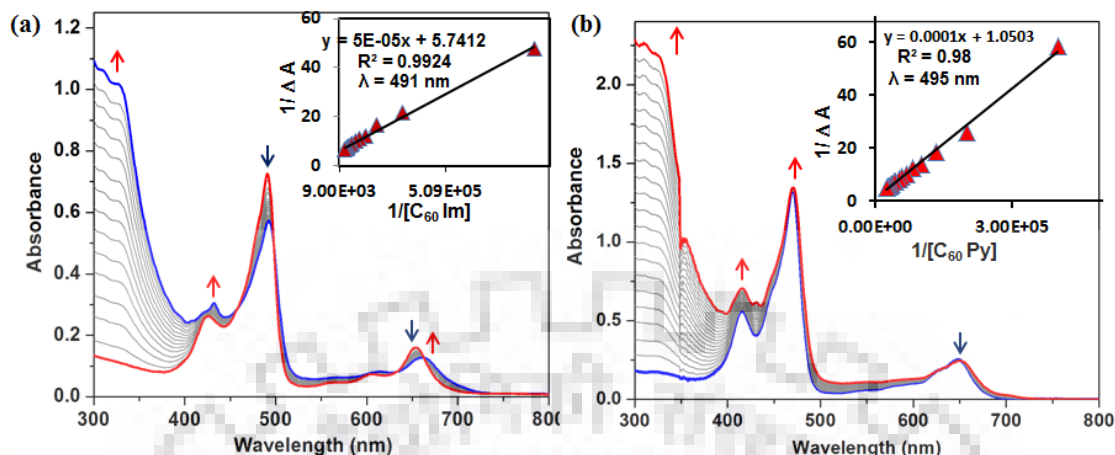


Figure 2.3 UV-Spectral Titration of ZnTPP(N-fusedPh)PE₂ with (a) C₆₀Im and (b) C₆₀Py in *o*-Dichlorobenzene at 298 K.

2.3.4 Emission Spectral Studies

The influence of the substitution at β -position of porphyrins was examined by emission spectral study. This study has been carried out in CH₂Cl₂ at 298 K. H₂TPP(NHPh)X₂ (X = H, Br, Ph and PE) exhibited 2-48 nm red shift in emission spectra and decreased intensity as compared to H₂TPP (Figure A50(a), Appendix-I). Whereas, ZnTPP(NHPh)X₂ (X = H, Br, Ph and PE) exhibited 6-22 nm blue shift in the emission spectra as compared to ZnTPP. Zn(II) derivatives of N-fusedporphyrins (ZnTPP(N-fusedPh)X₂ (X = H, Br, Ph, and PE) were characterized by fluorescence spectral studies to examine the influence of substitution at β -position of the macrocycle and porphyrin:C₆₀Im/C₆₀Py complex formation. Quantum yields of bromo substituted porphyrins were found to be very low due to heavy atom effect of bromo groups and nonplanar conformation of porphyrin. H₂TPP(N-fusedPh)X₂ (X = H, Br, Ph, and PE) exhibited 16-34 nm red shifts in emission bands as compared to H₂TPP in CH₂Cl₂ (Figure A50(b), Appendix-I). Emission spectra of ZnTPP(N-fusedPh)X₂ (X = H, Br, Ph and PE) has shown in Figure 2.4. An interesting trend in the emission band of free base N-fusedporphyrins was found which aligns in the following order H₂TPP < H₂TPP(N-fusedPh)Br₂ < H₂TPP(N-fusedPh) < H₂TPP(N-fusedPh)Ph₂ < H₂TPP(N-fusedPh)PE₂. After addition of C₆₀Im/C₆₀Py to porphyrin (ZnTPP(N-fusedPh)X₂ (X = H, Br, Ph, and PE)) in *o*-dichlorobenzene, a decrement in the fluorescence intensity of porphyrins was observed. The quenching of fluorescence intensity of ZnTPP(N-fusedPh)PE₂ with C₆₀Im and C₆₀Py are shown in Figure 2.5. Quenching of the fluorescence intensity of ZnTPP(N-fusedPh)PE₂ revealed the formation of self-assembled dyads.

Singlet excited state quenching of ZnTPP(N-fusedPh)X₂ (X = H, Br, Ph, and PE) revealed probable relaxation pathway from the first singlet excited state of porphyrin to C₆₀Im/C₆₀Py in *o*-dichlorobenzene which resulted in the decrement in the fluorescence intensity of porphyrin. Another reason for quenching of fluorescence intensity of porphyrin is the charge separation from porphyrin (ZnTPP(N-fusedPh)X₂ (X = H, Br, Ph and PE) to coordinated C₆₀Im/C₆₀Py in *o*-dichlorobenzene medium [36]. SV (Stern Volmer) quenching constant of ZnTPP(N-fusedPh)PE₂ was found higher (1.19×10^5) with C₆₀Im as compared to C₆₀Py (5.24×10^4). Fluorescence quenching of synthesized ZnTPP(N-fusedPh)X₂ (X = H, Br and Ph) are shown in Figures A21-A23 and A27-A29, Appendix-I. Quenching constants data of these porphyrins ZnTPP(N-fusedPh)X₂ (X = H, Br, Ph and PE) is listed in Table 2.2. After addition of C₆₀Im/C₆₀Py to these Zn(II) derivative of N-fused porphyrins solution exhibited shorter lifetime as compared to C₆₀Im/C₆₀Py free Zn(II) N-fusedporphyrins solution which revealed host-guest complex formation. Fluorescence lifetime study of these porphyrins has been carried out in non-coordinating *o*-dichlorobenzene.

Table 2.2 UV-visible and Fluorescence Titration Data of C₆₀Im/C₆₀Py with ZnTPP(N-fusedPh)X₂ (X = H, Br, Ph, PE) in *o*-Dichlorobenzene at 298 K.

Porphyrin	C ₆₀ Im		C ₆₀ Py	
	K, M ⁻¹	K _q , M ⁻¹	K, M ⁻¹	K _q , M ⁻¹
ZnTPP(N-fusedPh)	7.26×10^4	6.11×10^4	3.02×10^4	3.41×10^4
ZnTPP(N-fusedPh)Br ₂	4.51×10^5	8.24×10^4	5.39×10^3	4.52×10^4
ZnTPP(N-fusedPh)Ph ₂	2.22×10^4	1.08×10^5	1.02×10^4	8.02×10^4
ZnTPP(N-fusedPh)PE ₂	1.24×10^5	1.19×10^5	7.59×10^3	5.24×10^4

K = Association constant, **K_q** = Quenching constant

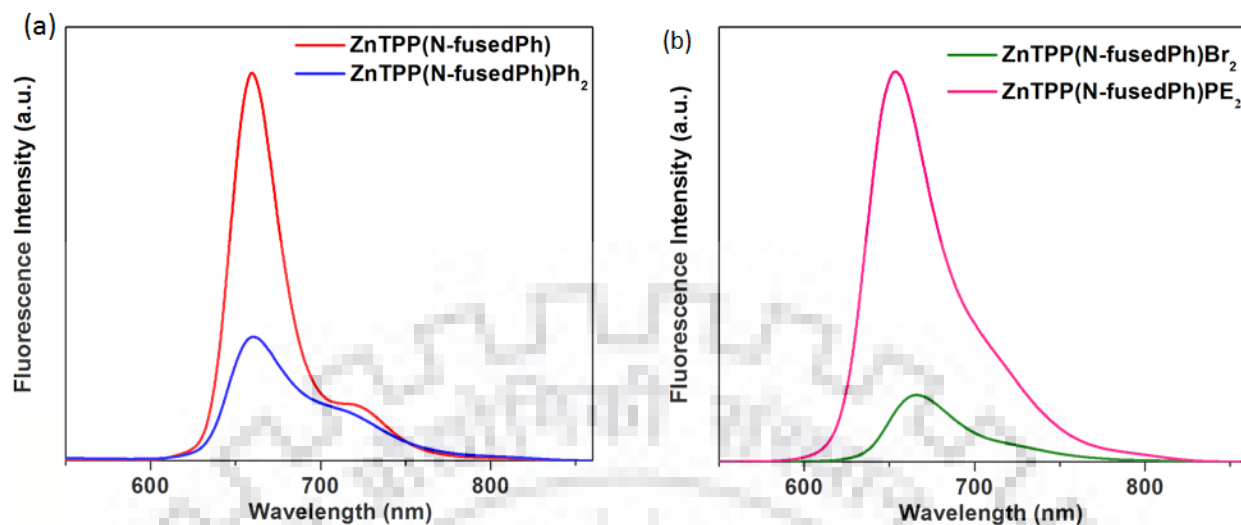


Figure 2.4 Fluorescence Spectra of (a) ZnTPP(N-fusedPh) and ZnTPP(N-fusedPh)Ph₂, (b) ZnTPP(N-fusedPh)Br₂ and ZnTPP(N-fusedPh)PE₂.

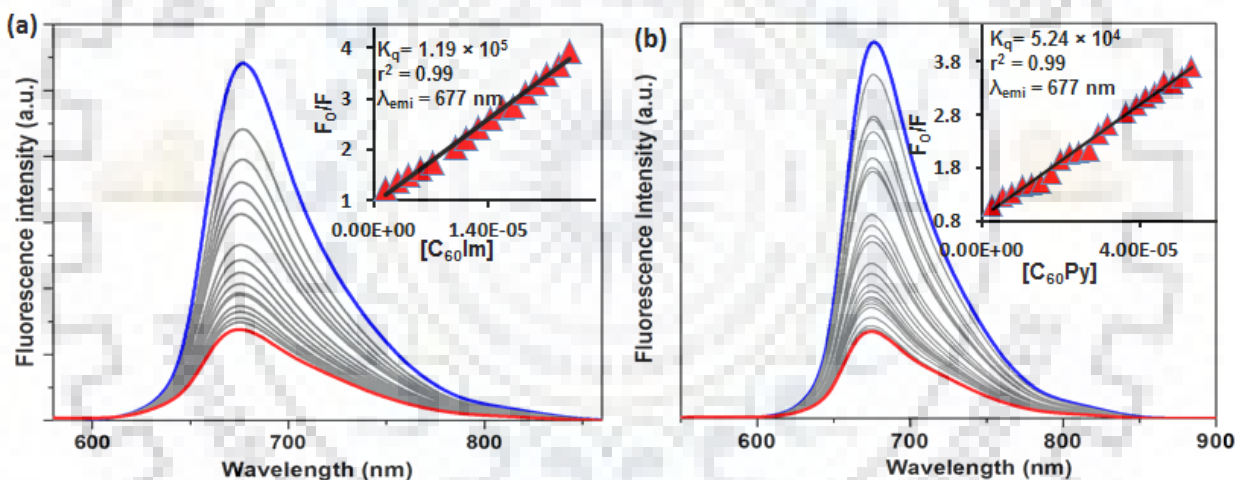


Figure 2.5 Quenching of Fluorescence Intensity of ZnTPP(N-fusedPh)PE₂ (**4d**) (a) $C_{60}Im$ and (b) $C_{60}Py$ in *o*-Dichlorobenzene at 298 K.

2.3.5 DFT Studies

The gas phase geometry optimization of synthesized porphyrins was performed by using B3LYP functional and LANL2DZ basis set. Due to mixed substitution at periphery of porphyrin, the bond length of $C_{\beta}-C_{\beta}$ and bond angle $C_{\beta}-C_{\alpha}-C_m$ increased while bond angle of $N-C_{\alpha}-C_m$ is decreased. $C_{\beta}-C_{\beta}$ bond length (1.387-1.405 Å) of β -pyrrole ($H_2TPP(NHPh)X_2$ ($X = H, Br, Ph$ and PE)) was found to be longer than $C_{\beta}-C_{\beta}$ (1.366-1.367 Å). The decrement in the bond angle of $N-C_{\alpha}-C_m$ was observed along with the increment in the bond angle of $C_{\beta}-C_{\alpha}-C_m$. All synthesized

porphyrins exhibited moderate nonplanarity because of the substitution at antipodal position of β -arylamino substituents. H₂TPP(NHPh)X₂ (X = H, Br, Ph and PE) exhibited deviation of β -pyrrole carbon ($\Delta C_{\beta} = \pm 0.129$ - 0.453 \AA) and 24 core atoms ($\Delta 24 = \pm 0.058$ - 0.220 \AA) from porphyrin mean plane. Among all synthesized porphyrins, H₂TPP(NHPh)Ph₂ exhibited highly nonplanar conformation ($\Delta C_{\beta} = \pm 0.453 \text{ \AA}$ and $\Delta 24 = \pm 0.220 \text{ \AA}$). Further, H₂TPP(NHPh) and H₂TPP(NHPh)PE₂ showed ΔC_{β} (± 0.129 and $\pm 0.249 \text{ \AA}$) while $\Delta 24$ (± 0.058 and $\pm 0.121 \text{ \AA}$), respectively which indicated that these both porphyrins have nearly planar conformation. ΔC_{β} and $\Delta 24$ of synthesized porphyrins follow the order: H₂TPP(NHPh) < H₂TPP(NHPh)PE₂ < H₂TPP(NHPh)Br₂ < H₂TPP(NHPh)Ph₂.

The ground state geometries for C₆₀Im/C₆₀Py:ZnTPP(N-fusedPh)X₂ (X = H, Br, Ph, PE) dyad were optimized in the gas phase by using G16 B3LYP/6-311G(d,p) method. D'souza *et al.* have reported the structures of various fullerene-porphyrin dyads [37]. Figure 2.6 shows optimized structure, electrostatic potential map and the frontier HOMO-LUMO orbital levels of ZnTPP(N-fusedPh). The formation of donor-acceptor dyads reveals photoinduced electron transfer (PET) from excited Zn(II) N-fusedporphyrin to C₆₀Py which lead to formation of charge separated state. In case of supramolecular dyads, the frontier HOMO was localized over the Zn(II) N-fusedporphyrin while LUMO existed on C₆₀ moiety which deduced that the most stable charge separated state of the dyads can be represent as C₆₀⁻Py to ZnTPP(N-fusedPh)Ph₂⁺. The localization of the HOMO over the Zn(II) N-fusedporphyrin revealed the stabilization of charge separated state of dyads. There is no HOMO exist on C₆₀ moiety and no LUMO exist on Zn(II)N-fusedporphyrin which results the partially charge displacement in both HOMO and LUMO can be represent as C₆₀ ^{δ^-} Py:ZnTPP(N-fusedPh) ^{δ^+} and there is no charge transfer interaction between both moieties (Zn(II) N-fusedporphyrin and C₆₀Py) in ground state. The HOMO-LUMO gap in ZnTPP(N-fusedPh) was found to be 2.45 eV, while after coordination with C₆₀Py HOMO-LUMO gap formed 1.00 eV due to stabilization of HOMO orbital. The distance of newly formed axial coordination of C₆₀Py to Zn metal of ZnTPP(N-fusedPh) was found 10.13 \AA and the distance between N of Py to Zn metal of ZnTPP(N-fusedPh) was 2.25 \AA . HOMO and LUMO orbital energies of ZnTPP(N-fusedPh) were found -4.75 eV and -2.30 eV, respectively. Optimized structure, electrostatic potential map and frontier HOMO-LUMO orbital levels of ZnTPP(N-fusedPh)X₂ (X = Br, Ph, PE) shown in Figures A33-A38, Appendix-I.

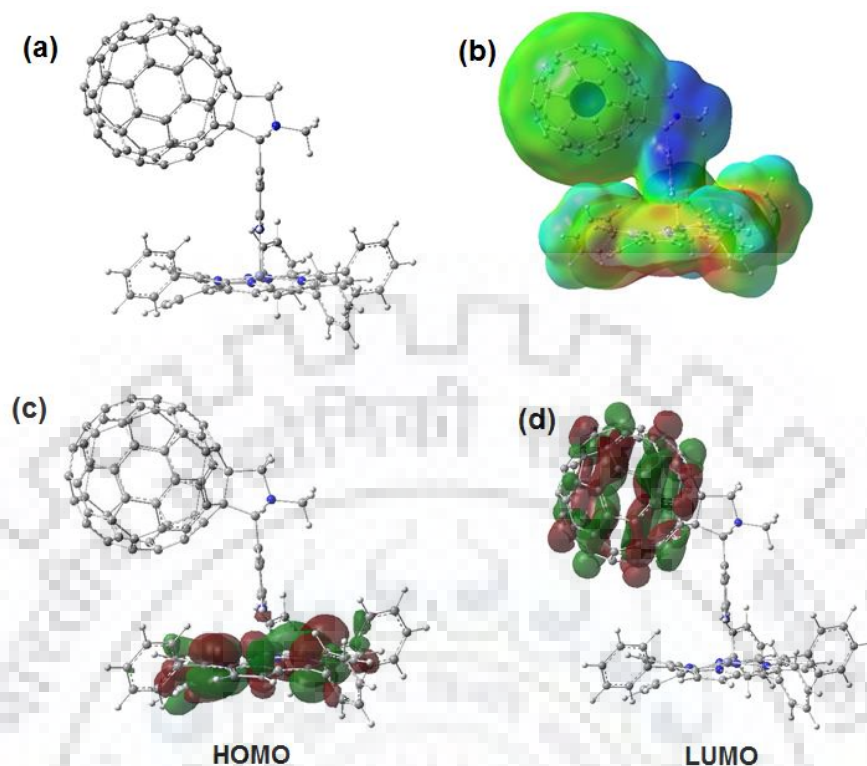


Figure 2.6 (a) Optimized Structure (b) Electrostatic Potential Map (c) Pictorial Representation of Frontier HOMO and (d) LUMO of ZnTPP(N-fusedPh): $C_{60}Py$.

2.3.6 Electrochemical Redox Studies

To examine the influence of mixed β -substitution, core metal ions, and nonplanarity on porphyrin π -system, we performed the cyclic voltammetric studies for all synthesized porphyrins in CH_2Cl_2 except Zn(II) derivatives of N-fused porphyrins which were performed in *o*-dichlorobenzene containing 0.1 M TBAPF₆ as supporting electrolyte at 298 K. The comparative cyclic voltammograms of ZnTPP(NHPh) X_2 and ZnTPP(N-fusedPh) X_2 ($X = H, Br, Ph$ and PE)) are shown in Figure A49, Appendix-I. The redox potential of newly synthesized porphyrins is listed in Tables A4 and A5, Appendix-I. Due to the presence of electron rich β -arylamino group, these macrocycle is easy to oxidized and difficult to reduce with respect to MTPP (where $M = 2H, Co(II), Ni(II), Cu(II)$ and Zn(II)). Co(II) porphyrins show metal centered redox behavior. The first oxidation potentials of ZnTPP(NHPh) X_2 ($X = H, Br, Ph$ and PE) were 20-130 mV cathodically shifted compared to ZnTPP which revealed that the external charge transfer from β -arylamino group to porphyrin core. ZnTPP(N-fusedPh)Ph₂ exhibited first oxidation potential at

0.71V which is 320 mV cathodically shifted as compared to ZnTPP(NHPh)Ph₂. ZnTPP(N-fusedPh)X₂ (X = H, Br, and PE) exhibited 210-230 mV cathodic shifts in the first oxidation potential with respect to ZnTPP(NHPh)X₂ (X = H, Br, PE) due to fusion of arylamino group to *meso*-phenyl ring and increase the external charge transfer to porphyrin core. ZnTPP(NHPh)PE₂ shows first reduction potential at 1.21V which is 150 mV anodically shifted than ZnTPP and 80-190 mV anodically shifted as compared to ZnTPP(NHPh)X₂ (X = H, Br, and Ph) this is due to extensive stabilization of LUMO whereas there is only marginal shift in first oxidation potential. H₂TPP(N-fusedPh)X₂ (X = H, Br, Ph, and PE) exhibited 260-410 mV cathodic shift in the first oxidation potential as compared to H₂TPP, due to the presence of electron rich arylamino group at the periphery of the porphyrin. The first oxidation potential of H₂TPP(N-fusedPh)Ph₂ was found 40-150 mV cathodically shifted with respect to other synthesized free base N-fused porphyrins. NiTPP(N-fusedPh)X₂ (X = H, Br, Ph, PE) exhibited 290-410 mV cathodic shift in first oxidation potential as compared to NiTPP. NiTPP(N-fusedPh) and NiTPP(N-fusedPh)Ph₂ exhibited a marginal 30-50 mV cathodic shift in the first reduction potential while NiTPP(N-fusedPh)Br₂ and NiTPP(N-fusedPh)PE₂ exhibited 70-80 mV anodic shift in first reduction as compared to NiTPP, due to electron withdrawing nature of Br and PE substituents. First oxidation potential of CuTPP(N-fusedPh)X₂ (X = H, Br, Ph, PE) 280-440 mV cathodically shifted than CuTPP whereas the first reduction potential 210-430 mV anodically shifted than CuTPP.

In order to determine the redox potentials of the newly synthesized (Zn(II) N-fusedporphyrin: $C_{60}Im/C_{60}Py$) dyads, we performed the cyclic voltammetric studies of Zn(II) N-fusedporphyrin and $C_{60}Im/C_{60}Py$ to explore the charge transfer interaction in the host-guest complexes in the ground state in *o*-dichlorobenzene as solvent containing 0.1M TBAPF₆ as supporting electrolyte. Plenty of research groups have reported the electrochemistry of porphyrin-fullerene dyad [38]. ZnTPP(N-fusedPh)X₂ (X = H, Br, Ph, and PE) exhibited two or three, one electron oxidations and one electron reductions potential. First oxidation potentials of porphyrins, ZnTPP(N-fusedPh)X₂ (X = H, Br, Ph and PE) were observed in the range of 0.44-0.70 V. These macrocycles oxidized very easily due to the external charge transfer from β -arylamino group to porphyrin core.

Figures 2.7 and A30-A32, Appendix-I, show the cyclic voltammograms of porphyrins ZnTPP(N-fusedPh)X₂ (X = H, Br, Ph, and PE) with and without $C_{60}Im/C_{60}Py$. Table A3, Appendix-I, lists

the redox potential of ZnTPP(N-fusedPh) X_2 ($X = H, Br, Ph$ and PE) porphyrins with and without $C_{60}Im/C_{60}Py$. ZnTPP(N-fusedPh) and ZnTPP(N-fusedPh) Br_2 exhibited a marginal anodic shift (10-20 mV) in the redox potentials after addition of $C_{60}Im/C_{60}Py$ to the Zn(II) N-fusedporphyrin in *o*-dichlorobenzene. ZnTPP(N-fusedPh) PE_2 exhibited its first oxidation potential at 0.70 V while addition of $C_{60}Im$ and $C_{60}Py$ showed 10-20 mV anodic shift in the first oxidation potential. The first reduction potential of ZnTPP(N-fusedPh) PE_2 exhibited 20-30 mV anodic shift after addition of $C_{60}Im/C_{60}Py$. The redox potential of Zn(II) N-fusedporphyrin- $C_{60}Im/C_{60}Py$ dyads exhibited small changes as compared to $C_{60}Im/C_{60}Py$ free Zn(II) N-fusedporphyrin. This study supports the formation of host-guest complex between fused porphyrin and $C_{60}Im/C_{60}Py$.

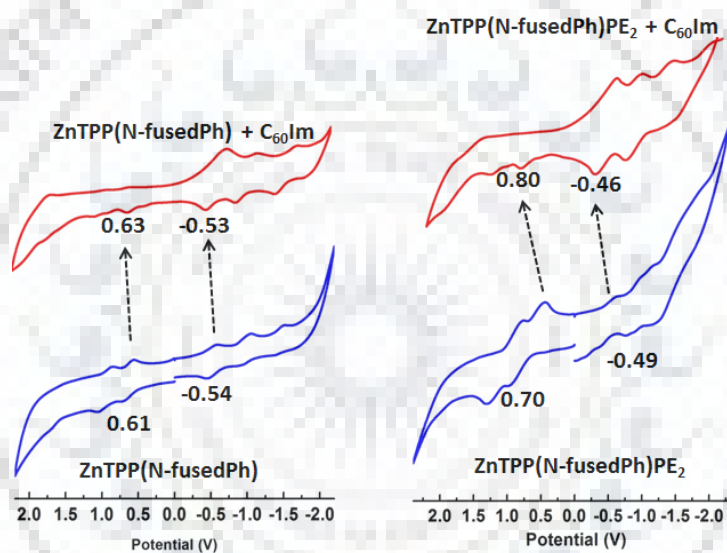


Figure 2.7 Cyclic Voltammograms of ZnTPP(N-fusedPh) and ZnTPP(N-fusedPh) PE_2 in the Presence and Absence of $C_{60}Im$ in *o*-Dichlorobenzene at 298 K.

2.3.7 Chemical Oxidation Studies

The chemical oxidation studies of synthesized Zn(II)N-fusedporphyrins were performed by using $NOBF_4$ in *o*-dichlorobenzene. N-fusedporphyrins (ZnTPP(N-fusedPh) X_2 ($X = H, Br, Ph,$ and PE)) worked as electron donor. Sequential addition of $NOBF_4$ in Zn(II)N-fusedporphyrins resulted into the continuous decrement in intensity of the Soret band as well as Q-bands with the generation of a new broad Q band in the longest wavelength region. The electron transfer from Zn(II)N-fusedporphyrin to NO^+ results in the formation of porphyrin cation radical. Figures 2.8 and A46-A48, Appendix-I, represent the chemical oxidation spectra of synthesized Zn(II)N-fused porphyrins (ZnTPP(N-fusedPh) X_2 ($X = H, Br, Ph, PE$)).

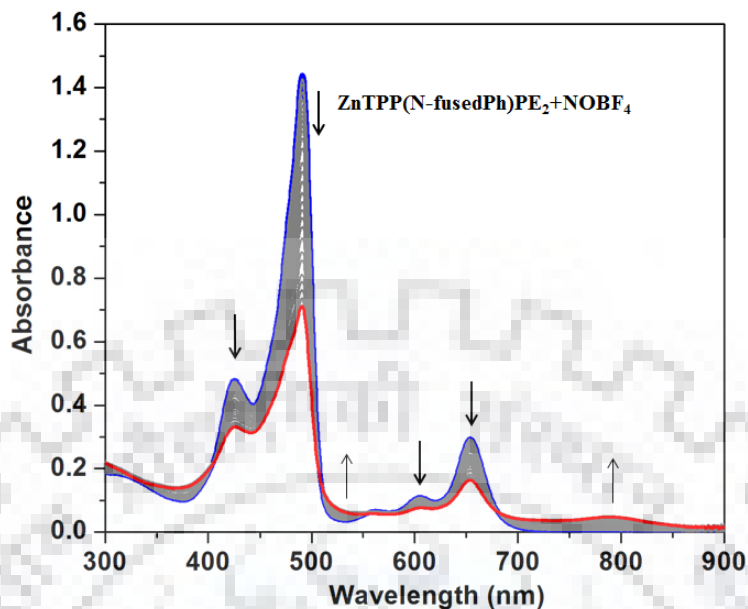


Figure 2.8 Chemical Oxidation of ZnTPP(N-fusedPh)PE₂ using NOBF₄ in *o*-Dichlorobenzene at 298 K.

2.3.8 ¹H NMR Studies

¹H NMR studies of synthesized porphyrins have been carried out in CDCl₃ at 298 K. These porphyrins exhibited characteristic peaks arising from β -pyrrole protons, *meso*-phenyl protons, β -pyrrole NH, N-fused phenyl protons, β -substituents (Ph and PE) and imino proton resonances. Figures A1-A8, Appendix-I, represent the ¹H NMR spectra of synthesized porphyrins in CDCl₃ at 298 K. β -H-3 Proton (β -proton adjacent to arylamine containing β -proton) of H₂TPP(NHPh)X₂ (X = H, Br, and PE) exhibited characteristic resonances in the range from 8.03-8.31 ppm as a singlet (appeared with multiplet in H₂TPP(NHPh)Ph₂). β -H-3 Proton resonance of H₂TPP(NHPh) appeared at 8.31 ppm while in case of H₂TPP(NHPh)Br₂ and H₂TPP(NHPh)PE₂ this peak raised in range of 8.03-8.09 ppm. β -H-3 Proton resonance of H₂TPP(NHPh)Br₂ and H₂TPP(NHPh)PE₂ is exhibited 0.22-0.28 ppm downfield shifted with respect to H₂TPP(NHPh) due to electron withdrawing effect of Br and PE substituents. The inner -NH core protons resonance of H₂TPP(NHPh) appeared at -2.53 ppm and show 0.08-0.27 ppm upfield shift as compared to H₂TPP(NHPh)Ph₂ and H₂TPP(NHPh)PE₂, respectively. H₂TPP(NHPh)Br₂, H₂TPP(NHPh)Ph₂ and H₂TPP(NHPh)PE₂ exhibited the inner core -NH protons resonance at -2.58, -2.26 and -2.45 ppm, respectively. There is only marginal shift in resonance (6.59-6.63

ppm) of outer -NH protons. The inner core -NHs of N-fused porphyrins lying in the range of -0.93 to -1.25 ppm as shown in Figure 2.9a. Inner NH proton peak of $H_2TPP(NHPh)Br_2$ show 1.44 ppm downfield shift after fusion with *meso*-phenyl ring, due to decreased ring current of macrocycle as shown in Figure 2.9b. β -H-3 Proton of $H_2TPP(N\text{-fusedPh})X_2$ (X = H, Br, Ph and PE) combined with *meso*-phenyl protons and appeared as multiplet in the range of 7.51-7.99 ppm. The β -pyrrole protons resonances arised sometimes as doublet and in some cases combined with *meso*-phenyl protons and appeared as multiplet. $H_2TPP(NHPh)X_2$ (X = H, Br, Ph, and PE) exhibited characteristic outer -NH proton peak with corresponding shifts in the ppm values according to the antipodal β -substituents which confirmed the synthesis of these substituted β -arylaminoporphyrins while there is no -NH proton peak observed in N-fused porphyrins which evidenced the formation of N-fusedporphyrins.

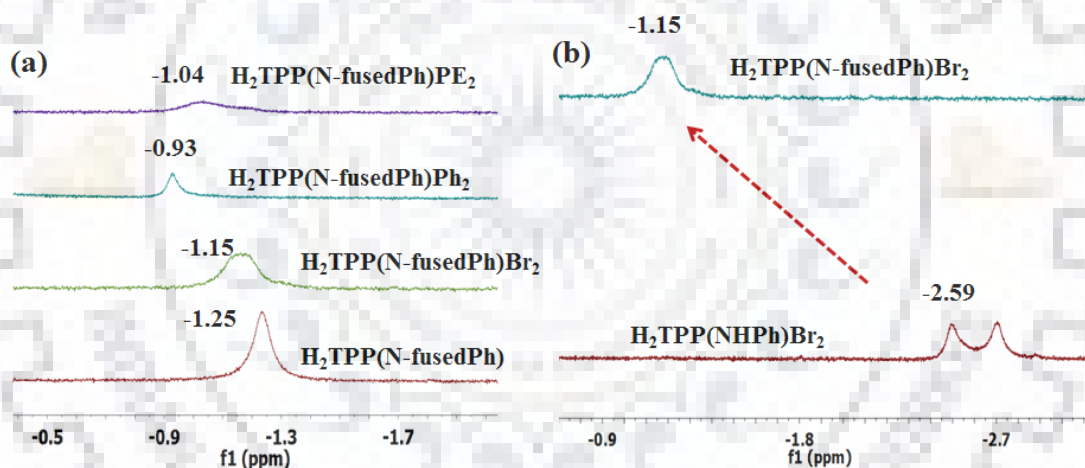


Figure 2.9 (a) 1H NMR Spectra of Imine Proton of $H_2TPP(N\text{-fusedPh})$, $H_2TPP(N\text{-fusedPh})Br_2$, $H_2TPP(N\text{-fusedPh})Ph_2$, $H_2TPP(N\text{-fusedPh})PE_2$ and (b) Comparative 1H NMR Spectra of Inner -NH Proton of $H_2TPP(N\text{-fusedPh})Br_2$ and $H_2TPP(NHPh)Br_2$.

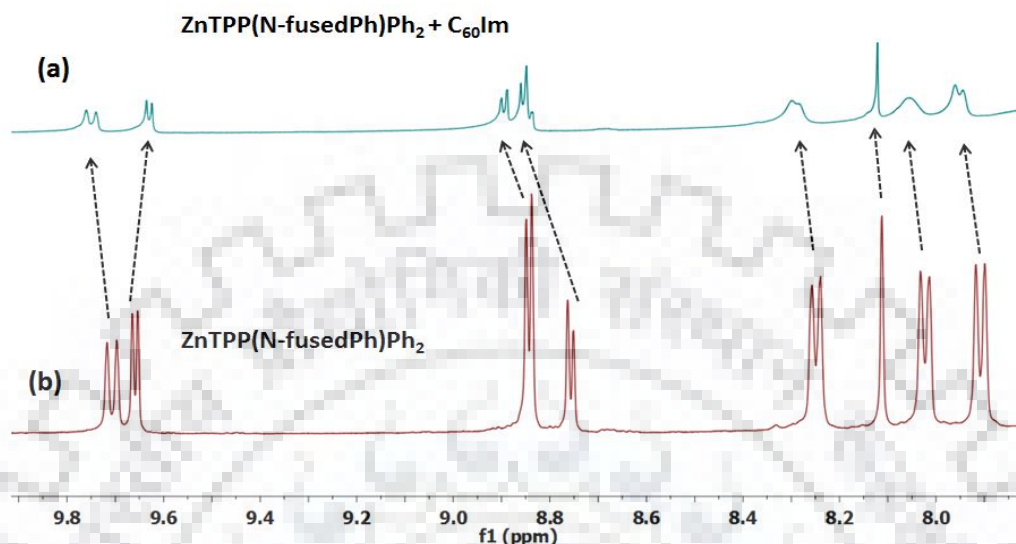


Figure 2.10 1H NMR Spectra of (a) ZnTPP(N-fusedPh) Ph_2 : $C_{60}Im$ Adduct (b) ZnTPP(N-fusedPh) Ph_2 in C_6D_6 at 298 K.

The 1H NMR titrations of ZnTPP(N-fusedPh) X_2 ($X = H, Br, Ph,$ and PE) with $C_{60}Im/C_{60}Py$ were carried out in C_6D_6 at 298 K. The 1H NMR titrations of synthesized Zn(II)N-fusedporphyrins with $C_{60}Im/C_{60}Py$ was performed by adding (0-2 equiv. of $C_{60}Im/C_{60}Py$) in benzene D_6 at 298 K. Shift in the peaks were saturated at 1.1 equiv. of $C_{60}Im/C_{60}Py$ which revealed the 1:1 Zn(II) N-fusedporphyrin and $C_{60}Im/C_{60}Py$ complex formation. While in case of ZnTPP(N-fusedPh) X_2 ($X = Br, Ph,$ and PE), β -proton peak exhibited upfield shift after addition of $C_{60}Im$. The proton signals of *meso-m,p*-phenyl protons, β -arylamino-phenyl protons merged with solvent (C_6D_6) peak. Figure 2.10 shows the marginal shift in porphyrin ZnTPP(N-fusedPh) Ph_2 after addition of $C_{60}Im$ in C_6D_6 . Figures A39-A45, Appendix-I, exhibit the comparative 1H NMR spectra of ZnTPP(N-fusedPh) X_2 ($X = H, Br,$ and PE), with $C_{60}Im$ and $C_{60}Py$ which show the marginal downfield shifts in the β -protons and *meso-o*-phenyl protons. The shift in the spectra is an evidence of formation of Zn(II) N-fusedporphyrins: $C_{60}Im/C_{60}Py$ (1:1) host-guest complex formation.

2.4 CONCLUSIONS

In the present work, we have synthesized β -arylamino and N-fused porphyrins (MTPP(NHPh) X_2 and MTPP(N-fusedPh) X_2 ($X = H, Br, Ph, PE$ and $M = 2H, Co(II), Ni(II), Cu(II), Zn(II)$). Synthesized porphyrins were characterized by various spectroscopic techniques. Optical absorption spectra indicated interesting features such as broad Soret band and intense Q bands. Emission spectra of these porphyrins featured redshifted and reduced spectra, due to nonplanar conformation of macrocyclic system and heavy atom effect of bromo groups. DFT study revealed moderate nonplanarity of these macrocycle and $H_2TPP(NHPh)Ph_2$ exhibited higher nonplanarity with respect to other synthesized β -arylamino porphyrins. The crystal structure of $H_2TPP(N-fusedPh)Br_2$ exhibited twisted conformation of the macrocycle. The binding of Zn(II) N-fused porphyrins (ZnTPP(N-fusedPh) X_2 : $X = 2H, Br, Ph, and PE$) with $C_{60}Im/Py$ was studied by 1H NMR, UV-visible and fluorescence spectroscopic techniques which revealed the 1:1 stoichiometry of Zn(II) N-fused porphyrin: $C_{60}Im/Py$ complexation. ZnTPP(N-fusedPh) PE_2 has shown the highest association constant and quenching constant as compared to other synthesized Zn(II)-N-fused porphyrins due to effective π - π interaction between porphyrins and C_{60} derivatives. The association constants of these Zn(II) N-fused porphyrins were found to be 10-100 times higher as compared to Zn(II) *meso*-tetra-methyl/ethylporphyrin. Positive shifts in the oxidation potentials of synthesized porphyrins also evidenced the supramolecular interaction between Zn(II) N-fused porphyrins and $C_{60}Im/Py$.

2.5 REFERENCES

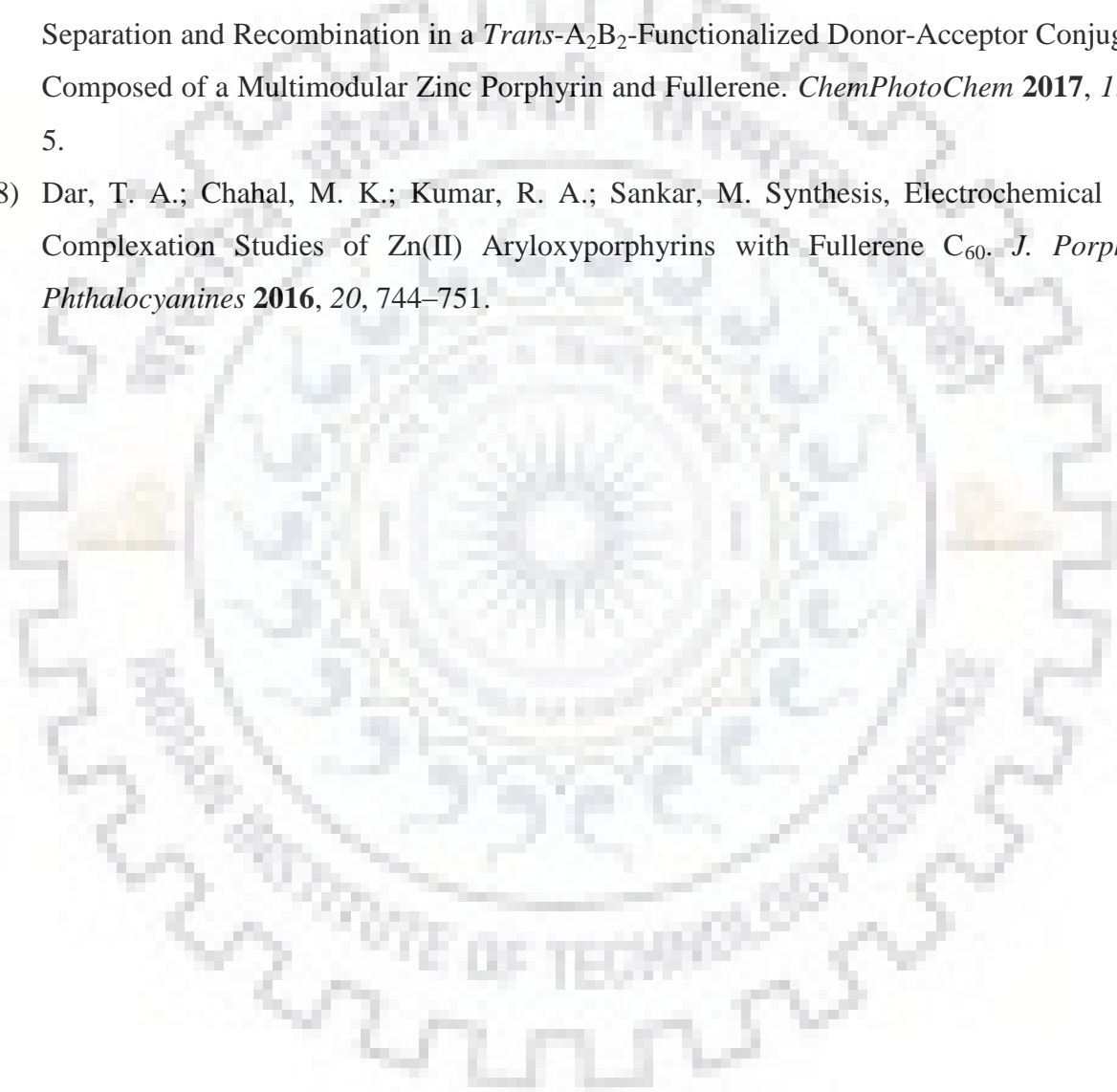
- (1) Karpuschkin, T.; Kappes, M. M.; Hampe, O. Binding of O_2 and CO to Metal Porphyrin Anions in the Gas Phase. *Angew. Chem. Int. Ed.* **2013**, *52*, 10374–10377.
- (2) Xiao-Fei, D.; Jin-Liang, W.; Jian, P. Organocatalytic Asymmetric Michael Addition of 2,4-Pentandione to Nitroolefins. *Org. Lett.* **2005**, *7*, 4713-4716.
- (3) Dar, T. A.; Uprety, B.; Sankar, M.; Maurya, M. R. Robust and Electron Deficient Oxidovanadium(IV) Porphyrin Catalysts for Selective Epoxidation and Oxidative Bromination Reactions in Aqueous Media. *Green Chem.* **2019**, *21*, 1757–1768.
- (4) Kou, J.; Dou, D.; Yang, L. Porphyrin Photosensitizers in Photodynamic Therapy and Its Applications. *Oncotarget* **2017**, *8*, 81591–81603.
- (5) Thompson, S. J.; Brennan, M. R.; Lee, S. Y.; Dong, G. Synthesis and Applications of

- Rhodium Porphyrin Complexes. *Chem. Soc. Rev.* **2018**, *47*, 929–981.
- (6) Yadav, P.; Anand, T.; Moram, S. S. B.; Bhattacharya, S.; Sankar, M.; Rao, S. V. Synthesis and Femtosecond Third Order Nonlinear Optical Properties of Push-Pull *Trans*-A₂B-Corroles. *Dye. Pigment.* **2017**, *143*, 324–330.
 - (7) Hiroto, S.; Miyake, Y.; Shinokubo, H. Synthesis and Functionalization of Porphyrins through Organometallic Methodologies. *Chem. Rev.* **2016**, *117*, 2910-3043.
 - (8) Kumar, S.; Jiang, X.; Shan, W.; Jinadasa, R. G. W.; Kadish, K. M.; Wang, H. β -Functionalized *Trans*-A₂B₂ Push-pull Tetrabenzoporphyrins. *Chem. Commun.* **2018**, *54*, 5303–5306.
 - (9) Jinadasa, R. G. W.; Fang, Y.; Kumar, S.; Osinski, A. J.; Jiang, X.; Ziegler, C. J.; Kadish, K. M.; Wang, H. β -Functionalized Push-Pull *Opp*-Dibenzoporphyrins. *J. Org. Chem.* **2015**, *80*, 12076–12087.
 - (10) Chen, Q.; Brambilla, L.; Daukiya, L.; Mali, K. S.; De Feyter, S.; Tommasini, M.; Müllen, K.; Narita, A. Synthesis of Triply Fused Porphyrin-Nanographene Conjugates. *Angew. Chem. Int. Ed.* **2018**, *57*, 11233–11237.
 - (11) Khusnutdinova, D.; Wadsworth, B. L.; Flores, M.; Beiler, A. M.; Reyes Cruz, E. A.; Zenkov, Y.; Moore, G. F. Electrocatalytic Properties of Binuclear Cu(II) Fused Porphyrins for Hydrogen Evolution. *ACS Catal.* **2018**, *8*, 9888–9898.
 - (12) Chaudhri, N.; Grover, N.; Sankar, M. Selective Conversion of Planar *Trans*-Chlorins into Highly Twisted Doubly Fused Porphyrins or Chlorins via Oxidative Fusion. *Inorg. Chem.* **2018**, *57*, 6658–6668.
 - (13) Davis, N. K. S.; Thompson, A. L.; Anderson, H. L. A Porphyrin Fused to Four Anthracenes. *J. Am. Chem. Soc.* **2011**, *133*, 30–31.
 - (14) Diev, V. V.; Hanson, K.; Zimmerman, J. D.; Forrest, S. R.; Thompson, M. E. Fused Pyrene-Diporphyrins: Shifting Near-Infrared Absorption to 1.5 μ m and Beyond. *Angew. Chem.* **2010**, *122*, 5655–5658.
 - (15) Denis, P. A. Theoretical Characterization of Supramolecular Complexes Formed by Fullerenes and Dimeric Porphyrins. *New J. Chem.* **2018**, *42*, 9956–9964.
 - (16) Boyd, P. D. W.; Reed, C. A. Fullerene–Porphyrin Constructs. **2005**, *38*, 235-242.
 - (17) Wang, R.; Qu, R.; Jing, C.; Zhai, Y.; An, Y.; Shi, L. Zinc Porphyrin/Fullerene/Block Copolymer Micelle for Enhanced Electron Transfer Ability and Stability. *RSC Adv.* **2017**,

- 7, 10100–10107.
- (18) D'Souza, F.; Ito, O. Supramolecular Donor–acceptor Hybrids of Porphyrins/Phthalocyanines with Fullerenes/Carbon Nanotubes: Electron Transfer, Sensing, Switching, and Catalytic Applications. *Chem. Commun.* **2009**, 33, 4913–4928.
- (19) Hu, Y.; Thomas, M. B.; Jinadasa, R. G. W.; Wang, H.; D'Souza, F. Competitive Energy and Electron Transfer in β -Functionalized Free-Base Porphyrin-Zinc Porphyrin Dimer Axially Coordinated to C₆₀: Synthesis, Supramolecular Formation and Excited-State Processes. *Chem. - A Eur. J.* **2017**, 23, 12805–12814.
- (20) Fukuzumi, S. Development of Bioinspired Artificial Photosynthetic Systems. *Phys. Chem. Chem. Phys.* **2008**, 10, 2283.
- (21) Sudhakar, K.; Gokulnath, S.; Giribabu, L.; Lim, G. N.; Trâm, T.; D'Souza, F. Ultrafast Photoinduced Charge Separation Leading to High-Energy Radical Ion-Pairs in Directly Linked Corrole-C₆₀ and Triphenylamine-Corrole-C₆₀ Donor-Acceptor Conjugates. *Chem. - An Asian J.* **2015**, 10, 2708–2719.
- (22) Zarrabi, N.; Obondi, C. O.; Lim, G. N.; Seetharaman, S.; Boe, B. G.; D'Souza, F.; Poddutoori, P. K. Charge-Separation in Panchromatic, Vertically Positioned Bis(Donor Styryl)BODIPY–aluminum(III) Porphyrin–fullerene Supramolecular Triads. *Nanoscale* **2018**, 10, 20723–20739.
- (23) Poddutoori, P. K.; Kandrashkin, Y. E.; Obondi, C. O.; D'Souza, F.; van der Est, A. Triplet Electron Transfer and Spin Polarization in a Palladium Porphyrin–fullerene Conjugate. *Phys. Chem. Chem. Phys.* **2018**, 20, 28223–28231.
- (24) Barrejón, M.; Arellano, L. M.; Gobeze, H. B.; Gómez-Escalonilla, M. J.; Fierro, J. L. G.; D'Souza, F.; Langa, F. N-Doped Graphene/C₆₀ Covalent Hybrid as a New Material for Energy Harvesting Applications. *Chem. Sci.* **2018**, 9, 8221–8227.
- (25) Obondi, C. O.; Lim, G. N.; Jang, Y.; Patel, P.; Wilson, A. K.; Poddutoori, P. K.; D'Souza, F. Charge Stabilization in High-Potential Zinc Porphyrin-Fullerene via Axial Ligation of Tetrathiafulvalene. *J. Phys. Chem. C* **2018**, 122, 13636–13647..
- (26) Follana-Berná, J.; Seetharaman, S.; Martín-Gomis, L.; Charalambidis, G.; Trapali, A.; Karr, P. A.; Coutsolelos, A. G.; Fernández-Lázaro, F.; D'Souza, F.; Sastre-Santos, Á. Supramolecular Complex of a Fused Zinc Phthalocyanine–zinc Porphyrin Dyad Assembled by Two Imidazole-C₆₀ Units: Ultrafast Photoevents. *Phys. Chem. Chem. Phys.*

- 2018**, *20*, 7798–7807.
- (27) Seetharaman, S.; Jang, Y.; KC, C. B.; Karr, P. A.; D'Souza, F. Peripheral Phenothiazine Induced Suppression of Charge Separation from the Singlet Excited Zinc Phthalocyanine to Coordinated C₆₀ in Supramolecular Donor–acceptor Conjugates. *J. Porphyr. Phthalocyanines* **2017**, *21*, 870–881.
- (28) Benitz, A.; Thomas, M. B.; D'Souza, F. Geometry-Controlled Photoinduced Charge Separation and Recombination in a *Trans*-A₂B₂ -Functionalized Donor-Acceptor Conjugate Composed of a Multimodular Zinc Porphyrin and Fullerene. *ChemPhotoChem* **2017**, *1*, 17–25.
- (29) Webre, W. A.; Gobeze, H. B.; Shao, S.; Karr, P. A.; Ariga, K.; Hill, J. P.; D'Souza, F. Fluoride-Ion-Binding Promoted Photoinduced Charge Separation in a Self-Assembled C₆₀ Alkyl Cation Bound Bis-Crown Ether-Oxoporphyrinogen Supramolecule. *Chem. Commun.* **2018**, *54*, 1351–1354.
- (30) Kumar, R.; Sankar, M. Synthesis, Spectral, and Electrochemical Studies of Electronically Tunable β -Substituted Porphyrins with Mixed Substituent Pattern. *Inorg. Chem.* **2014**, *53*, 12706–12719.
- (31) Pereira, A. M. V. M.; Alonso, C. M. A.; Neves, M. G. P. M. S.; Tomé, A. C.; Silva, A. M. S.; Paz, F. A. A.; Cavaleiro, J. A. S. A New Synthetic Approach to *N*-Arylquinolino[2,3,4-*at*]Porphyrins from β -Arylaminoporphyrins. *J. Org. Chem.* **2008**, *73*, 7353–7356.
- (32) Catalano, M. M.; Crossley, M. J.; Harding, M. M.; King, L. G. Control of Reactivity at the Porphyrin Periphery by Metal Ion Co-Ordination: A General Method for Specific Nitration at the β -Pyrrolic Position of 5,10,15,20-Tetra-Arylporphyrins. *J. Chem. Soc., Chem. Commun.* **1984**, *22*, 1535–1536.
- (33) Gao, G.-Y. ; Ruppel, J. V.; Allen, D. B.; Chen, Y.; Zhang, X. P. Synthesis of β -Functionalized Porphyrins via Palladium-Catalyzed Carbon–Heteroatom Bond Formations. Synthesis of β -Functionalized Porphyrins via Palladium-Catalyzed Carbon–Heteroatom Bond Formations: Expedient Entry into β -Chiral Porphyrins *J. Org. Chem.* **2007**, *72*, 9060-9066 .
- (34) Hauke, F.; Swartz, A.; Guldi, D. M.; Hirsch, A. Supramolecular Assembly of a Quasi-Linear Heterofullerene-porphyrin Dyad. *J. Mater. Chem.* **2002**, *12*, 2088–2094.
- (35) Grover, N.; Rathi, P.; Sankar, M. Spectral Investigations of *Meso*-Tetraalkylporphyrin-

- Fullerene Host-guest Complexes. *J. Porphyr. Phthalocyanines* **2015**, *19*, 997–1006.
- (36) D'Souza, F.; El-Khouly, M. E.; Gadde, S.; McCarty, A. L.; Karr, P. A.; Zandler, M. E.; Araki, Y.; Ito, O. Self-Assembled via Axial Coordination Magnesium Porphyrin-Imidazole Appended Fullerene Dyad: Spectroscopic, Electrochemical, Computational, and Photochemical Studies. *J. Phys. Chem. B* **2005**, *109*, 10107–10114.
- (37) Benitz, A.; Thomas, M. B.; D'Souza, F. Geometry-Controlled Photoinduced Charge Separation and Recombination in a *Trans*-A₂B₂-Functionalized Donor-Acceptor Conjugate Composed of a Multimodular Zinc Porphyrin and Fullerene. *ChemPhotoChem* **2017**, *1*, 5–5.
- (38) Dar, T. A.; Chahal, M. K.; Kumar, R. A.; Sankar, M. Synthesis, Electrochemical and Complexation Studies of Zn(II) Aryloxy porphyrins with Fullerene C₆₀. *J. Porphyr. Phthalocyanines* **2016**, *20*, 744–751.



CHAPTER 3

**HIGHLY ELECTRON DEFICIENT
TETRABENZOQUINONE APPENDED**

**Ni(II) AND Cu(II) PORPHYRINS:
SPECTRAL, SOLVATOCHROMISM,
ELECTROCHEMICAL REDOX AND
TUNEABLE F⁻ AND CN⁻ SENSING**



CHAPTER 3

HIGHLY ELECTRON DEFICIENT TETRABENZOQUINONE APPENDED Ni(II) AND Cu(II) PORPHYRINS: SPECTRAL, SOLVATOCHROMISM, ELECTROCHEMICAL REDOX AND TUNEABLE F⁻ AND CN⁻ SENSING

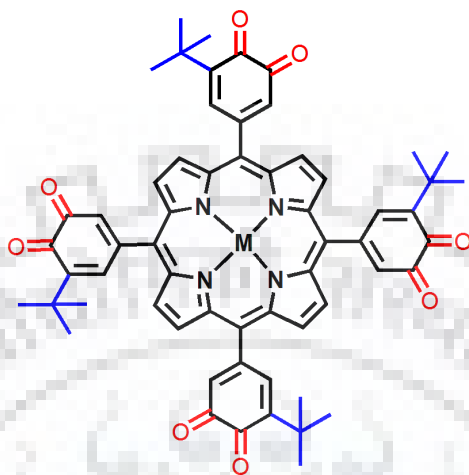
3.1 INTRODUCTION

Development of sensors for selective recognition of toxic anions, different metal ions, nitroaromatic explosives, organic ionic and neutral species or the enantiomers of chiral molecules through non-covalent bonding is of great importance due to applications in medical chemistry, environment protection, anti-terrorism and homeland security as well as pharmaceutical, food, cosmetic and pesticide industries [1]. Of the anionic species to be recognized and detected, CN⁻ and F⁻ have attracted considerable interest because the wide usage and toxicity associated with these ions [2]. In the last century the production and application of halides assumed an ever greater importance. In the fields of medicine, dentistry, plastics, pesticides, food, photography *etc.* many new halogen containing compounds have come into everyday use. Many assume that consuming fluoride is only an issue that involves dental health [3] and clinical treatment for osteoporosis [4,5]. But overexposure to fluoride is an endocrine disruptor that can affect bones, brain, thyroid gland, pineal gland and even blood sugar levels. Also, excess fluoride concentration causes acute gastric, fluorosis and kidney problems [6]. Cyanide anion is lethal in very small concentrations due to its ability to bind strongly to the active site of cytochrome c oxidase, which leads to the inhibition of the mitochondrial electron transport chain, and consequently to a decrease in the oxidative metabolism [7]. Cyanide ions could be absorbed through the lungs, skin, and gastrointestinal tract leading to vomiting, convulsions, loss of consciousness, and eventually death [8]. So the continuous release of cyanide ions into the environment through its increased usage in various industrial applications like metallurgy, mining, electroplating, polymer synthesis, petrochemicals and organic synthesis *etc.* is of great concern [9]. Hence both biological and

environmental aspects necessitate the development of cyanide and fluoride based receptors.

Porphyrinoids are a class of tetrapyrrole pigments that widely occur in nature. These pigments are highly coloured and exhibit varying degrees of π -conjugation leading to different nonplanar conformations of the porphyrin macrocycle, which are responsible for a variety of biological functions [10]. Porphyrins substituted with benzoquinone [11] and hemiquinone [12] groups were first prepared by Milgrom and co-workers. *Meso*-tetrakis(3,5-di-*tert*-butyl-4-oxo-2,5-cyclohexa-dienylidene)porphyrinogen exist as highly puckered species [13]. The chemistry of these porphyrinogens and their N,N'-substituted oxoporphyrinogens have been very much explored and also bind to various guest molecules at their pyrrolic -NH as well as quinonoid C=O. Oxoporphyrinogens are variously available as sensing probes for anions, [14] water in THF, [15] to differentiate organic solvents, [16] and chiral molecular recognition [17]. Among the class of the porphyrinoids, calixpyrroles, [18] phlorins, [19] corroles, [20] sapphyrins, [21] N-confused porphyrins, [22] oxoporphyrinogens [23] and tetraphenylporphyrins [24] are excellent multifunctional candidates for a great variety [25,26] of anion sensor applications *via*. -NH groups of the tetrapyrrole units. At earlier stage, porphyrin-*o*-quinone has been utilized for photoinduced electron transfer but its synthesis involves tedious multiple steps. In 2014, Hill *et al.* has reported the convenient synthesis of Cu(II) and Ni(II) complexes of 5,10,15,20-tetrakis(3,4-dioxo-5-*t*-butylcyclohexa-1,5-dienyl)porphyrin (diOxP) under β -nitration conditions for the Cu(II) or Ni(II) complexes of *meso*-tetrakis(3,5-di-*t*-butyl-4'-hydroxyphenyl)porphyrin [27]. Cu(II) or Ni(II) complexes of 5,10,15,20-tetrakis(3,4-dioxo-5-*t*-butylcyclohexa-1,5-dienyl)porphyrin (diOxPM, M = Ni(II), Cu(II)) was prepared by modified methods using copper nitrate in acetic anhydride-acetic acid mixture in chloroform. The rapid oxidation converts phenol substituents to electron withdrawing *o*-quinone groups. The electron-withdrawing effect of benzoquinone groups reduces the propensity of the macrocycle to undergo electrophilic substitution. The thorough investigation of electrochemical properties of OxP, diOxPM (M = Cu(II), Ni(II)) and their respective metallotetraphenylporphyrins leads us to a important observation that first reduction for diOxPM (M = Cu, Ni) is very much

anodically shifted as compared to oxoporphyrinogen (OxP) and porphyrin precursor. We have utilized these electron-deficient systems to interact with basic anions.



M = Ni(II); Ni-diOxP (1)
M = Cu(II); Cu-diOxP (2)

Chart 3.1 Molecular Structures of Synthesized Porphyrins.

3.2 EXPERIMENTAL SECTION

3.2.1 Reagents

3,5-di-*tert*-butyl-4-hydroxybenzaldehyde was purchased from HiMedia, India and used as received. All solvents employed in the present work were of analytical grade and distilled or dried before use. Silica gel (100-200 mesh) was purchased from Rankem and used as received. The tetrabutylammonium salts (TBAX, X = CN⁻, F⁻, Cl⁻, Br⁻, I⁻, HSO₄⁻, OAc⁻, H₂PO₄⁻, ClO₄⁻, PF₆⁻ and NO₃⁻) were purchased from Alfa Aesar and used as received. Dry CH₂Cl₂ for CV studies was distilled thrice from CaH₂ and toluene (for UV-Visible spectral studies) was dried and distilled from a sodium-benzophenone mixture. All measurements were performed in triple distilled CH₂Cl₂ containing 0.1M TBAPF₆ as supporting electrolyte, which was degassed by argon gas purging. Cyanide detection studies were carried out in distilled toluene at 298 K. Rest reagents and methods are same as discussed in Chapter 2.

3.2.2 Instrumentation and Methods

Optical absorption spectra were recorded using an Agilent Cary 100 spectrophotometer using a pair of quartz cells 10 mm path length. ¹H-NMR spectra were recorded using a Bruker AVANCE 500 MHz and JEOL ECX 400 MHz spectrometers in CDCl₃. MALDI-TOF-MS spectra were

measured using a Bruker UltrafleXtreme-TN MALDI-TOF/TOF spectrometer using HABA as a matrix. The ground state geometry optimization was carried out by DFT calculations using B3LYP functional with LANL2DZ basis set using G09 program suite. Electrochemical measurements were carried out using CH instrument (CH 620E). A three electrode assembly was used consisted of a platinum working electrode, Ag/AgCl as a reference electrode and a Pt-wire as a counter electrode. All measurements were performed in triple distilled CH₂Cl₂ containing 0.1M TBAPF₆ as supporting electrolyte, which was degassed by argon gas purging. Cyanide detection studies were carried out in distilled toluene at 298 K.

3.2.3 Synthetic Procedures

Preparation of 5,10,15,20-tetrakis(3,4-dioxo-5-*t*-butylcyclo-hexa-1,5-dienyl)porphyrinatocopper(II)/nickel(II):

5,10,15,20-*tetrakis*(3,5-di-*tert*-butyl-4-hydroxyphenyl)-porphyrinatocopper(II)/nickel(II) (100 mg) was dissolved in 20 mL of distilled chloroform. To this, 1 ml of acetic acid was added and stirred for 10 minutes. Solution of copper nitrate (12 mg) in acetic anhydride (5 ml) added dropwise after that reaction mixture was stirred at room temperature up to 2 h. After rota evaporation reaction mixture was washed with NaHCO₃ followed by extraction with CHCl₃. The crude product of porphyrin was chromatographed on silica gel column using CHCl₃/1-2% CH₃OH. A black amorphous powder of porphyrin obtained with (54-59 mg) 54-59% yield.

Ni-diOxP: Yield: 54%. UV-Vis. λ_{\max} (nm), (log ϵ): 397 (5.12), 501 (4.42), 611 (4.01). ¹H NMR in CDCl₃ δ (ppm): 9.27 (s, 8H, β -pyrrole-H), 7.54 (s, 4H, *meso-m*-phenyl-H), 6.95 (s, 4H, *meso-m*-phenyl-H), 1.37 (s, 36H, *meso-o-t*-butylphenyl-H) MALDI-TOF-MS (m/z): found [M+H]⁺ 1015.78, calcd. 1015.32.

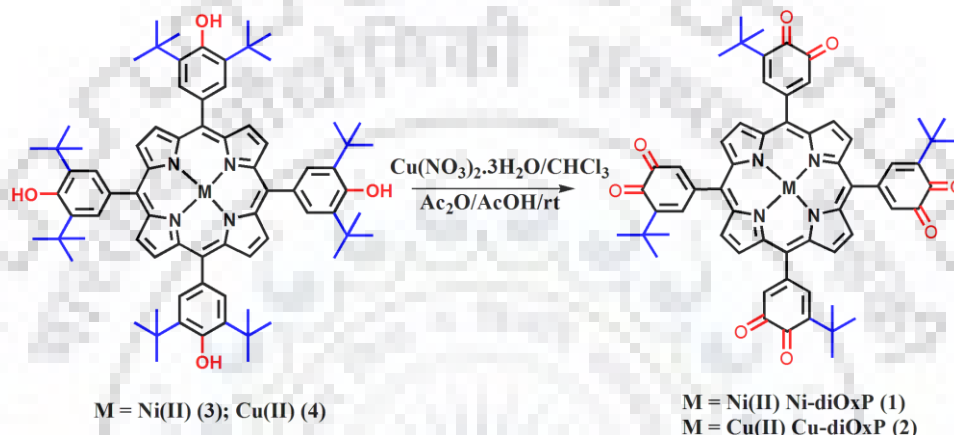
Cu-diOxP: Yield: 59%. UV-Vis. λ_{\max} (nm), (log ϵ): 401 (4.94), 509 (4.15), 630(3.76). MALDI-TOF-MS (m/z): found [M+H]⁺ 1020.76, calcd. 1020.32.

3.3 RESULTS AND DISCUSSION

3.3.1 Synthesis and Characterization

5,10,15,20-tetrakis(3,4-dioxo-5-*t*-butylcyclohexa-1,5-dienyl)porphyrinatonickel(II) (Ni-diOxP) and 5,10,15,20-tetrakis(3,4-dioxo-5-*t*-butylcyclohexa-1,5-

dienyl)porphyrinatocopper (Cu-diOxP) have been prepared from their respective nickel and copper 5,10,15,20-tetrakis(3,5-di-*t*-butyl-4-hydroxyphenyl)porphyrin under nitration conditions using acetic anhydride-acetic acid mixture in chloroform (Scheme 3.1). Ni-diOxP (**1**) and Cu-diOxP (**2**) exhibit brown-black colours in both solid and solution state in contrast to deep-purple of the parent porphyrins due to strong effect of the *o*-quinone substituents on the porphyrin chromophore relative to simple phenyl substituents.



Scheme 3.1 Synthetic Routes for the Ni-diOxP (**1**) and Cu-diOxP (**2**) under β -Nitration Conditions.

Electronic absorption spectra of porphyrins 1-3 are shown in Figure 3.1. The most important feature is the increased absorbance across the entire visible range from 350 to nearly 700 nm, which accounts for their dark colours.

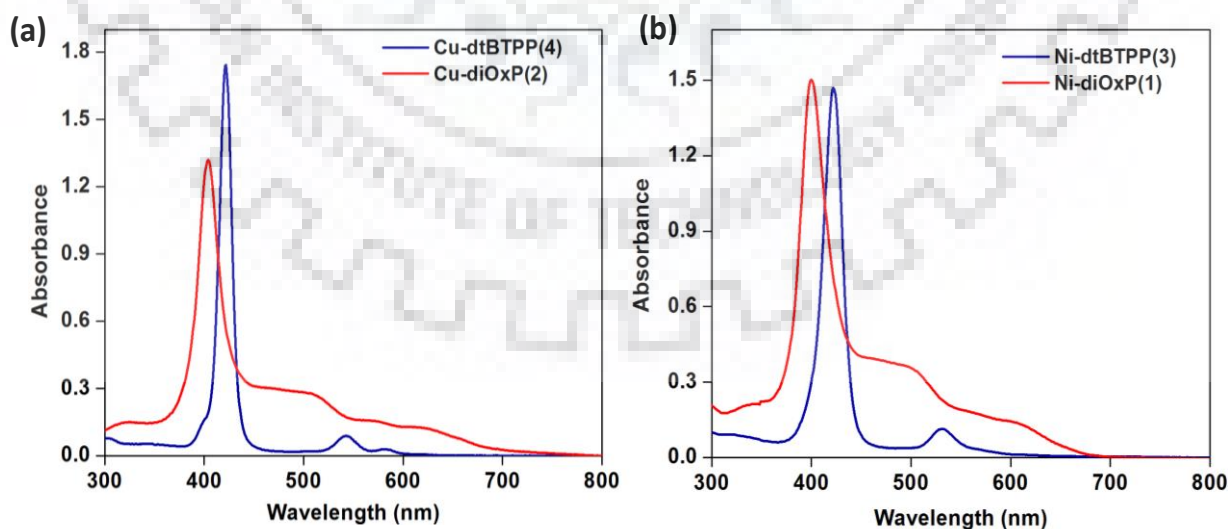


Figure 3.1 Absorption Spectra of **1-4** Porphyrins in CH_2Cl_2 at 298 K.

3.3.2 Cyclic Voltammetric Studies

To examine the effect of di-quinone and nonplanarity of the macrocycle on electrochemical redox potentials, we have carried out cyclic voltammetric studies. Cyclic voltammograms of **1–4** in CH_2Cl_2 containing 0.1 M TBAPF₆ as supporting electrolyte are shown in Figures 3.2 and A8, A9, Appendix-II. The cyclic voltammograms and differential pulse voltammetry of **1** and **2** in CH_2Cl_2 exhibit two well separated reductions under similar conditions, the corresponding MTPP (M = Ni(II) and Cu(II)) derivatives were also examined. The electrochemical redox data (vs Ag/AgCl) is listed in Table 3.1. The first two processes corresponding to the reduction of the appended benzoquinone are located at -0.372, -1.072 (for **1**) and -0.388, -1.204 (for **2**) vs. Ag/AgCl, respectively at a scan rate of 0.1 Vs⁻¹. Scanning the potential in the positive direction revealed the first porphyrin based oxidation at 1.384 V for **1** and 1.33 V for **2**, respectively.

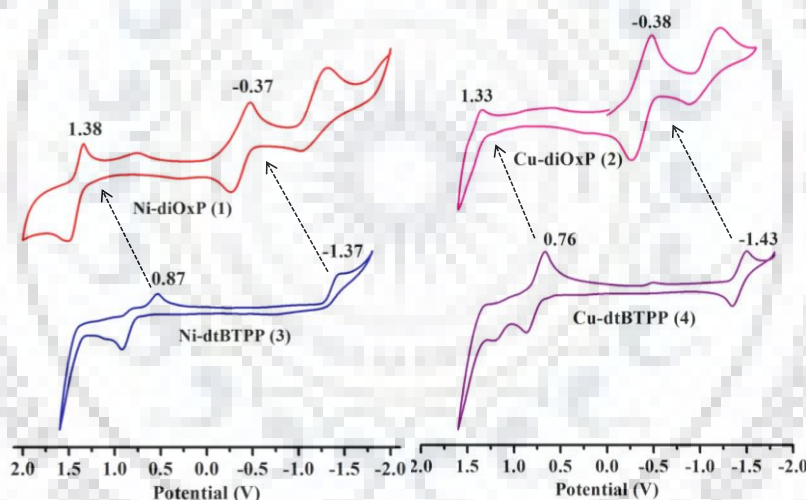


Figure 3.2 Cyclic Voltammograms of **1-4** in CH_2Cl_2 Containing 0.1 M TBAPF₆ as the Supporting Electrolyte using Ag/AgCl as the Reference Electrode.

These oxidations were more difficult compared to simple Cu and Ni porphyrins due to the presence of the four electron deficient *o*-quinone entities directly attached to the porphyrin macrocycle. The electrochemical studies revealed that *meso*-tetrakis(3,4-benzoquinone)-substituted metalloporphyrin ring is electron deficient by ~1.1 V as compared to TDtBPPM (M = Cu, Ni) and ~0.94 V as compared to oxoporphyrinogen, respectively.

Table 3.1 Electrochemical Redox Data (vs Ag/AgCl) of Synthesized Porphyrins (**1-4**) in CH₂Cl₂ Containing 0.1 M TBAPF₆ at 298 K with the Scan Rate of 0.1 V/s.

Porphyrin	Oxidation (V)		Reduction (V)		ΔE (V)
	I	II	I	II	
NiTPP	1.02	1.32	-1.28	-1.72	2.30
CuTPP	0.97	1.35	-1.30	-1.71 ^a	2.27
Ni-dtBTPP (3)	0.87 ^a		-1.37 ^a		2.24
Cu-dtBTPP (4)	0.76		-1.43		2.19
Ni-diOxP (1)	1.38		-0.37	-1.07 ^a	1.75
Cu-diOxP (2)	1.33		-0.38	-1.204 ^a	1.71
Ox[T(DtBHP)P]	0.48	0.27	-1.33		1.81

^a Irreversible peak potential

3.3.3 Solvatochromism Studies

Solvatochromism is the term for changes in electronic spectra of compounds when dissolved in different solvents and is related to changes in the electronic structure in the subject molecules caused by variation of solvent polarity or other interactions, especially hydrogen bonding [28,29]. We have taken the absorption spectra of **1** and **2** in different solvents such as polar, non-polar and basic. For compounds **1**, absorption maxima in different solvents appear in the range 395-445 nm, and this is illustrated by the spectra shown in Figure 3.3 while the positions of the absorption maxima in different solvents are summarized in Table A1-A2, Appendix-II. The *meso*-tetrakis(3,4-benzoquinone)-substituted metalloporphyrins (**1** and **2**) exhibited red-shifted absorption spectra in basic solvents like piperidine, Et₃N and pyridine unlike to other solvents like toluene, CHCl₃, ethyl acetate etc. The systems also showed change in hue for basic solvents such as piperidine, Et₃N and pyridine. This observation supports the axial ligation of basic solvents to metal atom of electron deficient benzoquinone system. This output directs to check the response of toxic anions towards these electron deficient *meso*-tetrakis(3,4-benzoquinone) appended porphyrin metal complexes (**1** and **2**).

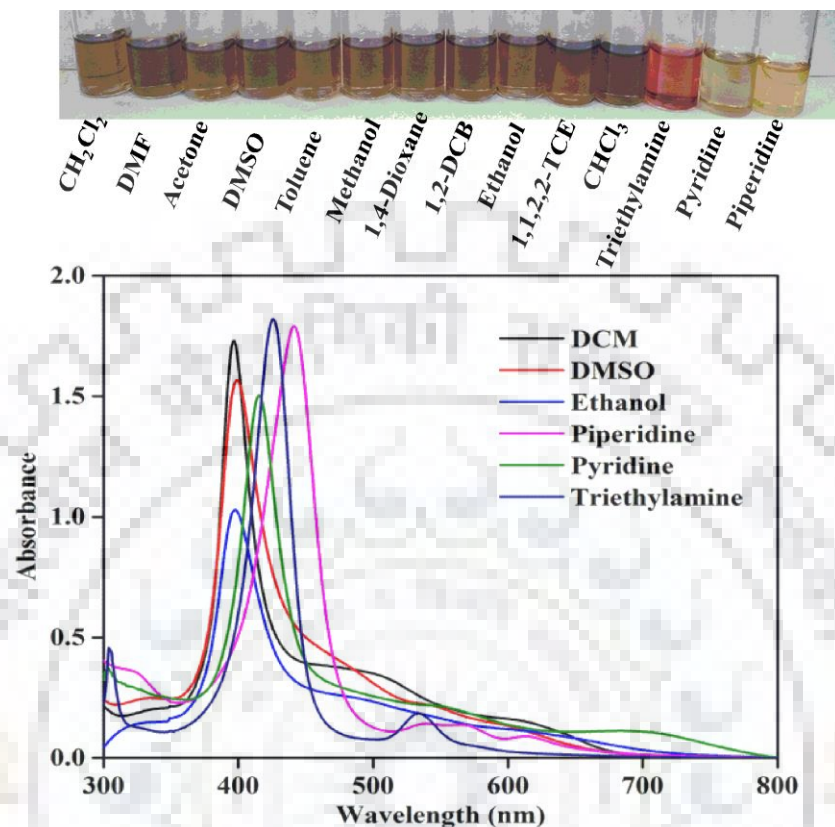


Figure 3.3 Electronic Absorption Spectrum of **1** in Solvents of Various Polarities.

3.3.4 Anion Binding Studies

The anion recognition properties of **1** and **2** were studied in toluene with different anions such as CN^- , F^- , Cl^- , Br^- , I^- , NO_3^- , HSO_4^- , PF_6^- , ClO_4^- , BF_4^- , CH_3COO^- and H_2PO_4^- ions using UV-visible spectroscopy with the addition of the aliquot anion in the form of TBA salt. Among all, CN^- and F^- selectively interacted with **1** and **2** by showing a considerable change in the UV-visible spectra, as shown in Figures 3.4 and A10, A11, Appendix-II, whereas there were no shifts observed for the other anions as shown in Figure 3.5 and A12, Appendix-II. As we increased the concentration of CN^- ions (0 - 1.53×10^{-4} M, 4.8 equiv.), the decrement in the absorbance of **1** was observed at 400 nm with the shift of wavelength at 427 nm with bathochromic shift of 27 nm. The B-H plot (Figure 3.4b inset) shows a straight line between $1/[\text{CN}^-]^2$ and $1/(A_0-A)$, which indicates 1 : 2 (porphyrin-to-anion) stoichiometry. The binding constant was found to be $5.01 \times 10^8 \text{ M}^{-2}$.

Upon addition of F^- ions ($0-1.41 \times 10^{-3}$ M, 45 equiv.) to **1**, the absorption band at 400 nm shifts to 424 nm with a binding constant of 2.5×10^6 M^{-2} . Moreover, the similar behaviour was observed for **2** with CN^- and F^- ions as shown in Figures A10, A11, Appendix-II. Table 3.2 lists the association constants obtained for CN^- , F^- ions with **1** and **2** in toluene at 298 K. From the binding constant and amount of toxic ions used to saturate the spectrum in each case lead us to important conclusion that cyanide ions interacts effectively with **1** and **2**. Our group has recently reported the ability of electron-deficient nickel porphyrins for cyanide sensing through axial ligation [30]. There are only few reports present in literature for the basic anions detection *via*. axial binding to metalloporphyrins [31]. These *meso*-tetrakis(3,4-benzoquinone) substituted metalloporphyrins (**1** and **2**) also binds to both F^- and CN^- ions axially.

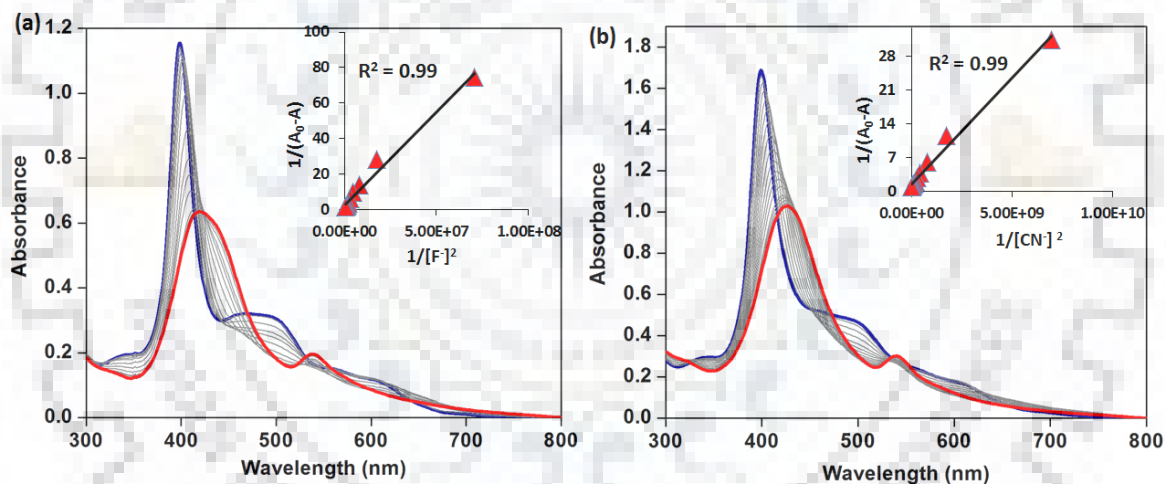


Figure 3.4 UV-Visible Titration of **1** (3.14×10^{-5} M) (a) Upon Addition of F^- Ions ($0-1.14 \times 10^{-3}$ M) and (b) Upon Addition of CN^- ions ($0-1.53 \times 10^{-3}$ M) in Toluene Medium at 298 K. Inset Shows the Corresponding B-H Plot.

Table 3.2 Binding Constant Data of Electron Deficient *Meso*-tetrakis(3,4-benzoquinone)-substituted Porphyrins in Toluene at 298 K

Porphyrin	Binding Constant (M^{-2})	
	CN^{-}	F^{-}
Ni-diOxP (1)	5.01×10^8	2.50×10^6
Cu-diOxP (2)	1.50×10^9	3.25×10^7

In order to evaluate the binding of only cyanide and fluoride ions with **1** and **2**, absorption spectral changes upon addition of excess of various anions including F^{-} , Cl^{-} , Br^{-} , NO_3^{-} , $H_2PO_4^{-}$, AcO^{-} , I^{-} , HSO_4^{-} , ClO_4^{-} , CN^{-} and PF_6^{-} were studied.

Characteristic spectral changes were observed only for cyanide and fluoride ions (Figures 3.5 and A12, Appendix-II). Competition experiments to ascertain the selectivity of the probes in the presence of the other interfering anions were performed in toluene. In these measurements, 10 equiv. of the other interfering anions (excess) were used. A representative selectivity bar charts observed for **1** and **2** are shown in Figures 3.6, 3.7 and A13, A14, Appendix-II.

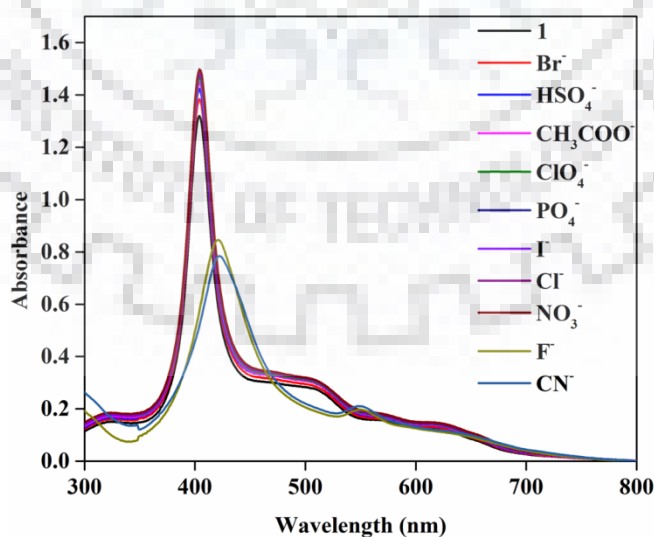


Figure 3.5 Absorption Spectra of **1** ($3.14 \times 10^{-5}M$) in the Presence of Different Anions.

It clearly confirms the exclusive cyanide and fluoride ion detecting ability of these porphyrins even in the presence of all interfering anions in the same solution. We have also recorded the ^1H NMR spectra after addition of CN^- and F^- ions into Ni-diOxP (**1**). On increasing the conc. of F^- ions from 0 to 2 equiv., there is no change in position of peaks. Even upto 20 equiv. of F^- ions does not change the spectrum and the similar behaviour is observed for CN^- ions also as shown in Figure A15, Appendix-II. To further support the binding mechanism, cyclic voltammetric studies have been done after addition of CN^- and F^- ions. The first reduction potential shifted cathodically after the addition of cyanide ions to **1** and **2** as shown in Figures A16-A17, Appendix-II. The cathodic shift in reduction potential supports the decrease of overall electron deficiency of complex. The spectral changes as well as CV and DPV changes lead to axial-ligation of F^- and CN^- ions to these metallated electron-deficient benzoquinone substituted porphyrins. But Ni-dtBTPP (**3**) and Cu-dtBTPP (**4**) do not show any axial-ligation with F^- and CN^- ions (Figures A18-A19, Appendix-II). The excess addition of F^- ions (> 200 equiv.) changed both Ni-dtBTPP (**3**) and Cu-dtBTPP (**4**) from porphyrin state to porphodimethene (Figures A20, A21, Appendix-II). The switching between porphyrin and porphodimethene state upon excess addition of fluoride ions are very well studied in literature in case of anti-oxidant porphyrins [32]. Whereas, addition of more than 200 equiv. of CN^- ions does not affect the spectra of **3** and **4** (Figures A22, A23, Appendix-II). In case of metallo-benzoquinone substituted porphyrin, anion sensing operation is based on the variation of its state from porphyrin to electron-deficient quinone and also *via* the ability of electron deficient dioxo-porphyrinogen to accommodate basic guests through axial-ligation. The electron deficiency of these systems concluded from the ability of benzoquinone substituted metalloporphyrin system towards fluoride ion in addition to most basic cyanide ions. Also, anion binding studies in different solvents shows only red-shift in absorption spectra for all the solvents except basic solvents. In basic solvents the bands are already red-shifted due to axial ligation of basic solvents. The broadening of UV-Vis spectrum was also observed after the addition of anions. So we can propose charge-transfer interactions between these donor-acceptor adducts. The FWHM for Cu-dtBTPP (39.7 nm) changes to 69 nm ($2 \cdot 2\text{F}^-$) and 63 nm ($2 \cdot 2\text{CN}^-$). FWHM for Ni-

dtBTPP (86 nm) changes to 69 nm ($1 \cdot 2F^-$) and 93 nm ($1 \cdot 2CN^-$) which supports the charge-transfer interactions between porphyrin metal centre and anions [33-34].

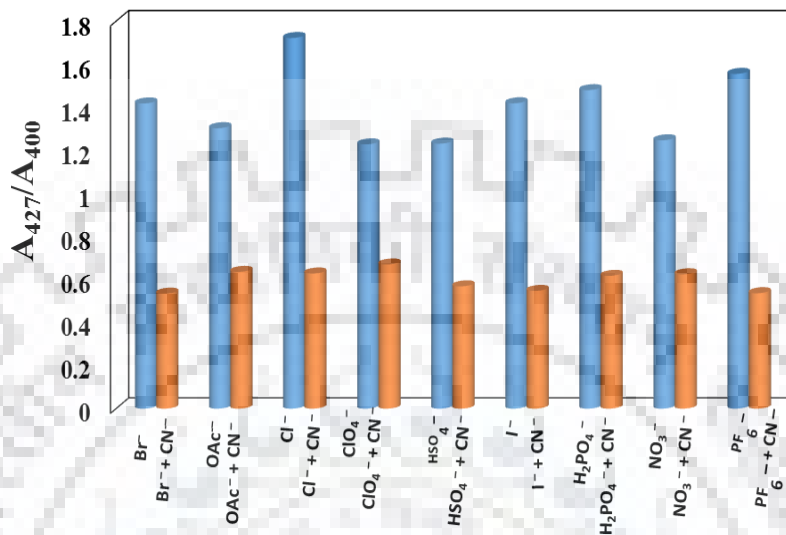


Figure 3.6 Ratiometric Absorbance Changes (A_{427}/A_{400}) of **1** ($3.14 \times 10^{-5}M$) on Addition of 4 equiv of CN^- and 10 equiv. of Other Anions. Blue Bars Indicate the Blank and in the Presence of Other Interfering Anions, and Brown Bars Indicate the Addition of CN^- to the Interfering Anions.

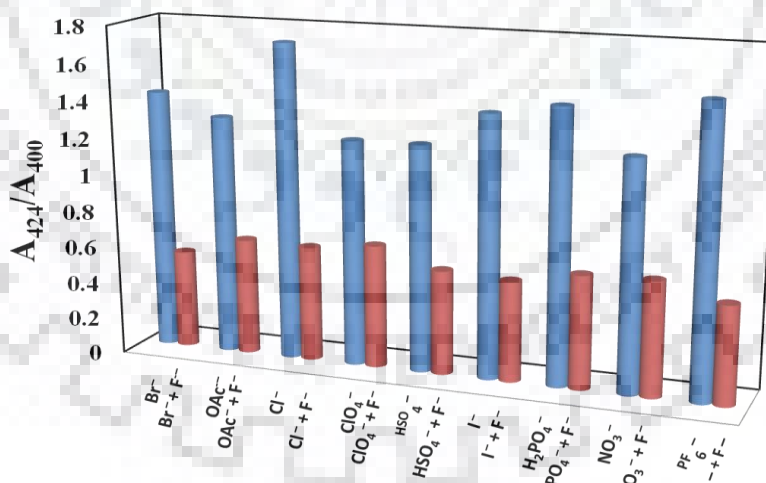


Figure 3.7 Ratiometric Absorbance Changes (A_{424}/A_{400}) of **1** ($3.14 \times 10^{-5}M$) on Addition of Excess equiv of F^- and Other Anions. Blue Bars Indicate the Blank and in the Presence of Other Interfering Anions, and Brown Bars Indicate the Addition of F^- to the Interfering Anions.

3.3.5 Computational Studies

The ground state geometry optimization of **1** and **2** in gas phase was carried out by DFT calculations using the B3LYP functional with LANL2DZ basis set. Notably, **1** exhibited quasi planar conformation with the displacement of β -pyrrole carbons, $\Delta C_{\beta} = \pm 0.212 \text{ \AA}$ and the 24 atoms core, $\Delta 24 = \pm 0.23 \text{ \AA}$, whereas **2** have shown planar conformation of the porphyrin macrocycle ($\Delta C_{\beta} = \pm 0.186 \text{ \AA}$ and $\Delta 24 = \pm 0.085 \text{ \AA}$). Figures A24, A25, Appendix-II, represents fully optimized geometries of **1** and **2**. Figure 3.8 represent the fully optimized geometry of **1**•2CN⁻ which exhibit planar conformation. The pictorial views of frontier molecular orbitals (FMOs) of **1**, and **1**•2CN⁻ are shown in Figure 3.9. As expected for porphyrins, the HOMOs and LUMOs of compounds **1-2** were all π -orbitals. But in contrast to porphyrins, the HOMO orbitals for compounds **1** and **2** were found to be mainly on the porphyrin 24-atom π -ring system, and LUMO spread only on benzoquinone rings. Switching of these orbitals occur upon cyanide binding. As shown in Figure 3.9, for **1**•2CN⁻, HOMO spreads all over the host-guest assembly.

3.3.6 Cyanide Sensing in Aqueous Media

Due to poisonous nature of cyanide ion and in order to find out the practical applicability of synthetic probe, we have tested the toxic ion ability of these systems in H₂O. Potassium cyanide was dissolved in water and after that 18-crown-6 was added into it, to capture K⁺. This solution was added into toluene solution of Ni-diOxP (**1**) and Cu-diOxP (**2**), respectively. The UV-Vis spectra shifted for each system due to axial ligation of cyanide ion as shown in Figure 3.10 and Figure A26, Appendix-II. However, addition of aqueous solution of KF and 18-crown-6 does not bring about any spectral changes **1** and **2** because of strong hydration of fluoride ion. These observations pave a new pathway for the selective detection of CN⁻ ions among other ions in aqueous medium. Ratiometric studies to check the selectivity of the probes towards CN⁻ ions in the presence of the other interfering anions were also performed. A representative selectivity bar charts observed for **1** and **2** clearly confirms the exclusive cyanide sensing ability of these porphyrins even in the presence of all interfering anions in aqueous media as shown in Figures A27, A28, Appendix-II.

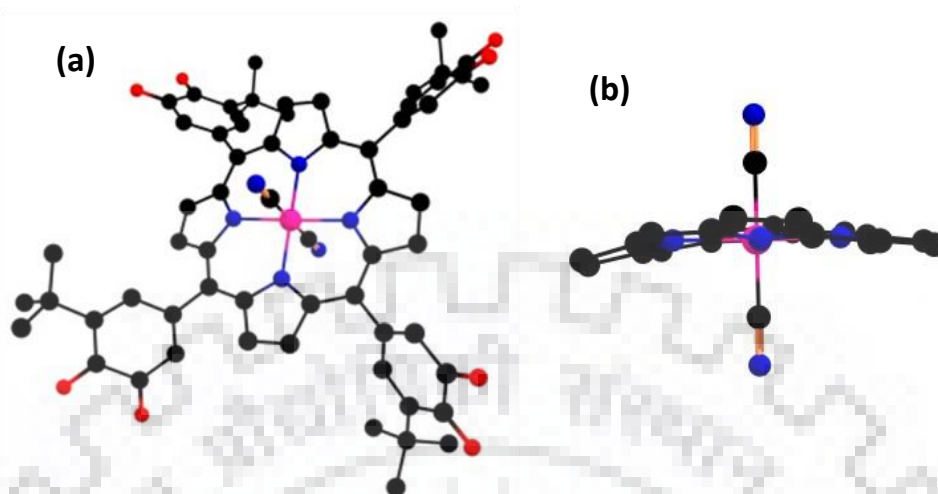


Figure 3.8 B3LYP/LANL2DZ-Optimized Geometry Showing (a) Top as well as (b) Side View of Ni-diOxP.2CN⁻; Hydrogen are Omitted for Clarity. In the Side View *Meso*-phenyl Substituents are not Shown Omitted for Clarity.

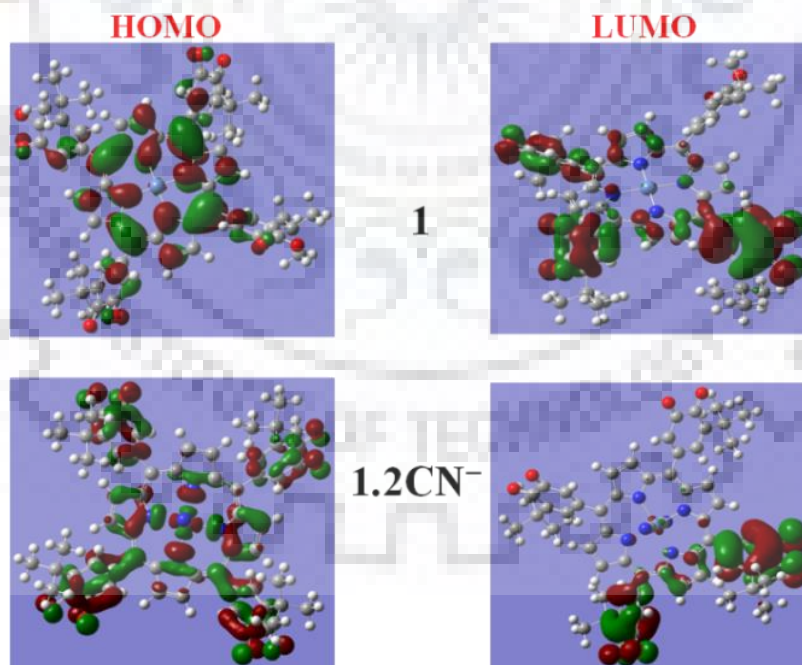


Figure 3.9 Pictorial Views of Frontier Molecular Orbitals (FMOs) of 1 and 1.2CN⁻.

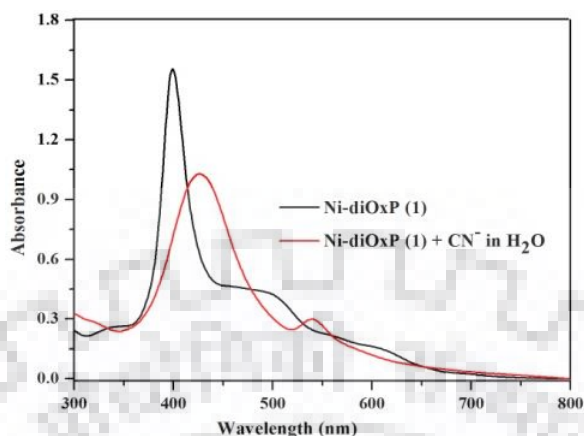


Figure 3.10 UV-Visible Spectra of **1** and 1.2CN^- . After Addition of Aqueous Solution of KCN and 18-crown-6.

3.4 CONCLUSIONS

In conclusion, we synthesized tetrabenzoquinone appended Ni(II) and Cu(II) porphyrins and characterized by various spectroscopic techniques. These porphyrins exhibited strong solvatochromism behavior in nitrogenous bases through axial coordination. Further, we studied the anion sensing properties of tetrabenzoquinone appended Ni(II) and Cu(II) porphyrins. The electrochemical studies revealed that *meso*-tetrakis(3,4-benzoquinone)-substituted metalloporphyrin ring is electron deficient by ~ 1.1 V as compared to TDtBPPM ($M = \text{Cu}$ and Ni) and nearly 0.94 V as compared to oxoporphyrinogen, respectively and therefore binds to less basic F^- ions also in addition to highly basic cyanide ions through axial ligation mechanism. These porphyrins act as F^- and CN^- chemosensor in nonaqueous media and selective CN^- sensor in aqueous medium due to high solvation of F^- ions in aqueous media even in presence of all other interfering anions in excess.

3.5 REFERENCES

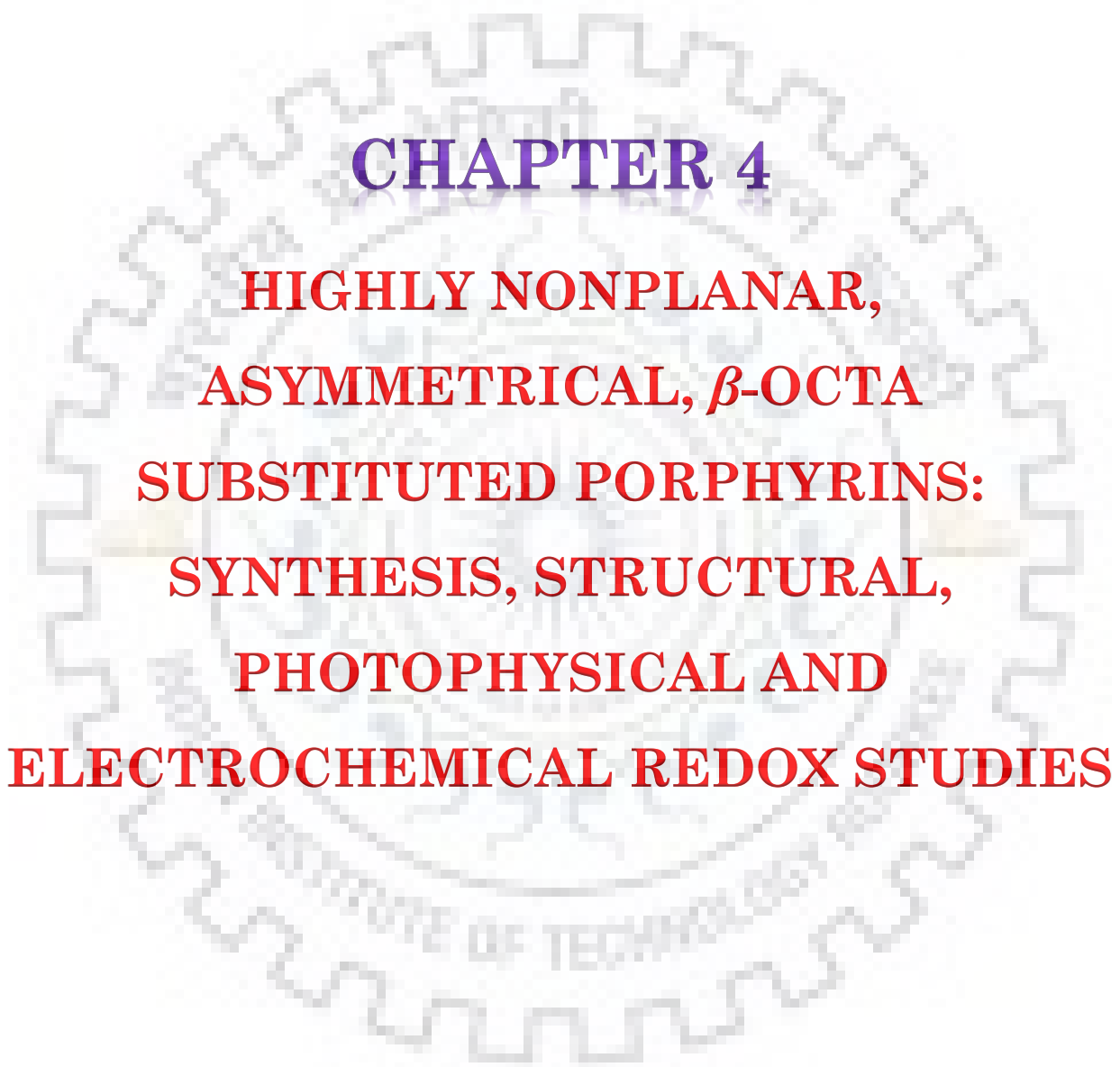
- (1) Ding, Y.; Zhu, W.-H.; Xie, Y. Development of Ion Chemosensors Based on Porphyrin Analogues. *Chem. Rev.* **2017**, *117*, 2203–2256.
- (2) Lin, Q.; Lu, T.-T.; Zhu, X.; Sun, B.; Yang, Q.-P.; Wei, T.-B.; Zhang, Y.-M. A Novel Supramolecular Metallogel-Based High-Resolution Anion Sensor Array. *Chem. Commun.*

- 2015, 51, 1635–1638.
- (3) Kirk, K. L. The Halogens: Discovery, Occurrence, and Biochemistry of the Free Elements. In *Biochemistry of the Elemental Halogens and Inorganic Halides*; Springer US: Boston, MA, 1991.
 - (4) Kleerekoper, M. The Role of Fluoride in the Prevention of Osteoporosis. *Endocrinol. Metab. Clin. North Am.* **1998**, 27, 441–452.
 - (5) Briançon, D. Fluoride and Osteoporosis: An Overview. *Rev. rhum.* **1997**, 64, 78–81.
 - (6) Michigami, Y.; Kuroda, Y.; Ueda, K.; Yamamoto, Y. Determination of Urinary Fluoride by Ion Chromatography. *Analytica Chimica Acta* **1993**, 274, 299–302.
 - (7) Wang, F.; Wang, L.; Chen, X.; Yoon, J. Recent Progress in the Development of Fluorometric and Colorimetric Chemosensors for Detection of Cyanide Ions. *Chem. Soc. Rev.* **2014**, 43, 4312–4324.
 - (8) Baud, F. J. Cyanide: Critical Issues in Diagnosis and Treatment. *Hum. Exp. Toxicol.* **2007**, 26, 191–201.
 - (9) Chahal, M. K.; Sankar, M. Porphyrin Chemodosimeters: Synthesis, Electrochemical Redox Properties and Selective “naked-Eye” Detection of Cyanide Ions. *RSC Adv.* **2015**, 5, 99028-99036.
 - (10) Shelnutt, J. A.; Song, X.-Z.; Ma, G.-J.; Jia, S.-L.; Jentzen, W.; Medforth, C. J. Nonplanar Porphyrins and their Significance in Proteins. *Chem. Soc. Rev.* **1998**, 27, 31–42.
 - (11) Milgrom, L. R. Synthesis of Some New Tetra-Aryl Porphyrins for Studies in Solar Energy Conversion. Part 2. Asymmetric Porphyrins. *J. Chem. Soc. Perkin Trans. 1*, **1984**, 1483–1487.
 - (12) Yamada, Y.; Hiraga, K.; Tanaka, K. Metal-Induced Dynamic Conformational and Fluorescence Switch of Quinone-Appended Zn-Porphyrin. *J. Porphyrins Phthalocyanines* **2015**, 19, 344–351.
 - (13) Hill, J. P.; Hewitt, I. J.; Anson, C. E.; Powell, A. K.; Mccarty, A. L.; Karr, P. A.; Zandler, M. E.; D’souza, F. Highly Nonplanar, Electron Deficient, N-Substituted Tetra-Oxocyclohexadienylidene Porphyrinogens: Structural, Computational, and Electrochemical Investigations. *J. Org. Chem.* **2004**, 69, 5861–5869.
 - (14) Chahal, M. K.; Sankar, M. Switching between Porphyrin, Porphodimethene and

- Porphyrinogen Using Cyanide and Fluoride Ions Mimicking Volatile Molecular Memory and the “NOR” Logic Gate. *Dalton Trans.* **2016**, *45*, 16404–16412.
- (15) Ishehara, S.; Iyi, N.; Labuta J.; Deguchi, K.; Ohki, S.; Tansho, M.; Shimizu, T.; Yamauchi, P.; Sahoo, M.; Naito M.; Abe, H.; Hill, J. P.; Ariga, K. Naked-Eye Discrimination of Methanol from Ethanol using Composite Film of Porphyrinogen and Layered Double Hydroxide. *ACS Appl. Mater. Interfaces.* **2013**, *5*, 5927-5930.
- (16) Ishihara, S.; Iyi, N.; Labuta, J.; Deguchi, K.; Ohki, S.; Tansho, M.; Shimizu, T.; Yamauchi, Y.; Sahoo, P.; Naito, M.; et al. Naked-Eye Discrimination of Methanol from Ethanol Using Composite Film of Oxoporphyrinogen and Layered Double Hydroxide. *ACS Appl. Mater. Interfaces* **2013**, *5*, 5927–5930.
- (17) Shundo, A.; Labuta, J.; Hill, J. P.; Ishihara, S.; Ariga, K. Nuclear Magnetic Resonance Signaling of Molecular Chiral Information Using an Achiral Reagent. *J. Am. Chem. Soc.* **2009**, *131*, 9494–9495.
- (18) Sessler, J. L.; Cho, W. S.; Gross, D. E.; Shriver, J. A.; Lynch, V. M.; Marquez M. Anion Binding Studies of Fluorinated Expanded Calixpyrroles. *J. Org. Chem.* **2005**, *70*, 5982-5986.
- (19) Bruce, A. M.; Weyburne, E. S.; Engle, J. T.; Ziegler, C. J.; Geier, G. R. Phlorins Bearing Different Substituents at the Sp³-Hybridized Meso-Position. *J. Org. Chem.* **2014**, *79*, 5664-5672.
- (20) Zhang, Z.; Yu, H.-J.; Huang, H.; Wang, H.-H.; Wu, S.; Liu, H.-Y.; Zhang, H.-T. The Photodynamic Activity and Toxicity Evaluation of 5,10,15-Tris(Ethoxycarbonyl)Corrole Phosphorus(V) in Vivo and in Vitro. *Eur. J. Med. Chem.* **2019**, *163*, 779–786.
- (21) Chatterjee, T.; Srinivasan, A.; Ravikanth, M.; Chandrashekar, T. K. Smaragdyrins and Sapphyrins Analogues. *Chem. Rev.* **2017**, *117*, 3329–3376.
- (22) Khodov, I. A.; Malteeva, O. V.; Klochkov, V. V.; Koifmanac, O. I.; Mamardashvili, N. Zh. N-Confused porphyrins: complexation and ¹H NMR studies. *New J. Chem* **2017**, *41*, 7932-7937.
- (23) Hill, J. P.; Labuta, J.; Ishihara, S.; Richards, G. J.; Xie, Y.; D’Souza, F.; Ariga, K. Tautomerism in Oxoporphyrinogens and Pyrazinacenes. In *Tautomerism*; **2016**, 203–228.
- (24) Alghooneh, L.; Eskandari, M.; Zakavi, S.; Omidyan, R. Optical Properties of β-

- Brominated *Meso* -Tetraphenylporphyrins: Comparative Experimental and Computational Studies. *J. Porphyrins Phthalocyanines* **2018**, 22, 646–657.
- (25) Jose, D. A.; Shukla, A. D.; Kumar, D. K.; Ganguly B.; Das. A. Synthesis, Characterization, Physicochemical, and Photophysical Studies of Redox Switchable NIR Dye Derived from a Ruthenium–Dioxolene–Porphyrin System. *Inorg. Chem.* **2005**, 44, 2414-2425.
- (26) Speck, M.; Kurreck, H.; Senge, M. O. Porphyrin-o-Quinones as Model Systems for Electron Transfer and Catecholase Reactions. *Eur. J. Org. Chem.* **2000**, 2000, 2303–2314.
- (27) Hill, J. P.; Van Rossom, W.; Ishihara, S.; Subbaiyan, N.; D'Souza, F.; Xie, Y.; Sanchez-Ballester, N. M.; Ariga, K. Unexpected but Convenient Synthesis of Soluble *Meso*-*Tetrakis* (3,4-Benzoquinone)-Substituted Porphyrins. *J. Porphyrins Phthalocyanines* **2014**, 18, 173–181.





CHAPTER 4
**HIGHLY NONPLANAR,
ASYMMETRICAL, β -OCTA
SUBSTITUTED PORPHYRINS:
SYNTHESIS, STRUCTURAL,
PHOTOPHYSICAL AND
ELECTROCHEMICAL REDOX STUDIES**



CHAPTER 4

UNSYMMETRICAL NONPLANAR 'PUSH-PULL' β -OCTA SUBSTITUTED PORPHYRINS: SYNTHESIS, STRUCTURAL, PHOTOPHYSICAL AND ELECTROCHEMICAL REDOX PROPERTIES

4.1 INTRODUCTION

Porphyrin is a colored, tetrapyrrolic pigment ubiquitous in nature. Porphyrin is highly aromatic 18- π electron system which is involved in many processes such as oxygen transport and storage, electron transfer and oxidative catalysis [1,2]. Due to nonplanar conformation, porphyrins are used as models for heme proteins. Porphyrins are conformationally flexible and have many peripheral positions available for functionalization [3]. The alternation in physicochemical properties of synthetic porphyrins can be studied by introduction of β -substituents either electron donor and/or electron acceptor at periphery of macrocycle since these substituents are in direct conjugation with porphyrin π -system [4]. β -Nitroporphyrins have been extensively used as starting material for further functionalization of macrocyclic core. Curiosity in the synthesis of new family of porphyrins arises due to application of these compounds in the field of biology, supramolecular chemistry and material science [5,6]. Mixed substituted porphyrins and their metal complexes have potential applications in molecular sensors [7–9], catalysis [10], dye-sensitized solar cells (DSSC) [11,12], photodynamic therapy (PDT) [12] and nonlinear optics (NLO) [13]. Increasing the number of β -substituents induces steric repulsion between the substituents and enhances the nonplanar conformation of the macrocyclic core which serves as model compounds of heme [14,15]. Perhalogenated metalloporphyrins exhibit enhanced robustness towards oxidative degradation and hence these porphyrins can serve as model compounds for heme enzymes such as cytochrome P450 [16]. The substitution at peripheral β -position of the macrocycle leads to modulation of physicochemical and electrochemical properties of porphyrins [17]. *Meso*-substituted porphyrin system exerts less steric and electronic effects on porphyrin π -system as compared to β -position. β -Substitution at periphery of porphyrin core exert the steric repulsion among the substituents as a result the pyrrole nitrogens incline from the plane of porphyrin core to reduce repulsion between peripheral substituents which results in nonplanarity of macrocycle core [18]. β -halo porphyrins are utilized as efficient

catalysts for epoxidation and hydroxylation reaction [19]. Highly substituted macrocycles exhibit exclusive physicochemical properties [20]. Kadish and other research groups have reported the electrochemical studies of various mixed substituted porphyrins [21–24]. Herein, we report the influence of mixed β -substitution on electrochemical redox and photophysical properties of porphyrin. Hence we synthesized two new family of free base mixed β -substituted porphyrins and their metal derivatives and studied their structural, photophysical and electrochemical redox properties of push-pull porphyrins viz. MTPP(Ph)₂Br₅X (X = NO₂ or Br and M = 2H, Co(II), Ni(II), Cu(II) and Zn(II)). These porphyrins were synthesized first time which shows highly bathochromic shift the in absorption spectra and enhanced nonplanarity of macrocyclic core as compared to MTPP (M = 2H, Co(II), Ni(II), Cu(II) and Zn(II)). Reports on β -substituted porphyrins are limited as compared to *meso*-substituted porphyrins due to lack of synthetic methodologies whereas latter ones have been widely explored due to their facile synthesis and functionalization [25,26].

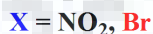
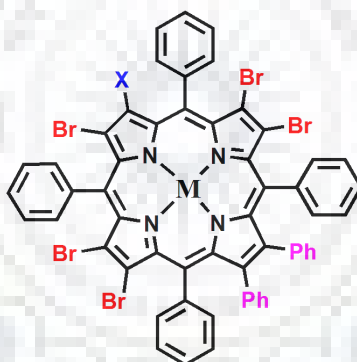


Chart 4.1 Molecular Structures of Synthesized Mixed β -Octasubstituted Porphyrins.

4.2 EXPERIMENTAL SECTION

4.2.1 Reagents

Pyrrole, N-bromosuccinamide, potassium carbonate, phenyl boronic acid, HCl, methanol and hexane, were purchased from Alfa Aesar Rankem, SRL and used without further purification. M(OAc)₂·nH₂O (M = Co^{II}, Cu^{II}, Ni^{II} and Zn^{II}), DMF, Na₂SO₄, TBAPF₆, P₂O₅ and Br₂ were purchased from HiMedia, and used as received. Pd(PPh₃)₄ was purchased from Sigma-Aldrich. Toluene, CHCl₃ and CH₂Cl₂ were distilled over P₂O₅.

NBS was used after recrystallized from hot water then dried under vacuum up to 8h at 75°C. TBAPF₆ was used after recrystallization twice from hot ethanol then dried at 25°C for 2 days.

4.2.2 Instrumentation and Methods

UV-vis and fluorescence spectra were recorded by Cary 100 spectrophotometer and Hitachi F-4600 spectrofluorometer, respectively. All ¹H NMR spectra were recorded using JEOL 400 MHz spectrometer in CDCl₃ at 298 K. Elementar EL III Instrument used to carry out elemental analysis. A Bruker UltrafleXtreme-TN MALDI-TOF/TOF mass spectrometer was used to record mass spectra of synthesized porphyrins using 2-(4'-hydroxybenzeneazo)benzoic acid as a matrix. Electrochemical studies were performed on CHI-620E electrochemical workstation. The electrode system, Pt-wire counter electrode, Pt working electrode and Ag/AgCl as a reference electrode. All measurement in electrochemical studies were carried out in triple distilled dichloromethane containing 0.1 M TBAPF₆ as supporting electrolytes. Computational studies of synthesized free base porphyrins were carried out in gas phase using LANL2DZ basis set and B3LYP functional.

4.2.3 Synthesis of 2,3,7,8,17,18-hexabromo-12,13-diphenyl-*meso*-tetraphenylporphyrin (H₂TPP(Ph)₂Br₆) and 2-nitro-3,7,8,17,18-pentabromo-12,13-diphenylporphyrin(H₂TPP(NO₂)(Ph)₂Br₅) and Their Metal Complexes:

NiTPP(NO₂)(Ph)₂ was synthesized according to the method developed in our lab [18]. NiTPP(NO₂)(Ph)₂ (0.120 g, 0.138 mmol) was taken in 40 ml of distilled CHCl₃ in 250 ml RB flask. To this solution, liquid bromine (40 eq.) was added drop wise and then reaction mixture stirred at room temperature for 4 h. After that, pyridine (1.24 ml) was added to the reaction mixture and again stirred for 6 h at room temperature. At the end of this period, reaction mixture was neutralized by sodium meta-bisulphite and washed with water. Finally, the organic layer dried over Na₂SO₄. The crude product was chromatographed on silica gel column in which CHCl₃/Hexane mixture (1:1 v/v) used as eluent, two fraction were obtained. The first fraction NiTPP(Ph)₂Br₆ was obtained with (0.051 g) 40% yield and NiTPP(NO₂)(Ph)₂Br₅ as second fraction with (0.042 g) 35% yield.

Demetalation of NiTPP(Ph)₂Br₅X (X = NO₂/Br):

75 mg of NiTPP(Ph)₂Br₅X (X = NO₂ or Br) was dissolved in minimum amount of chloroform. Few drops of conc. sulphuric acid was added dropwise in the solution and stir for 25 min at 0°C. Then 40 ml of distilled H₂O added to this solution. Water and 10% of aq. ammonia solution used to washed the organic layer and finally excess ammonia was removed with distilled water. Then organic layer was passed through the anhydrous Na₂SO₄ and then purified on silica gel chromatographed using chloroform as eluent. Yield: (57-62 mg) 86-88%.

H₂TPP(NO₂)(Ph)₂Br₅. UV-vis. λ_{\max} (nm), (log ϵ): 477(4.88), 644(3.69), 745(3.64). ¹H NMR in CDCl₃ (400MHz): δ (ppm) 8.24(t, 6H, *J* = 8.2 Hz, *meso-o*-Ph), 7.85-7.70(m, 10H, *meso-o* and *m*-Ph), 7.38-7.27(m, 4H, *meso-p*-Ph), 6.85-6.79(m, 10H β -Ph). MALDI-TOF-MS (m/z) = [M]⁺ 1204.89, calcd. 1204.84. Anal. calcd. for C₅₆H₃₂Br₅N₅O₂: C, 55.75; H, 2.67; N, 5.81%. Found: C, 55.05; H, 2.30; N, 5.32%.

20 mg, (0.016 mmol) H₂TPP(NO₂)Ph₂Br₅ was dissolved in 8 ml of CHCl₃. To this solution, 10 eq. of M(OAc)₂.nH₂O (M = Cu(II), Zn(II), Co(II)) in 2 ml of methanol was added and mixture was refluxed for 35 minutes. Then reaction mixture cooled to room temperature and washed with water, organic layer passed through anhydrous Na₂SO₄ and crude product was purified by column chromatographed using CHCl₃ as eluent. Yield: 90-94%.

NiTPP(NO₂)(Ph)₂Br₅: UV-vis. λ_{\max} (nm), (log ϵ): 454(4.86), 568(3.87), 617(3.68). ¹H NMR in CDCl₃ (400MHz): δ (ppm) 7.96-7.92(m, 4H, *meso-o*-Ph), 7.74-7.44(m, 12H, *meso-o,m*-Ph), 7.22-7.13(m, 4H, *meso-p*-Ph), 6.88-6.66(m, 10H β -Ph). MALDI-TOF-MS (m/z) = [M]⁺ 1263.91, calcd. 1263.76. Anal. calcd. for C₅₆H₃₂Br₅N₅NiO₂: C, 53.25; H, 2.39; N, 5.54%. Found: C, 53.92; H, 2.64; N, 5.02%.

CuTPP(NO₂)(Ph)₂Br₅: UV-vis. λ_{\max} (nm), (log ϵ): 465(4.79), 585(3.91), 635(3.64). MALDI-TOF-MS (m/z) = [M]⁺ 1268.93, calcd. 1268.76. Anal. calcd. for C₅₆H₃₀Br₅CuN₅O₂: C, 53.05; H, 2.38; N, 5.52%. Found: C, 52.94; H, 2.30; N, 5.32%.

CoTPP(NO₂)(Ph)₂Br₅: UV-vis. λ_{\max} (nm), (log ϵ): 455(4.88), 573(3.91). MALDI-TOF-MS (m/z) = [M+H]⁺ 1263.83, calcd. 1262.76. Anal. calcd. for C₅₆H₃₀Br₅CoN₅O₂: C, 53.24; H, 2.39; N, 5.54 %. Found: C, 53.15; H, 2.04; N, 5.14%.

ZnTPP(NO₂)(Ph)₂Br₅: UV-vis. λ_{\max} (nm), (log ϵ): 471(4.98), 605(3.71), 669(3.77). ¹H NMR in CDCl₃ (400MHz): δ (ppm) 8.12 (t, 4H, $J = 8$ Hz, *meso-o*-Ph), 7.82-7.60 (m, 12H, *meso-o,m*-Ph), 7.22-7.09 (m, 4H, *meso-p*-Ph), 6.80-6.60 (m, 10H, β -Ph). MALDI-TOF-MS (m/z) = [M+2H]⁺ 1270.85, calcd. 1270.75. Anal. calcd. for C₅₆H₃₀Br₅N₅O₂Zn: C, 52.97; H, 2.38; N, 5.52%. Found: C, 52.67; H, 2.20; N, 5.46 %.

H₂TPP(Ph)₂Br₆: UV-vis. λ_{\max} (nm), (log ϵ): 468(5.01), 571(3.64), 629(3.76), 738(3.85). ¹H NMR in CDCl₃ (400MHz): δ (ppm) 8.23(d, 6H, $J = 8$ Hz, *meso-o*-Ph), 7.83-7.74(m, 10H, *meso-o,m*-Ph), 7.34-7.28(m, 4H, *meso-p*-Ph), 6.83-6.76(m, 10H β -Ph), -1.64 (bs, 1H, imino-H). MALDI-TOF-MS (m/z) = [M+H]⁺ 1240.51, calcd. 1239.77. Anal. calcd. for C₅₆H₃₂Br₅N₅O₂: C, 55.75; H, 2.67; N, 5.81%. Found: C, 55.95; H, 2.97; N, 5.92%.

NiTPP(Ph)₂Br₆: UV-vis. λ_{\max} (nm), (log ϵ): 446 (5.18), 561 (4.06), 603 (3.74). ¹H NMR in CDCl₃ (400MHz): δ (ppm) 7.94(d, 4H, $J = 8$ Hz, *meso-o*-Ph), 7.75-7.62(m, 8H, *meso-o,m*-Ph), 7.53(d, 4H, $J = 8$, *meso-p*-Ph), 7.15(t, 4H $J = 8$ Hz, *meso-p*-Ph), 6.82-6.61(m, 10H β -Ph). MALDI-TOF-MS m/z) = [M+H]⁺ 1298.34, calcd. 1298.68. Anal. calcd. for C₅₆H₃₀Br₆N₅Ni: C, 51.86; H, 2.33; N, 4.32%. Found: C, 51.92; H, 2.94; N, 4.67%.

CuTPP(Ph)₂Br₆: UV-vis. λ_{\max} (nm), (log ϵ): 444(5.06), 461sh(5.01), 579(4.14), 626(3.73). MALDI-TOF-MS m/z = [M]⁺ 1301.97, calcd. 1301.68. Anal. calcd. for C₅₆H₃₀Br₆CuN₄: C, 51.67; H, 3.32; N, 4.30%. Found: C, 51.09; H, 3.76; N, 4.87%.

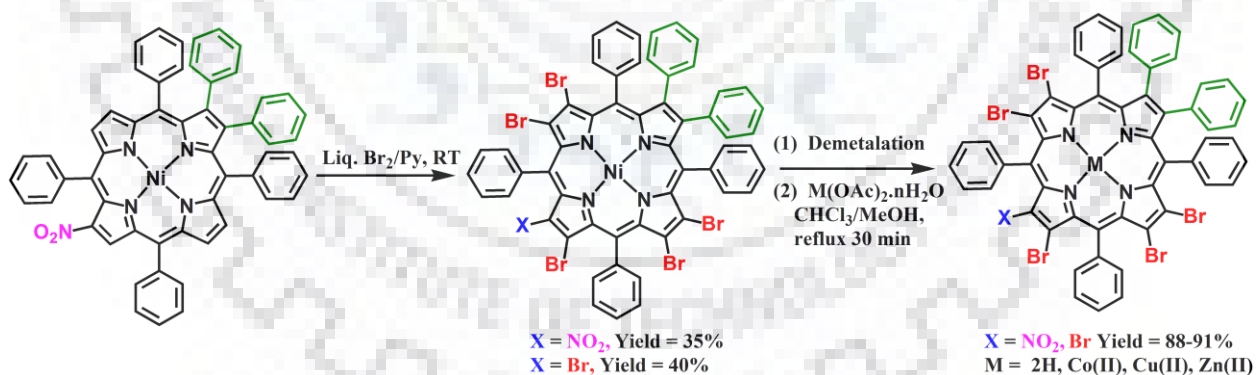
CoTPP(Ph)₂Br₆: UV-Vis. λ_{\max} (nm), (log ϵ): 445(5.02), 565(3.94). MALDI-TOF-MS m/z = [M+H]⁺ 1297.67, calcd. 1297.68 Anal. calcd. for C₅₆H₃₀Br₆CoN₄: C, 51.85; H, 2.33; N, 4.32%. Found: C, 51.99; H, 2.56; N, 4.67%.

ZnTPP(Ph)₂Br₆: UV-Vis. λ_{\max} (nm), (log ϵ): 463(5.07), 597(3.78), 653(3.68). ¹H NMR in CDCl₃ (400MHz): δ (ppm) 8.14(d, 4H, $J = 8$ Hz, *meso-o*-Ph), 7.79-7.71(m, 10H, *meso-o,m*-Ph), 7.32-7.27(m, 3H, *meso-p*-Ph), 7.23-7.18(m, 3H, *meso-p*-Ph), 7.79-7.64(m, 10H β -Ph). MALDI-TOF-MS m/z = [M]⁺ 1303.40, calcd. 1303.68. Anal. calcd. for C₅₆H₃₀Br₆N₄Zn: C, 51.59; H, 2.32; N, 54.30%. Found: C, 51.87; H, 2.45; N, 54.46 %.

4.3 RESULTS AND DISCUSSION

4.3.1 Synthesis and Characterization

Two new series of mixed β -octasubstituted porphyrins have been synthesized and characterized by using various spectroscopic techniques. Firstly, H₂TPP was synthesized according to the reported literature and followed by Cu(II) insertion in the core [27]. Then mono-nitration of CuTPP was carried out with 80% yield and followed by acid demetalation yielded H₂TPP(NO₂). Further, the regioselective dibromination of H₂TPP(NO₂) was carried out in order to synthesize H₂TPP(NO₂)Br₂ which again subjected for Pd catalyzed Suzuki cross-coupling reaction and resulted into the formation of H₂TPP(NO₂)Ph₂. Then Ni(II) insertion of H₂TPP(NO₂)(Ph)₂ was carried out in DMF. The bromination of NiTPP(NO₂)(Ph)₂ with 40 equivalents of liquid bromine resulted in to formation of NiTPP(NO₂)(Ph)₂Br₅ and NiTPP(Ph)₂Br₆. NiTPP(Ph)₂Br₆ was obtained as a first fraction with 40% yield and second fraction was NiTPP(NO₂)(Ph)₂Br₅ with 35% yield. The free base porphyrins were obtained by acid demetallation in good yield (86-88%). Metal (Co(II), Cu(II) and Zn(II)) complexes were prepared with excellent yields (90-94%) by conventional methods as described in the literature [18]. The synthesized porphyrins were characterized by various spectroscopic techniques such as UV-Vis, fluorescence, NMR, MALDI mass spectrometry, single-crystal X-ray and elemental analysis.



Scheme 4.1 Synthesis of Mixed β -Octasubstituted Porphyrins.

The mixed substituted porphyrins exhibited proton signals for *meso*-phenyl, β -substituents, and core imino protons. H₂TPP(NO₂)(Ph)₂ shows proton resonance for β -pyrrole protons in the range of 8.98-8.58 ppm, for *meso*-phenyl 8.30-7.23 ppm and for β -phenyl 6.90-6.80 ppm [18]. Due to more electron-withdrawing groups on periphery of

macrocycle, the *meso*-phenyl protons of $\text{H}_2\text{TPP}(\text{Ph})_2\text{Br}_5\text{X}$ ($\text{X} = \text{NO}_2$ or Br) were slightly upfield ($\Delta\delta = 0.1\text{-}0.4$ ppm) shifted than $\text{H}_2\text{TPP}(\text{NO}_2)(\text{Ph})_2$ whereas marginal shift was observed in case of β -phenyl protons of $\text{H}_2\text{TPP}(\text{Ph})_2\text{Br}_5\text{X}$ ($\text{X} = \text{NO}_2$ or Br). The core imino protons of $\text{H}_2\text{TPP}(\text{Ph})_2\text{Br}_6$ exhibited characteristic proton signal at -1.64 ppm which is 0.67 ppm downfield shifted as compared to $\text{H}_2\text{TPP}(\text{NO}_2)(\text{Ph})_2$, due to electron withdrawing nature of β -bromo groups and nonplanarity of the ring which reduces the ring current of porphyrin π -system [28]. In ^1H NMR spectra of $\text{MTPP}(\text{Ph})_2\text{Br}_5\text{X}$ ($\text{X} = \text{Br}$ or NO_2) ($\text{M} = \text{Zn}(\text{II})$ and $\text{Ni}(\text{II})$) complexes, no $-\text{NH}$ signal were found due to presence of metal ions in the porphyrin core. The resonances of *meso*-phenyl protons for $\text{NiTPP}(\text{Ph})_2\text{Br}_5\text{X}$ ($\text{X} = \text{Br}$ or NO_2) are slightly upfield shifted ($\Delta\delta = 0.14\text{-}0.28$ ppm) as compared to $\text{H}_2\text{TPP}(\text{Ph})_2\text{Br}_5\text{X}$ ($\text{X} = \text{Br}$ or NO_2). β -phenyl proton of $\text{NiTPP}(\text{Ph})_2\text{Br}_5\text{X}$ ($\text{X} = \text{Br}$ or NO_2) exhibits ($0.04\text{-}0.13$ ppm) upfield shift. While in case of $\text{ZnTPP}(\text{Ph})_2\text{Br}_5\text{X}$ ($\text{X} = \text{Br}$ or NO_2) *meso*-phenyl proton resonances are marginally upfield shifted ($0.11\text{-}0.17$ ppm) and β -phenyl protons exhibits ($0.06\text{-}0.15$ ppm) upfield shift than $\text{H}_2\text{TPP}(\text{Ph})_2\text{Br}_5\text{X}$ ($\text{X} = \text{Br}$ or NO_2). ^1H NMR spectra of synthesized porphyrins are shown in Figures A1-A3 and A5-A7, Appendix-III and the MALDI-TOF mass spectra of all synthesized porphyrins are shown in Figures A4 and A8, Appendix-III. The observed molecular ion peaks are matching with the proposed structures.

4.3.2 Single Crystal X-ray Structure

The X-ray quality single crystal of $\text{H}_2\text{TPP}(\text{NO}_2)(\text{Ph})_2\text{Br}_5$ were obtained by slow diffusion of CH_3OH in to CH_2Cl_2 solution of $\text{H}_2\text{TPP}(\text{NO}_2)(\text{Ph})_2\text{Br}_5$ at 298 K. ORTEP diagram of $\text{H}_2\text{TPP}(\text{NO}_2)(\text{Ph})_2\text{Br}_5$ is shown in Figure 4.1. Crystallographic data of $\text{H}_2\text{TPP}(\text{NO}_2)(\text{Ph})_2\text{Br}_5$ is listed in Table A1, Appendix-III. This porphyrin crystalized in monoclinic system with P 21/c space group. Crystal packing diagram of $\text{H}_2\text{TPP}(\text{NO}_2)(\text{Ph})_2\text{Br}_5$ is shown in Figure A13, Appendix-III. Selected average bond angles and bond distances are listed in Table A2, Appendix-III. Peripheral β -substitutions of free base porphyrin induced the nonplanarity of macrocyclic core. Further, two CH_3OH solvent molecule are having bonding with imino nitrogens. The $\text{C}_\beta\text{-C}_\beta$ bond length (1.366 \AA) of $\text{H}_2\text{TPP}(\text{NO}_2)\text{Ph}_2\text{Br}_5$ (bearing two Ph, one NO_2 and one Br groups) are longer than $\text{C}_\beta\text{-C}_\beta$ (1.273 \AA) (bearing four Br groups) due to the presence

of mixed β -substitutions by varying in shape and size at periphery of macrocycle. The pyrrole units of $\text{H}_2\text{TPP}(\text{NO}_2)(\text{Ph})_2\text{Br}_5$ tilted up and down alternatively from the mean plane of porphyrin core. $\text{C}_\beta\text{-C}_\beta$ substituents tilted to the one face of porphyrin and $\text{C}_{\beta'}\text{-C}_{\beta'}$ substituents tilted to other face of porphyrin. The increment in the $\text{C}_\beta\text{-C}_\alpha\text{-C}_m$ bond angle with decreament in the $\text{N-C}_\alpha\text{-C}_m$ revealed nonplanar conformation of the porphyrin core. $\text{H}_2\text{TPP}(\text{NO}_2)(\text{Ph})_2\text{Br}_5$ exhibited saddle shape nonplanar conformation with the deviation of 24 core atoms ($\Delta 24$) by $\pm 0.558 \text{ \AA}$ and the displacement of β -carbon (ΔC_β) by $\pm 1.23 \text{ \AA}$ from the mean plane of porphyrin core. So $\text{H}_2\text{TPP}(\text{NO}_2)\text{Ph}_2\text{Br}_5$ exhibited highly nonplanar conformation as compared to precursor ($\text{H}_2\text{TPP}(\text{NO}_2)(\text{Ph})_2$) ($\Delta \text{C}_\beta = \pm 0.673 \text{ \AA}$ and $\Delta 24 = \pm 0.320 \text{ \AA}$) due to the effect of five β -bromo substituents at periphery of the porphyrin [18].

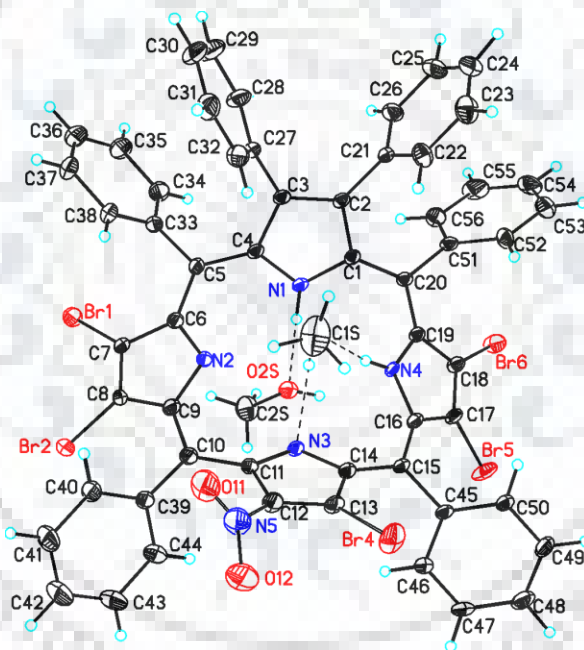


Figure 4.1 ORTEP Diagram of $\text{H}_2\text{TPP}(\text{NO}_2)(\text{Ph})_2\text{Br}_5$.

4.3.3 Electronic Spectral Studies

Optical absorption spectra of $\text{MTPP}(\text{Ph})_2\text{Br}_5\text{X}$ ($\text{M} = 2\text{H}, \text{Co}(\text{II}), \text{Ni}(\text{II}), \text{Cu}(\text{II}), \text{Zn}(\text{II})$ and $\text{X} = \text{NO}_2$ or Br) are influenced by the shape, size and electronic nature of β -substituents. The electronic spectra of all synthesized porphyrins were measured in CH_2Cl_2 at 298 K. The

increment in the number of substituents at β -pyrrole position of porphyrin leads to induce the nonplanarity of macrocyclic system which result into bathochromic shift in the absorptions spectra due to enhanced steric repulsion between the β -substituents which results into the destabilization of HOMOs [29]. The Soret band of $H_2TPP(Ph)_2Br_5X$ ($X = NO_2$ or Br) is broader than H_2TPP due to distortion of macrocyclic ring (nonplanar conformation) and intramolecular charge transfer. The Soret and longest wavelength $Q_x(0,0)$ bands of $H_2TPP(Ph)_2Br_5X$ ($X = NO_2$ or Br) exhibits ($\Delta\lambda_{max} = 53-61$ nm) and ($\Delta\lambda_{max} = 90-95$ nm) dramatic bathochromic shift, respectively as compared to H_2TPP . The optical absorption spectra of $H_2TPP(Ph)_2Br_6$, and $H_2TPP(NO_2)(Ph)_2Br_5$ are shown in Figure 4.2(a). The charge transfer from HOMO of porphyrin to LUMO of nitro group is attributed to a greater FWHM (full width half maximum) of $H_2TPP(NO_2)(Ph)_2Br_5$ as compared to H_2TPP and $H_2TPP(Ph)_2Br_6$. The bathochromic shift in Soret band and longest wavelength $Q_x(0,0)$ band was observed due to electron withdrawing nature of β -substituents and nonplanar conformation of macrocyclic core which follows the order $H_2TPP < H_2TPP(Ph)_2Br_6 < H_2TPP(NO_2)(Ph)_2Br_5$.

Synthesized $MTPP(Ph)_2Br_5X$ ($M = 2H, Zn, X = NO_2$ or Br) porphyrins were characterized by fluorescence spectroscopy studies to determine the effect of mixed substitution at β -position of porphyrin macrocycle. $H_2TPP(Ph)_2Br_5X$ ($X = NO_2$ or Br) exhibits extremely weak emission due to nonplanar conformation of porphyrin core and heavy atoms effect of bromo substituents. The comparative fluorescence spectra of H_2TPP , $H_2TPP(Ph)_2Br_6$, and $H_2TPP(NO_2)(Ph)_2Br_5$ are shown in Figure 4.2b. $H_2TPP(NO_2)(Ph)_2Br_5$ exhibited very low quantum yield as compared to H_2TPP due to heavy atom effect of bromo substituents and nonplanar conformation of porphyrin core. We were unable to calculate the quantum yield of $H_2TPP(Ph)_2Br_6$ due to feeble intensity of porphyrin. Fluorescence spectra of $H_2TPP(Ph)_2Br_5X$ ($X = NO_2$ or Br) and their Zn(II) derivative are shown in Figure A10, Appendix-III. The photophysical data of $MTPP(Ph)_2Br_5X$ ($X = NO_2$ or Br and $M = 2H, Zn$) is listed in Table 4.1.

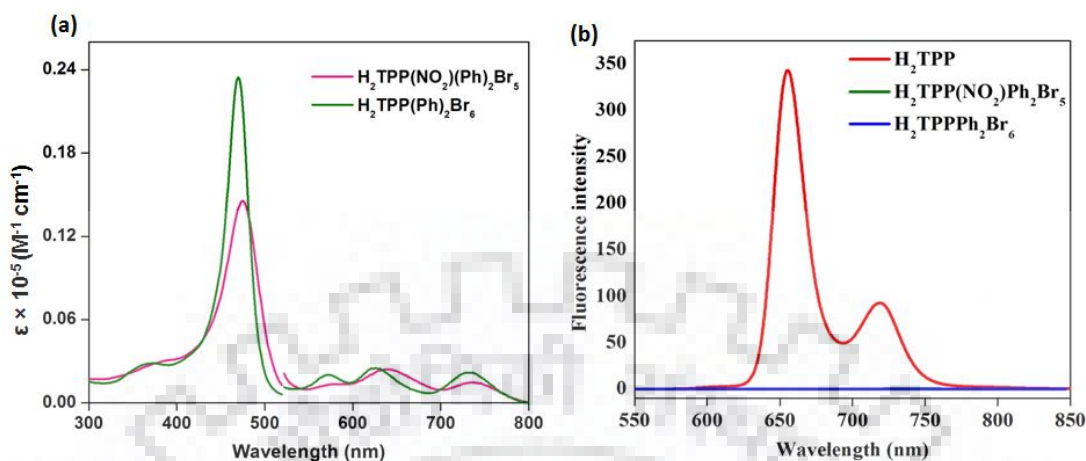


Figure 4.2 (a) Optical Absorption Spectra of $H_2TPP(NO_2)(Ph)_2Br_5$ and $H_2TPP(Ph)_2Br_6$ in CH_2Cl_2 (b) Emission Spectra of H_2TPP , $H_2TPP(NO_2)(Ph)_2Br_5$ and $H_2TPP(Ph)_2Br_6$ in CH_2Cl_2 at 298 K.

Table 4.1 Photophysical Data of Synthesized Free Base and Zn(II) Porphyrins in CH_2Cl_2 at 298 K.

Porphyrin	λ_{ex}	FWHM	λ_{em}	ϕ_f	τ (ns)
$H_2TPP(NO_2)(Ph)_2Br_5$	477	57	816	0.003	0.0985
$H_2TPP(Ph)_2Br_6$	469	39	808	-	0.0059
$ZnTPP(NO_2)(Ph)_2Br_5$	472	39	769, 807	0.001	0.0503
$ZnTPP(Ph)_2Br_6$	463	29	720	0.0016	0.176

λ_{ex} = Excitation wavelength (nm), λ_{em} = Emission wavelength (nm), FWHM- Full width half maximum, ϕ_f - Quantum yield relative to H_2TPP and $ZnTPP$ in CH_2Cl_2 , τ = represents excited state lifetime.

4.3.4 Protonation and Deprotonation Studies

The acid base properties can be tune by appending the mixed substituents at β -pyrrole position of the macrocycle. Many research groups have reported the acid-base properties of nonplanar porphyrins [30]. The protonation and deprotonation studies of $H_2TPP(Ph)_2Br_5X$ ($X = NO_2$ or Br) have been carried out to study the influence of mixed substitution on the porphyrin π -system. These studies were performed in toluene using TFA (trifluoroacetic acid) and TBAOH (tetrabutylammonium hydroxide), respectively. Figures 4.3 and A9, Appendix-III, show the

absorption spectral variations of $\text{H}_2\text{TPP}(\text{NO}_2)(\text{Ph})_2\text{Br}_5$ and $\text{H}_2\text{TPP}(\text{Ph})_2\text{Br}_6$, respectively in toluene. $\text{H}_2\text{TPP}(\text{NO}_2)(\text{Ph})_2\text{Br}_5$ has shown UV-Vis spectral changes while increasing the conc. of TFA ($0.42\text{-}9.31 \times 10^{-6}$ M) and tetrabutylammonium hydroxide ($0.39\text{-}2.34 \times 10^{-6}$ M), respectively. In case of $\text{H}_2\text{TPP}(\text{NO}_2)(\text{Ph})_2\text{Br}_5$, the absorption band at 477 nm with concomitant rise in the new band at 501 nm which shows 24 nm red shift in the Soret band while increasing the conc. of TFA. As protonation proceed, $\text{H}_2\text{TPP}(\text{NO}_2)(\text{Ph})_2\text{Br}_5$ exhibited a new Q band at 757 nm in place of multiple Q bands which was broader and 17 nm red shifted as compared to previous bands. Figure A9a, Appendix III, (inset) show the electronic spectral changes of $\text{H}_2\text{TPP}(\text{Ph})_2\text{Br}_6$ in toluene with rising the conc. of TFA ($0.12\text{-}1.14 \times 10^{-5}$ M) and TBAOH ($0.19\text{-}1.69 \times 10^{-5}$ M), respectively. In case of $\text{H}_2\text{TPP}(\text{Ph})_2\text{Br}_6$, the decrement in absorption intensity 469 nm and concomitant rise at 496 nm were observed while increasing the conc. of TFA. The red shift was found to be 27 and 13 nm bathochromic shift in Soret and $\text{Q}_x(0,0)$ bands, respectively. In both cases, the Hill plot showed the slope value 2 as shown in Figures 4.3a (inset) and A9a (inset), Appendix-III, (for $\text{H}_2\text{TPP}(\text{NO}_2)(\text{Ph})_2\text{Br}_5$ and $\text{H}_2\text{TPP}(\text{Ph})_2\text{Br}_6$, respectively) which indicates the formation of diprotonated porphyrin. As shown in Table 4.2, $\text{H}_2\text{TPP}(\text{NO}_2)(\text{Ph})_2\text{Br}_5$ has 87 fold lower protonation constant (β_2) value than $\text{H}_2\text{TPP}(\text{NO}_2)\text{Br}_6$ due to strong electron withdrawing nitro substituent. Figure 4.3b shows the decrement in the absorbance at 477 nm of $\text{H}_2\text{TPP}(\text{NO}_2)(\text{Ph})_2\text{Br}_5$ and arising of a new band at 521 nm while increasing the conc. of TBAOH. With disappearance of all Q bands, a new band arises at 779 nm of $\text{H}_2\text{TPP}(\text{NO}_2)(\text{Ph})_2\text{Br}_5$. Nonplanarity and the electronic nature of substituents at β -position of porphyrin core influences the deprotonation. $\text{H}_2\text{TPP}(\text{Ph})_2\text{Br}_6$ shows 89 fold higher protonation constant (β_2) than $\text{H}_2\text{TPP}(\text{NO}_2)(\text{Ph})_2\text{Br}_5$. Figure A9b, Appendix-III, (inset) shows the decrement in the absorption band at 469 nm of $\text{H}_2\text{TPP}(\text{Ph})_2\text{Br}_6$ while another band generated at 505 nm. The new band which arose at 740 nm with diminishing of multiple Q bands. Figure 4.3b (inset) and A9b, Appendix-III, (inset) show the Hill plots which exhibit slope value 2, resulting that the dianionic species are formed in both cases. $\text{H}_2\text{TPP}(\text{Ph})_2\text{Br}_6$ shows 83 fold higher deprotonation constant than $\text{H}_2\text{TPP}(\text{NO}_2)(\text{Ph})_2\text{Br}_5$. The $\log\beta_2$ value of free base porphyrins follows the order $\text{H}_2\text{TPP}(\text{Ph})_2\text{Br}_6 > \text{H}_2\text{TPP}(\text{NO}_2)(\text{Ph})_2\text{Br}_5$ which suggests that the effect of increased nonplanarity of porphyrin core and electronic effect of β -substituents influences the acid-base behavior of porphyrin core.

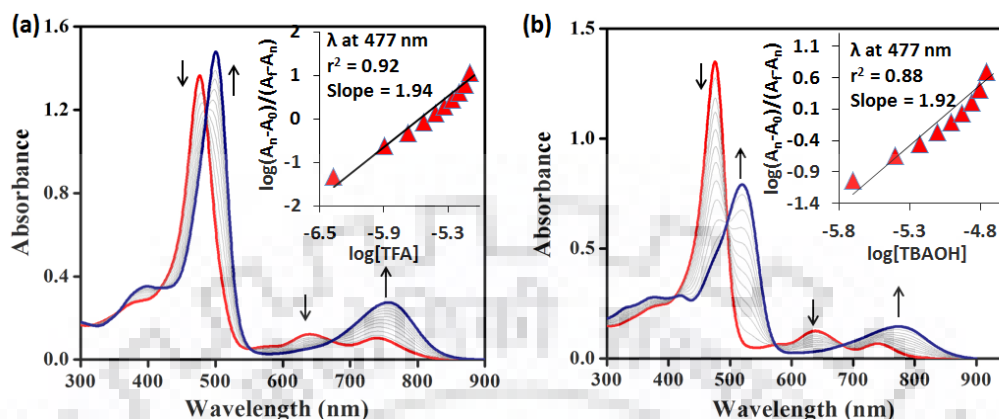


Figure 4.3 UV-Vis Spectral Titration of $\text{H}_2\text{TPP}(\text{NO}_2)(\text{Ph})_2\text{Br}_5$ with (a) TFA and (b) TBAOH in Toluene at 298K. Insets show the Consistent Hill Pots.

Table 4.2 Protonation and Deprotonation Constant of $\text{H}_2\text{TPP}(\text{NO}_2)(\text{Ph})_2\text{Br}_5$ and $\text{H}_2\text{TPP}(\text{Ph})_2\text{Br}_6$ in Comparison with $\text{H}_2\text{TPP}(\text{NO}_2)\text{Br}_6$ in Toluene at 298 K

Porphyrin	$\log\beta_2$	slope	r^2	$\log\beta_2$	slope	r^2
$\text{H}_2\text{TPP}(\text{Ph})_2\text{Br}_6$	12.15	2.20	0.85	12.23	2.30	0.93
$\text{H}_2\text{TPP}(\text{NO}_2)\text{Br}_6$	11.29	2.32	0.93	11.54	2.05	0.94
$\text{H}_2\text{TPP}(\text{NO}_2)\text{Ph}_2\text{Br}_5$	10.20	1.90	0.89	10.31	2.10	0.95

4.3.5 Electrochemical Redox Properties

To examine the influence of mixed electron-donor and acceptor substituents at β -position of porphyrin macrocycle, the electrochemical studies of mixed β -octasubstituted porphyrins were carried by using cyclic voltammetry (CV) in CH_2Cl_2 containing TBAPF_6 at 298 K. The electrochemical redox potential data (vs. Ag/AgCl) is summarized in Table 4.3.

All mixed substituted porphyrins exhibited two successive reversible one electron oxidation and one electron reduction potential waves in CV studies. The first ring reduction potential of CuTPP was found to be at -1.36 V. After nitration of CuTPP , the first ring reduction potential was 0.39 V anodically shifted as compared to CuTPP . Further diphenyl substitution at antipodal position of $-\text{NO}_2$ exhibited minimal shift in reduction potential as compared to CuTPPNO_2 whereas the

first oxidation potential is cathodically shifted (0.13 V) due to electron donating phenyl substituents. The first ring reduction potential of CuTPP(NO₂)(Ph)₂Br₅ is found at -0.740 V which shown a drastic anodic shift (0.62 V) as compared to CuTPP because of electron accepting substituents on β -pyrrole position of porphyrin while 0.22 and 0.23 V anodic shift as compared to CuTPPNO₂ and CuTPP(NO₂)(Ph)₂, respectively due to highly nonplanar conformation of macrocycle. While in case of CuTPP(Ph)₂Br₆ the first reduction potential exhibited 0.45 V anodically shifted as compared to CuTPP and 0.17 V cathodic shift than CuTPP(NO₂)(Ph)₂Br₅. These porphyrins follow the order of reduction potential such as CuTPP > CuTPPNO₂ > CuTPP(NO₂)(Ph)₂ > CuTPP(Ph)₂Br₆ > CuTPP(NO₂)(Ph)₂Br₅ as shown in Figure 4.4. Almost all porphyrins exhibited the same trend except Co(II) porphyrins as shown in Table 4.3. In general, Co(II) porphyrins undergo first metal centered oxidation Co^{II}/Co^{III} and reduction Co^{II}/Co^I followed by ring centered oxidation and reduction. The reactivity changes after metal centered oxidation and reduction that's why Co(II) porphyrins slightly deviates from the expected trend. The HOMO-LUMO variation is represented in Figure 4.5. As we increase the number of β -substituents (electron donor and electron acceptor) the HOMO-LUMO gap decreases gradually. The HOMO-LUMO energy gap of CuTPP(NO₂)(Ph)₂Br₅ was found 1.72 V which is 0.62 V less as compared to CuTPP due to stabilization of LUMO and electron withdrawing nitro and bromo substituents and destabilization of HOMO due to β -phenyl substituents and nonplanarity of the macrocycle. This huge reduction in HOMO-LUMO gap has been ascribed to mixed-substitution (Ph, NO₂, Br) on porphyrin macrocycle. Energy gap between these porphyrins follow the order CuTPP > CuTPPNO₂ > CuTPP(NO₂)(Ph)₂ > CuTPP(Ph)₂Br₆ > CuTPP(NO₂)(Ph)₂Br₅ due to push-pull β -substituents having differences in shape, size and electronic nature and nonplanarity of the macrocycle. These results suggest that the redox tunability can be achieved by the means of mixed β -substitution at the peripheries with reduced HOMO-LUMO gap.

Table 4.3 Redox Potential Data of Synthesized Porphyrins and their Precursors (V vs Ag/AgCl) in CH_2Cl_2 Containing 0.1 M TBAPF₆ with Scan Rate 0.1 Vs^{-1} at 298K

Porphyrin	Oxidation (V)		Reduction (V)			$\Delta E(\text{V})$	$\text{M}^{\text{II/III}}$	$\text{M}^{\text{II/I}}$
	I	II	I	II	III			
H ₂ TPP	1.00	1.34	-1.23	-1.54		2.23		
H ₂ TPPNO ₂	1.10	1.28	-0.87	-1.08		1.97		
H ₂ TPP(NO ₂)(Ph) ₂	1.00	1.13	-0.85	-1.03		1.85		
H ₂ TPP(NO ₂)(Ph) ₂ Br ₅	1.27	1.63 ⁱ	-1.06	-1.29		2.33		
H ₂ TPP(Ph) ₂ Br ₆	0.84	1.16	-0.80	-1.17		1.64		
CoTPP	1.06	1.31	-1.38			2.44	0.85	-0.86
CoTPPNO ₂	1.17	1.42	-1.30			2.47	0.91	-0.66
CoTPP(NO ₂)(Ph) ₂	1.13	1.34	-1.29			2.42	0.88	-0.64
CoTPP(NO ₂)(Ph) ₂ Br ₅	1.33	1.47	-1.16	-1.64 ^a		2.49	0.33 ^a	-0.34
CoTPP(Ph) ₂ Br ₆	1.35		-1.38 ^a			2.73	0.92	-0.42
NiTPP	1.02	1.32	-1.28	-1.72		2.30		
NiTPPNO ₂	1.19	1.32	-0.95	-1.21		2.14		
NiTPP(NO ₂)(Ph) ₂	1.12	1.24	-0.94	-1.20		2.06		
NiTPP(NO ₂)(Ph) ₂ Br ₅	1.27	1.95	-0.77	-1.03		2.04		
NiTPP(Ph) ₂ Br ₆	1.22		-0.92	-1.24		2.14		
CuTPP	0.99	1.36	-1.35	-1.73		2.35		
CuTPPNO ₂	1.08	1.44	-0.97	-1.22		2.05		
CuTPP(NO ₂)(Ph) ₂	0.96	1.38	-0.96	-1.21		1.92		
CuTPP(NO ₂)(Ph) ₂ Br ₅	0.98	1.55	-0.74	-1.01		1.72		
CuTPP(Ph) ₂ Br ₆	0.88	1.46	-0.91	-1.19		1.79		
ZnTPP	0.84	1.15	-1.36	-1.77		2.20		
ZnTPPNO ₂	0.91	1.22	-1.05 ⁱ	1.19	-1.50	1.96		
ZnTPP(NO ₂)(Ph) ₂	0.85	1.07	-1.06 ⁱ	-1.20	-1.49	1.91		
ZnTPP(NO ₂)(Ph) ₂ Br ₅	0.89	1.17	-0.98	-1.22		1.87		
ZnTPP(Ph) ₂ Br ₆	0.84	1.07	-0.98	-1.17		1.82		

ⁱrefers to irreversible potential; ^adata obtained from DPV

4.3.6 DFT Studies

The DFT studies of mixed β -octasubstituted free base porphyrins ($\text{H}_2\text{TPP}(\text{Ph})_2\text{Br}_5\text{X}$ ($\text{X} = \text{Br}$ or NO_2)) were carried out in gas phase using the B3LYP and LanL2DZ functional and basis set, respectively. Average bond angles and bond lengths are shown in Table A2, Appendix-III. Figure A11, Appendix-III, shows the optimized geometries of synthesized free base porphyrins (top view and side view) and deviation of core atoms from the mean plane of porphyrin. To reduce the repulsion between the substituents present at periphery, the pyrrole rings are tilted up and down (saddle shape conformation) with respect to the mean plane of porphyrin core. The bending of pyrrole ring increase $\text{C}_\beta\text{-C}_\alpha\text{-C}_m$ bond angles as well as $\text{C}_\beta\text{-C}_\beta$ bond length with decreasing in $\text{N-C}_\alpha\text{-C}_m$ bond angles. $\text{H}_2\text{TPP}(\text{Ph})_2\text{Br}_5\text{X}$ ($\text{X} = \text{NO}_2$ or Br) exhibits $3\text{-}4^\circ$ change in $\text{C}_\beta\text{-C}_\alpha\text{-C}_m$ as compared to H_2TPP this is showing that by appending the substituents on β -position, the nonplanarity of macrocycle is increased. While there is no more change in $\text{C}_\beta\text{-C}_\beta$ bond length of $\text{H}_2\text{TPP}(\text{Ph})_2\text{Br}_5\text{X}$ ($\text{X} = \text{NO}_2$ or Br). $\text{N-C}_\alpha\text{-C}_m$ bond angle of $\text{H}_2\text{TPP}(\text{Ph})_2\text{Br}_5\text{X}$ ($\text{X} = \text{NO}_2$ or Br) decreased to $1.4\text{-}1.8^\circ$ as compared to $\text{H}_2\text{TPP}(\text{NO}_2)(\text{Ph})_2$ and $3\text{-}4^\circ$ than H_2TPP . Due to increase the bond length of $\text{C}_\beta\text{-C}_\beta$ and bond angle of $\text{C}_\beta\text{-C}_\alpha\text{-C}_m$ and decrement in bond angles of $\text{N-C}_\alpha\text{-C}_m$ revealed the nonplanarity of porphyrin [18]. Further bromo substitution on remaining β -position exhibited high nonplanarity as compared to H_2TPP . The bond length of $\text{C}_\beta\text{-C}_\beta$ bond ($1.391\text{-}1.392 \text{ \AA}$) of bromo containing β -pyrrole in $\text{H}_2\text{TPP}(\text{Ph})_2\text{Br}_5\text{X}$ ($\text{X} = \text{NO}_2$ or Br) is longer relative to $\text{C}_\beta\text{-C}_\beta$ bond distance ($1.383\text{-}1.389 \text{ \AA}$) bearing four β -substituents. $\text{H}_2\text{TPP}(\text{Ph})_2\text{Br}_6$ exhibited higher ΔC_β as compared to $\text{H}_2\text{TPP}(\text{NO}_2)(\text{Ph})_2\text{Br}_5$ which indicates that $\text{H}_2\text{TPP}(\text{Ph})_2\text{Br}_6$ is more nonplanar than $\text{H}_2\text{TPP}(\text{NO}_2)(\text{Ph})_2\text{Br}_5$. $\text{H}_2\text{TPP}(\text{NO}_2)(\text{Ph})_2\text{Br}_5$ and $\text{H}_2\text{TPP}(\text{Ph})_2\text{Br}_6$ exhibited higher nonplanarity ($\Delta\text{C}_\beta = \pm 1.325$ and ± 1.328 , respectively) as compared to $\text{H}_2\text{TPP}(\text{NO}_2)(\text{Ph})_2$ ($\Delta\text{C}_\beta = \pm 0.671 \text{ \AA}$) porphyrins. Hence, optimized geometries of $\text{H}_2\text{TPP}(\text{Ph})_2\text{Br}_5\text{X}$ ($\text{X} = \text{NO}_2$ or Br) revealed the highly nonplanar and saddle shape conformation of macrocyclic ring.

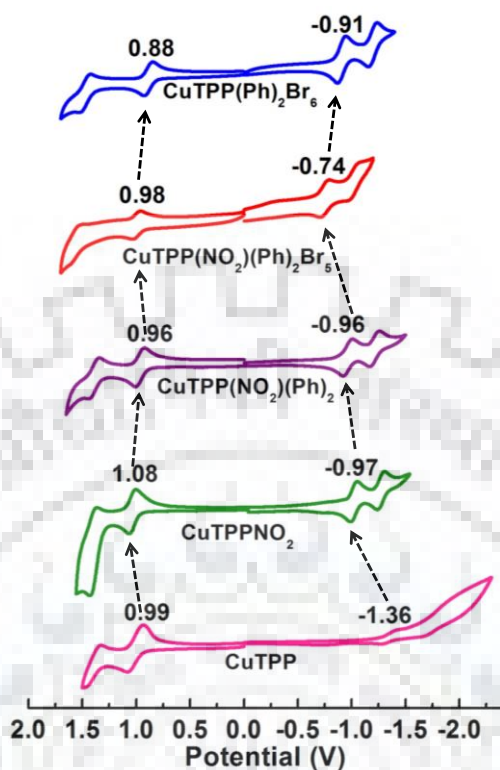


Figure 4.4 Cyclic Voltammograms of Cu(II) Porphyrins using Ag/AgCl as Reference Electrode in CH_2Cl_2 containing 0.1M TBAPF_6 at 298 K.

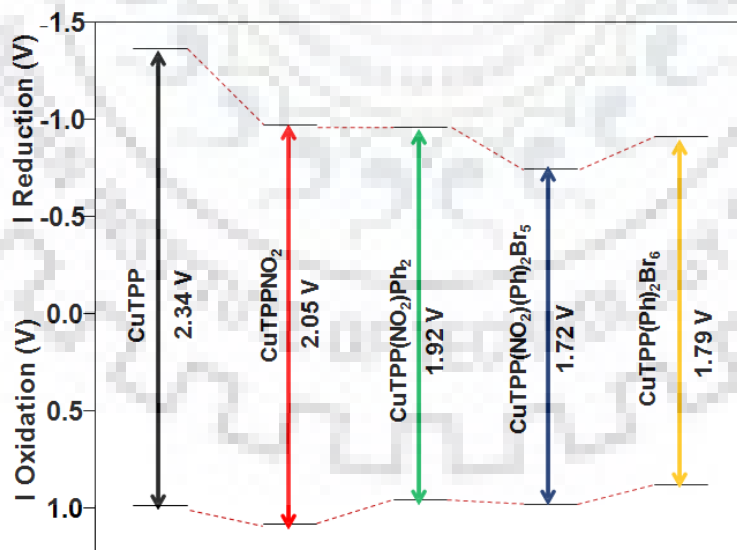


Figure 4.5 HOMO-LUMO Variation of Cu(II) Porphyrins.

4.4 CONCLUSIONS

Two new families of mixed substituted porphyrins have been synthesized and characterized by using various spectroscopic techniques. Crystal structure of $\text{H}_2\text{TPP}(\text{NO}_2)(\text{Ph})_2\text{Br}_5$ revealed the saddle shape nonplanar conformation with the deviation of 24 core atoms ($\Delta_{24} = \pm 0.558 \text{ \AA}$) and the displacement of β -carbon ($\Delta C_{\beta} = \pm 1.23 \text{ \AA}$) from the mean plane of porphyrin core. These unsymmetrical porphyrin exhibits 53-61 nm bathochromic shift in Soret band as compared to H_2TPP . These porphyrin show higher protonation and deprotonation constant due nonplanarity and electronic effect of β -substituents. The ^1H NMR spectra of $\text{H}_2\text{TPP}(\text{Ph})_2\text{Br}_6$ exhibited 0.67 ppm downfield shift in -NH protons as compared to $\text{H}_2\text{TPP}(\text{NO}_2)(\text{Ph})_2$. HOMO-LUMO gap of $\text{H}_2\text{TPP}(\text{NO}_2)(\text{Ph})_2\text{Br}_5$ is decreased about 0.62 V as compared to H_2TPP due to push-pull β -substituents having different shape, size and electronic nature and enhanced nonplanarity of the porphyrin core. Redox tunability of these porphyrins was accomplished by appending the electron donating/ accepting groups at periphery of porphyrin which results in push-pull effect of β -substituents at porphyrin π -system. The mixed push-pull β -substituents induces the higher order of nonplanarity which was confirmed by single crystal X-ray structure, DFT calculations and photophysical data as well as red-shifted spectral features with redox tunability.

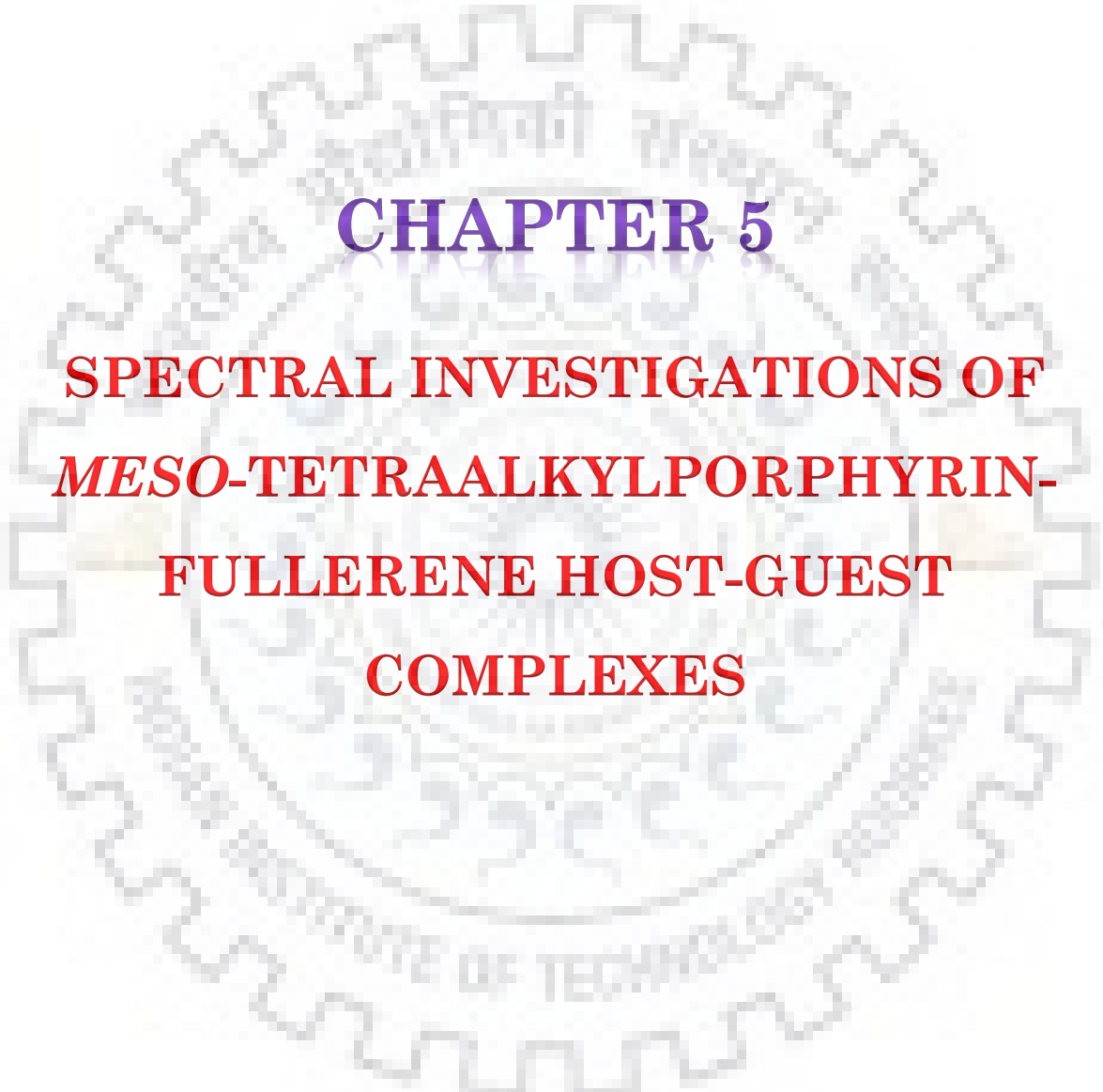
4.5 REFERENCES

- (1) Vakulya, B.; Varga, S.; Csámpai, A.; Soós, T. Highly Enantioselective Conjugate Addition of Nitromethane to Chalcones Using Bifunctional Cinchona Organocatalysts. *Org. Lett.* **2005**, *7*, 1967–1969.
- (2) Luo, J.; Chen, L.-F.; Hu, P.; Chen, Z.-N. Tetranuclear Gadolinium(III) Porphyrin Complex as a Theranostic Agent for Multimodal Imaging and Photodynamic Therapy. *Inorg. Chem.* **2014**, *53*, 4184–4191.
- (3) Kumar, S.; Jiang, X.; Shan, W.; Jinadasa, R. G. W.; Kadish, K. M.; Wang, H. β -Functionalized *Trans*- A_2B_2 Push-pull Tetrabenzoporphyrins. *Chem. Commun.* **2018**, *54*, 5303–5306.
- (4) Grover, N.; Chaudhri, N.; Sankar, M. Facile Conversion of Ni(II) Cyclopropylchlorins into Novel β -Substituted Porphyrins through Acid-Catalyzed Ring-Opening Reaction. *Inorg. Chem.* **2017**, *56*, 424–437.

- (5) Dar, T. A.; Sankar, M. Facile Synthesis of Nitrovanillin- Appended Porphyrin and Its Utilization as Potent, Recyclable, Naked-Eye CN^- and F^- Ion Sensor. *ChemistrySelect* **2017**, *2*, 6778–6783.
- (6) Smykalla, L.; Mende, C.; Fronk, M.; Siles, P. F.; Hietschold, M.; Salvan, G.; Zahn, D. R. T.; Schmidt, O. G.; Ruffer, T.; Lang, H. (Metallo)porphyrins for Potential Materials Science Applications. *Beilstein J. Nanotechnol.* **2017**, *8*, 1786–1800.
- (7) Wei, K.; Yao, F.; Kang, X.-F. Single-Molecule Porphyrin-Metal Ion Interaction and Sensing Application. *Biosens. Bioelectron.* **2018**, *109*, 272–278.
- (8) Kozitsina, A. N.; Svalova, T. S.; Malysheva, N. N.; Okhokhonin, A. V.; Vidrevich, M. B.; Brainina, K. Z. Sensors Based on Bio and Biomimetic Receptors in Medical Diagnostic, Environment, and Food Analysis. *Biosensors* **2018**, *8*, 35.
- (9) Ding, Y.; Zhu, W.-H.; Xie, Y. Development of Ion Chemosensors Based on Porphyrin Analogues. *Chem. Rev.* **2017**, *117*, 2203–2256.
- (10) Dar, T. A.; Uprety, B.; Sankar, M.; Maurya, M. R. Robust and Electron Deficient Oxidovanadium(IV) Porphyrin Catalysts for Selective Epoxidation and Oxidative Bromination Reactions in Aqueous Media. *Green Chem.* **2019**, *21*, 1757–1768.
- (11) Zhou, H.; Ji, J.-M.; Kang, S. H.; Kim, M. S.; Lee, H. S.; Kim, C. H.; Kim, H. K. PAPER Hwan Kyu Kim et Al. Molecular Design and Synthesis of D- π -A Structured Porphyrin Dyes with Various Acceptor Units for Dye-Sensitized Solar Cells Molecular Design and Synthesis of D- π -A Structured Porphyrin Dyes with Various Acceptor Units for Dye-Sensitized Solar Cells. *J. Mater. Chem. C* **2019**, *7*, 2843–2852.
- (12) Zeng, K.; Lu, Y.; Tang, W.; Zhao, S.; Liu, Q.; Zhu, W.; Tian, H.; Xie, Y. Efficient Solar Cells Sensitized by a Promising New Type of Porphyrin: Dye-Aggregation Suppressed by Double Strapping. *Chem. Sci.* **2019**, *10*, 2186–2192.
- (13) Tessore, F.; Biroli, A. O.; Di Carlo, G.; Pizzotti, M. Porphyrins for Second Order Nonlinear Optics (NLO): An Intriguing History. *Inorganics* **2018**, *6*, 81.
- (14) Grover, N.; Chaudhri, N.; Sankar, M. β -Functionalized Dibenzoporphyrins with Mixed Substituents Pattern: Facile Synthesis, Structural, Spectral, and Electrochemical Redox Properties. *Inorg. Chem.* **2019**, *58*, 2514–2522.
- (15) Grover, N.; Kumar, R.; Chaudhri, N.; Butcher, R.; Sankar, M. β -Heptasubstituted

- Porphyrins: Synthesis, Structural, Spectral, and Electrochemical Properties. *Eur. J. Inorg. Chem.* **2018**, 2018, 3338–3343.
- (16) Gotardo, M. C. A. F.; De Moraes, L. A. B.; Assis, M. D. Metalloporphyrins as Biomimetic Models for Cytochrome P-450 in the Oxidation of Atrazine. *J. Agric. Food Chem.* **2006**, 54, 10011–10018.
- (17) Bhyrappa, P. Recent Advances in Mixed β -Pyrrole Substituted *Meso*-Tetraphenylporphyrins. *Tetrahedron Lett.* **2016**, 57, 5150–5167.
- (18) Kumar, R.; Sankar, M. Synthesis, Spectral, and Electrochemical Studies of Electronically Tunable β -Substituted Porphyrins with Mixed Substituent Pattern. *Inorg. Chem.* **2014**, 53, 12706–12719.
- (19) Dias, L. D.; Carrilho, R. M. B.; Henriques, C. A.; Piccirillo, G.; Fernandes, A.; Rossi, L. M.; Filipa Ribeiro, M.; Calvete, M. J. F.; Pereira, M. M. A Recyclable Hybrid Manganese(III) Porphyrin Magnetic Catalyst for Selective Olefin Epoxidation Using Molecular Oxygen. *J. Porphyr. Phthalocyanines* **2018**, 22, 331–341.
- (20) Kielmann, M.; Flanagan, K. J.; Norvaiša, K.; Intrieri, D.; Senge, M. O. Synthesis of a Family of Highly Substituted Porphyrin Thioethers via Nitro Displacement in 2,3,7,8,12,13,17,18-Octaethyl-5,10,15,20-Tetranitroporphyrin. *J. Org. Chem.* **2017**, 82, 5122–5134.
- (21) Fang, Y.; Wang, L.; Xu, W.; Ou, Z.; Chen, M.; Cong, L.; Shan, W.; Ke, X.; Kadish, K. M. Spectral, Electrochemical, and ESR Characterization of Manganese Tetraarylporphyrins Containing Four β, β' -Pyrrole Fused Butano and Benzo Groups in Nonaqueous Media. *Inorg. Chem.* **2019**, 58, 2576–2587.
- (22) Shan, W.; Quesneau, V.; Desbois, N.; Blondeau-Patissier, V.; Naitana, M. L.; Rousselin, Y.; Gros, C. P.; Ou, Z.; Kadish, K. M. Synthesis, Electrochemistry, Protonation and X-Ray Analysis of *Meso*-Aryl Substituted Open-Chain Pentapyrroles. *J. Porphyr. Phthalocyanines.* **2019**, 23, 213–222.
- (23) Chaudhri, N.; Cong, L.; Grover, N.; Shan, W.; Anshul, K.; Sankar, M.; Kadish, K. M. Synthesis and Electrochemical Characterization of Acetylacetonate (Acac) and Ethyl Acetate (EA) Appended β -Trisubstituted Push-Pull Porphyrins: Formation of Electronically Communicating Porphyrin Dimers. *Inorg. Chem.* **2018**, 57, 13213–13224.

- (24) Ye, L.; Fang, Y.; Ou, Z.; Wang, L.; Xue, S.; Sun, J.; Kadish, K. M. Electrochemistry of Zinc Tetraarylporphyrins Containing Fused Butano and Benzo Groups. Effect of Solvent and Substituents on Spectra, Potentials and Mechanism in Nonaqueous Media. *J. Porphyr. Phthalocyanines* **2018**, *22*, 1129–1142.
- (25) Morone, M.; Beverina, L.; Abbotto, A.; Silvestri, F.; Collini, E.; Ferrante, C.; Bozio, R.; Pagani, G. A. Enhancement of Two-Photon Absorption Cross-Section and Singlet-Oxygen Generation in Porphyrins upon β -Functionalization with Donor-Acceptor Substituents. *Organic Lett.* **2006**, *8*, 2719–2722.
- (26) Campbell, W. M.; Jolley, K. W.; Wagner, P.; Wagner, K.; Walsh, P. J.; Gordon, K. C.; Schmidt-Mende, L.; Nazeeruddin, M. K.; Wang, Q.; Grätzel, M.; *et al.* Highly Efficient Porphyrin Sensitizers for Dye-Sensitized Solar Cells. *J. Phys. Chem. C* **2007**, *111*, 11760–11762.
- (27) Adleb, A. D.; Longo, F. R.; Finarelli, J. D.; Goldmacher, J.; Assour, J.; Korsakoff, L. A Simplified Synthesis for *Meso*-Tetraarylporphyrins. *J. Org. Chem.* **1967**, *32*, 476.
- (28) Bhyrappa, P.; Velkannan, V. β -Tetrakis(2-thienyl)-*meso*-tetraarylporphyrins: Synthesis, structural and electrochemical redox properties. *Inorg. Chim. Acta.* **2012**, *387*, 64–73.
- (29) Takeda, J.; Ohya, T.; Sato, M. Dodecaphenylporphyrin. Unusual Optical Properties of a Novel Sterically Hindered Hybrid Porphyrin. *Chem. Phys. Lett.* **1991**, *183*, 384–386.
- (30) Chaudhri, N.; Grover, N.; Sankar, M. Versatile Synthetic Route for β -Functionalized Chlorins and Porphyrins by Varying the Size of Michael Donors: Syntheses, Photophysical, and Electrochemical Redox Properties. *Inorg. Chem.* **2017**, *56*, 11532–11545.



CHAPTER 5
SPECTRAL INVESTIGATIONS OF
***MESO*-TETRAALKYLPORPHYRIN-**
FULLERENE HOST-GUEST
COMPLEXES



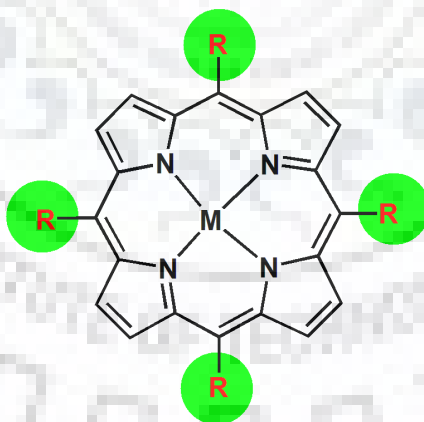
CHAPTER 5

SPECTRAL INVESTIGATIONS OF MESO-TETRAALKYLPORPHYRIN-FULLERENE HOST-GUEST COMPLEXES

5.1 INTRODUCTION

The manipulation of weak forces to assemble new molecular entity is one of the major areas of interest in modern chemistry [1]. Usually, H-bonding, electrostatics, labile metal-ligand bonds, and flat π - π^* interactions have been used to assemble new structures. The spontaneous interaction between simple donor-acceptor molecules leading to isolated nanostructures offers a great potential for straightforward discoveries and realistic applications. Further, non-covalent interactions play a very significant role in the execution of various molecular building blocks which can be utilized for the inception and implementation of advanced functional materials [2]. Such self-assemblies of carefully monitored and designed building blocks can lead to sophisticated photo-active systems [3-5]. Host molecules encapsulating fullerenes are of great importance because of their potential application to the extraction, solubilization and chemical modification of the fullerenes [6]. The cyclic oligomers consisting of electron-rich aromatic components, such as calixarenes, resorcinarenes and cyclotrimeratrylenes, have been reported as π -hosts for fullerenes [7]. One demanding class of compounds which has caught the awareness of many research groups and having vast positive aspect as well as potential is the porphyrin-fullerene conjugates [8-12]. This consideration results from the fact that a fullerene and a porphyrin are instinctively attracted to each other to form a host-guest complex both in the solid state and in solution despite the disparity in external shape between the planar porphyrin and the curved fullerene. Fullerenes [13] have been shown to be good candidates for electron acceptors due to their low reduction potentials [14], three-dimensional arrangement [15], and low reorganization energy involved in electron-transfer reactions [16]. Porphyrins have been utilized as electron donors due to their intense absorption in the visible region and due to the fact that they are easily oxidized [17]. As a result, extensive studies have been performed on covalently linked and self-assembled donor-acceptor dyads composed of porphyrin and fullerene as donor and acceptor entities. Sun *et al.* [18] reported the first structural characterization of a pyrrolidine-functionalized C₆₀ species, the crystal packing of the dyad revealed an intermolecular interaction

of the C₆₀ ball in remarkably close approach to the porphyrin plane. Later, unique cocrystallites of C₆₀ and C₇₀ fullerenes with various metal octaethylporphyrins (MOEPs) and metal tetraphenylporphyrins (MTPPs) have been reported and they shown distinct physicochemical properties. The intermolecular fullerene/porphyrin contacts range from 2.6 to 3.0 Å, which are shorter than typical π - π interactions (3.0-3.5 Å). Structures of supramolecular complexes featuring a single porphyrin-fullerene interaction have been characterized in the solid state (in the form of co-crystals) [19,20]. Nevertheless, these component of porphyrin-fullerene complexes readily detach in solution as a result of reduced thermodynamic stability. In spite of these few covalent macrocyclic metalloporphyrin dimers and one trimer capable of forming thermodynamically stable inclusion complexes with fullerenes in solution have been described. The gain in stability of these complexes not only derives from the macrocyclic effect as discussed above but is also due to the multivalency (several porphyrin units) built into the receptor's structure. *Meso*-tetraalkylporphyrins and their metal complexes are electron rich porphyrins having intense absorption and emission. Due to planar and electron rich nature these porphyrins formed supramolecular dyad with C₆₀. As a continuing effort to build novel supramolecular donor-acceptor systems, in the present study, we have developed donor-acceptor dyads using *meso*-tetraalkylporphyrins (**1-3**) and their Zn(II) complexes with fullerene C₆₀ and studied their spectroscopic as well as electrochemical redox properties.



R = Me, M = 2H; H₂TMeP (1)	R = Me, M = Zn; ZnTMeP (1a)
R = Et, M = 2H; H₂TETp (2)	R = Et, M = Zn; ZnTETp (2a)
R = Pr, M = 2H; H₂TPrP (3)	R = Pr, M = Zn; ZnTPrP (3a)

Chart 5.1 Molecular Structures of Synthesized *Meso*-Tetraalkylporphyrin.

5.2 EXPERIMENTAL SECTION

5.2.1 Reagents

Pyrrole purchased from Alfa Aesar and used as received. Acetaldehyde, propionaldehyde, butyraldehyde, pyridine, Zn(OAc)₂•2H₂O, Na₂SO₄ and NaHCO₃ were purchased from HiMedia, India and used as received. Fullerene (C₆₀) and benzene-d₆ was purchased from sigma-Aldrich and used as received. All solvents employed in this present work were of analytical grade and distilled or dried before use. Silica gel (100 - 200 mesh) was purchased from Thomas Baker, India and used as received. TBAPF₆ was recrystallised twice with ethanol and dried at 50°C under vacuum for 2 days. Toluene (for UV-Visible and fluorescence spectral studies) was dried and distilled from sodium-benzophenone mixture. Precoated thin layer silica gel chromatographic plates were purchased from E. Merck and used as received.

5.2.2 Instrumentation and Methods

Optical absorption spectra were recorded on Agilent Cary 100 spectrophotometer using a pair of quartz cells of 3.5 ml volume and 10 mm path length. Fluorescence spectra were recorded on Hitachi F-4600 spectrofluorometer using a quartz cell of 10 mm path length. ¹H NMR spectra were recorded on JEOL ECX 400 MHz spectrometers in CDCl₃. ESI mass spectra were recorded on Bruker Daltonics microTOF mass spectrometer in positive ion mode using CH₃CN as solvent. The X-ray quality single crystals of **3** were obtained by vapour diffusion of hexane into the tetrachloroethane solution of **3**. Single-crystal XRD data was collected on a Bruker Apex-II CCD diffractometer equipped with a liquid cryostat. The ground state geometry optimisation in gas phase was carried out by DFT calculations using B3LYP functional with 3-21G basis set. Electrochemical measurements were carried out using CH instruments (CHI 620E). A three electrode assembly was used consisted of a Platinum working electrode, Ag/AgCl as a reference electrode and a Pt-wire as a counter electrode.

5.2.3 Synthesis of MTMeP, MTETP, MTPrP (M = 2H, Zn).

(a) Synthesis of 5,10,15,20-tetramethylporphyrin(H₂TMeP) (1) and Their Zn(II) Derivative (1a): 300 ml of propionic acid was taken in 500 ml round bottom flask. To this, 2.3 ml of acetaldehyde, 12 ml of H₂O and 1 ml of pyridine were added and heated to 90°C for 5-10 minutes. To this hot mixture, 4 ml of pyrrole was added and heated to 80 °C for 30 minutes. Then, 1 ml acetaldehyde was added to the reaction mixture as

supplementary amount and heated for further 2 hrs. Reaction mixture was cooled and washed with hot sodium hydroxide solution followed by extraction with CHCl₃. The crude porphyrin was chromatographed on silica gel column using CHCl₃ as an eluent. Yield was found to be 0.28 g (8%).

UV-Vis. λ_{\max} (nm), (log ϵ): 415(5.07), 519(3.67), 555(3.50), 604(3.13), 661(3.37). ¹H NMR in CDCl₃ (δ in ppm): 9.46 (s, 8H, β -H), 4.57 (s, 12H, -CH₃), -2.41(s, 1H, NH) ESI-MS (m/z) found [M+H]⁺ 367.1902 calcd. 367.1878.

40 mg (0.108 mmol) of H₂TMeP was taken in 25 mL of CHCl₃. To this, 0.239 g (10 equiv., 1.08 mmol) of Zn(OAc)₂•2H₂O in 5 mL of methanol was added and refluxed for 30 minutes and then cooled to room temperature, washed with water, dried over anhydrous sodium sulphate. The crude product was purified by column chromatography on silica gel column using CHCl₃ as eluent. Yield: 36 mg (85%). UV-Vis. λ_{\max} (nm), (log ϵ): 418 (5.11), 555(3.68), 594(3.50). ¹H NMR in CDCl₃ (δ in ppm): 9.46 (s, 8H, β -H), 4.57 (s, 12H, -CH₃).

(b) Synthesis of 5,10,15,20-tetraethylporphyrin (H₂TETP) (2) and their Zn(II) derivative (2a):

300 ml of propionic acid was taken in 500 ml RB flask. To this, 2.1 ml of propionaldehyde, 12 ml of H₂O and 1 ml of pyridine were added and heated to 90°C for 5-10 minutes. To this mixture, 4 ml of pyrrole was added and heated to 80°C for 30 minutes. Then, 1 ml propionaldehyde was added to the reaction mixture as supplementary amount and heated for further 2 hrs. Reaction mixture was cooled, washed with hot sodium hydroxide solution followed by extraction with CHCl₃. The crude porphyrin was chromatographed on silica gel column using CHCl₃ as a eluent. Yield was found to be 0.38 g (10%). UV-Vis. λ_{\max} (nm), (log ϵ): 416(4.97), 517(3.60), 551(3.42), 599(3.06), 656(3.26) ¹H NMR in CDCl₃ (δ in ppm): 9.46 (s, 8H, β -H), 4.96-5.01(*J* = 7.6, 7.2, q, 8H, *meso*-CH₂), 2.12(*J* = 7.6, t, 12H, *meso*-CH₃), -2.65(s, 1H, -NH). ESI-MS (m/z) found [M+H]⁺ 423.2562 calcd. 423.2504.

50 mg (0.118 mmol) of H₂TETP was taken in 25 mL of CHCl₃. To this, 0.258 g (10 equiv., 1.18 mmol) of Zn(OAc)₂•2H₂O in 8 mL of methanol was added and refluxed for 30 minutes and then cooled to room temperature, washed with water, dried over anhydrous sodium sulphate. The crude product was purified by column chromatography on silica gel column using CHCl₃ as eluent. Yield: 42 mg (85%). UV-Vis. λ_{\max} (nm), (log ϵ): 418(5.08), 553(3.55), 592(3.13) ¹H

NMR in CDCl₃ (δ in ppm): 9.59 (s, 8H, β -H), 5.06-5.01 ($J = 7.6$, 7.6 q, 8H, *meso*-CH₂), 2.17 ($J = 7.6$, t, 12H, *meso*-CH₃) ESI-MS (m/z) found [M+H+CH₃OH]⁺ 517.5 calcd. 517.1941.

(c) Synthesis of 5,10,15,20-tetrapropylporphyrin (H₂TPrP) (3) and Their Zn(II) Derivative (3a):

300 ml of propionic acid was taken in 500 ml RB flask. To this, 2.3 ml of butyraldehyde, 12 ml of H₂O and 1 ml of pyridine were added and heated to 90 °C for 5-10 minutes. To this mixture, 4 ml of pyrrole was added and heated to 80°C for 30 minutes. Then, 1 ml butyraldehyde was added to the reaction mixture as supplementary amount and heated for further 2 hrs. Reaction mixture was cooled, washed with hot NaOH solution followed by extraction with CHCl₃. The crude porphyrin was chromatographed on silica column using CHCl₃ as a eluent. Yield was found to be 0.4 g (10%).

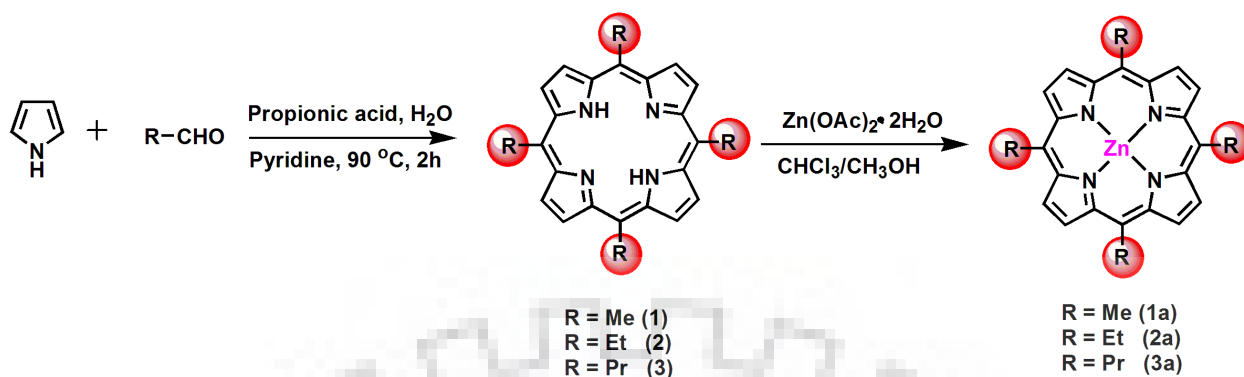
UV-Vis. λ_{\max} (nm), (log ϵ): 415(5.59), 518(4.13), 554(3.19), 559(3.62), 658(3.76). ¹H NMR in CDCl₃ (δ in ppm) 9.47 (s, 8H, β -H), 4.92 ($J = 3.2$, t, 8H, *meso*-CH₂), 2.48-2.58 (m, 8H, *meso*-CH₂), 1.32 ($J = 3.2$, t, 12H, *meso*-CH₃), -2.69 (s, 1H, NH). ESI-MS (m/z) found [M+K]⁺ 517.271 calcd. 517.7609.

50 mg (0.104 mmol) of H₂TPrP was taken in 25 mL of CHCl₃. To this, 0.230 g (10 equiv., 1.04 mmol) of Zn(OAc)₂•2H₂O in 10 mL of methanol was added and refluxed for 30 minutes and then cooled to room temperature, washed with water, dried over anhydrous sodium sulphate. The crude product was purified by column chromatography on silica gel column using CHCl₃ as eluent. Yield: 39 mg (83%). UV-Vis. λ_{\max} (nm), (log ϵ): 418(5.68), 554(4.16), 592(3.72). ¹H NMR in CDCl₃ (δ in ppm): 9.57 (s, 8H, β -H), 4.96 ($J = 7.6$, t, 8H, *meso*-CH₂), 2.63-2.54 (m, 8H, *meso*-CH₂), 1.36 ($J = 7.6$, t, 12H, *meso*-CH₃) ESI-MS (m/z) found [M]⁺ 540.6 calcd. 540.2231.

5.3 RESULTS AND DISCUSSION

5.3.1 Synthesis and Characterization

Meso-tetraalkylporphyrins (1-3) and their Zn(II) complexes (1a-3a) were synthesized according to the modified procedure reported in the literature [21].



Scheme 5.1 Synthesis of *Meso*-Tetraalkylporphyrins (**1-3**) and Their Corresponding Zn(II) complexes (**1a-3a**).

All synthesized porphyrins were characterized by UV-Vis, fluorescence, ¹H NMR spectroscopic techniques, mass spectrometry and cyclic voltammetric studies. ¹H NMR spectra of these porphyrins exhibited characteristic resonances arising from β-pyrrole protons (~ 9.5 δ ppm), and imino protons (for free base porphyrins, -2.4 to -2.8 δ ppm) as shown in Figures A1 to A6, Appendix-IV. *Meso*-alkyl group (methyl/methylene) which is directly attached to the porphyrin ring has shown considerable downfield shift in the range of 4-5 ppm. due to deshielding effect conjugated porphyrin π-system. The integrated intensities of the proton resonances of these porphyrins and mass spectrometry results (Figures A7 to A11, Appendix-IV) are consistent with the proposed structures of **1-3** and their corresponding Zn(II) complexes (**1a-3a**).

5.3.2 Crystal Structure Study of H₂TPrP

Crystallographic data of H₂TPrP (**3**) is listed in Table A1, Appendix-IV. ORTEP views (top and side) of **3** are shown in Figure 5.1. **3** has shown planar confirmation [22] as evidenced from the displacement of core atoms from the mean plane $\Delta_{24} = 0.031 \text{ \AA}$ and $\Delta_{C\beta} = 0.04 \text{ \AA}$. Two of the adjacent *meso*-propyl groups are oriented above the porphyrin plane and rest of the two are projected below the porphyrin plane as shown in Figure 5.1b. The crystal structure packing of **3** along the *a* and *b* crystallographic axes were shown in Figure A12, Appendix-IV. Notably, these porphyrins are held together by weak π-π interactions with a distance of ~ 3.66 Å.

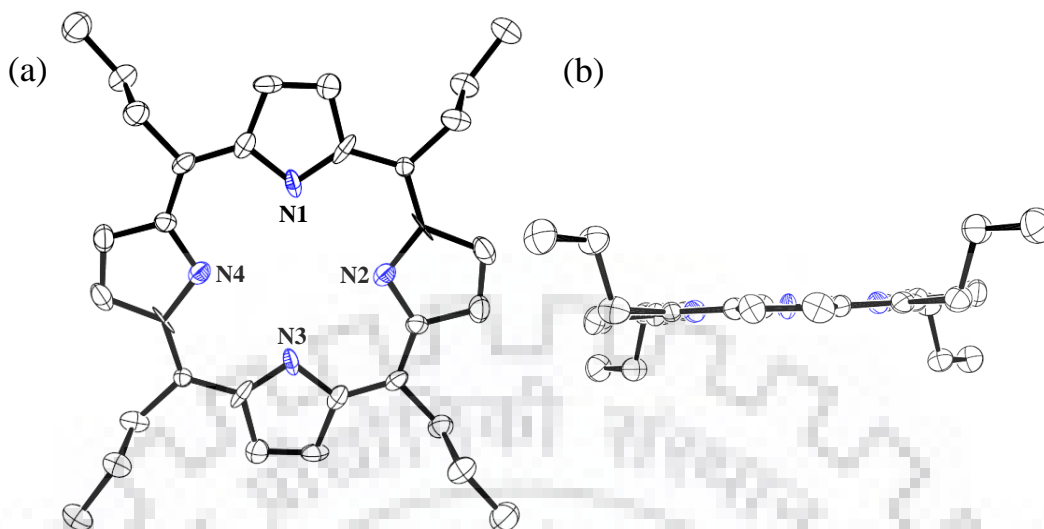


Figure 5.1 Crystal Structure Data of H₂TPrP (**3**) (a) Top View and (b) Side View

5.3.3 UV-Visible Spectral Studies

The UV-Vis absorption spectra of *meso*-tetraalkylporphyrins (**1-3**) and their Zn(II) complexes (**1a-3a**) were recorded in CH₂Cl₂ at 298 K. Table 5.2 lists the absorption spectral data of **1-3** and **1a-3a** in CH₂Cl₂. The UV-Vis spectra of H₂TetP and ZnTetP are shown in Figure 5.2. These porphyrins exhibited characteristic electronic absorption spectral features similar to H₂TPP and ZnTPP. The interaction between C₆₀ and *meso*-tetraalkylporphyrins (**1-3**) was studied by UV-visible spectral titrations by adding C₆₀ to each of the individual starting porphyrins in toluene as shown in Figure 5.3. The decrement in the intensity of Soret band (415 nm) and the concomitant increment in Q bands (518, 554 and 559 nm) revealed the host-guest complexation between porphyrin **3** and fullerene. The spectral intensity changes of the Soret band were used to construct a Benesi-Hildebrand plot as shown in Figure 5.3b. The association constant (K) for **3**:C₆₀ supramolecular complex was found to be $1.83 \times 10^4 \text{ M}^{-1}$ with 1:1 stoichiometry. The similar results were observed for **1-2** in toluene at 298 K as shown in Figures A13 and A14, Appendix-IV. The observed K values obtained from UV-Vis spectral titrations range from $10^4 - 10^5 \text{ M}^{-1}$ as listed in Table 5.1. These values are 10-100 times higher than H₂TPP ($K \sim 10^3 \text{ M}^{-1}$) and Zn-porphyrin dyad. The K values of free base porphyrins with C₆₀ follow the trend



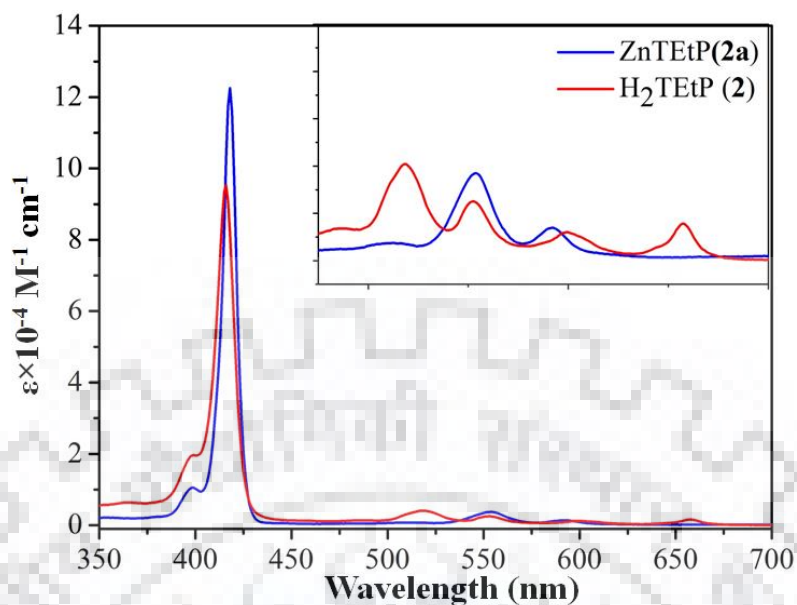


Figure 5.2 UV-Vis. Spectra of **2** (H₂TetP) and **2a** (ZnTetP) in CH₂Cl₂ at 298 K.

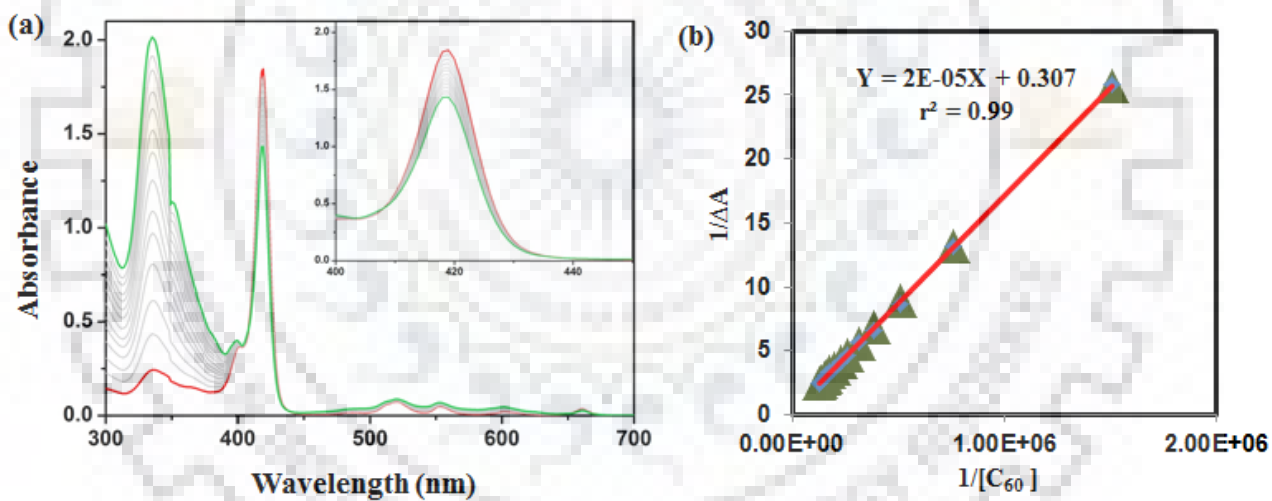


Figure 5.3 (a) Spectral Changes Observed During the Titration of Fullerene (C₆₀) to the Solution of H₂TPrP (**3**) in Toluene at 298 K. (b) Benesi-Hildebrand Plot Constructed for Evaluating the Binding Constant as well as Stoichiometry for **3**:C₆₀ Host-Guest Complex.

Table 5.1 Association Constants of Alkylporphyrin-C₆₀ Supramolecular Dyad in Toluene at 298 K

Porphyrin	Association constant (M ⁻¹)	logK
H ₂ TPP ^a	1×10 ³	3.00
H ₂ THexP ^a	1.7×10 ³	3.23
H ₂ TMeP	1.33×10 ⁵	5.12
H ₂ TEtP	4.84×10 ⁴	4.68
H ₂ TPrP	1.83×10 ⁴	4.26
ZnTMeP	2.18×10 ⁵	5.33
ZnTEtP	2.59×10 ⁴	4.41
ZnTPrP	5.4×10 ³	3.73

^adata taken from ref. 26; H₂THexP = *meso*-tetrahexylporphyrin.

H₂TMeP (**1**) exhibited highest binding constant among all free base porphyrins. As we increase the length of alkyl chain, the association constant decreases is possibly due to the free rotation of alkyl chains that can hinder the approach of C₆₀ towards the porphyrin plane as shown in Figure 5.3(b). Zn(II) porphyrins (**1a-3a**) exhibited similar spectral profiles as shown in Figures A15 to A17, Appendix-IV. All the plots exhibit straight lines with greater than 0.96 correlation coefficient, clearly indicating the 1:1 stoichiometry of C₆₀ and *meso*-tetraalkylporphyrins in the complex.

5.3.4 Fluorescence Spectral Studies

Table 5.2 UV-Vis and Fluorescence Spectral Data of *Meso*-Tetraalkylporphyrins (**1-3** and **1a-3a**) in CH₂Cl₂ at 298 K.

Porphyrin	λ_{abs}		λ_{em}	Φ_{f}
	Soret band	Q-bands		
H ₂ TMeP (1)	415(5.07)	519(3.67), 555(3.50), 604(3.13), 661(3.37)	673, 743	0.093
H ₂ TtEtP (2)	416(4.97)	517(3.60), 551(3.42), 599(3.06), 656(3.26)	666, 735	1.130
H ₂ TPrP (3)	415(5.59)	518(4.13), 554(3.19), 559(3.62), 658(3.76)	666, 736	0.091
ZnTMeP (1a)	418(5.11)	555(3.68), 594(3.50)	608, 661	0.029
ZnTtEtP (2a)	418(5.08)	553(3.55), 592(3.13)	605, 657	0.041
ZnTPrP (3a)	418(5.68)	554(4.16), 592(3.72)	604, 658	0.039

Values in parenthesis refer to log ϵ

The fluorescence spectra of *meso*-tetraalkylporphyrins (**1-3**) and their Zn(II) complexes (**1a-3a**) were recorded in CH₂Cl₂ at 298 K. Table 5.2 lists the emission spectral data of **1-3** and **1a-3a**. These porphyrins exhibited ~10 nm red-shift in their emission spectra as compared to H₂TPP and ZnTPP. The singlet excited state quenching of *meso*-tetraalkylporphyrin and C₆₀ was investigated to obtain the quenching behavior with respect to self assembled dyads. To this end, constant concentration of porphyrins (**1-3** and **1a-3a**) were titrated with increasing concentrations of fullerene C₆₀ in toluene at 298 K. By adding the fullerene, for example, to a solution of **3**, distinct quenching of the porphyrin emission band was observed. Figure 5.4 illustrates several characteristic changes at 666 nm and 736 nm occurred as the complex formation take place. There was an appreciable decrease of the Soret band extinction is observed which is probably due to the complex formation between *meso*-tetraalkylporphyrin and fullerene C₆₀. complexes. Quenching indicated a probable relaxation pathway from the first singlet excited state of the porphyrin to that of the fullerene in toluene as solvent, as a result fluorescence intensity decreases. Another probable explanation is that charge separation might also occur from the excited state of the porphyrin to the C₆₀ in toluene medium [23]. Mutual completion between

energy and electron transfer processes is a common prophecy in porphyrin-fullerene donor-acceptor dyads [24]. In conformationally flexible porphyrin-fullerene dyads, the arrangement of π -stacking interactions are assisted by through-space interactions between the two chromophores which has been reported and explained *via* quenching studies of porphyrin fluorescence and formation of fullerene excited states (by energy transfer) as shown with photophysical experiments in the literature [25]. Similar results were obtained for other complexes as shown in Figures A18 to A22, Appendix-IV. The photophysical experiments disclose that energy transfer route usually dominant over the electron transfer route in non-polar solvent like toluene attributed to deactivation of the photoexcited porphyrin-fullerene dyad. According to the results obtained in the performed optical absorption and emission experiments, the quenching event can be credited to photoinduced energy transfer from porphyrin moiety to the fullerene in the supramolecular complexes of **1-3** and **1a-3a** with C₆₀.

Figure 5.4 shows the fluorescence spectral change during the titration of H₂TPrP and C₆₀. Spectral changes are used to calculate the Stern-Volmer equation as.

$$F_0/F = 1 + K [\text{fullerene}] \quad (1)$$

Where F_0 is the fluorescence intensity in the absence of C₆₀, F is the fluorescence intensity in the presence of C₆₀ and K is the quenching constant. A plot between $(F_0-F)/F$ and [C₆₀] results into straight line reveals the 1:1 binding between these porphyrins and C₆₀.

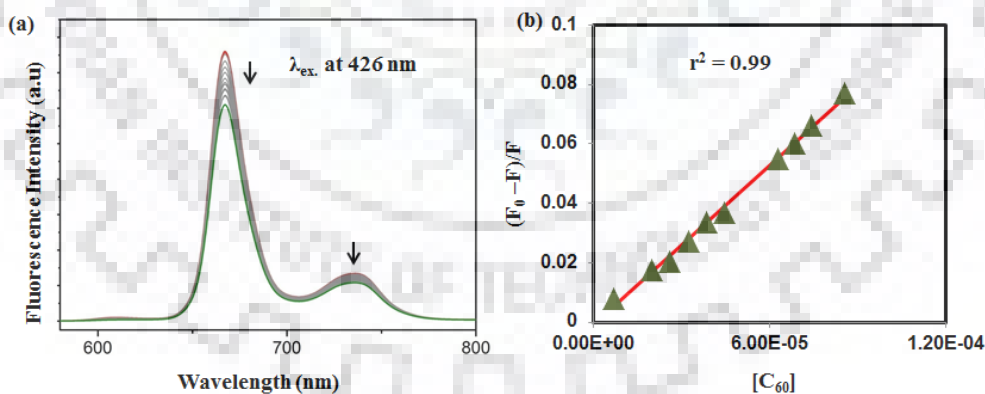


Figure 5.4 (a) Fluorescence Spectral Changes Observed During the Titration of Fullerene (C₆₀) to the Solution of H₂TPrP (**3**) in Toluene at 298 K. (b) Stern-Volmer Plot for **3**:C₆₀ Host-Guest Complex.

Interestingly, **2-3** and **2a-3a** exhibited lower binding constants as compared to **1** and **1a**, respectively which is due to the steric hindrance offered by *meso*-tetraalkyl chains. As we

increase the length of the alkyl chain from C₁ to C₆, the binding constant decreases considerably. In general, all alkyl substituted porphyrins (from propyl to methyl) have exhibited ~ 10 - 100 times higher binding constants as compared to H₂TPP is possibly due to electron-rich nature of porphyrin π -system and decrement in steric hindrance offered by alkyl chains.

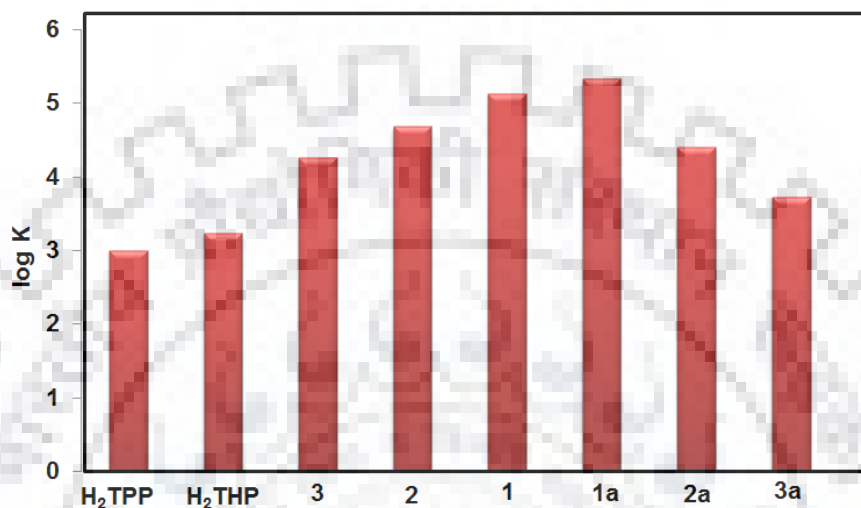


Figure 5.5 Bar Graph Represents logK Values of Differ Alkylporphyrins and Their Zn(II) Derivatives.

5.3.5 Cyclic Voltammetric Studies

Determination of redox potentials of these host-guest porphyrin-fullerene complexes is important to explore the existence of charge-transfer interactions between the porphyrin donor and fullerene acceptor in the ground state, and also to evaluate the energetic of electron-transfer reactions. Keeping this in mind, we have performed a systematic study to calculate the redox activities of the self-assembled dyads using cyclic voltammetric (CV) technique. CV studies were performed in benzonitrile containing 0.1 M TBAPF₆, as both porphyrins and C₆₀ are nicely soluble in benzonitrile. Table 5.3 represents electrochemical redox properties of dyad as compared to porphyrins. As revealed from redox data, alkyl porphyrins are electron-rich in nature. The cyclic voltammograms of the dyad formed by *meso*-tetraalkylporphyrins and C₆₀ show two or three reductions, among them, second is due to both porphyrin and C₆₀. The oxidation potentials of dyads are positively shifted (0.02-0.10 V) as compared to *meso*-tetraalkylporphyrin. The redox potentials of porphyrins and C₆₀ entities revealed small changes upon dyad formation suggesting the existence of weak charge transfer interactions. These

clarification are in concurrence with the earlier value reported for the other porphyrin-C₆₀ derivatives [26].

Table 5.3 Electrochemical Redox Data^a of **1-3** and **1a-3a** in Presence and Absence of C₆₀ in Benzonitrile at 298 K.

Porphyrin	Oxidation			Reduction		$\Delta E_{1/2}$
	P ^{I+/II+}	P ^{0/I+}	P ^{0/-}	P ^{I-/II-}	C ₆₀ ^{0/-}	
H ₂ TMeP		0.78	-0.86	-1.28		1.46
H ₂ TMeP+C ₆₀		0.80	-0.98	-1.49	-	1.78
H ₂ TEtP		0.78	-1.13	-1.35		1.91
H ₂ TEtP+ C ₆₀		0.82	-0.97	-1.39	-0.48	1.79
H ₂ TPrP		0.78	-0.98	-1.33		1.76
H ₂ TPrP+ C ₆₀	1.31	0.88	-0.88	-1.32	-0.45	1.76
ZnTMeP	1.08	0.74	-1.25			1.99
ZnTMeP+C ₆₀		0.70	-		-0.47	-0.91
ZnTEtP	1.05	0.61	-1.43			2.04
ZnTEtP+C ₆₀	1.09	0.59	-1.40		-0.47	-0.92
ZnTPrP	1.05	0.65	-1.53			2.18
ZnTPrP+ C ₆₀	1.01	0.58	-1.39		-0.46	-0.93

^aAg/AgCl taken as reference electrode and 0.1 M TBAPF₆ as supporting electrolyte. 0.01M solution of C₆₀ in PhCN was prepared.

5.3.6 ¹H NMR Studies

Association of Alkyl porphyrins (**1-3**) with C₆₀ was monitored by a ¹H NMR titration method in benzene-d₆. Addition of 1.1 eq. C₆₀ in solution of porphyrin results into upfield shift of β as well as *meso*-alkyl protons. Figure 5.6 shows the comparative ¹H NMR of **1** and **1:C₆₀**. Figure A25 to A29, Appendix-IV, represent the comparative ¹H NMR of **2**, **3**, **1a-3a** and their C₆₀ adduct respectively. These experimental results show upfield shift of protons signals due to interaction of porphyrins and C₆₀. Table A1, Appendix-IV, shows the change in chemical shift of protons by adding 1.1 eq. C₆₀ to the solution of alkyl porphyrins.

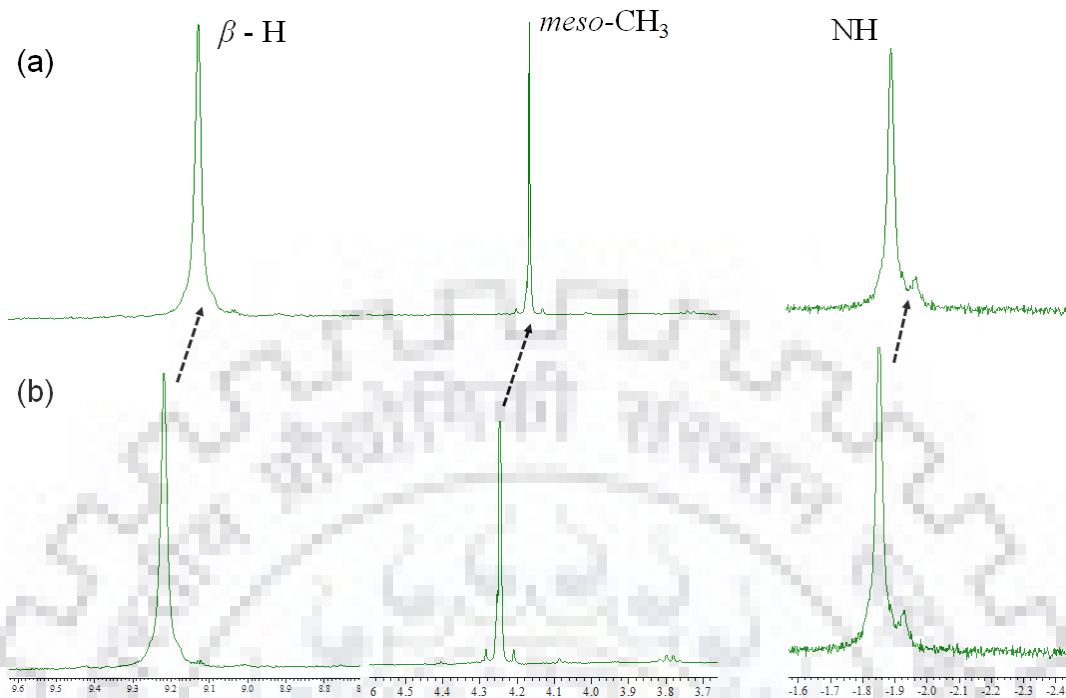


Figure 5.6 ¹H NMR Spectra of (a) **1**:C₆₀ Adduct (b) **1** in C₆D₆ at 298 K.

5.3.7 Computational Studies

The geometry and electronic structure of the dyad was probed by DFT calculations using the B3LYP functional and 3-21G basis set. D'souza *et al* have already reported the advantages of 3-21G basis set in predicting the structure of porphyrin-fullerene donor-acceptor dyad [26–29]. In our calculations, the starting compounds (porphyrin and C₆₀) were fully optimized and allowed to interact. Figure 5.7a represents the fully optimized **1**:C₆₀ dyad. The geometric parameters of the conjugates were obtained after complete energy optimization. The edge-to-edge distance and distance between the porphyrin to the fullerene spheroid were found to be 10.5 Å and 3.7 Å, respectively. These values were comparable to the earlier computed and calculated from X-ray structural studies of ZnTPP-C₆₀Im dyad [30]. The B3LYP/3-21G calculated HOMO and LUMO for the investigated dyad are shown in Figure 5.7b-c. The HOMO was found to be located on the porphyrin entity and LUMO was located on the C₆₀ entity. The absence of HOMOs on C₆₀ and LUMOs on the porphyrin macrocycle suggests weak charge transfer-type interactions between the donor and acceptor entities of the dyad in the ground state.

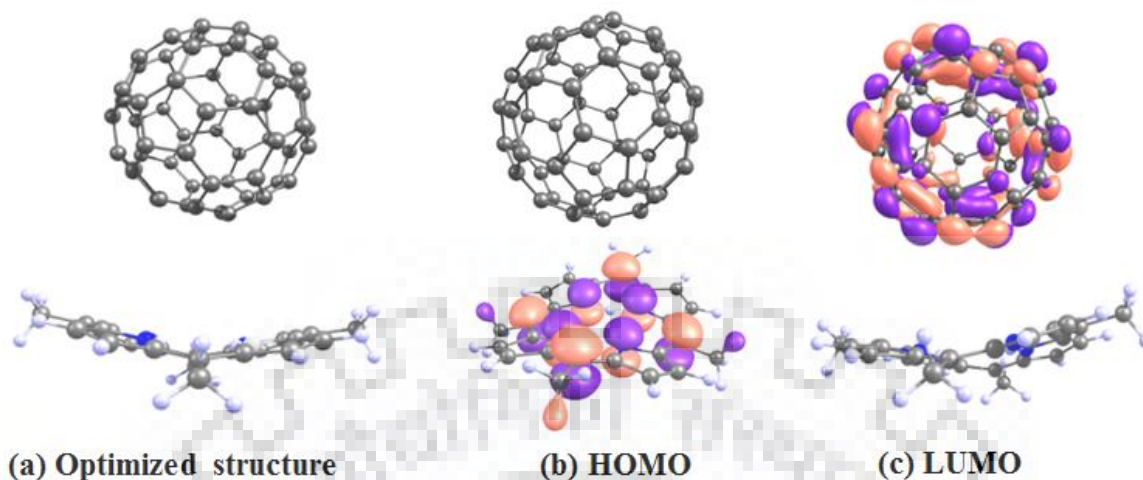


Figure 5.7 (a) B3LYP/3-21G Optimized Structure H₂TMeP (1):C₆₀ Supramolecular Dyad (b) Frontier HOMO Orbitals (c) Frontier LUMO Orbitals.

5.4 CONCLUSIONS

Meso-tetraalkylporphyrins with varying alkyl chain length were synthesized and characterized by various spectroscopic techniques. Crystal structure of *meso*-tetrapropylporphyrin exhibited planar confirmation of porphyrin macrocycle. The binding of C₆₀ with the **1-3** and their zinc complex was monitored by ¹H NMR, and fluorescence spectroscopic techniques. From UV-Vis and fluorescence titrations, the stoichiometry of complexation between porphyrin and fullerene (C₆₀) was found to be 1:1. These *meso*-tetraalkylporphyrins have shown 10-100 times higher association constants than H₂TPP and H₂THexP. As we increase the alkyl chain length from C₁ to C₆, a marked decrement (100 times) in the association constants was observed due to enhanced steric hindrance offered by alkyl chains. The anodic shift in oxidation potentials (20-100 mV) of porphyrin-fullerene dyads as compared to *meso*-tetraalkylporphyrins indicating the supramolecular interactions between the constituents in the ground state. The optimized geometry and electronic structure of **1**:C₆₀ supported the formation of supramolecular dyad and the possibility of charge transfer interactions between porphyrin host and fullerene C₆₀ guest.

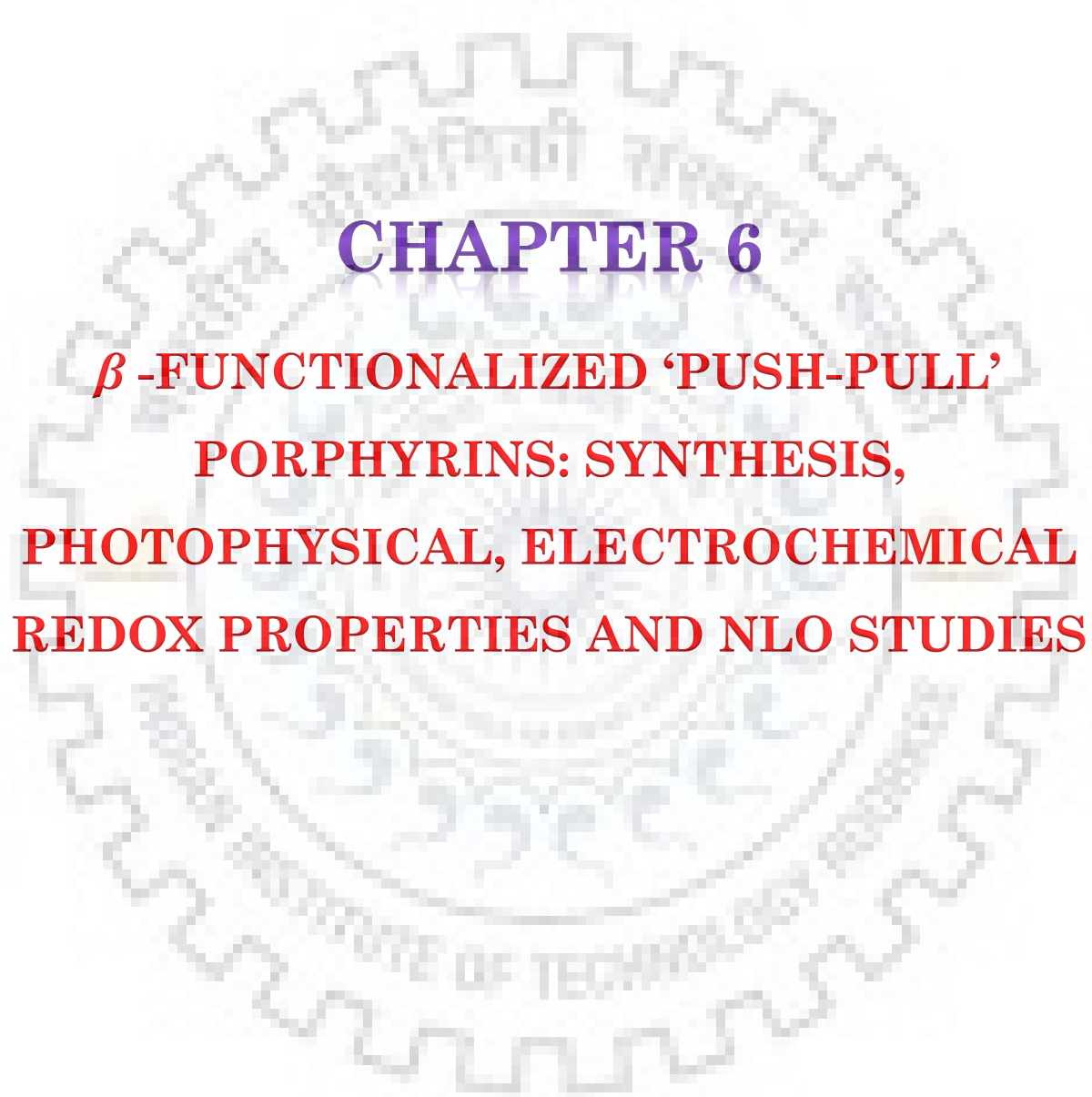
5.5 REFERENCES

- (1) Martín, N.; Nierengarten.; Jean-F. Supramolecular Chemistry of Fullerenes. *Tetrahedron* **2006**, *62*, 1919-2132.
- (2) Imahori, H.; Fukuzumi, S. Porphyrin-and Fullerene-Based Molecular Photovoltaic

- Devices. *Adv. Funct. Mater.* **2004**, *14*, 525–536.
- (3) Balzani, V.; Credi, A.; Silvi, S.; Venturi, M. Artificial Nanomachines Based on Interlocked Molecular Species: Recent Advances. *Chem. Soc. Rev.* **2006**, *35*, 1135–1149.
 - (4) Kira, A.; Umeyama, T.; Matano, Y.; Yoshida, K.; Isoda, S.; Park, J. K.; Kim, D.; Imahori, H. Supramolecular Donor-Acceptor Heterojunctions by Vectorial Stepwise Assembly of Porphyrins and Coordination-Bonded Fullerene Arrays for Photocurrent Generation. *J. Am. Chem. Soc.* **2009**, *131*, 3198–3200.
 - (5) Kotiaho, A.; Lahtinen, R. M.; Tkachenko, N. V.; Efimov, A.; Kira, A.; Imahori, H.; Lemmetyinen, H. Gold Nanoparticle Enhanced Charge Transfer in Thin Film Assemblies of Porphyrin-Fullerene Dyads. *Langmuir* **2007**, *23*, 13117–13125.
 - (6) Diederich, F.; Gómez-López, M. Supramolecular Fullerene Chemistry. *Chem. Soc. Rev.* **1999**, *28*, 263–277.
 - (7) Haino, T.; Yanase, M.; Fukazawa, Y. Fullerenes Enclosed in Bridged Calix[5]Arenes. *Angew. Chem. Int. Ed.* **1998**, *37*, 997–998.
 - (8) Denis, P. A. Theoretical Characterization of Supramolecular Complexes Formed by Fullerenes and Dimeric Porphyrins. *New. J. Chem.* **2018**, *42*, 9956–9964.
 - (9) García-Simón, C.; Costas, M.; Ribas, X. Metallosupramolecular Receptors for Fullerene Binding and Release. *Chem. Soc. Rev.* **2016**, *45*, 40–62.
 - (10) Ho, K. H. Le; Hijazi, I.; Rivier, L.; Gautier, C.; Jusselme, B.; De Miguel, G.; Romero-Nieto, C.; Guldi, D. M.; Heinrich, B.; Donnio, B.; *et al.* Host-Guest Complexation of [60] Fullerenes and Porphyrins Enabled by “Click Chemistry.” *Chem. Eur. J.* **2013**, *19*, 11374–11381.
 - (11) Kamimura, T.; Komura, M.; Komiyama, H.; Iyoda, T.; Tani, F. Linear Assembly of a Porphyrin-C₆₀ Complex Confined in Vertical Nanocylinders of Amphiphilic Block Copolymer Films. *Chem. Commun.* **2015**, *51*, 1685–1688.
 - (12) Chen, Y.; Zhao, D.; Liu, Y. Polysaccharide-Porphyrin-Fullerene Supramolecular Conjugates as Photo-Driven DNA Cleavage Reagents. *Chem. Commun.* **2015**, *51*, 12266–12269.
 - (13) Yadav, B. C.; Kumar, R. Structure, Properties and Applications of Fullerenes. *Int. J. Nanotechnol. Applications* **2008**, *2*, 15-24.
 - (14) Diao, G.; Li, L.; Zhang, Z. The Electrochemical Reduction of Fullerenes, C₆₀ and C₇₀.

- Talanta* **1996**, *43*, 1633–1637.
- (15) Graham, K. R.; Cabanetos, C.; Jahnke, J. P.; Idso, M. N.; El Labban, A.; Ngongang Ndjawa, G. O.; Heumueller, T.; Vandewal, K.; Salleo, A.; Chmelka, B. F.; *et al.* Importance of the Donor:Fullerene Intermolecular Arrangement for High-Efficiency Organic Photovoltaics. *J. Am. Chem. Soc.* **2014**, *136*, 9608–9618.
- (16) Hiroshi, I.; Kiyoshi, H.; Tsuyoshi, A.; Masanori, A.; Seiji, T.; Tadashi, O.; Masahiro, S.; Yoshiteru, S. The Small Reorganization Energy of C₆₀ in Electron Transfer. *Chem. Phys. Lett.* **2003**, *263*, 545–550.
- (17) Benitz, A.; Thomas, M. B.; D'Souza, F. Cover Picture: Geometry-Controlled Photoinduced Charge Separation and Recombination in a Trans -A₂B₂ -Functionalized Donor-Acceptor Conjugate Composed of a Multimodular Zinc Porphyrin and Fullerene. *ChemPhotoChem* **2017**, *1*, 1–1.
- (18) Sun, Y.; Drovetskaya, T.; Bolskar, R. D.; Bau, R.; Boyd, P. D. W.; Reed, C. A. Fullerides of Pyrrolidine-Functionalized C₆₀. *J. Org. Chem.* **2002**, *62*, 3642–3649.
- (19) Yamada, H.; Ohkubo, K.; Kuzuhara, D.; Takahashi, T.; Sandanayaka, A. S. D.; Okujima, T.; Ohara, K.; Ito, O.; Uno, H.; Ono, N.; *et al.* Synthesis, Crystal Structure, and Photodynamics of π -Expanded Porphyrin-Fullerene Dyads Synthesized by Diels-Alder Reaction. *J. Phys. Chem. B* **2010**, *114*, 14717–14728.
- (20) Lyons, D. M.; Mohanraj, J.; Accorsi, G.; Armaroli, N.; Boyd, P. D. W. A Supramolecular Porphyrin-Ferrocene-Fullerene Triad. *New. J. Chem.* **2011**, *35*, 632–639.
- (21) Neya, S.; Funasaki, N. A Facile Synthesis of the Lowest Homologues of Meso-Tetraalkylporphyrin. *J. Heterocycl. Chem.* **1997**, *34*, 689–690.
- (22) Coddling, P. W.; Tulinsky, A. Structure of Tetra-n-Propylporphine. An Average Structure for the Free Base Macrocycle from Three Independent Determinations. *J. Am. Chem. Soc.* **1972**, *94*, 4151–4157.
- (23) Zarrabi, N.; Agatemor, C.; Lim, G. N.; Matula, A. J.; Bayard, B. J.; Batista, V. S.; D'Souza, F.; Poddutoori, P. K. High-Energy Charge-Separated States by Reductive Electron Transfer Followed by Electron Shift in the Tetraphenylethylene- Aluminum(III) Porphyrin-Fullerene Triad. *J. Phys. Chem. C* **2019**, *123*, 131–143.
- (24) Martini, I. B.; Ma, B.; Da Ros, T.; Helgeson, R.; Wudl, F.; Schwartz, B. J. Ultrafast Competition between Energy and Charge Transfer in a Functionalized Electron

- Donor/Fullerene Derivative. *Chem. Phys. Lett.* **2000**, 327, 253–262.
- (25) Gust, D.; Moore, T. A.; Moore, A. L.; Kuciauskas, D.; Liddell, P. A.; Halbert, B. D. Mimicry of Carotenoid Photoprotection in Artificial Photosynthetic Reaction Centers: Triplet-Triplet Energy Transfer by a Relay Mechanism. *J. Photochem. Photobiol B.* **1998**, 43, 209–216.
- (26) D'Souza, F.; Deviprasad, G. R.; Zandler, M. E.; Hoang, V. T.; Klykov, A.; VanStipdonk, M.; Perera, A.; El-Khouly, M. E.; Fujitsuka, M.; Ito, O. Spectroscopic, Electrochemical, and Photochemical Studies of Self-Assembled via Axial Coordination Zinc Porphyrin-Fulleropyrrolidine Dyads. *J. Phys. Chem. A* **2002**, 106, 3243–3252.
- (27) Hu, Y.; Thomas, M. B.; Jinadasa, R. G. W.; Wang, H.; D'Souza, F. Competitive Energy and Electron Transfer in β -Functionalized Free-Base Porphyrin–Zinc Porphyrin Dimer Axially Coordinated to C₆₀: Synthesis, Supramolecular Formation and Excited-State Processes. *Chem. Eur. J.* **2017**, 23, 12805–12814.
- (28) Follana-Berná, J.; Seetharaman, S.; Martín-Gomis, L.; Charalambidis, G.; Trapali, A.; Karr, P. A.; Coutsolelos, A. G.; Fernández-Lázaro, F.; D'Souza, F.; Sastre-Santos, Á. Supramolecular Complex of a Fused Zinc Phthalocyanine-Zinc Porphyrin Dyad Assembled by Two Imidazole-C₆₀ Units: Ultrafast Photoevents. *Phys. Chem. Chem. Phys.* **2018**, 20, 7798–7807.
- (29) Obondi, C. O.; Lim, G. N.; Jang, Y.; Patel, P.; Wilson, A. K.; Poddutoori, P. K.; D'Souza, F. Charge Stabilization in High-Potential Zinc Porphyrin-Fullerene via Axial Ligation of Tetrathiafulvalene. *J. Phys. Chem. C* **2018**, 122, 13636–13647.
- (30) D'Souza, F.; Rath, N. P.; Deviprasad, G. R.; Zandler, M. E. Structural Studies of a Non-Covalently Linked Porphyrin-Fullerene Dyad. *Chem. Commun.* **2001**, 3, 267–268.



CHAPTER 6
 **β -FUNCTIONALIZED 'PUSH-PULL'
PORPHYRINS: SYNTHESIS,
PHOTOPHYSICAL, ELECTROCHEMICAL
REDOX PROPERTIES AND NLO STUDIES**



CHAPTER 6

β -FUNCTIONALIZED 'PUSH-PULL' PORPHYRINS: SYNTHESIS, PHOTOPHYSICAL, ELECTROCHEMICAL REDOX PROPERTIES AND NLO STUDIES

6.1 INTRODUCTION

The wide use of optical radiation which created from natural or artificial sources in the important applicative fields such as communication, machining, surgery, imaging and energy conversion urge the development of adequate tools to control the radiation features to achieve the desired function driven by the light in most durable, efficient and fast way. Sizeable attention has been focused dramatically on third order nonlinear optical (NLO) materials for their potential in optical communication, ultrahigh speed signal processing and aberration-corrected imaging [1-3]. NLO is described by a set of nonlinear response of properties such as polarization, frequency, phase and path of incident light consequently exhibiting by materials which can be further used for photonic applications [4]. NLO material have attracted physicists'/chemists'/material chemists' interest since past three decades due to their great potential in various applications such as optical limiting, optical communication, data storage devices, multi-photo imaging, fluorescence and surface-enhanced raman scattering [5,6]. Nonlinear optical activity was first investigated in inorganic crystal (LiNbO_3) and further extended to a variety of compounds [7]. Organic, inorganic and organometallic compounds with highly conjugated π -system, fascinating photophysical and electrochemical properties able to produce nonlinear optical properties [8]. Porphyrin and phthalocynines are suitable candidates for the NLO due to their high thermal and chemical stability, delocalized π -electronic system and good solubility. Further, they can generate a significant increment in hyper polarizability *via* facile electronic exchange through π -ring system or inserting the metal in core of porphyrin or through peripheral functionalization. Nonlinear response of porphyrin molecule can be enhances by peripheral substitution which tune the photophysical and electrochemical properties of porphyrin. Several porphyrins and corroles have been investigated for NLO studies [9,10]. A number of asymmetric porphyrins mainly reported for nonlinear optics. In 1998 Albert *et al.* reported NLO response on push-pull porphyrins and suggest that the NLO response obtained by (1) reducing the dihedral twist of

phenyl substituents with respect to the plane of porphyrin macrocycle, (2) β /*meso* functionalization of macrocycle *via* electron donor and acceptor substituents [11]. Molecule which containing large conjugated π -system with acceptor and donor groups at antipodal position, used as NLO materials. NLO properties can be tuned by β -functionalization of porphyrin molecules with both electron-withdrawing and electron-donating groups due to altered optoelectronic and redox properties. Triphenylamine, an electron-donating group, is a famous building block in material chemistry and use for the synthesis of such type of material which used in various applications including photovoltaic devices [12]. Triphenylamine used in optoelectronic material due to its good electron donating and hole transport mobility [13]. It is also found that many nitro group containing porphyrins are used for NLO application where nitro group act as acceptor and generate the asymmetry in porphyrin molecule. Porphyrin is a versatile functional molecule for its electrochemical and photophysical properties and which can be altered by changing the substituents at β /*meso* position of the macrocycle. Porphyrins and their metal complexes have been utilized in various fields such as materials, medicine and catalysis [14–17]. The studies on nonplanarity of porphyrin are of special interest, due to their biological significance. Herein, we report two series of tri- β -substituted push-pull porphyrins having formyl/nitro as an acceptor group and triphenylamine as a donor group. Triphenylamino group was attached at β -pyrrole position of porphyrin core by replacing bromo group via Pd(0) catalyzed coupling reaction. Synthesized porphyrin and their metal complexes were fully characterized by various spectroscopic techniques and their structural, optical and redox properties were studied. So, likewise in the present work, we have put forth the variation in two photon absorption, NLO coefficients and third order NLO susceptibility of $H_2TPP(TPA)_2NO_2$ and $H_2TPP(TPA)_2CHO$ for different wavelength by Z-scan experiment.

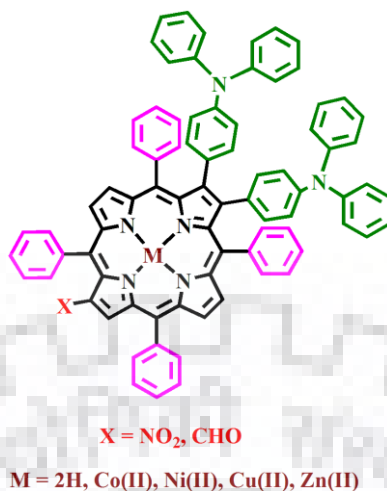


Chart 6.1 Molecular Structure of Synthesized Tri- β -substituted "Push-Pull" Porphyrins.

6.2 EXPERIMENTAL SECTION

6.2.1 Reagents

Benzaldehyde and pyrrole were received from HiMedia and Alfa Aesar, respectively and used as received. All metal salts, CaH_2 , N-bromosuccinimide and P_2O_5 were purchased from HiMedia. 4-(N,N-Diphenylamino)phenylboronic acid was prepared according to reported literature [18]. $\text{Pd}(\text{PPh}_3)_4$ was purchased from Sigma-Aldrich (India) and used as received. Toluene was of analytical grade, first dried and distilled over P_2O_5 to use. TBAPF_6 were purchased from HiMedia, India and recrystallized before use. Silica gel employed in this work purchased from Thomas Baker. H_2TPP , H_2TPPNO_2 , $\text{H}_2\text{TPPBr}_2\text{CHO}$ and $\text{H}_2\text{TPPBr}_2\text{NO}_2$ were synthesized according to the reported literature [19-22].

6.2.2 Instrumentation and Method

UV-Visible and emission spectra were recorded using Shimadzu spectrophotometer (UV-2600) and Hitachi F-4600 fluorescence spectrophotometer, respectively with quartz cell of 1 cm path length. All MALDI-TOF mass spectra were recorded with Bruker Ultra-fleXtreme TN MALDITOF/TOF spectrometer and HABA (2-(4-hydroxyphenylazo)benzoic acid) was used as matrix. ^1H and ^{13}C NMR spectra were recorded with Bruker AVENCE 400 MHz NMR spectrometer in CDCl_3 at 298 K. DFT study was carried out using B3LYP functional and LANL2DZ basis set. Electrochemical measurement were carried out using (CH 620E) CH instrument. Cyclic voltammetry studies were performed in distilled CH_2Cl_2 containing 0.1 M TBAPF_6 (tetrabutylammonium hexafluorophosphate) and three electrode assembly were used

containing Ag/AgCl as reference electrode, platinum wire counter electrode and platinum working electrode. We have utilized a Ti-sapphire laser (Chameleon, Coherent) for Z scan experiment having 150 fs pulse duration, repetition rate of 80 MHz, beam diameter 2 mm, along with 680-1080 nm spectral range feasibility. We engaged a 10 cm lens for focusing the beam onto the sample. We carried out the experiment for 680-850 nm range with corresponding Rayleigh range 0.5-1 mm using neutral density filters for input pulse energy attenuation. The fine powder-like samples were utilized making them dissolved in Toluene (10 mM concentration) and they resulted in a linear transmittance of 70-80% in 680-850 nm wavelength range. We have used a 1mm glass cuvette for containing the sample solution while scanning with a linear translation stage and we fed the transmittance data to a photo-diode connected to a power meter. For the closed aperture mode, a varying aperture was kept in front of photodiode and the experiment was repeated several times to obtain the averaged best data for extracting the NLO coefficients.

6.2.3 Synthesis of $\text{H}_2\text{TPP}(\text{TPA})_2\text{NO}_2$ and $\text{H}_2\text{TPP}(\text{TPA})_2\text{CHO}$:

Free base 2-nitro-12,13-dibromo-5,10,15,20-tetraphenylporphyrin (0.16 g, 0.196 mmol) was taken in two neck round bottom (RB) flask. To this, a solution of 4-(N,N-Diphenylamino)phenylboronic acid (0.676 g, 2.35 mmol) in toluene (80 ml) and K_2CO_3 (0.648 g, 4.68 mmol) were added and argon was purged for 15 min. Further, $\text{Pd}(\text{PPh}_3)_4$ (0.045 g, 0.039 mmol) was added under inert atmosphere and the reaction mixture was heated to 95 °C for 20 h. After completion of reaction, reaction mixture was cooled to room temperature and reduce to concentrate by rotary evaporation. Then, residue was dissolved in chloroform and washed with aqueous sodium bicarbonate followed by brine solution. The organic layer was separated, dried over anhydrous Na_2SO_4 and evaporated to reduce. The crude product was purified by silica gel column chromatography using CHCl_3 /hexane mixture (3:1 v/v) and the polarity was enhanced up to 100% CHCl_3 . The product was found with yield 65% (105 mg, 0.091 mmol).

$\text{H}_2\text{TPP}(\text{TPA})_2\text{CHO}$ was also synthesized by similar procedure and yield was found to be 30% (30 mg, 0.042 mmol).

$\text{H}_2\text{TPP}(\text{TPA})_2\text{NO}_2$: UV-Vis. λ_{max} (nm), (log ϵ): 308 (4.65), 438 (5.13), 539 (4.12), 660 (3.83). ^1H NMR in CDCl_3 , 400 MHz: δ (ppm): 8.98 (s, 1H, β -H), 8.79-8.83 (m, 2H, β -H), 8.62 (t, $J = 4$ Hz, 2H, β -H), 8.29 (dd, $J = 4$ Hz, 8 Hz, 4H, *meso-o*-Ph-H), 7.93-7.99 (m, 8H, *meso-o*-Ph-H),

7.73-7.80 (m, 6H, *meso-m*-Ph-H), 7.51 (m, 2H, *meso-m*-Ph-H), 7.42-7.45 (m, 4H, *meso-p*-Ph-H), 7.28 (s, 2H, TPA-H), 7.24 (s, 2H, TPA-H), 6.98-7.03(m, 12H, TPA-H), 6.78-6.81(m, 4H, TPA-H), 6.65 (d, $J = 8$ Hz, 4H,TPA) -2.29 (s, 2H, -NH). MALDI-TOF-MS (m/z): found $[M+H]^+$ 1146.825, calcd. 1146.44. Elemental analysis calcd. for $C_{80}H_{55}N_7O_2$: C, 83.82%; H, 4.84%; N, 8.55% and found: C, 84.28%; H, 5.12%; N, 8.77%.

H₂TPP(TPA)₂CHO: UV-Vis. λ_{max} (nm), (log ϵ): 308 (4.59), 438 (5.24), 535 (4.06), 576 (3.88), 612(3.72), 678(3.61). ¹H NMR in CDCl₃, 400 MHz: δ (ppm): 9.34 (s, 1H, CHO), 9.24(s, 1H, β -H), 8.76 (d, $J = 4$ Hz, 2H, β -H), 8.58 (t, $J = 8$ Hz, 2H, β -H), 8.25 (dd, $J = 8$ Hz, 4 Hz 4H, *meso-o*-Ph-H), 7.81-7.95 (t, $J = 4$ Hz, 4H, *meso-o*-Ph-H), 7.74-7.80 (m, 8H, *meso-m*-Ph-H), 7.50-7.54 (t, $J = 4$ Hz, 2H, *meso-p*-Ph-H), 7.33-7.39 (m, 2H, *meso-p*-Ph-H), 7.31 (m, 4H, TPA-H), 6.98-7.13 (s, 16H, TPA-H), 6.81-6.86(m, 4H, TPA-H), 6.66(d, $J = 4$ Hz, 4H, TPA-H), -2.26 (s, 2H, -NH). MALDI-TOF-MS (m/z): found $[M+H]^+$ 1129.53, calcd. 1129.45. Elemental analysis calcd. for $C_{81}H_{56}N_6O$: C, 85.90%; H, 5.06%; N, 7.03% and found: C, 85.97%; H, 5.19%; N, 7.36%.

6.2.4 Synthesis of MTPP(TPA)₂NO₂ and MTPP(TPA)₂CHO, where M = Co(II), Ni(II), Cu(II), Zn(II).

In a 100 ml RB, H₂TPP(TPA)₂NO₂/H₂TPP(TPA)₂CHO (0.052 mmol) was taken and dissolved in 12 ml of chloroform. To this, 10 equiv. of M(OAc)₂·nH₂O (where M = Co, Cu and Zn) dissolved in CH₃OH was added, then reaction mixture was allowed to reflux for half an hour. Reaction mixture was washed with water to remove excess metal salt. The organic layer was separated, dried over anhydrous Na₂SO₄ and the solvent was removed by rotatory evaporation. The product was subjected to silica column chromatography for purification using CHCl₃ as an eluent. Further, NiTPP(TPA)₂NO₂ complex was prepared by refluxing H₂TPP(TPA)₂NO₂ or H₂TPP(TPA)₂CHO and Ni(OAc)₂·2H₂O in the DMF for 3 h. Then it was cooled to room temperature, added water to get precipitate and filtered on G-4 crucible. The crude product was further purified via silica gel column chromatography using CHCl₃ as eluent. Yield was found to be 80-90%.

CoTPP(TPA)₂NO₂: UV-Vis. λ_{max} (nm), (log ϵ): 308 (4.76), 432 (5.01), 551 (4.11), 597 (4.10). MALDI-TOF-MS (m/z): found $[M+H]^+$ 1203.257, calcd. 1203.36. Elemental analysis calcd. for $C_{80}H_{53}CoN_7O_2$: C, 79.85%; H, 4.44%; N, 8.15% and found: C, 79.26%; H, 4.99%; N, 8.42%.

NiTPP(TPA)₂NO₂: UV-Vis. λ_{\max} (nm), (log ϵ): 309 (4.77), 438 (5.11), 553 (4.17), 602 (4.14). ¹H NMR in CDCl₃, 400 MHz: δ (ppm): 8.91 (s, 1H, β -H), 8.56 (d, J = 4 Hz, 1H, β -H), 8.45 (d, J = 4 Hz, 1H, β -H), 8.32 (d, J = 4 Hz, 1H, β -H), 8.26 (d, J = 4 Hz, 1H, β -H), 7.96-7.99 (m, 4H, *meso-o*-Ph-H), 7.56-7.70 (m, 12H, *meso-o*. *m* and *p*-Ph-H), 7.41-7.45 (m, 3H, *meso-p*-Ph-H), 7.28-7.30 (m, 4H, TPA), 7.23-7.25 (m, 4H, TPA-H), 6.98-7.05 (m, 12H, TPA-H), 6.60-6.75 (m, 8H, TPA-H). MALDI-TOF-MS (m/z): found [M]⁺ 1201.626, calcd. 1201.36. Elemental analysis calcd. for C₈₀H₅₃N₇NiO₂: C, 79.87%; H, 4.44%; N, 8.15% and found: C, 79.20%; H, 4.78%; N, 8.79%.

CuTPP(TPA)₂NO₂: UV-Vis. λ_{\max} (nm), (log ϵ): 309 (4.73), 432 (5.17), 559 (4.16), 606 (4.10). MALDI-TOF-MS (m/z): found [M+H]⁺ 1207.819, calcd. 1207.37. Elemental analysis calcd. for C₈₀H₅₃CuN₇O₂: C, 79.55%; H, 4.42%; N, 8.12% and found: C, 79.70%; H, 4.80%; N, 8.55%.

ZnTPP(TPA)₂NO₂: UV-Vis. λ_{\max} (nm), (log ϵ): 309 (4.85), 434 (5.50), 560 (4.47), 609 (4.36). ¹H NMR in CDCl₃, 400 MHz: δ (ppm): 9.16 (s, 1H, β -H), 8.86 (d, J = 8 Hz, 1H, β -H), 8.83 (d, J = 4 Hz, 1H, β -H), 8.59-8.61 (m, 2H, β -H), 8.17-8.21 (m, 4H, *meso-o*-Ph-H), 7.84-7.88 (m, 4H, *meso-o*-Ph-H), 7.66-7.79 (m, 6H, *meso-m*-Ph-H), 7.49-7.52 (m, 2H, *meso-m*-Ph-H), 7.32-7.36 (m, 4H, *meso-p*-Ph-H), 7.27-7.29 (m, 6H, TPA-H), 7.25 (s, 2H, TPA-H), 6.98-7.07 (m, 12H, TPA-H) 6.86 (d, J = 8 Hz, 4H, TPA-H), 6.69 (d, J = 8 Hz, 4H, TPA-H). MALDI-TOF-MS (m/z): found [M+H]⁺ 1208.750, calcd. 1208.36. Elemental analysis calcd. for C₈₀H₅₃N₇NiO₂: C, 79.43%; H, 4.42%; N, 8.10% and found: C, 79.66%; H, 4.76%; N, 8.44%.

CoTPP(TPA)₂CHO: UV-Vis. λ_{\max} (nm), (log ϵ): 308 (4.70), 434(5.11), 555 (4.16), 593 (4.09). MALDI-TOF-MS (m/z): found [M+H]⁺ 1186.82, calcd. 1186.37. Elemental analysis calcd. for C₈₁H₅₄CoN₆O: C, 80.18%; H, 4.49%; N, 6.56% and found: C, 79.97%; H, 4.62%; N, 6.69%.

NiTPP(TPA)₂CHO: UV-Vis. λ_{\max} (nm), (log ϵ): 309 (4.76), 437 (5.34), 554 (4.11), 598 (4.08). ¹H NMR in CDCl₃, 400 MHz: δ (ppm): 9.24 (s, 1H, CHO), 9.18(s, 1H, β -H), 8.56-8.59(m, 2H, β -H), 8.31-8.35 (m, 2H, β -H), 7.98 (dd, J = 4Hz, 4 Hz 2H, *meso-o*-Ph-H), 7.95 (dd, J = 4 Hz, 4 Hz 2H, *meso-o*-Ph-H), 7.65-7.72 (m, 10 H, *meso-o*- and *m*-Ph-H), 7.57 (d, J = 8Hz, 4H, *meso- m* and *p*-Ph-H), 7.40-7.44 (m, 2H, *meso-p*-Ph-H), 7.23 (s, 4H, TPA-H), 6.98-7.07 (m, 16H, TPA-H), 6.72 (d, J = 4Hz, 4H, TPA-H), 6.62 (d, J = 4Hz, 4H, TPA-H). MALDI-TOF-MS (m/z):

found $[M+H]^+$ 1185.70, calcd. 1185.37. Elemental analysis calcd. for $C_{80}H_{53}N_7NiO_2$: C, 80.20%; H, 4.49%; N, 6.56% and found: C, 80.87%; H, 4.69%; N, 6.47%.

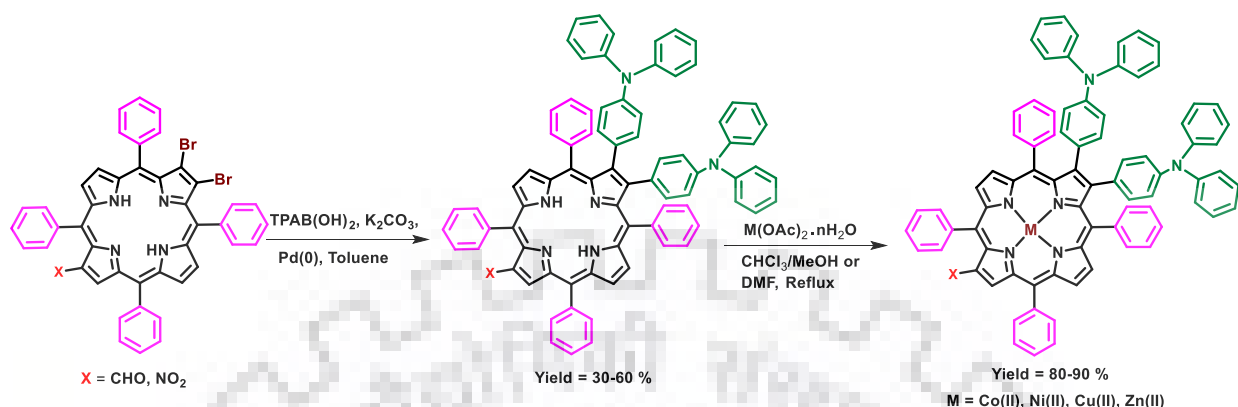
CuTPP(TPA)₂CHO: UV-Vis. λ_{max} (nm), (log ϵ): 309 (4.81), 434 (5.46), 559 (4.25), 600 (4.20). MALDI-TOF-MS (m/z): found $[M+H]^+$ 1190.49, calcd. 1190.38. Elemental analysis calcd. for $C_{81}H_{54}CuN_6O$: C, 79.75%; H, 4.46%; N, 6.53% and found: C, 79.97%; H, 4.82%; N, 6.67%.

ZnTPP(TPA)₂CHO: UV-Vis. λ_{max} (nm), (log ϵ): 311 (4.42), 434 (5.16), 562 (3.91), 603 (3.83). ¹H NMR in CDCl₃, 400 MHz: δ (ppm): 9.51(s, 1H, CHO), 9.29 (s, 1H, β -H), 8.84 (d, $J = 4$ Hz, 2H, β -H), 8.61-8.64 (m, 2H, β -H), 8.24 (d, $J = 8$ Hz, 2H, *meso-o*-Ph-H), 8.17 (d, $J = 8$ Hz, 2H, *meso-o*-Ph-H), 7.85-7.88 (m, 4H, *meso-m*-Ph-H), 7.69-7.81 (m, 10H, *meso-m* and *p*-Ph-H), 7.47-7.52 (m, 2H, *meso-p*-Ph-H), 7.24-7.35 (m, 4H, TPA-H), 7.06 (d, $J = 8$ Hz, 2H, TPA-H), 6.99 (t, $J = 8$ Hz, 6H, TPA-H) 6.88 (d, $J = 4$ Hz, 4H, TPA-H), 6.69 (d, $J = 8$ Hz, 4H, TPA-H). MALDI-TOF-MS (m/z): found $[M+H]^+$ 1191.94, calcd. 1191.37. Elemental analysis calcd. for $C_{80}H_{53}N_7NiO_2$: C, 79.58%; H, 4.45%; N, 6.51% and found: C, 79.69%; H, 4.47%; N, 6.94%.

6.3 RESULTS AND DISCUSSION

6.3.1 Synthesis and Characterization

Two new family of free base asymmetric β -trisubstituted porphyrins (MTPP(TPA)₂X, M = 2H, Zn(II), Co(II), Ni(II) and Cu(II); X = CHO/NO₂) were synthesized using Suzuki cross coupling reaction of H₂TPPBr₂X (X = CHO/NO₂) with 4-(N,N-Diphenylamino)phenylboronic acid where bromo substituents were replaced by triphenylamine groups. Metal complexes of these two porphyrins were prepared by reported procedure. As per our knowledge, it is the first time that β -triphenylamine substituted porphyrins were reported. All the synthesized porphyrins were characterized by various spectroscopic techniques such as UV-Vis, fluorescence, ¹H NMR spectroscopic techniques, MALDI-TOF mass spectrometry and elemental analysis. ¹H NMR spectra of MTPP(TPA)₂X (where X = NO₂/CHO and M = 2H, Ni, Zn) exhibited resonance arising from β -triphenylamine, *meso*-phenyl, β -pyrrole, -CHO proton and inner -NH protons. ¹H and ¹³C NMR spectra have shown in Figures A1-A11, Appendix-V. Integrated intensity and position of protons found in closed agreements with the proposed structure. MALDI-TOF-mass spectra of synthesized porphyrins shown in Figures A12-A21, Appendix-V.



Scheme 6.1 Synthesis of Mixed Tri- β -Substituted ‘Push-Pull’ Porphyrins.

6.3.2 Optical Absorption and Emission Spectral Studies

Absorption and emission properties of porphyrin were influenced by electronic nature of β -substituents (electron donor/electron acceptor), core metal ions and nonplanarity of macrocyclic core [23-26]. The optical absorption and emission spectra of synthesized porphyrins are shown in Figure 6.1. Table 6.1 lists the absorption and emission data of all synthesized porphyrins. The Soret band of these porphyrins was found in range of $\lambda = 432$ -438 nm and last Q bands are in 593-690 nm. MTPP(TPA)₂X (X = NO₂/CHO, M = 2H, Co, Ni, Cu, Zn) exhibited 16-22 nm red shift in the Soret band and 39-58 nm shift in last Q band as compared to MTPP due to resonance and inductive effect of β -substituents on π -system of porphyrin and it is well known that the nonplanar conformation of porphyrin also induces the unusual red shift in their spectral properties [27,28]. The full width half maximum (FWHM) of MTPP(TPA)₂X (X = NO₂/CHO; M = 2H, Zn) are greater than MTPPs (M = 2H, Zn) which reflected the greater extent of charge transfer from HOMO of triphenylamine moieties (electron donor) to π^* orbitals of -NO₂/CHO group (electron acceptor) [29] and revealed the intramolecular charge-transfer from donor to acceptor group. The emission spectra of MTPP(TPA)₂X (X = NO₂/CHO, M = 2H and Zn(II)) were recorded in the dichloromethane at 298 K. These porphyrins exhibited broad and red shifted emission spectra due to asymmetric arrangement of β -substituents. The fluorescence maxima of free base and Zn(II) derivatives of synthesized porphyrins observed red shifted than H₂TPP and ZnTPP, respectively. H₂TPP(TPA)₂NO₂ and H₂TPP(TPA)₂CHO exhibited emission spectra at 754 and 700 nm, respectively which are found 50-100 nm red shifted as compared to

H₂TPP. These porphyrins exhibited reduced quantum yield and shorter lifetime, due to nonplanar conformation of porphyrin macrocycle [30].

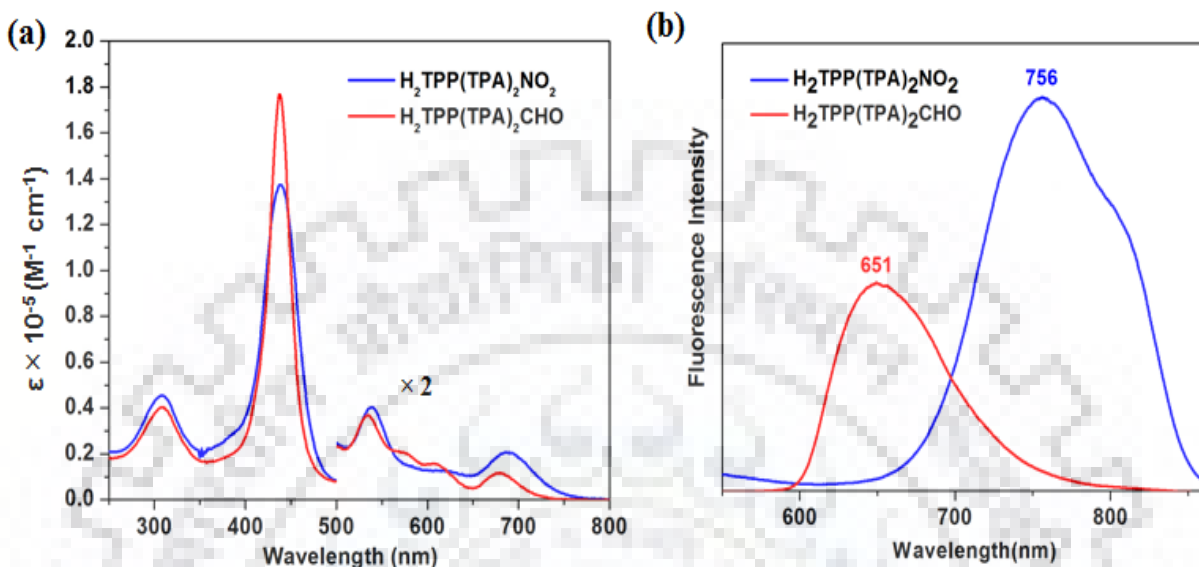


Figure 6.1 (a) UV-visible and (b) Fluorescence Spectra of H₂TPP(TPA)₂NO₂ and H₂TPP(TPA)₂CHO in CH₂Cl₂ at 298 K.

Table 6.1 Photophysical Data of MTPP(TPA)₂NO₂ and MTPP(TPA)₂CHO (M = 2H, Co(II), Ni(II), Cu(II), Zn(II)) in CH₂Cl₂ at 298 K

Porphyrin	$\lambda_{\text{excitation}}$, nm	$\lambda_{\text{emission}}$, nm	Φ_f	FWHM	τ [ns]
H ₂ TPP(TPA) ₂ NO ₂	308(4.65), 438(5.13), 539(4.12), 690(3.83)	754	0.0019	40	0.52
H ₂ TPP(TPA) ₂ CHO	308(4.69), 438(5.24), 535(4.06), 576(3.88), 612(3.72), 678(3.61)	649	0.019	29	4.88
CoTPP(TPA) ₂ NO ₂	308(4.76), 432(5.01), 551(4.11), 597(4.10)			60	
CoTPP(TPA) ₂ CHO	308(4.70), 434(5.11), 555(4.16), 593(4.09)			45	
NiTPP(TPA) ₂ NO ₂	309(4.77), 438(5.11), 553(4.17), 602(4.14)			44	
NiTPP(TPA) ₂ CHO	309(4.76), 437(5.34), 554(4.11), 598(4.08)			32	
CuTPP(TPA) ₂ NO ₂	309(4.73), 432(5.17), 559(4.16), 606(4.10)			41	

CuTPP(TPA) ₂ CHO	309(4.81), 434(5.46), 559(4.25), 600(4.20)			25	
ZnTPP(TPA) ₂ NO ₂	309(4.85), 434(5.50), 560(4.47), 609(4.36)	701	0.003	37	0.58
ZnTPP(TPA) ₂ CHO	311(4.42), 434(5.16), 562(3.91), 603(3.83)	644	0.009	23	0.89

*Value in the parentheses denote to $\log \epsilon$

6.3.3 NLO Studies using Femtosecond Pulses

We have obtained prominent Z-scan experimental results for different wavelengths and were able to extract various parameters like Two photon absorption coefficient [31] (β) (cm W^{-1}), absorption cross section σ_{2PA} (GM), nonlinear refractive index (n_2) ($\text{cm}^2 \text{W}^{-1}$) and nonlinear optical susceptibility index ($\chi^{(3)}$). For all four samples we have noticed RSA behavior in open aperture experimental data, whereas in closed aperture mode curves have displayed always peak-valley nature revealing about the negative refractive index as well as the defocusing nature of the H₂TPP(TPA)₂NO₂ and H₂TPP(TPA)₂CHO.

Figure 6.2(i)a-e illustrates about the open aperture mode data obtained for the porphyrin H₂TPP(TPA)₂NO₂ for different wavelengths. Figure 6.2(i)a displays the OA data for the mentioned sample with peak intensity $4.54 \times 10^8 \text{ W/cm}^2$ and calculated 2PA coefficient (β) is $5.5 \times 10^{-8} \text{ cm W}^{-1}$ at 680 nm. Figure 6.2(i)b exhibits the data for open aperture with applied peak intensity $4.02 \times 10^8 \text{ W/cm}^2$ and calculated β is $8 \times 10^{-8} \text{ cmW}^{-1}$ at 700 nm. Figure 6.2(i)c presents the OA data with peak intensity $3.73 \times 10^8 \text{ W/cm}^2$ and calculated β is $0.16 \times 10^{-8} \text{ cmW}^{-1}$ at 750 nm. In Figure 6.2(i)d we found OA data with peak intensity $3.22 \times 10^8 \text{ W/cm}^2$ and calculated β is $0.73 \times 10^{-8} \text{ cmW}^{-1}$ at 800 nm and Figure 6.2(i)e will give the OA data having peak intensity $2.92 \times 10^8 \text{ W/cm}^2$ as well calculated β $0.2 \times 10^{-8} \text{ cm W}^{-1}$ at 850 nm. Now, for CA mode we have extracted the value of NLO refractive index (n_2) for 750 nm (Figure 6.2(i)f) to be $6.80 \times 10^{-13} \text{ cm}^2 \text{W}^{-1}$ and for 800 nm (Figure 6.2(i)g) to be $0.22 \times 10^{-13} \text{ cm}^2 \text{W}^{-1}$.

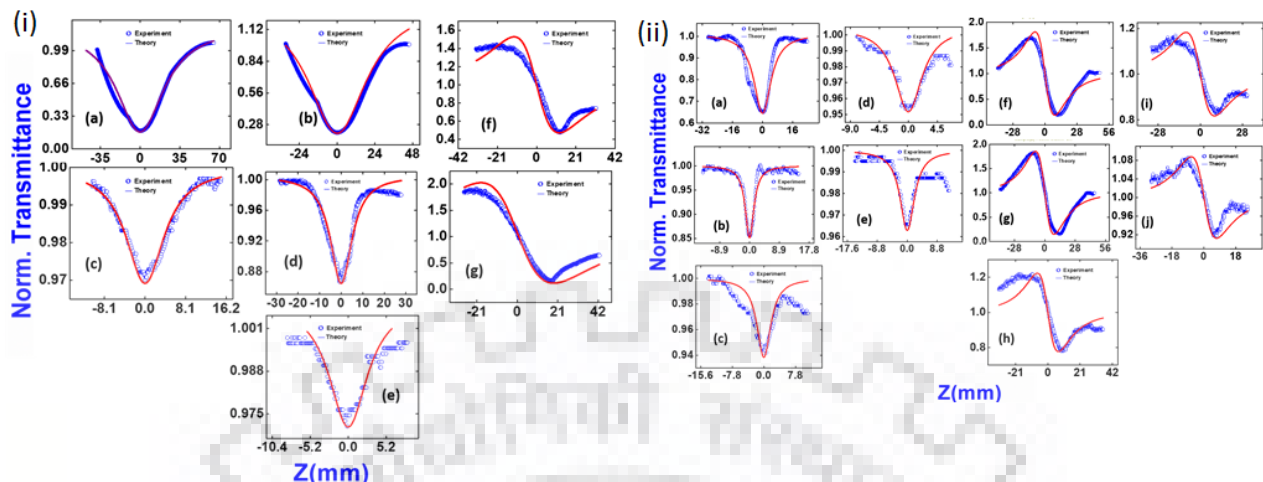


Figure 6.2 Experimental and Theoretically fitted Z scan data for sample (i) $\text{H}_2\text{TPP}(\text{TPA})_2\text{NO}_2$ in OA mode at (a) 680 nm (b) 700 nm (c) 750 nm (d) 800 nm (e) 850 nm and CA mode at (f) 750 nm (g) 800 nm (ii) $\text{H}_2\text{TPP}(\text{TPA})_2\text{CHO}$ in OA mode at (a) 680 nm (b) 700 nm (c) 750 nm (d) 800 nm (e) 850 nm and CA mode at (f) 680 nm (g) 700 nm (h) 750 nm (i) 800 nm (j) 850 nm.

Table 6.2 NLO coefficient data of $\text{H}_2\text{TPP}(\text{TPA})_2\text{NO}_2$ and $\text{H}_2\text{TPP}(\text{TPA})_2\text{CHO}$.

λ (nm)	$\beta \times 10^{-8}$ (cm W^{-1})	$\sigma_{2\text{PA}}(\text{GM})$ $\times 10^5$	$\text{Im}(\chi^{(3)})$ $\times 10^{-11}$ (e.s.u.)	$n_2 \times 10^{-13}$ ($\text{cm}^2 \text{W}^{-1}$)	$\text{Re}(\chi^{(3)})$ $\times 10^{-11}$ (e.s.u.)	Total $(\chi^{(3)}) \times 10^{-11}$ (e.s.u.)
$\text{H}_2\text{TPP}(\text{TPA})_2\text{NO}_2$						
680	5.5	2.65	2.538	--	--	--
700	8	3.75	3.8	--	--	--
750	0.16	0.07	0.081	6.8	5.797	5.798
800	0.73	0.29	0.39	0.22	0.187	0.433
850	0.2	0.0773	0.115	--	--	--
$\text{H}_2\text{TPP}(\text{TPA})_2\text{CHO}$						
680	1.9	0.918	0.88	7.9	6.73	6.787
700	0.77	0.362	0.37	9.7	8.27	8.28
750	0.39	0.171	0.19	2.97	2.53	2.54
800	0.41	0.168	0.22	3.27	2.79	2.798
850	0.3	0.116	0.173	1.66	1.415	1.426

For $\text{H}_2\text{TPP}(\text{TPA})_2\text{CHO}$ we performed the same Z-scan studies in both OA, CA mode and obtained nonlinear absorption and refractive index coefficients (Figure 6.2ii). For broad band (680-850 nm) wavelength using this sample we achieved the coefficients as follows- at 680 nm, 700 nm, 750 nm, 800 nm and 850 nm we got β with values of $1.9 \times 10^{-8} \text{ cm W}^{-1}$, $0.77 \times 10^{-8} \text{ cm W}^{-1}$, $0.39 \times 10^{-8} \text{ cm W}^{-1}$, $0.41 \times 10^{-8} \text{ cm W}^{-1}$, $0.3 \times 10^{-8} \text{ cm W}^{-1}$ respectively as

well as the n_2 values being $7.9 \times 10^{-13} \text{ cm}^2 \text{ W}^{-1}$, $9.7 \times 10^{-13} \text{ cm}^2 \text{ W}^{-1}$, $2.97 \times 10^{-13} \text{ cm}^2 \text{ W}^{-1}$, $3.27 \times 10^{-13} \text{ cm}^2 \text{ W}^{-1}$ and $1.66 \times 10^{-13} \text{ cm}^2 \text{ W}^{-1}$ respectively.

6.3.4 Electrochemical Redox Properties

Triphenylamine is a highly conjugated tertiary amine group which acts as very good electron donating group in its initial state. Triphenylamine also stabilizes the charge transfer in excited state [32]. So to probe the effect of β -triphenylamine on MTPP(TPA)₂NO₂/CHO (M = 2H, Zn, Cu, Co and Ni), the electrochemical redox behavior was studied in CH₂Cl₂ at 298 K (Figure A22, Appendix-V) and compared the result with reported MTPP, MTPPBr₂NO₂ and MTPPBr₂CHO derivatives under similar experimental condition. The electrochemical redox potential data of porphyrins are listed in the Table 6.2. It is seen from the Table 6.2 the presence of two bromo group and one CHO or NO₂ group in MTPPBr₂NO₂ and MTPPBr₂CHO (M = 2H, Zn, Cu, Co and Ni) resultant into the anodic shift in their redox potential corresponding their MTPP porphyrins as electron-withdrawing nature of both group make oxidation harder and reduction easier. Further, if both bromo group were replaced with triphenylamino substituents in MTPP(TPA)₂X (X = CHO/NO₂), then TPA group will give opposite effect than bromo substituent and change their redox properties accordingly. A comparative representation of CVs of CuTPP, CuTPPBr₂NO₂ and CuTPP(TPA)₂NO₂ (Figure 6.3a) and NiTPP, NiTPPBr₂CHO and NiTPP(TPA)₂CHO (Figure 6.3b) are shown in Figure 6.3. It is found that CuTPP exhibited two reversible reduction potential at -1.33 and -1.72 V and two oxidation potential found at 0.97 and 1.35 V. CuTPPBr₂NO₂ exhibited anodic shift in the first oxidation and reduction potential by 0.10 V and 0.48 V from CuTPP. Further, CuTPP(TPA)₂NO₂ showed two reversible oxidation potential at 1.00 and 1.50 V and three reversible reduction potential at -0.89, -1.14 and -1.34 V. CuTPP(TPA)₂NO₂ exhibited first oxidation and first reduction potential cathodically shifted by 0.07 and 0.04 V, respectively as compared to CuTPPBr₂NO₂ due to electron-donating nature of TPA group whereas the first reduction potentials of CuTPP(TPA)₂NO₂ are anodically shifted as compared to CuTPP due to the effect of nitro group. Similarly, the first reduction potential of NiTPP(TPA)₂CHO was cathodically shifted as compared to NiTPPBr₂CHO but anodically shifted as compared to NiTPP. Other MTPP(TPA)₂X porphyrin followed the same trend. The order of first reduction potential is follows as: MTPPBr₂X < MTPP(TPA)₂X < MTPP and the order of first oxidation potential is as follows: MTPP < MTPP(TPA)₂X < MTPPBr₂X where X = CHO/NO₂ and M = 2H, Zn, Cu, Co, Ni indicating the cathodic shift in their redox potential of

MTPP(TPA)₂X as compared to MTPPBr₂X due to electron-donating effect TPA substituent. Surprisingly, ZnTPP(TPA)₂X porphyrins did not follow the trend observed in first oxidation potential and showed anodic shift in their first oxidation potential as compared to ZnTPPBr₂X where the first oxidation potential of ZnTPP(TPA)₂CHO and ZnTPP(TPA)₂NO₂ are 0.06 and 0.03 V anodically shifted from ZnTPPBr₂CHO and ZnTPPBr₂NO₂ respectively. Overall, in case of MTPP(TPA)₂X, the attachment of TPA group on porphyrin core in place of bromo substituents leads to cathodic shift in their redox potential as compared to MTPPBr₂X due to electron donating nature and inductive effect of TPA group but the presence of electron-withdrawing -CHO/NO₂ group in these porphyrins still favor harder oxidation and easier reduction as compared to corresponding MTPPs and The tunable redox behavior of MTPP(TPA)NO₂/CHO revealed a “push-pull” effect of β -substituents (TPA, NO₂/CHO) at periphery of porphyrin system.

By appending electron releasing TPA groups and electron accepting nitro or formyl group at β -position of macrocycle, the HOMO-LUMO gap got reduced as compared to MTPPs. The HOMO-LUMO energy variation of the synthesized β -trisubstituted porphyrins was compared with MTPP (M = 2H, Co, Ni, Cu, Zn), mono and tri- β -substituted porphyrins as shown in Figure 6.4. The values have been taken from the literature [33]. The highest HOMO-LUMO gap is found for MTPPs and linearly decreased as moving from MTPPX to MTPPBr₂X and MTPP(TPA)₂X where X = CHO/NO₂. HOMO-LUMO decrement can be ascribed due to the presence of electron-withdrawing effect and structural effect as steric crowding increase around the porphyrin macrocycle. The presence of formyl, nitro or bromo substituents (electron pulling group) at porphyrin lead to stabilization of LUMO level which decrease HOMO-LUMO energy gap. As opposite, triphenylamino group stabilize the HOMO level and destabilize the LUMO level. The HOMO-LUMO gap of MTPP(TPA)₂NO₂ is lower than MTPPBr₂NO₂ but MTPP(TPA)₂CHO has higher HOMO-LUMO gap as compared to MTPPBr₂CHO. The order of HOMO-LUMO is observed as follows: MTPPs > MTPPX > MTPPBr₂X and MTPP(TPA)₂X. The trend is more consistent in case of nitro substituted porphyrin as compared with formyl substituted porphyrins due to the higher electron-withdrawing nature of nitro substituent.

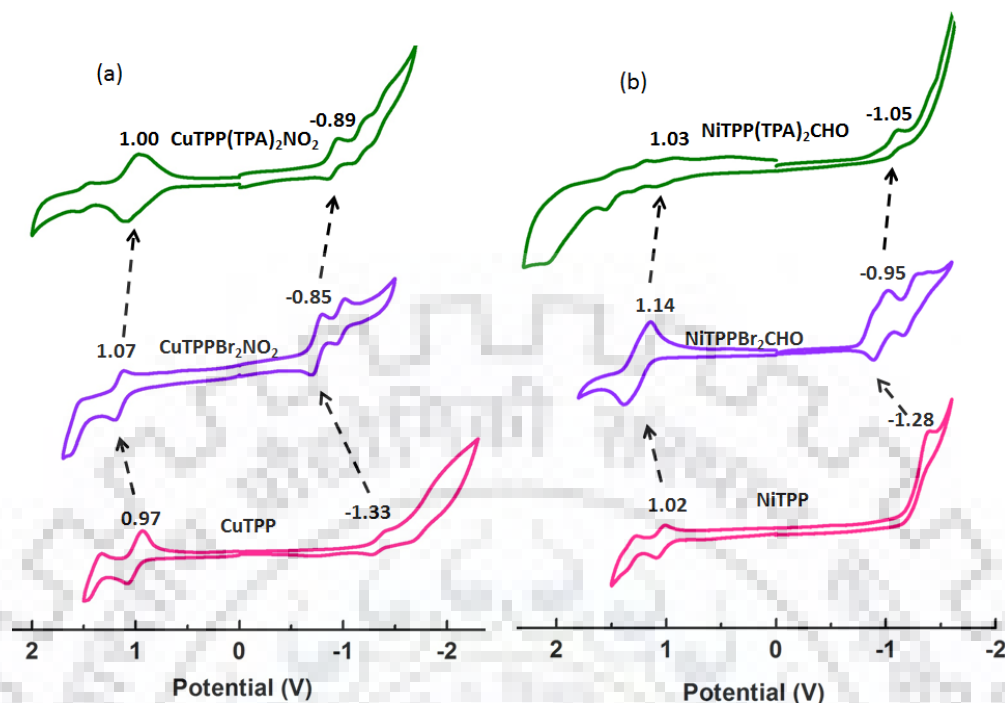


Figure 6.3 Cyclic Voltammograms of (a) CuTPP, CuTPPBr₂NO₂ and CuTPP(TPA)₂NO₂ and (b) NiTPP, NiTPPBr₂CHO and NiTPP(TPA)₂CHO in CH₂Cl₂ with a Scan Rate of 0.1 V/s at 298 K.

Table 6.3 Redox Potential Data of all Synthesized Porphyrins with Comparative Porphyrins (MTPPs and MTPPBr₂X; (X = NO₂/CHO)) Where (M = 2H, Ni(II), Co(II), Cu(II) and Zn(II)) in CH₂Cl₂ at 298 K.

Porphyrin	Oxidation				ΔE	Reduction			Metal Centre		
	I	II	III	IV		I	II	III	Oxi./Red.	I	II
H ₂ TPP	1.00	1.34			2.23	-1.23	-1.54				
H ₂ TPPBr ₂ NO ₂	1.11	1.21			1.87	-0.75	-0.82				
H ₂ TPP(TPA) ₂ NO ₂	1.02	1.62			1.85	-0.83	-0.98				
H ₂ TPPBr ₂ CHO	1.11	1.22			2.00	-0.89					
H ₂ TPP(TPA) ₂ CHO	1.10				2.05	-0.94					
CoTPP	1.06	1.31			2.44	-1.38			0.85	-0.86	
CoTPPBr ₂ NO ₂	1.22	1.44			2.43	-1.20			0.92	-0.51	
CoTPP(TPA) ₂ NO ₂	1.22	1.51			2.47	-1.25			0.96	-0.60	
CoTPPBr ₂ CHO	1.26	1.41			2.28	-1.02	-1.49		0.95	-0.57	
CoTPP(TPA) ₂ CHO	1.23	1.45			2.36	-1.13			0.98	-0.67	

NiTPP	1.02	1.32			2.30	-1.28	-1.72	
NiTPPBr ₂ NO ₂	1.24				2.07	-0.83	-1.06	
NiTPP(TPA) ₂ NO ₂	0.95	1.23			1.82	-0.87	-1.14	-1.38
NiTPPBr ₂ CHO	1.14				2.09	-0.95	-1.21	
NiTPP(TPA) ₂ CHO	1.03	1.26	1.50	2.00	2.09	-1.05	-1.05	
CuTPP	0.97	1.35			2.30	-1.33	-1.70	
CuTPPBr ₂ NO ₂	1.07	1.49			1.92	-0.85	-1.07	
CuTPP(TPA) ₂ NO ₂	1.00	1.50			1.89	-0.89	-1.14	-1.34
CuTPPBr ₂ CHO	1.08	1.47			2.02	-0.94	-1.20	
CuTPP(TPA) ₂ CHO	1.06	1.47			2.03	-0.97	-1.34	
ZnTPP	0.84	1.15			2.20	-1.36	-1.77	
ZnTPPBr ₂ NO ₂	0.94	1.18			1.88	-0.93	-1.08	
ZnTPP(TPA) ₂ NO ₂	0.98	1.23			2.05	-1.07	-1.30	
ZnTPPBr ₂ CHO	0.97	1.22			2.02	-1.05	-1.20	
ZnTPP(TPA) ₂ CHO	1.04	1.55			2.16	-1.11	-1.36	

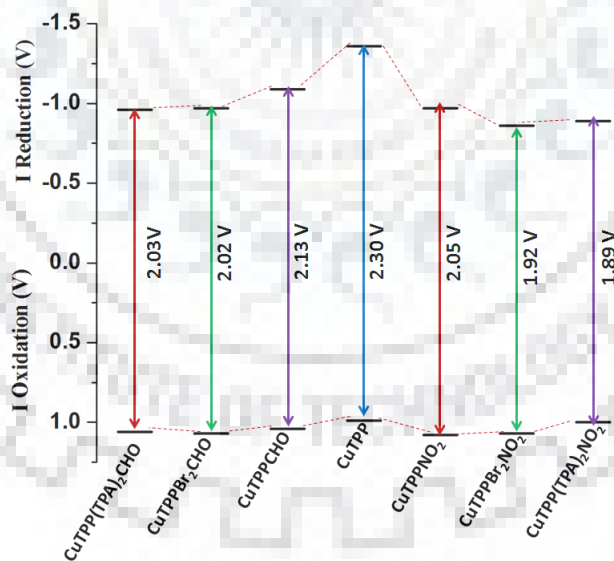


Figure 6.4 Comparative HOMO-LUMO Variation of CuTPP, CuTPPNO₂, CuTPPBr₂NO₂, CuTPP(TPA)₂NO₂, CuTPPCHO, CuTPPBr₂CHO and CuTPP(TPA)₂CHO.

6.3.5 DFT Studies

The porphyrin core structure of MTPP(TPA)₂X (X = CHO/NO₂ and M = 2H, Zn, Cu, Co, Ni) must be more nonplanar as compared to their corresponding MTPPBr₂X porphyrins as two bromo substituents were replaced with bulky triphenylamino group at the β -pyrrole position. To further investigate the conformational changes these porphyrins, the gas phase geometry for H₂TPP(TPA)₂X, X = CHO/NO₂ were optimized with B3LYP functional and LANL2DZ basis set and compared with H₂TPPBr₂X reported in literature [34–36]. The optimized geometries of H₂TPP(TPA)₂X (X = CHO or NO₂) are shown in Figure 6.5 and frontier molecular orbitals (FMOs) are shown in Figure A23, Appendix-V. The Selected average bond lengths and bond angles of H₂TPP(TPA)₂X and H₂TPPBr₂X (X = CHO or NO₂) were listed in Table A1, Appendix-V. Both porphyrins exhibited saddle shape nonplanar conformation of porphyrin macrocycle due to two triphenylamino group. H₂TPP(TPA)₂CHO has $\Delta C_{\beta} = \pm 0.636 \text{ \AA}$ and the 24 core atoms $\Delta_{24} = \pm 0.312 \text{ \AA}$ which is comparatively higher from H₂TPPBr₂CHO. H₂TPPBr₂NO₂ shows $\Delta C_{\beta} = \pm 0.642 \text{ \AA}$ and $\Delta_{24} = \pm 0.317 \text{ \AA}$ which is similar to H₂TPPBr₂NO₂. These porphyrins showed increment in C_{β} - C_{β} bond length along with increment in C_{β} - C_{α} - C_m by 3^o (Table A1, Appendix-V) which clearly indicating that pyrrole ring tilted from the mean plane

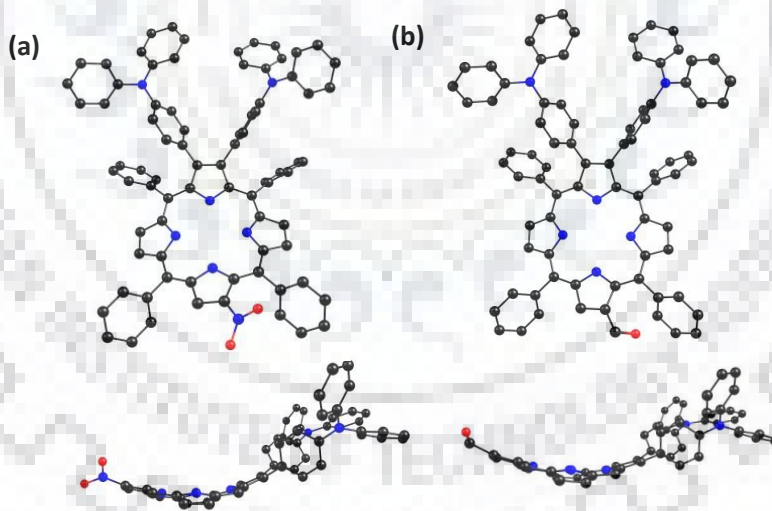


Figure 6.5 Optimized Gas Phase Geometries of H₂TPP(TPA)₂NO₂ and H₂TPP(TPA)₂CHO.

of porphyrin core to adjust the two new bulky group at β -position and saddle shape non-planar conformation arise. From Figure A23, Appendix-V, it can be seen that the electron density of HOMO and HOMO + 1 levels were spread only at triphenylamino unit and the electron density of LUMO and LUMO + 1 levels spread only at porphyrin core and β -CHO or NO₂ groups. Thus,

triphenylamine act as donor group and formyl or nitro groups act as acceptor groups which make "push-pull" nature of porphyrin. This electron density distribution also suggests the possibility of intramolecular charge transfer from triphenylamino donors to acceptor porphyrin unites. The pictorial representations of resultant dipole moment of both tri- β -substituted porphyrins were shown in the Figure 6.6, Appendix-V. $H_2TPP(TPA)_2NO_2$ have a higher dipole moment ($\mu = 7.66$ D) as compared to $H_2TPP(TPA)_2CHO$ ($\mu = 4.55$ D) due to the more electron-withdrawing nature of nitro substituent. These porphyrins exhibited higher dipole moment as compared to H_2TPP ($\mu = 0.052$ D) due to nonplanarity of porphyrin macrocycle and nature of substituents at β -position of porphyrin.

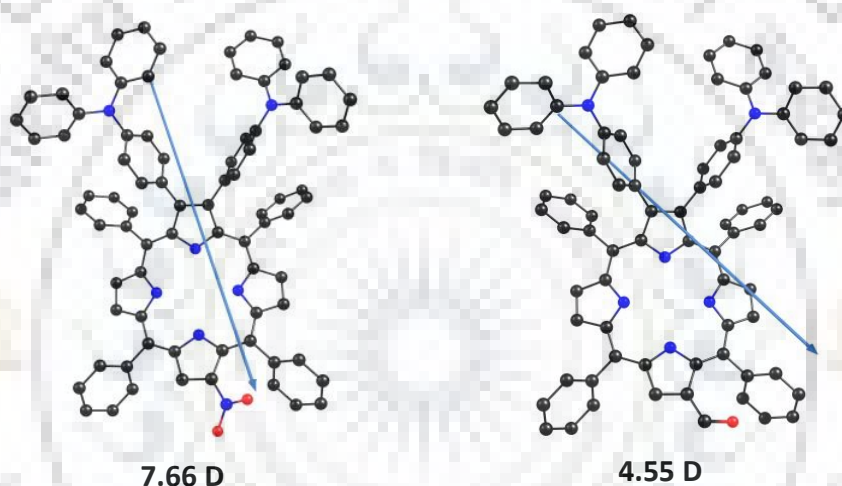


Figure 6.6 Theoretically Calculated Dipole Moment Direction of $H_2TPP(TPA)_2NO_2$ and $H_2TPP(TPA)_2CHO$.

6.4 CONCLUSIONS

We have synthesized successfully two new families of asymmetric β -trisubstituted porphyrins ($MTPP(TPA)_2X$ ($X = NO_2/CHO$ and $M = 2H, Co, Ni, Cu, Zn$)) using Pd(0) catalyzed Suzuki cross-coupling reaction and the synthesized porphyrins were characterized by various spectroscopic techniques, mass spectrometry, ultrafast NLO properties, DFT and electrochemical studies. $MTPP(TPA)_2NO_2/CHO$ ($M = 2H, Co(II), Cu(II), Ni(II), Zn(II)$) exhibited 16-22 nm and 39-58 nm redshift in the Soret and $Q_{x(0,0)}$ bands, respectively as compared to $MTPPs$ due to resonance and inductive effect of β -substituents on porphyrin π -system. The quantum yields as well as fluorescence lifetime of nitro substituted porphyrins have been found to be less as

compared to those of formyl substituted porphyrins which clearly suggests larger extent of charge-transfer from donor moiety to nitro group *via* porphyrin spacer due to better electronic coupling of nitro group. H₂TPP(TPA)₂NO₂ and H₂TPP(TPA)₂CHO revealed large resultant dipole moment (7.62 D and 4.55 D, respectively) as compared to H₂TPP(0.052 D) due to nonplanarity of macrocycle core and cross polarized 'push-pull' effect of β -substituents. H₂TPP(TPA)₂NO₂ exhibited nonplanar saddle shape conformation of the macrocyclic core as it was confirmed by DFT calculations. The first reduction potential of CuTPP(TPA)₂NO₂ and CuTPP(TPA)₂CHO was found 0.44 and 0.36 V anodically shifted as referenced to CuTPP, respectively due to the electronic nature of β -substituents (NO₂ and CHO) which made them easy to reduce than CuTPP. Redox potentials were found to be less altered in case of formyl substituted porphyrins compared to those of nitro substituted porphyrins. HOMO-LUMO energy levels were also found to be modulated due to peripheral substitutions of macrocycle. Ultrafast NLO properties of investigated porphyrins in visible range were estimated using femtosecond Z-scan technique. Photophysical, electrochemical and DFT studies suggest that these porphyrins have good potentiality in the nonlinear optics (NLO).

6.5 REFERENCES

- (1) He, G. S.; Tan, L.-S.; Zheng, Q.; Prasad, P. N. Multiphoton Absorbing Materials: Molecular Designs, Characterizations, and Applications. *Chem. Rev.* **2008**, *108*, 1245–1330.
- (2) Pawlicki, M.; Collins, H. A.; Denning, R. G.; Anderson, H. L. Two-Photon Absorption and the Design of Two-Photon Dyes. *Angew. Chemie. Int. Ed.* **2009**, *48*, 3244–3266.
- (3) Samoć, M. Third-Order Nonlinear Optical Materials: Practical Issues and Theoretical Challenges. In *J. Mol. Model.* **2011**, *17*, 2183–2189.
- (4) Maaza, M.; Mongwaketsi, N.; Genene, M.; Hailu, G.; Garab, G.; Sahraoui, B.; Hamidi, D. Nonlinear Photonics Properties of Porphyrins Nanocomposites and Self-Assembled Porphyrins. *J. Porphyr. and Phthalocyanines* **2012**, *16*, 985–995.
- (5) Gautam, P.; Dhokale, B.; Shukla, V.; Singh, C. P.; Bindra, K. S.; Misra, R. Optical Limiting Performance of *Meso*-Tetraferrocenyl Porphyrin and Its Metal Derivatives. *J. Photochem. Photobiol. A: Chemistry* **2012**, *239*, 24–27.
- (6) Kanis, D. R.; Ratner, M. A.; Marks, T. J. Design and Construction of Molecular

- Assemblies with Large Second-Order Optical Nonlinearities. Quantum Chemical Aspects. *Chem. Rev.* **1994**, *94*, 195–242.
- (7) de la Torre, G.; Vázquez, P.; Agulló-López, F.; Torres, T. Role of Structural Factors in the Nonlinear Optical Properties of Phthalocyanines and Related Compounds. *Chem. Rev.* **2004**, *104*, 3723–3750.
- (8) Biswal, B. P.; Valligatla, S.; Wang, M.; Banerjee, T.; Saad, N. A.; Mariserla, B. M. K.; Chandrasekhar, N.; Becker, D.; Addicoat, M.; Senkovska, I.; Berger, R.; Rao, D. N.; Kaskel, S.; Feng, X. Nonlinear Optical Switching in Regioregular Porphyrin Covalent Organic Frameworks. *Angew. Chem. Int. Ed.* **2019**, *58*, 6896–6900.
- (9) Santos, C.; Barata, J.; Calvete, M.; Vale, L.; Dini, D.; Meneghetti, M.; Neves, M.; Faustino, M.; Tomé, A.; Cavaleiro, J. Synthesis and Functionalization of Corroles. An Insight on Their Nonlinear Optical Absorption Properties. *Curr. Org. Synth.* **2014**, *11*, 29–41.
- (10) Biswal, B. P.; Valligatla, S.; Wang, M.; Banerjee, T.; Saad, N. A.; Mariserla, B. M. K.; Chandrasekhar, N.; Becker, D.; Addicoat, M.; Senkovska, I.; et al. Nonlinear Optical Switching in Regioregular Porphyrin Covalent Organic Frameworks. *Angew. Chem. Int. Ed.* **2019**, *58*, 6896–6900.
- (11) Albert, I. D. L.; Marks, T. J.; Rather, M. A. Remarkable NLO Response and Infrared Absorption in Simple Twisted Molecular π -Chromophores. *J. Am. Chem. Soc.* **1998**, *120*, 11174–11181.
- (12) Le, T. H.; Dao, Q. D.; Nghiê, M. P.; Peralta, S.; Guillot, R.; Pham, Q. N.; Fujii, A.; Ozaki, M.; Goubard, F.; Bui, T. T. Triphenylamine–Thienothiophene Organic Charge-Transport Molecular Materials: Effect of Substitution Pattern on Their Thermal, Photoelectrochemical, and Photovoltaic Properties. *Chem. Asian J.* **2018**, *13*, 1302–1311.
- (13) Pham, H. D.; Jain, S. M.; Li, M.; Manzhos, S.; Feron, K.; Pitchaimuthu, S.; Liu, Z.; Motta, N.; Wang, H.; Durrant, J. R.; et al. Dopant-Free Novel Hole-Transporting Materials Based on Quinacridone Dye for High-Performance and Humidity-Stable Mesoporous Perovskite Solar Cells. *J. Mater. Chem. A* **2019**, *7*, 5315–5323.
- (14) Maeda, C.; Ogawa, K.; Sadanaga, K.; Takaishi, K.; Ema, T. Chiroptical and Catalytic Properties of Doubly Binaphthyl-Strapped Chiral Porphyrins. *Chem. Commun.* **2019**, *55*, 1064–1067.

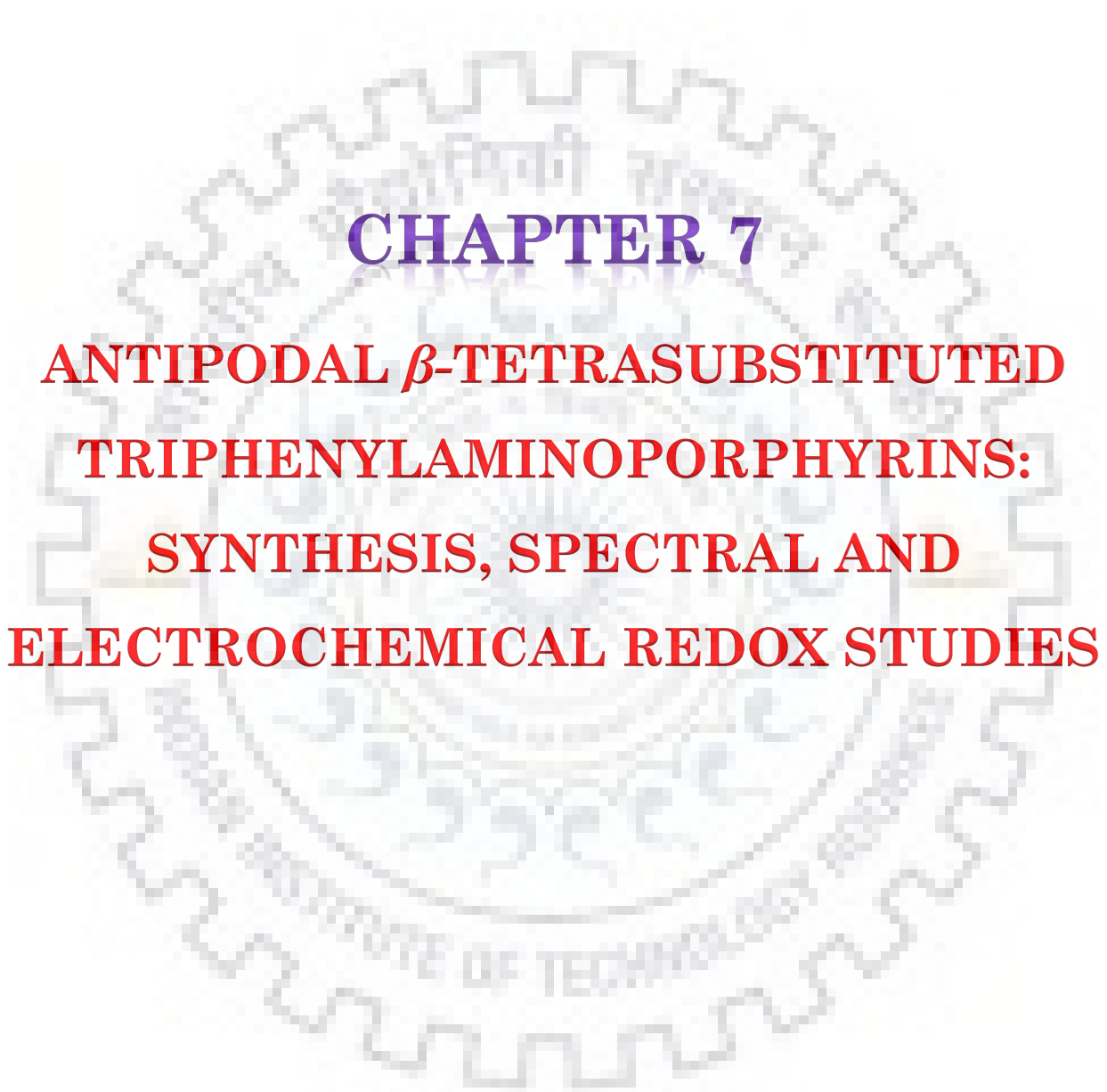
- (15) Dar, T. A.; Uprety, B.; Sankar, M.; Maurya, M. R. Robust and Electron Deficient Oxidovanadium(IV) Porphyrin Catalysts for Selective Epoxidation and Oxidative Bromination Reactions in Aqueous Media. *Green Chem.* **2019**, *21*, 1757–1768.
- (16) Reddy, G.; Katakam, R.; Devulapally, K.; Jones, L. A.; Della Gaspera, E.; Upadhyaya, H. M.; Islavath, N.; Giribabu, L. Ambient Stable, Hydrophobic, Electrically Conductive Porphyrin Hole-Extracting Materials for Printable Perovskite Solar Cells. *J. Mater. Chem. C* **2019**, *7*, 4702–4708.
- (17) Wang, B.; Rudnick, S.; Cengia, B.; Bonkovsky, H. L. Acute Hepatic Porphyrins: Review and Recent Progress. *Hepatol. Commun.* **2019**, *3*, 193–206.
- (18) Wang, J.; Yang, C. J.; Peng, H. N.; Deng, Y. S.; Gao, X. C. Synthesis of Triphenylamine-Modified Arylates and Ketones via Suzuki Coupling Reactions. *Synth. Commun.* **2011**, *41*, 832–840.
- (19) Yadav, P.; Kumar, R.; Saxena, A.; Butcher, R. J.; Sankar, M. β -Trisubstituted "Push-Pull" Porphyrins-Synthesis and Structural, Photophysical, and Electrochemical Redox Properties. *Eur. J. Inorg. Chem.* **2017**, *2017*, 3269–3274.
- (20) Giraudeau, A.; Ezhar, I.; Gross, M.; Callot, H. J.; Jordan, J. Substituent Effects in the Electroreduction of Porphyrins and Metalloporphyrins. *J. Am. Chem. Soc.* **1979**, *101*, 3857–3862.
- (21) Jaquinod, L.; Khoury, R. G.; Shea, K. M.; Smith, K. M. Regioselective Syntheses and Structural Characterizations of 2,3-Dibromo- and 2,3,7,8,12,13-Hexabromo-5,10,15,20-Tetraphenylporphyrins. *Tetrahedron* **1999**, *55*, 13151–13158.
- (22) Kumar, R.; Sankar, M. Synthesis, Spectral, and Electrochemical Studies of Electronically Tunable β -Substituted Porphyrins with Mixed Substituent Pattern. *Inorg. Chem.* **2014**, *53*, 12706–12719.
- (23) Bakar, M. A.; Sergeeva, N. N.; Juillard, T.; Senge, M. O. Synthesis of Ferrocenyl Porphyrins via Suzuki Coupling and Their Photophysical Properties. *Organometallics* **2011**, *30*, 3225–3228.
- (24) Kumar, P. R.; Britto, N. J.; Kathiravan, A.; Neels, A.; Jaccob, M.; Mothi, E. M. Synthesis and Electronic Properties of A₃B-Thienyl Porphyrins: Experimental and Computational Investigations. *New J. Chem.* **2019**, *43*, 1569–1580.
- (25) Slenczka, A. Electronic Spectroscopy of Phthalocyanine and Porphyrin Derivatives in

- Superfluid Helium Nanodroplets. *Molecules.*, **2017**, 22, 1244.
- (26) Reddy, K. S. K.; Liu, Y. C.; Chou, H. H.; Kala, K.; Wei, T. C.; Yeh, C. Y. Synthesis and Characterization of Novel β -Bis(N, N-Diarylamino)-Substituted Porphyrin for Dye-Sensitized Solar Cells under 1 Sun and Dim Light Conditions. *ACS Appl. Mater. Interfaces* **2018**, 10, 39970-39982.
- (27) Zhou, Z.; Liu, Q.; Yan, Z.; Long, G.; Zhang, X.; Cao, C.; Jiang, R. Conversion of Electron Configuration of Iron Ion through Core Contraction of Porphyrin: Implications for Heme Distortion. *Org. Lett.* **2013**, 15, 606-609.
- (28) DiMugno, S. G.; Wertsching, A. K.; Ross, C. R. Electronic Consequences of Nonplanar Core Conformations in Electron-Deficient Porphyrins: The Structure and Spectroscopic Properties of [5,10,15,20-Tetrakis(Heptafluoropropyl)-Porphinato]Cobalt(II). *J. Am. Chem. Soc.* **1995**, 117, 8279-8280.
- (29) Karelson, M.; Pihlaja, K.; Tamm, T.; Uri, A.; Zerner, M. C. UV-Visible Spectra of Some Nitro-Substituted Porphyrins. *J. Photochem. Photobiol. A: Chemistry* **1995**, 85, 119-126.
- (30) Grover, N.; Kumar, R.; Chaudhri, N.; Butcher, R.; Sankar, M. β -Heptasubstituted Porphyrins: Synthesis, Structural, Spectral, and Electrochemical Properties. *Eur. J. Inorg. Chem.* **2018**, 2018, 3338-3343.
- (31) Swain, D.; Rana, A.; Panda, P. K.; Rao, S. V. Strong two-photon absorption properties and ultrafast pump-probe studies of novel porphyrin derivatives. *Chem. Phys. Lett.* **2014**, 610, 310-315.
- (32) D'Souza, F.; Gadde, S.; Shafiqul Islam, D. M.; Wijesinghe, C. A.; Schumacher, A. L.; Zandler, M. E.; Araki, Y.; Ito, O. Multi-Triphenylamine-Substituted Porphyrin-Fullerene Conjugates as Charge Stabilizing "Antenna - Reaction Center" Mimics. *J. Phys. Chem. A* **2007**, 111, 8552-8560.
- (33) Prakash, K.; Kumar R.; Sankar, M. Mono- and tri- β -substituted unsymmetrical metalloporphyrins: synthesis, structural, spectral and electrochemical properties. *RSC Adv.* **2015**, 5, 66824-66832.
- (34) Alemayehu, A. B.; Hansen, L. K.; Ghosh, A. Nonplanar, Noninnocent, and Chiral: A Strongly Saddled Metalloporphyrin. *Inorg. Chem.* **2010**, 49, 7608-7610.
- (35) Thomas, K. E.; Wasbotten, I. H.; Ghosh, A. Copper β -Octakis(Trifluoromethyl)Corroles: New Paradigms for Ligand Substituent Effects in Transition Metal Complexes. *Inorg.*

Chem. **2008**, *47*, 10469-10478.

- (36) Ghosh, A. Transition Metal Spin State Energetics and Noninnocent Systems: Challenges for DFT in the Bioinorganic Arena. *J. Biol. Inorg. Chem.* **2006**, *11*, 712-724.





CHAPTER 7
ANTIPODAL β -TETRASUBSTITUTED
TRIPHENYLAMINOPORPHYRINS:
SYNTHESIS, SPECTRAL AND
ELECTROCHEMICAL REDOX STUDIES



CHAPTER 7

ANTIPODAL β -TETRASUBSTITUTED TRIPHENYLAMINOPORPHYRIN: SYNTHESIS, SPECTRAL AND ELECTROCHEMICAL REDOX STUDIES

7.1 INTRODUCTION

Nonplanar porphyrins are a class of compounds of continued interest owing to their use in model of naturally occurring macrocycle [1,2]. Several reports are available in literature related to similar type of substitution at periphery of porphyrin [3,4]. Highly conjugated π -system, thermal stability, diverse coordination chemistry and versatility in the synthesis of porphyrins make them potentially attractive molecular synthons for several material applications [5]. Steric repulsive interaction between the peripheral substituents causes the nonplanar conformation of porphyrin macrocycle. It reveals that the nonplanarity of porphyrin macrocycle can be modulated by varying the shape, size, and the number of the substituents at periphery of the porphyrin [6,7]. Kadish *et al.* and other research groups have already reported the electrochemical redox properties of similar types of β -substituted porphyrins [8–11]. β -Substituted porphyrins exhibit unique physicochemical properties [12,13]. *Meso*-tetraphenylporphyrin is broadly explored system, due to facile synthesis and ease of functionalization as compared to β -functionalized porphyrins. Peripheral functionalization of porphyrin is one of the appropriate methodology to obtain novel functionalized porphyrins [14,15]. Nowadays, synthesis of functionalized porphyrins attracting the researchers due to their widespread applications in various field including dyes-sensitized solar cells [16], photodynamic therapy [17], catalysis [18,19], molecular sensing [20] and nonlinear optics [21] and owing to their significant photophysical properties such as strong absorption in visible region and their thermochemical stability. TPA is a strong electron donating chromophore which absorb radiation at 300 nm in dichloromethane due to $n\text{-}\pi^*$ electronic transition [22]. TPA is not a component of naturally occurring photosynthetic system but it is very potential material in modeling photosynthetic system [23]. TPA based materials are used in optoelectronic devices due to its reversible redox behavior, low oxidation potential, and good film forming properties. TPA based materials used as photovoltaic devices because organic photovoltaic devices are considered the promising renewable energy

sources [24,25]. This is known that TPA can easily modify and modulate the photophysical properties of porphyrin π -system. The efficient synthesis of arylamine substituted porphyrins using palladium catalyst was developed by Zhang *et al.* [26]. Chen *et al.* have prepared Cu(II) diphenylamine substituted porphyrins and also studied their thermal stability. Triphenylamine is a good electron donating and flexible conjugated group that imparts better charge transfer to porphyrin as good donor materials [27,28]. In this regard, we report the synthesis, spectral, and electrochemical redox properties of antipodal β -tetrasubstituted triphenylaminoporphyrin ($H_2TPP(TPA)_4$) and its metal derivatives (Co(II), Ni(II), Cu(II) and Zn(II)). All the synthesized porphyrins were characterized by UV-Visible, fluorescence, NMR, MALDI-TOF mass spectrometry, electrochemical studies and elemental analysis.

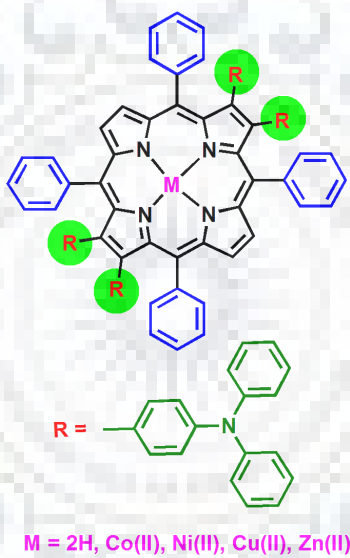


Chart 7.1 Molecular Structure of Antipodal β -Tetrasubstituted Triphenylaminoporphyrins.

7.2 EXPERIMENTAL SECTION

7.2.1 Reagents

Benzaldehyde and pyrrole were obtained from HiMedia and Alfa Aesar, respectively and used without further purification. All metal salt including $Co(OAc)_2 \cdot 4H_2O$, $Cu(OAc)_2 \cdot 3H_2O$, $Ni(OAc)_2 \cdot 4H_2O$ and $Zn(OAc)_2 \cdot 2H_2O$, N-bromosuccinimide (NBS), P_2O_5 , CaH_2 , DMF and $TBAPF_6$ were purchased from HiMedia. $Pd(PPh_3)_4$ was purchased from Sigma-Aldrich. Analytical grade toluene was first dried and distilled over P_2O_5 to use. NBS was used after recrystallization from hot water then dried under vacuum up to 8h at 75 °C. $TBAPF_6$ was used

after recrystallization twice from hot ethanol then dried at 25 °C for 2 days. Triphenylamine-4-boronic acid prepared according to the reported literature [29].

7.2.2 Instrumentation and Methods

Optical absorption and fluorescence spectral studies were carried out in CH₂Cl₂ using Cary 100 spectrophotometer and Hitachi F-4600 spectrofluorimeter, respectively. Elementary EL III Instrument used to elemental analysis. ¹H NMR spectra were recorded in CDCl₃ using JEOL 400 MHz spectrometer. DFT studies were carried out in gas phase using LANL2DZ as basis set with B3LYP functional. A Bruker UltrafleXtreme-TN MALDI-TOF/TOF mass spectrometer was used to recorded mass spectra by using 2-(4'-hydroxyphenylazo)benzoic acid as a matrix. Electrochemical studies were performed on CHI-620 electrochemical workstation. The electrode system consist of Pt-wire counter electrode, Pt working electrode and Ag/AgCl (SHE) as a reference electrode. All measurement in electrochemical studies were carried out in triple distilled dichloromethane containing 0.1 M TBAPF₆ as supporting electrolytes. DFT studies were carried out in gas phase using LANL2DZ as basis set with B3LYP functional.

7.2.3 Synthetic Procedure

Synthesis of 2,3,12,13-tetrakis(triphenylamino)-5,10,15,20-tetraphenylporphyrin and Its Metal Derivatives (MTPP(TPA)₄, M = Co(II), Ni(II), Cu(II), Zn(II)):

Two neck RB flask charged with 40 ml toluene. To this, H₂TPPBr₄ (100 mg, 0.107 mmol), 4-(N,N-diphenylamino)phenylboronic acid (0.100 g, 0.107 mmol) and K₂CO₃ (0.400 g, 2.58 mmol) were added under of inert atmosphere and purging was continued for 15 min. Then, Pd(PPh₃)₄ (0.040 g, 0.026 mmol) was added under inert atmosphere and reaction mixture was allowed to refluxed at 95 °C for 20 h. After completion of the reaction, solvent (toluene) was removed by rotary evaporation. The residue was dissolved in chloroform and washed with NaHCO₃ followed by (30 %) NaCl solution. The crude product was purified by silica column chromatography using C₆H₆/CHCl₃ mixture (1:3 v/v) followed by 100% CHCl₃. Product was formed with 40% yield (40 mg, 0.025 mmol).

H₂TPP(TPA)₄:UV-Vis. λ_{\max} (nm), (log ϵ): 308(4.65), 438(5.13), 539(4.12), 660(3.83). ¹H NMR (CDCl₃) (400 MHz): (δ , ppm) 8.40 (s, 4H, β -H), 7.97 (d, J = 8 Hz, 8H, *meso-o*-Ph-H), 7.51(t, J = 8 Hz, 4H, *meso-m*-Ph-H), 7.39 (t, J = 8 Hz, 8H, *meso-m* and *p*-Ph-H), 7.28 (s, 4H, TPA-H), 7.24

(s, 4H, TPA-H), 6.98-7.04 (m, 32H, TPA-H), 6.84 (d, $J = 8$ Hz, 8H, TPA-H), 6.66 (d, $J = 8$ Hz, 8H, TPA) -2.07 (s, 2H, -NH). MALDI-TOF-MS (m/z): found $[M+H]^+$ 1588.89, calcd. 1588.67. Anal. calcd. for $C_{116}H_{82}N_8$: C, 87.74%; H, 5.20%; N, 7.06% and found: C, 87.28%; H, 5.78%; N, 7.56%.

$H_2TPP(TPA)_4$ (0.020 g, 0.012 mmol) was dissolved in 8 ml of chloroform. To this, 10 equiv. of $M(OAc)_2 \cdot nH_2O$ (Co(II), Cu(II) and Zn(II)) in CH_3OH was added and refluxed for 30 min. Then, the solvent was evaporated to dryness and redissolved in $CHCl_3$ washed with H_2O to remove excess of metal salts and dried over Na_2SO_4 , then purified on silica column using $CHCl_3$ as eluent. While $NiTPP(TPA)_4$ complex was prepared by refluxing $H_2TPP(TPA)_4$ and $Ni(OAc)_2 \cdot 2H_2O$ in the DMF (10 ml) for 3h. Then water (50 ml) was added and the porphyrin precipitate filtered and dried under vacuum. The crude product was purified on silica gel column using $CHCl_3$ as eluent. The yield of metal complexes was found to be 80-90%.

CoTPP(TPA)₄: UV-Vis. λ_{max} (nm), (log ϵ): 308(4.76), 432(5.01), 551(4.11), 597(4.10). MALDI-TOF-MS (m/z): found $[M+H]^+$ 1645.47, calcd. 1645.59. Anal. calcd. for $C_{116}H_{80}CoN_8$: C, 84.70%; H, 4.90%; N, 6.83% and found: C, 84.98%; H, 5.01%; N, 6.42%.

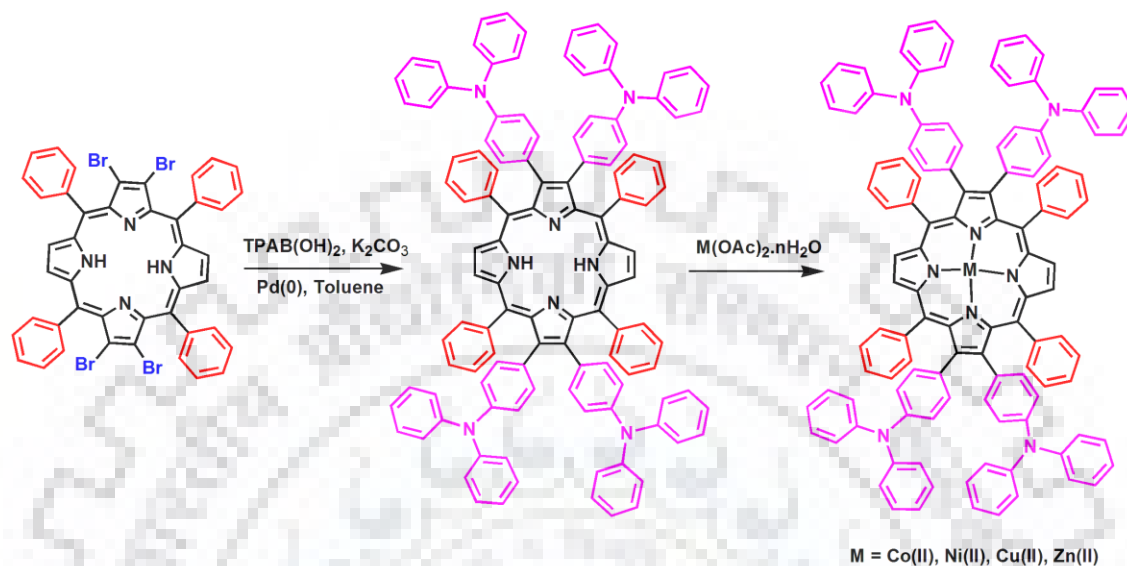
NiTPP(TPA)₄: UV-Vis. λ_{max} (nm), (log ϵ): 309(4.77), 438(5.11), 553(4.17), 602 (4.14). 1H NMR ($CDCl_3$) (400 MHz): (δ , ppm) 8.23 (s, 4H, β -H), 7.60 (d, $J = 4$ Hz, 8H, *meso-o*-Ph-H), 7.40(t, $J = 8$ Hz, 4H, *meso-m*-Ph-H), 7.25-7.27 (m, 8H, *meso-m* and *p*-Ph-H), 7.23 (s, 8H, TPA-H), 6.69-7.04 (m, 32H, TPA-H), 6.75 (d, 8H, TPA-H), 6.63 (d, $J = 8$ Hz, 8H, TPA-H), MALDI-TOF-MS (m/z): found $[M+H]^+$ 1644.48, calcd. 1644.59. Anal. calcd. for $C_{116}H_{80}N_8Ni$: C, 84.71%; H, 4.90%; N, 6.81% and found: C, 84.88%; H, 4.67%; N, 6.90%.

CuTPP(TPA)₄: UV-Vis. λ_{max} (nm), (log ϵ): 309(4.73), 432(5.17), 559(4.16), 606(4.10). MALDI-TOF-MS (m/z): found $[M+H]^+$ 1649.92, calcd. 1649.59. Anal. calcd. for $C_{116}H_{80}CuN_8$: C, 84.47%; H, 4.89%; N, 6.79% and found: C, 84.98%; H, 4.98%; N, 6.99%.

ZnTPP(TPA)₄: UV-Vis. λ_{max} (nm), (log ϵ): 309(4.85), 434(5.50), 560(4.47), 609(4.36). 1H NMR ($CDCl_3$) (400 MHz): (δ , ppm) 8.57 (s, 4H, β -H), 7.90 (d, $J = 8$ Hz, 8H, *meso-o*-Ph-H), 7.47-7.51(m, 4H, *meso-m*-Ph-H), 7.33 (t, $J = 8$ Hz, 8H, *meso-m* and *p*-Ph-H), 7.28 (s, 4H, TPA-H), 7.24 (s, 4H, TPA-H), 7.06 (d, $J = 8$ Hz, 20H, TPA-H), 6.99 (t, $J = 8$ Hz, 12H, TPA-H), 6.89 (d, $J = 8$ Hz, 8H, TPA-H), 6.68 (d, $J = 8$ Hz, 8H, TPA-H), MALDI-TOF-MS (m/z): found $[M]^+$ 1649.92, calcd. 1649.58. Anal. calcd. for $C_{116}H_{80}N_8Zn$: C, 84.37%; H, 4.88%; N, 6.79% and found: C, 84.67%; H, 4.99%; N, 6.95%.

7.3 RESULTS AND DISCUSSION

7.3.1 Synthesis and Characterization



Scheme 7.1 Synthesis of $H_2TPP(TPA)_4$ and its Metal Derivatives.

A series of antipodal β -tetrasubstituted triphenylaminoporphyrin have been synthesized using H_2TPPBr_4 as the precursor. The route for the synthesis of β -tetrasubstituted porphyrin is shown in scheme 7.1. H_2TPPBr_4 was synthesized according to the reported procedure [30]. $H_2TPP(TPA)_4$ was synthesized with 40% yield by Suzuki cross-coupling reaction using H_2TPPBr_4 , K_2CO_3 , $TPAB(OH)_2$ and $Pd(PPh_3)_4$ under inert atmosphere. Metal derivatives (Co^{II} , Cu^{II} and Zn^{II}) of $H_2TPP(TPA)_4$ were synthesized by refluxing 10 equiv. of $M(OAc)_2 \cdot nH_2O$ ($M = Co^{II}$, Cu^{II} and Zn^{II}) in $CHCl_3/CH_3OH$ mixture whereas $NiTPP(TPA)_4$ was prepared by refluxing 10 equiv. of $Ni(OAc)_2 \cdot 4H_2O$ in DMF. All synthesized porphyrins were characterized by various spectroscopic techniques, mass spectrometry and elemental analysis. 1H NMR spectra of $MTPP(TPA)_4$, $M = 2H$, $Ni(II)$ and $Zn(II)$ revealed resonances arising from β -triphenylamine, β -pyrrole, *meso*-phenyl and inner imino protons. 1H NMR spectra of synthesized porphyrins are shown in Figures A1-A3, Appendix-VI. Inner core imino protons signal of $H_2TPP(TPA)_4$ found at -2.07 ppm which is 0.69 ppm downfield shifted with respect to H_2TPP , possibly due to nonplanarity of porphyrin core and electronic effect of β -triphenylamine groups. MALDI-TOF mass spectra of these porphyrins are in good consent with the introduced structures as shown in Figures A4-A8, Appendix-VI.

7.3.2 Electronic Spectral Studies

UV-visible absorption spectra of synthesized porphyrin and its metal derivatives were recorded in CH_2Cl_2 at 298 K. All derivatives exhibited characteristic spectral features of porphyrin derivatives. The electronic absorption spectra were influenced by electron donating triphenylamino groups. Photophysical data of these porphyrins are listed in Table 7.1. Representative optical absorption spectra of $\text{H}_2\text{TPP}(\text{TPA})_4$ and $\text{ZnTPP}(\text{TPA})_4$ are shown in the Figure 7.1a. Optical absorption spectra of porphyrin was influenced by electronic nature of β -substituents (electron donor and electron acceptor groups) at periphery of macrocycle. $\text{H}_2\text{TPP}(\text{TPA})_4$ exhibited 16 nm and 34 nm red-shift in Soret band and last Q band, respectively as compared to H_2TPP due to +I effect of triphenylamine with porphyrin π -system and nonplanar conformation of porphyrin macrocycle which resulted in to the significantly reduced HOMO-LUMO energy gap. $\text{MTPP}(\text{TPA})_4$ exhibited absorption peak at 308 nm which revealed the TPA substitution at β -position of MTPP. The increase in size and number of β -substituents enhanced the steric crowding around the peripheral position of porphyrin which results the nonplanarity of macrocycle. The emission spectra of $\text{H}_2\text{TPP}(\text{TPA})_4$ and $\text{ZnTPP}(\text{TPA})_4$ were recorded to elucidate the effect of β -triphenylamino groups on the macrocyclic core and nonplanarity. Emission spectra of $\text{H}_2\text{TPP}(\text{TPA})_4$ and $\text{ZnTPP}(\text{TPA})_4$ shown in Figure 7.1b. Emission studies of these porphyrins were characterized in CH_2Cl_2 at 298 K. $\text{H}_2\text{TPP}(\text{TPA})_4$ and $\text{ZnTPP}(\text{TPA})_4$ exhibited 29 and 12 nm red shifted emission spectra than H_2TPP and ZnTPP , respectively. The red shift in the sterically crowded porphyrins has been account to the nonplanarity of porphyrin ring in conjugation with inductive and resonance interaction of the substituents that are in direct conjugation with porphyrin π -system.

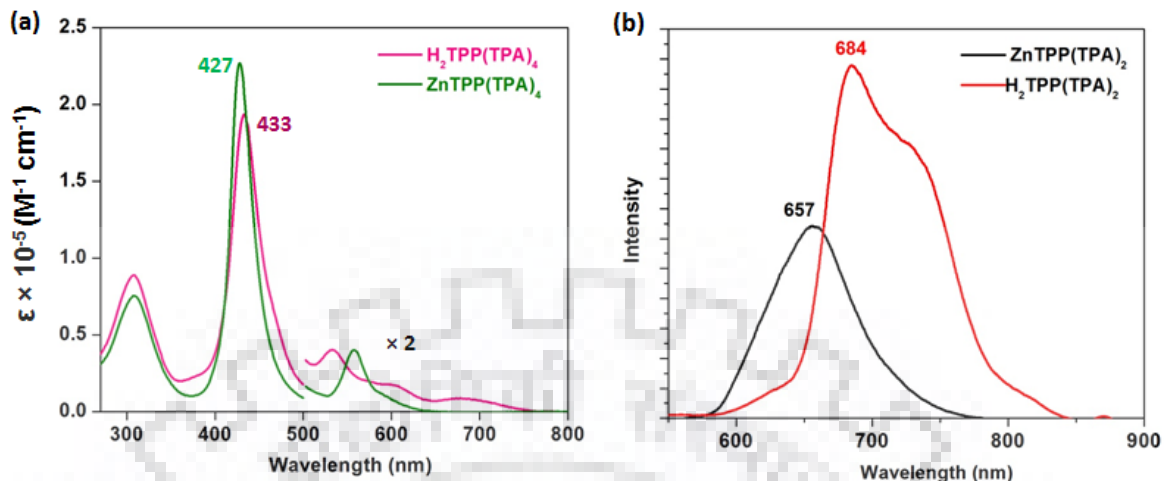


Figure 7.1 (a) UV-visible and (b) Emission Spectra of $\text{H}_2\text{TPP}(\text{TPA})_4$ and $\text{ZnTPP}(\text{TPA})_4$ in CH_2Cl_2 at 298 K.

Table 7.1 Photophysical Data of $\text{H}_2\text{TPP}(\text{TPA})_4$ and its Metal in CH_2Cl_2 at 298 K.

Porphyrin	λ_{abs} [nm]	λ_{em} [nm]	Φ_f	η [ns]
$\text{H}_2\text{TPP}(\text{TPA})_4$	308(4.94), 432(5.28), 533(4.29), 602(3.96), 680(3.56)	684	0.031	3.03
$\text{CoTPP}(\text{TPA})_4$	308(4.88), 425(5.19), 550(4.37)			
$\text{NiTPP}(\text{TPA})_4$	309(4.91), 432(5.14), 550(4.28), 588 (4.10)			
$\text{CuTPP}(\text{TPA})_4$	308(4.82), 426(5.22), 556 (4.20)			
$\text{ZnTPP}(\text{TPA})_4$	308 (4.87), 428(5.35), 557(4.87)	657	0.007	0.42

The values in parentheses denote to $\log \epsilon$

7.3.3 DFT Studies

To study the effect of triphenylamine at β -position and nonplanarity of porphyrins macrocycle, we have optimized the geometry of synthesized free base porphyrin ($\text{H}_2\text{TPP}(\text{TPA})_4$) in gas phase using LANL2DZ and B3LYP basis set and functional, respectively [31,32]. DFT study indicated that the HOMOs are contributed from *meso*-position of macrocyclic core and HOMO-1 and HOMO-2 have contribution from triphenylamine moieties whereas LUMOs exist at porphyrin core. Selected average bond angle and bond lengths are shown in Table A1, Appendix-VI. $\text{H}_2\text{TPP}(\text{TPA})_4$ exhibited saddle shaped nonplanar conformation of macrocycle. $\text{H}_2\text{TPP}(\text{TPA})_4$

exhibited $\Delta_{24} = \pm 0.377 \text{ \AA}$ and $\Delta_{C_{\beta}} = \pm 0.760 \text{ \AA}$ mean plane deviation from 24 carbon atoms and β -carbon atoms of porphyrin core, respectively. Top and side views of $\text{H}_2\text{TPP}(\text{TPA})_4$ are shown in Figure 7.2. The $\text{C}_{\beta}\text{-C}_{\beta'}$ bond distance (1.403 \AA) bearing triphenylamine moieties are longer than $\text{C}_{\beta}\text{-C}_{\beta'}$ (1.378 \AA) distance of unsubstituted β -positions due to interelectronic repulsion between the β -substituents. FMOs of $\text{H}_2\text{TPP}(\text{TPA})_4$ are shown in the Figure 7.3. Nonplanar conformation arises by the tilting of pyrrole rings to prevent the steric repulsive interaction among the substituents (triphenylamino groups), and this results in an increase of the bond angle of $\text{C}_{\beta}\text{-C}_{\alpha}\text{-C}_m$ as well as decreasing of $\text{N-C}_{\alpha}\text{-C}_m$.

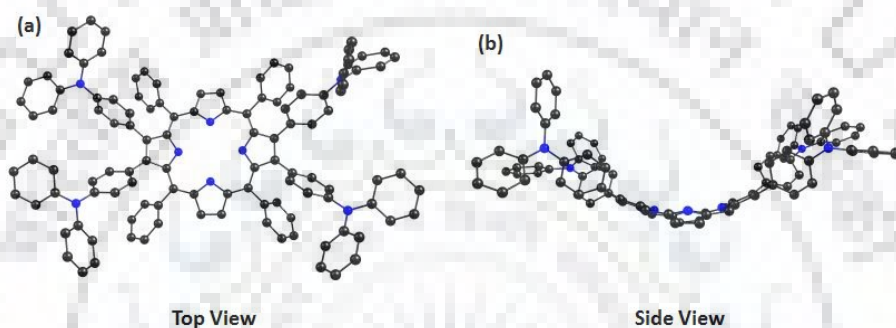


Figure 7.2 Optimized Geometry of $\text{H}_2\text{TPP}(\text{TPA})_4$ (a) Top and (b) Side View.

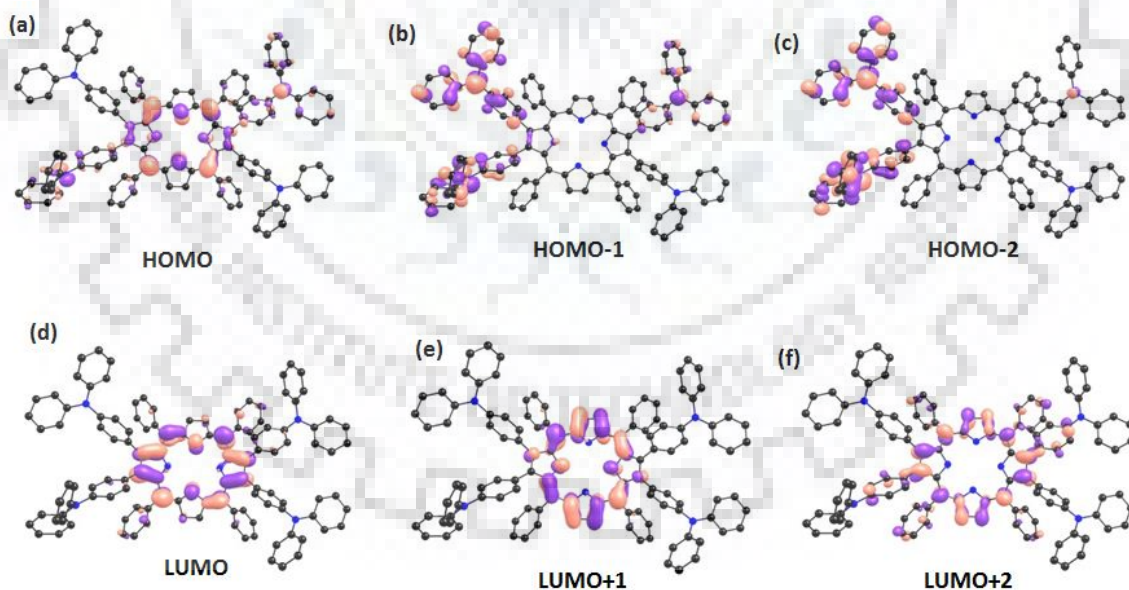


Figure 7.3 Frontier Molecular Orbitals of $\text{H}_2\text{TPP}(\text{TPA})_4$.

7.3.4 Electrochemical Redox Studies

To probe the effect of β -triphenylamino groups, on conformation of the macrocycle and the extended π -conjugation on porphyrin π -system, the electrochemical redox studies were carried out by cyclic voltammetry (CVs) in distilled CH_2Cl_2 having 0.1 M TBAPF₆ at 298 K. The electrochemical redox data of synthesized porphyrins is compared with MTPPs (Table 7.2). Redox potentials of NiTPP(TPA)₄ were compared with NiTPP and NiOPP as shown in Figure 7.4. The redox potential data exhibited that these porphyrin are easy to oxidized and difficult to reduced, due to strong electron donating effect of TPA moieties. The redox potential of β -arylamino porphyrin was influenced by electronic nature of peripheral substituents, core metal ion as well as solvent polarity. The introduction of TPA groups at backbone of macrocycle leads to cathodic shift in oxidation and reduction potential due to pushing effect of TPA groups. NiTPP exhibited first oxidation potential at 1.05 V and first reduction potential at -1.28 V. NiTPP(TPA)₄ exhibited first oxidation potential at 0.76 V which revealed 0.29 V cathodically shifted with respect to NiTPP and 0.04 V cathodic shift in first reduction potential than NiTPP due to destabilization of HOMO. The introduction of four phenyl groups at β -pyrrole positions of NiTPP made the macrocycle system difficult to reduce and easier to oxidize as compared to NiTPP. The first oxidation potential of NiOPP exhibited 0.140 V cathodically shifted whereas a marginal shift observed in the first reduction potential than corresponding NiTPP. NiTPP(TPA)₄ exhibited 0.15 V and 0.030 V cathodic shifts in the first oxidation and first reduction potential as compared to NiOPP. This is due to the +I effect of TPA groups.

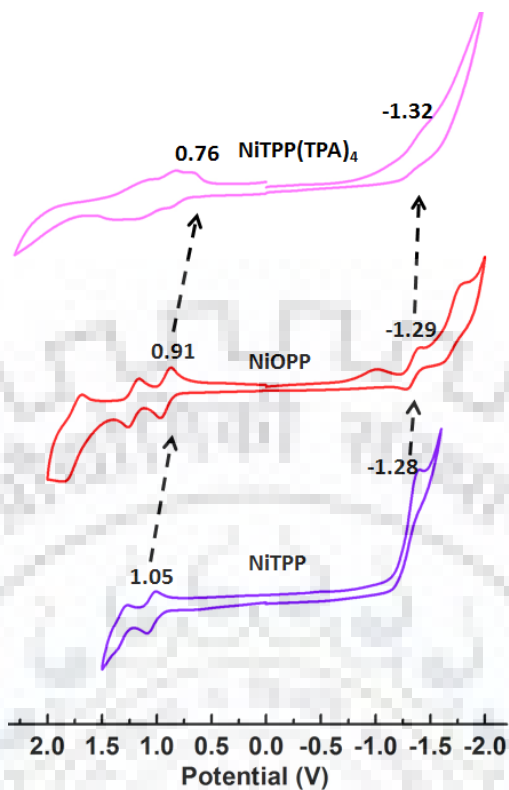


Figure 7.4 Cyclic Voltammograms of NiTPP, NiOPP and NiTPP(TPA)₄ in CH₂Cl₂ at 298 K.

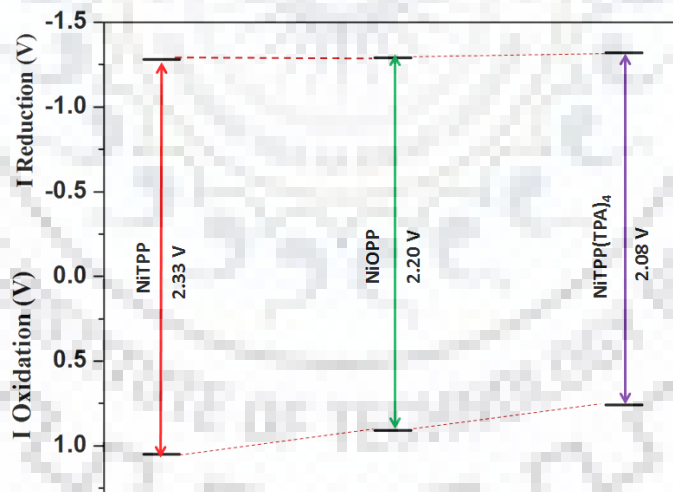


Figure 7.5 HOMO-LUMO Variation of NiTPP(TPA)₄ with respect to NiTPP and NiOPP.

Table 7.2 Electrochemical Redox Data of MTPP(TPA)₄ (Where M = 2H, Co, Ni, Cu, and Zn) in CH₂Cl₂ at 298 K.

Porphyrin	Oxidation				ΔE	Reduction		Metal Centered	
	I	II	III	IV		I	II	Oxdn.	Red.
								I	II
H ₂ TPP	1.00	1.34			2.23	-1.23	-1.54		
H ₂ TPP(TPA) ₄	0.86	1.09	1.27		1.95	-1.32			
CoTPP	1.06	1.31			2.44	-1.38		0.85	-0.86
CoTPP(TPA) ₄	1.02	1.47	2.01		2.46	-1.44		0.82	-0.71
NiTPP	1.05	1.32			2.33	-1.28	-1.72		
NiTPP(TPA) ₄	0.76	1.00	1.25		2.08	-1.32			
CuTPP	0.97	1.35			2.27	-1.30	-1.70		
CuTPP(TPA) ₄	0.96	1.10	1.41	1.90	2.29	-1.33			
ZnTPP	0.84	1.15			2.20	-1.36	-1.77		
ZnTPP(TPA) ₄	0.84	1.05	1.43	1.99	2.15	-1.31			

H₂TPP(TPA)₄ exhibited 0.14 V and 0.09 V cathodic shift in first oxidation and reduction potential with referenced to H₂TPP due to electron releasing conjugative effect of triphenylamine units and the nonplanar conformation of porphyrin core. The similar trends were observed for other metal derivatives, whereas ZnTPP(TPA)₄ exhibited marginal cathodic shift in the first reduction potential and marginal shift was observed in first oxidation potential with respect to ZnTPP. HOMO-LUMO energy level diagram for NiTPP(TPA)₄ in comparisons do NiTPP and NiOPP are shown in Figure 7.5. Overall, β -substituted triphenylaminoporphyrins exhibited cathodic shift in the redox potentials as compared to MTPPs. Nonplanarity of synthesized porphyrins leads to reduce HOMO-LUMO energy gap. NiTPP(TPA)₄ exhibited HOMO-LUMO energy gap reduced 0.25 V and 0.12 V as compared to NiTPP and NiOPP, respectively due to destabilization of HOMO.

7.4 CONCLUSIONS

A new family of antipodal β -tetrasubstituted triphenylaminoporphyrins (H₂TPP(TPA)₄) was synthesized *via* Suzuki cross-coupling reaction. Also, its metal derivatives were synthesized and characterized using various spectroscopic techniques. β -Tetrasubstituted

triphenylaminoporphyrins exhibited nonplanar conformation of the macrocyclic core. Due the β -substitution, the synthesized porphyrins exhibited tunable redox potentials. These porphyrins are found to be easy to oxidize as compared to MTPPs. NiTPP(TPA)₄ exhibited 0.15-0.29 V cathodic shift in the first oxidation potential and marginal shift in the first reduction potential as compared to NiTPP and NiOPP due destabilization of HOMOs. UV-vis and fluorescence spectral studies revealed significant bathochromic shift with respect to MTPPs due to electron donating nature of TPA, extended π -conjugation and nonplanarity of the macrocyclic core.

7.5 REFERENCES

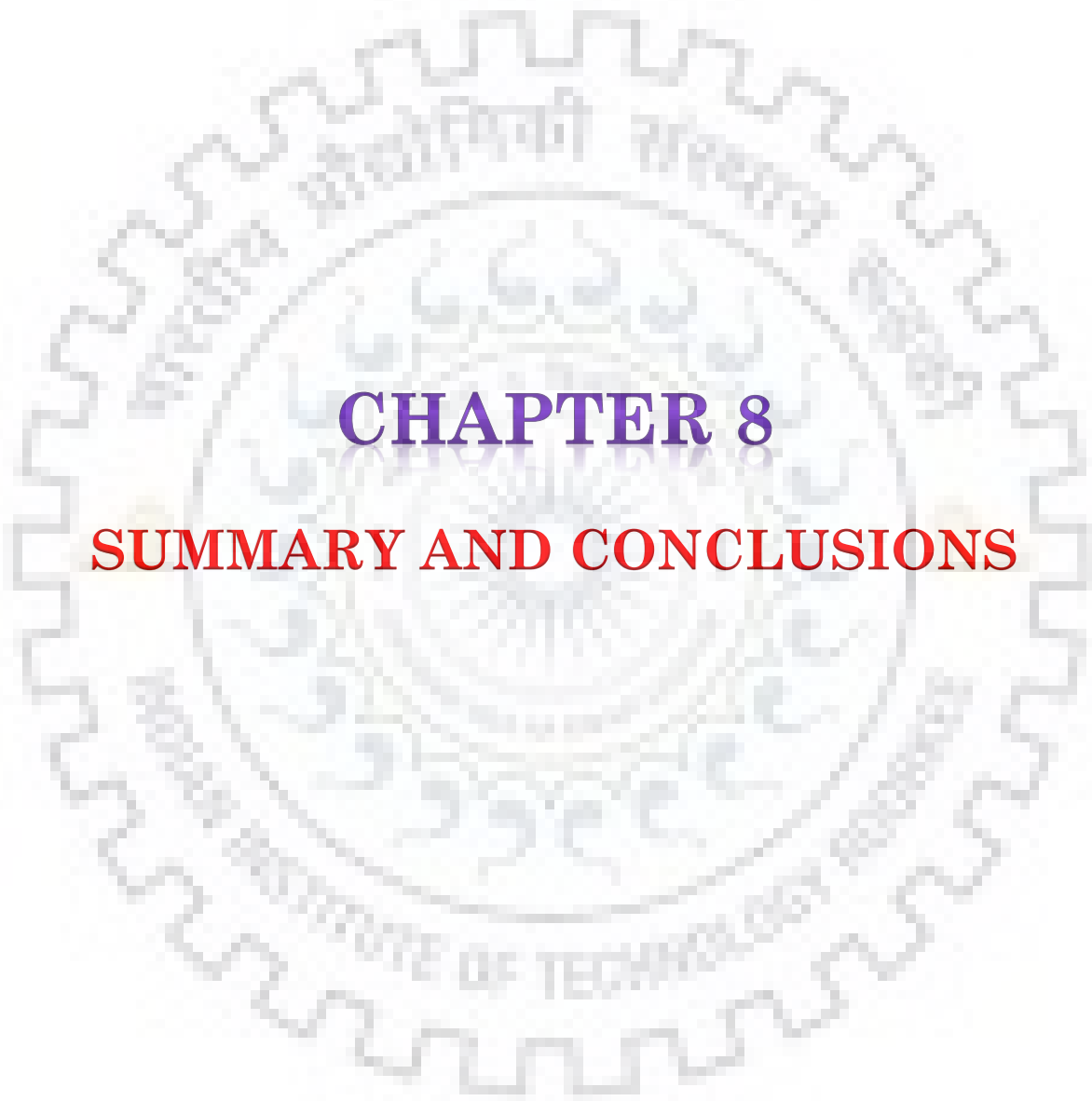
- (1) Kadish, K. M.; Smith, K. M.; Guillard, R. *The Porphyrin Handbook*; Academic Press, 2000.
- (2) Bhyrappa, P.; Arunkumar, C. Structural and Electrochemical Properties of β -Tetrabromo-Meso-tetrakis(4-Alkyloxyphenyl)Porphyrins and Their Metal Complexes. *J. Chem. Sci.* **2010**, *122*, 233–238.
- (3) Berthelot, M.; Hoffmann, G.; Bousfiha, A.; Echaubard, J.; Roger, J.; Cattey, H.; Romieu, A.; Lucas, D.; Fleurat-Lessard, P.; Devillers, C. H. Oxidative C-N Fusion of Pyridinyl-Substituted Porphyrins. *Chem. Commun.* **2018**, *54*, 5414–5417.
- (4) Antoniuk-Pablant, A.; Terazono, Y.; Brennan, B. J.; Sherman, B. D.; Megiatto, J. D.; Brudvig, G. W.; Moore, A. L.; Moore, T. A.; Gust, D. A New Method for the Synthesis of β -Cyano Substituted Porphyrins and Their Use as Sensitizers in Photoelectrochemical Devices. *J. Mater. Chem. A* **2016**, *4*, 2976–2985.
- (5) Smykalla, L.; Mende, C.; Fronk, M.; Siles, P. F.; Hietschold, M.; Salvan, G.; Zahn, D. R. T.; Schmidt, O. G.; Ruffer, T.; Lang, H. (Metallo)Porphyrins for Potential Materials Science Applications. *Beilstein J. Nanotechnol.* **2017**, *8*, 1786–1800.
- (6) Ochsenein, P.; Ayougou, K.; Mandon, D.; Fischer, J.; Weiss, R.; Austin, R. N.; Jayaraj, K.; Gold, A.; Ternner, J.; Fajer, J. Conformational Effects on the Redox Potentials of Tetraarylporphyrins Halogenated at the β -Pyrrole Positions. *Angew. Chem. Int. Ed. Engl.* **1994**, *33*, 348–350.
- (7) Kumar, R.; Sankar, M. Synthesis, Spectral, and Electrochemical Studies of Electronically Tunable β -Substituted Porphyrins with Mixed Substituent Pattern. *Inorg. Chem.* **2014**, *53*, 12706–12719.

- (8) Chaudhri, N.; Cong, L.; Grover, N.; Shan, W.; Anshul, K.; Sankar, M.; Kadish, K. M. Synthesis and Electrochemical Characterization of Acetylacetone (Acac) and Ethyl Acetate (EA) Appended β -Trisubstituted Push–Pull Porphyrins: Formation of Electronically Communicating Porphyrin Dimers. *Inorg. Chem.* **2018**, *57*, 13213–13224.
- (9) Ye, L.; Fang, Y.; Ou, Z.; Wang, L.; Xue, S.; Sun, J.; Kadish, K. M. Electrochemistry of Zinc Tetraarylporphyrins Containing Fused Butano and Benzo Groups. Effect of Solvent and Substituents on Spectra, Potentials and Mechanism in Nonaqueous Media. *J. Porphyrins and Phthalocyanines* **2018**, *22*, 1129–1142.
- (10) Kumar, S.; Jiang, X.; Shan, W.; Jinadasa, R. G. W.; Kadish, K. M.; Wang, H. β -Functionalized *Trans*-A₂B₂ Push–pull Tetrabenzoporphyrins. *Chem. Commun.* **2018**, *54*, 5303–5306.
- (11) Chaudhri, N.; Grover, N.; Sankar, M. Nickel-Induced Skeletal Rearrangement of Free Base *Trans*-Chlorins into Monofused Ni^{II}-Porphyrins: Synthesis, Structural, Spectral, and Electrochemical Redox Properties. *Inorg. Chem.* **2018**, *57*, 11349–11360.
- (12) Bhyrappa, P.; Sankar, M.; Varghese, B. Mixed Substituted Porphyrins: Structural and Electrochemical Redox Properties. *Inorg. Chem.* **2006**, *45*, 4136–4149.
- (13) Antoniuk-Pablant, A.; Terazono, Y.; Brennan, B. J.; Sherman, B. D.; Megiatto, J. D.; Brudvig, G. W.; Moore, A. L.; Moore, T. A.; Gust, D. A New Method for the Synthesis of β -Cyano Substituted Porphyrins and Their Use as Sensitizers in Photoelectrochemical Devices. *J. Mater. Chem. A*, **2016**, *4*, 2976–2985.
- (14) Jin, J.; Dong, Z.; He, J.; Li, R.; Ma, J. Synthesis of Novel Porphyrin and Its Complexes Covalently Linked to Multi-Walled Carbon Nanotubes and Study of Their Spectroscopy. *Nanoscale Res. Lett.* **2009**, *4*, 578–583.
- (15) Hiroto, S.; Miyake, Y.; Shinokubo, H. Synthesis and Functionalization of Porphyrins through Organometallic Methodologies. *Chem. Rev.* **2017**, *117*, 2910–3043.
- (16) Kumar, R.; Sudhakar, V.; Prakash, K.; Krishnamoorthy, K.; Sankar, M. Tuning the Photovoltaic Performance of DSSCs by Appending Various Donor Groups on *Trans* - Dimesityl Porphyrin Backbone. *ACS Appl. Energy Mater.* **2018**, *1*, 2793–2801.
- (17) Kou, J.; Dou, D.; Yang, L. Porphyrin Photosensitizers in Photodynamic Therapy and Its Applications. *Oncotarget* **2017**, *8*, 81591–81603.
- (18) Dar, T. A.; Uprety, B.; Sankar, M.; Maurya, M. R. Robust and Electron Deficient

- Oxidovanadium(IV) Porphyrin Catalysts for Selective Epoxidation and Oxidative Bromination Reactions in Aqueous Media. *Green Chem.* **2019**, *21*, 1757-1768.
- (19) Rybicka-Jasińska, K.; Shan, W.; Zawada, K.; Kadish, K. M.; Gryko, D. Porphyrins as Photoredox Catalysts: Experimental and Theoretical Studies. *J. Am. Chem. Soc.* **2016**, *138*, 15451–15458.
- (20) Intriери, D.; Damiano, C.; Rizzato, S.; Paolesse, R.; Venanzi, M.; Monti, D.; Savioli, M.; Stefanelli, M.; Gallo, E. Sensing of Diclofenac by a Porphyrin-Based Artificial Receptor. *New J. Chem.* **2018**, *42*, 15778–15783.
- (21) Tessore, F.; Biroli, A. O.; Di Carlo, G.; Pizzotti, M. Porphyrins for Second Order Nonlinear Optics (NLO): An Intriguing History. *Inorganics* **2018**, *6*, 81.
- (22) Yeh, S. J.; Tsai, C. Y.; Huang, C.-Y.; Liou, G.-S.; Cheng, S.-H. Electrochemical Characterization of Small Organic Hole-Transport Molecules Based on the Triphenylamine Unit. *Electrochem. Commun.* **2003**, *5*, 373–377.
- (23) El-Khouly, M. E.; Ju, D. K.; Kay, K.-Y.; D'Souza, F.; Fukuzumi, S. Supramolecular Tetrad of Subphthalocyanine-Triphenylamine-Zinc Porphyrin Coordinated to Fullerene as an “Antenna-Reaction-Center” Mimic: Formation of a Long-Lived Charge-Separated State in Nonpolar Solvent. *Chem. Eur. J.* **2010**, *16*, 6193–6202.
- (24) Kozlov, O. V.; Liu, X.; Luponosov, Y. N.; Solodukhin, A. N.; Toropynina, V. Y.; Min, J.; Buzin, M. I.; Peregudova, S. M.; Brabec, C. J.; Ponomarenko, S. A.; *et al.* Triphenylamine-Based Push–Pull Molecule for Photovoltaic Applications: From Synthesis to Ultrafast Device Photophysics. *J. Phys. Chem. C* **2017**, *121*, 6424–6435.
- (25) Kozlov, O. V.; Liu, X.; Luponosov, Y. N.; Solodukhin, A. N.; Toropynina, V. Y.; Min, J.; Buzin, M. I.; Peregudova, S. M.; Brabec, C. J.; Ponomarenko, S. A.; *et al.* Triphenylamine-Based Push–Pull Molecule for Photovoltaic Applications: From Synthesis to Ultrafast Device Photophysics. *J. Phy. Chem. C* **2017**, *121*, 6424–6435.
- (26) Gao, G. Y.; Chen, Y.; Zhang, X. P. General and Efficient Synthesis of Arylamino- and Alkylamino-Substituted Diphenylporphyrins and Tetraphenylporphyrins *via* Palladium-Catalyzed Multiple Amination Reactions. *J. Org. Chem.* **2003**, *68*, 6215–6221.
- (27) Huang, C.-W.; Yuan Chiu, K.; Cheng, S.-H. Novel Spectral and Electrochemical Characteristics of Triphenylamine-Bound Zinc Porphyrins and Their Intramolecular Energy and Electron Transfer. *Dalton Trans.* **2005**, *0*, 2417-2422.

- (28) Ning, Z.; Tian, H. Triarylamine: A Promising Core Unit for Efficient Photovoltaic Materials. *Chem. Commun.* **2009**, *0*, 5483-5495.
- (29) Wang, J.; Yang, C. J.; Peng, H. N.; Deng, Y. S.; Gao, X. C. Synthesis of Triphenylamine-Modified Arylates and Ketones via Suzuki Coupling Reactions. *Synth. Commun.* **2011**, *41*, 832-840.
- (30) Kumar, P. K.; Bhyrappa, P.; Varghese, B. An Improved Protocol for the Synthesis of Antipodal β -Tetrabromo-tetraphenylporphyrin and the Crystal Structure of its Zn(II) Complex. *Tetrahedron Lett.* **2003**, *44*, 4849-4851.
- (31) Thomas, K. E.; Wasbotten, I. H.; Ghosh, A. Copper β -Octakis(Trifluoromethyl)Corroles: New Paradigms for Ligand Substituent Effects in Transition Metal Complexes. *Inorg. Chem.* **2008**, *47*, 10469-10478.
- (32) Alemayehu, A. B.; Hansen, L. K.; Ghosh, A. Nonplanar, Noninnocent, and Chiral: A Strongly Saddled Metalloporphyrin. *Inorg. Chem.* **2010**, *49*, 7608-7610.





CHAPTER 8

SUMMARY AND CONCLUSIONS



CHAPTER 8

SUMMARY AND CONCLUSIONS

Porphyrins have many interesting properties which caught the attention of researchers and hence the study of porphyrinoids has seen enormous surge in terms of various publication in the last decade or so. Porphyrins are the chemically and thermally stable compounds but their photophysical and electrochemical properties can be very easily tuned *via* modification and functionalization at periphery of porphyrin core. *Meso* and β -Functionalized porphyrins with appropriate functional groups have been successfully explored for their use in photodynamic therapy (PDT), anion sensing, catalysis, dye-sensitized solar cells (DSSCs), molecular, biomedical imaging, nonlinear optical materials and in medicine. In chapter 1, we have described the synthesis of various functionalized porphyrins and their medical and material applications.

In chapter 2, we have synthesized β -arylamino and N-fused porphyrins (MTPP(NHPh) X_2 and MTPP(N-fusedPh) X_2 ($X = H, Br, Ph, PE$ and $M = 2H, Co(II), Ni(II), Cu(II), Zn(II)$). Synthesized porphyrins were characterized by various spectroscopic techniques. Optical absorption spectra indicated interesting features such as broad Soret band and intense Q bands. Emission spectra of these porphyrins featured redshifted with reduced intensity, due to nonplanar conformation of macrocyclic system and heavy atom effect of bromo groups. DFT study revealed that moderate nonplanarity of these macrocycle and $H_2TPP(NHPh)Ph_2$ exhibited higher nonplanarity with respect to other synthesized β -arylamino porphyrins. The crystal structure of $H_2TPP(N-fusedPh)Br_2$ exhibited twisted conformation of the macrocycle. The binding of Zn(II) N-fused porphyrins ($ZnTPP(N-fusedPh)X_2$: $X = 2H, Br, Ph, and PE$) with $C_{60}Im/Py$ was studied by 1H NMR, UV-visible and fluorescence spectroscopic techniques which revealed the 1:1 stoichiometry of Zn(II) N-fused porphyrin: $C_{60}Im/Py$ complexation. $ZnTPP(N-fusedPh)PE_2$ has shown the highest association constant and quenching constant as compared to other synthesized Zn(II)-N-fused porphyrins due to effective π - π interaction between porphyrins and C_{60} derivatives. The association constants of these Zn(II) N-fused porphyrins were found to be 10-100 times higher as compared to Zn(II) *meso*-tetra-methyl/ethylporphyrin. Positive shifts in the oxidation potentials of synthesized porphyrins also evidenced the supramolecular interaction between Zn(II) N-fused porphyrins and $C_{60}Im/Py$.

In chapter 3, we have synthesized tetrabenzoquinone appended Ni(II) and Cu(II) porphyrins and characterized by various spectroscopic techniques. These porphyrins exhibited strong solvatochromism behavior in nitrogenous bases through axial coordination. Further, we studied the anion sensing properties of tetrabenzoquinone appended Ni(II) and Cu(II) porphyrins. The electrochemical studies revealed that *meso*-tetrakis(3,4-benzoquinone)-substituted metalloporphyrin macrocycle is electron deficient by ~ 1.1 V as compared to TDtBPPM (M = Cu and Ni) and nearly 0.94 V as compared to oxoporphyrinogen, respectively and therefore binds to less basic F^- ions also in addition to highly basic cyanide ions through axial ligation mechanism. These porphyrins act as F^- and CN^- chemosensor in nonaqueous media and selective CN^- sensor in aqueous medium due to high solvation of F^- ions in aqueous media even in presence of all other interfering anions in excess.

In chapter 4, we have developed new families of mixed substituted porphyrins and characterized by various spectroscopic techniques. Crystal structure of $H_2TPP(NO_2)(Ph)_2Br_5$ revealed the saddle shape nonplanar conformation with the deviation of 24 core atoms ($\Delta_{24} = \pm 0.558 \text{ \AA}$) and the displacement of β -carbon ($\Delta C_\beta = \pm 1.23 \text{ \AA}$) from the mean plane of porphyrin core. These unsymmetrical porphyrin exhibits 53-61 nm bathochromic shift in Soret band as compared to H_2TPP . These porphyrin show higher protonation and deprotonation constant due nonplanarity of the macrocyclic core and the electronic effect of β -substituents. The 1H NMR spectra of $H_2TPP(Ph)_2Br_6$ exhibited 0.67 ppm downfield shift in -NH protons as compared to $H_2TPP(NO_2)(Ph)_2$. HOMO-LUMO gap of $H_2TPP(NO_2)(Ph)_2Br_5$ is decreased about 0.62 V as compared to H_2TPP due to push-pull β -substituents having different shape, size and electronic nature and enhanced nonplanarity of the porphyrin core. Redox tunability of these porphyrins was accomplished by appending electron donating/ accepting groups at the periphery of the porphyrin which results in push-pull effect of β -substituents at porphyrin π -system. The mixed push-pull β -substituents induces the higher order of nonplanarity which was confirmed by single crystal X-ray structure, DFT calculations and photophysical data as well as red-shifted spectral features with redox tunability.

In chapter 5, *meso*-tetraalkylporphyrins with varying alkyl chain length were synthesized and characterized by various spectroscopic techniques. Crystal structure of *meso*-tetrapropylporphyrin exhibited planar confirmation of porphyrin macrocycle. The binding of C_{60} with the *meso*-tetramethyl/ethyl/propylporphyrin (**1-3**) and their zinc complexes was monitored

by ^1H NMR, and fluorescence spectroscopic techniques. From UV-Vis and fluorescence titrations, the stoichiometry of complexation between porphyrin and fullerene (C_{60}) was found to be 1:1. These *meso*-tetraalkylporphyrins have shown 10-100 times higher association constants than H_2TPP and H_2THexP . As we increase the alkyl chain length from C_1 to C_6 , a marked decrement (100 times) in the association constants was observed due to enhanced steric hindrance offered by alkyl chains. The anodic shift in oxidation potentials (20-100 mV) of porphyrin-fullerene dyads as compared to *meso*-tetraalkylporphyrins indicating the supramolecular interactions between the constituents in the ground state. The optimized geometry and electronic structure of $1:\text{C}_{60}$ supported the formation of supramolecular dyad and the possibility of charge transfer interactions between porphyrin host and fullerene C_{60} guest.

In chapter 6, we have designed and synthesized successfully two new families of asymmetric β -trisubstituted ‘push-pull’ porphyrins ($\text{MTPP}(\text{TPA})_2\text{X}$ ($\text{X} = \text{NO}_2/\text{CHO}$ and $\text{M} = 2\text{H}$, Co^{II} , Ni^{II} , Cu^{II} , Zn^{II})) through Pd catalyzed Suzuki cross-coupling reaction and characterized by various spectroscopic techniques, mass spectrometry, NLO properties, DFT and electrochemical studies. These porphyrins exhibited 16-22 nm and 39-58 nm redshift in the Soret and $\text{Q}_{\text{x}(0,0)}$ bands, respectively as compared to MTPPs due to resonance and inductive effect of β -substituents on porphyrin π -system. The quantum yields as well as fluorescence lifetime of nitro substituted porphyrins have been found to be less as compared to those of formyl substituted porphyrins which clearly suggests larger extent of charge-transfer from donor moiety to nitro group *via* porphyrin spacer due to better electronic coupling of nitro group. $\text{H}_2\text{TPP}(\text{TPA})_2\text{NO}_2$ and $\text{H}_2\text{TPP}(\text{TPA})_2\text{CHO}$ revealed large resultant dipole moment (7.62 D and 4.55 D, respectively) as compared to H_2TPP (0.052 D) due to nonplanarity of macrocycle core and cross polarized ‘push-pull’ effect of β -substituents. $\text{H}_2\text{TPP}(\text{TPA})_2\text{NO}_2$ exhibited nonplanar saddle shape conformation of the macrocyclic core as it was confirmed by DFT calculations. The first reduction potential of $\text{CuTPP}(\text{TPA})_2\text{NO}_2$ and $\text{CuTPP}(\text{TPA})_2\text{CHO}$ was found 0.44 and 0.36 V anodically shifted as referenced to CuTPP , respectively due to the electron withdrawing nature of NO_2 and CHO groups which made them easy to reduce than CuTPP . Redox potentials were found to be less altered in case of formyl substituted porphyrins as compared to those of nitro substituted porphyrins. HOMO-LUMO energy levels were also found to be modulated due to peripheral substitutions of macrocycle. Third order nonlinear optical properties of $\text{H}_2\text{TPP}(\text{TPA})_2\text{NO}_2$ and $\text{H}_2\text{TPP}(\text{TPA})_2\text{CHO}$ were investigated in a broad spectral range (680-850 nm) using the Z-scan

technique with femtosecond, 80 MHz pulses. We have noticed RSA behavior in open aperture experimental data whereas in closed aperture case, the data displayed a peak-valley nature revealing the defocusing nature (suggesting negative refractive index) for both $\text{H}_2\text{TPP}(\text{TPA})_2\text{NO}_2$ and $\text{H}_2\text{TPP}(\text{TPA})_2\text{CHO}$. The NLO coefficients (and cross-sections) of $\text{H}_2\text{TPP}(\text{TPA})_2\text{NO}_2$ were found to be higher compared to $\text{H}_2\text{TPP}(\text{TPA})_2\text{CHO}$, which clearly suggests the role of nitro group (electron withdrawing).

In chapter 7, we have reported a new family of antipodal β -tetrasubstituted triphenylaminoporphyrins ($\text{H}_2\text{TPP}(\text{TPA})_4$) via Suzuki cross-coupling reaction. Also, its metal derivatives were synthesized and characterized using various spectroscopic techniques. β -Tetrasubstituted triphenylaminoporphyrins exhibited nonplanar conformation of the macrocyclic core. Due the β -substitution, the synthesized porphyrins exhibited tunable redox potentials. These porphyrins are found to be easy to oxidize as compared to MTPPs. $\text{NiTPP}(\text{TPA})_4$ exhibited 0.15-0.29 V cathodic shift in the first oxidation potential and marginal shift in the first reduction potential as compared to NiTPP and NiOPP due destabilization of HOMOs. UV-vis and fluorescence spectral studies revealed significant bathochromic shift with respect to MTPPs due to electron donating nature of TPA, extended π -conjugation and nonplanarity of the macrocyclic core.

Future Perspectives

Our work on β /*meso*-functionalized porphyrins **paves a way** to synthesize electronically tunable porphyrins for various application including NLO, anion sensing and porphyrin-fullerene dyads. We have developed electron rich mixed β -arylamino porphyrin and β -N-fused porphyrins. These porphyrins exhibited interesting photophysical and electrochemical properties and have asymmetrical pattern which reveals that these porphyrins can be used in nonlinear optical application in future. β -N-fused porphyrins used as electron donor to mimic natural photosynthesis. We used these (β -N-fused porphyrins) porphyrins for the complexation with fullerene and form porphyrin-fullerene dyads. Two most important applications of these models (porphyrin-**fullerene** dyads) (i) the conversion of light energy in to electrical energy and (ii) optoelectronic devices development. **Hence these types** of assemblies can be used in light harvesting applications. We have also developed electron rich *meso*-tetraalkylporphyrin and investigated their supramolecular donor-acceptor dyads formation. Our work on anion sensing

depicted that the highly electron deficient porphyrin can be synthesized by appending benzoquinone groups at *meso*-position which make the macrocycle electron deficient and CN^- and F^- coordinate *via* axial ligation and exhibited very high binding constant. Mixed β -substituted porphyrin exhibit very interesting electrochemical and photophysical properties. We have synthesized unsymmetrical mixed β -octasubstituted porphyrins *via* Suzuki cross-coupling reaction. The unsymmetrical pattern and ‘push-pull’ effect of β -substituents reflect that these porphyrins can be used in nonlinear optical application. Triphenylamine is good electron donating group which is a famous building block in material chemistry and used for the synthesis of such type of material in various application such as photovoltaic devices. We have synthesized β -trisubstituted ‘push-pull’ porphyrins. These porphyrins exhibited largest dipole moment, unsymmetrical pattern and highly conjugated system which depicted that these types of porphyrins can be used in nonlinear optical application due to the presence of electron rich (triphenylamino group). These porphyrins can be used in the complexation with fullerene. Nonplanar porphyrins are used in model of naturally occurring macrocycle. Steric repulsive interaction between the peripheral substituents leads the nonplanarity of macrocyclic ring. So, the nonplanarity of porphyrin ring can be modulated *via* varying the shape, size, and the number of substituents at the periphery. The presence of triphenylamino group at periphery of porphyrin leads the nonplanarity of porphyrin core. TPA based material used as photovoltaic devices exhibit low oxidation potential. Triphenylamine groups at periphery of porphyrin make them electron rich macrocyclic system which can be used in the complexation with fullerene. Thus, our work **describes** useful synthetic methods for the functionalization and also **suggests** the new pathway to **get electronically tunable porphyrins for various applications**.







APPENDIX-I

Synthesis, Structural, Spectral and Electrochemical Redox Properties of β -arylamino and N-Fused Porphyrins and Photoinduced Electron Transfer Studies of N-Fused Porphyrins with C_{60} Derivatives

Table of Contents	Page No.
Figure A1-A4. 1H NMR spectrum of $H_2TPP(NHPh)X_2$, X = H, Br, Ph, PE in $CDCl_3$ at 298 K.	189-190
Figure A5-A8. 1H NMR spectrum of $H_2TPP(N-fusedPh)X_2$, X = H, Br, Ph, PE in $CDCl_3$ at 298 K.	191-192
Figure A9-A12. MALDI-TOF mass spectra of $H_2TPP(NHPh)X_2$, X = H, Br, Ph, PE.	193-194
Figure A13-A16. MALDI-TOF mass spectra of $H_2TPP(N-fusedPh)X_2$, X = H, Br, Ph, PE.	195-196
Table A1. Selected average bond lengths and bond angles of $H_2TPP(N-fusedPh)Br_2$.	197
Table A2. Crystal structure data of $H_2TPP(N-fusedPh)Br_2$.	198
Figure A17. UV-Visible spectra of (a) $H_2TPP(NHPh)$ and $H_2TPP(NHPh)Ph_2$, (b) $H_2TPP(NHPh)Br_2$ and $H_2TPP(NHPh)PE_2$.	199
Figure A18-A20. UV-visible titration of $ZnTPP(N-fusedPh)$, $ZnTPP(N-fusedPh)Br_2$ and $ZnTPP(N-fusedPh)Ph_2$ with $C_{60}Im$ in <i>o</i> -dichlorobenzene at 298 K and inset corresponding to Benesi-Hildebrand plot.	199-200
Figure A21-A23. UV-visible titration of $ZnTPP(N-fusedPh)$, $ZnTPP(N-fusedPh)Br_2$ and $ZnTPP(N-fusedPh)Ph_2$ with $C_{60}Py$ in <i>o</i> -dichlorobenzene at 298 K and inset corresponding to Benesi-Hildebrand plot.	201-202
Figure A24-A26. Quenching of fluorescence intensity of $ZnTPP(N-fusedPh)$, $ZnTPP(N-fusedPh)Br_2$ and $ZnTPP(N-fusedPh)Ph_2$ with $C_{60}Im$ in <i>o</i> -dichlorobenzene at 298 K and inset corresponding to Stern-Volmer plot.	202-203
Figure A27-A29. Quenching of fluorescence intensity of $ZnTPP(N-fusedPh)$, $ZnTPP(N-fusedPh)Br_2$ and $ZnTPP(N-fusedPh)Ph_2$ with $C_{60}Py$ in <i>o</i> -dichlorobenzene at 298 K and inset corresponding to Stern-Volmer plot.	204-205
Figure A30. Cyclic voltammetric studies of $ZnTPP(N-fusedPh)Br_2$ and $ZnTPP(N-fusedPh)Ph_2$ in the presence and absence of $C_{60}Im$ in <i>o</i> -dichlorobenzene at 298 K.	205

- Table A3.** Electrochemical data of Zn(II) derivatives of ZnTPP(N-fusedPh) X_2 , X = H, Br, Ph, PE) with and without $C_{60}Im$ and $C_{60}Py$ in *o*-dichlorobenzene containing 0.1 M TBAPF₆ with scan rate of 0.1V/s at 298 K. 206
- Figure A31.** Cyclic voltammetric studies of ZnTPP(N-fusedPh) and ZnTPP(N-fusedPh)PE₂ in the presence and absence of $C_{60}Py$ in *o*-dichlorobenzene at 298 K. 206
- Figure A32.** Cyclic voltammetric studies of ZnTPP(N-fusedPh)Br₂ and ZnTPP(N-fusedPh)Ph₂ in the presence and absence of $C_{60}Py$ in *o*-dichlorobenzene at 298 K. 207
- Figure A33.** (a) Optimized structure (b) electrostatic potential map (c) Pictorial representation of frontier HOMO (d) LUMO of ZnTPP(N-fusedPh)Br₂: $C_{60}Py$ 207
- Figure A34.** (a) Optimized structure (b) electrostatic potential map (c) Pictorial representation of frontier HOMO (d) LUMO of ZnTPP(N-fusedPh)Ph₂: $C_{60}Py$ 208
- Figure A35.** (a) Optimized structure (b) electrostatic potential map (c) Pictorial representation of frontier HOMO (d) LUMO of ZnTPP(N-fusedPh)PE₂: $C_{60}Py$ 208
- Figure A36.** (a) Optimized structure (b) electrostatic potential map (c) Pictorial representation of frontier HOMO (d) LUMO of ZnTPP(N-fusedPh): $C_{60}Im$ 209
- Figure A37.** (a) Optimized structure (b) electrostatic potential map (c) Pictorial representation of frontier HOMO (d) LUMO of ZnTPP(N-fusedPh)Br₂: $C_{60}Im$ 209
- Figure A38.** (a) Optimized structure (b) electrostatic potential map (c) Pictorial representation of frontier HOMO (d) LUMO of ZnTPP(N-fusedPh)Ph₂: $C_{60}Im$ 210
- Figure A39.** ¹H NMR spectra of (a) ZnTPP(N-fusedPh): $C_{60}Im$ adduct (b) ZnTPP(N-fusedPh) in C_6D_6 at 298 K. 210
- Figure A40.** ¹H NMR spectra of (a) ZnTPP(N-fusedPh)Br₂: $C_{60}Im$ adduct (b) ZnTPP(N-fusedPh)Br₂ in C_6D_6 at 298 K. 211
- Figure A41.** ¹H NMR spectra of (a) ZnTPP(N-fusedPh)PE₂: $C_{60}Im$ adduct (b) ZnTPP(N-fusedPh)PE₂ in C_6D_6 at 298 K. 211
- Figure A42.** ¹H NMR spectra of (a) ZnTPP(N-fusedPh): $C_{60}Py$ adduct (b) ZnTPP(N-fusedPh) in C_6D_6 at 298 K. 212
- Figure A43.** ¹H NMR spectra of (a) ZnTPP(N-fusedPh)Br₂: $C_{60}Py$ adduct (b) ZnTPP(N-fusedPh)Br₂ in C_6D_6 at 298 K. 212
- Figure A44.** ¹H NMR spectra of (a) ZnTPP(N-fusedPh)Ph₂: $C_{60}Py$ adduct (b) ZnTPP(N-fusedPh)Ph₂ in C_6D_6 at 298 K. 213

- Figure A45.** 1H NMR spectra of (a) ZnTPP(N-fusedPh)PE₂:C₆₀Py adduct (b) ZnTPP(N-fusedPh)PE₂ in C₆D₆ at 298 K. 213
- Figure A46.** Chemical oxidation of ZnTPP(N-fusedPh) using NOBF₄ in *o*-dichlorobenzene at 298 K. 214
- Figure A47.** Chemical oxidation of ZnTPP(N-fusedPh)Br₂ using NOBF₄ in *o*-dichlorobenzene at 298 K. 214
- Figure A48.** Chemical oxidation of ZnTPP(N-fusedPh)Ph₂ using NOBF₄ in *o*-dichlorobenzene at 298 K. 215
- Figure A49.** Comparative cyclic voltammograms of (a) ZnTPP(NHPh)X₂ (b) ZnTPP(N-fusedPh)X₂, where X = H, Br, Ph and PE. 215
- Figure A50.** Fluorescence spectra of (a) H₂TPP(NHPh)X₂ (b) H₂TPP(N-fusedPh)X₂, where X = H, Br, Ph and PE. 216
- Table A4.** Electrochemical redox data of MTPP(NHPh)X₂, X = H, Br, Ph, PE and M = 2H, Co, Ni, Cu, Zn in CH₂Cl₂ containing 0.1 M TBAPF₆ at scan rate 0.1V/s at 298 K. 217
- Table A5.** Electrochemical redox data of MTPP(N-fusedPh)X₂ (M = 2H, Co (II), Ni (II), Cu (II), Zn (II) and X = H, Br, Ph, PE) in CH₂Cl₂ containing 0.1 M TBAPF₆ with scan rate of 0.1V/s at 298 K. 218

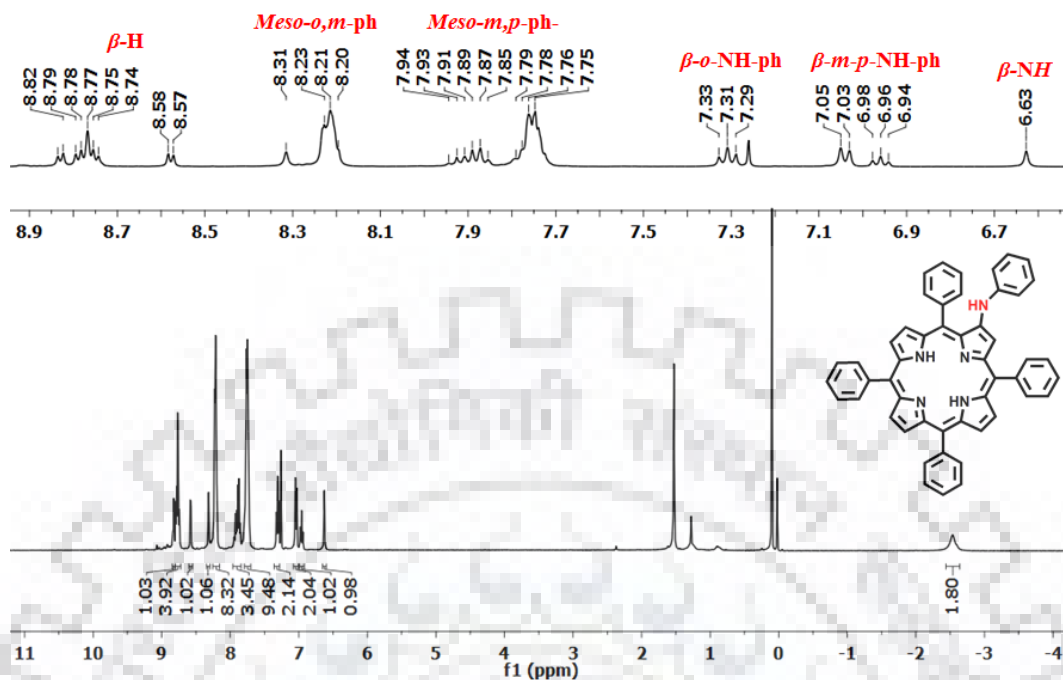


Figure A1. ^1H NMR spectrum of $\text{H}_2\text{TPP}(\text{NHPh})$ in CDCl_3 at 298 K.

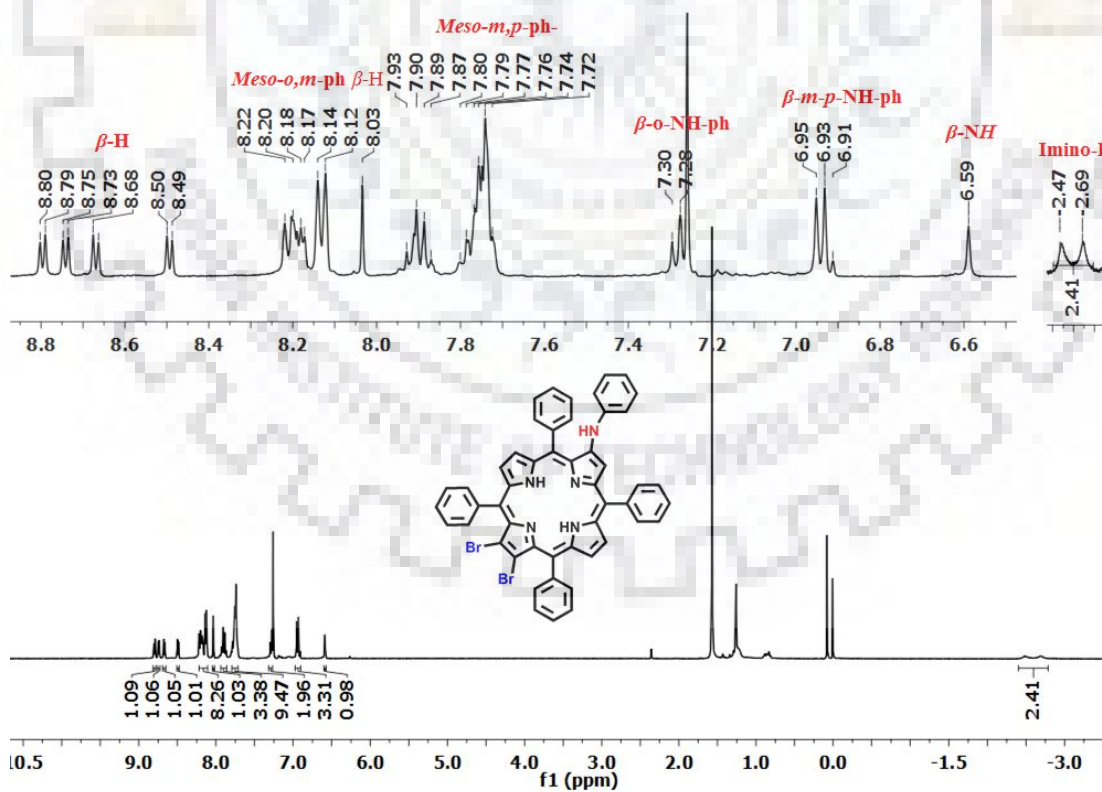


Figure A2. ^1H NMR spectrum of $\text{H}_2\text{TPP}(\text{NHPh})\text{Br}_2$ in CDCl_3 at 298 K.

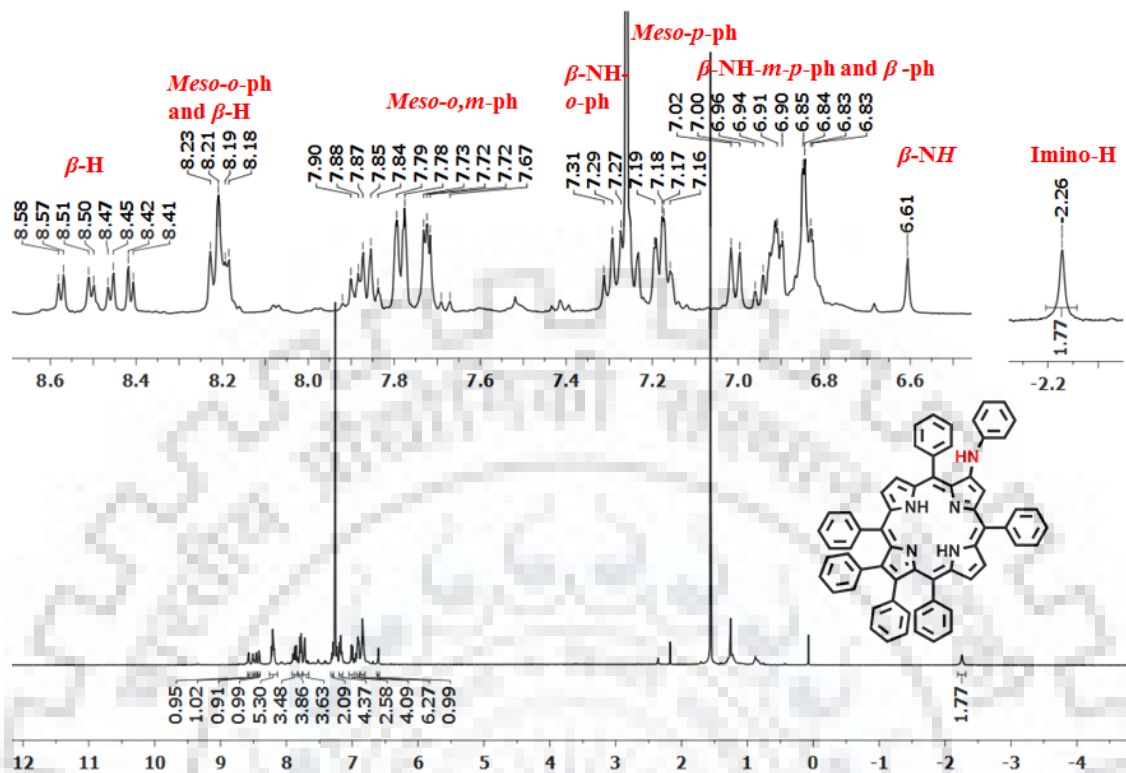


Figure A3. ^1H NMR spectrum of $\text{H}_2\text{TPP}(\text{NHPh})\text{Ph}_2$ in CDCl_3 at 298 K.

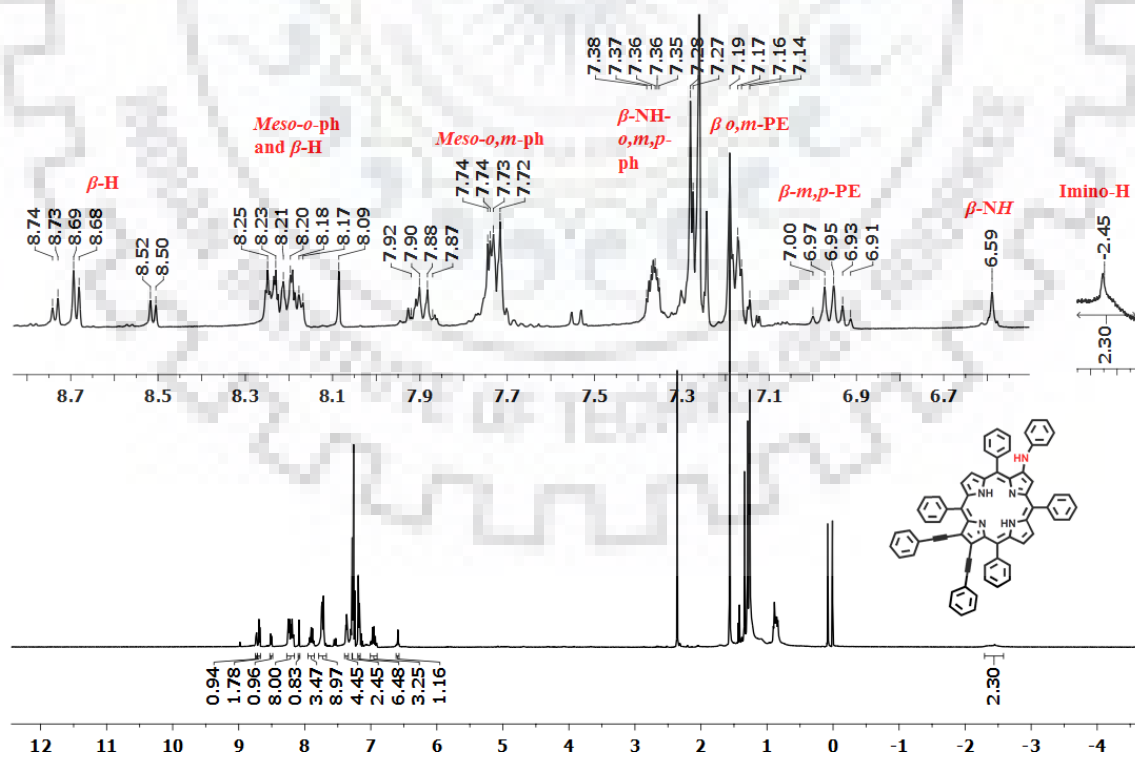


Figure A4. ^1H NMR spectrum of $\text{H}_2\text{TPP}(\text{NHPh})\text{PE}_2$ in CDCl_3 at 298 K.

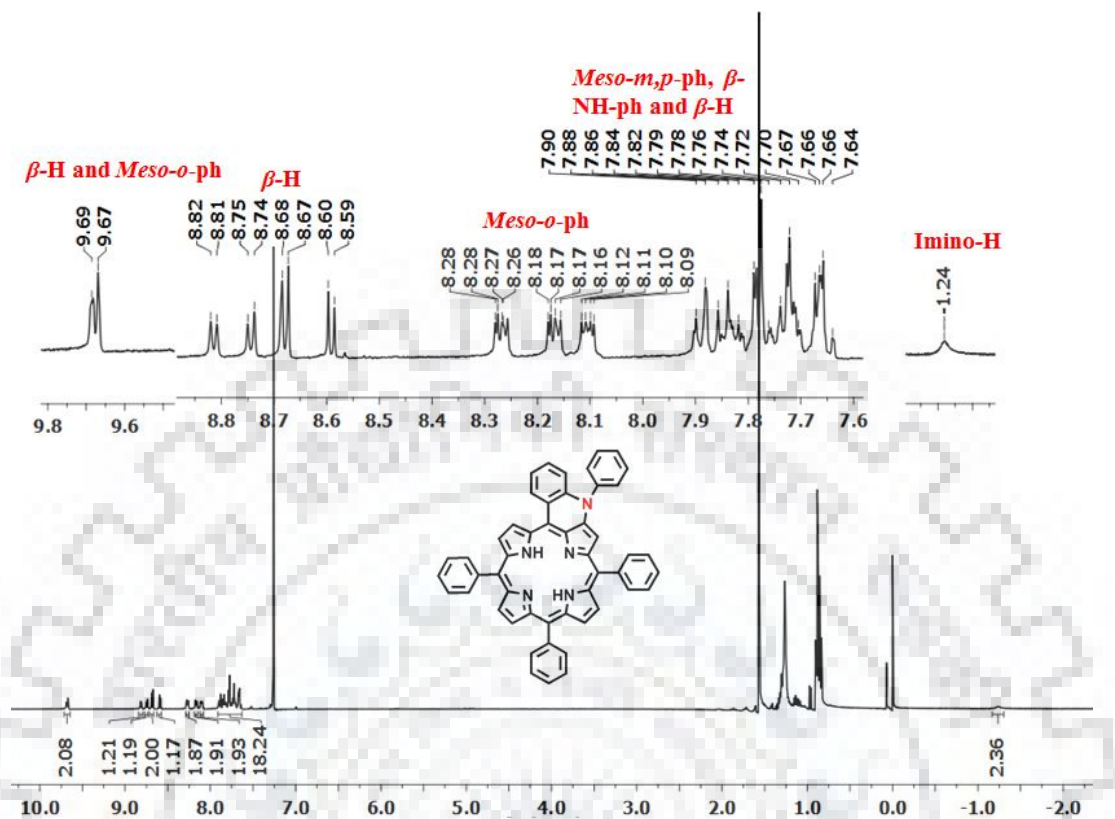


Figure A5. ^1H NMR spectrum of $\text{H}_2\text{TPP}(\text{N-fusedPh})$ in CDCl_3 at 298 K.

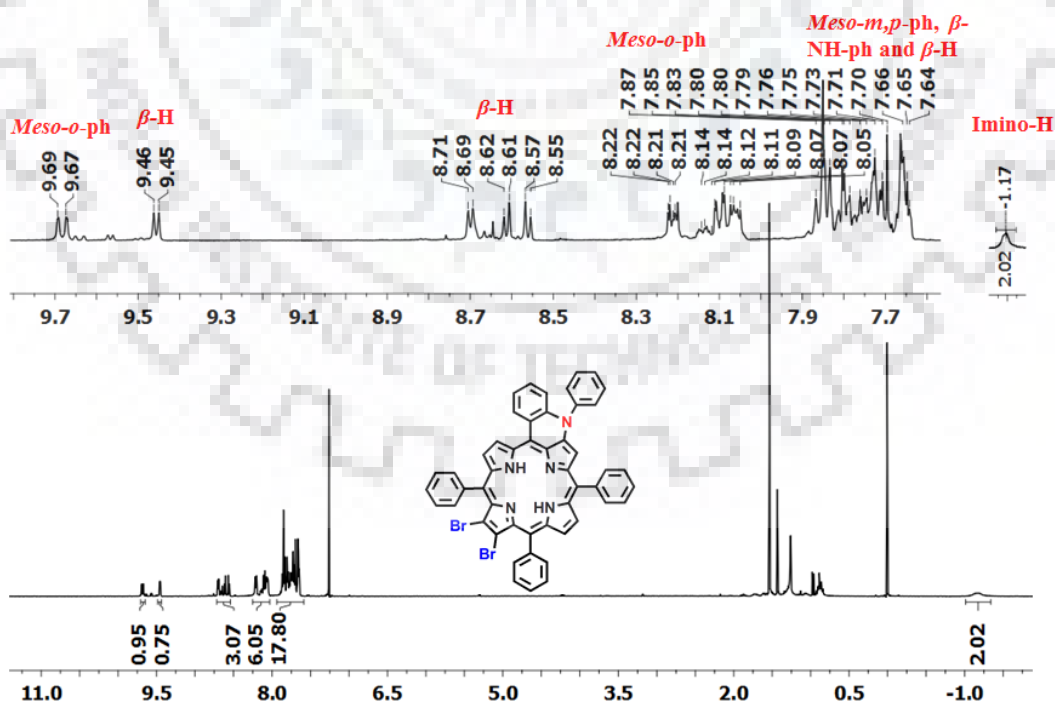


Figure A6. ^1H NMR spectrum of $\text{H}_2\text{TPP}(\text{N-fusedPh})\text{Br}_2$ in CDCl_3 at 298 K.

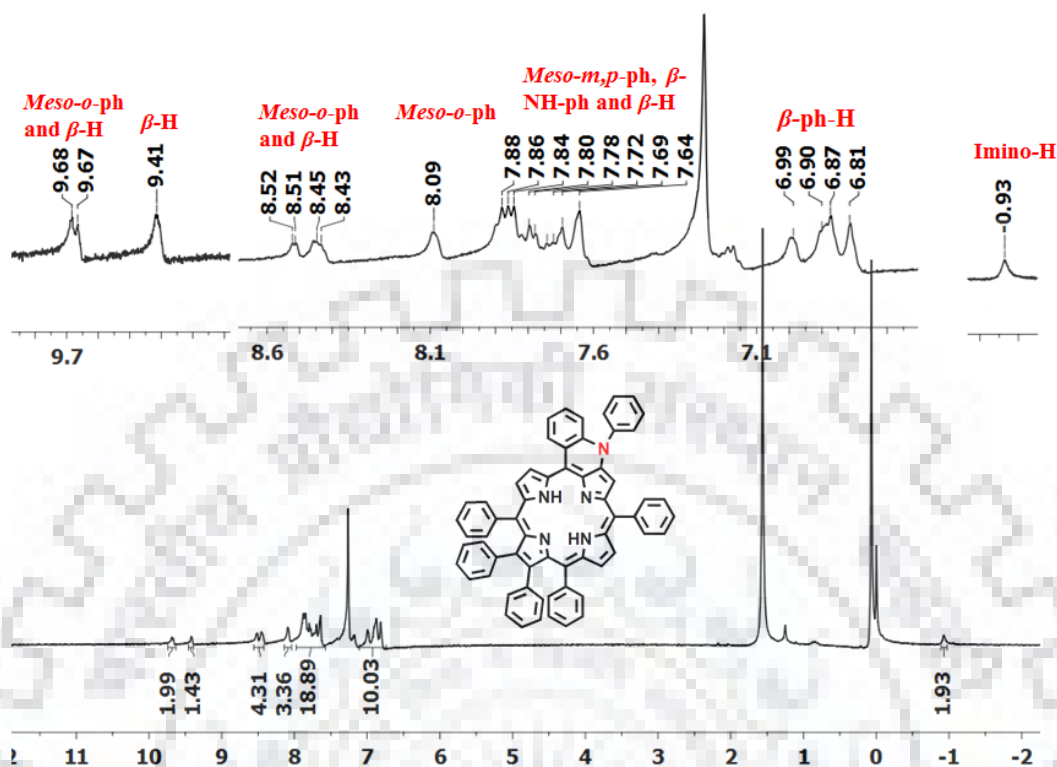


Figure A7. 1H NMR spectrum of $H_2TPP(N\text{-fusedPh})Ph_2$ in $CDCl_3$ at 298 K.

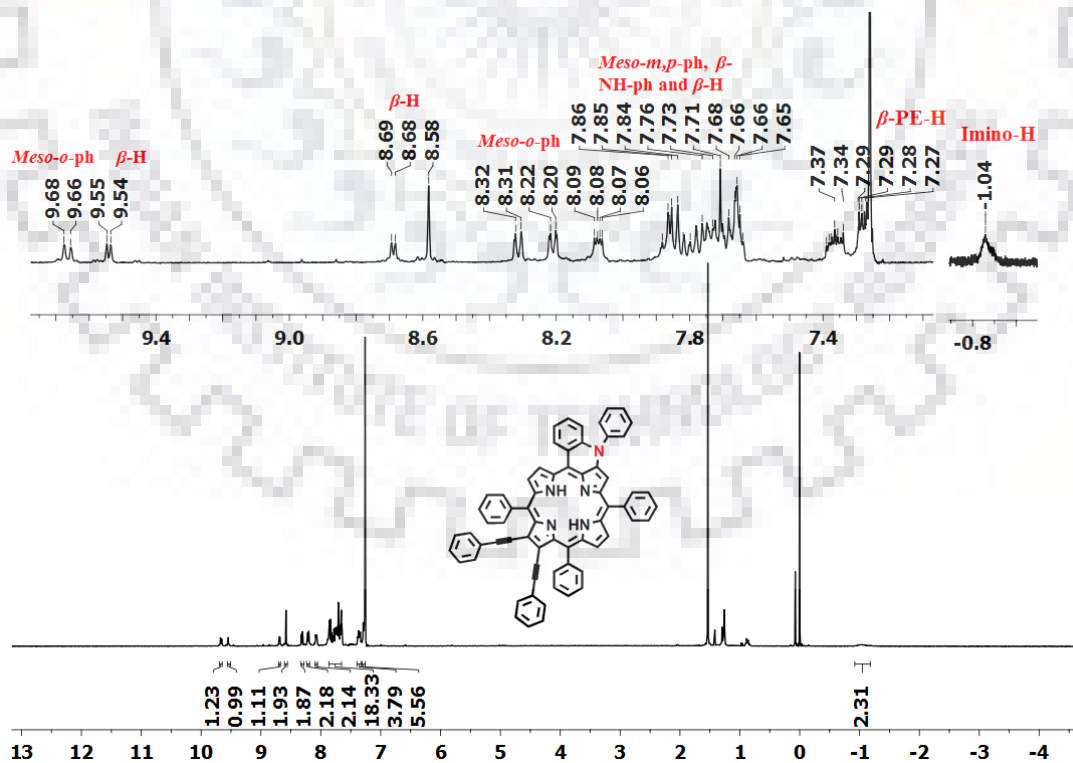


Figure A8. 1H NMR spectrum of $H_2TPP(N\text{-fusedPh})PE_2$ in $CDCl_3$ at 298 K.

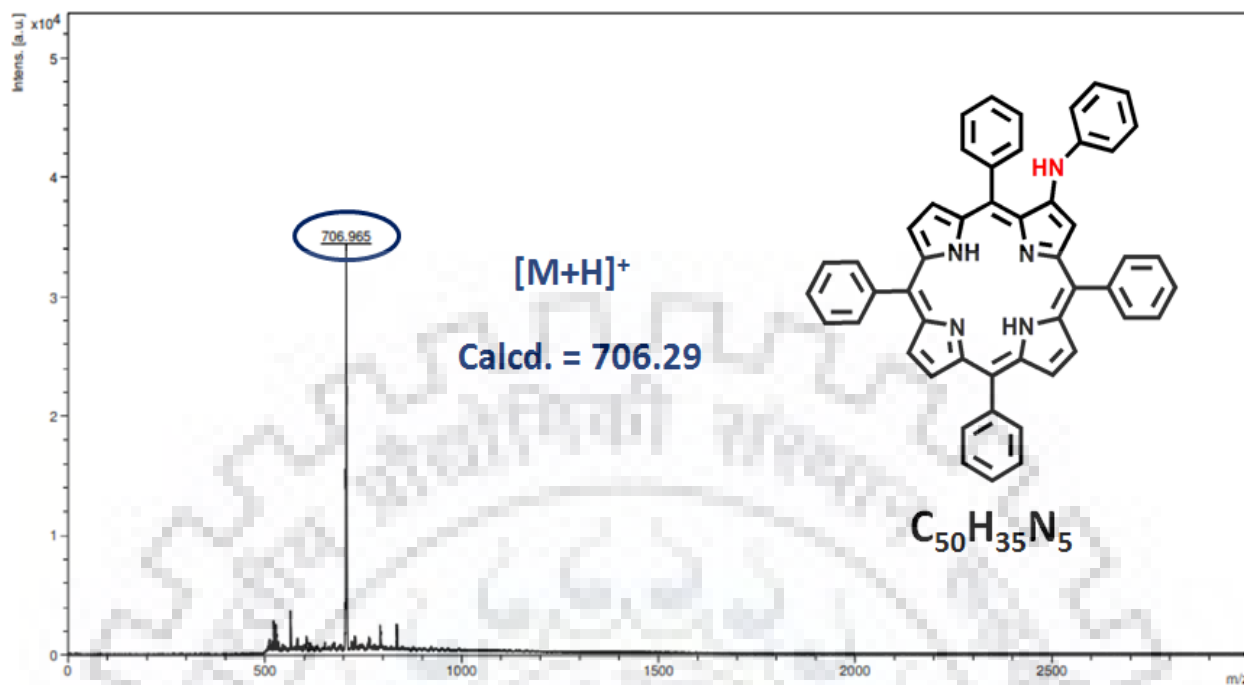


Figure A9. MALDI-TOF mass spectrum of $H_2TPP(NHPh)$ in CH_2Cl_2 at 298K.

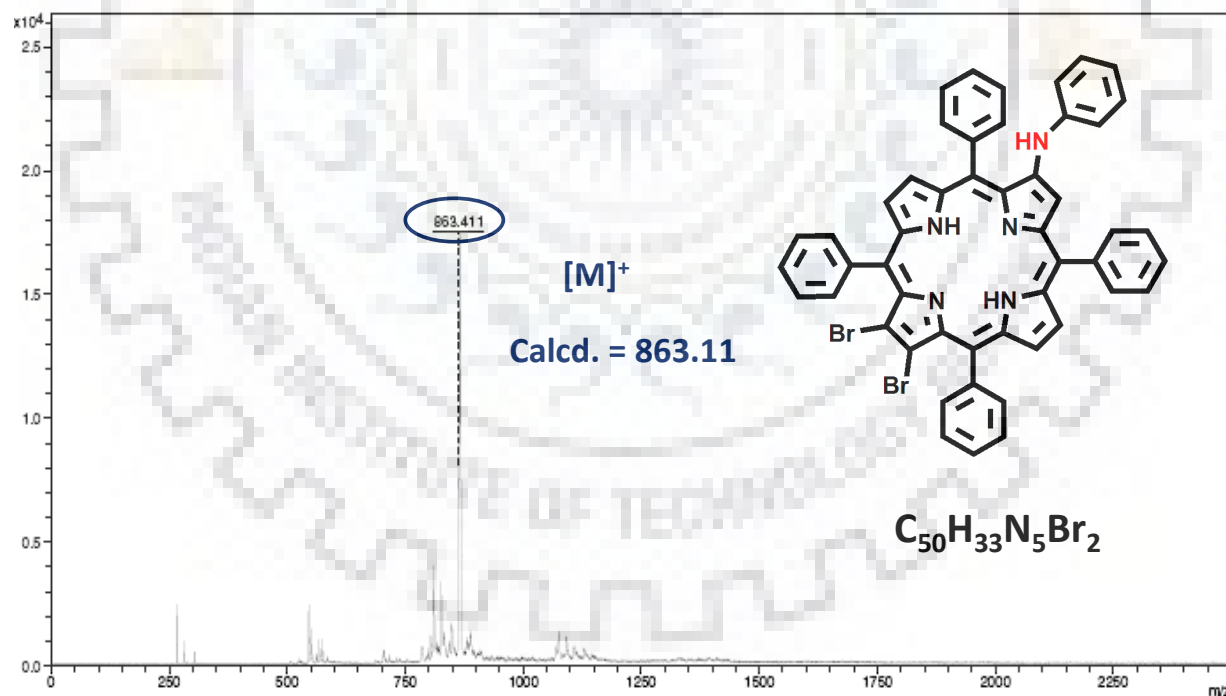


Figure A10. MALDI-TOF mass spectrum of $H_2TPP(NHPh)Br_2$ in CH_2Cl_2 at 298K.

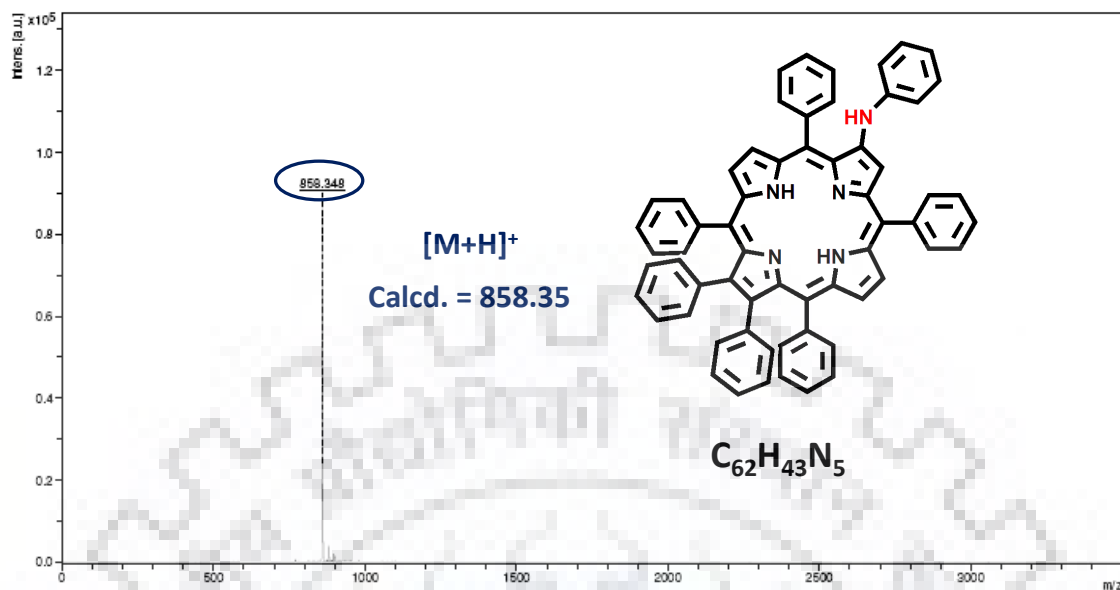


Figure A11. MALDI-TOF mass spectrum of $H_2TPP(NHPh)Ph_2$ in CH_2Cl_2 at 298K.

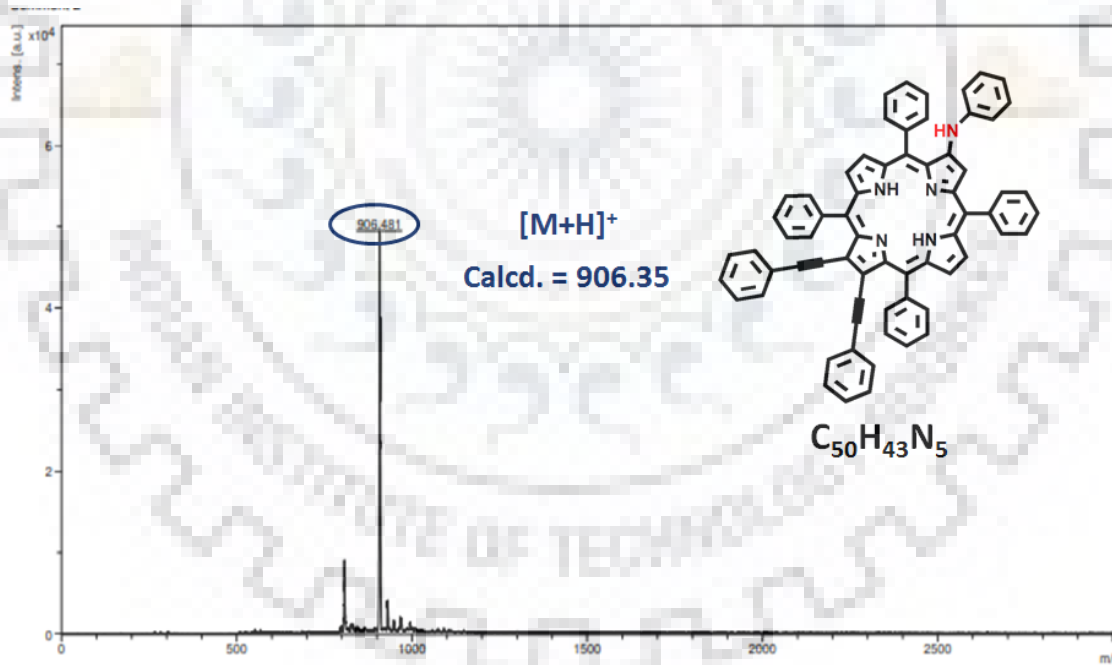


Figure A12. MALDI-TOF mass spectrum of $H_2TPP(NHPh)PE_2$ in CH_2Cl_2 at 298K.

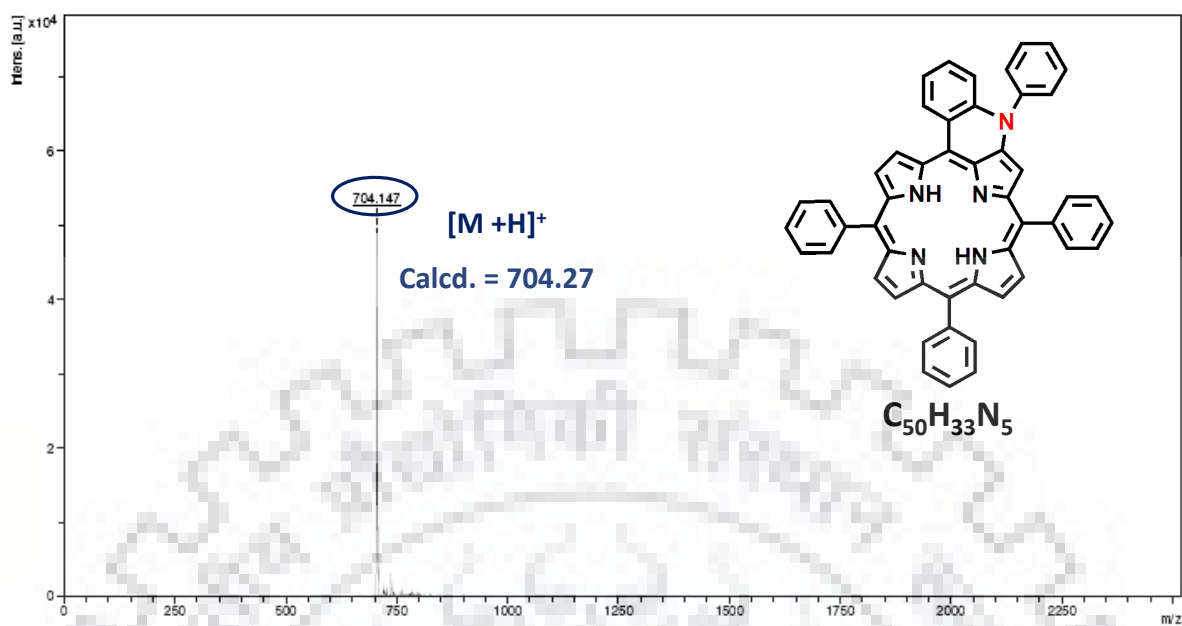


Figure A13. MALDI-TOF mass spectrum of $H_2TPP(N\text{-fusedPh})$ in CH_2Cl_2 at 298K.

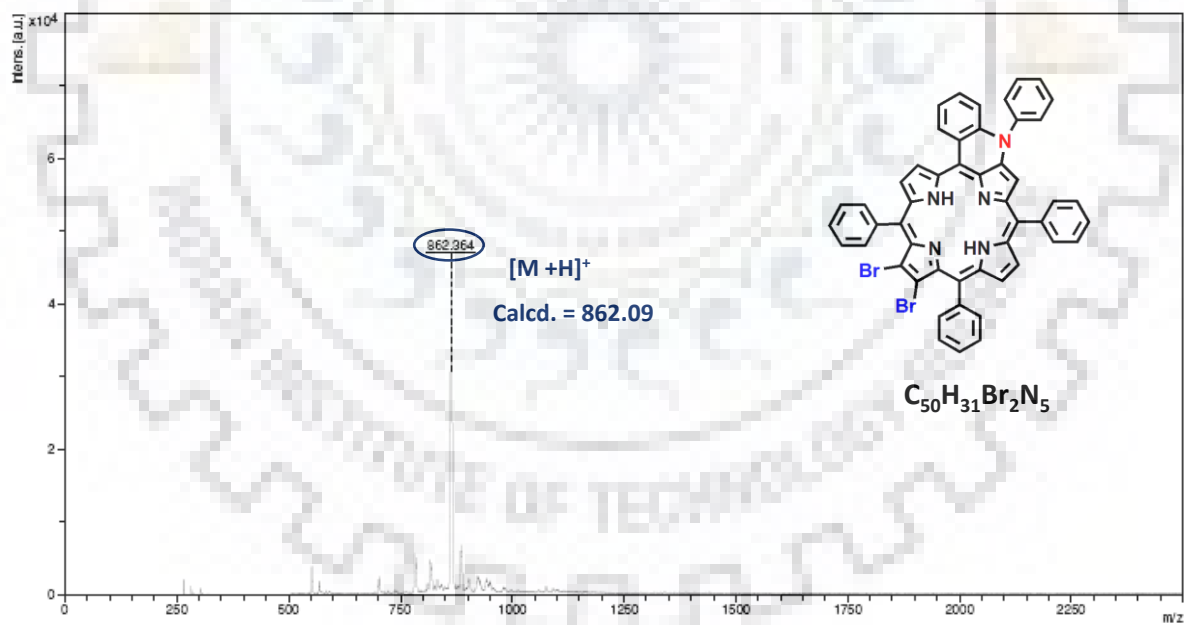


Figure A14. MALDI-TOF mass spectrum of $H_2TPP(N\text{-fusedPh})Br_2$ in CH_2Cl_2 at 298K.

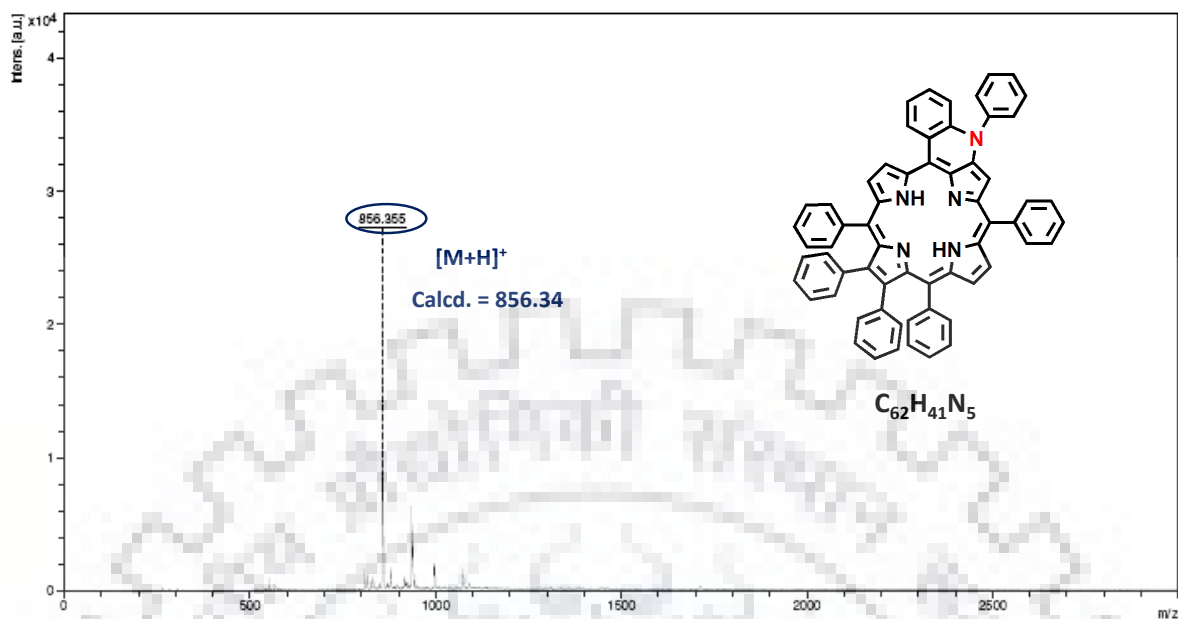


Figure A15. MALDI-TOF mass spectrum of $H_2TPP(N\text{-fusedPh})Ph_2$ in CH_2Cl_2 at 298K.

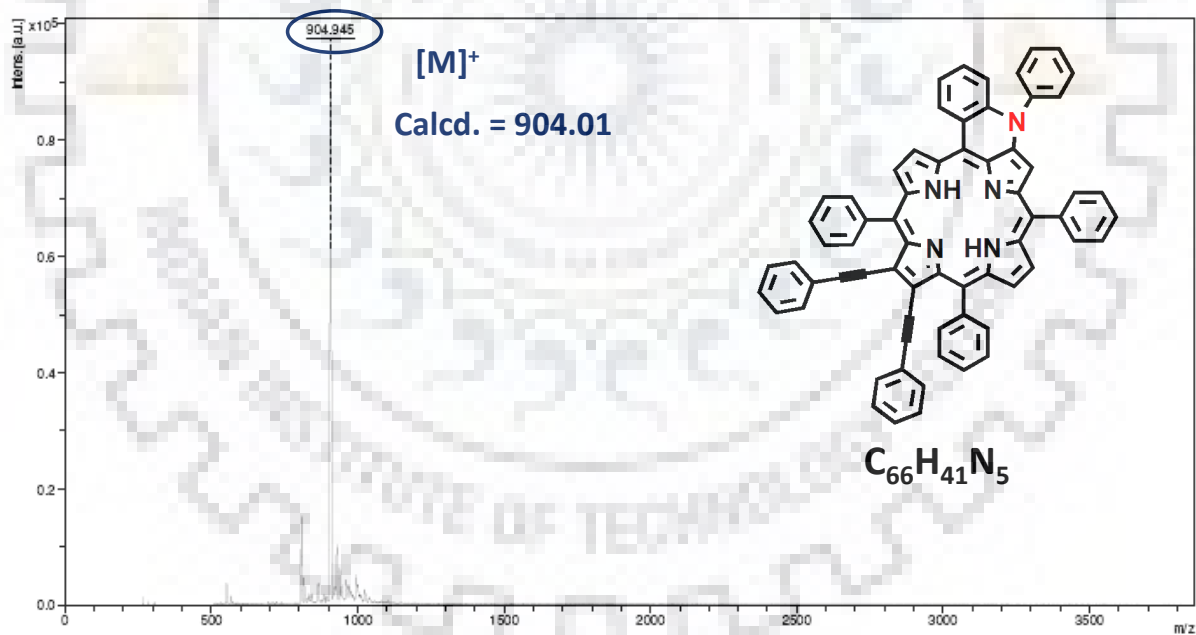


Figure A16. MALDI-TOF mass spectrum of $H_2TPP(N\text{-fusedPh})PE_2$ in CH_2Cl_2 at 298K.

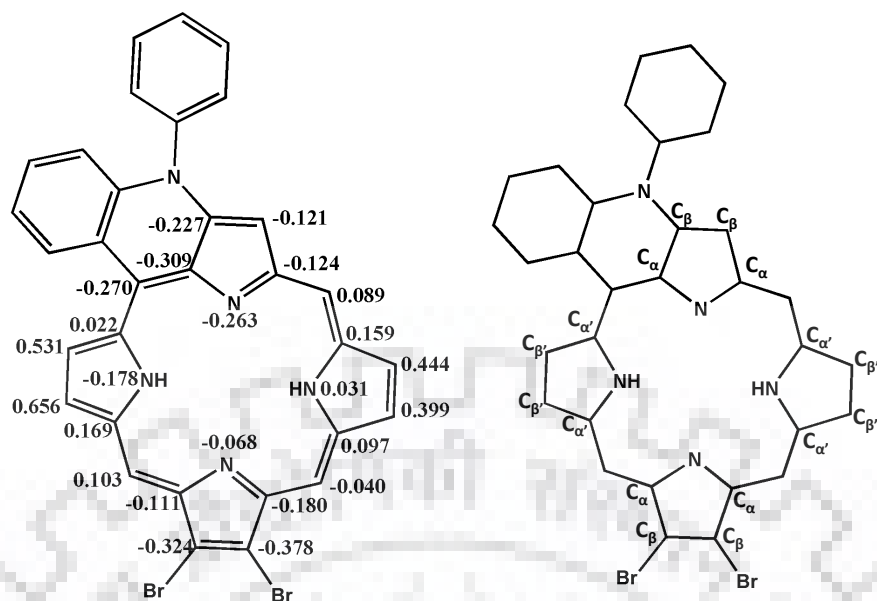


Table A1. selected average bond lengths and bond angles of $H_2TPP(N\text{-fusedPh})Br_2$

$H_2TPP(N\text{-fusedPh})Br_2$	
Bond Length (Å)	
$N-C_\alpha$	1.357
$N'-C_{\alpha'}$	1.370
$C_\alpha-C_\beta$	1.450
$C_{\alpha'}-C_{\beta'}$	1.429
$C_\beta-C_\beta$	1.368
$C_{\beta'}-C_{\beta'}$	1.346
$C_\alpha-C_m$	1.406
$C_{\alpha'}-C_m$	1.394
ΔC_β (Å)	0.385
$\Delta 24$ (Å)	0.220
Bond Angle (deg)	
$N-C_\alpha-C_m$	125.54
$N'-C_{\alpha'}-C_m$	127.05
$N-C_\alpha-C_\beta$	110.16
$N'-C_{\alpha'}-C_{\beta'}$	106.13
$C_\beta-C_\alpha-C_m$	124.06
$C_{\beta'}-C_{\alpha'}-C_m$	126.74
$C_\alpha-C_m-C_{\alpha'}$	124.73
$C_\alpha-C_\beta-C_\beta$	106.68
$C_{\alpha'}-C_{\beta'}-C_{\beta'}$	108.48
$C_\alpha-N-C_\alpha$	106.23
$C_{\alpha'}-N'-C_{\alpha'}$	110.68

ΔC_β refers mean plane deviation of β -carbon atoms, $\Delta 24$ refers mean plane deviation of 24 core atoms.

Table A2. Crystal structure data of $H_2TPP(N\text{-fusedPh})Br_2$.	
Empirical formula	$C_{50}H_{31}Br_2N_5$
Formula wt.	861.60
Crystal system	triclinic
Space group	P- 2
a (Å)	10.712(3)
b (Å)	12.660(4)
c (Å)	15.982(5)
α ($^\circ$)	70.276(16)
β ($^\circ$)	81.620(17)
γ ($^\circ$)	71.761(18)
Volume (Å ³)	1935.8(10)
Z	2
Decald (mg/m ³)	1.478
λ (Å)	0.71073
T (K)	293(2)
No. of total reflns.	9617
No. of indepnt. reflns.	5247
R	0.0663
Rw	0.2087
GOOF	0.985
CCDC	1944532

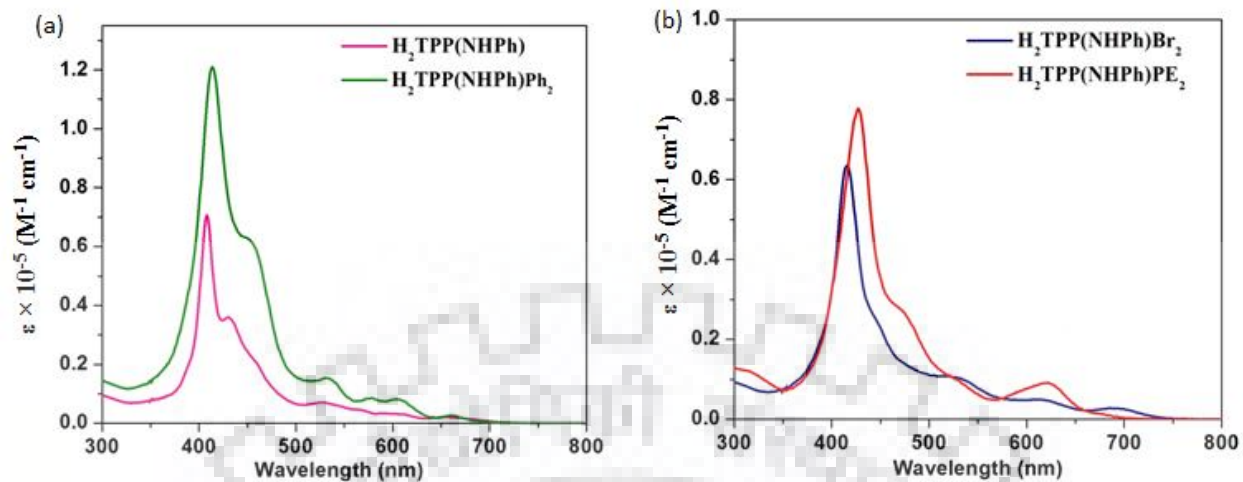


Figure A17. UV-Visible spectra of (a) $H_2TPP(NHPh)$ and $H_2TPP(NHPh)Ph_2$, (b) $H_2TPP(NHPh)Br_2$ and $H_2TPP(NHPh)PE_2$.

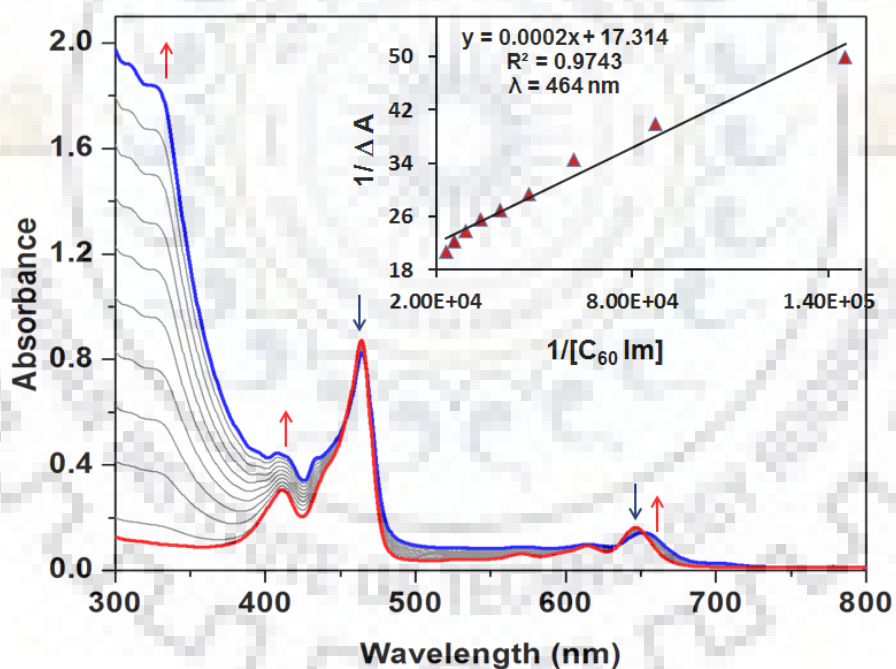


Figure A18. UV-visible titration of $ZnTPP(N-fusedPh)$ with $C_{60}Im$ in *o*-dichlorobenzene at 298 K and inset corresponding to Benesi-Hildebrand plot.

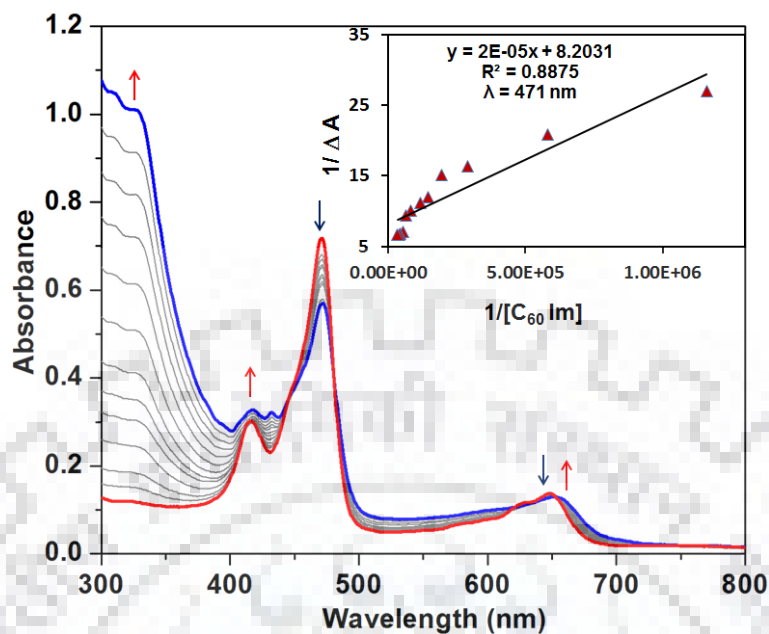


Figure A19. UV-visible titration of ZnTPP(N-fusedPh)Br₂ with C₆₀Im in *o*-dichlorobenzene at 298 K and inset corresponding to Benesi-Hildebrand plot.

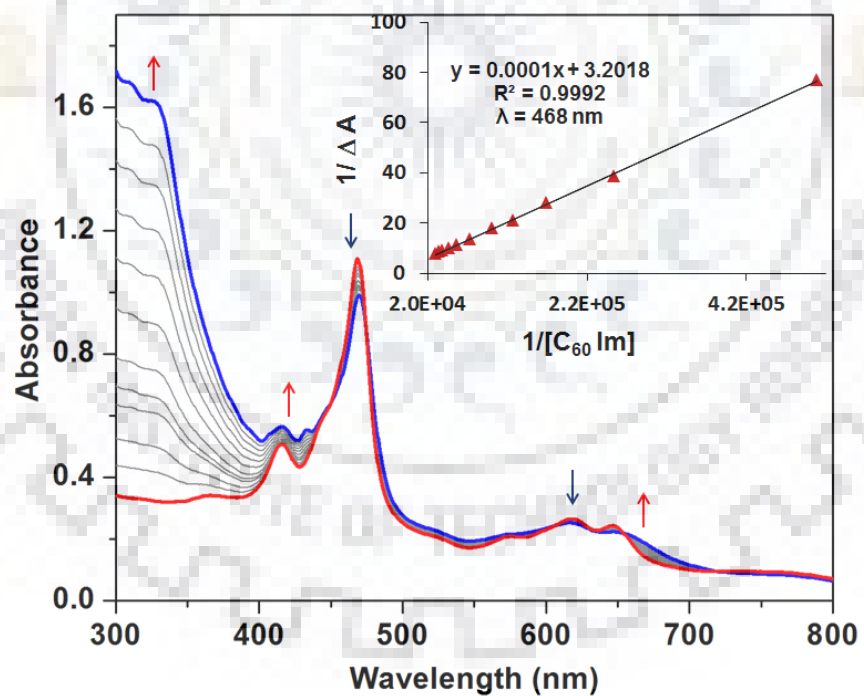


Figure A20. UV-visible titration of ZnTPP(N-fusedPh)Ph₂ with C₆₀Im in *o*-dichlorobenzene at 298 K and inset corresponding to Benesi-Hildebrand plot.

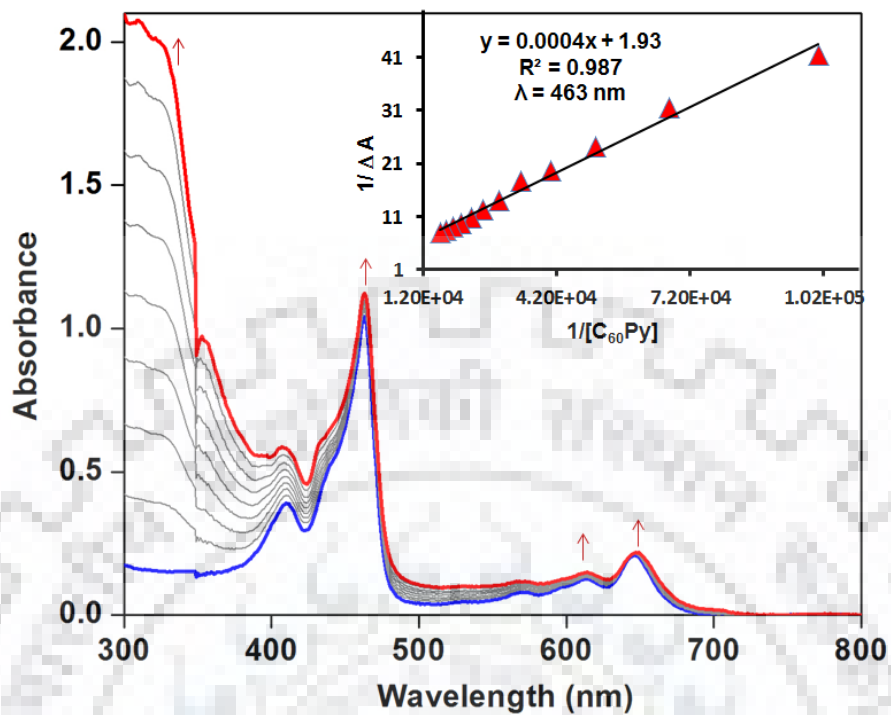


Figure A21. UV-visible titration of ZnTPP(N-fusedPh) with $C_{60}Py$ in *o*-dichlorobenzene at 298 K and inset corresponding to Benesi-Hildebrand plot.

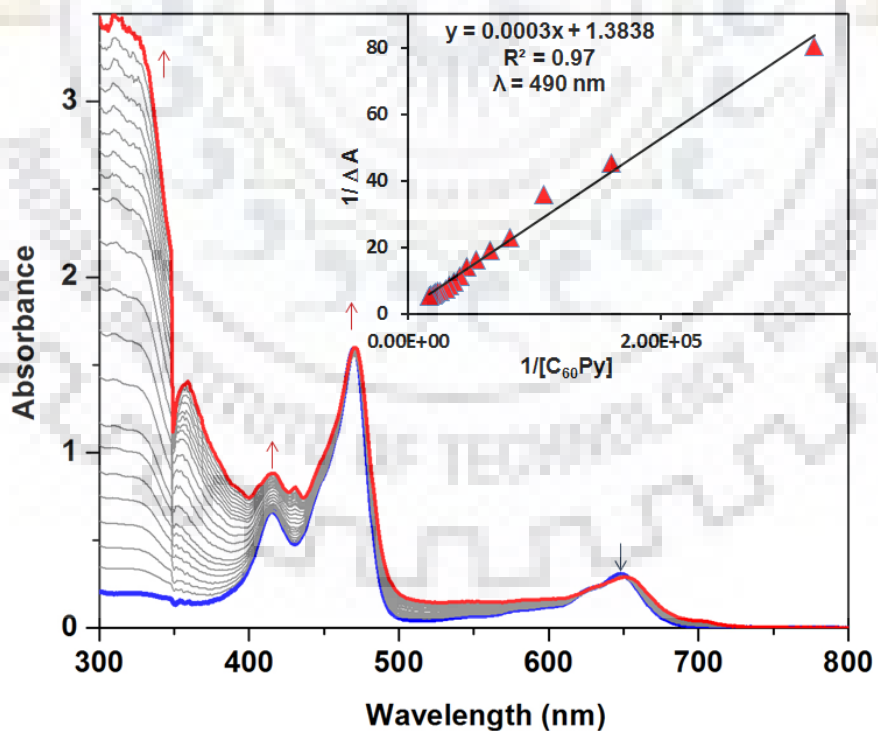


Figure A22. UV-visible titration of ZnTPP(N-fusedPh) Br_2 with $C_{60}Py$ in *o*-dichlorobenzene at 298 K and inset corresponding to Benesi-Hildebrand plot.

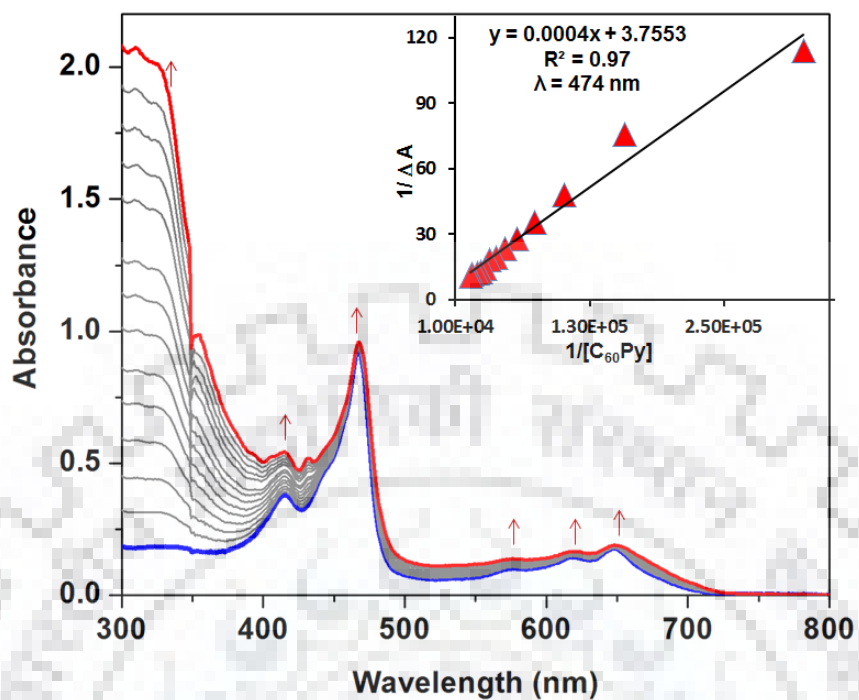


Figure A23. UV-visible titration of ZnTPP(N-fusedPh)Ph₂ with C₆₀Py in *o*-dichlorobenzene at 298 K and inset corresponding to Benesi-Hildebrand plot.

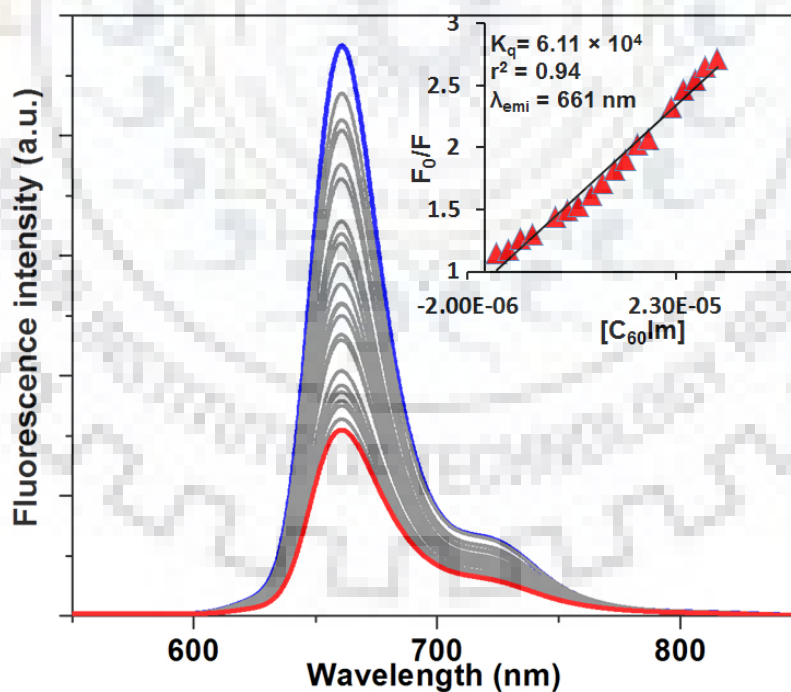


Figure A24. Quenching of fluorescence intensity of ZnTPP(N-fusedPh) with C₆₀Im in *o*-dichlorobenzene at 298 K and inset corresponding to Stern-Volmer plot.

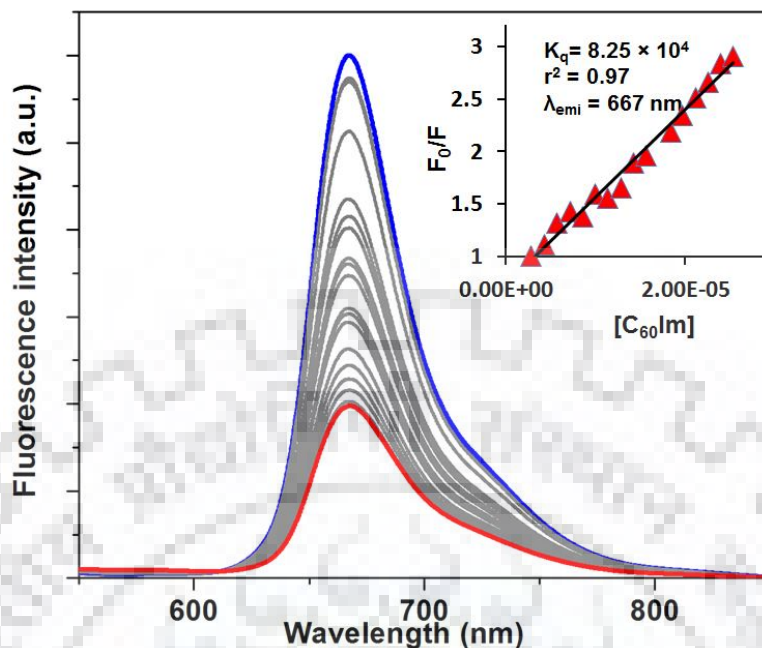


Figure A25. Quenching of fluorescence intensity of ZnTPP(N-fusedPh)Br₂ with C₆₀Im in *o*-dichlorobenzene at 298 K and inset corresponding to Stern-Volmer plot.

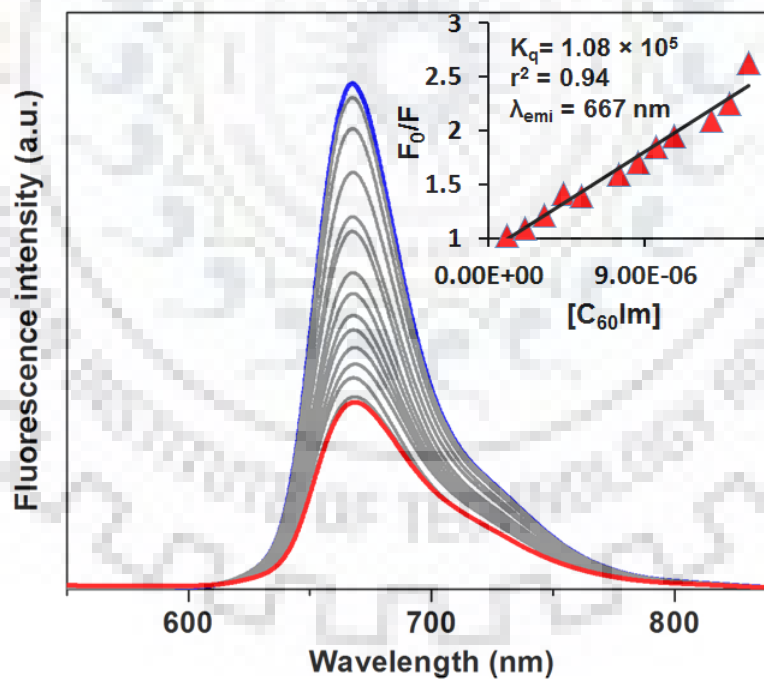


Figure A26. Quenching of fluorescence intensity of ZnTPP(N-fusedPh)Ph₂ with C₆₀Im in *o*-dichlorobenzene at 298 K and inset corresponding to Stern-Volmer plot.

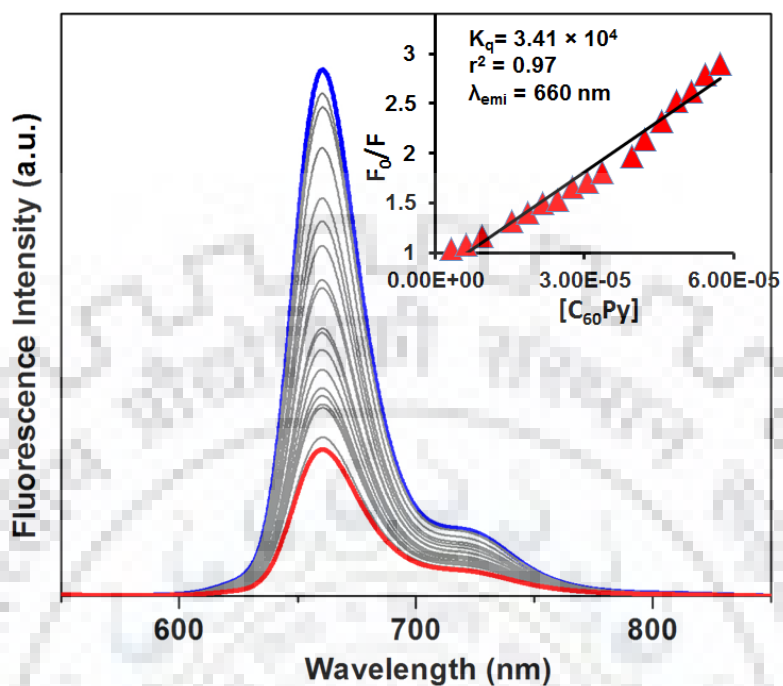


Figure A27. Quenching of fluorescence intensity of ZnTPP(N-fusedPh) with $C_{60}Py$ in *o*-dichlorobenzene at 298 K and inset corresponding to Stern-Volmer plot.

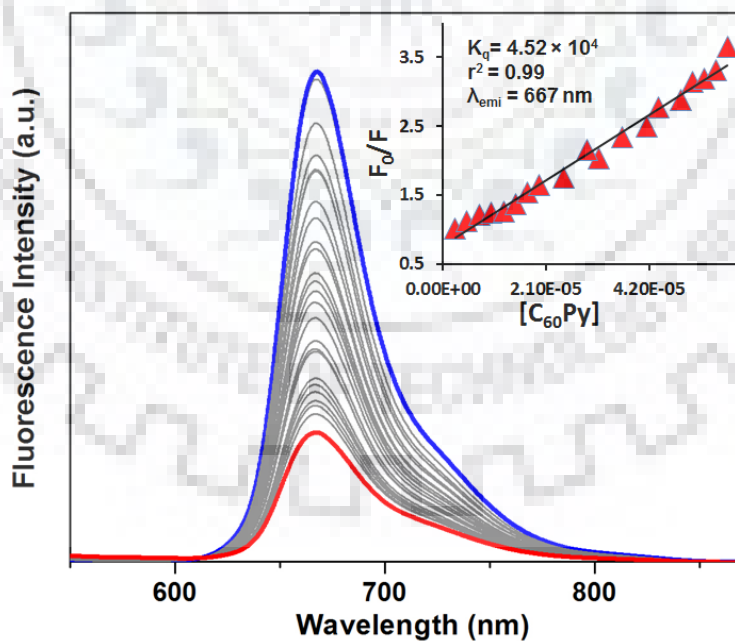


Figure A28. Quenching of fluorescence intensity of ZnTPP(N-fusedPh) Br_2 with $C_{60}Py$ in *o*-dichlorobenzene at 298 K and inset corresponding to Stern-Volmer plot.

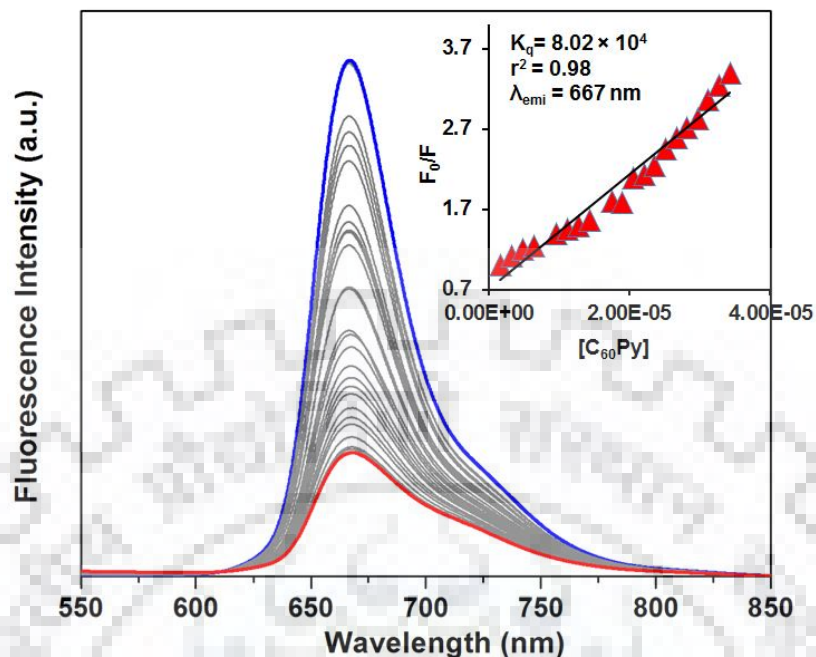


Figure A29. Quenching of fluorescence intensity of ZnTPP(N-fusedPh)Ph₂ with C₆₀Py in *o*-dichlorobenzene at 298 K and inset corresponding to Stern-Volmer plot.

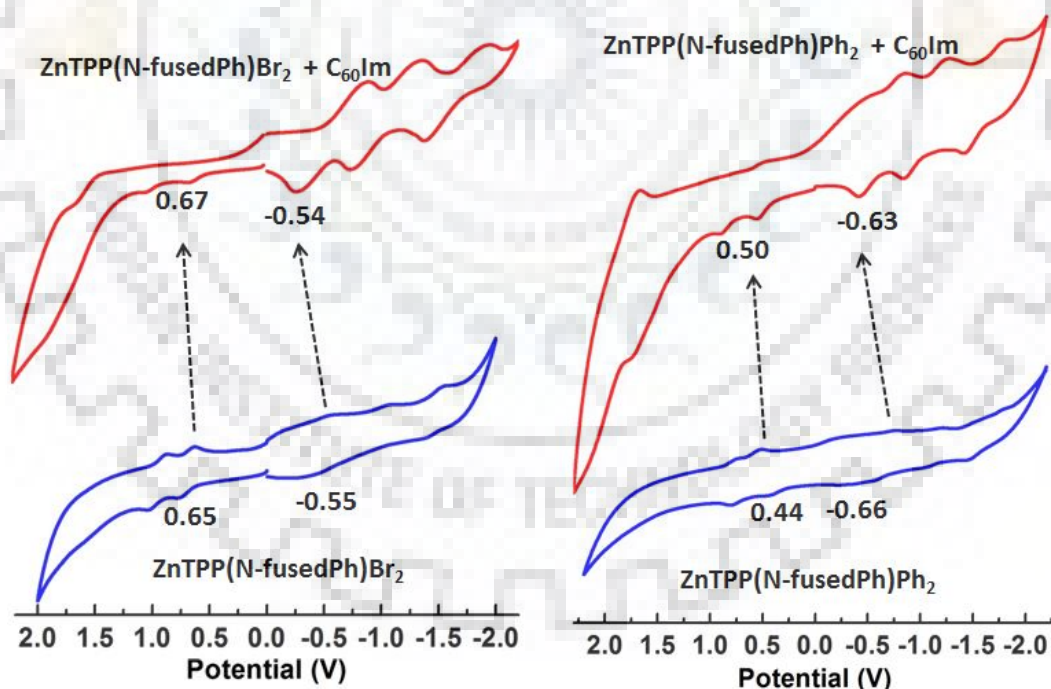
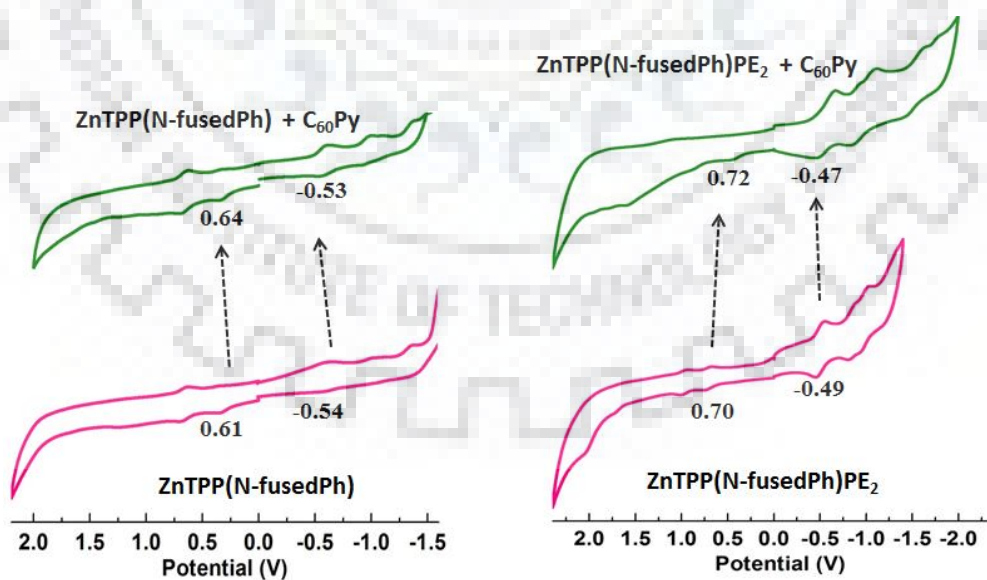


Figure A30. Cyclic voltammetric studies of ZnTPP(N-fusedPh)Br₂ and ZnTPP(N-fusedPh)Ph₂ in the presence and absence of C₆₀Im in *o*-dichlorobenzene at 298 K.

Table A3. Electrochemical data of Zn(II) derivatives of ZnTPP(N-fusedPh) X_2 , X = H, Br, Ph, PE) with and without $C_{60}Im$ and $C_{60}Py$ in *o*-dichlorobenzene containing 0.1 M TBAPF₆ with scan rate of 0.1 V/s at 298 K.

Porphyrin	Oxidation (V)			Reduction (V)			$\Delta E(V)$
	I	II	III	I	II	III	
ZnTPP(N-fusedPh)	0.61	0.92	1.62	-0.54	-0.99	-1.44	1.15
ZnTPP(N-fusedPh): $C_{60}Im$	0.63	1.06	1.70	-0.53	-1.02	-1.58	1.16
ZnTPP(N-fusedPh): $C_{60}Py$	0.64	0.85	1.85	-0.53	-0.90	-1.47	1.20
ZnTPP(N-fusedPh)Br ₂	0.65	0.95	1.58	-0.54	-0.97	-1.47	1.19
ZnTPP(N-fusedPh)Br ₂ : $C_{60}Im$	0.67	1.02	1.76	-0.55	-1.03	-1.64	1.22
ZnTPP(N-fusedPh)Br ₂ : $C_{60}Py$	0.66	0.99	1.73	-0.54	-0.98	-1.32	1.20
ZnTPP(N-fusedPh)Ph ₂	0.44	0.78	1.68	-0.66	-1.15	-1.59	1.10
ZnTPP(N-fusedPh)Ph ₂ : $C_{60}Im$	0.50	0.89	1.70	-0.63	-1.05	-1.60	1.13
ZnTPP(N-fusedPh)Ph ₂ : $C_{60}Py$	0.48	0.68	1.78	-0.65	-0.99	-1.50	1.13
ZnTPP(N-fusedPh)PE ₂	0.70	1.03	1.70	-0.49	-0.90	-1.41	1.19
ZnTPP(N-fusedPh)PE ₂ : $C_{60}Im$	0.80	1.22	1.87	-0.46	-0.88	-1.42	1.26
ZnTPP(N-fusedPh)PE ₂ : $C_{60}Py$	0.72	1.10	1.59	-0.47	-0.98	-1.52	1.19

**Figure A31.** Cyclic voltammetric studies of ZnTPP(N-fusedPh) and ZnTPP(N-fusedPh)PE₂ in the presence and absence of $C_{60}Py$ in *o*-dichlorobenzene at 298 K.

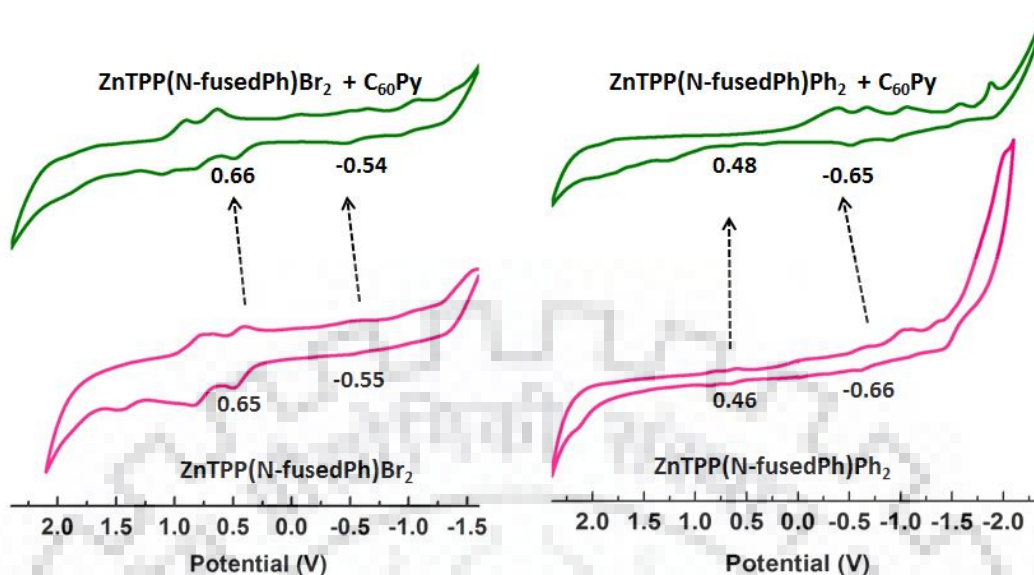


Figure A32. Cyclic voltammetric studies of ZnTPP(N-fusedPh)Br₂ and ZnTPP(N-fusedPh)Ph₂ in the presence and absence of C₆₀Py in *o*-dichlorobenzene at 298 K.

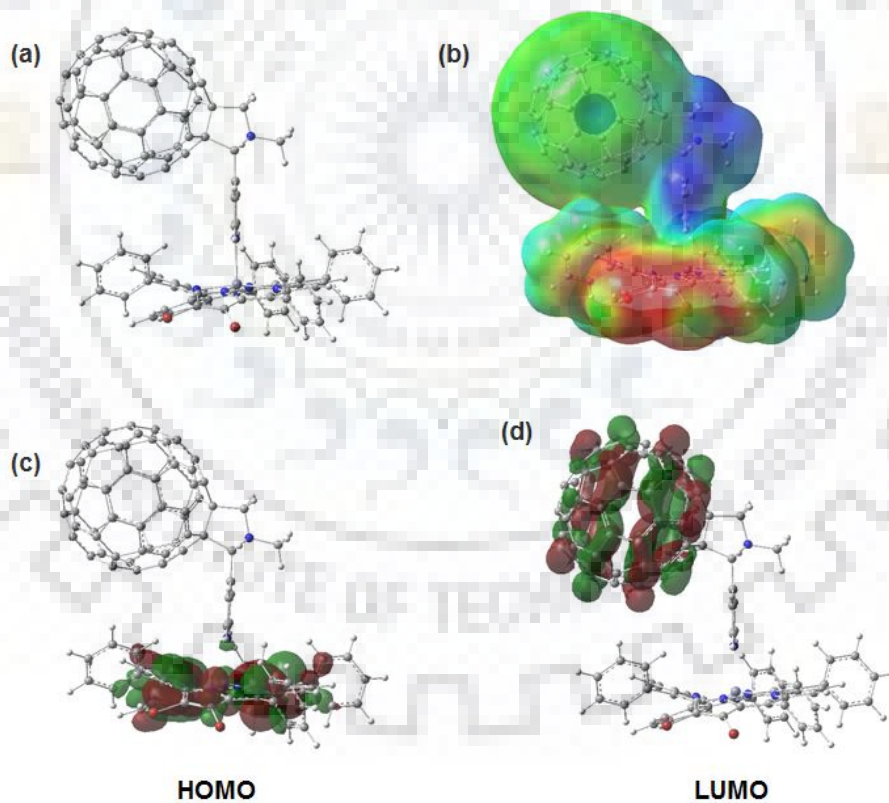


Figure A33. (a) Optimized structure (b) electrostatic potential map (c) Pictorial representation of frontier HOMO (d) LUMO of ZnTPP(N-fusedPh)Br₂:C₆₀Py.

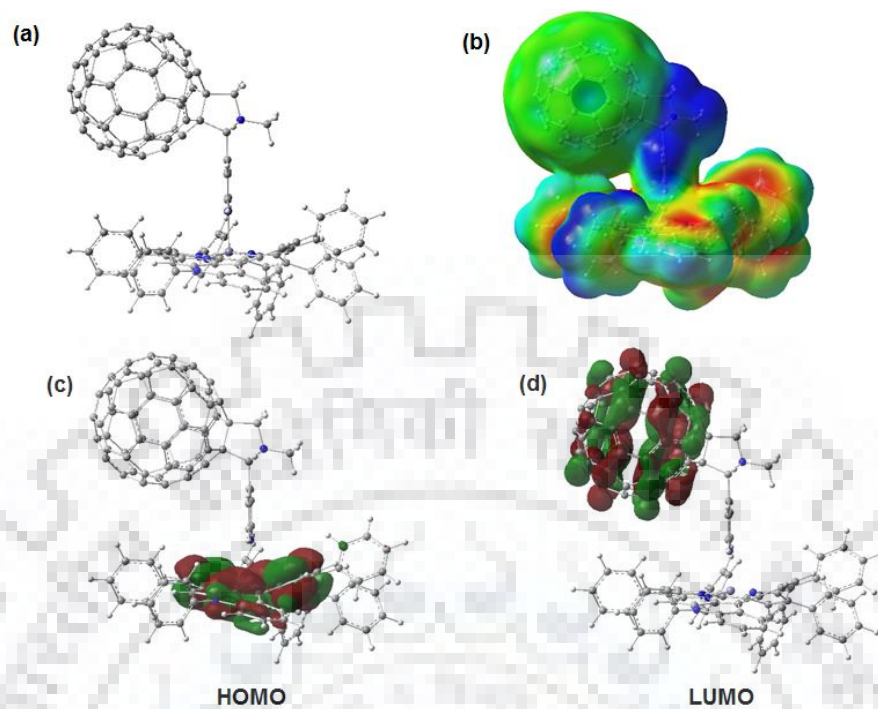


Figure A34. (a) Optimized structure (b) electrostatic potential map (c) Pictorial representation of frontier HOMO (d) LUMO of ZnTPP(N-fusedPh)Ph₂:C₆₀Py.

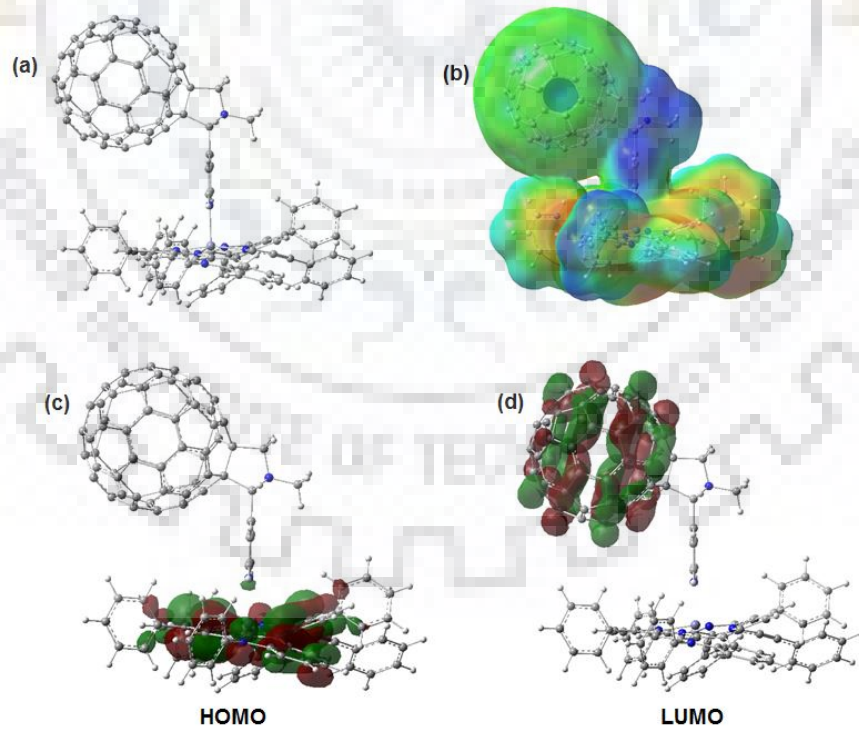


Figure A35. (a) Optimized structure (b) electrostatic potential map (c) Pictorial representation of frontier HOMO (d) LUMO of ZnTPP(N-fusedPh)PE₂:C₆₀Py.

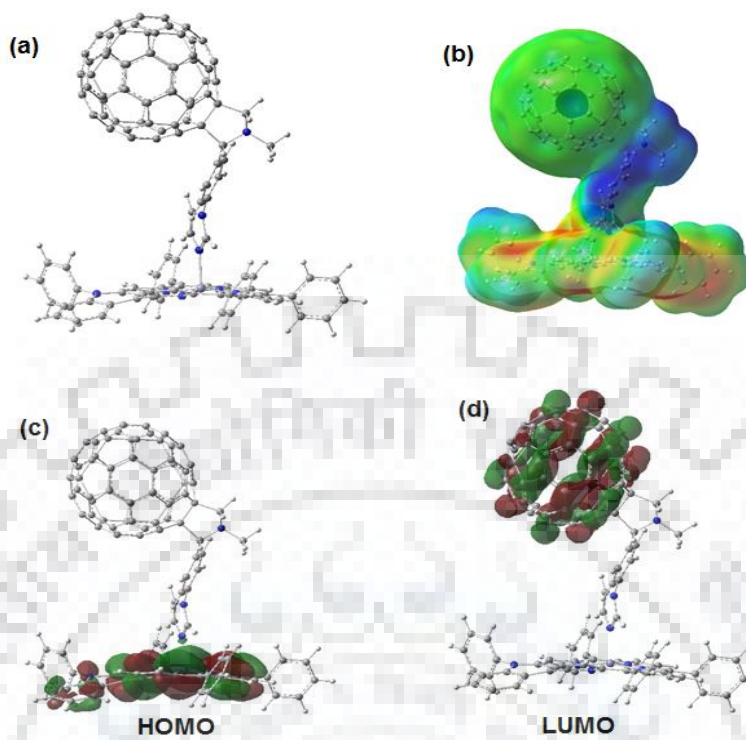


Figure A36. (a) Optimized structure (b) electrostatic potential map (c) Pictorial representation of frontier HOMO (d) LUMO of ZnTPP(N-fusedPh): $C_{60}Im$.

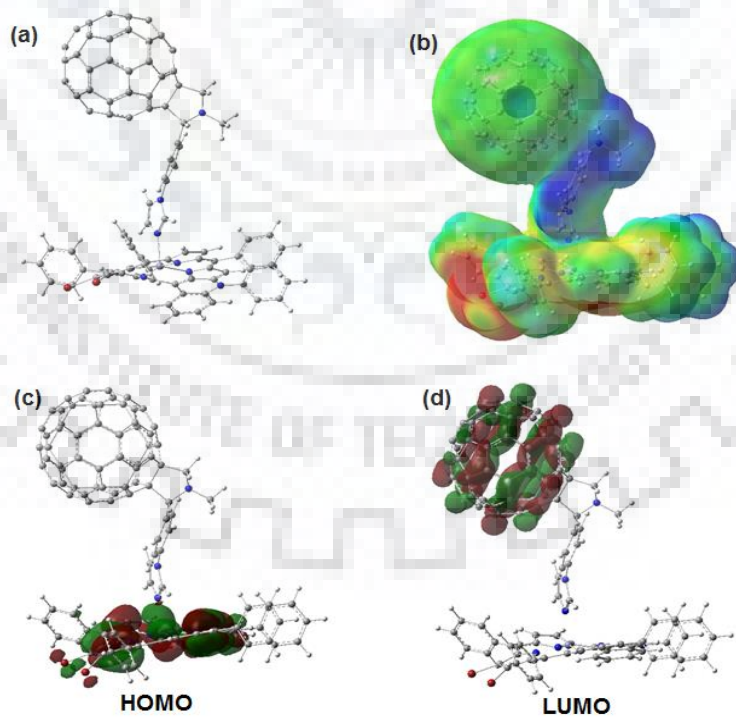


Figure A37. (a) optimized structure (b) electrostatic potential map (c) Pictorial representation of frontier HOMO (d) LUMO of ZnTPP(N-fusedPh)Br₂: $C_{60}Im$.

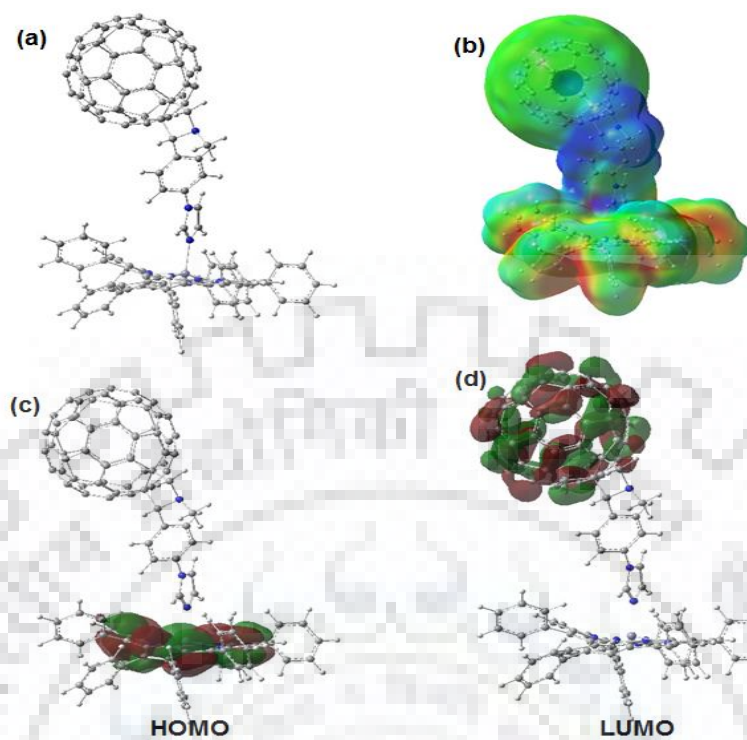


Figure A38. (a) optimized structure (b) electrostatic potential map (c) Pictorial representation of frontier HOMO (d) LUMO of ZnTPP(N-fusedPh)Ph₂:C₆₀Im.

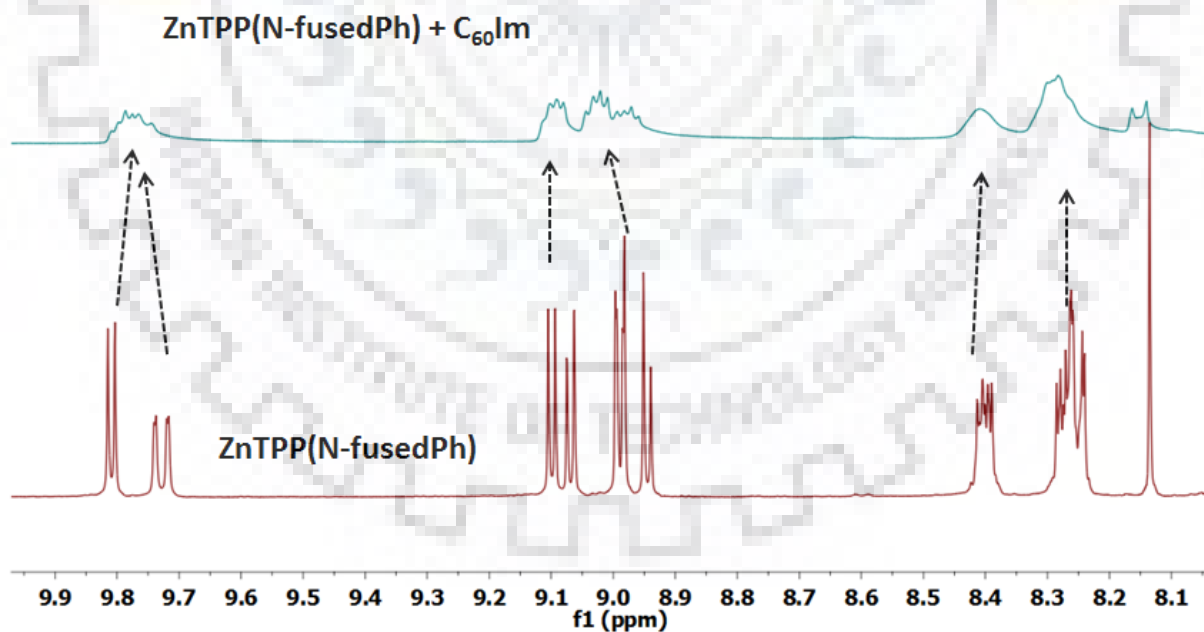


Figure A39. ¹H NMR spectra of (a) ZnTPP(N-fusedPh):C₆₀Im adduct (b) ZnTPP(N-fusedPh) in C₆D₆ at 298 K.

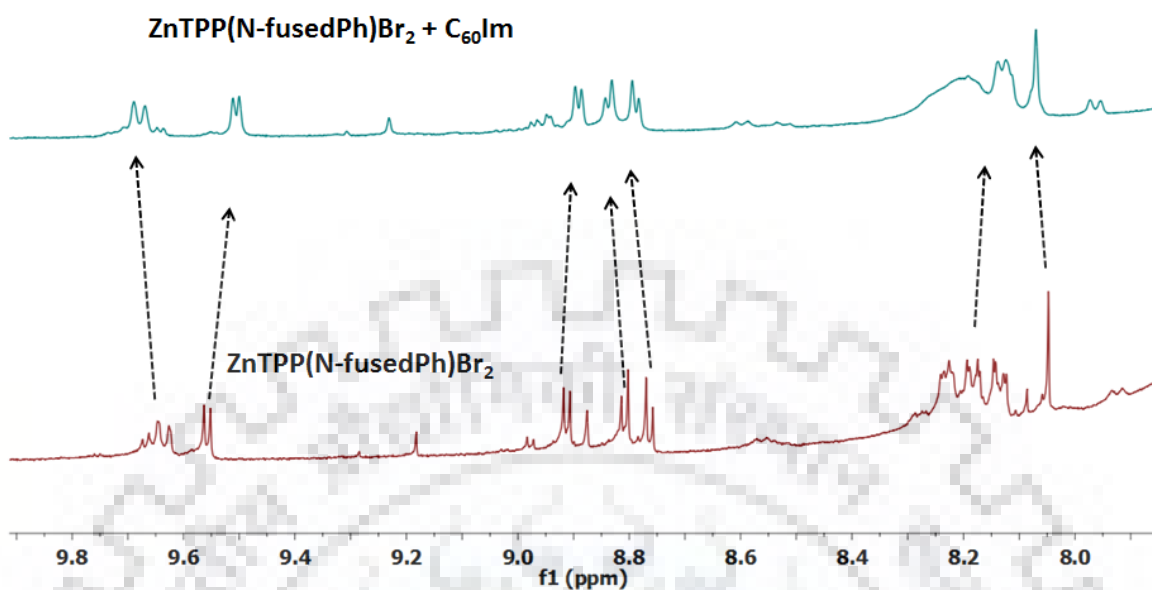


Figure A40. 1H NMR spectra of (a) ZnTPP(N-fusedPh)Br₂:C₆₀Im adduct (b) ZnTPP(N-fusedPh)Br₂ in C₆D₆ at 298 K.

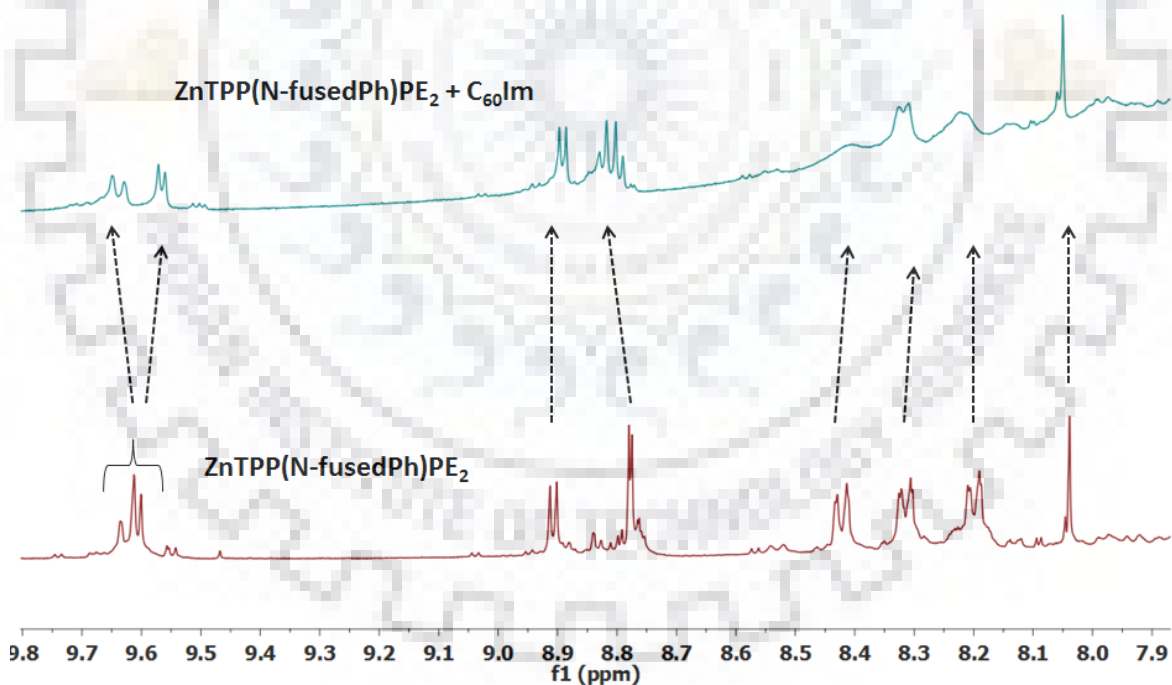


Figure A41. 1H NMR spectra of (a) ZnTPP(N-fusedPh)PE₂:C₆₀Im adduct (b) ZnTPP(N-fusedPh)PE₂ in C₆D₆ at 298 K.

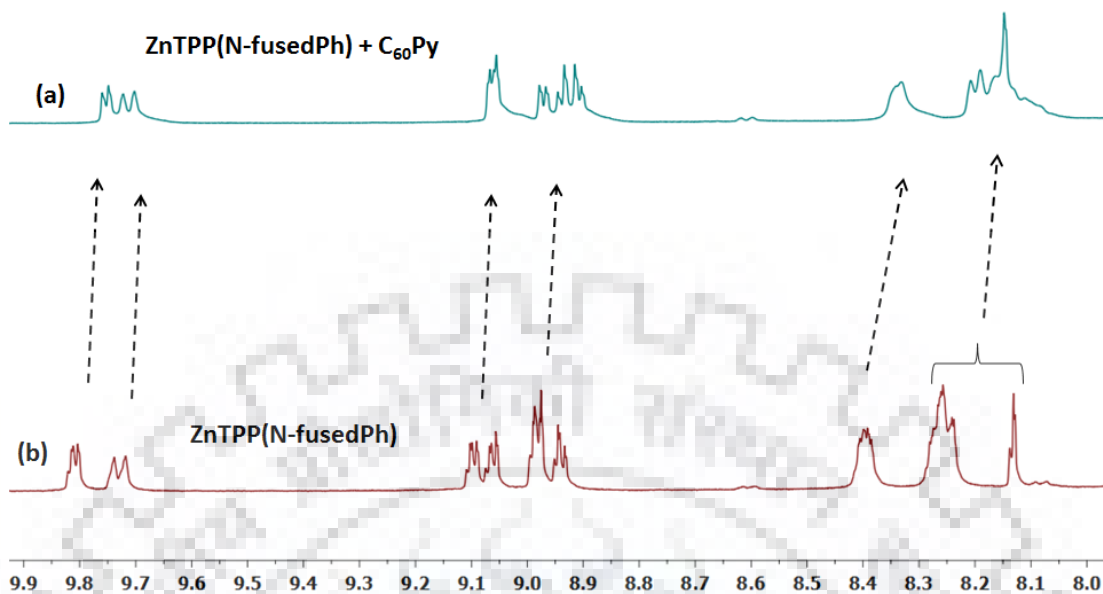


Figure A42. 1H NMR spectra of (a) ZnTPP(N-fusedPh): $C_{60}Py$ adduct (b) ZnTPP(N-fusedPh) in C_6D_6 at 298 K.

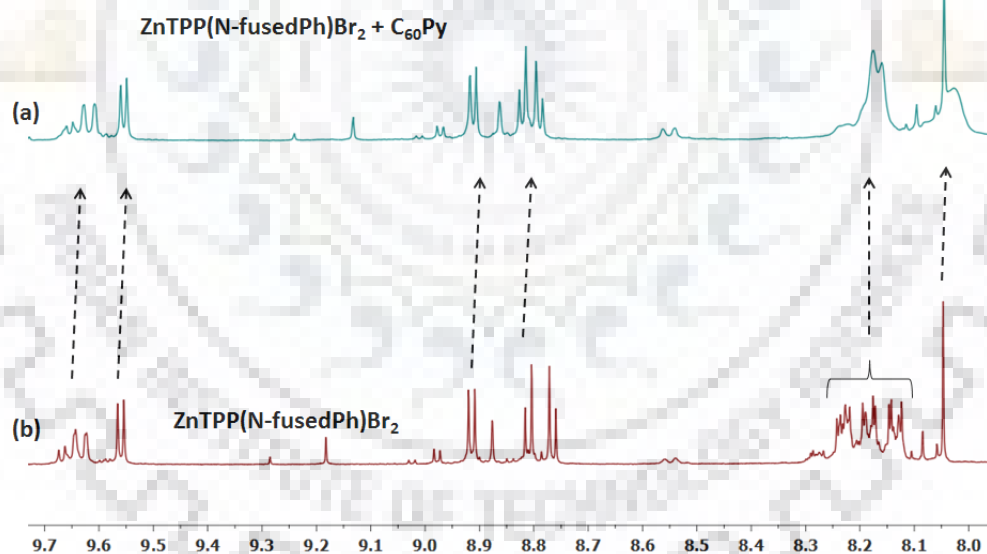


Figure A43. 1H NMR spectra of (a) ZnTPP(N-fusedPh)Br₂: $C_{60}Py$ adduct (b) ZnTPP(N-fusedPh)Br₂ in C_6D_6 at 298 K.

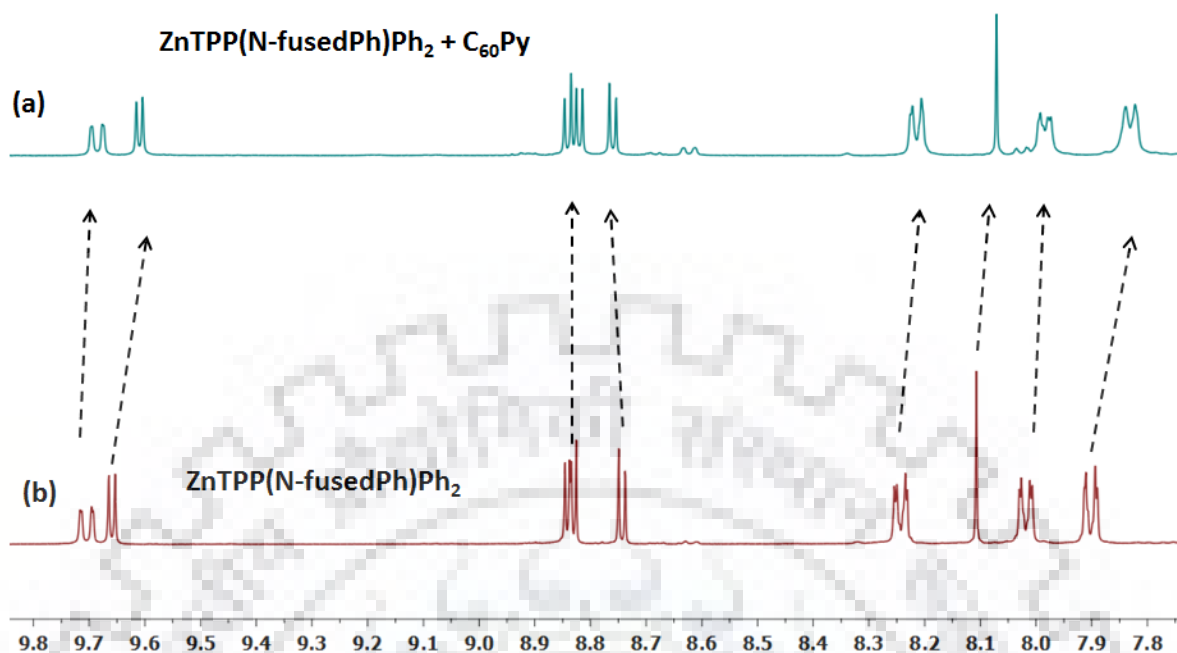


Figure A44. 1H NMR spectra of (a) ZnTPP(N-fusedPh)Ph₂:C₆₀Py adduct (b) ZnTPP(N-fusedPh)Ph₂ in C₆D₆ at 298 K.

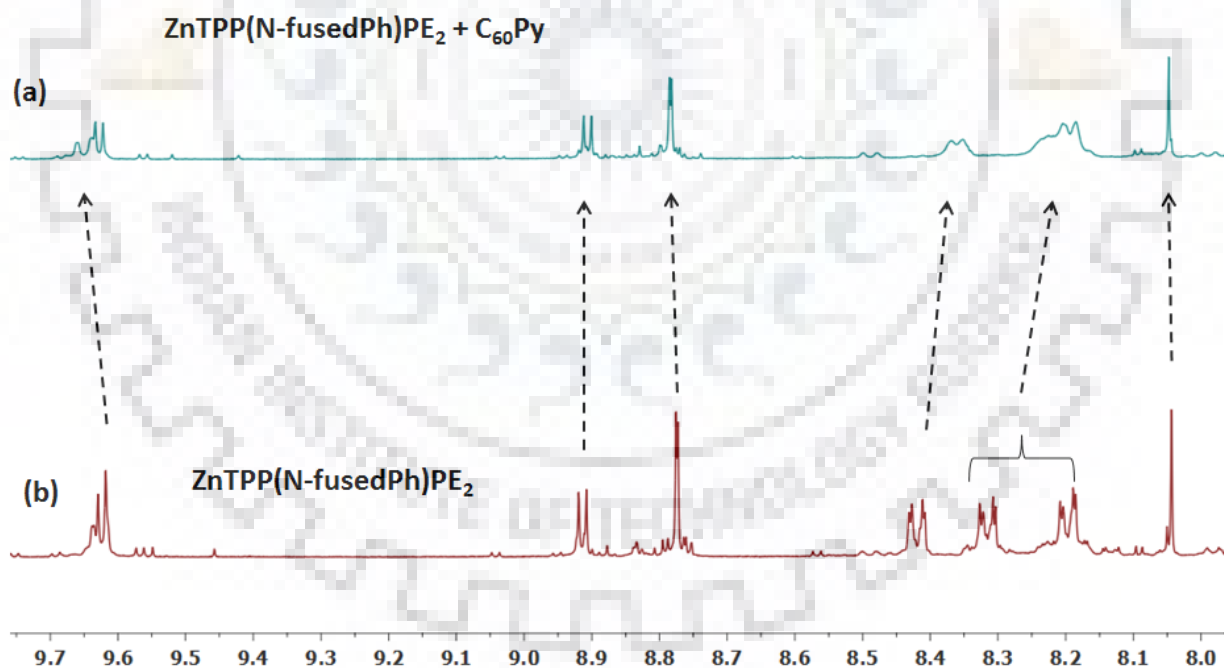


Figure A45. 1H NMR spectra of (a) ZnTPP(N-fusedPh)PE₂:C₆₀Py adduct (b) ZnTPP(N-fusedPh)PE₂ in C₆D₆ at 298 K.

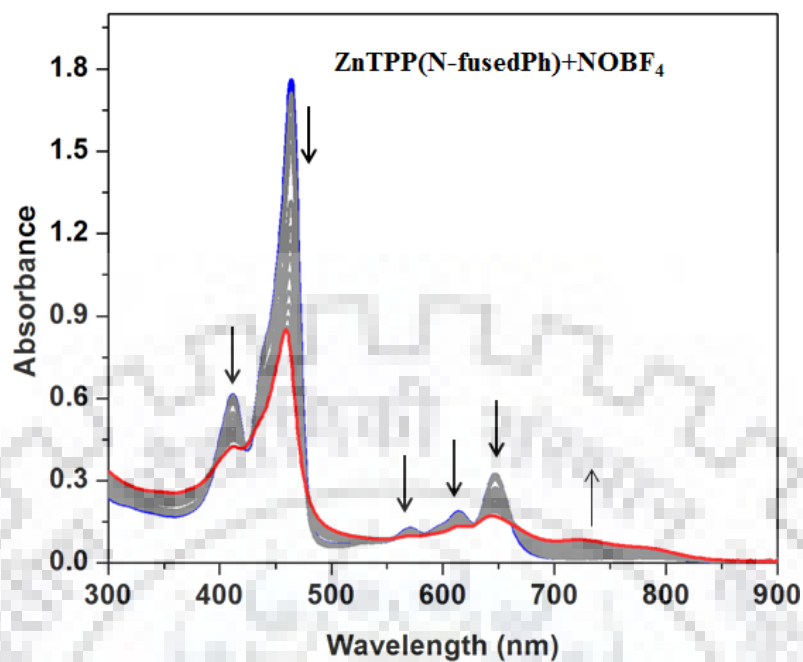


Figure A46. Chemical oxidation of ZnTPP(N-fusedPh) using NOBF₄ in *o*-dichlorobenzene at 298 K.

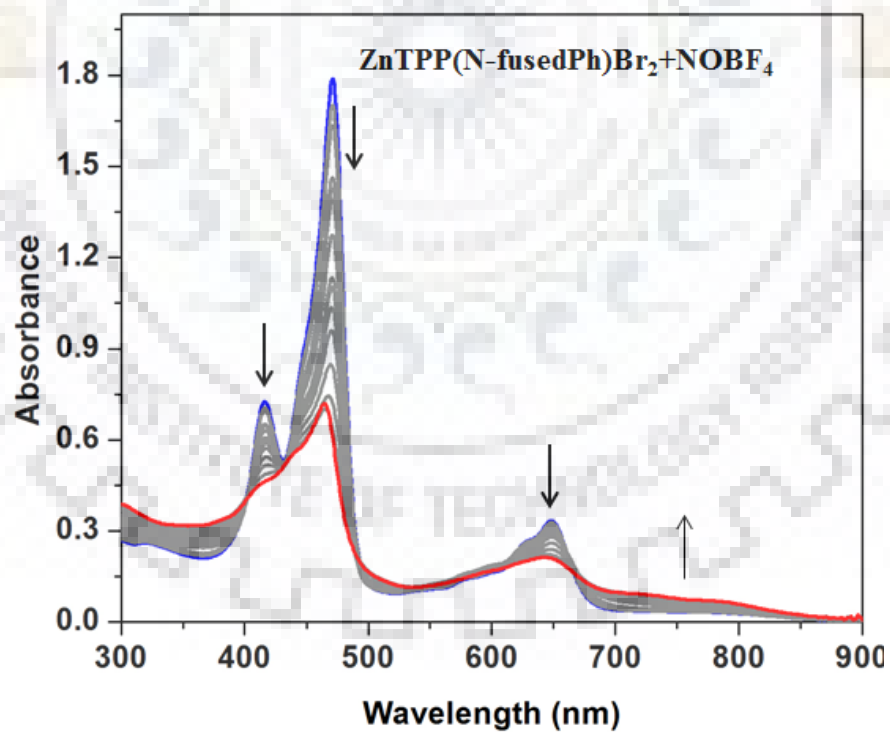


Figure A47. Chemical oxidation of ZnTPP(N-fusedPh)Br₂ using NOBF₄ in *o*-dichlorobenzene at 298 K.

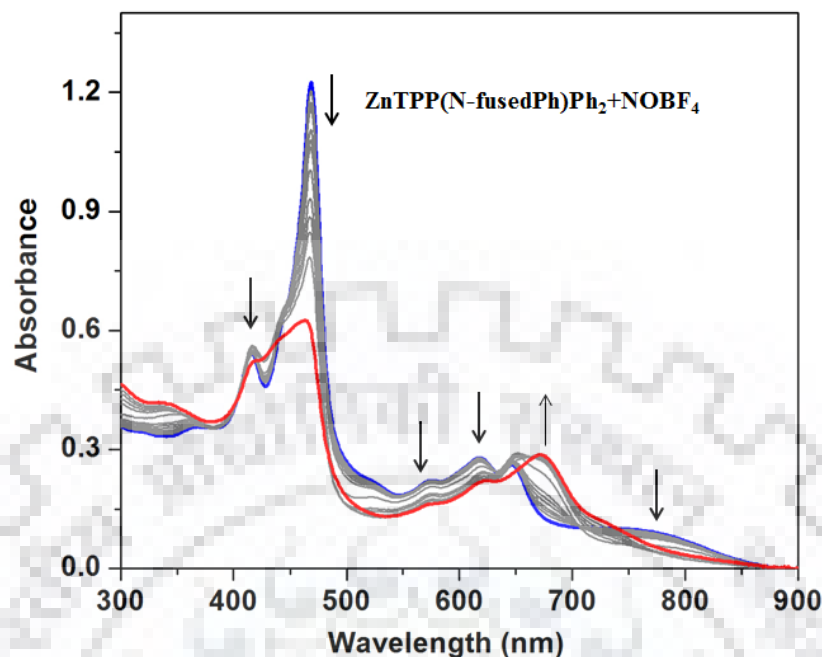


Figure A48. Chemical oxidation of $ZnTPP(N-fusedPh)Ph_2$ using $NOBF_4$ in *o*-dichlorobenzene at 298 K.

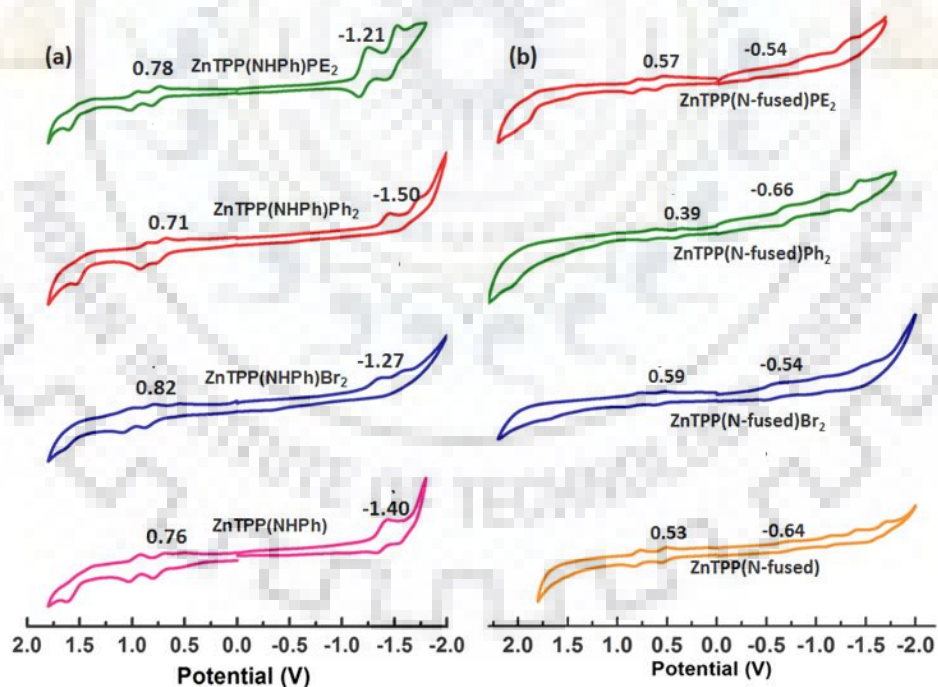


Figure A49. Comparative cyclic voltammograms of (a) $ZnTPP(NHPh)X_2$ (b) $ZnTPP(N-fusedPh)X_2$, where $X = H, Br, Ph$ and PE .

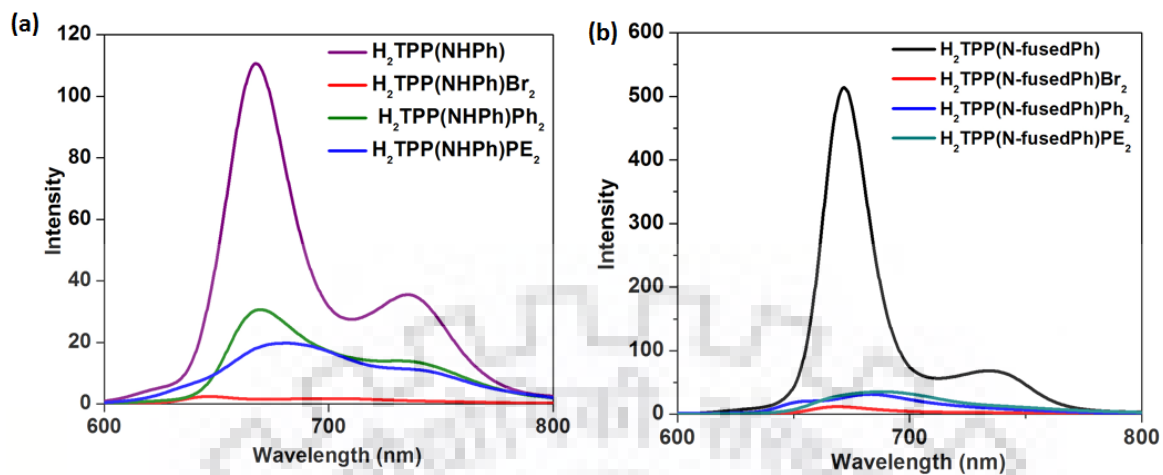


Figure A50. Fluorescence spectra of (a) $H_2TPP(NHPh)X_2$ (b) $H_2TPP(N-fusedPh)X_2$, where $X = H, Br, Ph$ and PE .

Table A4. Electrochemical redox data of MTPP(NHPh) X_2 , X = H, Br, Ph, PE and M = 2H, Co, Ni, Cu, Zn in CH_2Cl_2 containing 0.1 M TBAPF₆ at scan rate 0.1V/s at 298 K.

Porphyrins	Oxidation (V)				Reduction (V)			ΔE (V)
	I	II	III	IV	I	II	III	
H ₂ TPP(NHPh)	1.01	1.28	1.48	1.67	-1.25 ^d	-1.55 ^d		2.26
H ₂ TPP(NHPh)Br ₂	0.93 ^d	1.14 ^d	1.45 ^d	1.71 ^d	-1.0 ⁶	-1.20	-1.43	1.93
H ₂ TPP(NHPh)Ph ₂	0.82 ^d	1.14 ^d	1.43 ^d	1.92 ^d	-1.21	-1.47		2.03
H ₂ TPP(NHPh)PE ₂	0.89	1.14	1.41	1.66	-1.05	-1.22		1.94
CoTPP(NHPh)	0.75	0.99	1.22	1.78	-0.89	-1.23	-1.57	2.22
CoTPP(NHPh)Br ₂	0.78	1.03	1.17		-0.75	-0.97 ^d	-1.32 ^d	2.00
CoTPP(NHPh)Ph ₂	0.69	0.95	1.09	1.75	-0.85	-1.36	-1.96	2.31
CoTPP(NHPh)PE ₂	0.74	0.98	1.16		-0.77	-1.13		2.11
NiTPP(NHPh)	0.87	1.20	1.54 ^d		-1.35 ^d			2.22
NiTPP(NHPh)Br ₂	0.86	1.21	1.60		-1.16	-1.58		2.02
NiTPP(NHPh)Ph ₂	0.76	1.08	1.69	1.92	-1.35	-1.67	1.91	2.11
NiTPP(NHPh)PE ₂	0.85	1.15			-1.18	-1.42		2.03
CuTPP(NHPh)	0.81	1.21	1.72		-1.30			2.11
CuTPP(NHPh)Br ₂	0.87	1.19	1.64		-1.18 ^d	-1.46 ^d	-1.63 ^d	2.05
CuTPP(NHPh)Ph ₂	0.75	1.05			-1.36	-1.67	1.77	2.11
CuTPP(NHPh)PE ₂	0.83	1.17	1.66		-1.22	-1.46		2.05
ZnTPP(NHPh)	0.76	1.00	1.62 ^d		-1.40	-1.58		2.16
ZnTPP(NHPh)Br ₂	0.82	1.01	1.56		-1.27	-1.46		2.09
ZnTPP(NHPh)Ph ₂	0.71	0.87	1.45	1.98	-1.50	-1.64		2.21
ZnTPP(NHPh)PE ₂	0.78	0.97	1.55		-1.21	-1.48		1.99

Table A5. Electrochemical redox data of MTPP(N-fusedPh) X_2 (M = 2H, Co (II), Ni (II), Cu (II), Zn (II) and X = H, Br, Ph, PE) in CH_2Cl_2 containing 0.1 M TBAPF₆ with scan rate of 0.1V/s at 298 K.

Porphyrins	Oxidation (V)						Reduction(V)			Metal centred		$\Delta E(V)$
	I			II			I			Oxdn. Redn.		
	I	II	III	I	II	III	I	II				
H ₂ TPP(N-fusedPh)	0.63	0.94	1.33	-1.04	-1.25	-1.57						1.67
H ₂ TPP(N-fusedPh)Br ₂	0.74	0.96	1.19	-1.06	-1.36							1.80
H ₂ TPP(N-fusedPh)Ph ₂	0.59 ^d	0.82	1.55	-0.80	-1.23	-1.56						1.39
H ₂ TPP(N-fusedPh)PE ₂	0.72	0.95	1.12	-0.81	-1.37	-1.76						1.53
CoTPP(N-fusedPh)	0.74	1.00	1.71	-1.26	1.53		0.55	-0.91				2.00
CoTPP(N-fusedPh)Br ₂	0.99	1.146		-1.03	-1.29		0.66	-0.83				2.02
CoTPP(N-fusedPh)Ph ₂	0.78	0.95	1.80	-1.17	-1.47		0.52	-0.89				1.95
CoTPP(N-fusedPh)PE ₂	0.95	1.10	1.93	-1.12	-1.76		0.60	-0.84				2.07
NiTPP(N-fusedPh)	0.63	1.07	1.94	-1.33	-1.72							1.96
NiTPP(N-fusedPh)Br ₂	0.73	1.14	1.84	-1.21	-1.55	-1.73						1.94
NiTPP(N-fusedPh)Ph ₂	0.61	0.98	1.86	-1.31	-1.72							1.92
NiTPP(N-fusedPh)PE ₂	0.70	1.10	1.87	-1.20	-1.55							1.90
CuTPP(N-fusedPh)	0.63	1.034	1.47	-1.13	-1.38	-1.70						1.76
CuTPP(N-fusedPh)Br ₂	0.71	1.09	2.10	-1.15	-1.58							1.86
CuTPP(N-fusedPh)Ph ₂	0.55	0.91	1.99	-1.04	-1.35	1.72						1.59
CuTPP(N-fusedPh)PE ₂	0.65	1.034	1.98	-0.93	-1.25	-1.60						1.58
ZnTPP(N-fusedPh)	0.53	0.79		-1.13	-1.47	-1.68						1.66
ZnTPP(N-fusedPh)Br ₂	0.59	0.84		-0.54	-1.02	-1.51						1.13
ZnTPP(N-fusedPh)Ph ₂	0.39	0.66	1.15	-0.66	-1.08	1.59						1.05

Appendix-I: Host-Guest Assemblies of Fused Porphyrin-C₆₀Im/C₆₀Py

ZnTPP(N-fusedPh)PE ₂	0.57	0.81	1.83	-0.77	-1.26	-1.48	1.34
---------------------------------	------	------	------	-------	-------	-------	------



APPENDIX-II

Highly Electron Deficient Tetrabenzoquinone Appended Ni(II) and Cu(II) Porphyrins: Spectral, Solvatochromism, Electrochemical Redox and Tuneable F⁻ and CN⁻ Sensing Properties

Table of Contents	Page No.
Figure A1. ¹ H NMR spectrum of <i>meso</i> -tetrakis(3,5-di- <i>tert</i> -butyl-4-hydroxy)porphyrin in CDCl ₃ at 298 K.	223
Figure A2. MALDI-TOF mass spectrum of <i>meso</i> -tetrakis(3,5-di- <i>tert</i> -butyl-4-hydroxy)porphyrin.	223
Figure A3. ¹ H NMR spectrum of Ni-diOxP (1) in CDCl ₃ at 298 K.	224
Figure A4. MALDI-TOF mass spectrum of Ni-diOxP (1).	224
Figure A5. IR spectra of Ni-diOxP (1) and Ni-dtBTPP (3).	225
Figure A6. MALDI-TOF mass spectrum of Cu-diOxP (2).	225
Figure A7. IR spectra of Cu-diOxP (2) and Cu-dtBTPP (4).	226
Figure A8. DPV traces of Ni-dtBTPP (3) and Cu-dtBTPP (4) in CH ₂ Cl ₂ containing 0.1 M TBAPF ₆ at 298 K.	226
Figure A9. DPV traces of Ni-diOxP (1) and Cu-diOxP (2) in CH ₂ Cl ₂ containing 0.1 M TBAPF ₆ at 298 K.	227
Figure A10. UV-Vis spectral response of 2 (3.15 × 10 ⁻⁵ M) upon incremental addition of CN ⁻ (0-4.78 × 10 ⁻⁵ M, 1.5 equiv.) in toluene. Inset show BH-plot.	227
Figure A11. UV-Vis spectral response of 2 (3.15 × 10 ⁻⁵ M) upon incremental addition of F ⁻ (0-7.29 × 10 ⁻⁴ M, 23 equiv.) in toluene. Inset show BH-plot.	228
Figure A12. Absorption spectra of 2 (3.15 × 10 ⁻⁵ M) in the presence of different anions.	228
Figure A13. Ratiometric absorbance changes (A ₄₂₂ /A ₄₀₅) of 2 (3.15 × 10 ⁻⁵ M) on addition of 1.5 equiv. of CN ⁻ and 10 equiv. of other anions. Green has indicated the blank and the presence of other interfering anions and red indicated the addition of CN ⁻ to interfering anions.	229

- Figure A14.** Ratiometric absorbance changes (A_{422}/A_{405}) of **2** (3.15×10^{-5} M) on addition of 1.5 equiv. of F^- and 10 equiv. of other anions. Green has indicated the blank and the presence of other interfering anions and red indicated the addition of F^- to interfering anions. 229
- Figure A15.** 1H NMR spectra of **1** in the presence and absence of (a) F^- and (b) CN^- in $CDCl_3$ at 298 K. 230
- Figure A16.** (a) Cyclic voltammetry (b) DPV (in V vs Ag/AgCl) traces recorded for **1** (black) and **1**• $2CN^-$ (red) in CH_2Cl_2 containing 0.1 M TBAPF₆ with scan rate of 0.1 V/s at 298 K. 231
- Figure A17.** (a) Cyclic voltammetric (b) DPV (in V vs Ag/AgCl) traces recorded for **2** (black) and **2**• $2CN^-$ (red) in CH_2Cl_2 containing 0.1 M TBAPF₆ with scan rate of 0.1 V/s at 298 K. 231
- Figure A18.** Absorption spectra of Ni-dtBTPP (**3**) in the presence and absence of 150 equiv. of F^- ions. 232
- Figure A19.** Absorption spectra of Cu-dtBTPP (**4**) in the presence and absence of 150 equiv. of F^- ions. 232
- Figure A20.** Absorption spectra of Ni-dtBTPP (**3**) in the presence and absence of > 200 equiv. of F^- ions. 233
- Figure A21.** Absorption spectra of Cu-dtBTPP (**4**) in the presence of > 200 equiv. of F^- ions. 233
- Figure A22.** Absorption spectra of Ni-dtBTPP (**3**) in the presence and absence of > 200 equiv. of CN^- ions. 234
- Figure A23.** Absorption spectra of Cu-dtBTPP (**4**) in the presence and absence of > 200 equiv. of CN^- ions. 234
- Figure A24.** B3LYP/LANL2DZ optimized geometry showing (a) top as well as (b) side views of Ni-diOxP (**1**); H atoms are omitted for the clarity. In the side view, the *meso*-phenyl substituents are not shown for clarity. 235
- Figure A25.** B3LYP/LANL2DZ optimized geometry showing (a) top as well as (b) side views of Cu-diOxP (**2**); H atoms are omitted for the clarity. In the side view, the *meso*-phenyl substituents are not shown for clarity. 235

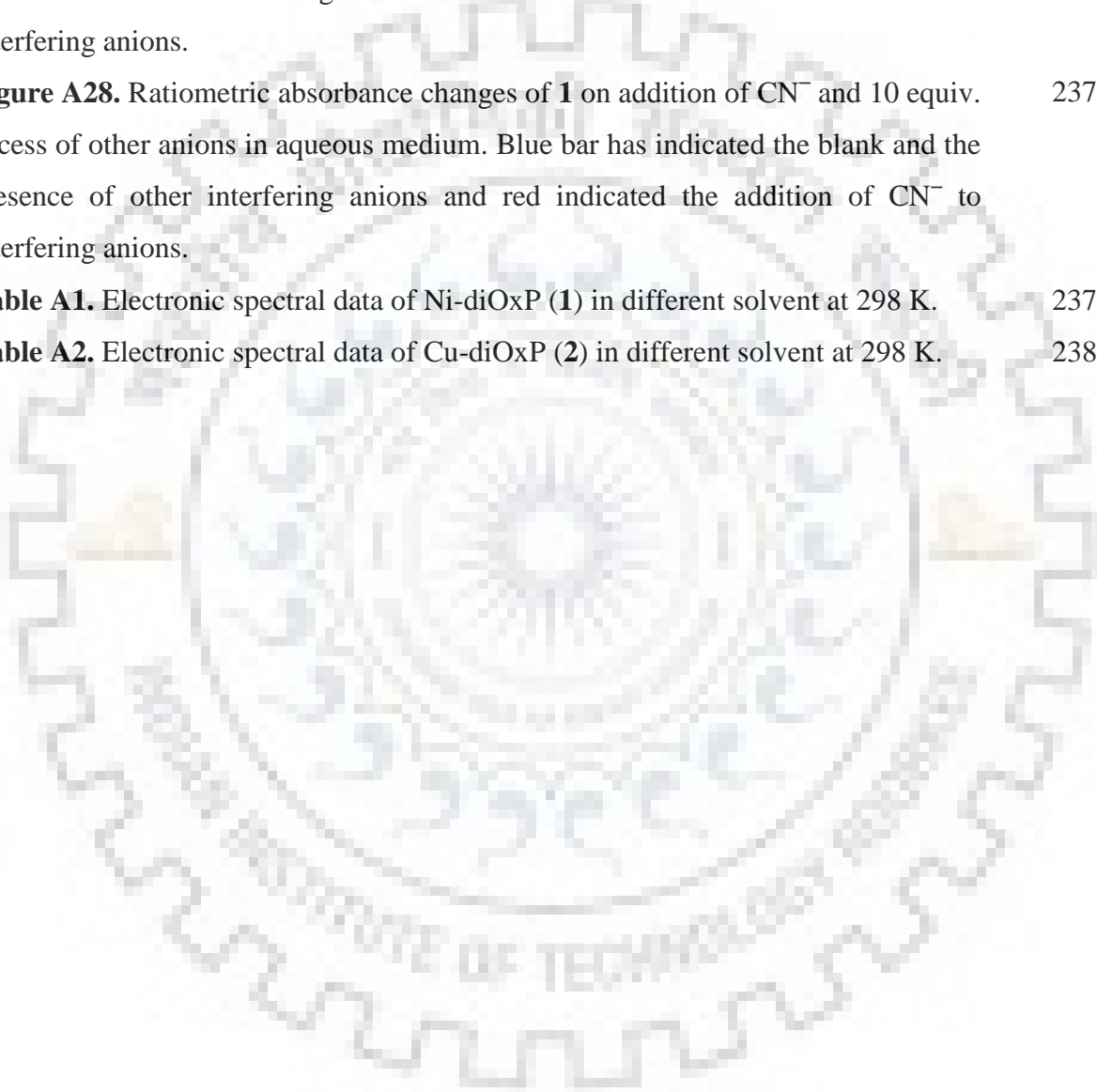
Figure A26. UV-vis spectra of Cu-diOxP (**2**) after addition of aqueous solution of KCN and 18-crown-6. 236

Figure A27. Ratiometric absorbance changes of **2** on addition of CN^- and 10 equiv. excess of other anions in aqueous medium. Blue bar has indicated the blank and the presence of other interfering anions and red indicated the addition of CN^- to interfering anions. 236

Figure A28. Ratiometric absorbance changes of **1** on addition of CN^- and 10 equiv. excess of other anions in aqueous medium. Blue bar has indicated the blank and the presence of other interfering anions and red indicated the addition of CN^- to interfering anions. 237

Table A1. Electronic spectral data of Ni-diOxP (**1**) in different solvent at 298 K. 237

Table A2. Electronic spectral data of Cu-diOxP (**2**) in different solvent at 298 K. 238



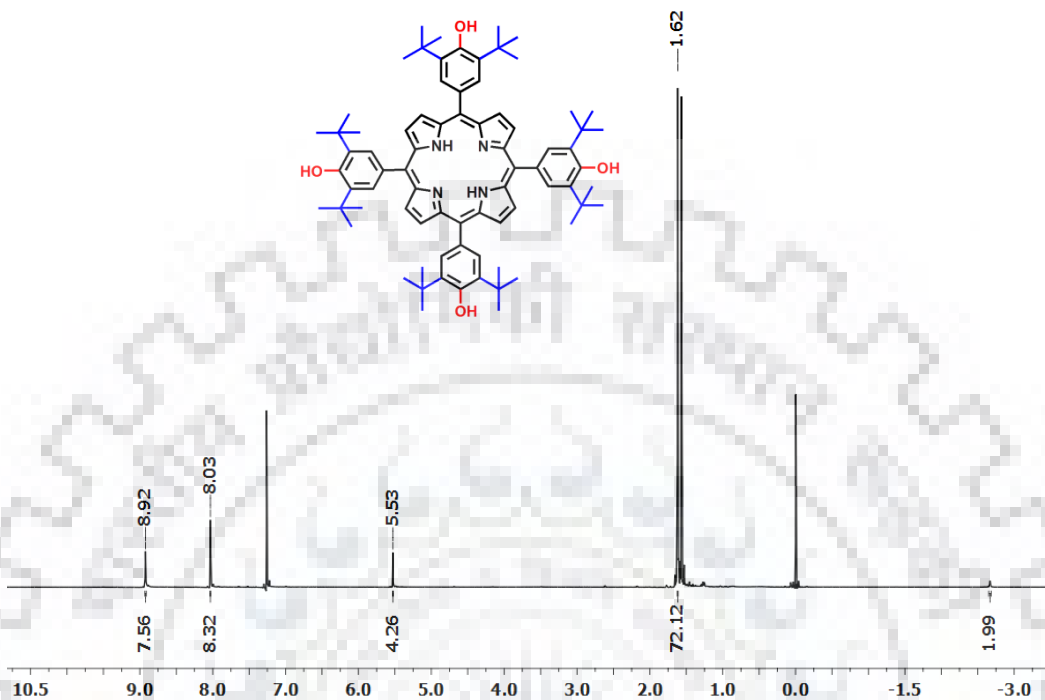


Figure A1. ^1H NMR spectrum of *meso*-tetrakis(3,5-di-*tert*-butyl-4-hydroxy)porphyrin in CDCl_3 at 298 K.

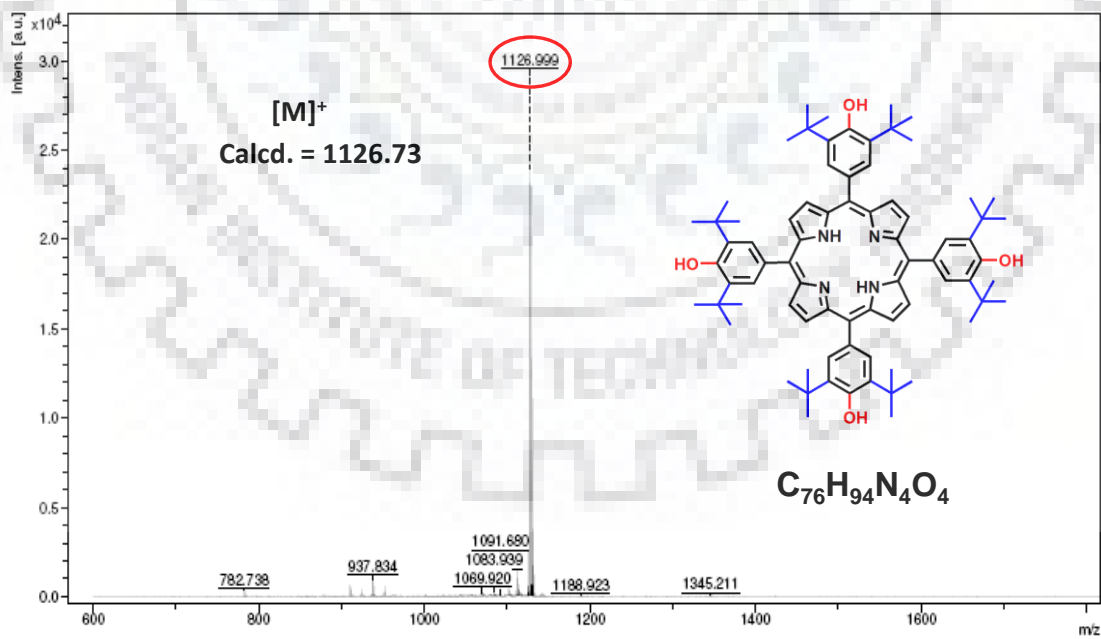


Figure A2. MALDI-TOF mass spectrum of *meso*-tetrakis(3,5-di-*tert*-butyl-4-hydroxy)porphyrin.

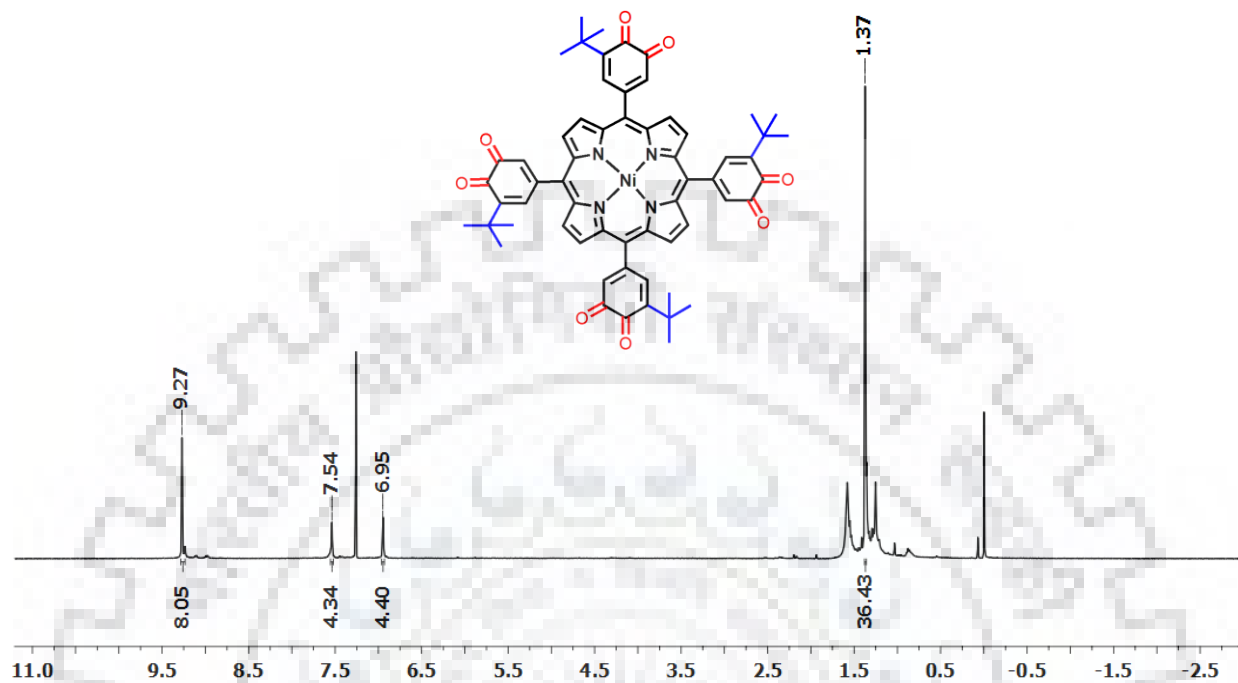


Figure A3. ^1H NMR spectrum of Ni-diOxP (1) in CDCl_3 at 298 K.

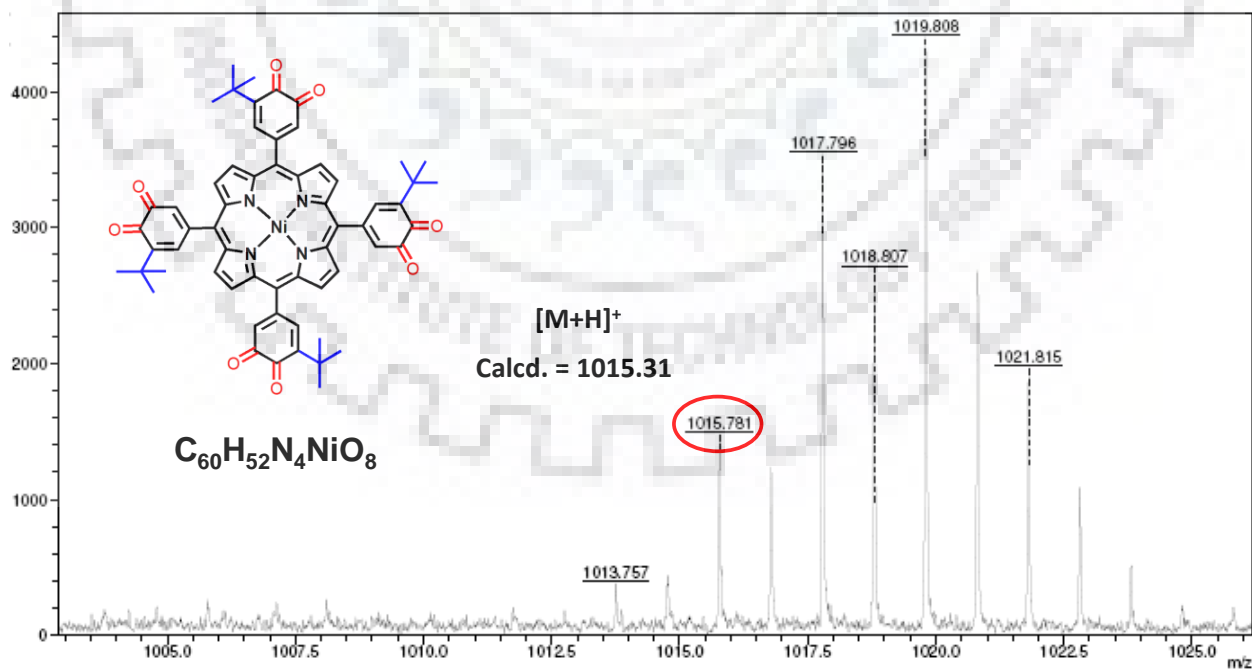


Figure A4. MALDI-TOF mass spectrum of Ni-diOxP (1).

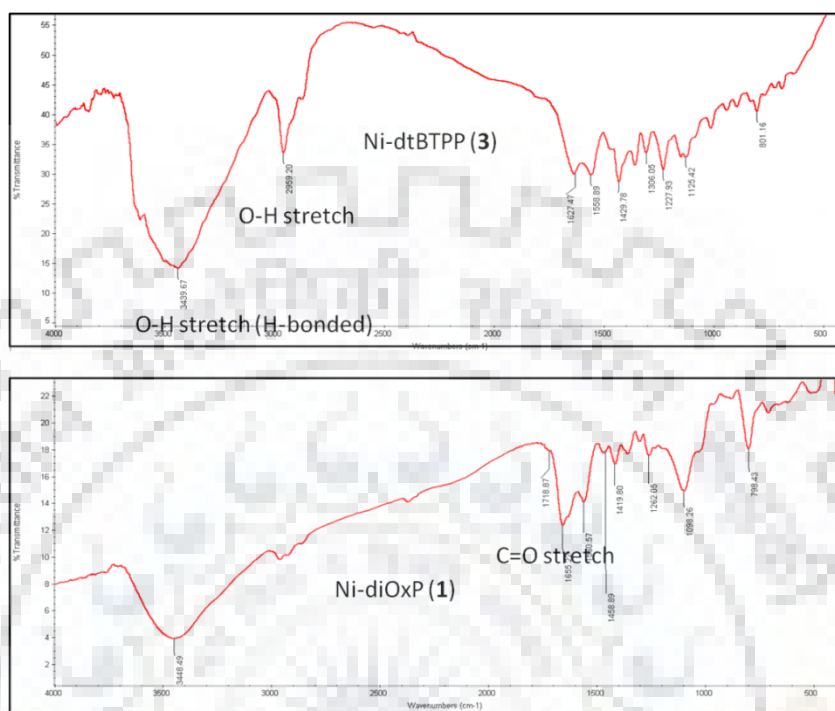


Figure A5. IR spectra of Ni-diOxP (1) and Ni-dtBTTP (3).

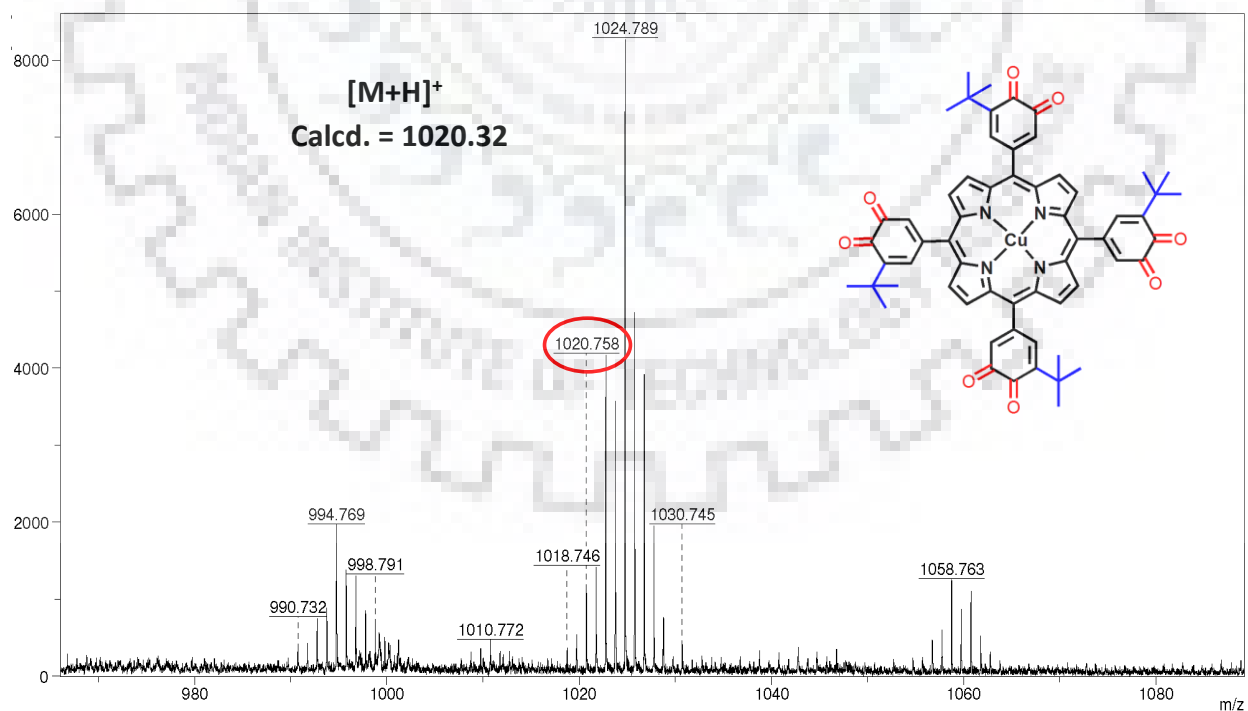


Figure A6. MALDI-TOF mass spectrum of Cu-diOxP (2).

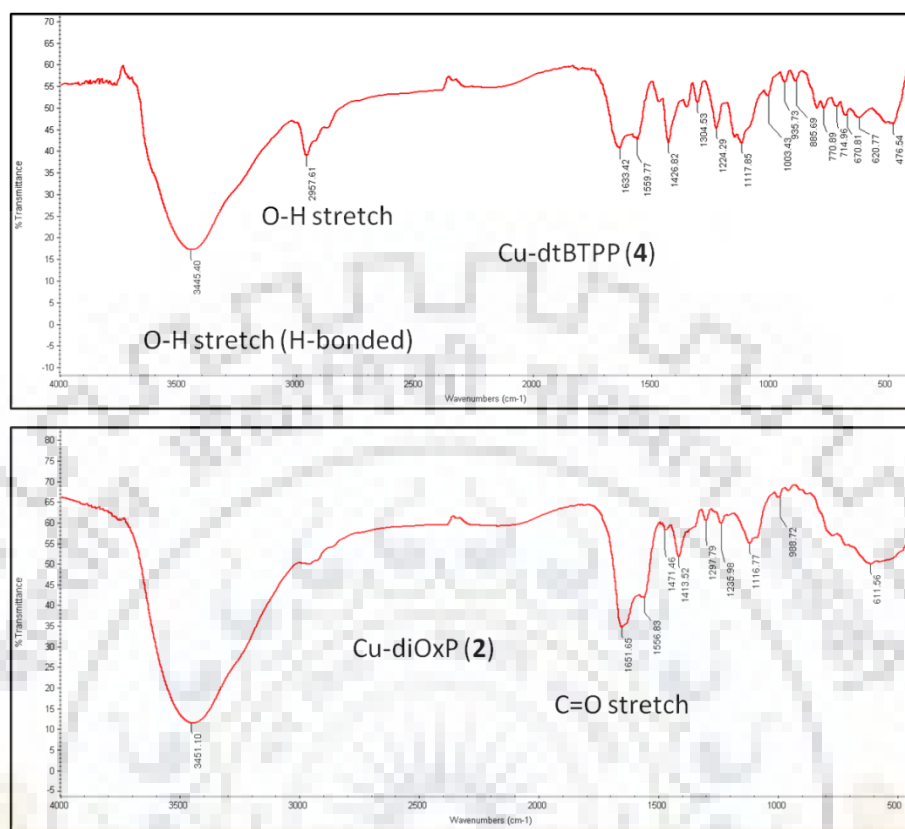


Figure A7. IR spectra of Cu-diOxP (2) and Cu-dtBTTP (4).

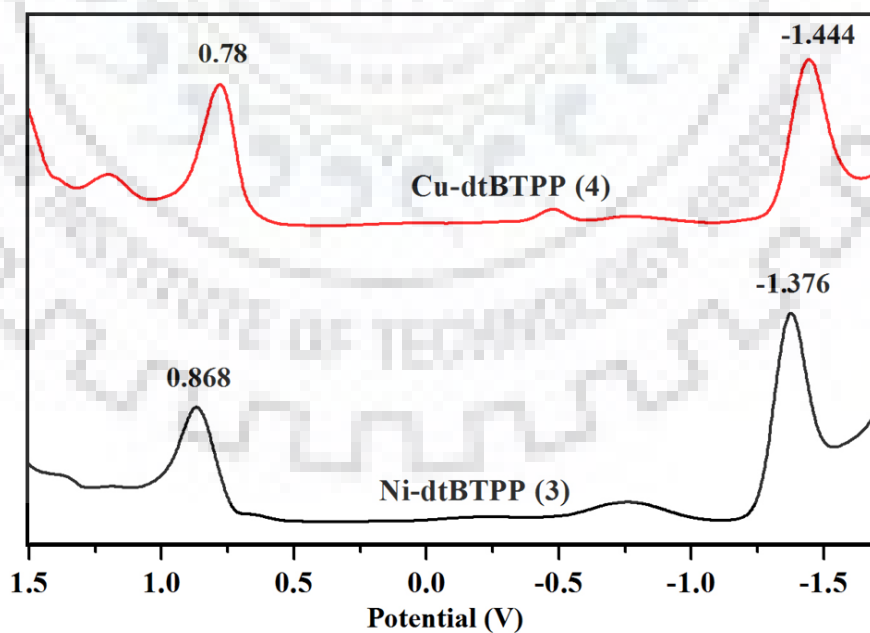


Figure A8. DPV traces of Ni-dtBTTP (3) and Cu-dtBTTP (4) in CH_2Cl_2 containing 0.1 M TBAPF₆ at 298 K.

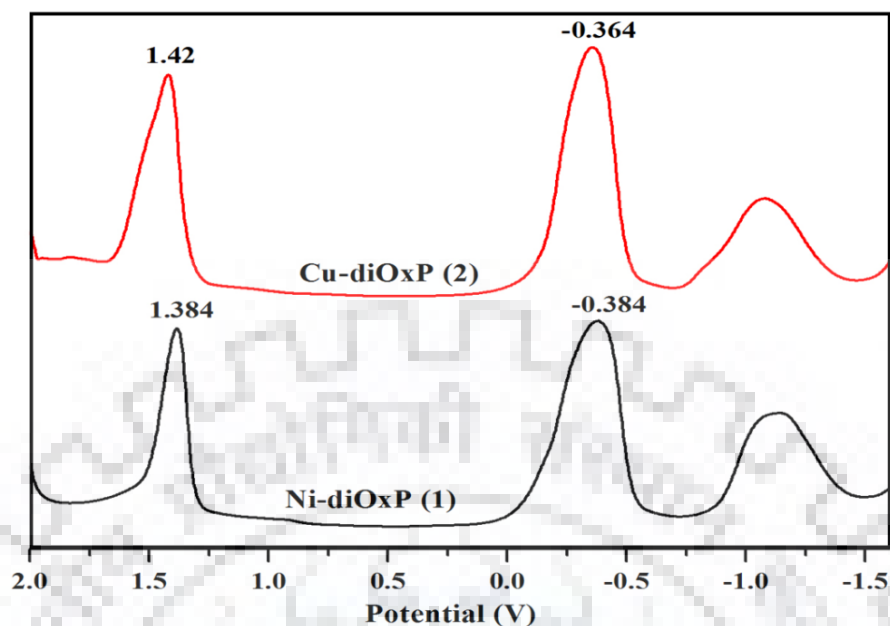


Figure A9. DPV traces of Ni-diOxP (1) and Cu-diOxP (2) in CH_2Cl_2 containing 0.1 M TBAPF_6 at 298 K.

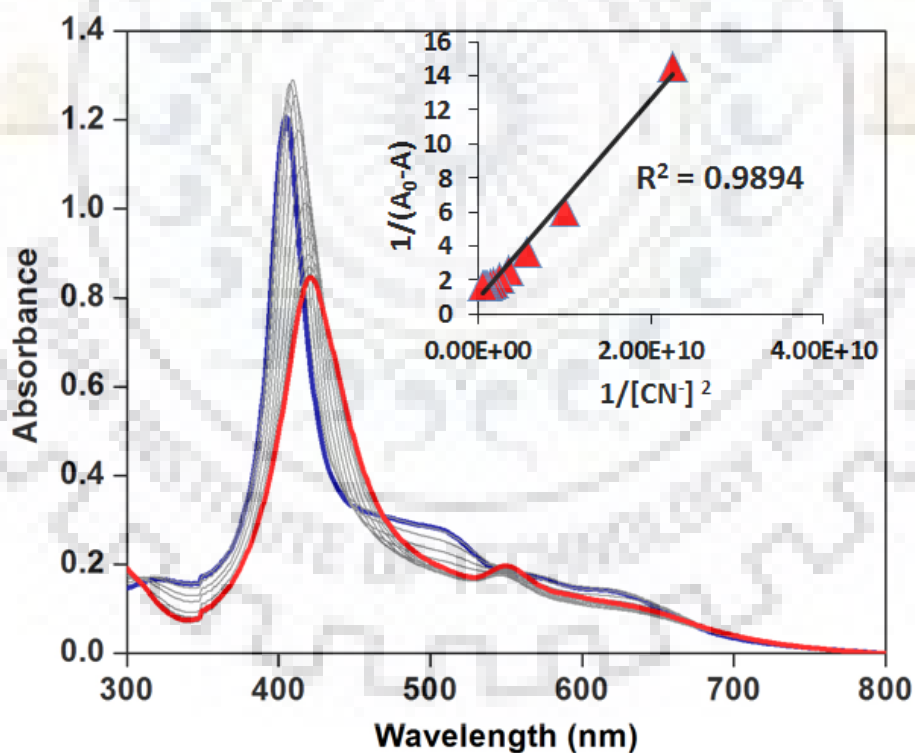


Figure A10. UV-Vis spectral response of **2** (3.15×10^{-5} M) upon incremental addition of CN^- (0 - 4.78×10^{-5} M, 1.5 equiv.) in toluene. Inset show BH-plot.

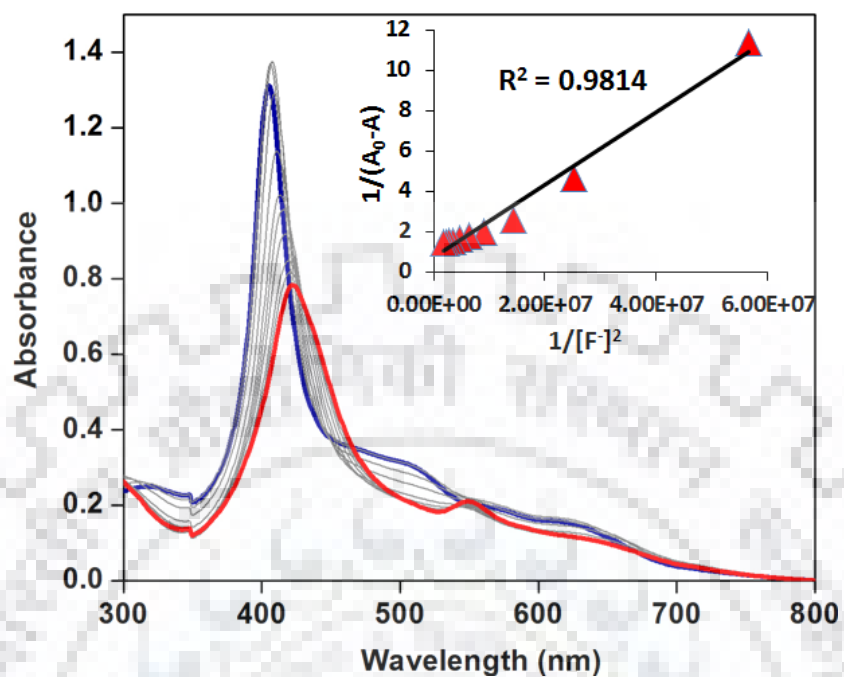


Figure A11. UV-Vis spectral response of **2** (3.15×10^{-5} M) upon incremental addition of F⁻ ($0-7.29 \times 10^{-4}$ M, 23 equiv.) in toluene. Inset show BH-plot.

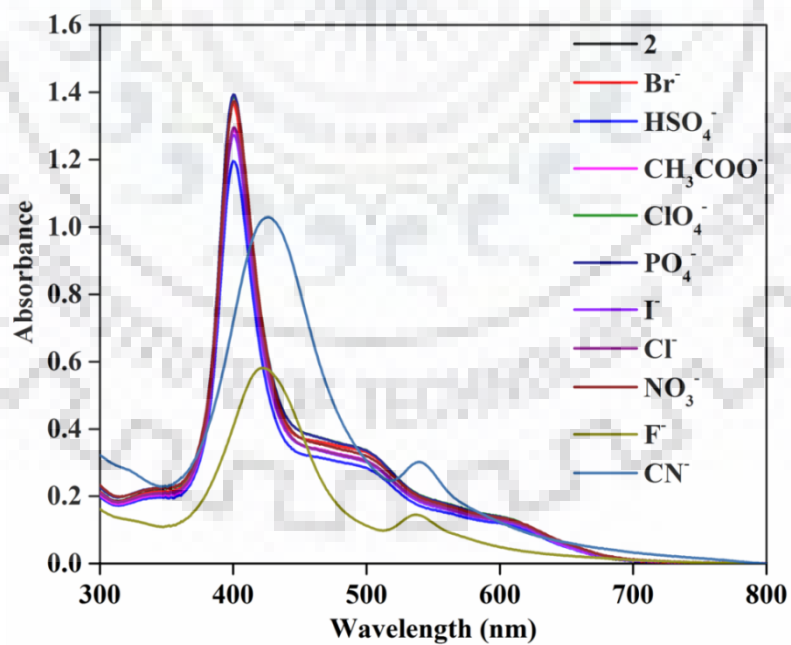


Figure A12. Absorption spectra of **2** (3.15×10^{-5} M) in the presence of different anions.

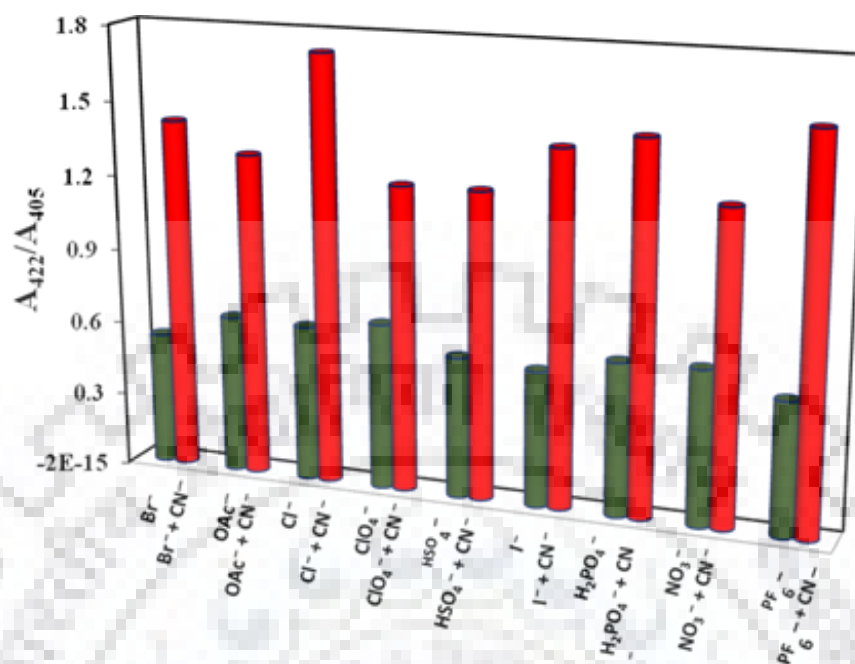


Figure A13. Ratiometric absorbance changes (A_{422}/A_{405}) of **2** (3.15×10^{-5} M) on addition of 1.5 equiv. of CN^- and 10 equiv. of other anions. Green has indicated the blank and the presence of other interfering anions and red indicated the addition of CN^- to interfering anions.

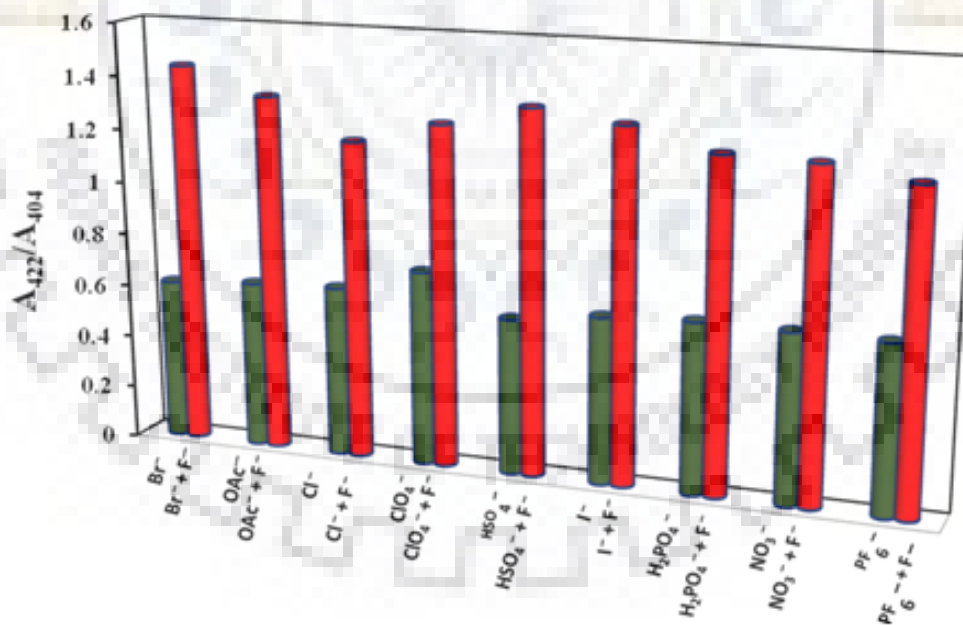


Figure A14. Ratiometric absorbance changes (A_{422}/A_{404}) of **2** (3.15×10^{-5} M) on addition of 1.5 equiv. of F^- and 10 equiv. of other anions. Green has indicated the blank and the presence of other interfering anions and red indicated the addition of F^- to interfering anions.

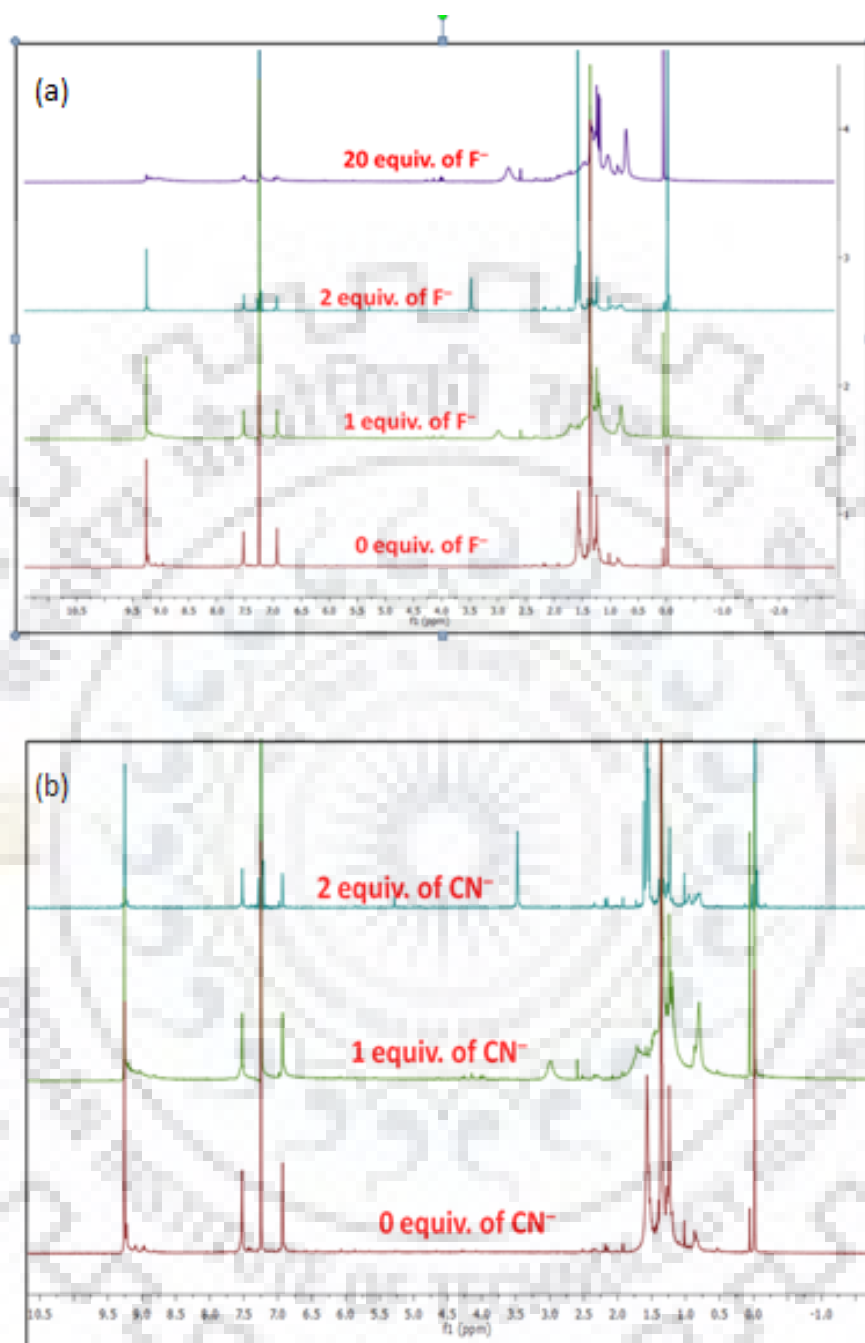


Figure A15. ^1H NMR spectra of **1** in the presence and absence of (a) F^- and (b) CN^- in CDCl_3 at 298 K.

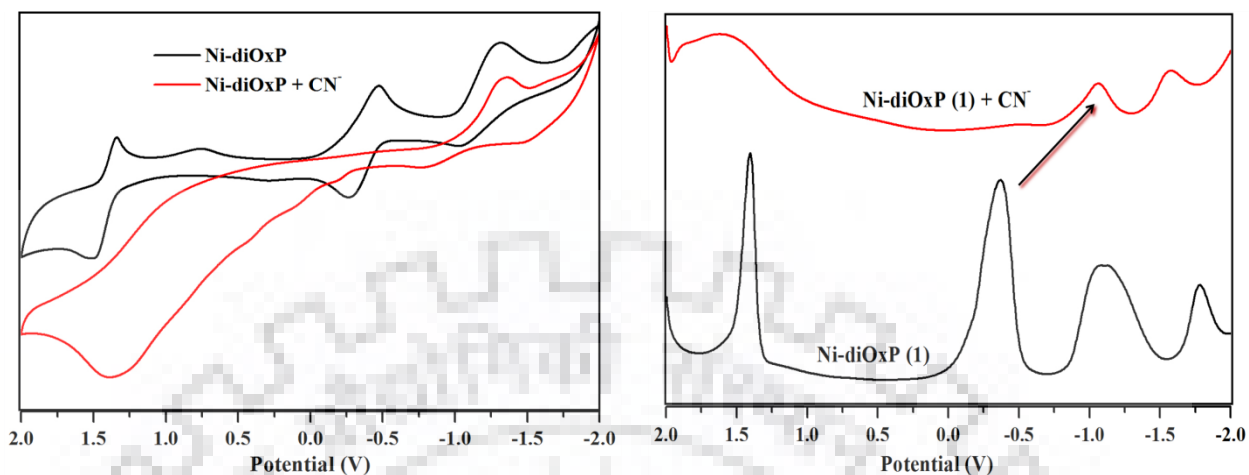


Figure A16. (a) Cyclic voltammetric (b) DPV (in V vs Ag/AgCl) traces recorded for **1** (black) and **1**•2CN⁻ (red) in CH₂Cl₂ containing 0.1 M TBAPF₆ with scan rate of 0.1 V/s at 298 K.

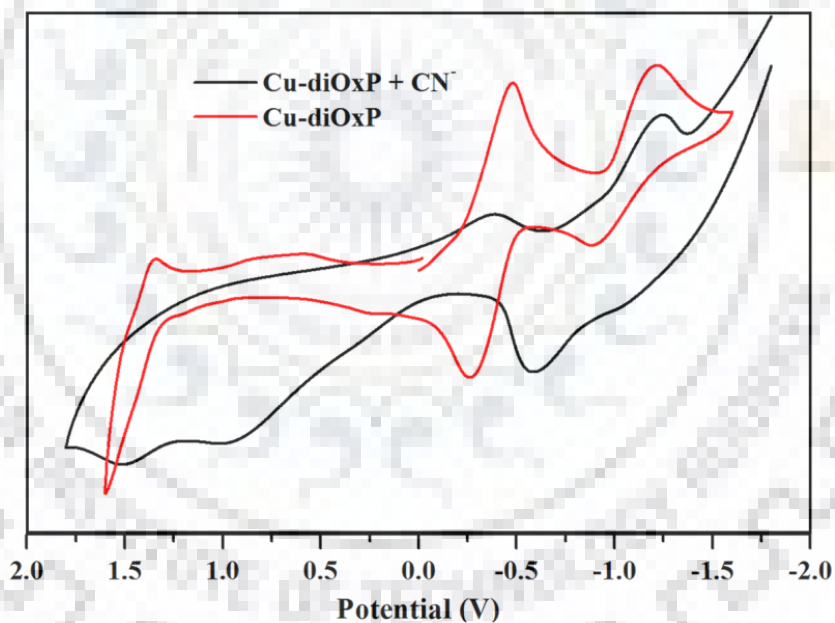


Figure A17. (a) Cyclic voltammetric (b) DPV (in V vs Ag/AgCl) traces recorded for **2** (black) and **2**•2CN⁻ (red) in CH₂Cl₂ containing 0.1 M TBAPF₆ with scan rate of 0.1 V/s at 298 K.

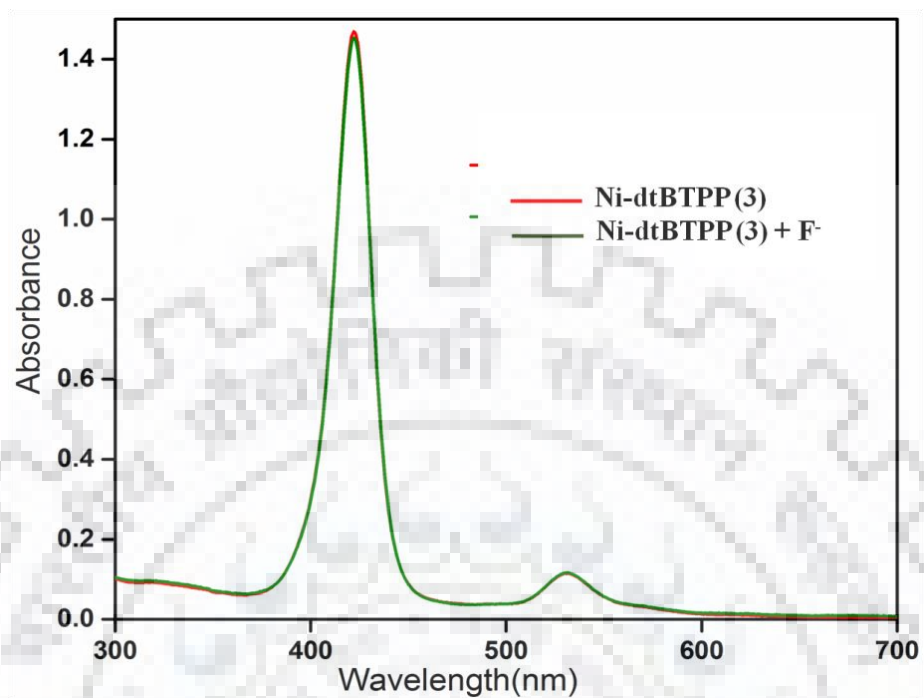


Figure A18. Absorption spectra of Ni-dtBTPP (3) in the presence and absence of 150 equiv. of F⁻ ions.

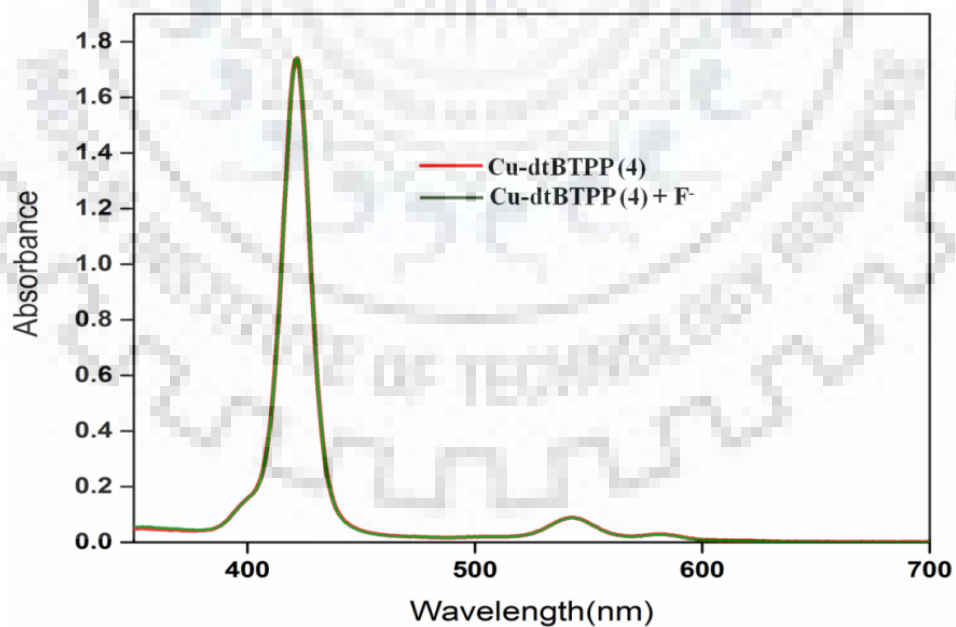


Figure A19. Absorption spectra of Cu-dtBTPP (4) in the presence and absence of 150 equiv. of F⁻ ions.

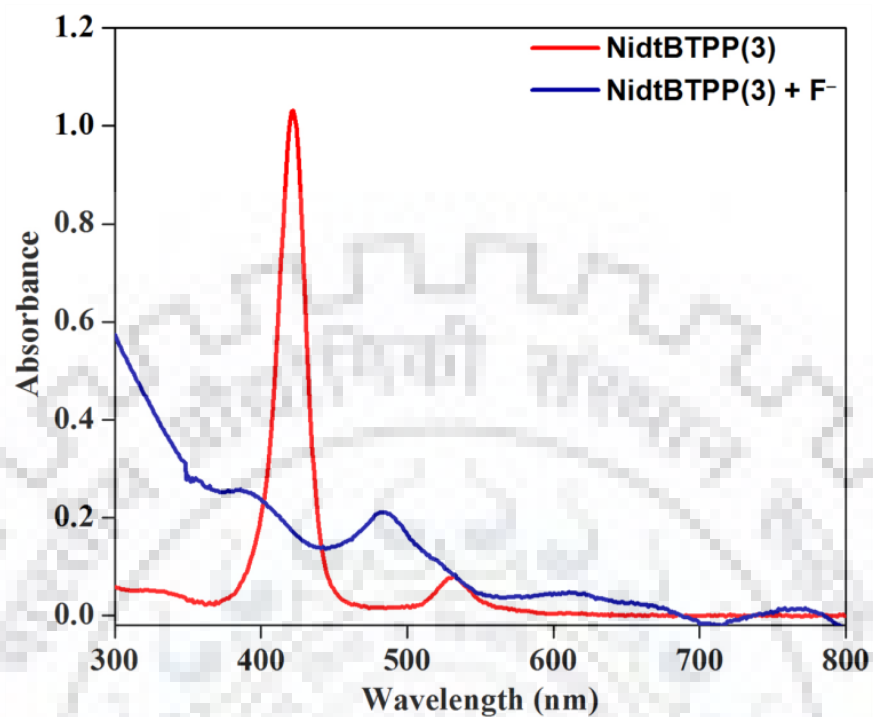


Figure A20. Absorption spectra of Ni-dtBTPP (3) in the presence and absence of > 200 equiv. of F^- ions.

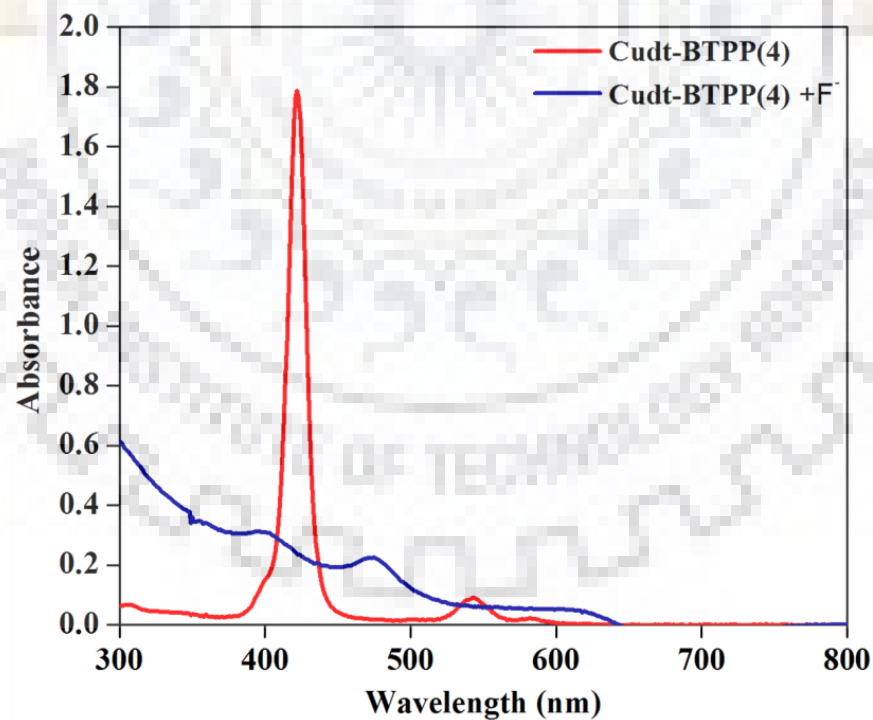


Figure A21. Absorption spectra of Cu-dtBTPP (4) in the presence of > 200 equiv. of F^- ions.

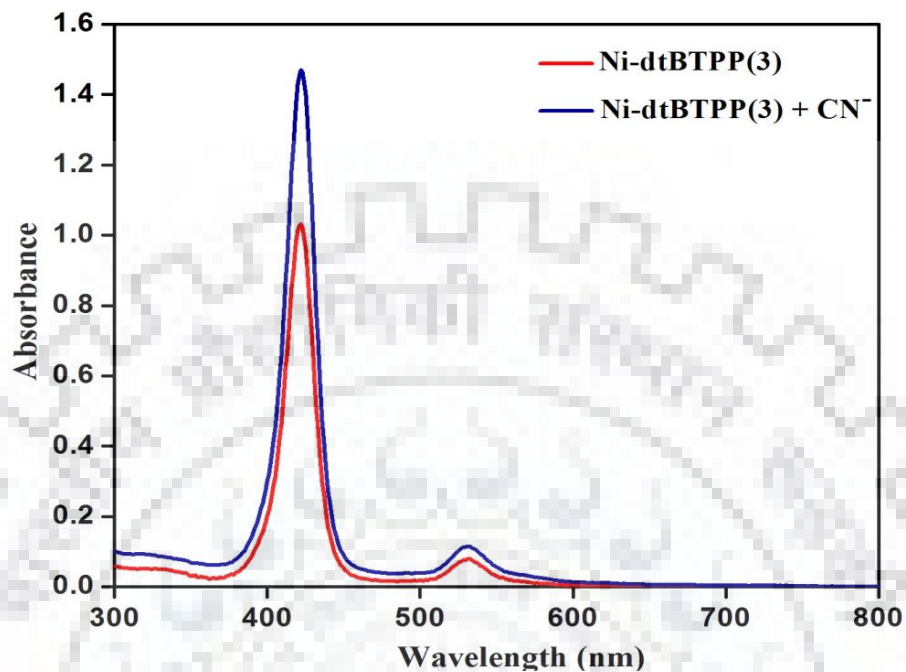


Figure A22. Absorption spectra of Ni-dtBTPP (3) in the presence and absence of > 200 equiv. of CN⁻ ions.

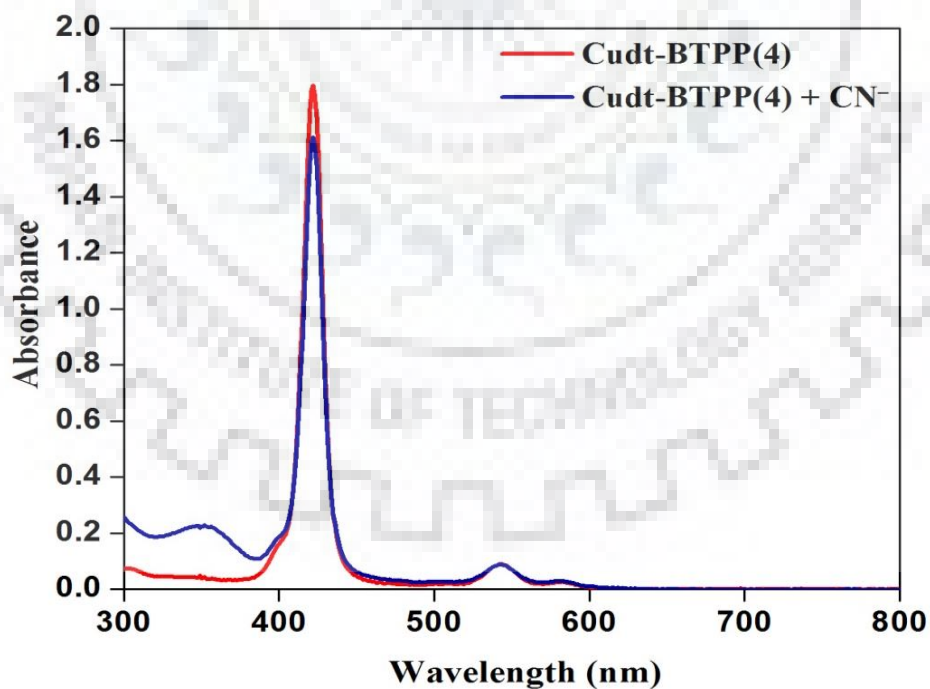


Figure A23. Absorption spectra of Cu-dtBTPP (4) in the presence and absence of > 200 equiv. of CN⁻ ions.

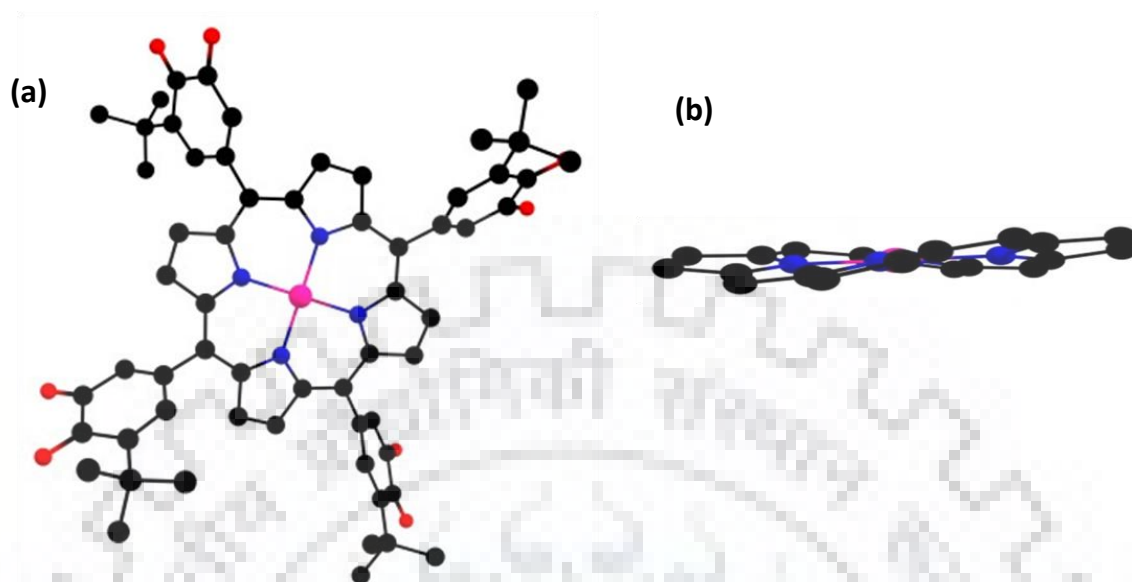


Figure A24. B3LYP/LANL2DZ optimized geometry showing (a) top as well as (b) side views of Ni-diOxP (**1**); H atoms are omitted for the clarity. In the side view, the *meso*-phenyl substituents are not shown for clarity.

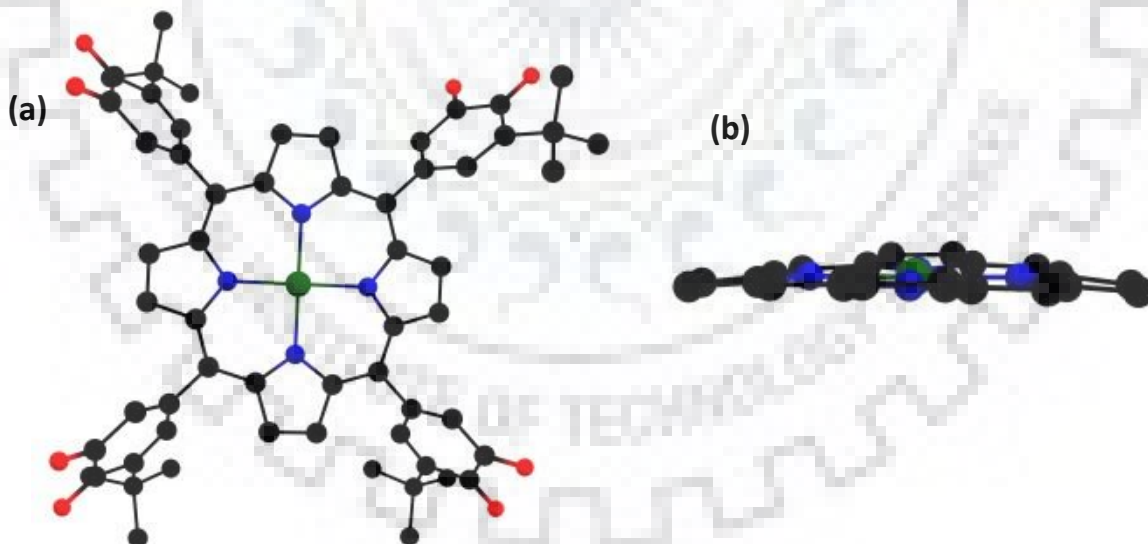


Figure A25. B3LYP/LANL2DZ optimized geometry showing (a) top as well as (b) side views of Cu-diOxP (**2**); H atoms are omitted for the clarity. In the side view, the *meso*-phenyl substituents are not shown for clarity.

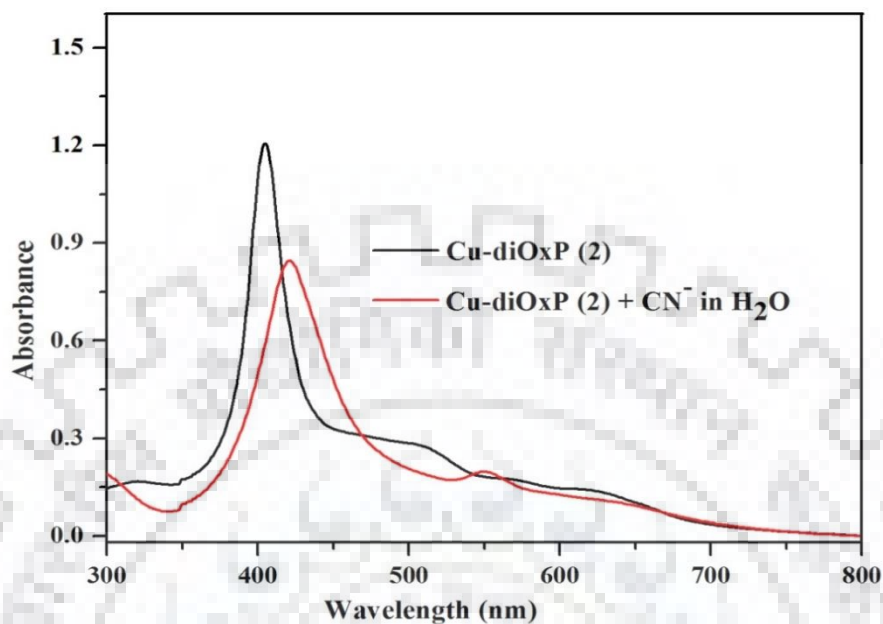


Figure A26. UV-vis spectra of Cu-diOxP (**2**) after addition of aqueous solution of KCN and 18-crown-6.

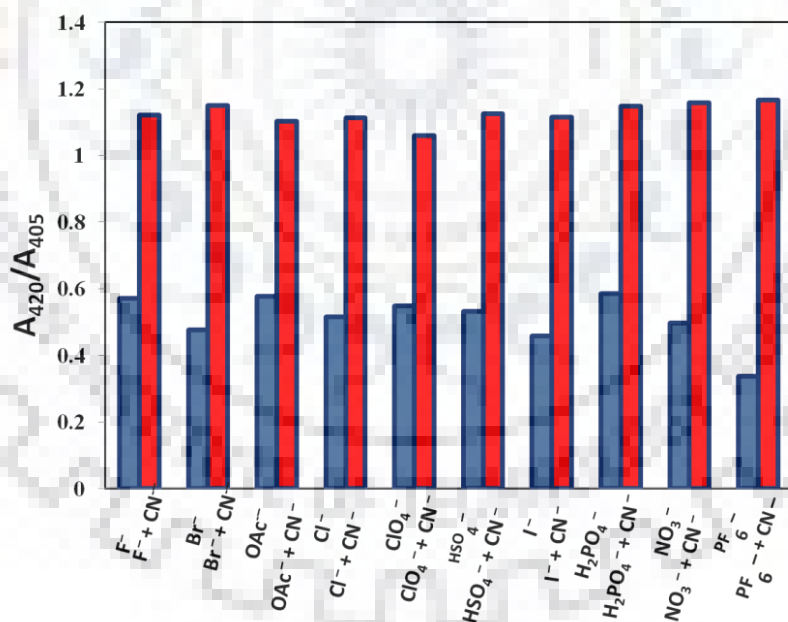


Figure A27. Ratiometric absorbance changes of **2** on addition of CN⁻ and 10 equiv. excess of other anions in aqueous medium. Blue bar has indicated the blank and the presence of other interfering anions and red indicated the addition of CN⁻ to interfering anions.

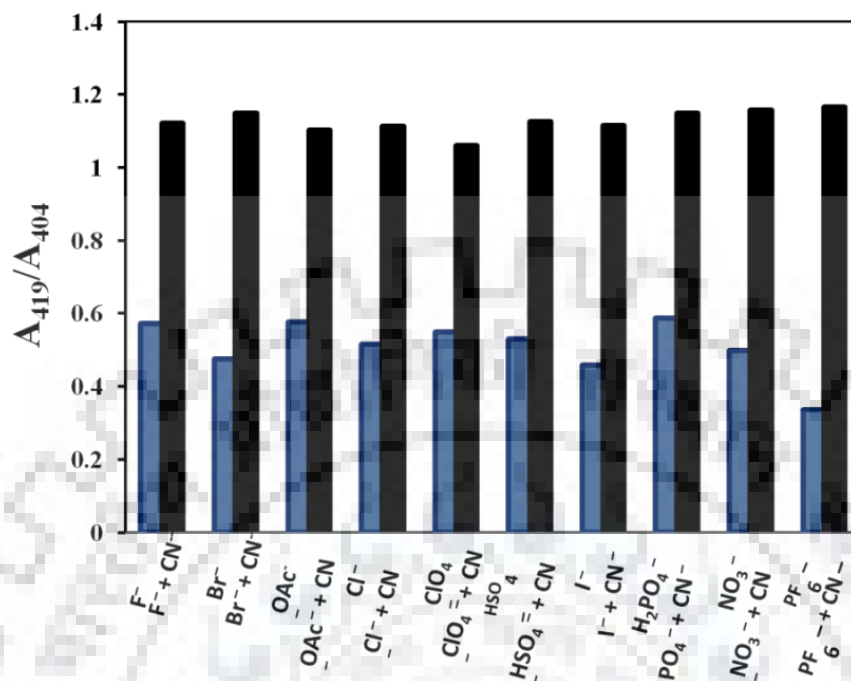


Figure A28. Ratiometric absorbance changes of **1** on addition of CN^- and 10 equiv. excess of other anions in aqueous medium. Blue bar has indicated the blank and the presence of other interfering anions and red indicated the addition of CN^- to interfering anions.

Table A1. Electronic spectral data of Ni-diOxP (**1**) in different solvents at 298 K.

Solvent	B and Q bands, nm
Ethyl acetate	398 (4.85), 557 (3.88), 610 (3.62)
Dimethyl formamide (DMF)	405 (4.85), 553 (3.88), 620 (3.62)
Acetone	398 (4.83), 558 (3.82), 614 (3.6)
DMSO	406 (4.83), 560 (3.88), 631 (3.69)
THF	401 (4.86), 560 (3.88), 618 (3.68)
Toluene	403 (4.72), 568 (3.81), 618 (3.7)
Methanol	401 (4.83), 562 (3.84), 622 (3.67)
1,4-dioxane	401 (4.81), 560 (3.87), 612 (3.67)
1,2-dichlorobenzene (1,2-DCB)	404 (4.86), 519 (4.1), 642 (3.74)
Ethanol	402 (4.83), 555 (3.94), 626 (3.76)
Triethylamine	424 (4.96), 543 (3.87), 585 (3.28)
Piperdine	435 (4.9), 554 (3.88), 600 (3.49)
Chloroform	401 (4.94), 509 (4.15), 630(3.76)
Pyridine	410 (4.77), 568 (3.88), 642(3.67)
1,1,2,2-Tetrachloroethane	402 (4.94), 518 (4.1), 638 (3.78)

Table A2. Electronic spectral data of Cu-diOxP (**2**) in different solvents at 298 K.

Solvent	B and Q bands, nm
Ethyl acetate	398 (4.85), 557 (3.88), 610 (3.62)
Dimethyl formamide (DMF)	405 (4.85), 553 (3.88), 620 (3.62)
Acetone	398 (4.83), 558 (3.82), 614 (3.6)
DMSO	406 (4.83), 560 (3.88), 631 (3.69)
THF	401 (4.86), 560 (3.88), 618 (3.68)
Toluene	403 (4.72), 568 (3.81), 618 (3.7)
Methanol	401 (4.83), 562 (3.84), 622 (3.67)
1,4-dioxane	401 (4.81), 560 (3.87), 612 (3.67)
1,2-dichlorobenzene (1,2-DCB)	404 (4.86), 519 (4.1), 642 (3.74)
Ethanol	402 (4.83), 555 (3.94), 626 (3.76)
Triethylamine	424 (4.96), 543 (3.87), 585 (3.28)
Piperidine	435 (4.9), 554 (3.88), 600 (3.49)
Chloroform	401 (4.94), 509 (4.15), 630(3.76)
Pyridine	410 (4.77), 568 (3.88), 642(3.67)
1,1,2,2-Tetrachloroethan	402 (4.94), 518 (4.1), 638 (3.78)

APPENDIX-III

Unsymmetrical Non-planar 'Push-Pull' Octa β -Substituted Porphyrins:
Synthesis, Photophysical and Electrochemical Spectroscopic Properties

Table of Contents	Page No.
Figure A1-A3. ^1H NMR spectrum of $\text{MTPP}(\text{Ph})_2\text{Br}_6$ ($\text{M} = 2\text{H}, \text{Ni}, \text{Zn}$) in CDCl_3 at 298 K.	240-241
Figure A4. MALDI-TOF mass spectrum of $\text{H}_2\text{TPP}(\text{Ph})_2\text{Br}_6$.	241
Figure A5-A7. ^1H NMR spectrum of $\text{MTPP}(\text{NO}_2)(\text{Ph})_2\text{Br}_2$ ($\text{M} = 2\text{H}, \text{Ni}, \text{Zn}$) in CDCl_3 at 298 K.	242-243
Figure A8. MALDI-TOF mass spectrum of $\text{H}_2\text{TPP}(\text{NO}_2)(\text{Ph})_2\text{Br}_2$.	243
Figure A9. UV-visible spectral titration of $\text{H}_2\text{TPP}(\text{Ph})_2\text{Br}_2$ with TFA (a) and TBAOH (b) in toluene at 298 K respectively. inset shows the corresponding Hill plots.	244
Figure A10. Fluorescence spectra of (a) $\text{MTPP}(\text{NO}_2)(\text{Ph})_2\text{Br}_5$ and (b) $\text{MTPP}(\text{Ph})_2\text{Br}_6$ ($\text{M} = 2\text{H}, \text{Zn}(\text{II})$) in CH_2Cl_2 at 298 K.	244
Figure A11. B3LYP/LANL2DZ optimized geometry showing the top views as well as side views of $\text{H}_2\text{TPP}(\text{NO}_2)(\text{Ph})_2\text{Br}_5$ (a) and (b), for $\text{H}_2\text{TPP}(\text{Ph})_2\text{Br}_6$ (d) and (e), respectively. The displacement of porphyrin core atoms from mean plane are shown in figures (c) and (f) for $\text{H}_2\text{TPP}(\text{NO}_2)(\text{Ph})_2\text{Br}_5$ and $\text{H}_2\text{TPP}(\text{Ph})_2\text{Br}_6$, respectively	245
Figure A12. Cyclic Voltametric (in V vs Ag/ AgCl) traces recorded for porphyrins (a) $\text{MTPP}(\text{Ph})_2\text{Br}_6$ ($\text{M} = 2\text{H}, \text{Co}(\text{II}), \text{Cu}(\text{II}), \text{Ni}(\text{II}), \text{Zn}(\text{II})$) and $\text{MTPP}(\text{NO}_2)(\text{Ph})_2\text{Br}_6$ ($\text{M} = 2\text{H}, \text{Co}(\text{II}), \text{Cu}(\text{II}), \text{Ni}(\text{II}), \text{Zn}(\text{II})$) in CH_2Cl_2 containing 0.1 M TBAPF ₆ with a scan rate of 0.1 V/s at 298 K.	246
Figure A13. Crystal structure packing diagram of $\text{H}_2\text{TPP}(\text{NO}_2)(\text{Ph})_2\text{Br}_5$.	246
Table A1. Crystallographic data of $\text{H}_2\text{TPP}(\text{NO}_2)(\text{Ph})_2\text{Br}_5$	247
Table A2. Selected average bond lengths (\AA) and bond angles ($^\circ$) for the single crystal of $\text{H}_2\text{TPP}(\text{NO}_2)(\text{Ph})_2\text{Br}_5$.	248
Table A3. Selected bond lengths (\AA) and bond angles ($^\circ$) for the B3LYP/LanLD2Z	249

optimized geometries of $H_2TPP(Ph)_2Br_5X$ ($X = NO_2, Br$).

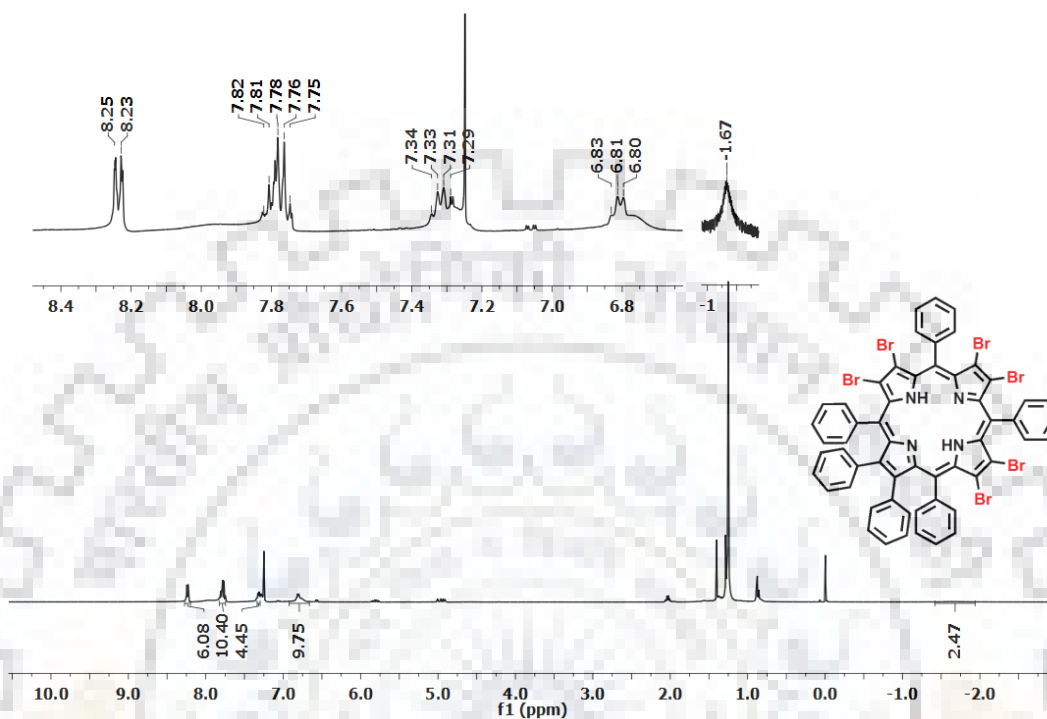


Figure A1. 1H NMR spectrum of $H_2TPP(Ph)_2Br_6$ in $CDCl_3$ at 298 K.

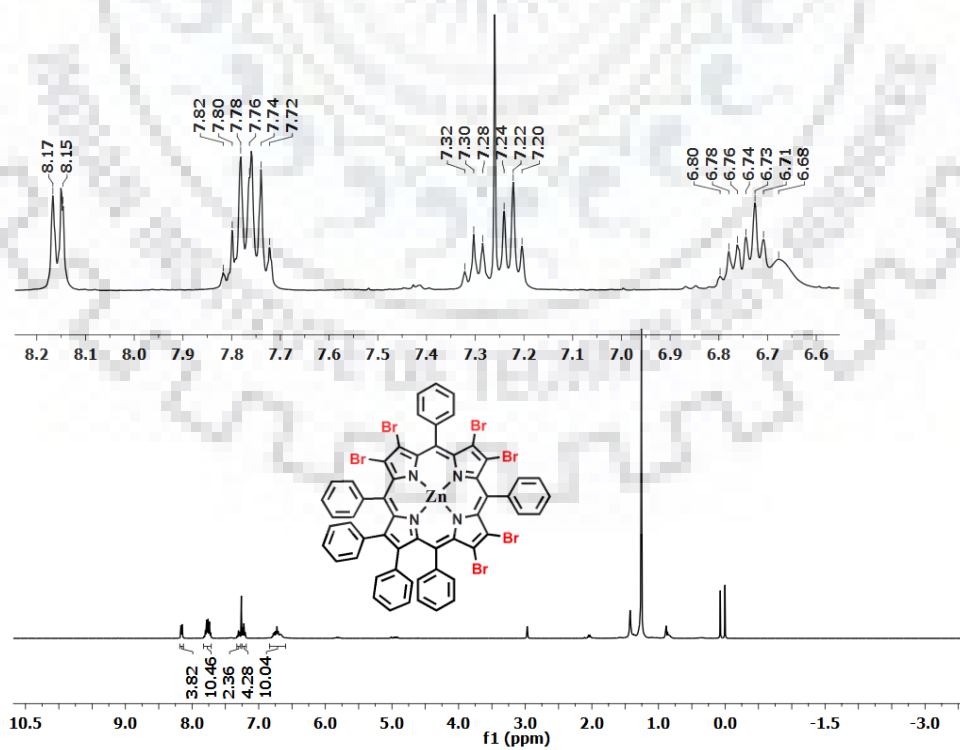


Figure A2. ^1H NMR spectrum of $\text{ZnTPP}(\text{Ph})_2\text{Br}_6$ in CDCl_3 at 298 K.

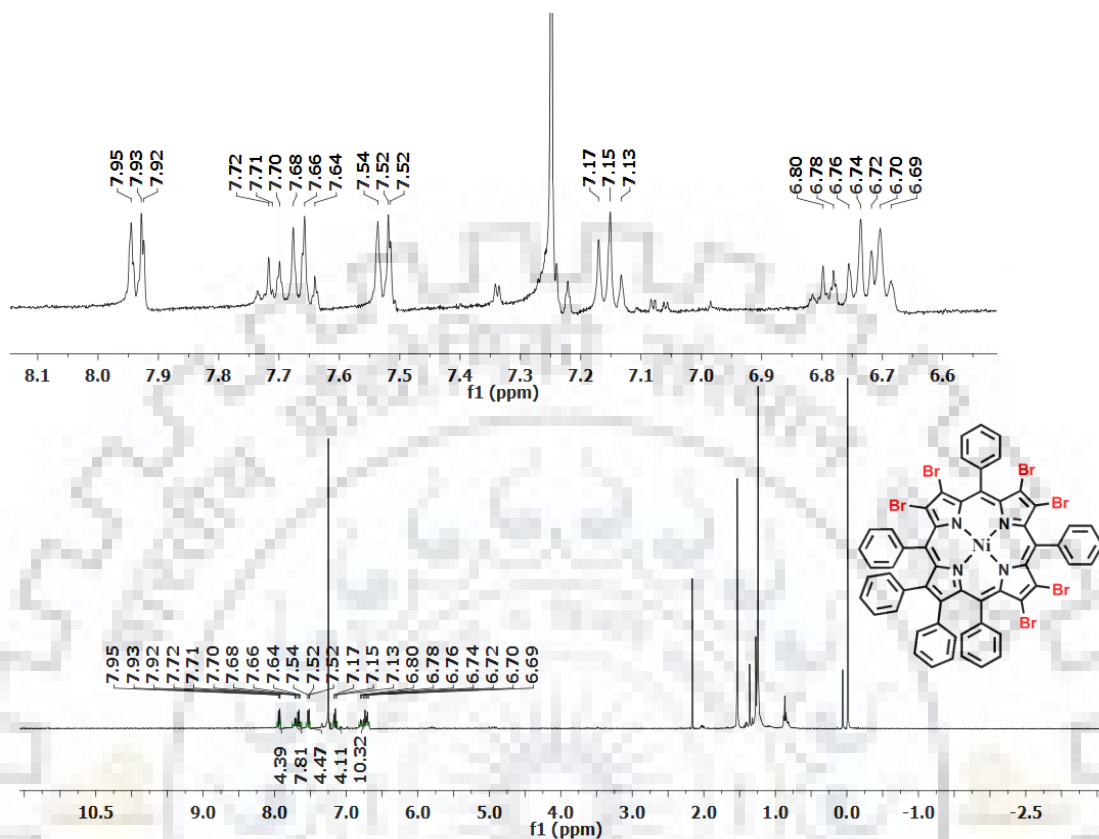


Figure A3. ^1H NMR spectrum of $\text{NiTPP}(\text{Ph})_2\text{Br}_6$ in CDCl_3 at 298 K.

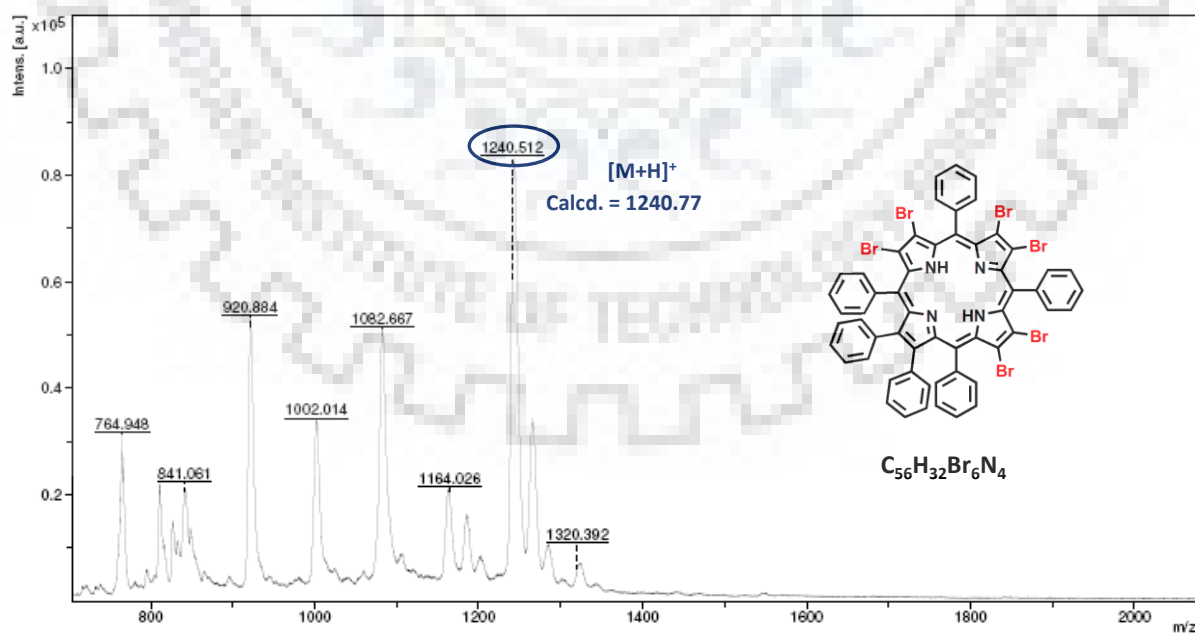
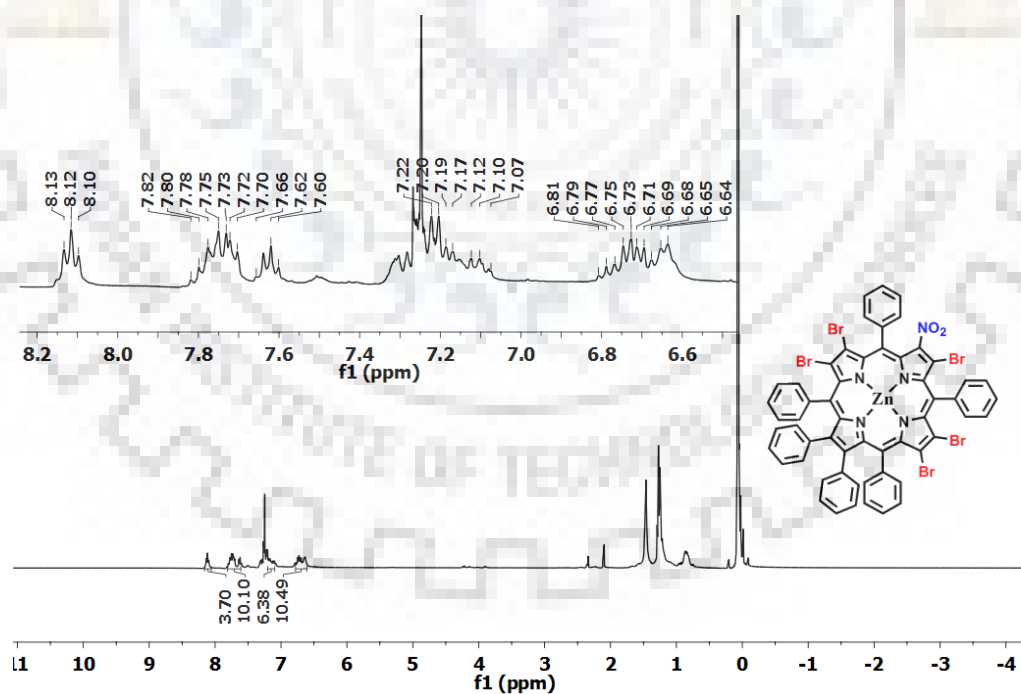
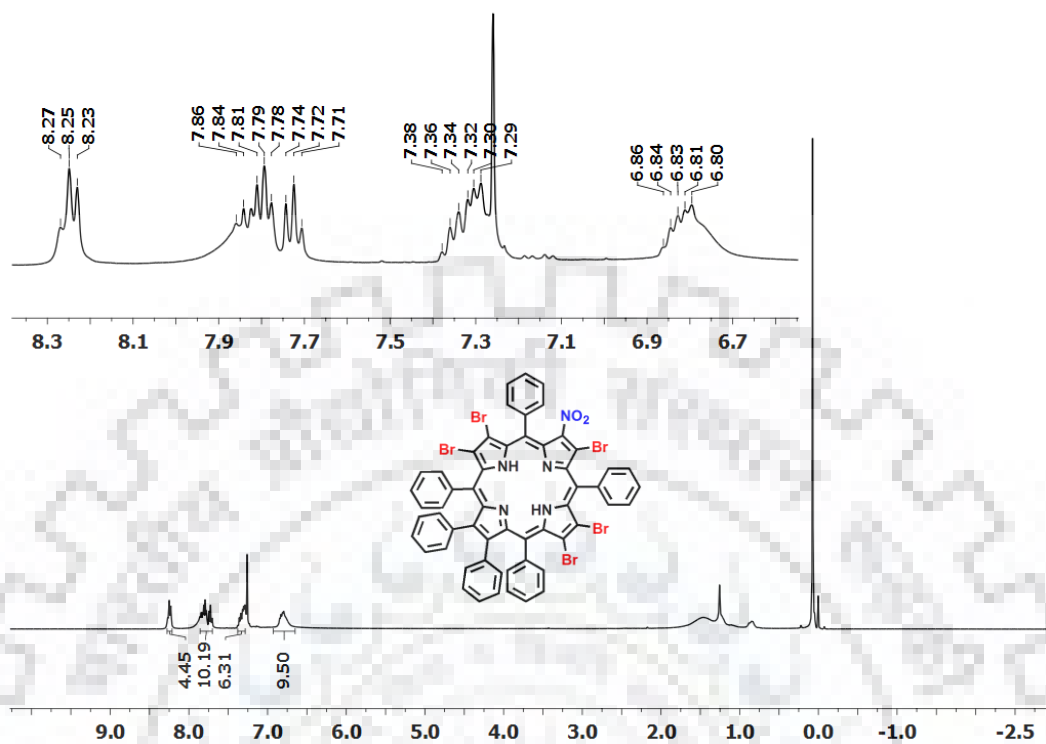


Figure A4. MALDI-TOF mass spectrum of $\text{H}_2\text{TPP}(\text{Ph})_2\text{Br}_6$.



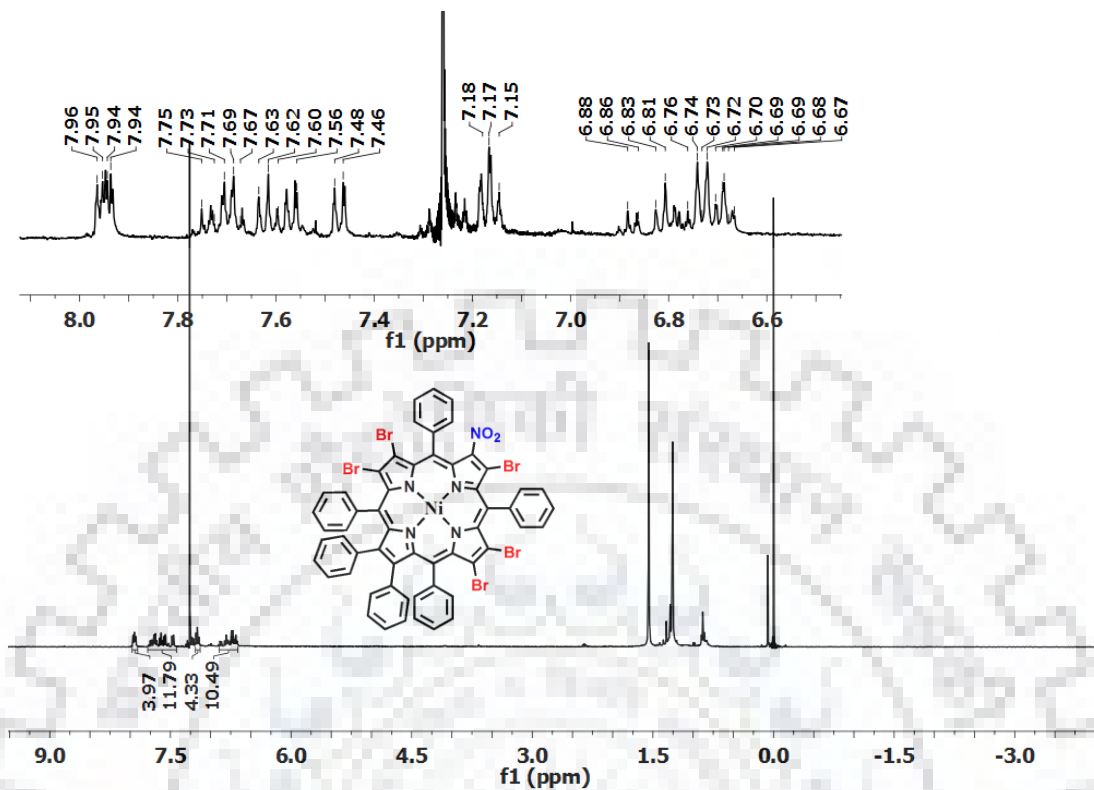


Figure A7. ^1H NMR spectrum of NiTPP(NO₂)(Ph)₂Br₂ in CDCl₃ at 298 K.

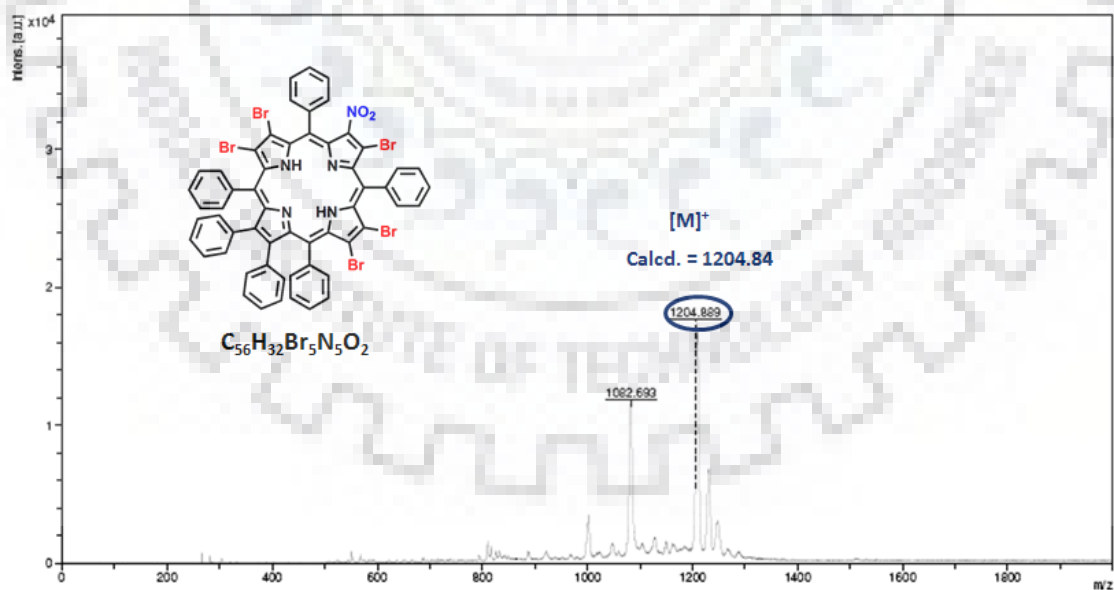


Figure A8. MALDI-TOF mass spectrum of H₂TPP(NO₂)(Ph)₂Br₅.

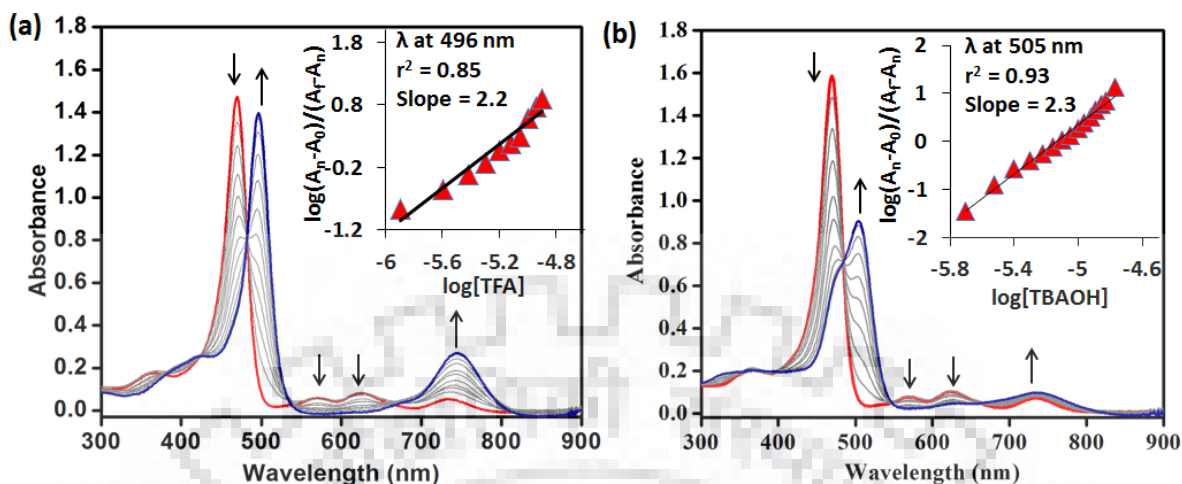


Figure A9. UV-visible spectral titration of $H_2TPP(Ph)_2Br_6$ with TFA (a) and TBAOH (b) in toluene at 298 K respectively. insets shows the corresponding Hill plots.

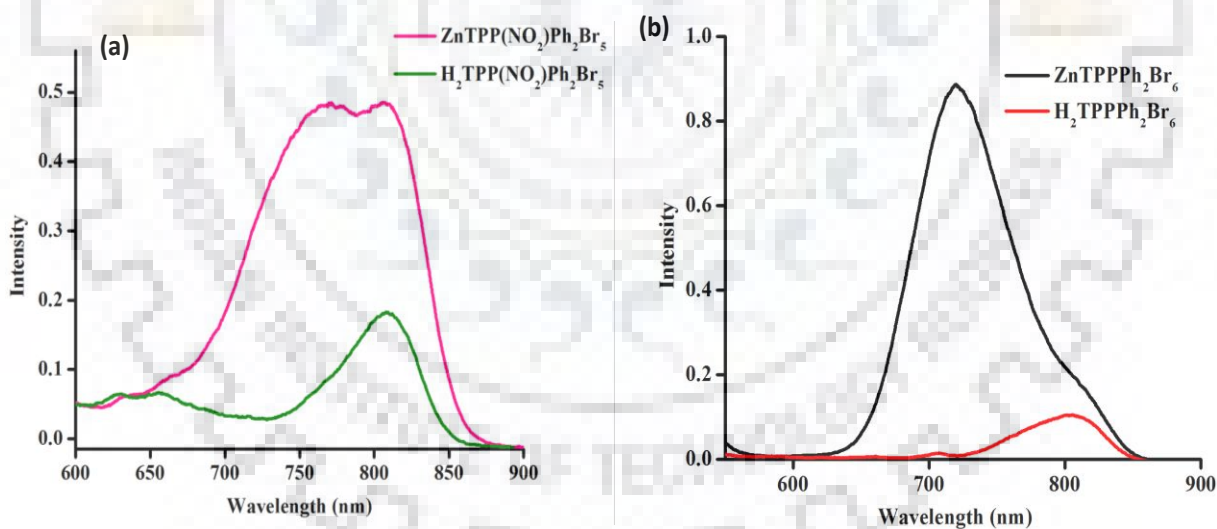


Figure A10. Fluorescence spectra of (a) $MTPP(NO_2)Ph_2Br_5$ and (b) $MTPP(Ph)_2Br_6$ ($M = 2H, Zn$ (II)) in CH_2Cl_2 at 298 K.

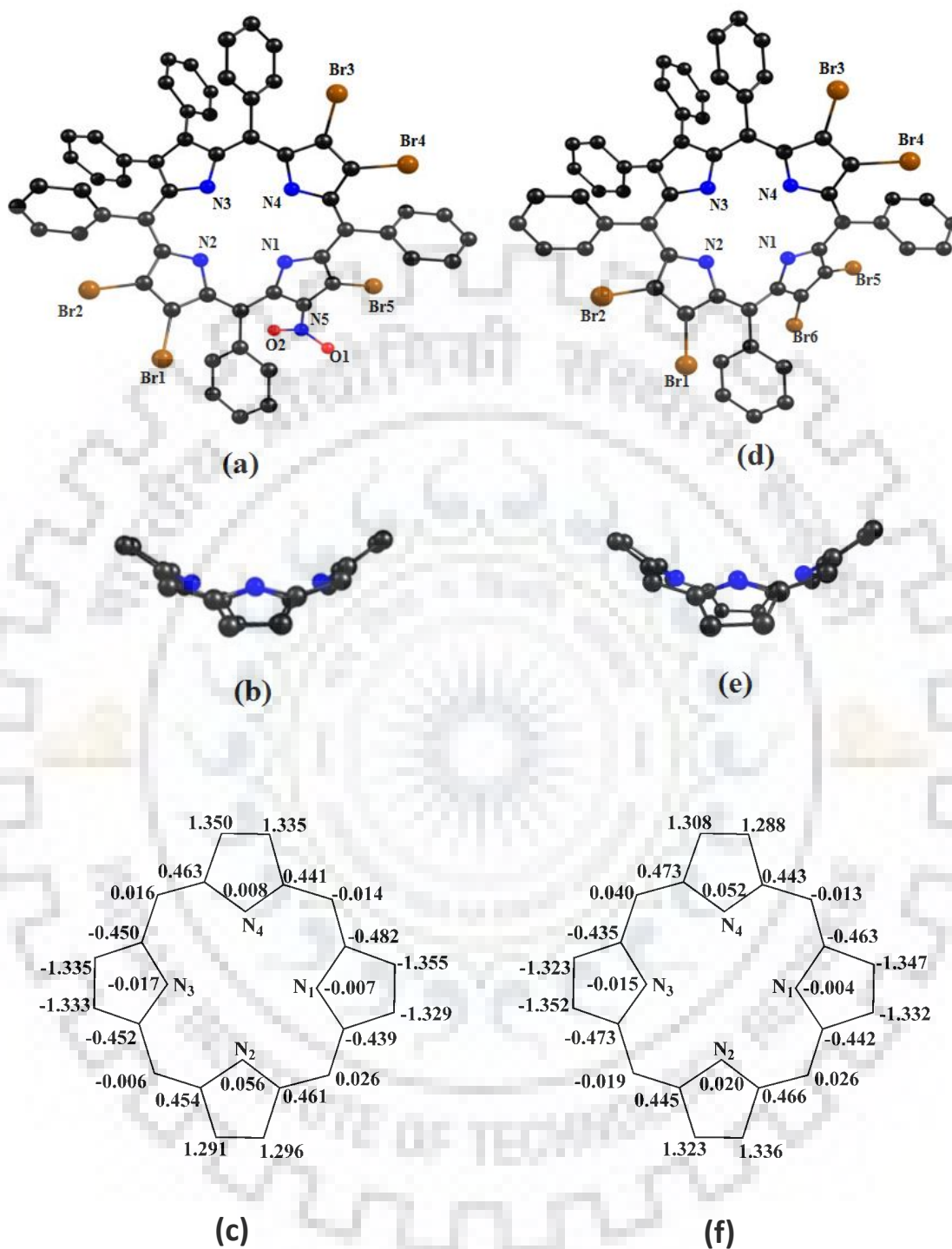


Figure A11. B3LYP/LANL2DZ optimized geometry showing the top views as well as side views of $\text{H}_2\text{TPP}(\text{NO}_2)(\text{Ph})_2\text{Br}_5$ (a) and (b), for $\text{H}_2\text{TPP}(\text{Ph})_2\text{Br}_6$ (d) and (e), respectively. The displacement of porphyrin core atoms from mean plane are shown in figures (c) and (f) for $\text{H}_2\text{TPP}(\text{NO}_2)(\text{Ph})_2\text{Br}_5$ and $\text{H}_2\text{TPP}(\text{Ph})_2\text{Br}_6$, respectively.

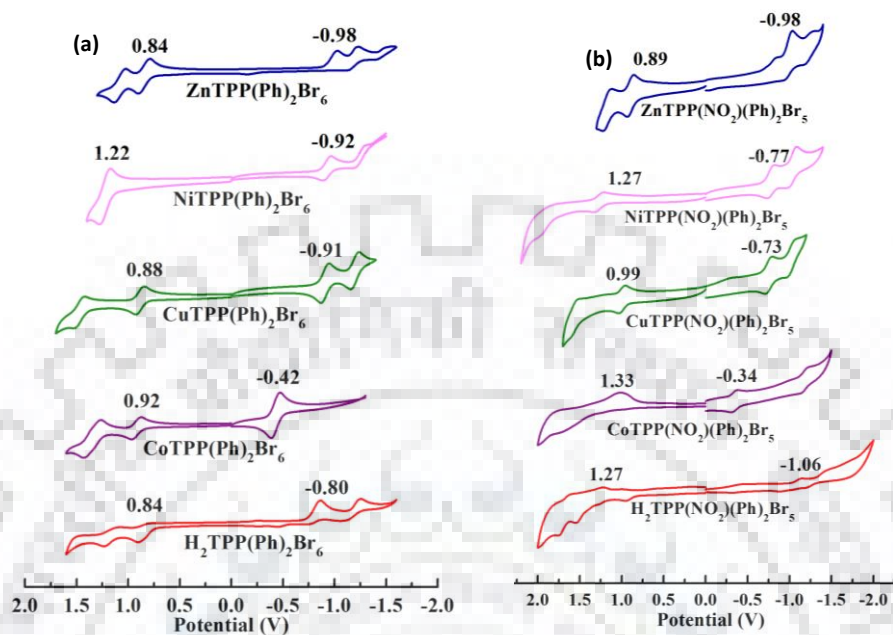


Figure A12. Cyclic Voltammetric (in V vs Ag/ AgCl) traces recorded for porphyrins (a) MTPPP₂Br₆ (M = 2H, Co(II), Cu(II), Ni(II), Zn(II)) and MTPP(NO₂)(Ph)₂Br₅ (M = 2H, Co(II), Cu(II), Ni(II), Zn(II)) in CH₂Cl₂ containing 0.1 M TBAPF₆ with a scan rate of 0.1 V/s at 298 K.

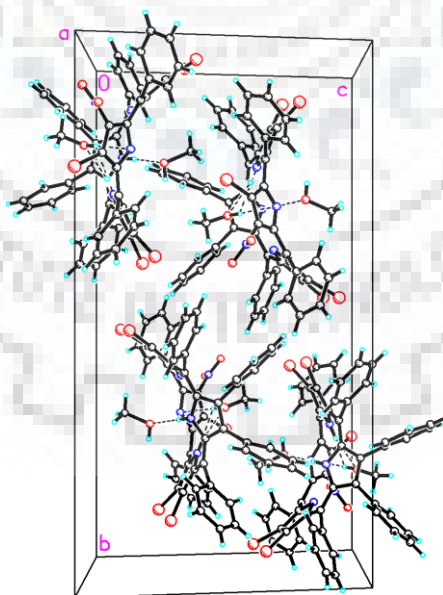
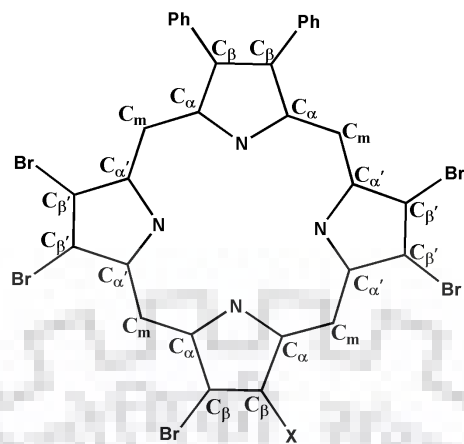


Figure A13. Crystal structure packing diagram of H₂TPP(NO₂)(Ph)₂Br₅.

Table A1. Crystallographic data of $\text{H}_2\text{TPP}(\text{NO}_2)(\text{Ph})_2\text{Br}_5$.	
	$\text{H}_2\text{TPP}(\text{NO}_2)(\text{Ph})_2\text{Br}_5$
Empirical Formula	$\text{C}_{58}\text{H}_{40}\text{Br}_5\text{N}_5\text{O}_4$
Formula wt.	1270.50
Crystal system	Monoclinic
Space group	P 21/c
a (Å)	13.7272(4) Å
b (Å)	27.1133(10) Å
c (Å)	14.7309(5) Å
α (°)	90°
β (°)	101.409(2)°
γ (°)	90°
Volume (Å ³)	5374.4(3) Å ³
Z	4
D _{calc} (mg/m ³)	1.570 mg/m ³
λ (Å)	0.71073 Å
T (°C)	296(2) K
No. of total reflns.	72230
No. of indepnt. reflns.	9721
R	0.1082
R _w	0.1638
GOOF	1.027
CCDC No.	1921730

Table A2. Selected average bond lengths (\AA) and bond angles ($^\circ$) for the single crystal of $\text{H}_2\text{TPP}(\text{NO}_2)\text{Ph}_2\text{Br}_5$.	
Bond Length(\AA)	
	$\text{H}_2\text{TPP}(\text{NO}_2)(\text{Ph})_2\text{Br}_5$
N- C_α	1.354
N'- $\text{C}_{\alpha'}$	1.311
C_α - C_β	1.428
$\text{C}_{\alpha'}$ - $\text{C}_{\beta'}$	1.465
C_β - C_β	1.366
$\text{C}_{\beta'}$ - $\text{C}_{\beta'}$	1.273
C_α - C_m	1.411
$\text{C}_{\alpha'}$ - C_m	1.332
ΔC_β (\AA)	1.23
$\Delta 24$ (\AA)	0.558
Bond Angle (deg)	
N- C_α - C_m	125.42
N'- $\text{C}_{\alpha'}$ - C_m	119.01
N- C_α - C_β	106.88
N'- $\text{C}_{\alpha'}$ - $\text{C}_{\beta'}$	111.35
C_β - C_α - C_m	127.53
$\text{C}_{\beta'}$ - $\text{C}_{\alpha'}$ - C_m	129.60
C_α - C_m - $\text{C}_{\alpha'}$	123.34
C_α - C_β - C_β	107.63
$\text{C}_{\alpha'}$ - $\text{C}_{\beta'}$ - $\text{C}_{\beta'}$	106.01
C_α -N- C_α	110.94
$\text{C}_{\alpha'}$ -N'- $\text{C}_{\alpha'}$	105.16



X = NO₂, Br

Table A3. Selected bond lengths (Å) and bond angles (°) for the B3LYP/LanLD2Z optimized geometries of H₂TPP(Ph)₂Br₅X (X = NO₂, Br).

	H ₂ TPP(Ph) ₂ Br ₆	H ₂ TPP(NO ₂)(Ph) ₂ Br ₅
Bond Length (Å)		
N-C _α	1.385	1.384
N'-C _{α'}	1.391	1.391
C _α -C _β	1.477	1.475
C _{α'} -C _{β'}	1.450	1.451
C _β -C _β	1.382	1.384
C _{β'} -C _{β'}	1.393	1.391
C _α -C _m	1.426	1.427
C _{α'} -C _m	1.420	1.418
ΔC_{β} (Å)	1.251	1.238
$\Delta 24$ (Å)	0.594	0.581
Bond Angle (deg)		
N-C _α -C _m	122.80	123.13
N'-C _{α'} -C _m	123.45	123.45
N-C _α -C _β	109.64	109.64

Appendix-III: Unsymmetrically Octa β -Substituted Porphyrins

$N'-C_{\alpha'}-C_{\beta'}$	105.05	105.09
$C_{\beta}-C_{\alpha}-C_m$	127.26	118.81
$C_{\beta'}-C_{\alpha'}-C_m$	131.43	131.31
$C_{\alpha}-C_m-C_{\alpha'}$	121.90	121.84
$C_{\alpha}-C_{\beta}-C_{\beta}$	106.59	106.58
$C_{\alpha'}-C_{\beta'}-C_{\beta'}$	108.51	108.50
$C_{\alpha}-N-C_{\alpha}$	106.89	107.00
$C_{\alpha'}-N'-C_{\alpha'}$	112.47	112.41



APPENDIX-IV

SPECTRAL INVESTIGATIONS OF MESO-TETRAALKYLPORPHYRIN-FULLERENE HOST-GUEST COMPLEXES

Table of Contents	Page No.
Figure A1. ¹ H NMR spectrum of H ₂ TMeP (1) in CDCl ₃ at 298 K.	254
Figure A2. ¹ H NMR spectrum of H ₂ TEtP (2) in CDCl ₃ at 298 K.	254
Figure A3. ¹ H NMR spectrum of H ₂ TPrP (3) in CDCl ₃ at 298 K.	255
Figure A4. ¹ H NMR spectrum of ZnTMeP (1a) in CDCl ₃ at 298 K.	255
Figure A5. ¹ H NMR spectrum of ZnTEtP (2a) in CDCl ₃ at 298 K.	256
Figure A6. ¹ H NMR spectrum of ZnTPrP (3a) in CDCl ₃ at 298 K.	256
Figure A7. ESI-MS spectrum of H ₂ TMeP (1) in CH ₃ CN.	257
Figure A8. ESI-MS spectrum of H ₂ TEtP (2) in CH ₃ CN.	257
Figure A9. ESI-MS spectrum of H ₂ TPrP (3) in CH ₃ CN.	258
Figure A10. ESI-MS spectrum of ZnTEtP (2a) in CH ₃ CN.	258
Figure A11. ESI-MS spectrum of ZnTPrP (3a) in CH ₃ CN.	259
Table A1. Crystal data of H ₂ TPrP (3).	259
Figure A12. Molecular crystal packing of H ₂ TPrP (3) along (a) a axis and (b) b axis, respectively.	260
Figure A13. (a) Spectral changes observed during the titration of Fullerene (C ₆₀) to the solution of containing H ₂ TMeP (1) in toluene at 298 K. (b) Benesi-Hildebrand plot constructed for evaluating the binding constant as well as stoichiometry for 2 :C ₆₀ host-guest complex.	260
Figure A14. (a) Spectral changes observed during the titration of Fullerene (C ₆₀) to the solution of containing H ₂ TEtP (2) in toluene at 298 K. (b) Benesi-Hildebrand plot constructed for evaluating the binding constant as well as stoichiometry for 1 :C ₆₀ host-guest complex.	261
Figure A15. (a) Spectral changes observed during the titration of Fullerene (C ₆₀) to the solution of containing ZnTMeP (1a) in toluene at 298 K. (b) Benesi-Hildebrand plot constructed for evaluating the binding constant as well as	261

stoichiometry for **2a**:C₆₀ host-guest complex.

Figure A16. (a) Spectral changes observed during the titration of Fullerene (C₆₀) to the solution of containing ZnTEtP (**2a**) in toluene at 298 K. (b) Benesi-Hildebrand plot constructed for evaluating the binding constant as well as stoichiometry for **1a**:C₆₀ host-guest complex. 262

Figure A17. (a) Spectral changes observed during the titration of Fullerene (C₆₀) to the solution of containing ZnTPrP (**3a**) in toluene at 298 K. (b) Benesi-Hildebrand plot constructed for evaluating the binding constant as well as stoichiometry for **3a**:C₆₀ host-guest complex. 262

Figure A18. (a) Fluorescence spectral changes observed during the titration of Fullerene (C₆₀) to the solution of H₂TMeP (**1**) in toluene at 298 K. (b) Stern-Volmer plot for **1**:C₆₀ host-guest complex. 263

Figure A19. (a) Fluorescence spectral changes observed during the titration of Fullerene (C₆₀) to the solution of H₂TEtP (**2**) in toluene at 298 K. (b) Stern-Volmer plot for **2**:C₆₀ host-guest complex. 263

Figure A20. (a) Fluorescence spectral changes observed during the titration of Fullerene (C₆₀) to the solution of ZnTMeP (**1a**) in toluene at 298 K. (b) Stern-Volmer plot for **2a**:C₆₀ host-guest complex. 264

Figure A21. (a) Fluorescence spectral changes observed during the titration of Fullerene (C₆₀) to the solution of ZnTEtP (**2a**) in toluene at 298 K. (b) Stern-Volmer plot for **1a**:C₆₀ host-guest complex. 264

Figure A22. (a) Fluorescence spectral changes observed during the titration of Fullerene (C₆₀) to the solution of ZnTPrP (**3a**) in toluene at 298 K. (b) Stern-Volmer plot for **3a**:C₆₀ host-guest complex. 265

Figure A23. (a) Spectral changes observed during the titration of Fullerene (C₆₀) to the solution of H₂TEtP (**2**) in PhCN at 298 K. (b) Benesi-Hildebrand plot constructed for evaluating the binding constant as well as stoichiometry for **3**:C₆₀ host-guest complex. 265

Figure A24. (a) Spectral changes observed during the titration of Fullerene (C₂₅₄₆₀) to the solution of H₂TPrP (**3**) in PhCN at 298 K. (b) Benesi-Hildebrand plot constructed for evaluating the binding constant as well as stoichiometry for 266

2:C₆₀ host-guest complex.

Figure A25. ¹H NMR spectra in C₆D₆ (a) **2**:C₆₀ adduct (b) **2**. 266

Figure A26. ¹H NMR spectra in C₆D₆ (a) **3**:C₆₀ adduct (b) **3**. 267

Figure A27. ¹H NMR spectra in C₆D₆ (a) **1a**:C₆₀ adduct (b) **1a**. 267

Figure A28. ¹H NMR spectra in C₆D₆ (a) **2a**:C₆₀ adduct (b) **2a**. 268

Figure A29. ¹H NMR spectra in C₆D₆ (a) **3a**:C₆₀ adduct (b) **3a**. 268

Figure A30. Change in the chemical shift of β-pyrrole proton in **3** by addition of C₆₀ in C₆D₆. The solid line is the theoretical isotherm obtained by nonlinear curve-fitting to experimental data points. The observed association constant (K) $3.4 \times 10^4 \text{ M}^{-1}$ which is close to the value obtained from UV-Vis titration in toluene at 298 K. 269

Table A2. Change in chemical shift of protons by adding 1.1 eq. C₆₀ to the solution of **1-3** and **1a-3a** in C₆D₆ 270

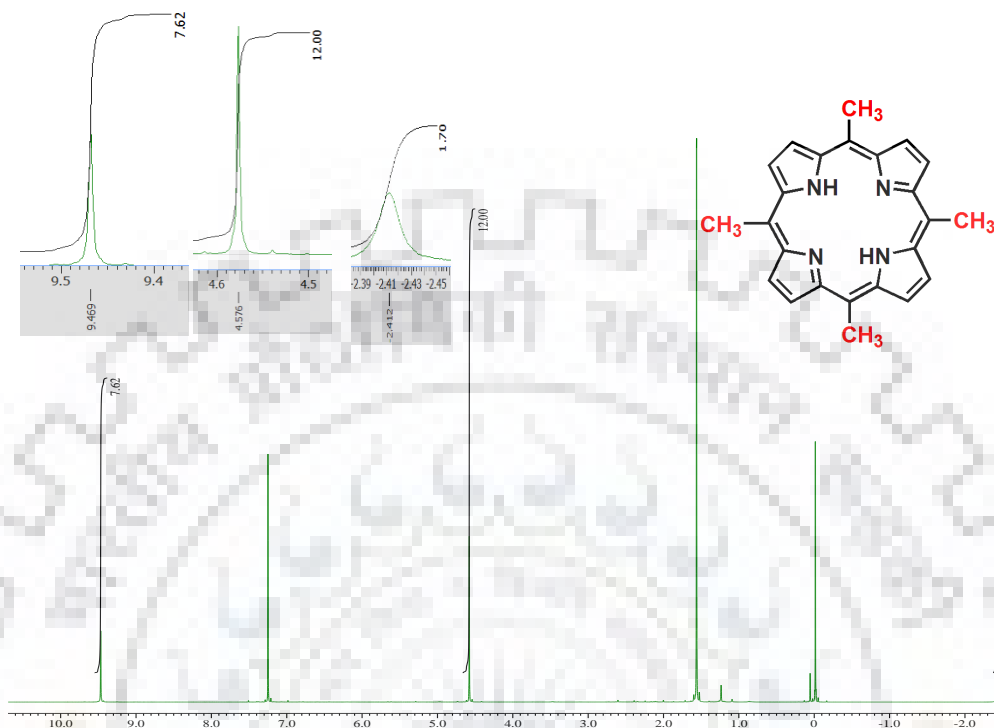


Figure A1. ¹H NMR spectrum of H₂TMeP (1) in CDCl₃ at 298 K.

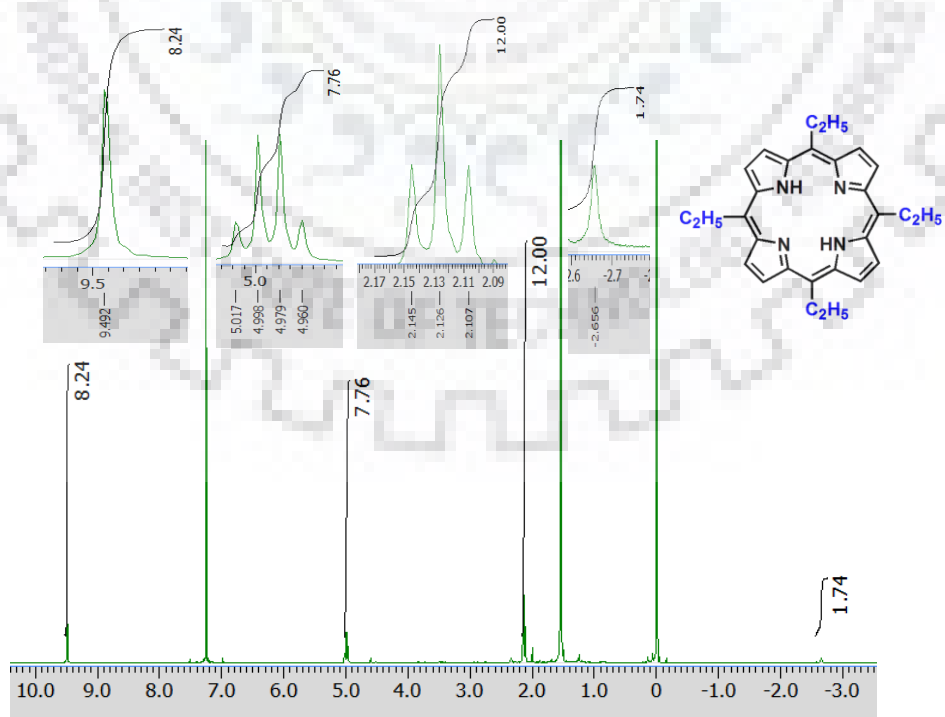


Figure A2. ^1H NMR spectrum of H_2TetP (**2**) in CDCl_3 at 298 K.

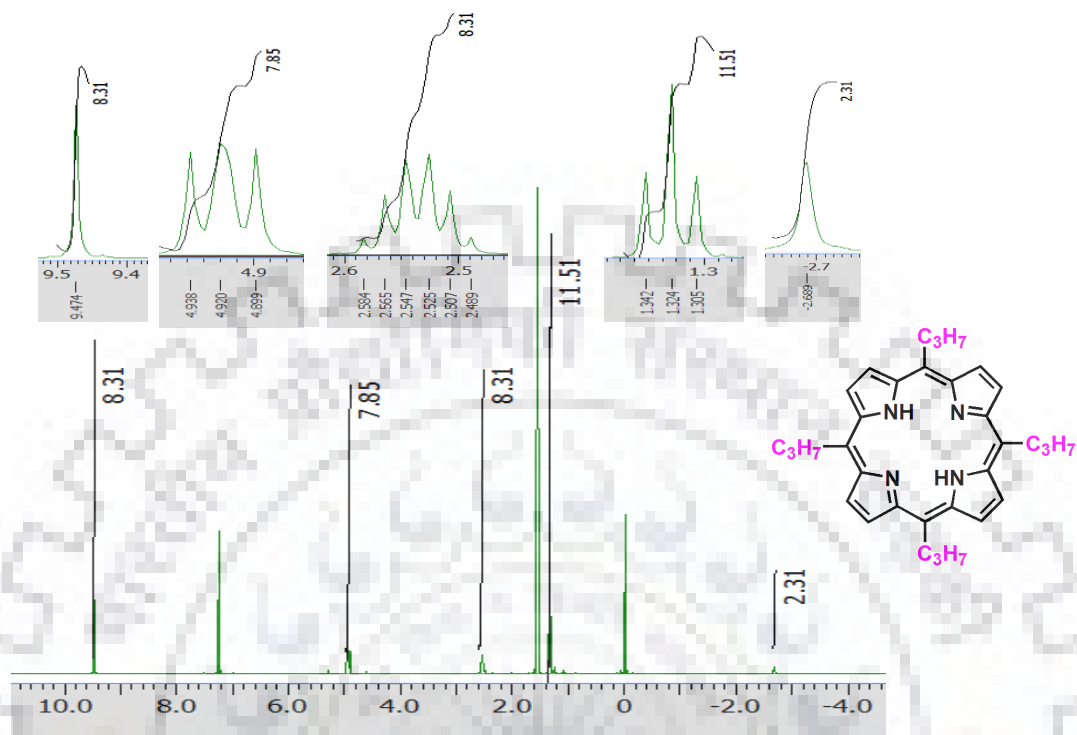


Figure A3. ^1H NMR spectrum of H_2TPrP (**3**) in CDCl_3 at 298 K.

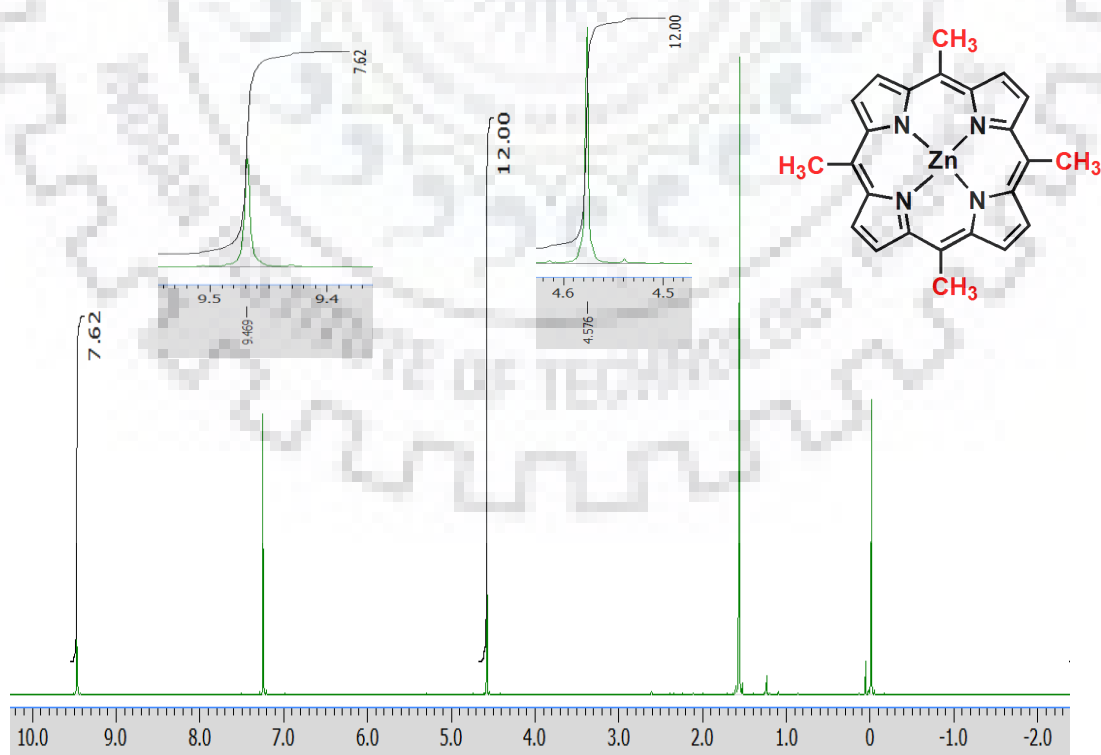


Figure A4. ^1H NMR spectrum of ZnTMeP (**1a**) in CDCl_3 at 298 K.

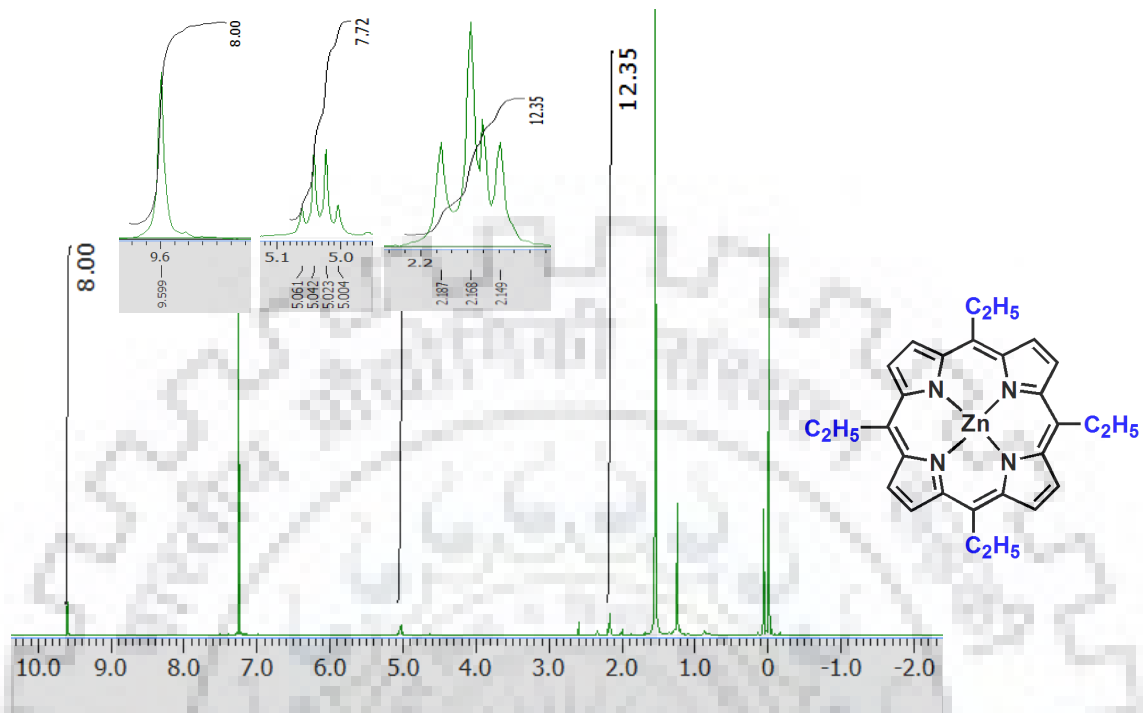


Figure A5. ^1H NMR spectrum of ZnTtEtP (**2a**) in CDCl_3 at 298 K.

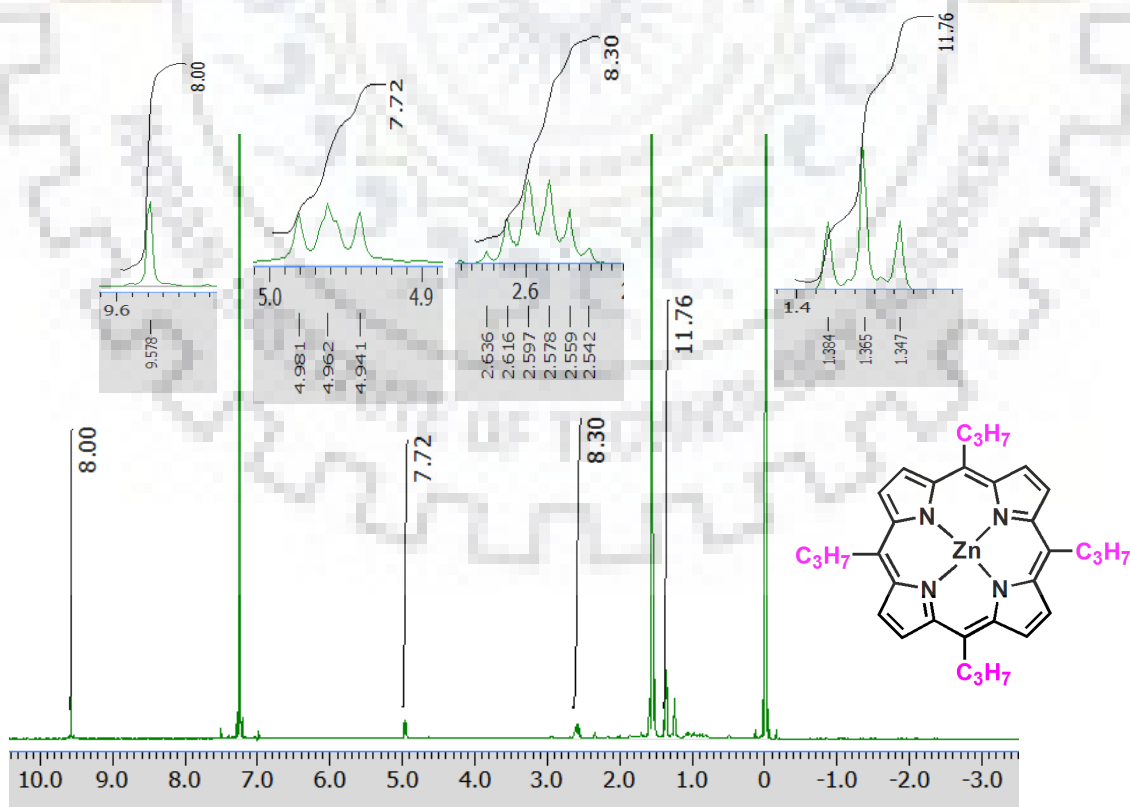


Figure A6. ^1H NMR spectrum of ZnTPrP (**3a**) in CDCl_3 at 298 K.

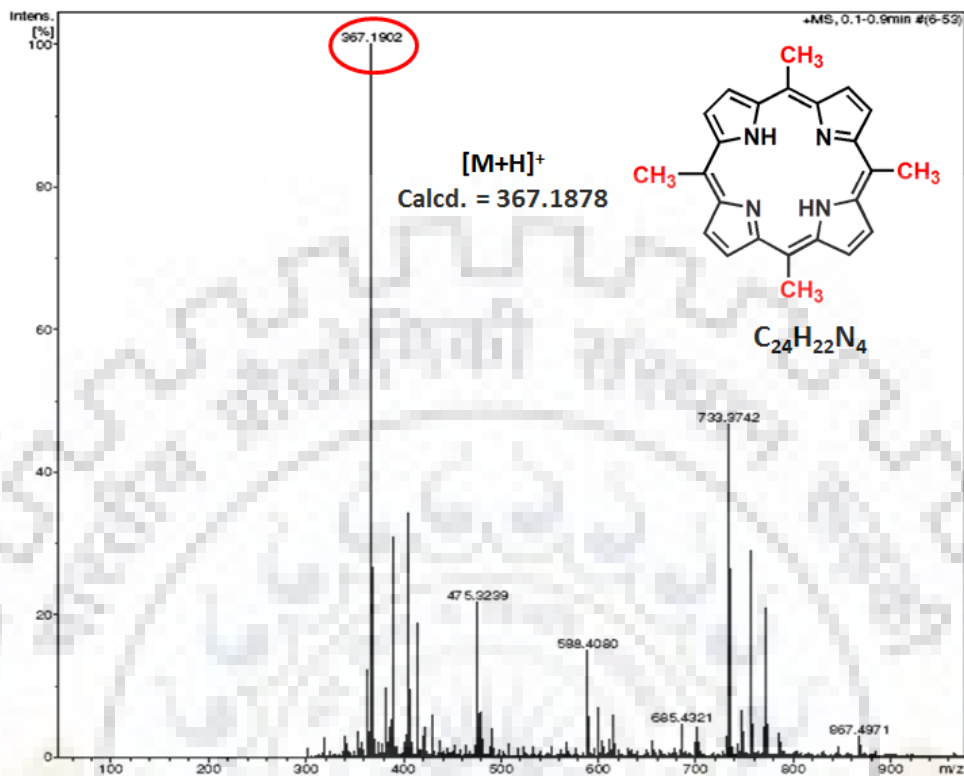


Figure A7. ESI-MS spectrum of H₂TMeP (**1**) in CH_3CN .

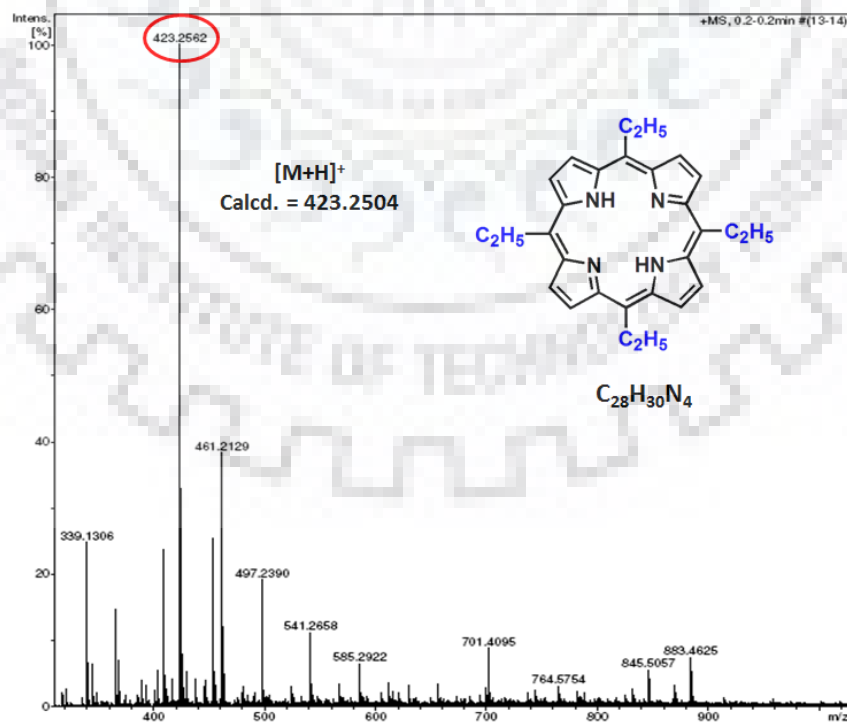


Figure A8. ESI-MS spectrum of H₂TtP (2) in CH₃CN.

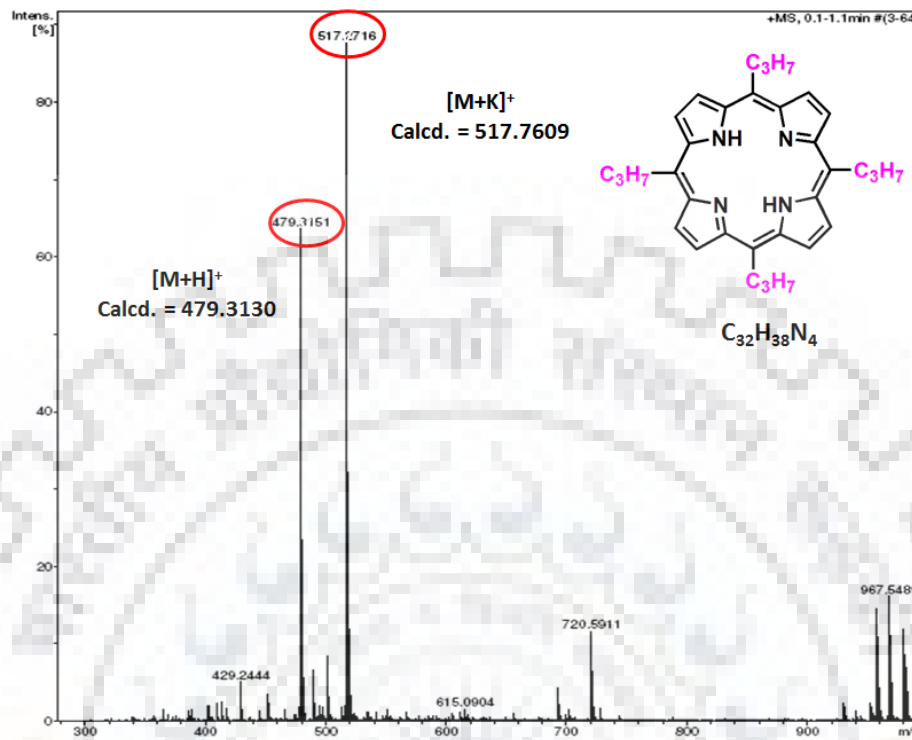


Figure A9. ESI-MS spectrum of H₂TPrP (3) in CH₃CN.

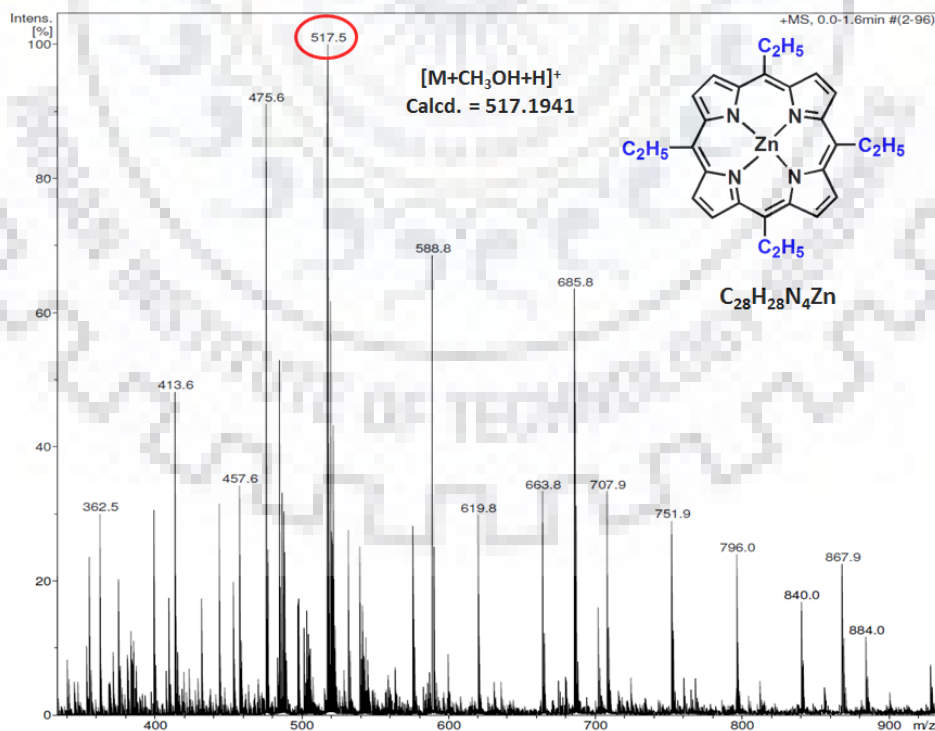
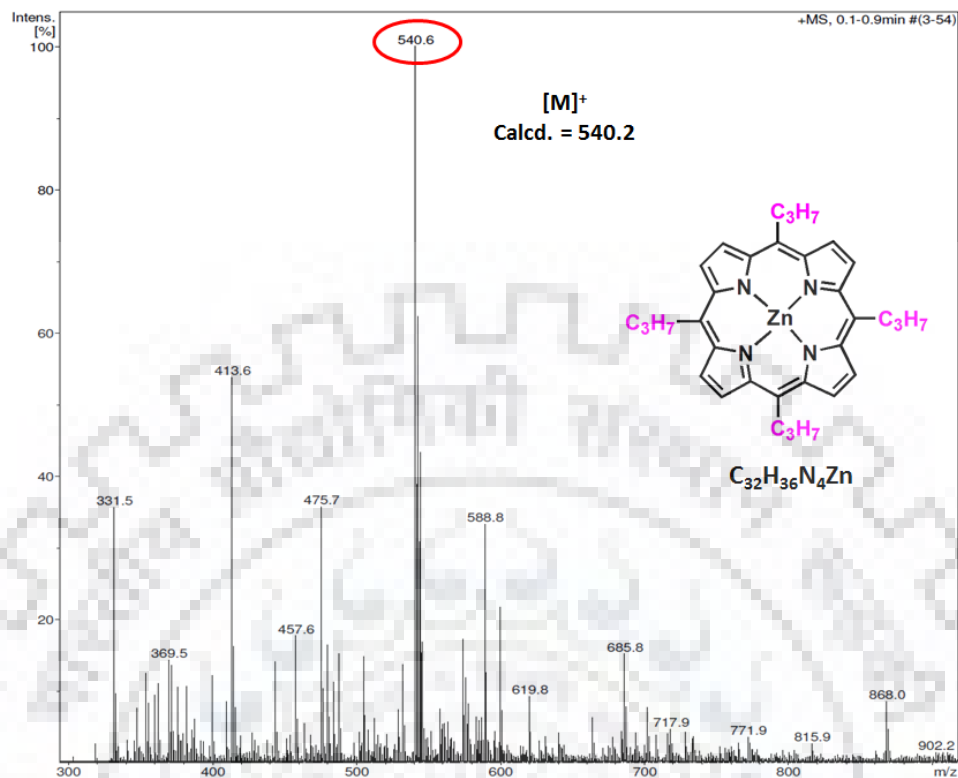


Figure A10. ESI-MS spectrum of ZnTtP (2a) in CH₃CN.

Figure A11. ESI-MS spectrum of ZnTPrP (**3a**) in CH₃CN.

Empirical formula	C ₃₂ H ₃₈ N ₄
Formula Wt.	478.66
Crystal system	monoclinic
Space group	P 21/n
a (Å)	5.0843
b (Å)	11.6075
c (Å)	22.1697
α (°)	90
B (°)	93.53
γ (°)	90
Volume (Å ³)	1305.88
Z	2
D _{calcd} (mg/m ³)	1.217
Wavelength	0.71073
T	293 K
No. of total refins	575
No. of indent. refins	515
R ^a	0.0533
R _w ^b	0.1313
CCDC	1051569

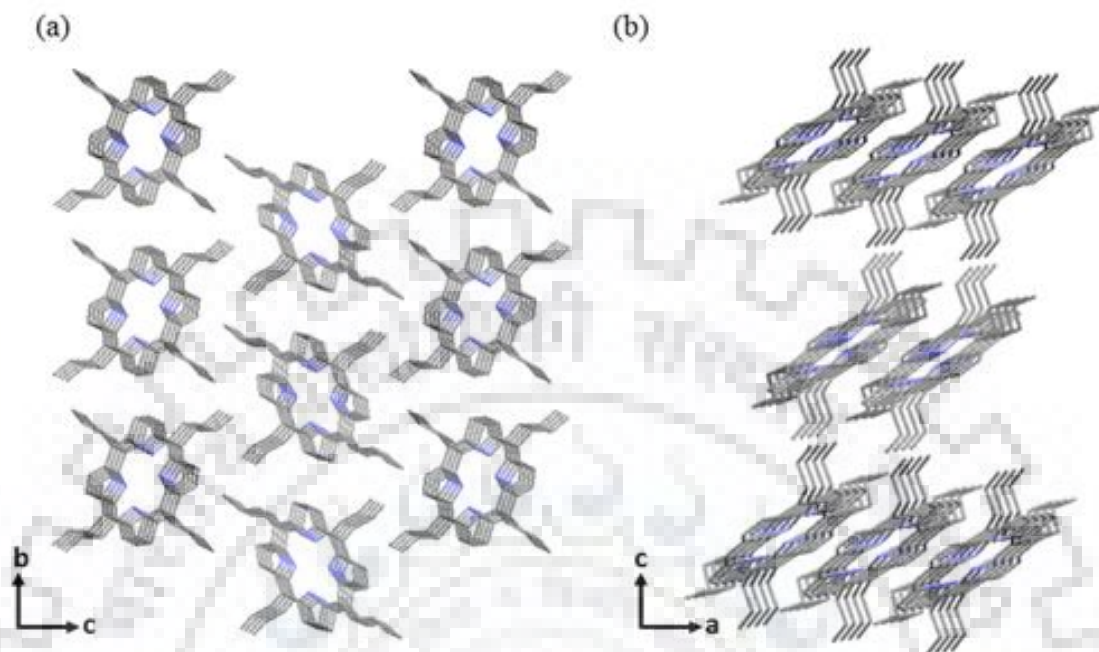


Figure A12. Molecular crystal packing of H_2TPrP (**3**) along (a) a axis and (b) b axis, respectively.

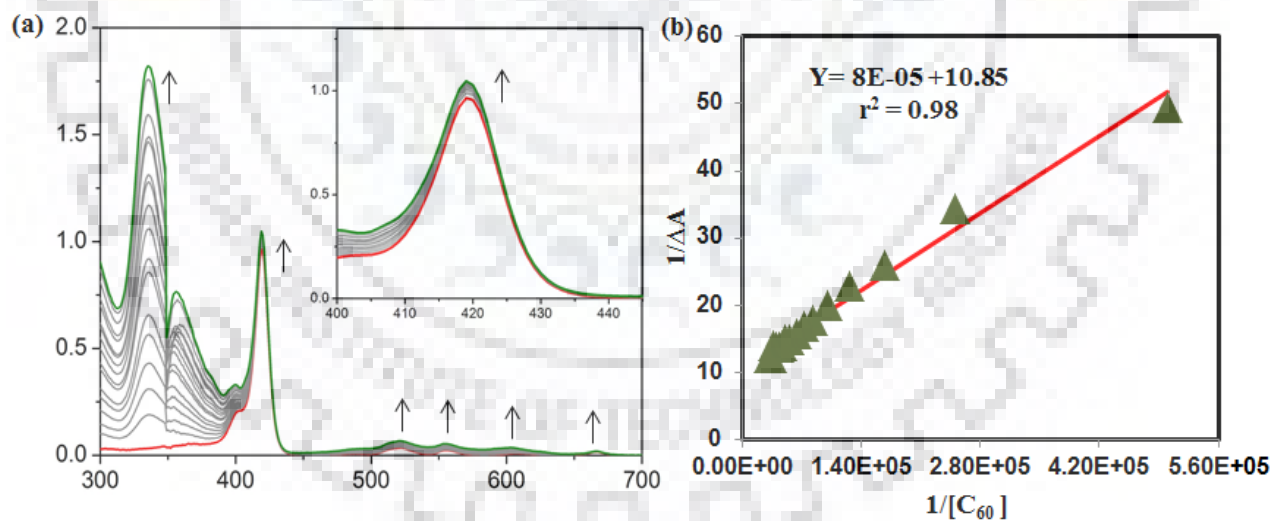


Figure A13. (a) Spectral changes observed during the titration of Fullerene (C_{60}) to the solution of containing H_2TMeP (**1**) in toluene at 298 K. (b) Benesi-Hildebrand plot constructed for evaluating the binding constant as well as stoichiometry for **1**: C_{60} host-guest complex.

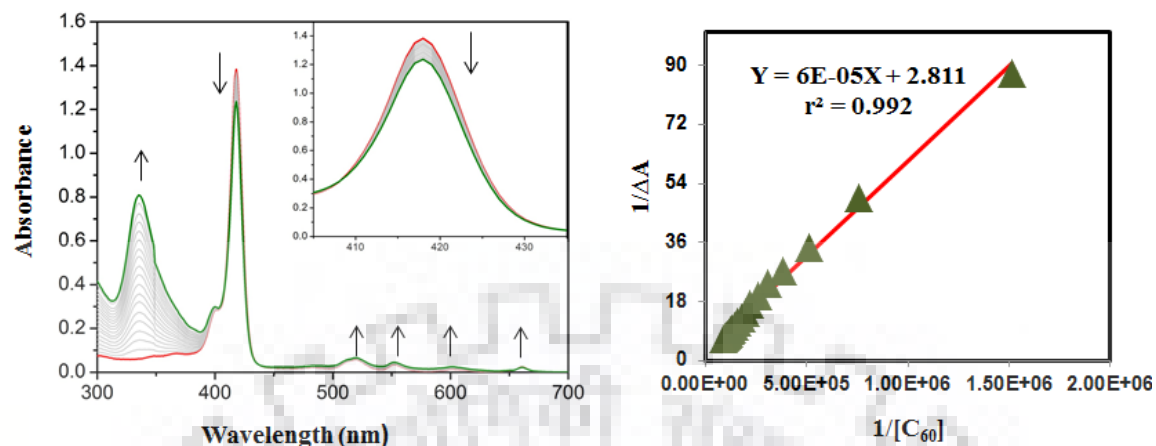


Figure A14. (a) Spectral changes observed during the titration of Fullerene (C₆₀) to the solution of containing H₂TEtP (**2**) in toluene at 298 K. (b) Benesi-Hildebrand plot constructed for evaluating the binding constant as well as stoichiometry for **2**:C₆₀ host-guest complex.

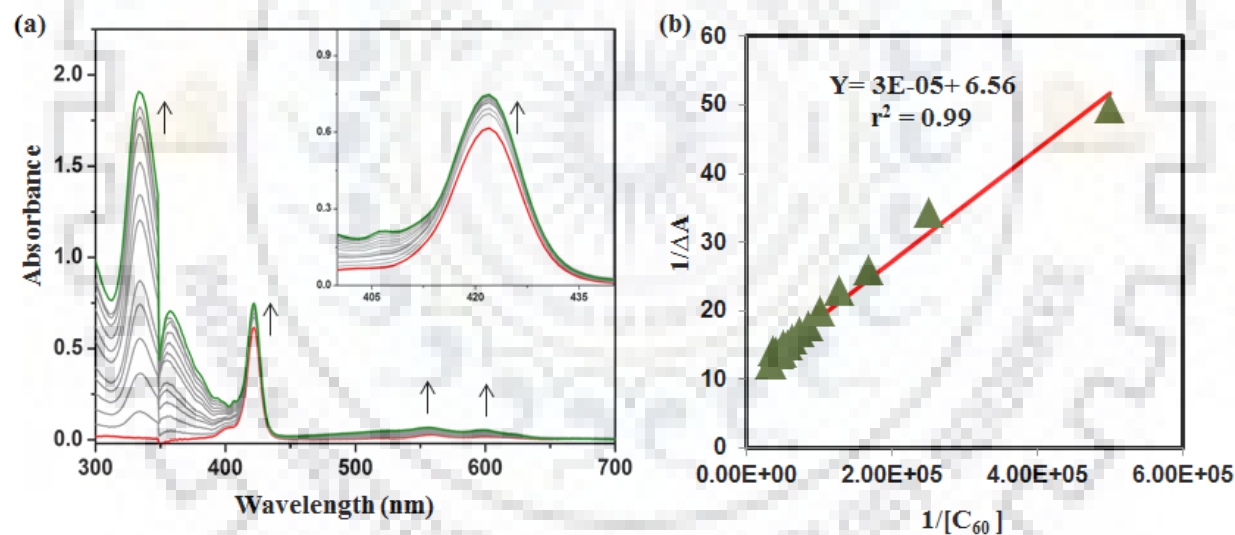


Figure A15. (a) Spectral changes observed during the titration of Fullerene (C₆₀) to the solution of containing ZnTMeP (**1a**) in toluene at 298 K. (b) Benesi-Hildebrand plot constructed for evaluating the binding constant as well as stoichiometry for **1a**:C₆₀ host-guest complex.

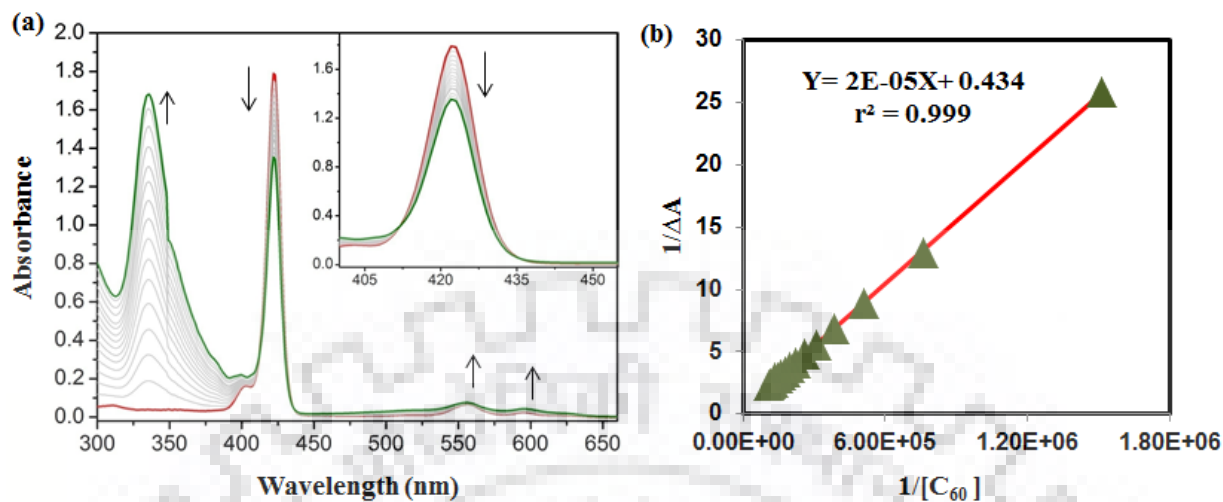


Figure A16. (a) Spectral changes observed during the titration of Fullerene (C₆₀) to the solution of containing ZnTEtP (**2a**) in toluene at 298 K. (b) Benesi-Hildebrand plot constructed for evaluating the binding constant as well as stoichiometry for **2a**:C₆₀ host-guest complex.

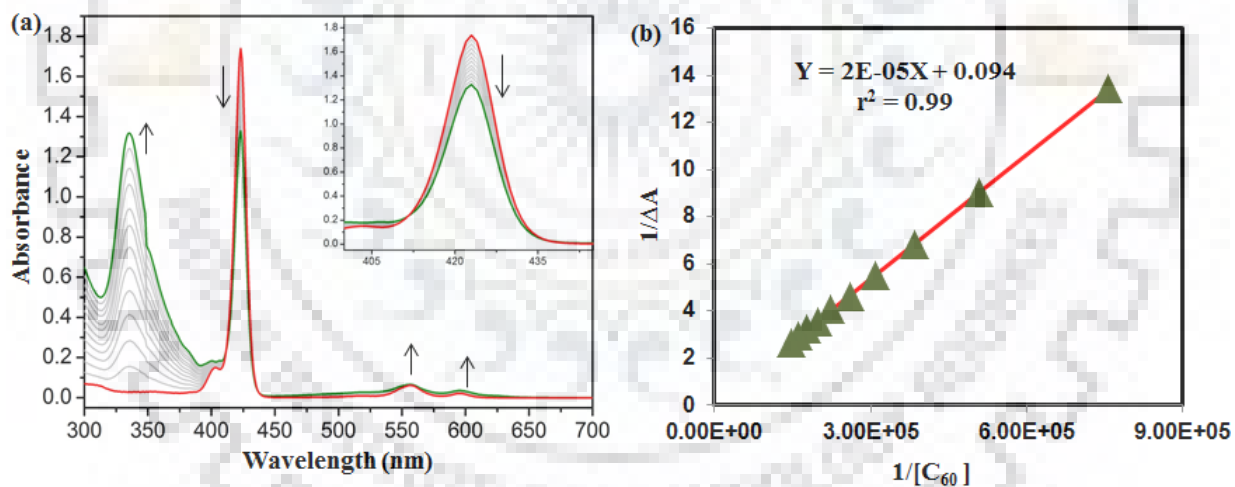


Figure A17. (a) Spectral changes observed during the titration of Fullerene (C₆₀) to the solution of containing ZnTPrP (**3a**) in toluene at 298 K. (b) Benesi-Hildebrand plot constructed for evaluating the binding constant as well as stoichiometry for **3a**:C₆₀ host-guest complex.

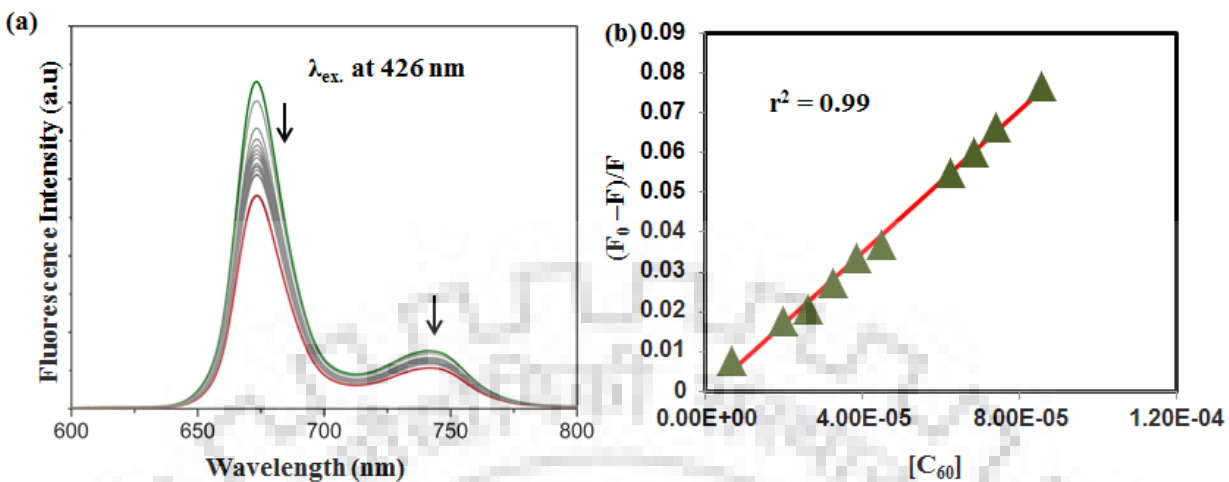


Figure A18. (a) Fluorescence spectral changes observed during the titration of Fullerene (C₆₀) to the solution of H₂TMeP (**1**) in toluene at 298 K. (b) Stern-Volmer plot for **1**:C₆₀ host-guest complex.

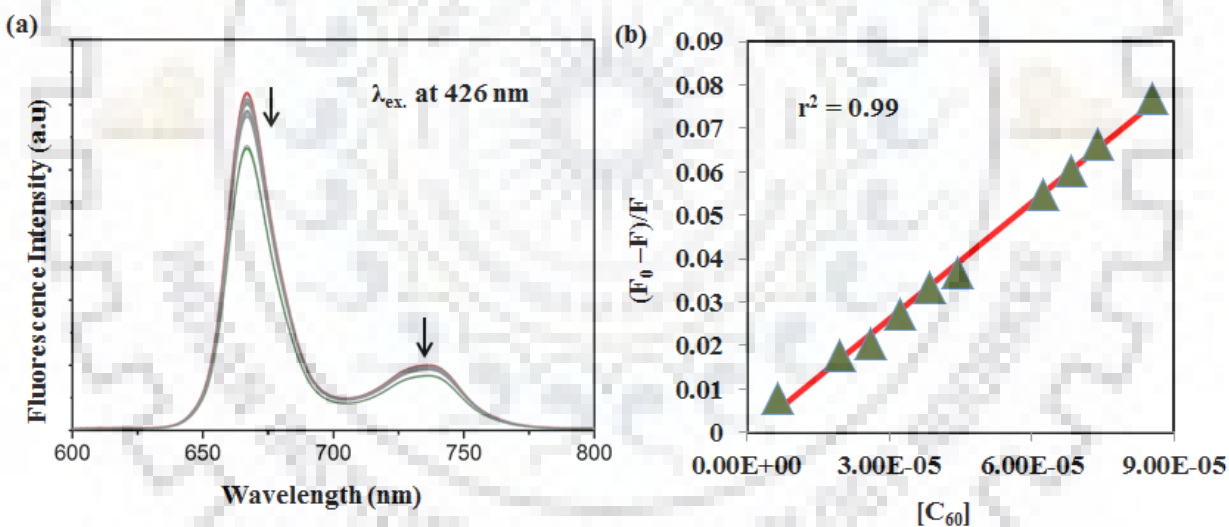


Figure A19. (a) Fluorescence spectral changes observed during the titration of Fullerene (C₆₀) to the solution of H₂TEtP (**2**) in toluene at 298 K. (b) Stern-Volmer plot for **2**:C₆₀ host-guest complex.

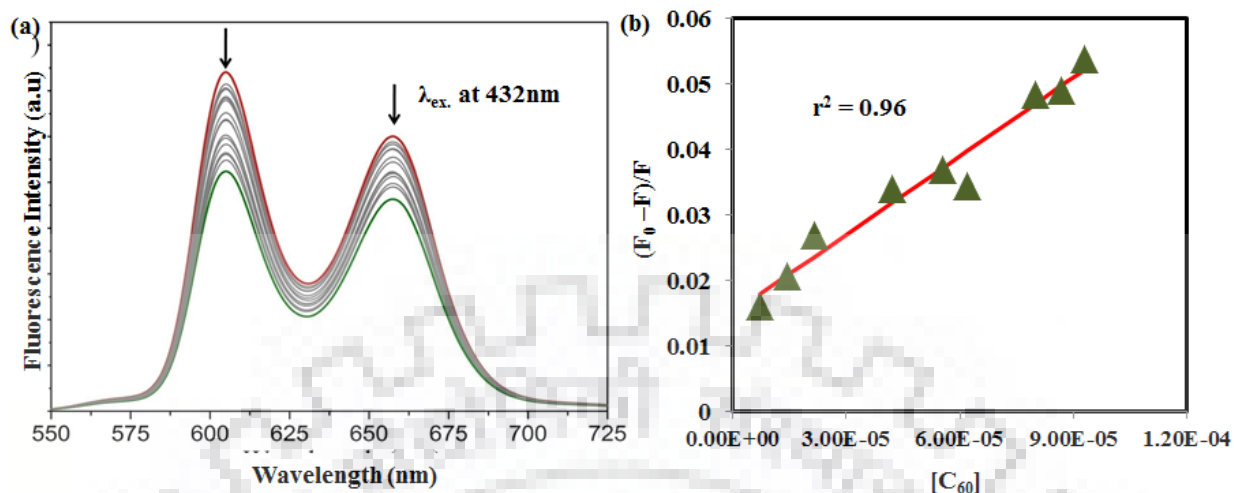


Figure A20. (a) Fluorescence spectral changes observed during the titration of Fullerene (C₆₀) to the solution of ZnTMeP (**1a**) in toluene at 298 K. (b) Stern-Volmer plot for **1a**:C₆₀ host-guest complex.

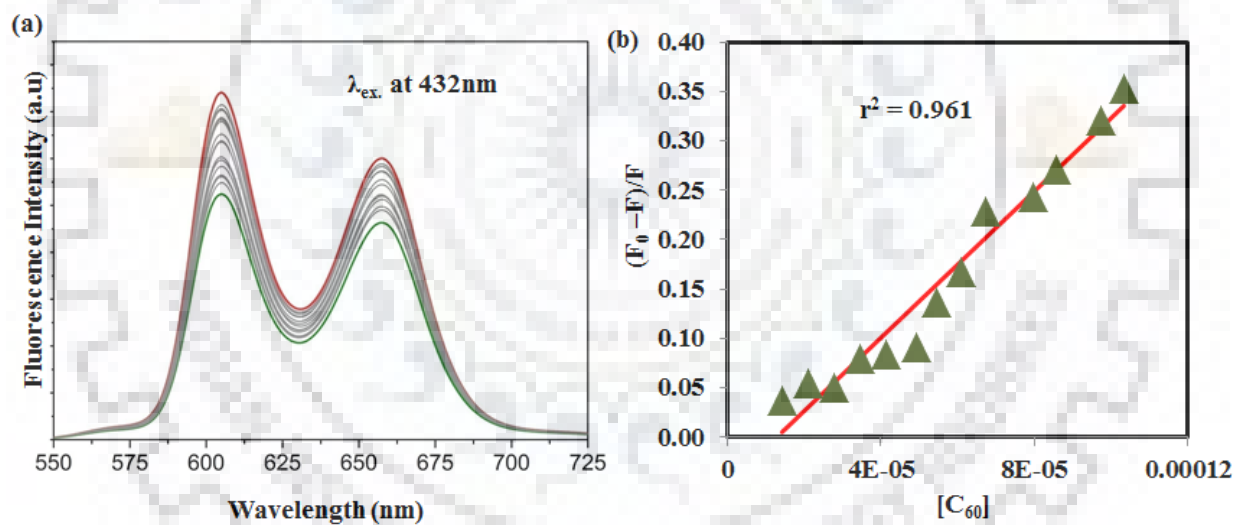


Figure A21. (a) Fluorescence spectral changes observed during the titration of Fullerene (C₆₀) to the solution of ZnTEtP (**2a**) in toluene at 298 K. (b) Stern-Volmer plot for **2a**:C₆₀ host-guest complex.

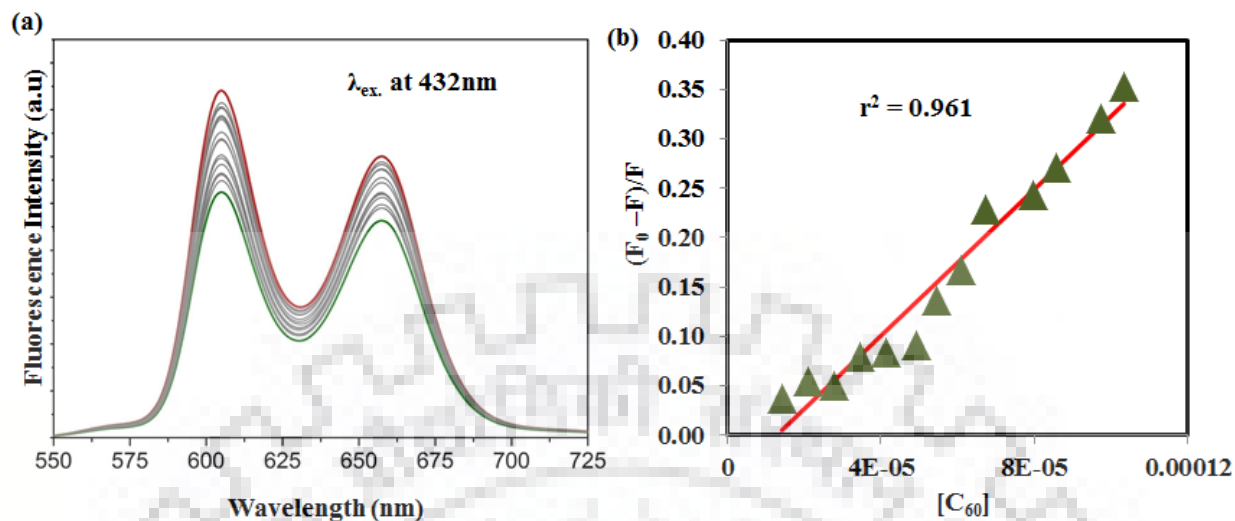


Figure A22. (a) Fluorescence spectral changes observed during the titration of Fullerene (C_{60}) to the solution of ZnTPrP (**3a**) in toluene at 298 K. (b) Stern-Volmer plot for **3a**: C_{60} host-guest complex.

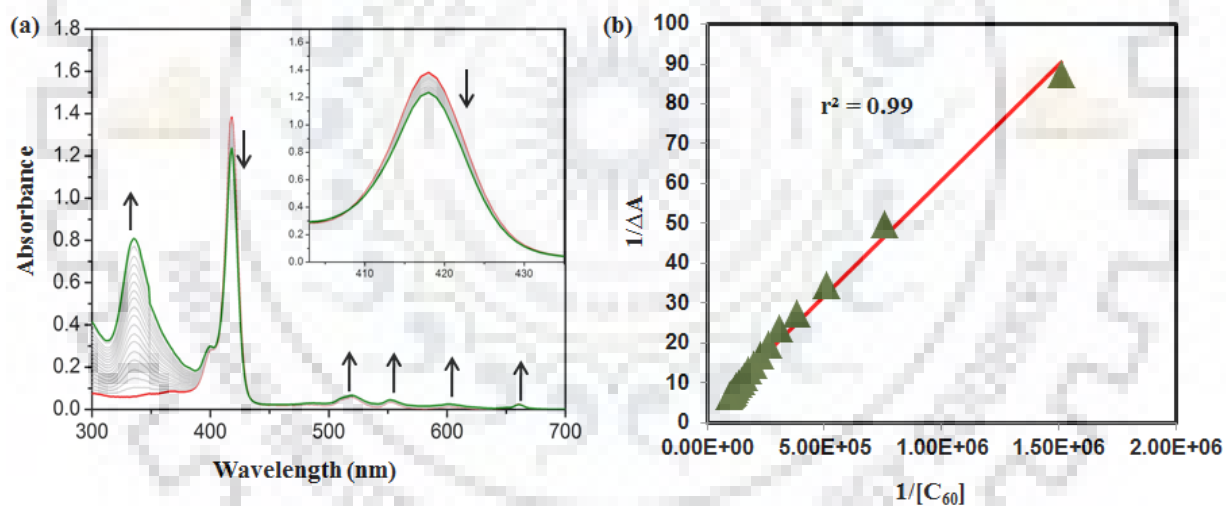


Figure A23. (a) Spectral changes observed during the titration of Fullerene (C_{60}) to the solution of H_2TetP (**2**) in PhCN at 298 K. (b) Benesi-Hildebrand plot constructed for evaluating the binding constant as well as stoichiometry for **2**: C_{60} host-guest complex.

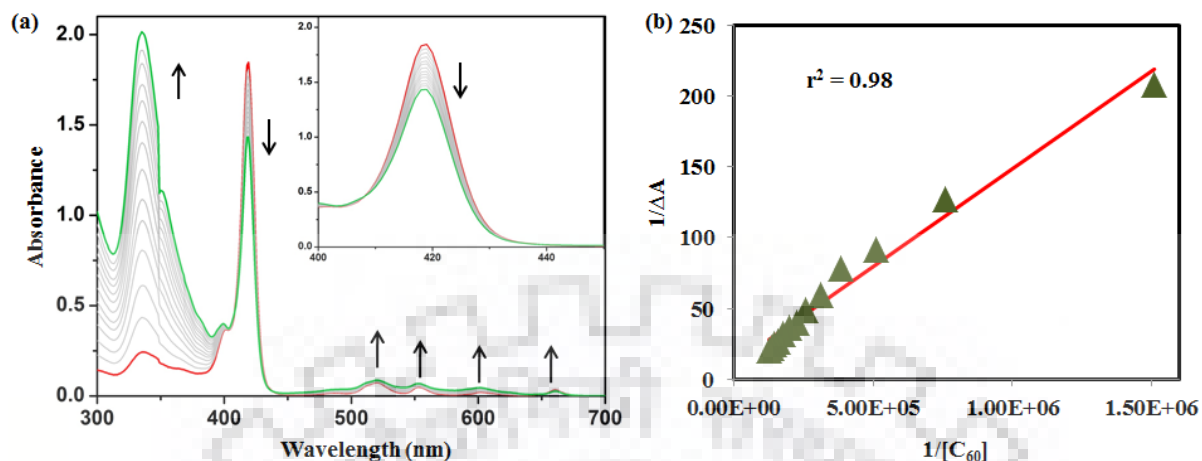


Figure A24. (a) Spectral changes observed during the titration of Fullerene (C₆₀) to the solution of H₂TPrP (**3**) in PhCN at 298 K. (b) Benesi-Hildebrand plot constructed for evaluating the binding constant as well as stoichiometry for **3**:C₆₀ host-guest complex.



Figure A25. ¹H NMR spectra of (a) **2**:C₆₀ adduct (b) **2** in C₆D₆ at 298 K.

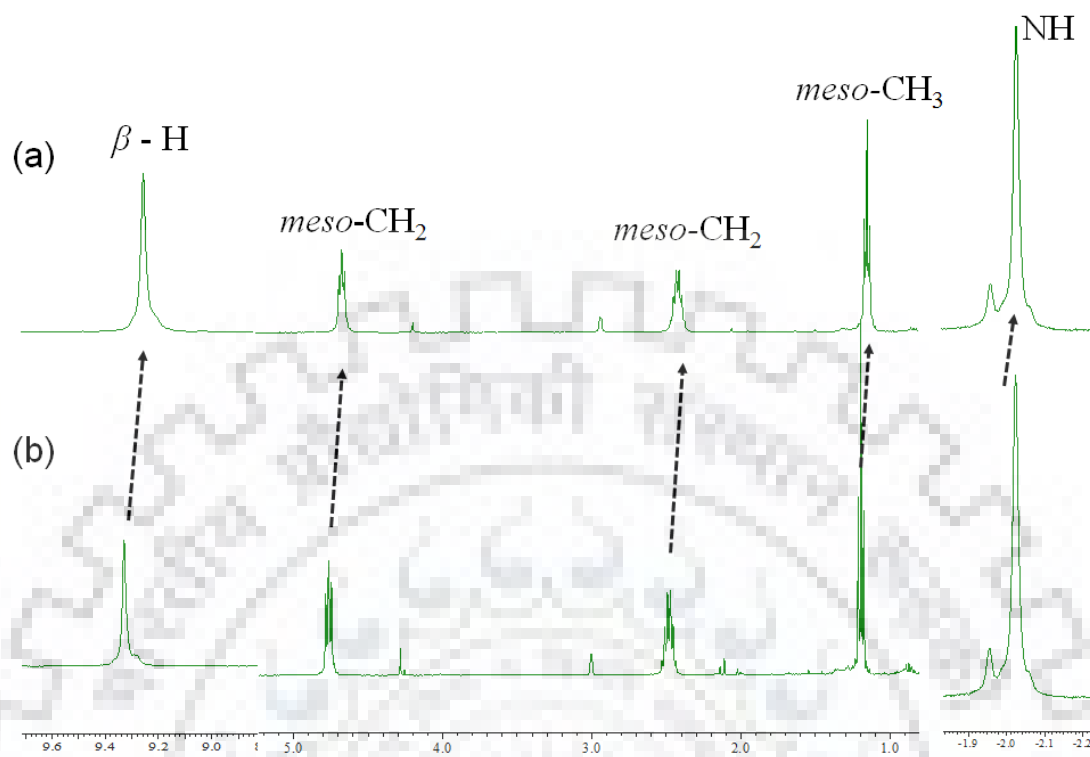


Figure A26. ¹H NMR spectra of (a) **3**:C₆₀ adduct (b) **3** in C₆D₆ at 298 K.

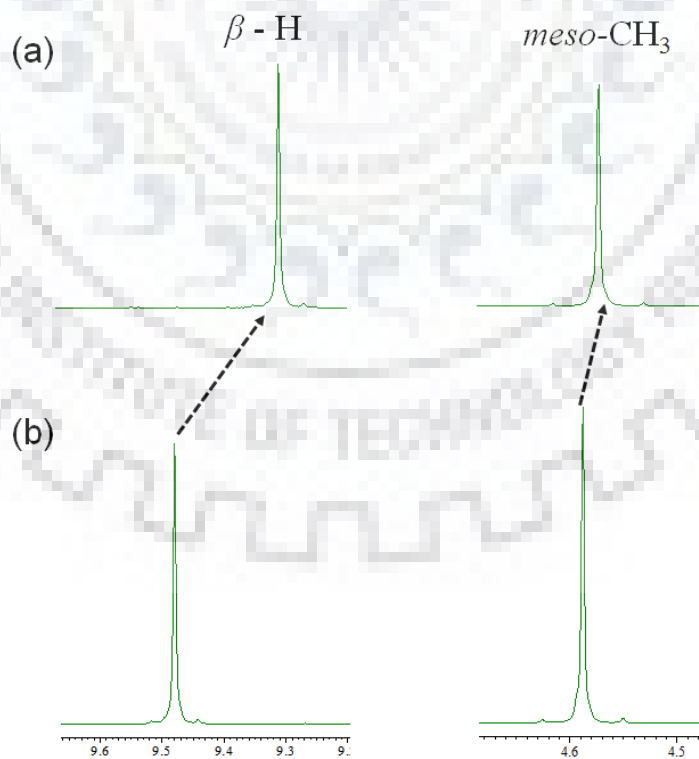


Figure A27. ¹H NMR spectra of (a) **1a**:C₆₀ adduct (b) **1a** in C₆D₆ at 298 K.

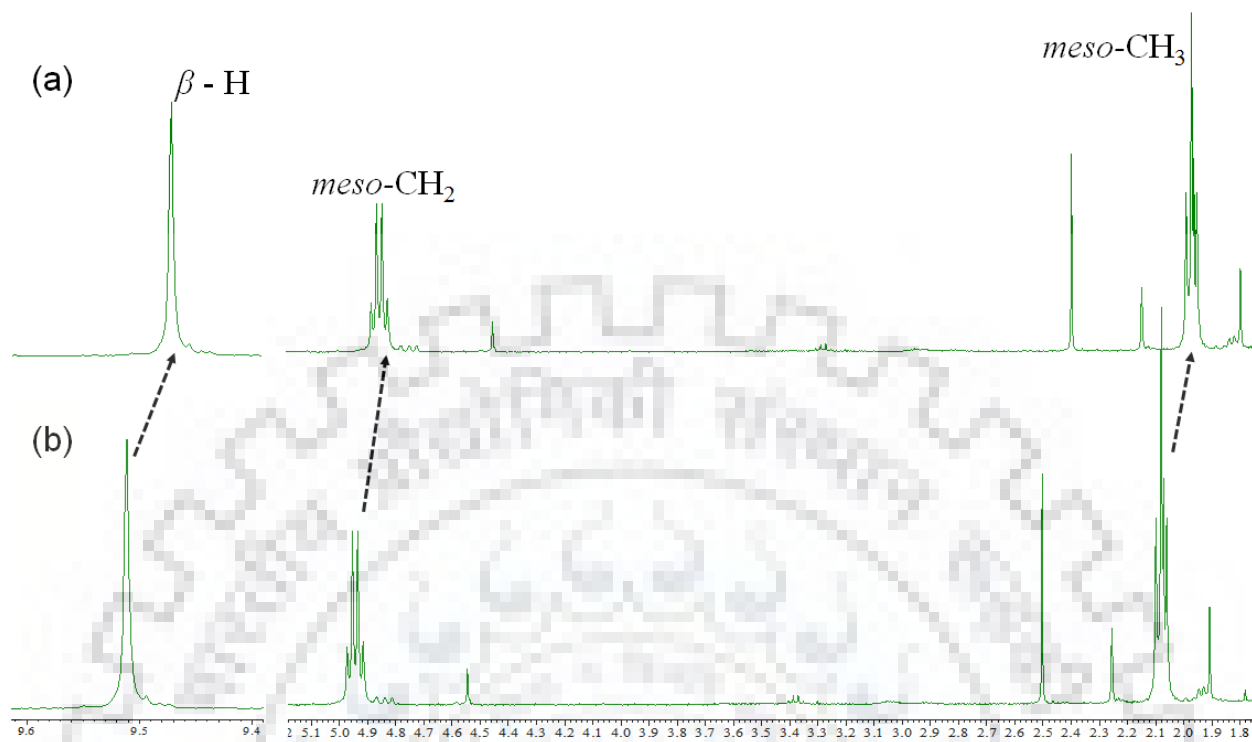


Figure A28. ¹H NMR spectra of (a) **2a**:C₆₀ adduct (b)**2a** in C₆D₆ at 298 K.

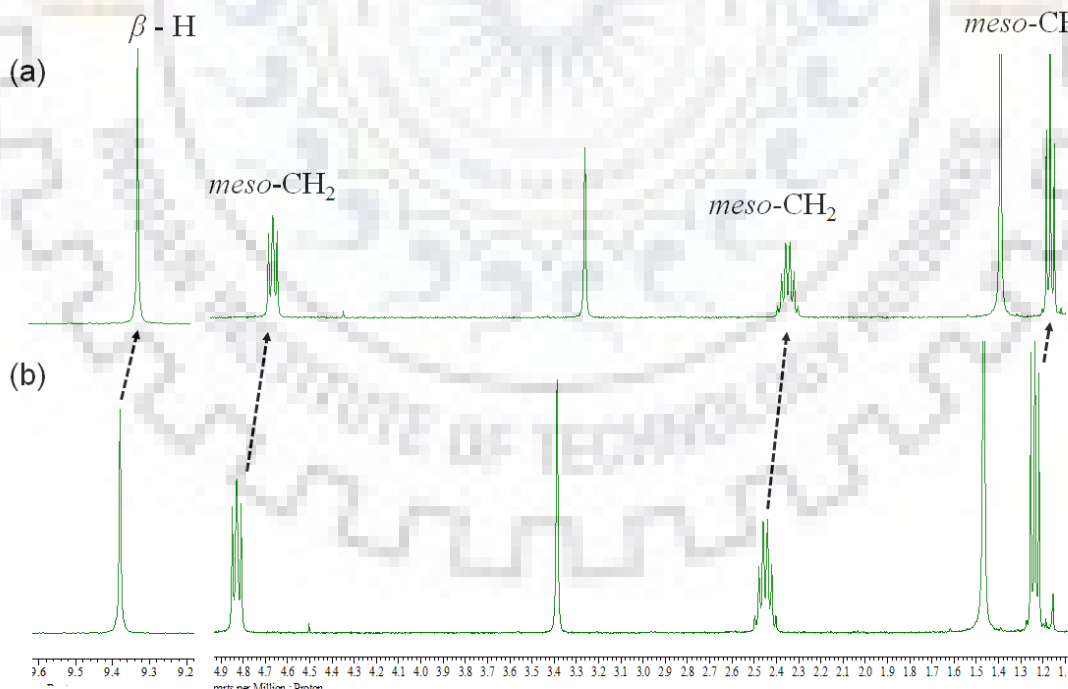


Figure A29. ¹H NMR spectra of (a) **3a**:C₆₀ adduct (b)**3a** in C₆D₆ at 298 K.

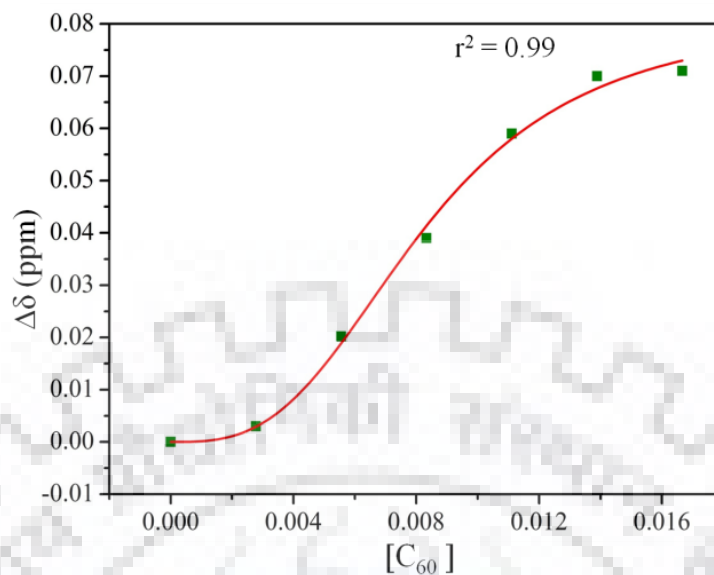


Figure A30. Change in the chemical shift of β -pyrrole proton in **3** by addition of C₆₀ in C₆D₆. The solid line is the theoretical isotherm obtained by nonlinear curve-fitting to experimental data points. The observed association constant (K) $3.4 \times 10^4 \text{ M}^{-1}$ which is close to the value obtained from UV-Vis titration in toluene at 298 K.

Table A2. Change in chemical shift of protons by adding 1.1 eq. C₆₀ to the solution of 1-3 and 1a-3a in C₆D₆.

Porphyrin	Chemical Shift (δ ppm)				
	β -H	<i>meso</i> -CH ₃	<i>meso</i> -CH ₂	<i>meso</i> -CH ₂	NH
1	9.220	4.247			-1.744
1:C₆₀	9.113	4.140			-1.851
2	9.404	2.038	4.929-4.872		-2.745
2:C₆₀	9.334	1.968	4.859-4.802		-2.815
3	9.330	1.195	4.765	2.53-2.43	-2.023
3:C₆₀	9.260	1.125	4.695	2.46-2.36	-2.093
1a	9.480	4.588			
1a:C₆₀	9.310	4.418			
2a	9.511	2.080	4.973-4.916		
2a:C₆₀	9.441	2.010	4.903-4.846		
3a	9.380	1.237	4.829	2.497-2.403	
3a:C₆₀	9.310	1.167	4.759	2.420-2.330	

APPENDIX-V

β -Functionalized 'Push-Pull' Porphyrins: Synthesis, Photophysical and Electrochemical Redox Properties and NLO Studies

Table of Contents	Page No.
Figure A1. ^1H NMR spectrum of $\text{H}_2\text{TPP}(\text{TPA})_2\text{NO}_2$ in CDCl_3 at 298 K.	273
Figure A2. ^1H NMR spectrum of $\text{NiTPP}(\text{TPA})_2\text{NO}_2$ in CDCl_3 at 298 K.	273
Figure A3. ^1H NMR spectrum of $\text{ZnTPP}(\text{TPA})_2\text{NO}_2$ in CDCl_3 at 298 K.	274
Figure A4. ^1H NMR spectrum of $\text{H}_2\text{TPP}(\text{TPA})_2\text{CHO}$ in CDCl_3 at 298 K.	274
Figure A5. ^1H NMR spectrum of $\text{NiTPP}(\text{TPA})_2\text{CHO}$ in CDCl_3 at 298 K.	275
Figure A6. ^1H NMR spectrum of $\text{ZnTPP}(\text{TPA})_2\text{CHO}$ in CDCl_3 at 298 K.	275
Figure A7. ^{13}C NMR spectrum of $\text{H}_2\text{TPP}(\text{TPA})_2\text{NO}_2$ in CDCl_3 at 298 K	276
Figure A8. ^{13}C NMR spectrum of $\text{NiTPP}(\text{TPA})_2\text{NO}_2$ in CDCl_3 at 298 K	276
Figure A9. ^{13}C NMR spectrum of $\text{ZnTPP}(\text{TPA})_2\text{NO}_2$ in CDCl_3 at 298 K	277
Figure A10. ^{13}C NMR spectrum of $\text{H}_2\text{TPP}(\text{TPA})_2\text{CHO}$ in CDCl_3 at 298 K	277
Figure A11. ^{13}C NMR spectrum of $\text{NiTPP}(\text{TPA})_2\text{CHO}$ in CDCl_3 at 298 K	278
Figure A12. MALDI-TOF mass spectrum of $\text{H}_2\text{TPP}(\text{TPA})_2\text{NO}_2$.	278
Figure A13. MALDI-TOF mass spectrum of $\text{CoTPP}(\text{TPA})_2\text{NO}_2$.	279
Figure A14. MALDI-TOF mass spectrum of $\text{NiTPP}(\text{TPA})_2\text{NO}_2$.	279
Figure A15. MALDI-TOF mass spectrum of $\text{CuTPP}(\text{TPA})_2\text{NO}_2$.	280
Figure A16. MALDI-TOF mass spectrum of $\text{ZnTPP}(\text{TPA})_2\text{NO}_2$.	280
Figure A17. MALDI-TOF mass spectrum of $\text{H}_2\text{TPP}(\text{TPA})_2\text{CHO}$.	281
Figure A18. MALDI-TOF mass spectrum of $\text{CoTPP}(\text{TPA})_2\text{CHO}$.	281
Figure A19. MALDI-TOF mass spectrum of $\text{NiTPP}(\text{TPA})_2\text{CHO}$.	282
Figure A20. MALDI-TOF mass spectrum of $\text{CuTPP}(\text{TPA})_2\text{CHO}$.	282
Figure A21. MALDI-TOF mass spectrum of $\text{ZnTPP}(\text{TPA})_2\text{CHO}$.	283
Table A1. Selected average bond lengths and bond angles for B3LYP/LANL2DZ optimized geometry of $\text{H}_2\text{TPP}(\text{TPA})_2\text{CHO}/\text{NO}_2$.	284
Figure A22. Cyclic Voltammograms of Porphyrins (a) $\text{MTPP}(\text{TPA})_2\text{NO}_2$ and $\text{MTPP}(\text{TPA})_2\text{CHO}$ ($\text{M} = 2\text{H}, \text{Co(II)}, \text{Ni(II)}, \text{Cu(II)}$ and Zn(II)) and CH_2Cl_2 with Scan	285

Appendix V: β -Functionalized 'Push-Pull' Porphyrins for NLO Application

Rate of 0.1 V/s at 298 K.



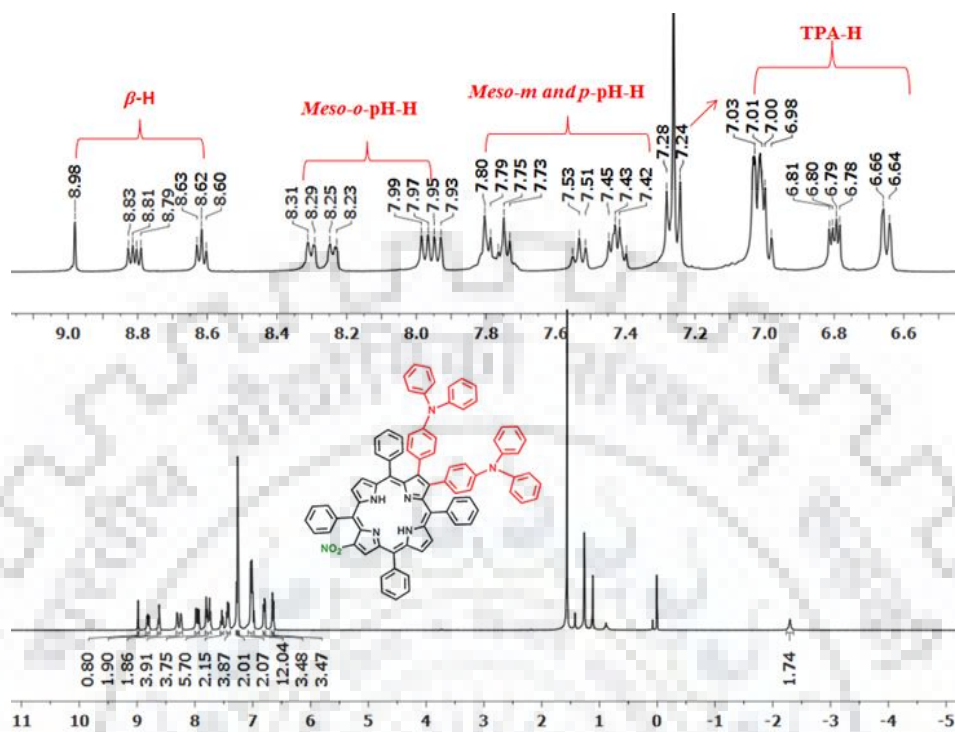


Figure A1. ^1H NMR spectrum of $\text{H}_2\text{TPP}(\text{TPA})_2\text{NO}_2$ in CDCl_3 at 298 K.

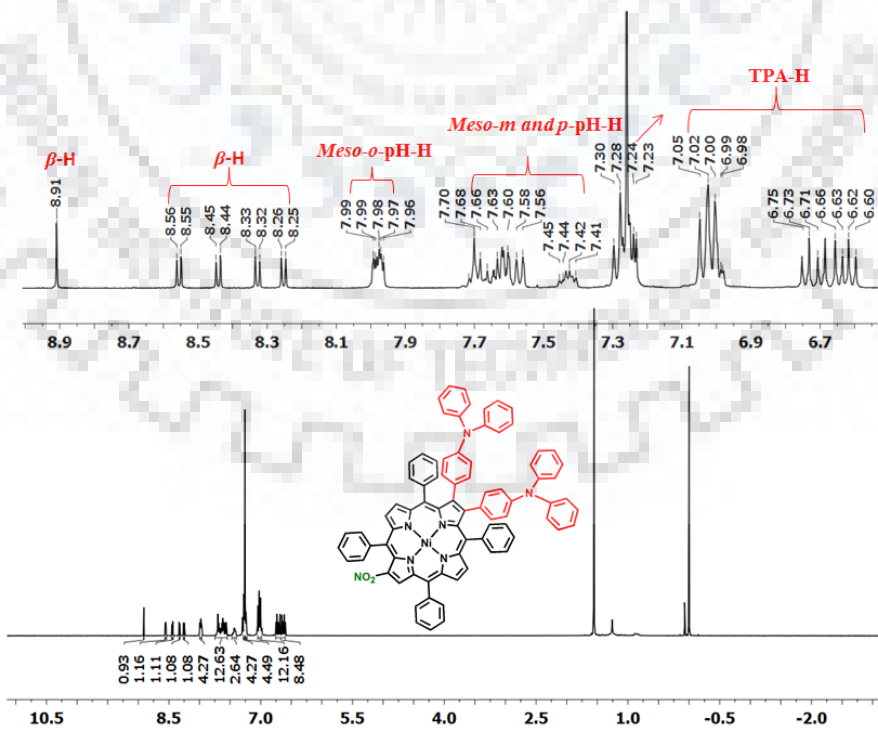


Figure A2. ^1H NMR spectrum of NiTPP(TPA) $_2$ NO $_2$ in CDCl $_3$ at 298 K.

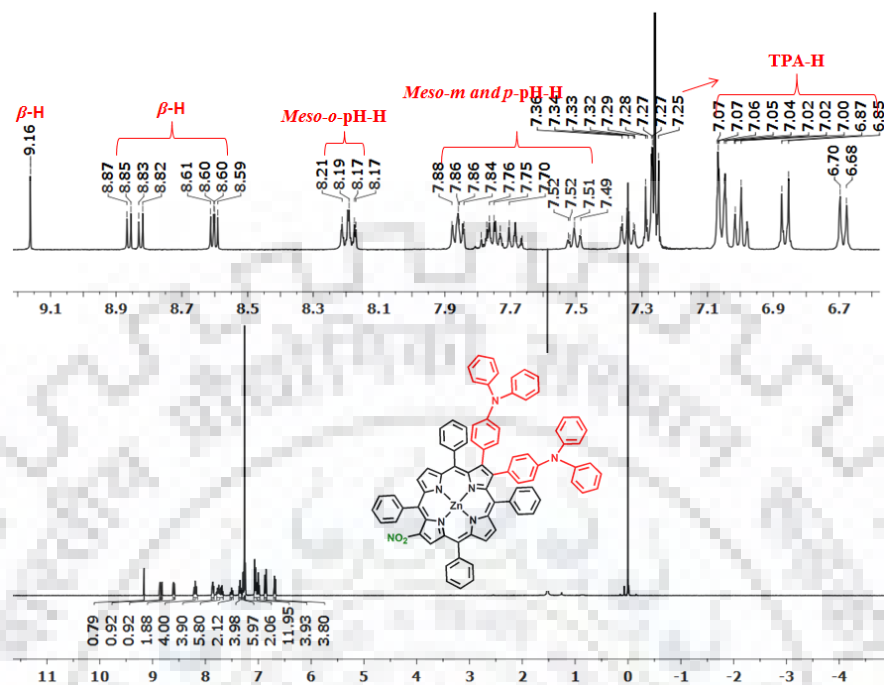


Figure A3. ^1H NMR spectrum of ZnTPP(TPA) $_2$ NO $_2$ in CDCl $_3$ at 298 K.

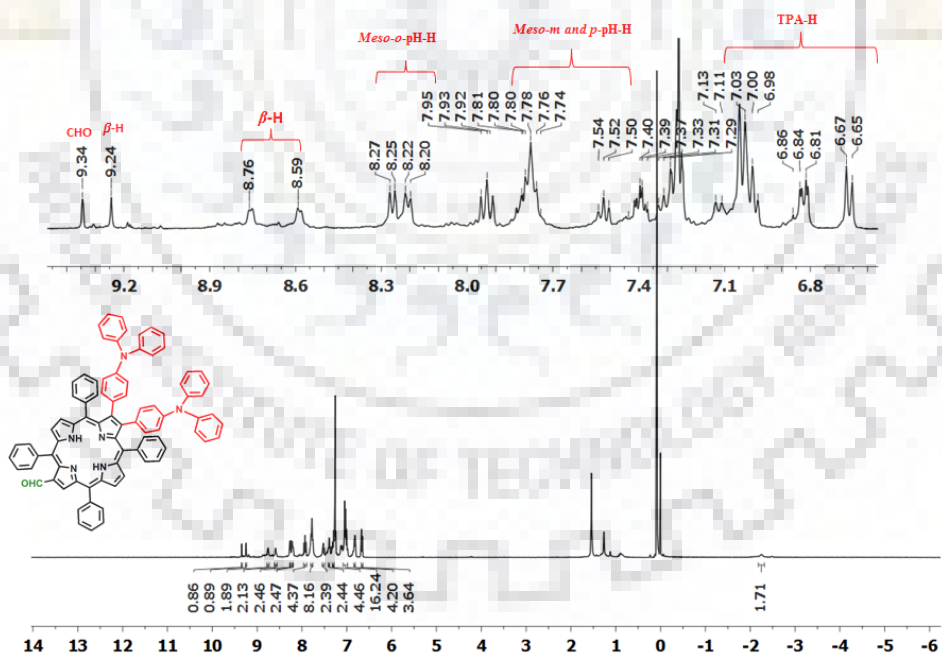


Figure A4. ^1H NMR spectrum of H $_2$ TPP(TPA) $_2$ CHO in CDCl $_3$ at 298 K.

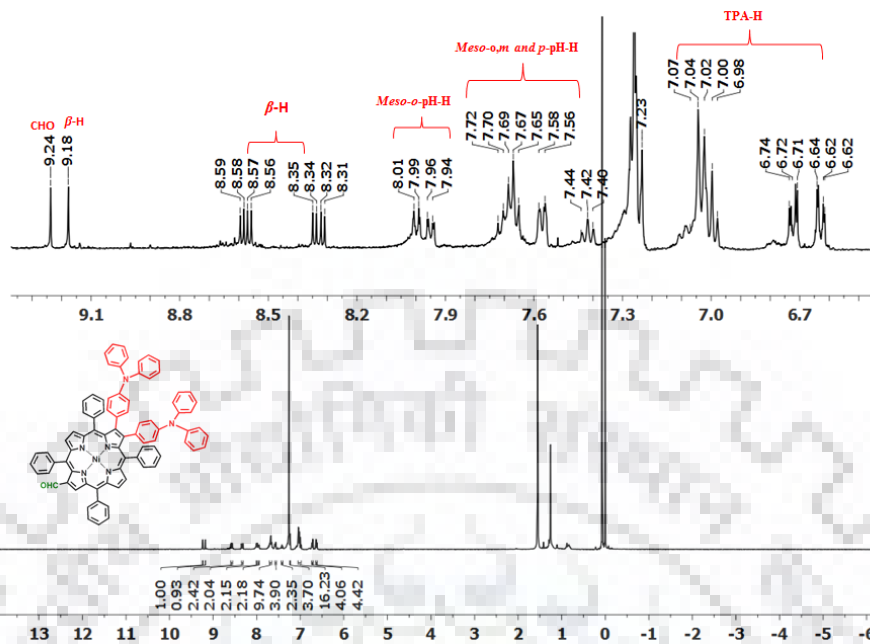


Figure A5. ^1H NMR spectrum of NiTPP(TPA) $_2$ CHO in CDCl_3 at 298 K.

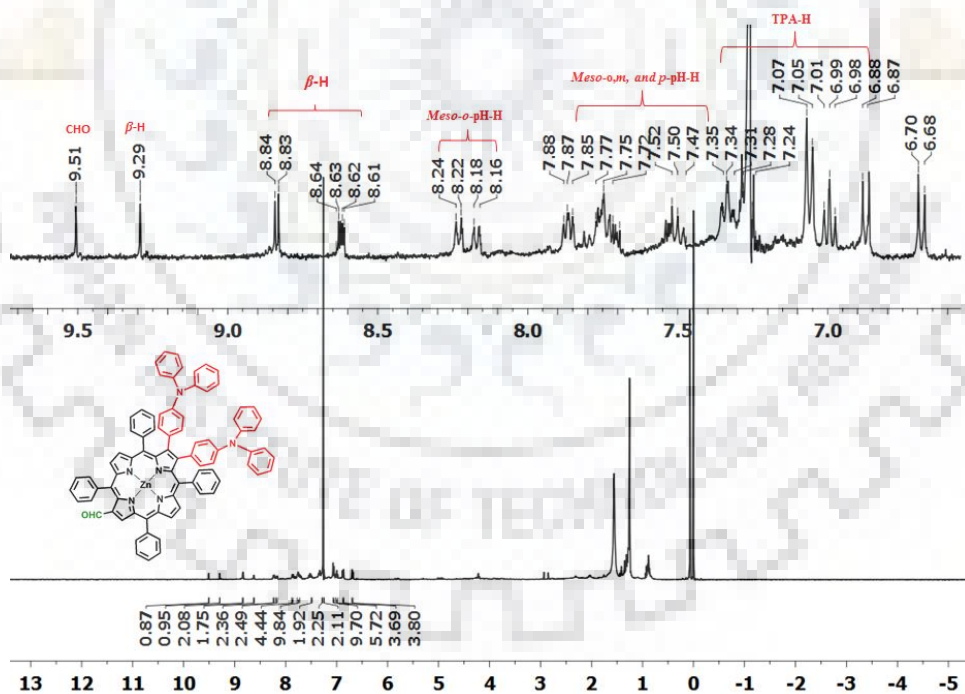


Figure A6. ^1H NMR spectrum of ZnTPP(TPA) $_2$ CHO in CDCl_3 at 298 K.

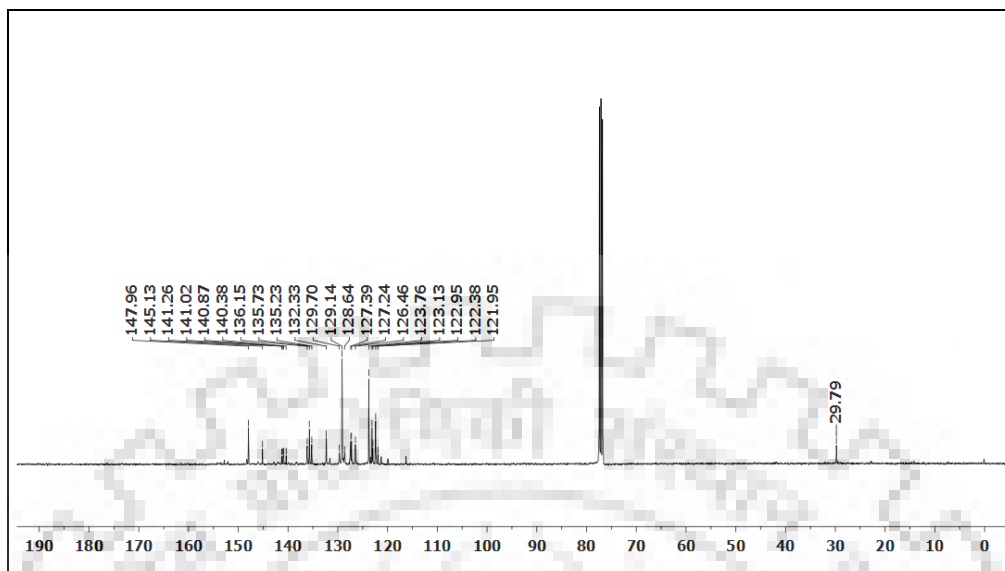


Figure A7. ^{13}C NMR spectrum of $\text{H}_2\text{TPP}(\text{TPA})_2\text{NO}_2$ in CDCl_3 at 298 K

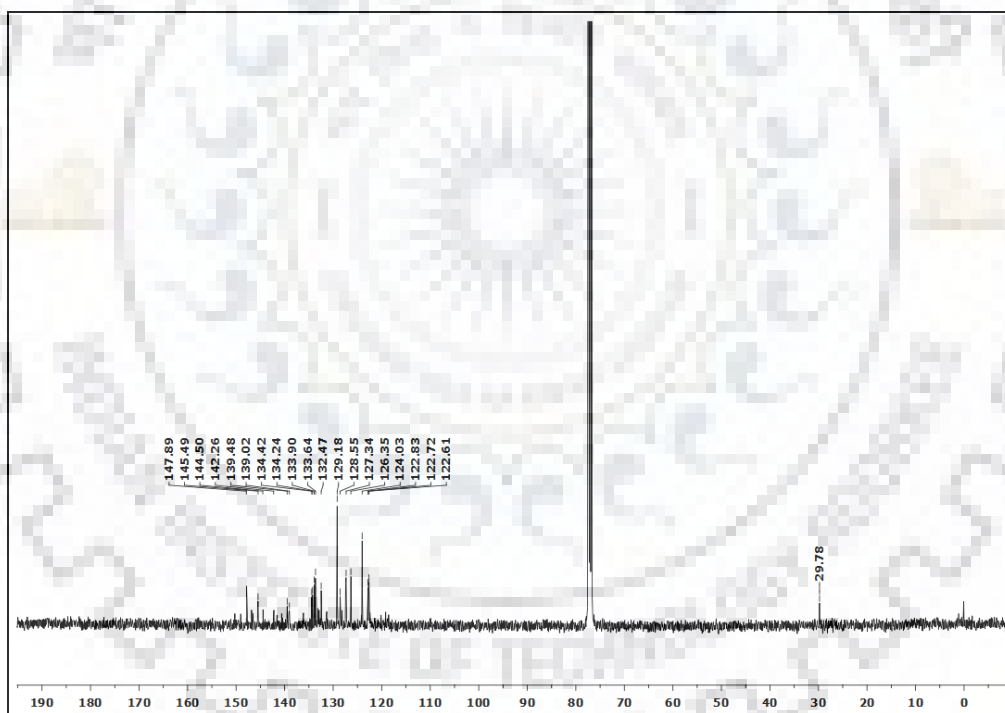


Figure A8. ^{13}C NMR spectrum of $\text{NiTPP}(\text{TPA})_2\text{NO}_2$ in CDCl_3 at 298 K

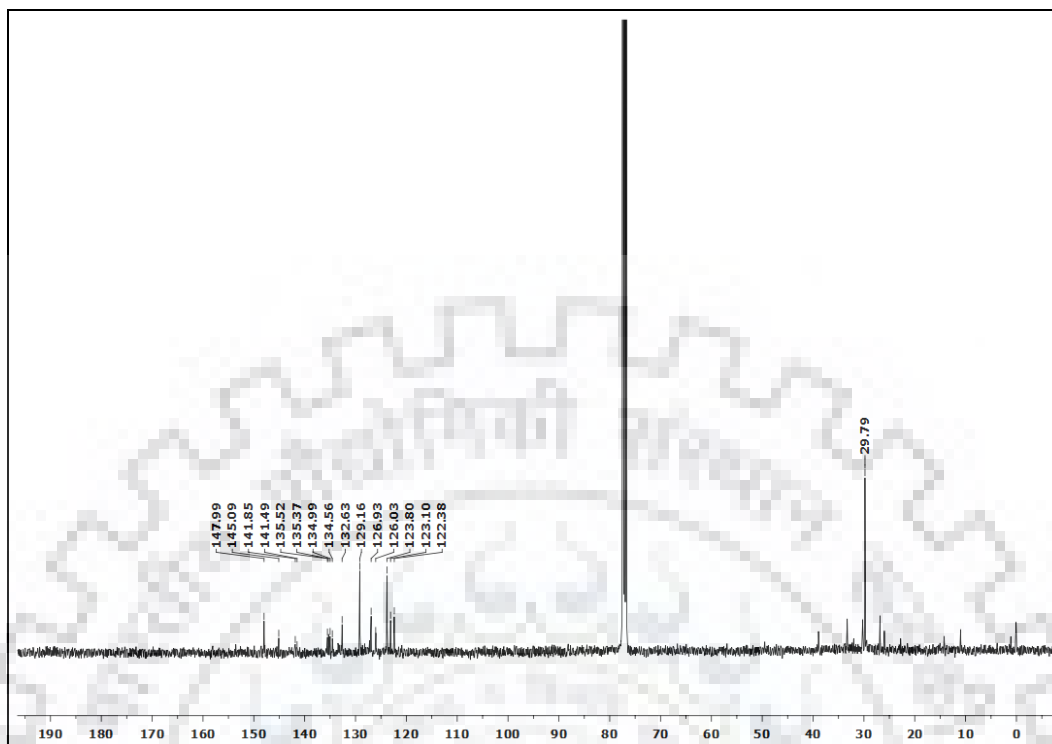


Figure A9. ^{13}C NMR spectrum of ZnTPP(TPA)₂NO₂ in CDCl₃ at 298 K

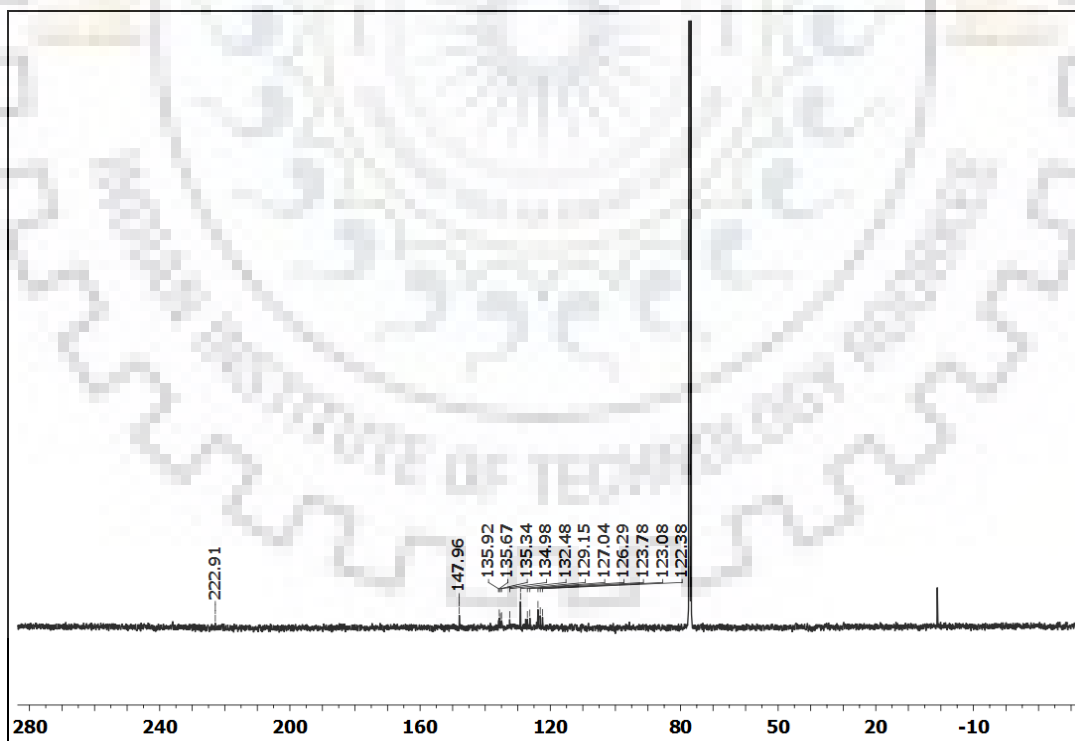


Figure A10. ^{13}C NMR spectrum of H₂TPP(TPA)₂CHO in CDCl₃ at 298 K

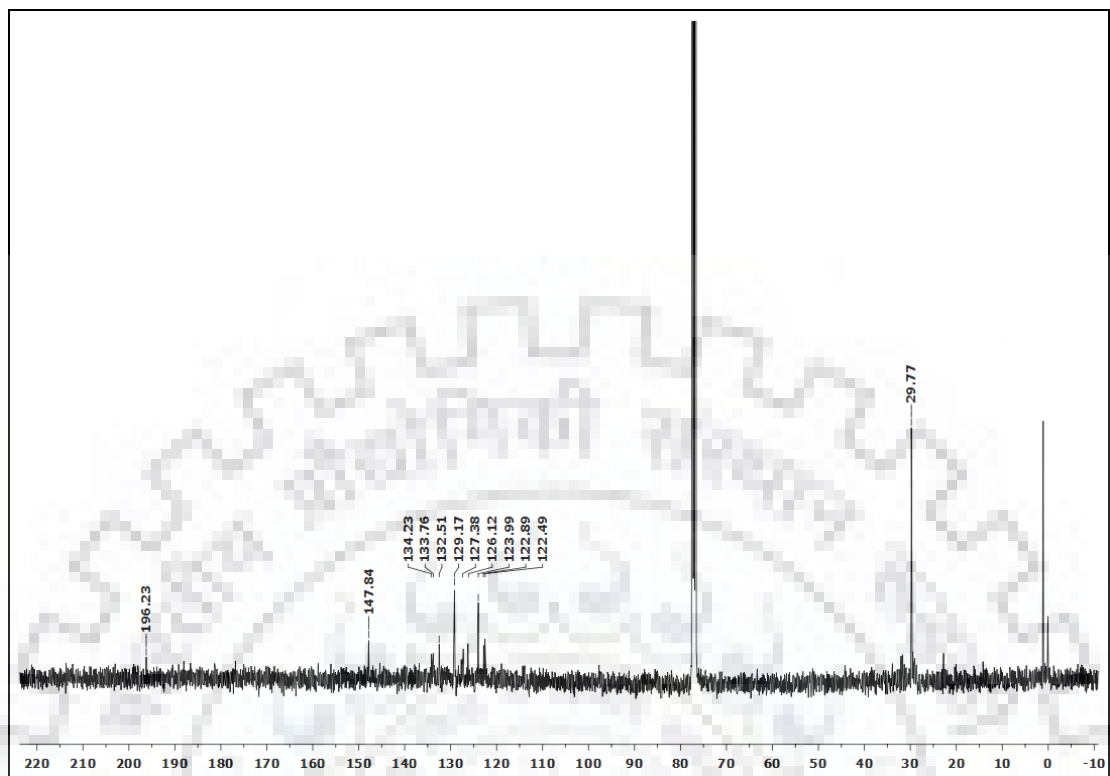


Figure A11. ^{13}C NMR spectrum of NiTPP(TPA) $_2$ CHO in CDCl_3 at 298 K

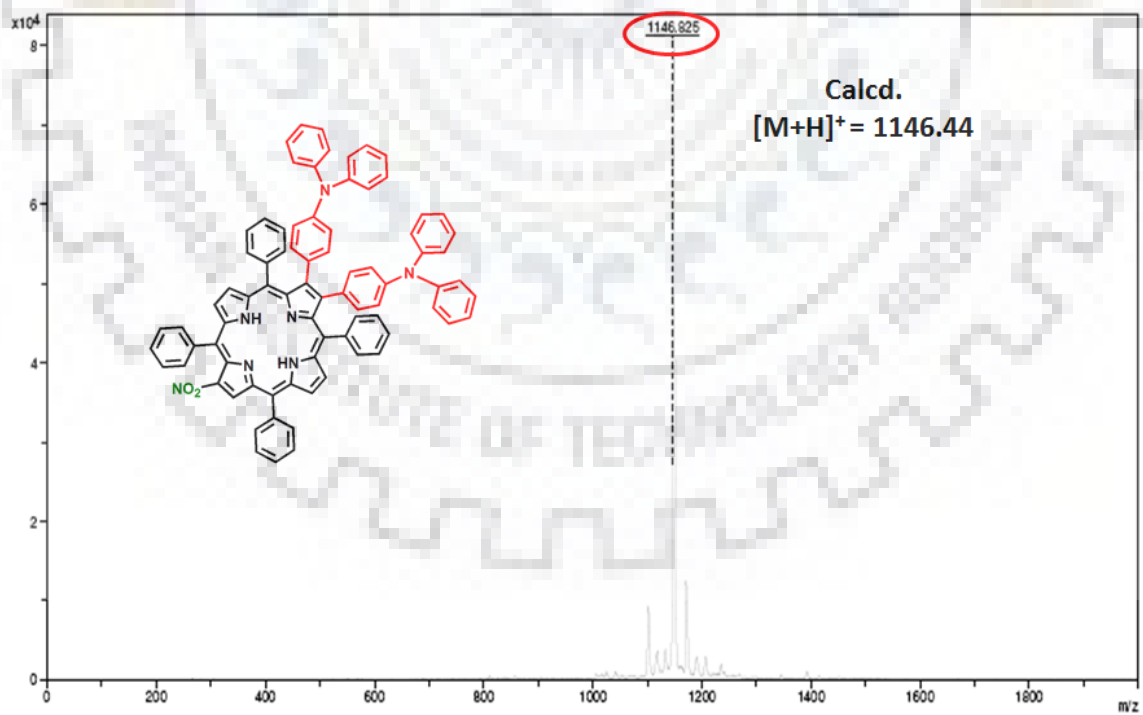


Figure A12. MALDI-TOF mass spectrum of $\text{H}_2\text{TPP}(\text{TPA})_2\text{NO}_2$.

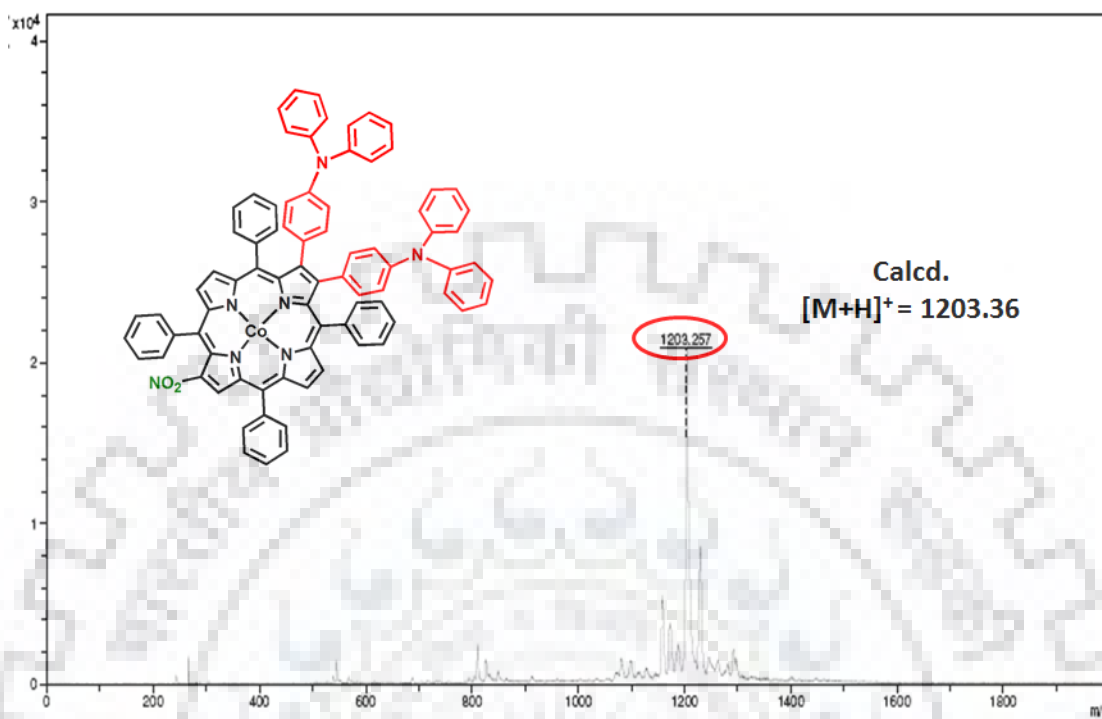


Figure A13. MALDI-TOF mass spectrum of CoTPP(TPA)₂NO₂.

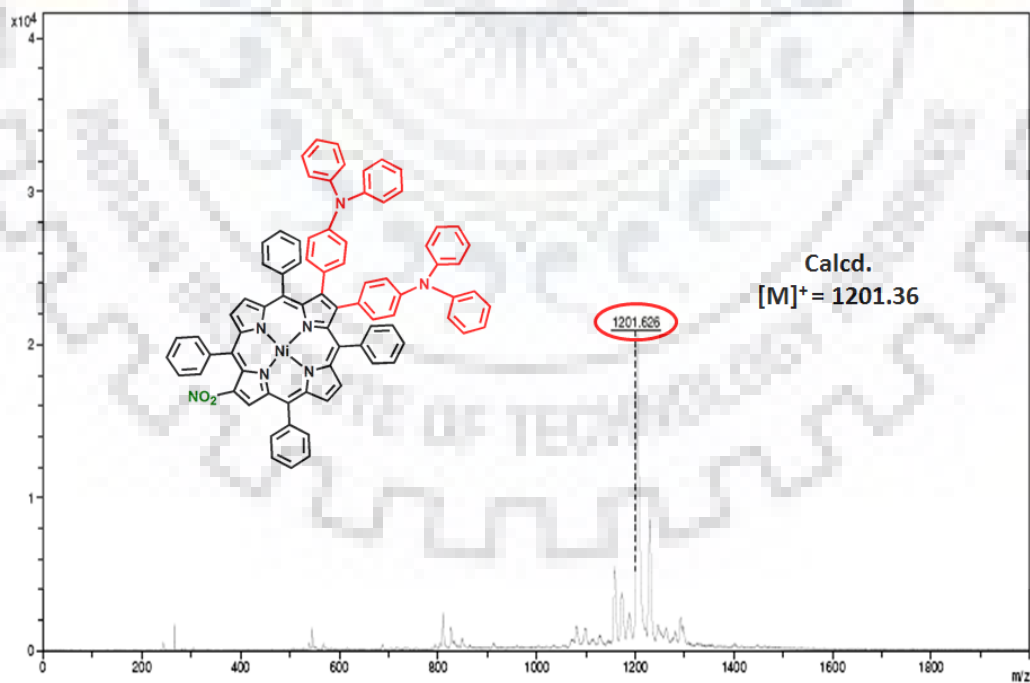


Figure A14. MALDI-TOF mass spectrum of NiTPP(TPA)₂NO₂.

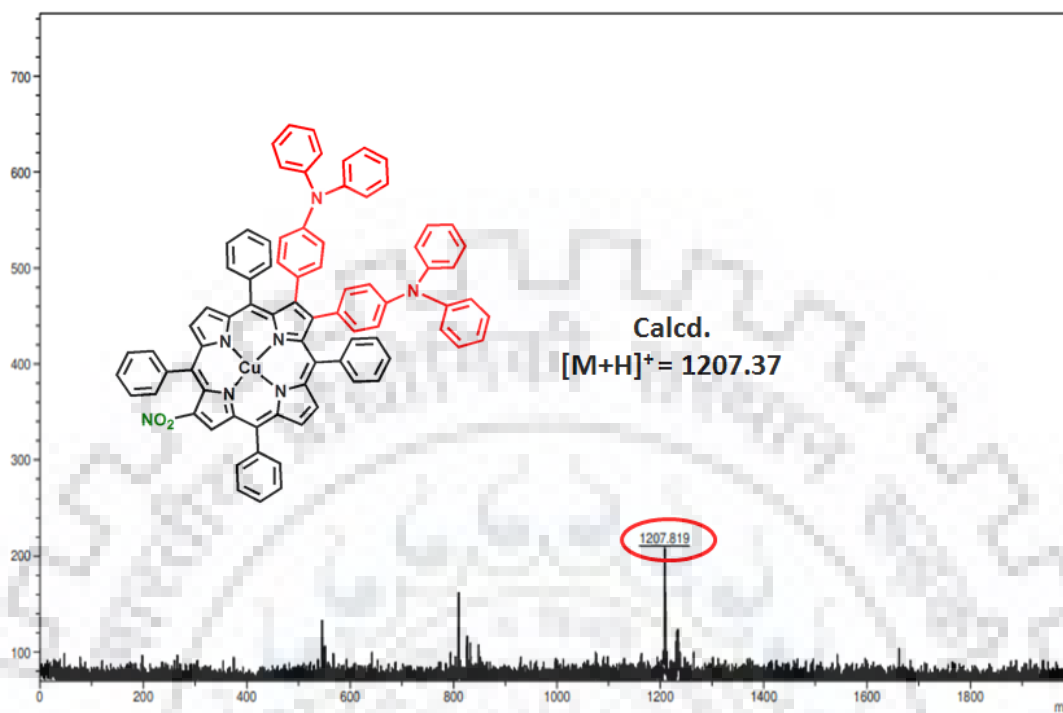


Figure A15. MALDI-TOF mass spectrum of CuTPP(TPA)₂NO₂.

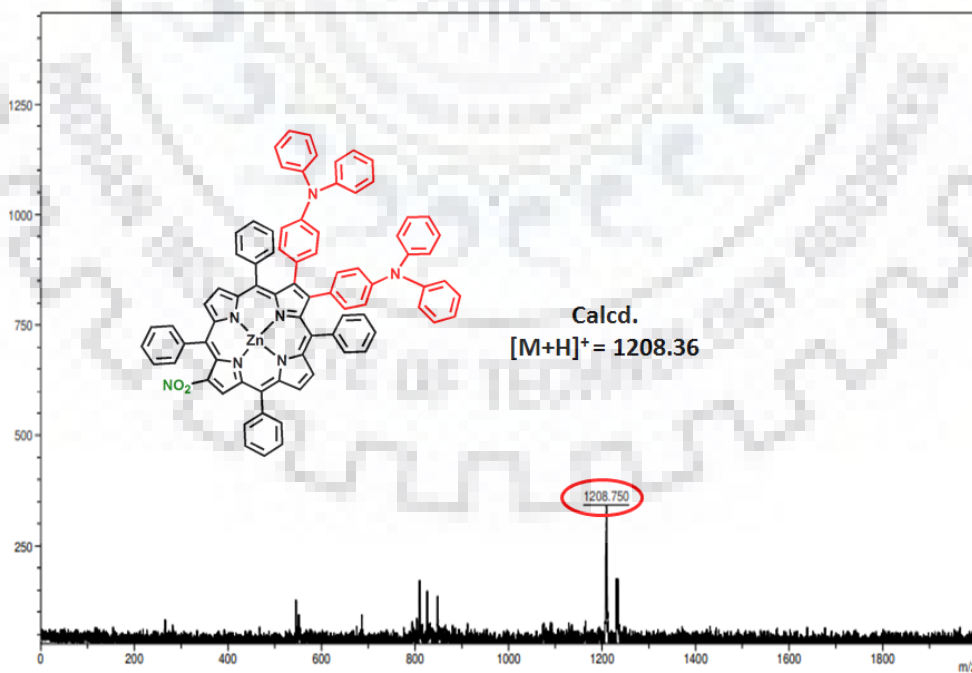


Figure A16. MALDI-TOF mass spectrum of ZnTPP(TPA)₂NO₂.

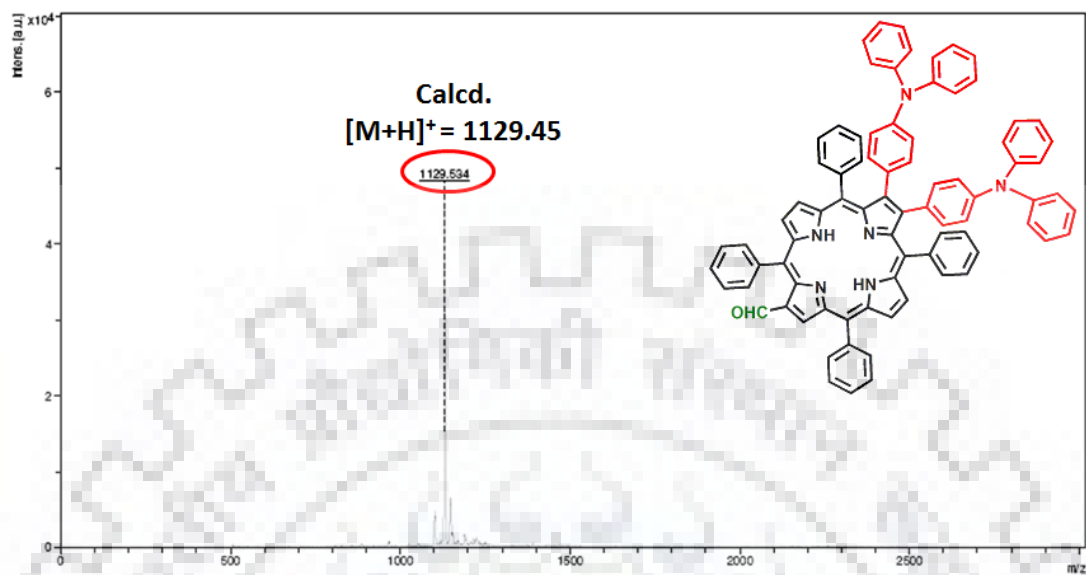


Figure A17. MALDI-TOF mass spectrum of $H_2TPP(TPA)_2CHO$.

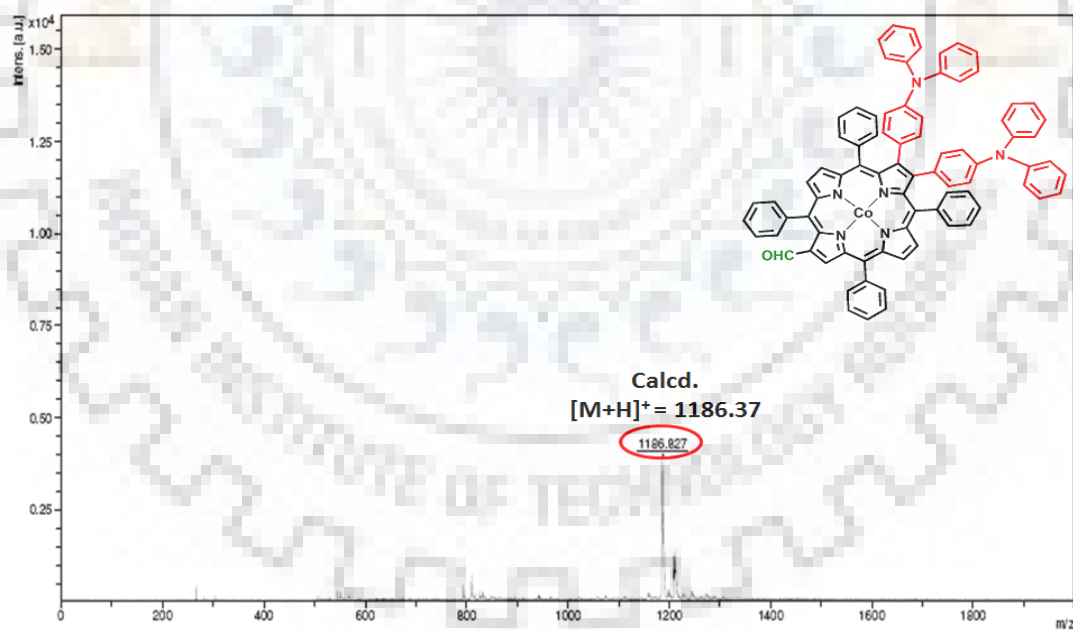


Figure A18. MALDI-TOF mass spectrum of $CoTPP(TPA)_2CHO$.

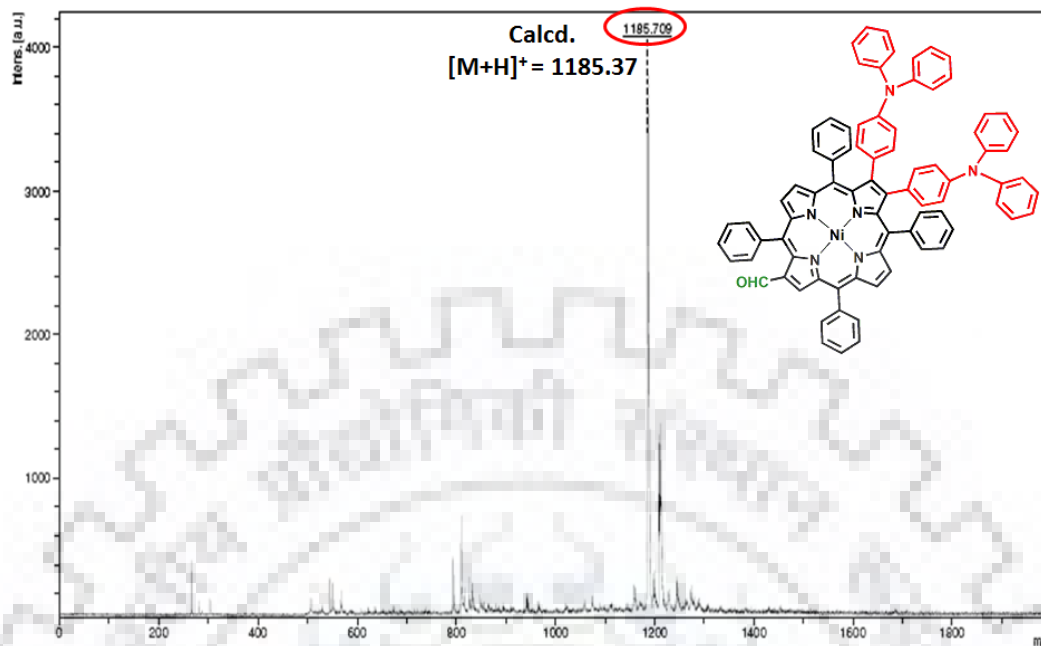


Figure A19. MALDI-TOF mass spectrum of NiTPP(TPA)₂CHO.

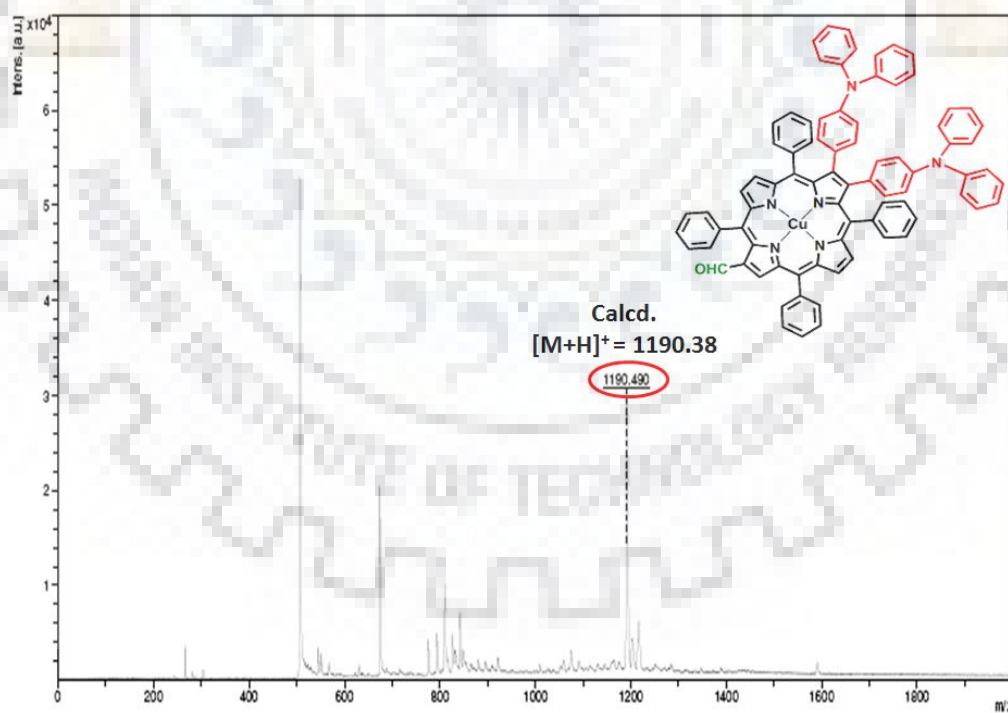


Figure A20. MALDI-TOF mass spectrum of CuTPP(TPA)₂CHO.

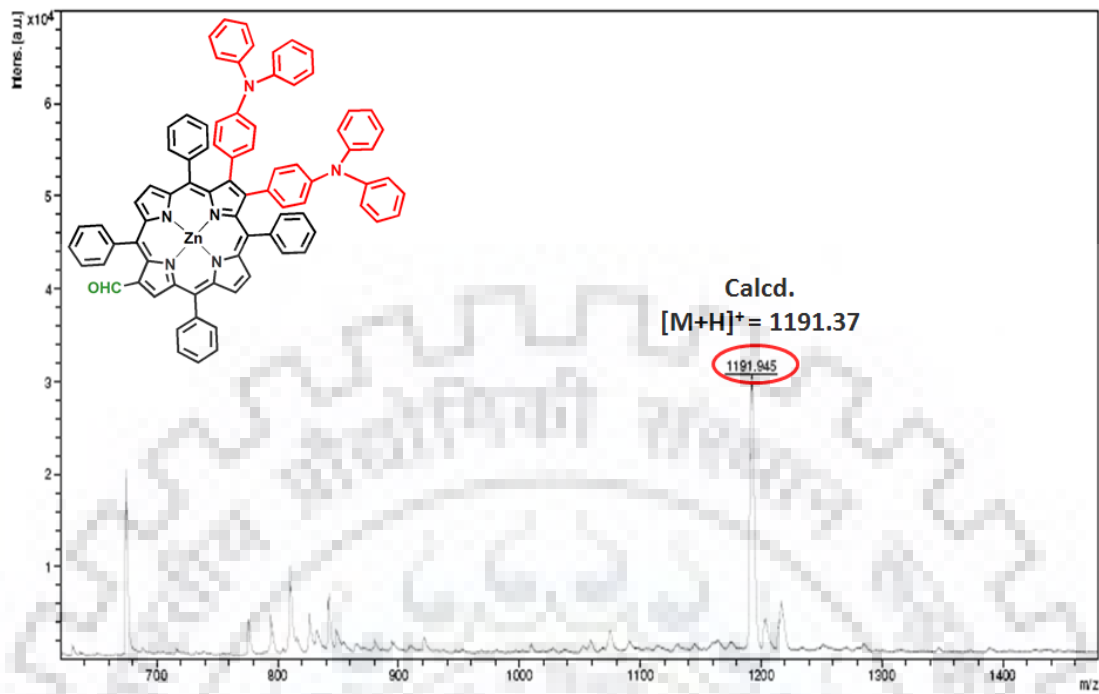


Figure A21. MALDI-TOF mass spectrum of ZnTPP(TPA)₂CHO.

Appendix V: β -Functionalized 'Push-Pull' Porphyrins for NLO Application

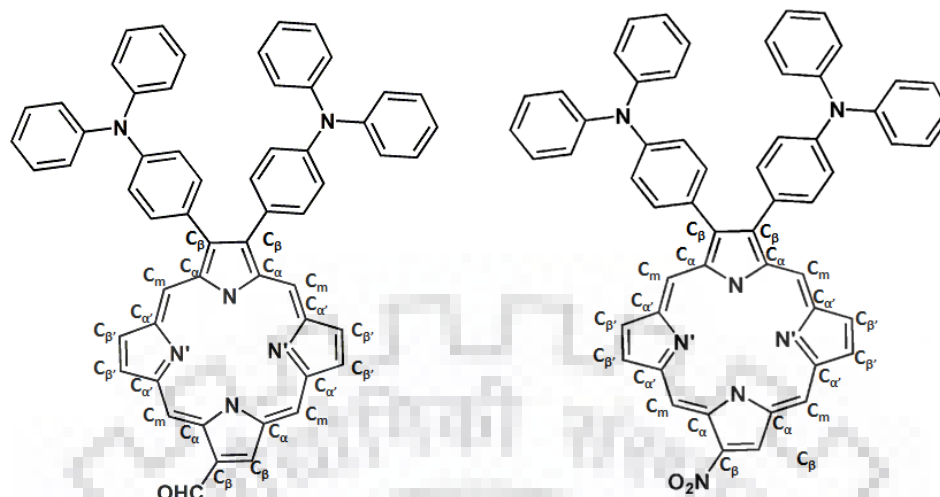


Table A1. Selected Average Bond Lengths (Å) and Bond Angles ($^{\circ}$) for the B3LYP/LANL2DZ Optimized Geometry of $H_2TPP(TPA)_2NO_2$ and $H_2TPP(TPA)_2CHO$

	$H_2TPP(NO_2)(TPA)_2$	$H_2TPP(CHO)(TPA)_2$
Bond Length (Å)		
N- C_{α}	1.391	1.390
N'- $C_{\alpha'}$	1.390	1.390
C_{α} - C_{β}	1.440	1.450
$C_{\alpha'}$ - $C_{\beta'}$	1.472	1.471
C_{β} - C_{β}	1.394	1.399
$C_{\beta'}$ - $C_{\beta'}$	1.366	1.367
C_{α} - C_m	1.417	1.417
$C_{\alpha'}$ - C_m	1.418	1.419
ΔC_{β} (Å)	0.642	0.636
$\Delta 24$ (Å)	0.317	0.312
Bond Angle (deg)		
N- C_{α} - C_m	125.12	124.97
N'- $C_{\alpha'}$ - C_m	126.33	126.37
N- C_{α} - C_{β}	106.11	106.33
N'- $C_{\alpha'}$ - $C_{\beta'}$	110.28	110.26
C_{β} - C_{α} - C_m	128.58	128.56

Appendix V: β -Functionalized 'Push-Pull' Porphyrins for NLO Application

$C_{\beta'}-C_{\alpha'}-C_m$	123.34	123.33
$C_{\alpha}-C_m-C_{\alpha'}$	123.95	124.13
$C_{\alpha}-C_{\beta}-C_{\beta}$	108.12	107.96
$C_{\alpha'}-C_{\beta'}-C_{\beta}$	106.78	106.80
$C_{\alpha}-N-C_{\alpha}$	110.95	111.11
$C_{\alpha'}-N'-C_{\alpha'}$	110.73	105.76

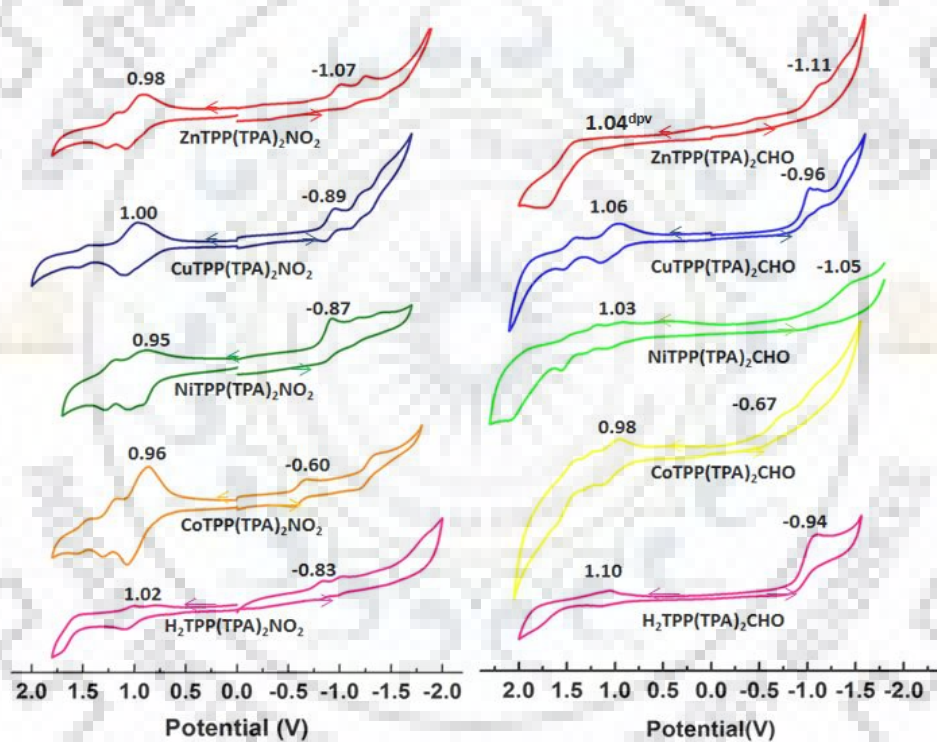


Figure A22. Cyclic Voltammograms of Porphyrins (a) MTPP(TPA)₂NO₂ and MTPP(TPA)₂CHO (M = 2H, Co(II), Cu(II), Ni(II), Zn(II)) and in CH₂Cl₂ with a Scan Rate of 0.1 V/s at 298 K.

APPENDIX-VI

Antipodal β -Tetrasubstituted Triphenylaminoporphyrin: Synthesis, Spectral and Electrochemical Redox Studies

Table of Contents	Page No.
Figure A1. ^1H NMR spectrum of $\text{H}_2\text{TPP}(\text{TPA})_4$ in CDCl_3 at 298 K.	287
Figure A2. ^1H NMR spectrum of $\text{NiTPP}(\text{TPA})_4$ in CDCl_3 at 298 K.	287
Figure A3. ^1H NMR spectrum of $\text{ZnTPP}(\text{TPA})_4$ in CDCl_3 at 298 K.	288
Figure A4. MALDI-TOF-Mass spectrum of $\text{H}_2\text{TPP}(\text{TPA})_4$.	288
Figure A5. MALDI-TOF-Mass spectrum of $\text{CoTPP}(\text{TPA})_4$.	289
Figure A6. MALDI-TOF-Mass spectrum of $\text{CuTPP}(\text{TPA})_4$.	289
Figure A7. MALDI-TOF-Mass spectrum of $\text{NiTPP}(\text{TPA})_4$.	290
Figure A8. MALDI-TOF-Mass spectrum of $\text{ZnTPP}(\text{TPA})_4$.	290
Figure A9. Cyclic voltammograms of synthesized porphyrins in CH_2Cl_2 at 298 K.	291
Table A1. Selected bond lengths (\AA) and bond angles ($^\circ$) for the B3LYP/LANL2DZ optimized geometry of $\text{H}_2\text{TPP}(\text{TPA})_4$.	292

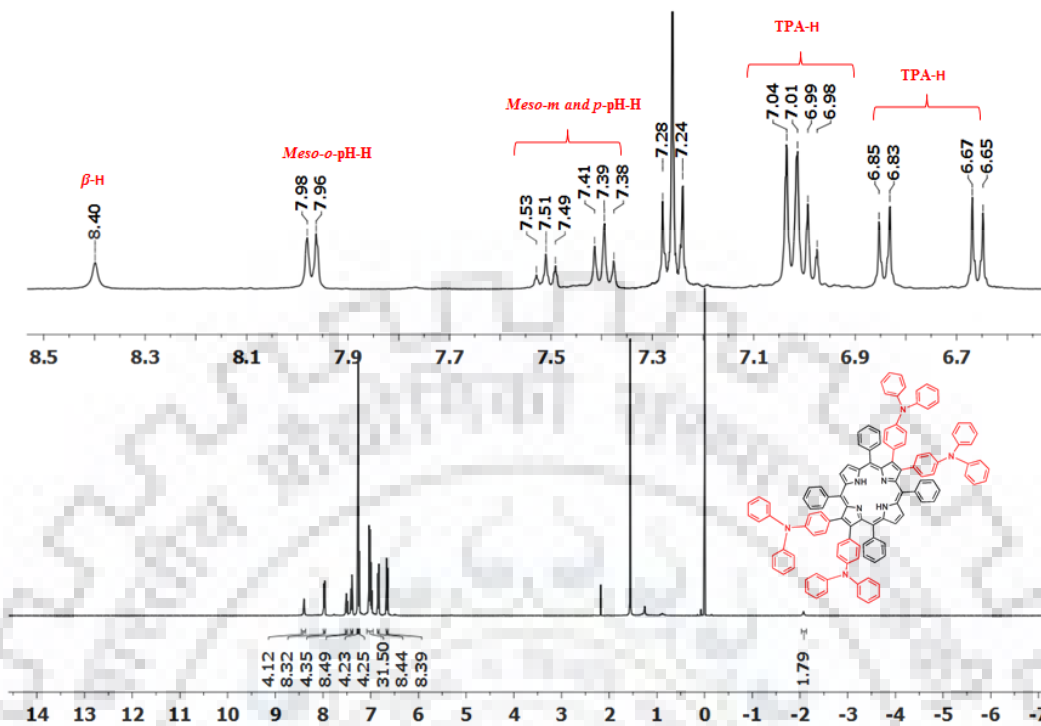


Figure A1. ^1H NMR Spectrum of $\text{H}_2\text{TPP}(\text{TPA})_4$ in CDCl_3 at 298 K.

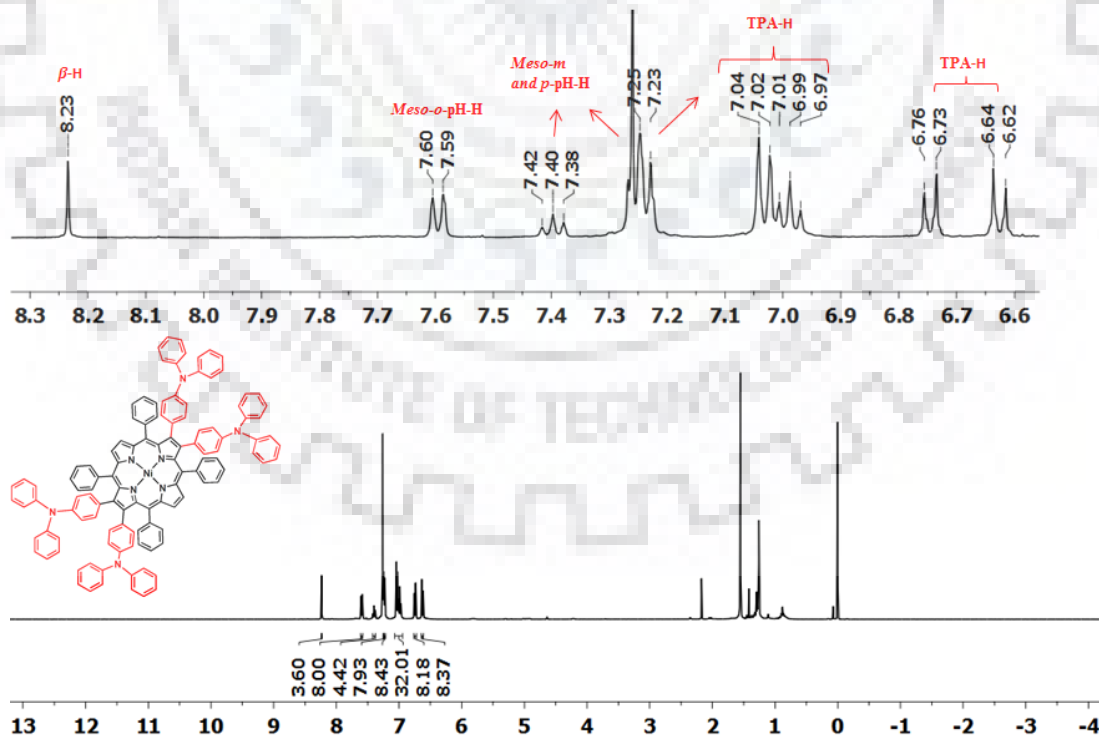


Figure A2. ^1H NMR spectrum of $\text{NiTPP}(\text{TPA})_4$ in CDCl_3 at 298 K.

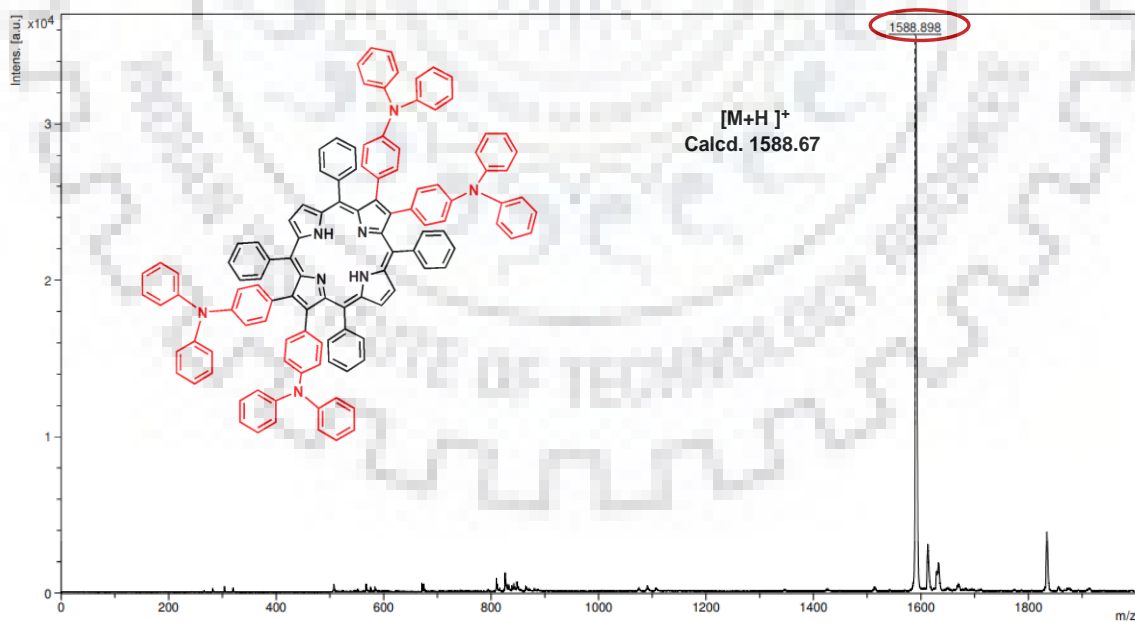
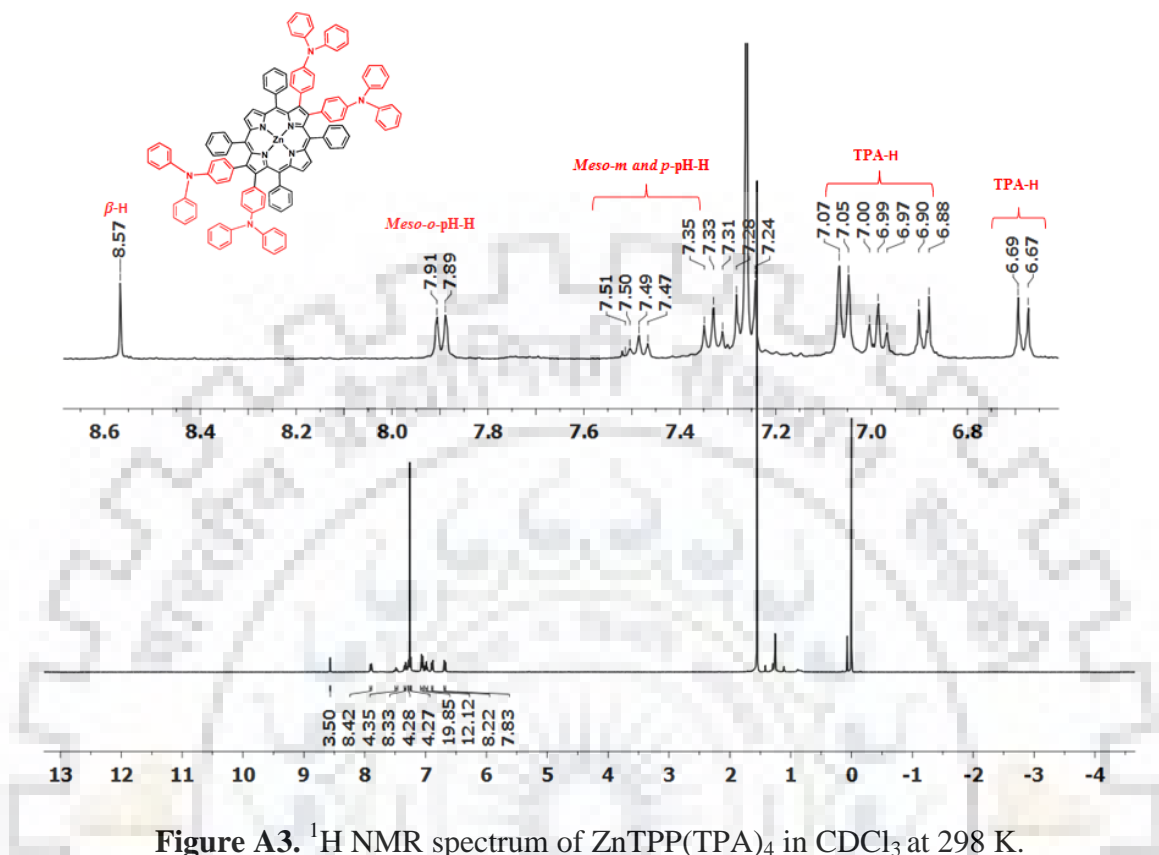


Figure A4. MALDI-TOF-MASS Spectrum of $\text{H}_2\text{TPP}(\text{TPA})_4$.

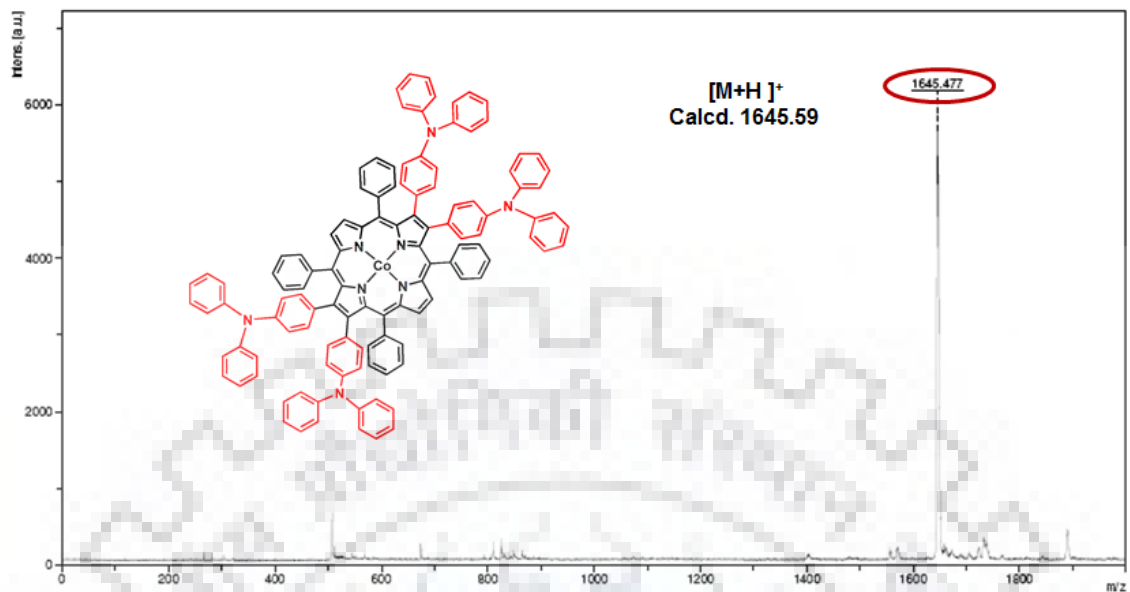


Figure A5. MALDI-TOF-Mass spectrum of CoTPP(TPA)₄.

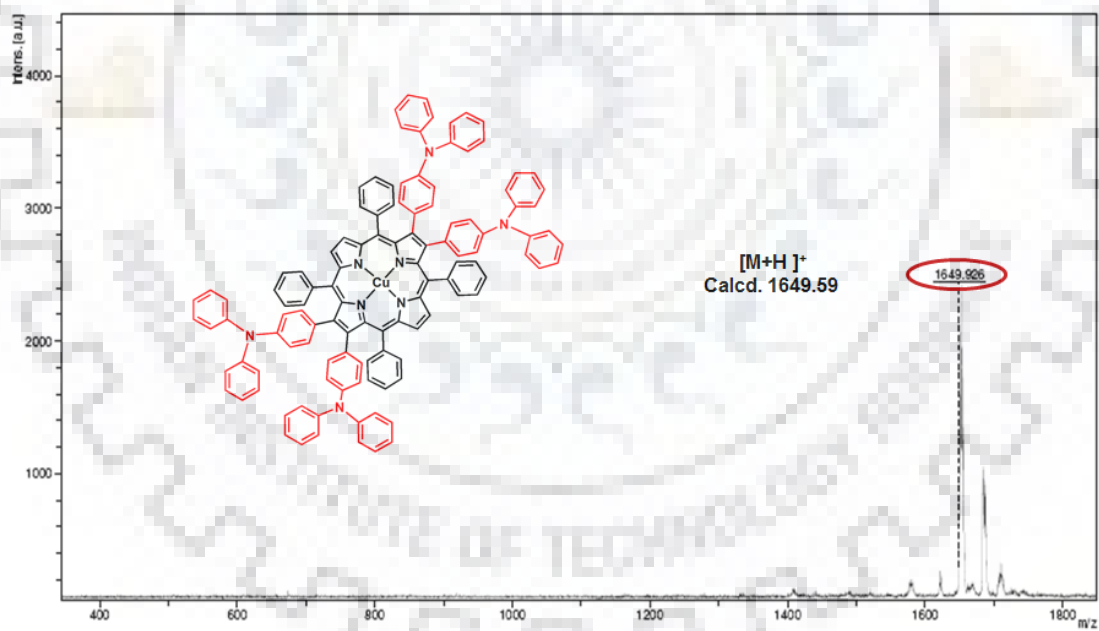


Figure A6. MALDI-TOF-Mass spectrum of CuTPP(TPA)₄.

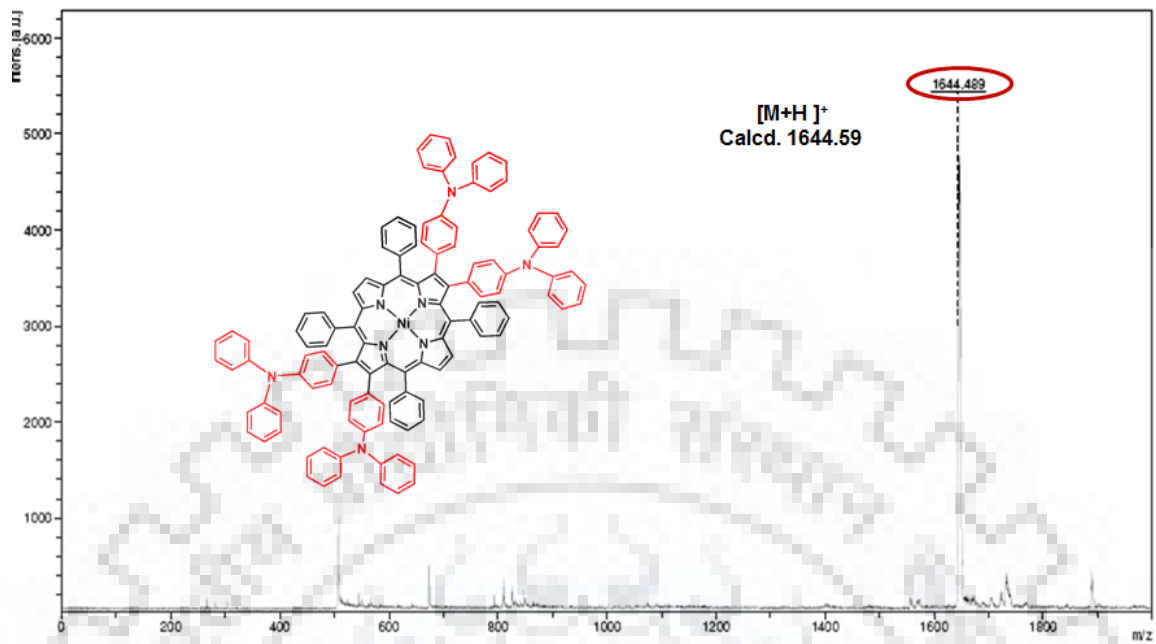


Figure A7. MALDI-TOF-Mass spectrum of NiTPP(TPA)₄.

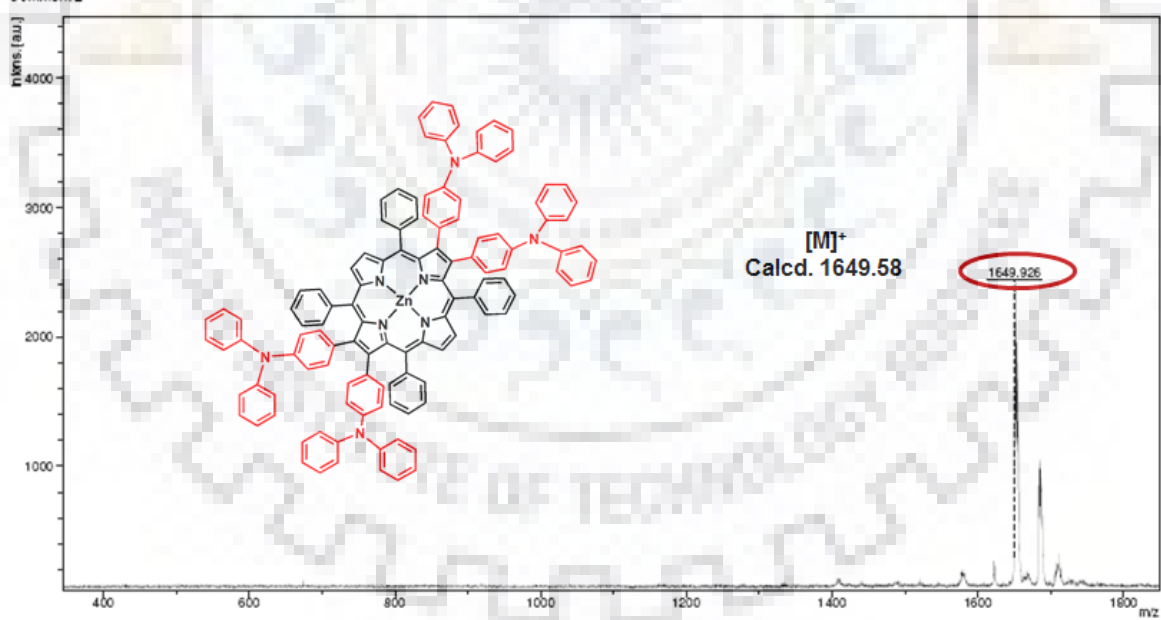


Figure A8. MALDI-TOF-Mass spectrum of ZnTPP(TPA)₄.

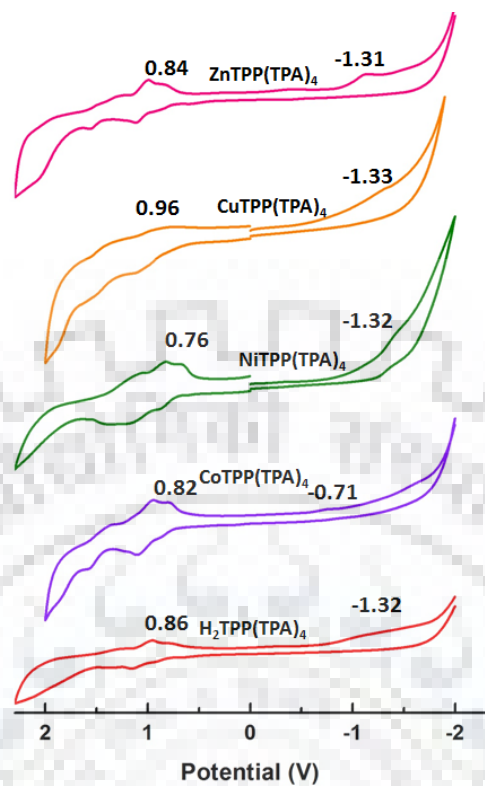


Figure A9. Cyclic voltammograms of synthesized porphyrins in CH_2Cl_2 at 298 K.

Appendix VI: Symmetrically β -Tetrasubstitutedporphyrins

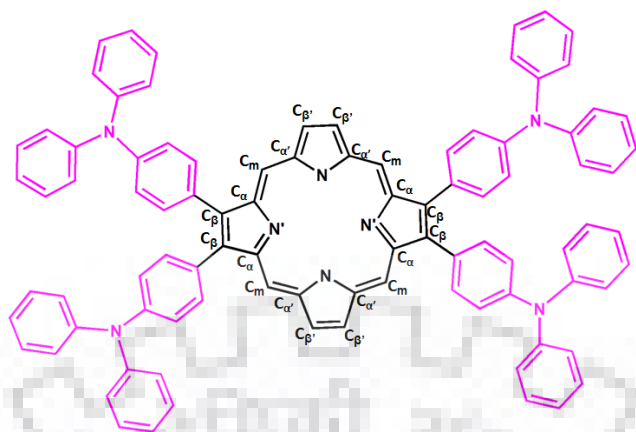


Table A1. Selected bond lengths (Å) and bond angles (°) for the B3LYP/LANL2DZ optimized geometry of $H_2TPP(TPA)_4$.

Bond Length(Å)	
	$H_2TPP(TPA)_4$
N-C _{α}	1.388
N'-C _{α'}	1.39
C _{α} -C _{β}	1.454
C _{α'} -C _{β'}	1.470
C _{β} -C _{β}	1.403
C _{β'} -C _{β'}	1.368
C _{α} -C _{m}	1.418
C _{α'} -C _{m}	1.420
ΔC_{β} (Å)	0.760
$\Delta 24$ (Å)	0.377
Bond Angle (deg)	
N-C _{α} -C _{m}	124.09
N'-C _{α'} -C _{m}	126.20
N-C _{α} -C _{β}	106.56
N'-C _{α'} -C _{β'}	110.18
C _{β} -C _{α} -C _{m}	129.2
C _{β'} -C _{α'} -C _{m}	123.56
C _{α} -C _{m} -C _{α'}	123.89
C _{α} -C _{β} -C _{β}	107.71
C _{α'} -C _{β'} -C _{β'}	106.80
C _{α} -N-C _{α}	111.01
C _{α'} -N'-C _{α'}	105.88